

UNIVERSITÉ DE STRASBOURG

ÉCOLE DOCTORALE DES SCIENCES DE LA VIE ET DE LA SANTÉ

UMR 7199 CNRS

Laboratoire de **Conception et Application de Molécules Bioactives**

Equipe de **Chimie et Neurobiologie Moléculaire**

THESIS

presented by:

Kate DUNNING

To obtain the degree of: Doctor of Philosophy of the University of Strasbourg

Speciality: Molecular Neurobiology

Structural and functional studies of P2X7 receptors.

Thesis supervised by:

Dr. GRUTTER Thomas

Directeur de recherche, CNRS, Université de Strasbourg

Examinors:

Dr. RASSENDREN François

Directeur de recherche, CNRS, Institut de Génomique Fonctionnelle

Dr. NICKE Annette

Professor, Ludwig-Maximilians-Universität München

President of the jury:

Dr. POISBEAU Pierrick

Professeur, Université de Strasbourg

ACKNOWLEDGMENTS

I would like to firstly thank the members of my jury for accepting to judge this thesis work; Dr. François Rassendren and Prof. Dr. Annette Nicke as examiners, and Dr. Pierrick Poisbeau as the president of the jury.

Je tiens à remercier, tout d'abord, mon directeur de thèse le docteur Thomas Grutter, pour la confiance qu'il m'a accordée dans ces projets de thèse, sa disponibilité au quotidien et son encadrement qui m'ont permis de prendre confiance en mes capacités. Merci pour le soutien et l'enthousiasme sans faille, même quand la science est dure, et d'avoir créé un environnement de recherche au sein duquel on se sent libre de poser des questions, de discuter et d'explorer nos idées sans jugement. Ce laboratoire me manquera.

Je remercie également le docteur Alexandre Specht pour son aide, ses conseils et sa disponibilité au quotidien. Merci à tout.e.s les autres permanent.e.s du laboratoire et de l'UMR, qui ont toujours été prêts à m'aider pendant ces trois années. Un grand merci à Adeline en particulier qui m'a beaucoup aidée pendant ma dernière année et sans qui le projet du chapitre trois n'aurait pu aboutir. Merci également à tous les anciens membres du laboratoire que j'ai pu croiser, qui m'ont chacun.e transmis des connaissances et de précieux conseils pour cette thèse. Aux "nouveaux" arrivants, merci de m'avoir soutenue durant la fameuse période « single channel » avec tous les cafés apportés au bureau, les blagues et les visites en patch pour vérifier que je tenais le coup ! Je vous souhaite le meilleur pour vos fins de thèses.

A mes « ami.e.s du labo » a.k.a les docteurs Laurie, Juline et Seb, un énorme merci pour ces années passées ensemble, merci de m'avoir soutenue dans les moments difficiles (les pauses café comme les petits dej de crise !), pour toutes les sorties, apéros et voyages ensemble, pour les montages qui me font encore rire, et bien sûr les conseils et discussions scientifiques. Merci de m'avoir encouragée et de m'avoir rassurée quand je ne voyais pas la fin, et de m'avoir aidée à enfin passer la ligne d'arrivée ! Je me considère chanceuse d'avoir pu vivre ma thèse en telle bonne compagnie. Vivement la prochaine sortie entre végan.e.s !

A mes colocs, à Rue Sellénick et à la 101, qui sont devenu.e.s des vrai.e.s ami.e.s pour la vie, merci de m'avoir soutenue dans les moments difficiles, de thèse et autres, d'avoir su me changer des idées au quotidien et de me faire relativiser après les longues journées de patch, de m'avoir apportée chacun.e énormément. On a vécu cette rédaction ensemble, merci pour tous les repas ramenés au bureau, les goûters et les debriefs dans ma chambre qui m'ont permis de garder une vie sociale pendant ces mois difficiles !

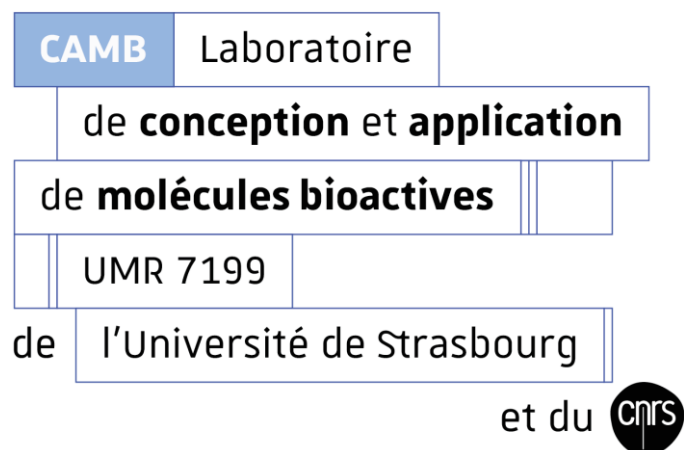
Thank you to my friends “back home”, the Aldryngton mandem and ME betches (yes, I have just written that in my manuscript), for always being there despite the distance, for making time for me in the diary when I’m back, for the voice notes (which have given us some real gems), for the care packages sent over in crisis moments, and the visits to Strassy B equipped with a supply of Cadburys and Marmite. How lucky I am to have you.

A small shoutout to Erykah, Sade, Debussy and Ravel for the soundtrack which kept me going through many, many hours of patch.

Finally, and most importantly, I would like to thank my family, my Mum and Dad, my brother, my Granny and Papa, who have always supported me and been there for me at any time, any cost and any distance. I love you and I appreciate you, and I could not have done any of it without you.

PREFACE

This work has been realised in the Laboratory of Conception and Application of Bioactive Molecules (UMR7199), within the group of Chemistry and Molecular Neurobiology, under the direction of Dr. Thomas Grutter.



Funding was provided by a doctoral scholarship, awarded by the French Ministry for Higher Education and Research (**Ministère de l'Enseignement Supérieure et de la Recherche**).



TABLE OF CONTENTS

ACKNOWLEDGMENTS	2
PREFACE	4
TABLE OF CONTENTS	5
LIST OF FIGURES	12
LIST OF TABLES	16
ABBREVIATIONS	17
INTRODUCTION	22
1. Ion channels	22
1.1. Ligand-Gated Ion Channels (LGICs)	23
1.1.1. Historical context	23
1.1.2. LGIC superfamily	24
1.2. Study of ion channels: patch clamp electrophysiology	26
2. P2X receptors	28
2.1. Purinergic signalling	28
2.1.1. Discovery	28
2.1.2. Sources of extracellular ATP	29
2.2. P2X receptors: historical context and generalities	31
2.3. Seven P2X subtype variants	32
2.4. Localisation	34
2.4.1. Heteromeric P2XRs	35
2.5. Physiological roles	36
2.5.1. Neuromodulation: P2X2, P2X4, P2X6, P2X7	36
2.5.2. Smooth muscle contraction: P2X1	37
2.5.3. Vasodilation: P2X4	38
2.5.4. Sensory functions: P2X4	39
2.5.4.1. Sensory functions in pathological states: P2X4 in neuropathic pain	40
2.6. Structural features	41

2.6.1.	Global architecture	43
2.6.2.	Extracellular domain.....	45
2.6.3.	Transmembrane helices and the gate	45
2.6.4.	Ion conduction pathway.....	46
2.6.5.	Intracellular domain: cytoplasmic cap.....	47
2.7.	Allosteric conformational states.....	48
2.7.1.	Pore opening (<i>gating</i>).....	48
2.7.2.	Desensitised state.....	49
2.7.3.	“Dilated” state.....	50
3.	P2X7	50
3.1.	Historical aspect.....	50
3.2.	Localisation	50
3.3.	Structure	51
3.3.1.	Overall architecture	52
3.3.2.	The extracellular domain: ATP binding site	53
3.3.3.	The TM domains	53
3.3.4.	The intracellular domains: cytoplasmic cap, Ccys anchor and the ballast region.....	54
3.4.	Function	57
3.4.1.	Single channel level activity	59
3.5.	Pharmacology	60
3.5.1.	Agonists	60
3.5.1.1.	Non – nucleotide agonists.....	61
3.5.2.	Antagonists	62
3.5.3.	Modulators	64
3.5.4.	Species differences.....	64
3.6.	Protein partners.....	65
3.7.	P2X7R variants	66
3.7.1.	Splice variants.....	66

3.7.2.	Single Nucleotide Polymorphisms (SNPs).....	67
3.8.	Physiological and pathophysiological roles.....	68
3.8.1.	P2X7 knock-out mouse models.....	68
3.8.2.	Physiological roles	69
3.8.2.1.	Inflammation	69
3.8.2.2.	Cell life: proliferation	70
3.8.3.	Cell death: apoptosis and necrosis.....	71
3.8.4.	Pathological roles.....	72
3.8.4.1.	Neuropathic and inflammatory pain.....	72
3.8.4.2.	Alzheimer’s disease	72
3.9.	Therapeutic outlook.....	73
GENERAL THESIS OBJECTIVES.....		74
CHAPTER ONE: TOWARDS A STRUCTURE OF P2X7 BY SINGLE PARTICLE CRYO ELECTRONMICROSCOPY		76
INTRODUCTION		76
1.	Methods of membrane protein production.....	77
1.1.	Recombinant expression in yeast host system: <i>Pichia pastoris</i>	78
1.2.	Recombinant expression in insect cell systems: <i>Spodoptera frugiperda</i>	79
1.3.	Recombinant expression in mammalian cell systems.....	80
2.	Extraction, reconstitution and purification of membrane proteins.....	81
2.1.	Advance construct design	81
2.1.1.	Use of fusion tags	81
2.1.2.	Modifications of target protein	82
2.2.	Extraction and reconstitution of membrane proteins.....	82
2.2.1.	Nanodiscs	84
2.2.2.	Amphipols	84
2.3.	Purification of membrane proteins	84
3.	Structural determination of membrane proteins: principal methods	86
3.1.	NMR spectroscopy.....	86

3.2.	X-ray crystallography.....	86
3.3.	Single particle cryo-EM	87
3.4.	Comparative analysis of the different methods	88
3.5.	Global considerations.....	88
4.	Structural studies of P2X receptors.....	88
4.1.	Structures obtained by X-ray crystallography	89
4.1.1.	zfP2X4 <i>apo</i> resting state structure (2009)	89
4.1.2.	zfP2X4 <i>apo</i> and ATP-bound open state structures (2012).....	90
4.1.3.	amP2X.....	90
4.1.4.	hP2X3	91
4.1.5.	pdP2X7	92
4.1.6.	ckP2X7	93
4.2.	Limitations of the crystallographic structures	94
4.3.	Structures obtained by cryo-EM	95
4.3.1.	rP2X7.....	95
	OBJECTIVES AND STRATEGY	97
1.	Objectives.....	97
2.	General strategy.....	97
	EXPERIMENTAL SECTION	99
	RESULTS.....	101
1.	Generation of hP2X7-8His constructs and functionality test.....	101
2.	Sf9/Baculovirus system expression tests	101
3.	<i>P. pastoris</i> expression tests.....	104
	DISCUSSION AND OUTLOOK	106
	CHAPTER TWO: USE OF PHOTOISOMERISABLE TOOLS TO PROBE STRUCTURE AND FUNCTION OF P2X7 RECEPTORS	108
	INTRODUCTION	108
1.	Photoswitches for ion channel studies	108
1.1.	Azobenzene as a photoswitchable core motif.....	109

1.2. Optopharmacology	110
1.3. Optogenetic pharmacology.....	113
2. Optogenetic pharmacological tools for P2X receptors	115
2.1. Optogating: MEA-TMA	116
2.2. Optotweezers: MAM.....	118
OBJECTIVES AND STRATEGIES.....	121
1. Optogating of P2X7	121
2. Extension of optotweezers strategy to P2X7	123
3. Apparatus: irradiation-coupled patch clamp electrophysiology	124
EXPERIMENTAL SECTION	125
RESULTS.....	127
1. Use of MEA-TMA photoswitch: optogating and optoblock of rP2X7	127
1.1. Optogating for light-controlled P2X7 activity	127
1.2. Use of a TM cavity-bordering tyrosine-to-serine mutation to enable P2X7 optogating.....	130
1.2.1. Background.....	130
1.2.2. Characterisation of P2X7 I331C/Y343S mutant optogating	131
1.3. Use of optoblocking to investigate P2X7 facilitation behaviour.	134
2. Use of MAMs: optotweezers strategy applied to P2X7	137
DISCUSSION AND OUTLOOK	140
1. MEA-TMA optogating and optoblock strategies	140
2. MAM optotweezers strategy	145
CONCLUSION.....	147
CHAPTER THREE: STUDIES ON THE PHENOMENA OF FACILITATION AND MACROPORE FORMATION IN P2X7 RECEPTORS	148
INTRODUCTION	148
1. Facilitation phenomenon of P2X7 receptors	148
1.1. Context.....	148
1.2. Modulation by cholesterol.....	149
1.2.1. Cholesterol: a P2X7 inhibitor	149

1.2.2.	P2X7 in cholesterol-rich lipid raft environments	151
1.3.	Modulation by the Ccys anchor	153
1.4.	Modulation by Calmodulin	154
1.5.	Species differences concerning facilitation	155
1.6.	Role of the N-terminus	156
1.7.	General comments	156
2.	The P2X7 macropore.....	157
2.1.	Brief historical context	157
2.2.	Methodologies to study macropore formation and their caveats	158
2.3.	Classic theories behind macropore formation.....	159
2.3.1.	Intrinsic P2X7 permeation	159
2.3.2.	Recruitment of an annexe channel.....	160
2.4.	Pannexin-1 as a possible annexe channel	162
2.5.	Permeating species and characterisation	162
2.6.	General remarks	163
3.	TMEM16 channels : a possible P2X7 complex with implications for facilitation and macropore formation ?	164
OBJECTIVES.....		168
EXPERIMENTAL SECTION		170
RESULTS.....		175
1.	Molecular characterisation of the rP2X7 facilitated state.....	175
1.1.	Mathematical kinetic modelling (<i>Dr. Thomas Grutter</i>).....	179
1.2.	Probing the pore diameter of the facilitated state.....	181
2.	Studies on a possible rP2X7/TMEM16s complex and its implication in facilitation and macropore formation.....	184
2.1.	Probing the regulation of channel gating by an rP2X7/TMEM16 protein complex.	184
2.2.	Probing the role of rP2X7/TMEM16 protein complex in macropore formation.....	187
2.3.	Contribution of TMEM16F subtype to rP2X7 activity.....	189

2.4. Contribution of TMEM16F to rP2X7 channel gating.....	191
2.5. Study of P451L mutant to probe the link between facilitation and macropore formation.....	193
2.6. A molecular model supporting rP2X7/TMEM16F complex formation.	196
DISCUSSION AND OUTLOOK	197
CONCLUSION.....	202
GENERAL CONCLUSIONS.....	203
BIBLIOGRAPHY.....	205
ANNEXES.....	246
ANNEXE 1: Rate and dissociation constants obtained from simulations.	246
ANNEXE 2: Publications.....	247

LIST OF FIGURES

Figure 1. Ligand gated ion channel superfamily.....	24
Figure 2. Different modes of patch clamp electrophysiology.....	27
Figure 3. Chemical structure of ATP in its protonated form.....	29
Figure 4. The "purinergic world".	30
Figure 5. P2X receptors.....	31
Figure 6. Relationship of P2X subunit variants to one another.....	32
Figure 7. Desensitisation kinetics in homomeric P2XRs.	33
Figure 8. Neuromodulatory role of P2XRs: synaptic scaling.	37
Figure 9. Purinergic receptor involvement in vasodilation and vasoconstriction.....	38
Figure 10. Implication of P2X4 in light touch and nociceptive signal transmission <i>via</i> keratinocytes.....	40
Figure 11. Crystallographic structures of zfP2X4.....	43
Figure 12. Individual monomer of zfP2X4.....	44
Figure 13. ATP binding site of zfP2X4.....	45
Figure 14. Ion conduction pathway of P2XRs.....	46
Figure 15. Crystallographic structure of ATP-bound hP2X3: TM domains and cytoplasmic cap.	47
Figure 16. Principal allosteric conformational states of P2XRs.....	48
Figure 17. Cryo-EM structure of rP2X7R.....	52
Figure 18. ATP binding site of rP2X7 as compared to hP2X3.....	53
Figure 19. TM domains and pore of rP2X7R.....	54
Figure 20. Ccys anchor and lipid binding site of rP2X7.....	55
Figure 21. The rP2X7 ballast region.....	56
Figure 22. Possible pathways for P2X7 macropore-mediated large molecule permeabilisation.	58
Figure 23. Sensitisation of P2X7.....	59
Figure 24. Permeating characteristics of hP2X7R at the single channel level.....	59
Figure 25. P2X7 agonists: ATP analogues.....	61
Figure 26. Non-competitive and competitive antagonists in complex with P2X7Rs.....	62
Figure 27. Coding exons of <i>P2RX7</i>	67
Figure 28. P2X7R in the NLRP3 inflammasome.....	70
Figure 29. Implication of P2X7R in cellular energy metabolism mechanisms.....	71
Figure 30. Overview of the principal steps of protein structure determination.....	77

Figure 31. Non–exhaustive presentation of common reconstitution methods for structural determination.	83
Figure 32. Three dimensional reconstructions of a TRPV1 channel nanodisc complex.	84
Figure 33. Co-ordination of histidine residues by a Co ²⁺ -carboxymethylaspartate (CMA) resin.	85
Figure 34. Structures of zfP2X4 solved by X-ray crystallography.....	89
Figure 35. Crystallographic structures of zfP2X4.....	90
Figure 36. Crystallographic structure of ampP2X highlighting M1 and M2 divalent metal binding sites.....	91
Figure 37. Structures of the (a) <i>apo</i> , (b) ATP-bound open and (c) ATP-bound desensitised states of hP2X3 receptor.....	92
Figure 38. Crystallographic structures of pdP2X7.....	93
Figure 39. Structural studies of ckP2X7 in complex with TNP-ATP.....	94
Figure 40. Cryo-EM structures of full length rP2X7.....	95
Figure 41. Schematic representation of the hP2X7-8His construct to be employed in these studies.....	97
Figure 42. Whole cell electrophysiological traces of hP2X7-8His and hP2X7 WT.....	101
Figure 43. Western blots of (a) SDS-PAGE and (b) native electrophoresis gels of hP2X7-8His expressing Sf9 cells.	102
Figure 44. Western Blot of hP2X7-8His protein isolated from Sf9 membranes infected with a viral titer of 1, 5, or 10 Pfu.	103
Figure 45. Western Blot of SDS-PAGE analysis of hP2X7-8His isolated from Sf9 membranes in different conditions.....	104
Figure 46. Expression tests of C _{term} 10His-tagged hP2X7 constructs in <i>P. pastoris</i>	105
Figure 47. Azobenzene isomerisation.....	109
Figure 48. Schematic diagram describing the use of azobenzene for optopharmacology and optogenetic pharmacology.	110
Figure 49. AAQ as a PCL targeting K _v channels.....	111
Figure 50. Cell-targeted QAQ strategy.....	112
Figure 51. Example of the MAQ PTL system as applied to Shaker K ^o channels.....	114
Figure 52. Chemical structure and isomerisation of MEA-TMA.....	116
Figure 53. MEA-TMA optogating and optoblock(a).....	117
Figure 54. MAM photoswitch and the optotweezers strategy.....	118
Figure 55. Optotweezers strategy as applied to P2X2 receptors.	119
Figure 56. Refinement of the zfP2X4 crystallographic structure.....	120
Figure 57. Sequence alignment of the TM2 domain regions of rat P2X subtypes 1-7.....	121
Figure 58. Extension of optogating to other homomeric P2X subtypes.....	122

Figure 59. Range of MAMs of differing lengths and rigidities available for use.....	123
Figure 60. LED-coupled patch clamp electrophysiology apparatus.....	124
Figure 61. Strategy for rP2X7R optogating.	127
Figure 62. Optogating and optoblocking of rP2X7.	128
Figure 63. I331C/Y343S P2X7 mutant.....	130
Figure 64. Optogating of rP2X7 mutant I331C/Y343S.	131
Figure 65. Optogating of I331C/Y343S P2X7 mutant in the presence of inhibitors.	133
Figure 66. Lateral view of optoblocking residues on rP2X7R.	134
Figure 67. Facilitation profile of D329C mutant.	135
Figure 68. Optoblock of D329C mutant during the facilitation process.	135
Figure 69. Photoregulation of rP2X7 by MAMs.	137
Figure 70. Hypotheses concerning the nature of the optoblock during facilitation.	142
Figure 71. Possible sites of MAM tethering to endogenous cysteine residues in rP2X7.....	145
Figure 72. Characteristics of facilitation in rP2X7.....	149
Figure 73. Methyl- <i>beta</i> -cyclodextrin (MCD) and its cholesterol chelating action	150
Figure 74. Modulation of facilitation and initial currents of hP2X7 by cholesterol depletion with MCD.....	151
Figure 75. Characteristics of P2X7 receptors lacking the Ccys region.	153
Figure 76. Location of Ccys anchor and behaviour of Ccys mutants.....	154
Figure 77. Calcium-dependent and -independent facilitation of rP2X7.....	155
Figure 78. Difference in facilitation profile for rP2X7 and hP2X7 receptors.	156
Figure 79. Incorporation of YO-PRO-1 into HEK293 cells expressing rP2X2.....	159
Figure 80. Fast-scanning AFM images of P2X4 receptor.....	159
Figure 81. Identity of various species known to pass the P2X7 macropore.....	163
Figure 82. Cryo-EM structure of mTMEM16F.	165
Figure 83. Possible P2X7/TMEM16F interaction mechanisms.....	165
Figure 84. Effects of TA on facilitation of P2X7 currents in human macrophages.	166
Figure 85. Effect of chloride channel blockers on P2X7 currents and YO-PRO-1 uptake in microglia.....	167
Figure 86. Probing facilitation of rP2X7R with single channel recordings.....	176
Figure 87. BzATP-evoked current facilitation results in a cholesterol-dependent increase of single channel open probability.	177
Figure 88. Increase of mean open time of rP2X7 unitary conductances during facilitation..	178
Figure 89. Effect of MCD on initial rP2X7R current responses.....	179
Figure 90. Kinetic modelling of single channel and whole cell currents.....	180
Figure 91. MTSR modification of rP2X7 cysteine mutants in the naive and facilitated state.	181

Figure 92. Differing MTSR modifications of native and MCD-treated S339C mutant receptors.	182
Figure 93. CaCC inhibitors employed in this study.	184
Figure 94. Effects of CaCC inhibitors on rP2X7 single channel and whole cell currents.	185
Figure 95. Effects of CaCC inhibitors on BzATP-elicited currents in rP2X7-expressing Axolotl oocytes. (<i>Dr. Eric Boué-Grabot</i>).	185
Figure 96. Effects of CaCC inhibitors on BzATP-evoked whole cell rP2X7 currents.	186
Figure 97. Probing TA inhibition of rP2X7 whole cell currents.....	187
Figure 98. rP2X7-induced dye uptake and its regulation by CaCC inhibitors.	188
Figure 99. Dye uptake in rP2X7-expressing 16F-null cells.....	190
Figure 100. A possible rP2X7/TMEM16F complex with implications for dye uptake.	191
Figure 101. Channel gating properties of rP2X7 in TMEM16F-void cells.	192
Figure 102. Effects of CaCC inhibitors on whole cell rP2X7 currents in 16F-null cells.	193
Figure 103. Characterisation of facilitation and macropore formation in P451L mutant.	195
Figure 104. Molecular model of rP2X7 and mTMEM16F in complex.	196

LIST OF TABLES

Table 1. P2XR pharmacology.....	34
Table 2. Localisation of P2XRs.....	35
Table 3. Summary of heteromeric P2XR assemblies.....	35
Table 4. Modulators of P2X7 activity.	64
Table 5. Summary of splice variants identified in human and rodent P2X7 genes.	66
Table 6. Comparative table of the three major protein structural determination techniques. .	88
Table 7 Recapitulative table of all resolved P2X receptor structures.....	96

ABBREVIATIONS

2-MeSATP	2-methylthio-adenosine-5'-triphosphate
5-HT ₃ R	5-hydroxytryptamine receptors
9AC	9-anthracene carboxylic acid
Å	angstrom
AAQ	acrylamide azobenzene quaternary ammonium
ADP	adenosine diphosphate
AMP	adenosine monophosphate
AMPA	α-amino-3-hydroxy-5-methyl-4-isoxazolepropionic acid receptor
AOX1	alcohol oxidase 1 promoter
ASIC	acid-sensing ion channel
ATP	adenosine-5'-triphosphate
ATPγS	adenosine 5'-(3-thiotriphosphate)
AZ106	AZ10606120
BDNF	brain-derived neurotrophic factor
bp	base pairs
BSA	bovine serum albumin
BzATP	2'(3')-O-(4-benzoylbenzoyl) adenosine-5'-triphosphate
CaM	calmodulin
CHAPS	3-((3-cholamidopropyl) dimethylammonio)-1-propanesulfonate
CHO	chinese hamster ovary cells
CHS	cholesteryl hemisuccinate
CMV	cytomegalovirus
CNS	central nervous system
Cryo-EM	cryo electron microscopy

D	Debye
Da	dalton
DAMP	damage associated molecular pattern
DDM	n-dodecyl- β -D-maltoside
DIDS	4,4'-diisothiocyano-2,2'-stilbenedisulfonic acid
DLS	dynamic light scattering
DMEM	Dulbecco's Modified Eagle Medium
DNA	deoxyribose nucleic acid
DRM	detergent resistant membrane
DTT	dithiothreitol
EDTA	ethylenediaminetetraacetic acid
eGFP	enhanced green fluorescent protein
ELIC	<i>Erwinia chrysanthemi</i> ligand-gated ion channel
FBS	fetal bovine serum
FFA	flufenamic acid
FRET	Forster resonance energy transfer
FSEC	fluorescence-detected size exclusion chromatography
GABA _A	γ -aminobutyric acid type A receptor
GDP	guanosine diphosphate
GFP	green fluorescent protein
GLIC	gleobacter ligand-gated ion channel
GluK1	ionotropic kainate-type 1 glutamate receptor
GlyR	glycine receptor
HEK293T	human embryonic kidney cells (stably expressing SV40 large T antigen)
iGluR	ionotropic glutamate receptors
IL-1 β	interleukin 1 <i>beta</i>

IMAC	immobilised metal affinity chromatography
IP ₅ I	diinosine pentaphosphate
KN-62	1-[N,O-bis(5-isoquinoline-sulfonyl)-N-methyl-L-tyrosyl]-4-phenylpiperazine
K _v	voltage-gated potassium channel
LB	lysogeny broth
LDS	lithium dodecyl sulphate
LED	light emitting diode
LGIC	ligand-gated ion channel
LPS	lipopolysaccharide
MAM	maleimide azobenzene maleimide
MAQ	maleimide azobenzene quaternary ammonium
MCD	methyl-β-cyclodextrin
MEA-TMA	maleimide ethylene azobenzene trimethyl ammonium derivative
mEPC	miniature excitatory postsynaptic currents
MGlur	metabotropic glutamate receptor
MNG	maltose-neopentyl glycol
MSP	membrane spanning protein
MTSEA	2-aminoethyl methanethiosulfonate
MTSET	2-(trimethylammonium)ethyl methanethiosulfonate
MTSR	methanethiosulfonate rhodamine
MW	molecular weight
MyD88	myeloid differentiation primary response 88
NA	noradrenaline
nAChR	nicotinic acetylcholine receptor
NAD ⁺	nicotinamide adenine dinucleotide
NES	normal extracellular solution

NFA	niflumic acid
NFATc1	Nuclear Factor Of Activated T Cells 1
NF-κB	Nuclear Factor kappa-light-chain-enhancer of activated B cells
NLRP3	NOD-like receptor family, pyrin domain containing 3
NMDAR	N-methyl-D-aspartate receptor
NMDG ⁺	N-methyl-D-glucamine
NMR	nuclear magnetic resonance
NPC	neuronal progenitor cell
NPY	neuropeptide Y
OD	optical density
PAGE	polyacrylamide gel electrophoresis
PAMP	pathogen associated molecular pattern
PANX1	pannexin 1
PBS	phosphate buffered saline
PCL	photochromic ligand
PCR	polymerase chain reaction
PDB	protein data bank
PhENAQ	phenylethylamino azobenzene quaternary ammonium
PI3K	phosphoinositide 3-kinases
PIP	phosphatidylinositol
PMP	post mastectomy pain
PPADS	pyridoxal phosphate-6-azophenyl-2-4-disulphonic acid
PS	phosphatidylserine
PTL	phototethered ligand
PTM	post-translational modification
PVAT	perivascular adipose tissue

QAQ	quaternary ammonium-azobenzene-quaternary ammonium
rpm	repetitions per minute
SDS	sodium dodecyl sulphate
SEC	size exclusion chromatography
Sf21	IPLB-Sf21-AE cell line, ovarian cells of <i>Spodoptera frugiperda</i>
Sf9	clonal isolate of IPLB-Sf21-AE cell line, ovarian cells of <i>Spodoptera frugiperda</i>
SMase	sphingomyelinase
SNP	single nucleotide polymorphism
SPARK	synthetic photoisomerizable azobenzene-regulated K ⁺ channels
TA	tannic acid
TCP	targeted covalent photoswitches
TEA	tetraethyl ammonium
TEV	tobacco etch virus
TLR4	toll-like receptor 4
TM	transmembrane
TMEM16	transmembrane protein 16 family
TNP-ATP	2',3'-O-(2,4,6-trinitrophenyl) adenosine-5'-triphosphate
TRPV1	transient receptor potential cation channel, subfamily V, member 1
UV	ultraviolet
WT	wild type
ZAC	zinc activated channel
α,β -MeATP	α , β -methylene adenosine 5'-triphosphate
β,γ -MeATP	β,γ -methylene adenosine 5'-triphosphate

INTRODUCTION

Life, in all its forms, exists as an amalgamation of highly complex, intercommunicating networks. From unicellular organisms to higher eukaryotes, these networks are intricate, interlaced and require tight regulation to guarantee proper organism function and adequate response to external influences. Such biological networks exist on all manner of scales, whether this be molecular, cellular, or indeed networks within whole tissues and those which tie entire systems within a given organism together. These networks, of an astounding complexity, are finely tuned and as such, their functioning may be acutely influenced by the precise combination of a multitude of influential factors. Mastering an intimate understanding of these systems is therefore highly challenging, and the subject of biological research across the world.

In order for these networks to be maintained in a harmonious balance, intra- and inter-network communication *via* biological signals is of great importance. Such biological signals, an abundance of which are being sent and received at any one moment, are wide and varied in nature, involving a plethora of biological entities. One such class of biological entities involved in signal reception and transmission are ion channels; pore-forming membrane proteins, allowing the passive transport of ions along their electrochemical gradient in response to physiological stimuli. The passage of these ions between extra- and intracellular space constitutes in itself a biological signal, whether this be by inducing a transition in the membrane polarity or by way of activation of secondary messengers and pathways within or external to the cell.

1. Ion channels

As the signals to which biological networks must respond, both environmental and within the organism, are highly diverse, so must be the receptors waiting to receive them. Ion channels can be classed according to the stimulus to which they respond, this response being the “gating” of the channel: a series of stimulus-triggered conformational changes resulting in the opening of an ion-permeable pore. As such, a number of families can be resolved: voltage-gated channels, sensitive to changes in membrane polarisation; mechanosensitive channels, gated by changes in pressure; light-sensitive channels, such as channelrhodopsin, which are gated by photons; temperature-sensitive channels, and finally those which are gated in response to the binding of specific molecules or *ligands*.

It is this last class of channels which we will be interested in over the course of this manuscript; those activated by the binding of a particular ligand, the so-called ligand-gated ion channels (LGICs).

1.1. Ligand-Gated Ion Channels (LGICs)

1.1.1. Historical context

The very first origins of LGICs can be traced back to the 1850s, when Claude Bernard investigated the effects of *curare*, an alkaloid plant extract used by indigenous South American tribes as arrowhead poison, on the sciatic nerves of frogs. His experiments gave the first indication that some kind of junctional structure exists between nerve and muscular fibres, transmission across which may be blocked by application of a substance (Bennett, 2001). In the early 1900s, Paul Ehrlich developed the side chain theory, in the context of immunological studies, proposing that living cells possess side chains capable of binding to toxins. This theory of receptors was equally supported by the work of John Newport Langley, who proposed the presence of *receptive substances*. Around the same period, a student of Langley, Thomas Renton Elliot, who was working with adrenalin, presented the idea that this was a “chemical stimulant liberated on each occasion when the [nervous] impulse arrives at the periphery” (Maehle, 2004), what we now know today as neurotransmitters.

The Nobel prize winning work of Hodgkin and Huxley in the 1950s, who established the voltage-clamp technique to directly measure currents flowing across the membrane of a giant squid axon (Hodgkin et al., 1952), was the first of many landmark events in the global field of ion channels, which allowed their study in much finer precision. The development of the patch clamp technique, equally recognised by a Nobel prize, by Neher and Sakmann (Neher and Sakmann, 1976), allowed the first recordings of single channel conductances, whilst the first example of a biochemically purified LGIC was achieved in the laboratory of Changeux, who used α -bungarotoxin, a toxin found in snake venom, to purify the nicotinic acetylcholine receptor (Changeux et al., 1970). Following Rod MacKinnon’s crystallographic resolution of the KcsA potassium channel, again a Nobel-prize winning work (Doyle et al., 1998), advancing structural techniques have given rise to an large and growing number of ion channel structures, with those of each member of the LGIC superfamily having now been determined (Lemoine et al., 2012). In under 200 years, therefore, our knowledge of how chemical agents can interact in biological systems in specific and selective ways has advanced to such a point that we are now able to probe these ligand – receptor interactions on the atomic level, in terms of both structure and function. We will now consider the variety of ligand-gated ion channels which exist.

1.1.2. LGIC superfamily

Within the LGIC superfamily, three subfamilies exist, of distinct architecture and nature (Figure 1). They can be classed according to their oligomeric organisation: trimeric P2X receptors, tetrameric glutamate receptors and pentameric “cys-loop” receptors (Donnelly-Roberts & Jarvis, 2007; Ferrari et al., 2006).

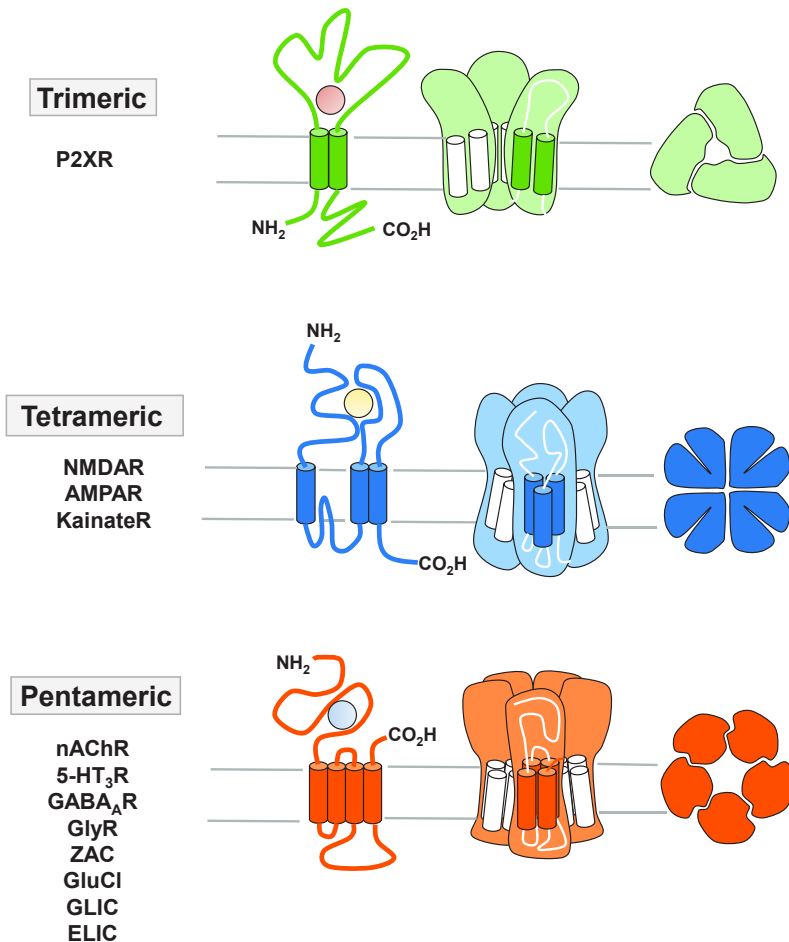


Figure 1. Ligand gated ion channel superfamily.

Schematic representations of the LGIC superfamily, comprising three subfamilies, classed according to their oligomeric organisation: trimeric P2X receptors, tetrameric glutamate receptors and pentameric “cys-loop” receptors. P2XR = P2X receptors, NMDAR = N-methyl-D-aspartate receptor, AMPAR = α -amino-3-hydroxy-5-methyl-4-isoxazoleprionic acid receptor, KainateR = kainate receptor, nAChR = nicotinic acetylcholine receptor, 5-HT₃R = 5-hydroxytryptamine (serotonin) receptor, GABA_AR = γ -aminobutyric acid receptor, GlyR = glycine receptor, ZAC = zinc activatec channels, GluCl = invertebrate glutamate-gated chloride channels, GLIC = gleobacter ligand gated ion channel, ELIC = *Erwinia chrysanthemi* ligand gated ion channel.

Trimeric P2X receptors

P2X receptors are non-selective cationic receptors, of which there exists 7 subtype variants in mammals. A common monomeric structure is present, intracellular terminal domains linked by two transmembrane spanning helical domains, and a large extracellular domain, location of the agonist binding site. Homo- and heterotrimers are possible depending on the specific

subtype in question. They are activated by the binding of extracellular ATP, and possess roles in the modulation of neurotransmission, as well as within the immune system (North, 2002).

Tetrameric glutamate receptors

The tetrameric family of ionotropic glutamate receptors comprises the NMDA, AMPA and kainate subtypes, designated according to their favoured agonist. Cation-selective tetramers are assembled from a range of structurally differing subunits, in a homomeric or heteromeric fashion depending on the receptor type. The common topology of these subunits is the following: an extracellular N-terminus, three transmembrane helical domains, with a re-entrant *p-loop* between the first and second helices, dipping back into the membrane, and finally an intracellularly located C-terminus (Alexander et al., 2017; Armstrong et al., 1998). Located in neuronal and non-neuronal cells, these receptors mediate fast excitatory synaptic transmission in the central nervous system (Traynelis et al., 2010).

Pentameric cys-loop receptors

The third member of the LGIC superfamily are the pentameric receptors. This subfamily is vast, and can be further divided into different groups. Firstly, the excitatory, cation-selective nicotinic acetylcholine receptors (nAChRs), 5-HT₃ or serotonin receptors and zinc-activated channels. Secondly, inhibitory, anion-selective γ -aminobutyric acid-sensitive receptors (GABA_AR), glycine receptors (GlyR) and invertebrate glutamate-gated chlorine channels (GluCl). These channels are abundant in both the central and periphery nervous system and have a wide ranging sensitivity to different pharmacological agents.

Various combinations of subunit assemblies exist, but a common topology is visible between subunit variants: four transmembrane helices, followed by a large extracellular domain, flanked by extracellular N- and C-termini. Within this extracellular domain is the presence of the “cys-loop”, a loop structure of thirteen residues framed by two conserved cysteines forming an intrasubunit disulphide bridge (Lemoine et al., 2012). A number of other, related pentameric receptors have been identified in prokaryotes (GLIC, ELIC).

Other than their importance in normal physiological functions, various dysfunctions of LGICs are at the origin of a vast range of pathologies, known as channelopathies (Kim, 2014). For this reason, the study of LGICs is of importance not only from a viewpoint of fundamental research, but also in terms of therapeutic potential. Our study is focussed on just one of these subfamilies, the trimeric P2X receptors, and the work described herein is focussed more precisely on one particular member of this family: P2X7.

1.2. Study of ion channels: patch clamp electrophysiology

At this point, we will undertake a brief detour to consider the techniques employed to investigate ion channel function. In the study of ion channels, patch clamp electrophysiology is one of the principal techniques employed, due to its ability to record current passing through channels, across the membrane in a finely controlled, sensitive and high resolute manner. First developed in the seventies by Neher and Sakmann (Neher and Sakmann, 1976), which would later win them the 1991 Nobel prize, the technique of patch clamp electrophysiology works on the premise that limiting the area within which current is measured to a small, electrically isolated membrane patch, reduces any background noise to a point at which the resolution of currents flowing through single channels becomes possible. This is achieved by using glass pipettes of μm diameter, filled with the desired composition of intracellular solution, and containing an electrode. Further advances in this technique added even more sensitivity and resolute power, notably the introduction of the “gigaseal”, whereby the resistance of the seal between the pipette and membrane patch reaches values in the giga Ohm range (Hamill et al., 1981; Sigworth and Neher, 1980). This made possible the high degree of versatility in this technique, whereby four principal configurations can be accessed:

- (i) **Cell attached mode:** in the cell attached mode, the pipette is giga-sealed to a patch of membrane, and the currents recorded therefore pertain to ion channels which are contained within this patch, often giving rise to single channel recordings. The remainder of the cell stays intact, allowing these ion channels to be studied under physiological cytosolic conditions, where interactions with intracellular components and signalling pathways are maintained (Figure 2a).
- (ii) **Whole cell mode:** the whole cell configuration is widely used, as it provides robust read-outs of the activity of ion channels across the entire surface of the cell membrane studied. It can be accessed by entering cell attached mode, and subsequently piercing the cell membrane by a brief application of negative pressure (e.g. by suction), rendering the electrode contained within the pipette in direct contact with the cytosol. The intrapipette solution thus dialyses the interior of the cell, and in this way, precise control of the intracellular composition can be achieved. Recordings in the whole cell mode are the culmination of the currents produced by all of the channels of interest expressed at the cell surface membrane. As such, a global, average view is obtained, with no resolution of individual populations of channels, should they exist (Figure 2b).

- (iii) **Outside-out mode:** the outside-out configuration is another mode which allows the recording of conductances pertaining to single channels. Starting from the whole cell configuration, outside-out mode is achieved by gently withdrawing the pipette from the cell surface. Due to the presence of the giga-seal, the cell membrane is thus also drawn away from the remainder of the cell, until the point at which it “breaks” and becomes disconnected, reforming a seal around the surface of the pipette. In this way, the extracellularly facing side of the channel is located outside the pipette, and the intracellularly facing side is located in the intrapipette region. This mode allows the study of single channel conductances, whilst probing the response of channels to stimuli applied extracellularly (Figure 2c).
- (iv) **Inside-out mode:** as in outside-out mode, this configuration allows the recording of single channels, this time with the extracellular domains of the channel contained within the pipette, and the intracellular side of the channel facing outwards. This configuration can be accessed by starting in cell-attached mode and gently withdrawing the pipette until the breaking point of the membrane, effectively excising a patch of membrane for study. This configuration allows the application of various stimuli to the intracellularly facing domains of the channel (Figure 2d).

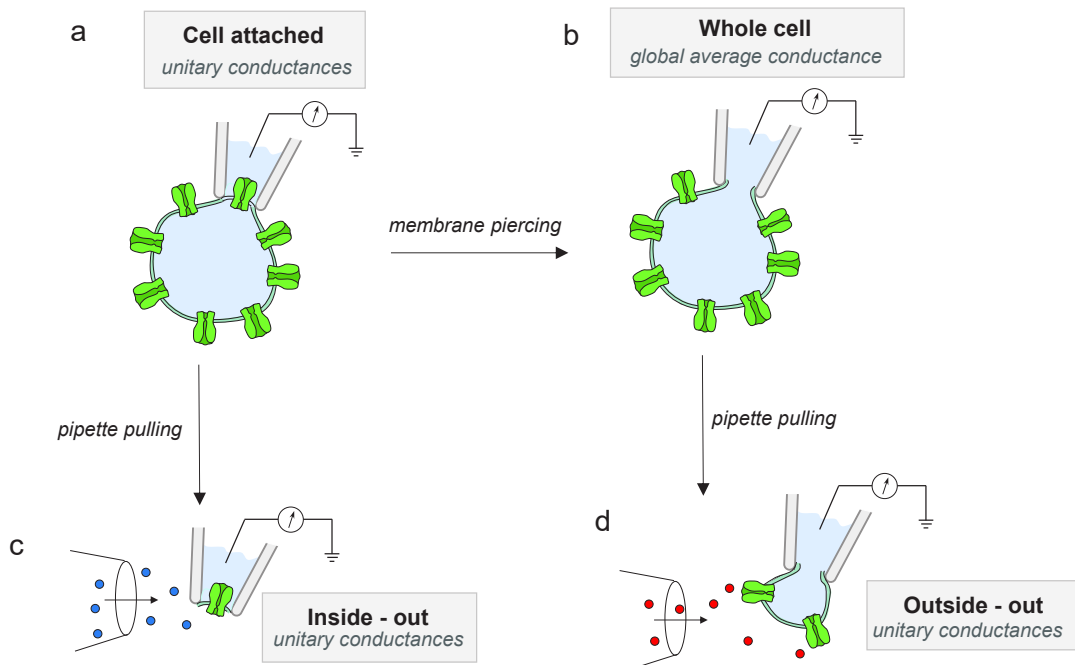


Figure 2. Different modes of patch clamp electrophysiology.

Schematic representation of the four principal configurations used in patch clamp electrophysiology, and how they are accessed.

Patch clamp electrophysiology, therefore, represents a highly versatile, sensitive technique whereby ion channel function can be probed in controlled environments. This allows the investigation of channel responses to a range of stimuli, applied from both sides of the membrane, and the measurement of various parameters to characterise these responses: current amplitudes, unitary conductances, kinetic parameters and relative permeabilities with respect to the ions transiting through the channel.

This is the primary technique which is employed in our laboratory, and within this thesis work, to study the activity of P2X receptors.

2. P2X receptors

2.1. Purinergic signalling

Despite its fairly recent discovery compared to that of the cholinergic or adrenergic systems, the purinergic signalling system is suggested to be one of the oldest in terms of evolutionary origins (Burnstock and Verkhatsky, 2009). ATP-mediated signalling in some form is found in almost all tissues and cell types, rendering it an omnipresent signalling molecule.

2.1.1. Discovery

The role of ATP as a signalling molecule, and not just the ubiquitous cellular source of energy, was first alluded to in the late 1920s, when Drury and Szent-Györgyi described the effects of extracellular purines on the mammalian heart (Drury and Szent-Györgyi, 1929). Years later, Pamela Holton identified the release of ATP following the antidromic stimulation of rabbit sensory nerves (Holton, 1959), but it was not until the 1970s when Geoffrey Burnstock discovered ATP as a neurotransmitter in non-adrenergic, non-cholinergic nerve transmission in the gut and coined the term *purinergic signalling* (Burnstock, 1972; Burnstock et al., 1970). Despite almost twenty years of opposition to this theory, the purinergic signalling system as we know it today has been characterised and its corresponding receptors classed into subfamilies: P2 receptors, activated by ATP and ADP, and P1 receptors, activated by adenosine (Burnstock, 1978). The division of P2 receptors into two subfamilies, ionotropic P2X and metabotropic P2Y receptors swiftly followed (Abbracchio and Burnstock, 1994; Burnstock and Kennedy, 1985). Recently, the P0 family of receptors has also been identified and characterised, activated by adenine (Thimm et al., 2015, 2013).

2.1.2. Sources of extracellular ATP

ATP, as the primary energy source of the cell, is present in physiological conditions, at concentrations ranging from 3 - 10 mM within the cytosol. Meanwhile, the extracellular concentration of ATP ([eATP]) is much reduced, at just 10 nM (Trautmann, 2009). The electrochemical gradient promoting the passage of ATP from intracellular regions into extracellular space is, therefore, particularly strong, but by nature of its size and charge (as ATP is found in physiological conditions as its deprotonated 4- form), ATP is unable to simply pass across hydrophobic cell membranes. A number of pathways, therefore, exist to effect the passage of ATP into extracellular space. In pathological conditions, cell death and subsequent lysis is one of the primary sources of ATP release, whether this be by necrotic cell death or apoptosis, where a role for pannexin-1 (PANX-1) has been also determined (Qu et al., 2011). In this sense, release of eATP through injured or damaged cells is in the context of a danger signal, whereby ATP acts as a damage-associate molecular pattern (DAMP) (Tanaka et al., 2014). Non-lytic, release pathways also exist, for example, PANX1 and other hemichannels such as connexins have also been determined as conductive pathways through which ATP can exit the cell (Barbe et al., 2006; Eltzschig et al., 2006), and interestingly, it has also been suggested that P2X7 itself constitutes a pathway for ATP-induced ATP release (Pellegatti et al., 2005). Finally, exocytotic release by secretory vesicles has been found in a number of different cell types (Lazarowski et al., 2011; Montana et al., 2006).

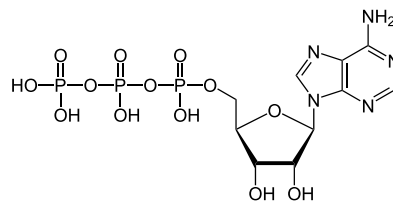


Figure 3. Chemical structure of ATP in its protonated form.

Once present in extracellular space, a number of enzymes are involved in the metabolism of ATP into its related purinergic signalling compounds: ecto-nucleoside triphosphate diphosphohydrolases (e-NTDPases), named CD39s, catalyse the degradation of ATP to ADP as well as ADP to AMP, and ecto-5'-nucleotidases, CD73s, catalyse the formation of adenosine from AMP (Colgan et al., 2006; Zimmermann, 2006). Equally, alkaline phosphatases may also catalyse the formation of adenosine from any of its related nucleotides (Fields and Burnstock, 2006). The formation of adenine, meanwhile, is catalysed by purine nucleoside phosphorylase enzyme (Kaebisch et al., 2015).

The interactions between purine signalling molecules and their receptor targets are summarised in Figure 4.

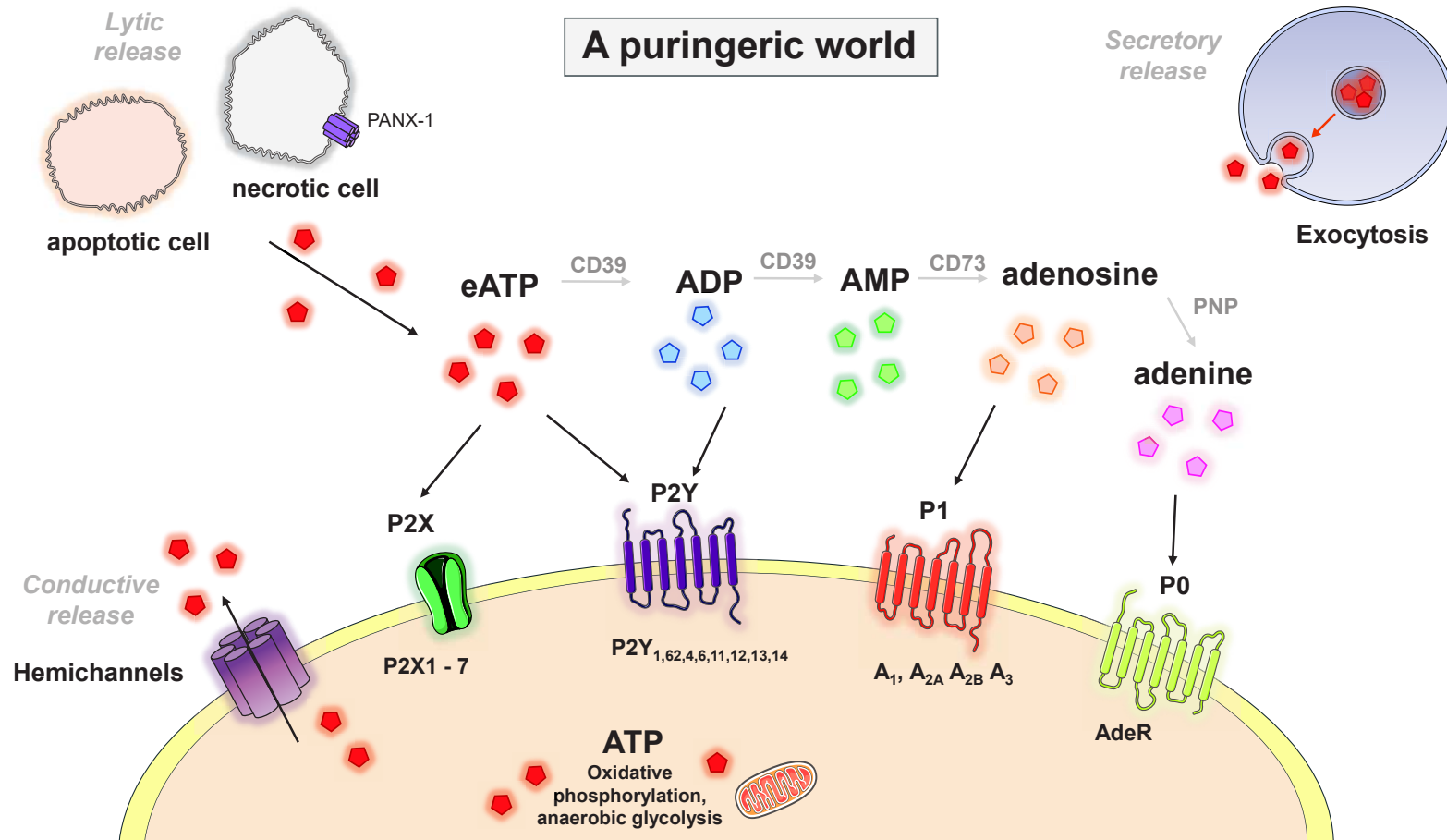


Figure 4. The "purinergic world".

Schematic representation of the key entities and interactions involved in purinergic signalling pathways. ATP is synthesised in the cell, primarily by oxidative phosphorylation in the mitochondria, but also by anaerobic glycolysis. Different pathways exist for the release of ATP into extracellular space: lytic release pathways (cell death due to apoptosis or necrosis), secretory release by vesicle exocytosis and conductive release pathways, through channels such as pannexins and connexions. ATP is metabolised by a network of enzymes, CD39 = ecto-nucleoside triphosphate diphosphohydrolases, CD73 = ecto-5'-nucleotidases and PNP = purine nucleoside phosphorylases. ATP and its metabolic derivatives have differing targets: ATP activates ionotropic P2X and metabotropic P2Y receptors, ADP equally activates P2Y receptors, adenosine activates P1 receptors, and adenine activates the newly classed P0 AdeR receptors. P2Y receptors are also activated by UTP and UDP (not shown here).

2.2. P2X receptors: historical context and generalities

Within this purinergic signalling system, the family of ionotropic P2X receptors (P2XRs) occupy a number of wide-ranging, key roles. The molecular identification of the first P2X receptors took place relatively recently, in the 1990s, when P2X1 (Valera et al., 1994) and P2X2 (Brake et al., 1994) were first cloned. In quick succession, the entire seven-member P2X family had been identified (Buell et al., 1996; Chen et al., 1995; Collo et al., 1996; Lê et al., 1997; Lewis et al., 1995; Rassendren et al., 1997; Soto et al., 1996; Surprenant et al., 1996). P2X receptors have thus far been identified exclusively in eukaryotic organisms, including invertebrates and primitive unicellular organisms such as amoeba, but have an unusual phylogeny given that they are missing from *Drosophila* and *C. elegans*, species where other common mammalian ionotropic receptors are found (Fountain, 2013).

P2X receptors possess a relatively simple, common architecture, comprising intracellular N- and C-terminal domains, of differing length according to the specific subtype, two transmembrane helical domains, TM1 and TM2, linked by a large ectodomain, which is held in structure by disulphide bridges formed between pairs of ten conserved cysteine residues (Figure 5a). The ATP binding site is found within this extracellular domain. These P2X monomers assemble into homotrimers, or heteromers in the case of some subunit variants (see section 2.4.1).

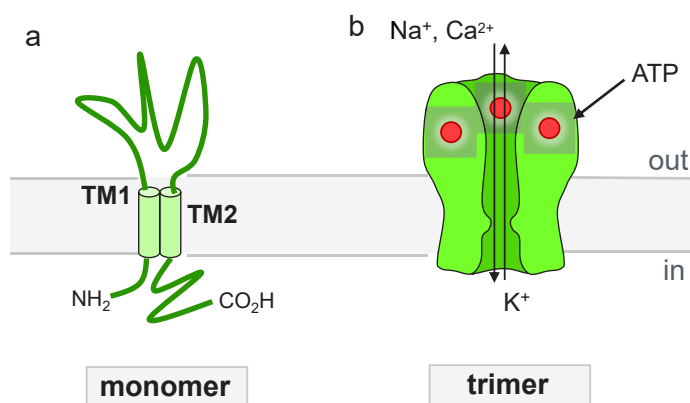


Figure 5. P2X receptors.

Schematic representation of P2X receptor topology in their monomeric (a) and trimeric (b) forms, showing the direction of ion permeation upon ATP-activation (ATP indicated by red spheres). In typical physiological conditions, Ca^{2+} and Na^{+} flow into the cell, whilst K^{+} transits outwards.

Comprising seven members, with ATP sensitivities ranging from the μM to mM range, as well as distinct kinetic properties, the family of P2X receptors constitutes a versatile and finely tuned collective, able to respond in differing manners to a common stimulus, that of extracellular ATP.

Here, key aspects of P2X receptor structure and function will be briefly considered before we explore one subtype in particular in greater detail; P2X7.

2.3. Seven P2X subtype variants

Seven P2X genes exist, coding for seven subunit variants. These different subtypes vary in their similarity to another, ranging from 40 – 55% pairwise amino acid sequence similarity, with the most similar to other subtypes being the P2X4 receptor, and the least similar to other family members being the P2X7 receptor (highlighted in green, Figure 6) (North, 2002).

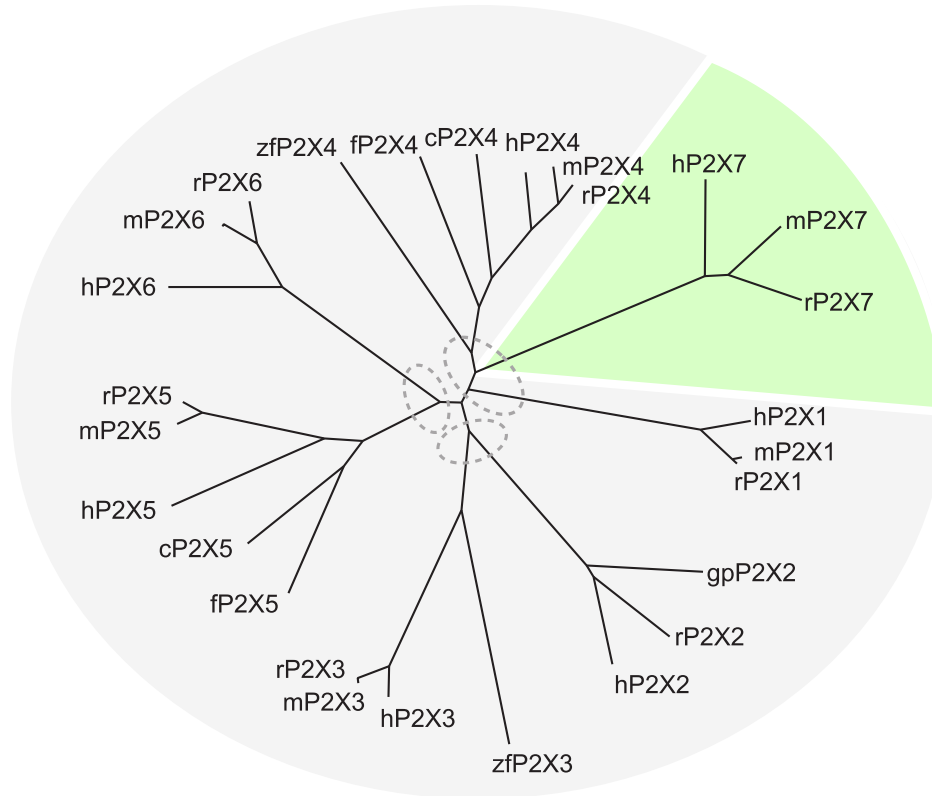


Figure 6. Relationship of P2X subunit variants to one another.

(a) Dendrogram to show relatedness of 29 selected P2X receptor subunits. h = human, r = rat, c = chicken, m = mouse, gp = guinea pig, zf = zebrafish, f = fugu. Adapted from (North, 2002).

Each P2X subtype variant is able to assemble into homotrimeric receptor units, P2X1R – P2X7R. This is with the exception of P2X6, which is considered a “silent” subunit, becoming functional only when in heterotrimeric assemblies with other subtypes, such as P2X2/6 (Torres et al., 1999) and P2X4/6 (K.-T. Lê et al., 1998).

P2XRs are non-selective cationic channels, and upon activation become permeable to Na^+ and Ca^{2+} , both of which flow along their electrochemical gradients into the cell, as well as to K^+ , which transits from intra- to extracellular space (see Figure 5b) (Samways et al., 2014). The result of these movements is membrane depolarisation, in addition to the activation of a plethora of Ca^{2+} -activated intracellular pathways, owing to the fact that P2XRs are highly permeable to Ca^{2+} (Egan and Khakh, 2004). The P2X5 subtype also exhibits an additional

permeability to chloride ions (P_{Cl^-}/P_{Na^+} = approximately 0.5 in hP2X5) (Bo et al., 2003; Ruppelt et al., 2001).

Whilst these receptors possess certain similarities, there are a number of features which can be used to distinguish family members from one another. Desensitisation, the phenomenon of channel closure despite the presence of agonist, for example, is a characteristic of varying nature between P2X subtypes (Figure 7). P2X1 and P2X3 exhibit fast desensitisation kinetics, with channel closure occurring on the ms time scale, whilst P2X2 and P2X4 are slowly desensitising channels. As for the P2X7 subtype, it is unique amongst its family members in that it does not experience desensitisation, but rather, a sensitisation or facilitation of currents which increase in magnitude upon prolonged ATP application (North, 2002). We will come back to this unique feature several times over the course of this manuscript.

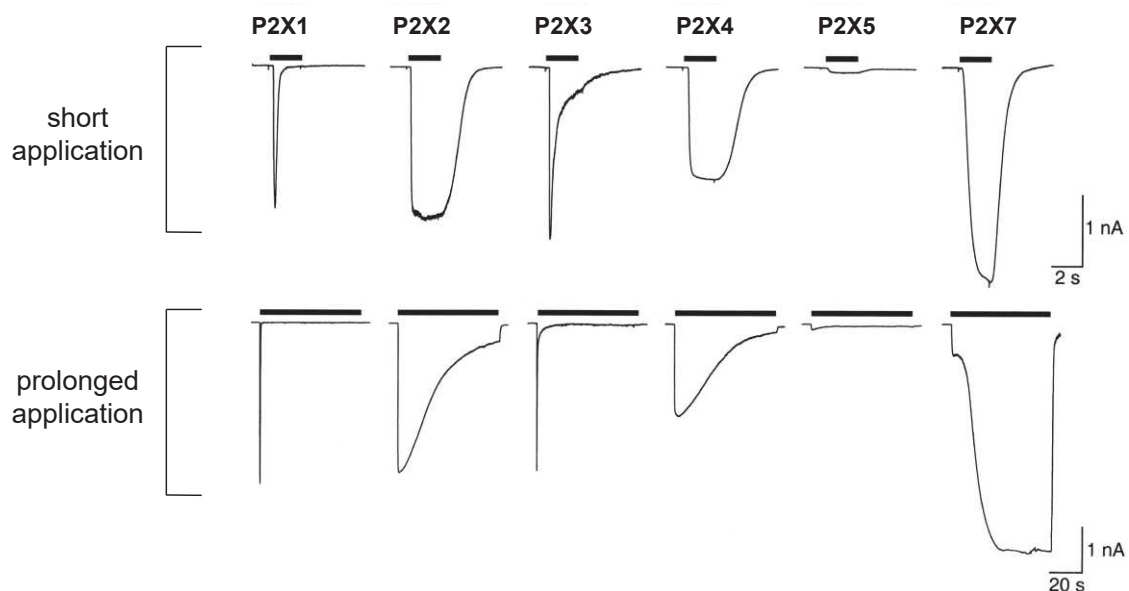


Figure 7. Desensitisation kinetics in homomeric P2XRs.

Desensitisation as a result of short (top, 2s) or prolonged (bottom, 60s) ATP application, in homomeric rat P2XRs, stimulated with 30 μ M ATP (P2X1 – P2X5) or 1 mM (P2X7) compared for homomeric rat P2X receptors. Adapted from (North, 2002).

Aside from these desensitisation profiles and relative permeability characteristics, the pharmacological profile of P2XRs also varies between receptor subtypes in terms of agonists, antagonists and allosteric modulators. A non-comprehensive summary relating to homotrimeric P2X pharmacology is shown in Table 1.

	P2X1	P2X2	P2X3	P2X4	P2X5	P2X7
Agonists (EC₅₀ μM)						
ATP	0.07	1.2	0.5	10	10	100
2-meSATP	0.07	1.2	0.3	10	10	100
αβ-meATP	0.3	>300	0.8	>300	>300	>300
BzATP	0.003	0.75	0.08	7	>500	20
Antagonists (EC₅₀ μM)						
Suramin	1	10	3	>500	4	500
PPADS	1	1	1	>500	3	50
TNP-ATP	0.006	1	0.001	15	-	>30
IP ₅ I	0.003	>300	2.8	(+)	-	N.D
KN-62	-	-	-	-	-	0.3
Modulators (potentiation (+) or inhibition (-))						
Zn ²⁺	(-)	(+)	(+)	(+)	(+)	(-)
Cu ²⁺	N.D	(+)	N.D	(-)	N.D	(-)
Cd ²⁺	(-)	(+)	(-)	(+)	N.D	(-)
H ⁺	(-)	(+)	(-)	(-)	(-)	(-)
Ivermectin	N.D	none	none	(+)	N.D	(+)
Ethanol	N.D	(-)	(+)	(-)	N.D	N.D
Phosphoinos- -itides	(+)	Desensitis- ation reduced	(+)	(+)	(+)	(+)

Table 1. P2XR pharmacology.

A non-comprehensive summary of P2X pharmacology, as described in (Coddou et al., 2011a; Jarvis and Khakh, 2009). ATP, adenosine 5'-triphosphate; 2-meSATP, 2-methylthioadenosine 5'-triphosphate; α,β-meATP, α,β-methyleneadenosine 5'-triphosphate, BzATP, 2,3-O-(4-benzoylbenzoyl)-ATP; PPADS, pyridoxal-5'-phosphate-6-azophenyl-2'',4''-disulphonic acid; TNP-ATP, 2',3'-O-(2,4,6-trinitrophenyl) adenosine 5'-triphosphate; IP₅I, diinosine pentaphosphate; KN-62, 1-[N,O-bis(5-isoquinoline-sulfonyl)-N-methyl-L-tyrosyl]-4-phenylpiperazine.

2.4. Localisation

P2XRs are expressed in wide range of cell types, according to the specific subtype in question. For example, P2X7Rs are highly expressed in cells of the immune system, whereas P2X2Rs are widely found within the central nervous system (CNS). Table 2 summarises the principal locations of different homomeric P2XR assemblies.

P2XR	Cellular localisation	Primary roles
P2X ₁	Smooth muscle, platelets, cerebellum, dorsal horn spinal neurons	Smooth muscle contraction; platelet activation
P2X ₂	Smooth muscle, CNS, retina, chromaffin cells, autonomic and sensory ganglia, pancreas	Sensory transmission & modulation of synaptic function
P2X ₃	Sensory neurons, NTS neurons, some sympathetic neurons	Mediates sensory transmission; facilitates glutamate release in CNS
P2X ₄	CNS, testis, colon, endothelial cells, microglia	Modulates chronic inflammatory & neuropathic pain
P2X ₅	Proliferating cells in skin, gut, bladder, thymus, spinal cord, heart, adrenal medulla	Inhibits proliferation & increases differentiation
P2X ₆	CNS, motor neurons in spinal cord	Functions as a heteromeric channel in combination with P2X ₂ & P2X ₄ subunits
P2X ₇	Immune cells including dendritic cells (mast cells, macrophages), pancreas, skin, microglia	Mediates apoptosis, cell proliferation & pro-inflammatory cytokine release

Table 2. Localisation of P2XRs.

Summary of the primary cellular localisations and accompanying roles of homomeric P2XRs (with the exception of P2X6 which is an obligatory heteromer). Adapted from (Burnstock, 2008, 2018).

2.4.1. Heteromeric P2XRs

In addition to the homomeric assemblies, it has been shown, by co-immunoprecipitation, crosslinking and electrophysiological characterisation experiments, that a multitude of heteromeric assembly possibilities exist. These are shown in Table 3, shaded green for those possibilities observed *in vitro*, and in orange for those heteromers for which strong evidence has been found to indicate their presence in native tissues.

	P2X ₁	P2X ₂	P2X ₃	P2X ₄	P2X ₅	P2X ₆	P2X ₇
P2X ₁	+	+	+	+	+	+	-
P2X ₂		+	+	-	+	+	-
P2X ₃			+	-	+	-	-
P2X ₄				+	+	+	-
P2X ₅					+	+	-
P2X ₆						-	-
P2X ₇							+

Table 3. Summary of heteromeric P2XR assemblies.

Adapted from (Torres et al., 1999). According to (Lê et al., 1998; Lewis et al., 1995; Nicke et al., 1998; Nicke, 2008; Saul et al., 2013)

The definitive presence of P2X heteromers in native tissues is poorly characterised, but those for whom the strongest evidence exists are present in a range of cell types; P2X1/5 was identified in mouse cortical astrocytes (Lalo et al., 2011), P2X2/3 in sensory neurons such as nodose ganglia neurons and autonomic ganglia neurons (Cockayne et al., 2005; Lewis et al., 1995), P2X4/6 heteromers have been proposed as present in the mammalian CNS (Lê et al., 1998).

2.5. Physiological roles

Accompanying the wide-ranging cellular distribution of P2XRs are numerous physiological roles (Table 2). In this section, a select few of these roles will be considered as pertinent examples.

2.5.1. Neuromodulation: P2X2, P2X4, P2X6, P2X7

A prime example of neuromodulation by P2X receptors is within the hypothalamus, within magnocellular neurons (MCNs), where the likely P2X variants involved are P2X2, P2X4 and P2X7 (Vavra et al., 2011). The role of P2XRs in this network is to modulate synaptic scaling, in this case to reinforce synaptic strength by promoting the insertion of AMPA receptors into the postsynaptic terminals, the ultimate result of which being an increase in miniature excitatory postsynaptic currents (mEPCs) (Gordon et al., 2005, 2009). Presynaptic release of glutamate and noradrenaline (NA), which are recognised by mGluR and α -1 adrenoreceptors respectively, located in neighbouring astrocytes, induce an increase in intracellular Ca^{2+} , by way of the intermediate IP3 (inositol 1,4,5-trisphosphate). Subsequent release of ATP occurs, activating extrasynaptic P2XRs, through which an influx of Ca^{2+} causes activation of phosphatidylinositol 3-kinase (PI3K), which ultimately promotes the insertion of AMPA receptors into the postsynaptic dendritic spine, thus increasing synaptic strength. This modulation network is summarised in Figure 8.

Equally, Pougnet *et al* identified a further P2X-modulation of synaptic strength, this time in hippocampal neurons, whereby NA-modulated ATP release from glial cells this time had the opposing effect, to induce internalisation of AMPA receptors in dendrites *via* a Ca^{2+} -dependent, phosphatase and CAMKII-dependent pathway (Pougnet et al., 2014). This likely involves P2X2, P2X4 and/or P2X6Rs, as these subtypes have been identified in CA1 pyramidal cells of the hippocampus (Soto et al., 1996).

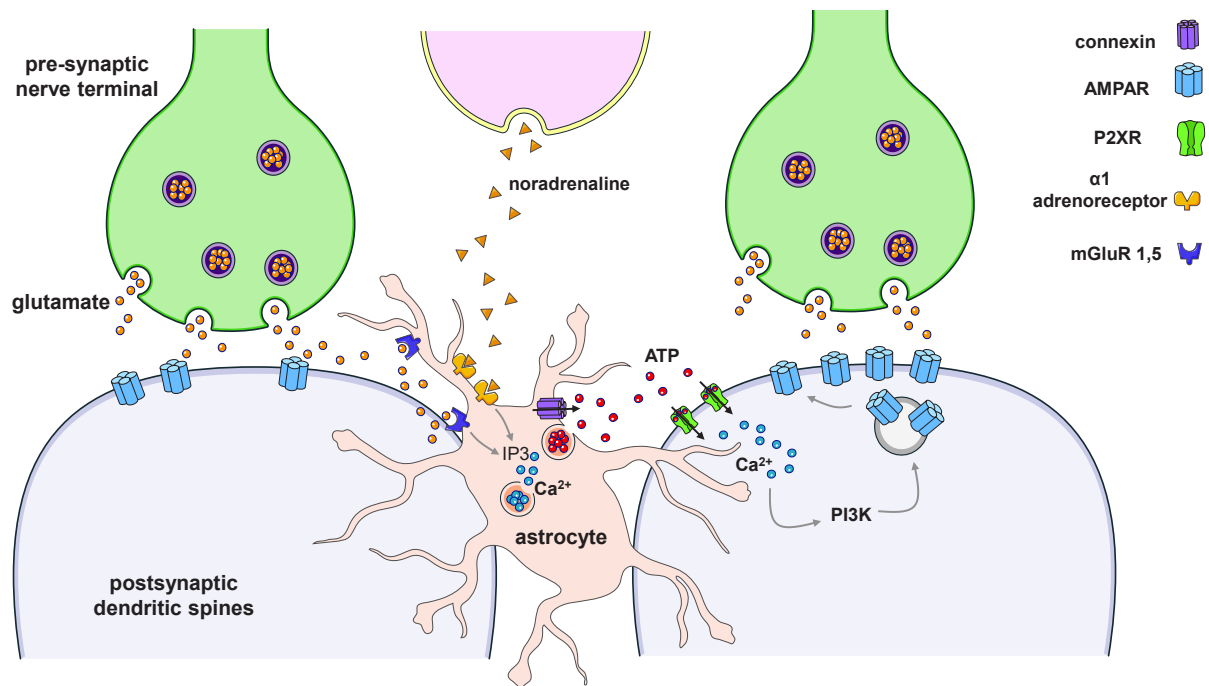


Figure 8. Neuromodulatory role of P2XRs: synaptic scaling.

Release of noradrenaline (NA) and glutamate from pre-synaptic sources causes an IP₃-mediated release in Ca²⁺ of astrocytes, following recognition at mGluR (glutamate) and α₁-adrenoreceptor (NA) receptors. This triggers glial release of ATP, which acts upon P2XRs in postsynaptic dendritic spines, causing an influx of calcium, activation of PI3K and subsequent promotion of postsynaptic AMPA insertion. Recreated from (Khakh and North, 2012).

2.5.2. Smooth muscle contraction: P2X₁

A role has also been determined for P2XRs, specifically P2X₁, in the contraction of arterial smooth muscle cells (Burnstock and Ralevic, 2014; Ralevic, 2012). In this context, ATP and NA are co-released from sympathetic nerve varicosities in proximity to smooth muscle cells. ATP activates P2X₁ receptors, which are located in clusters adjacent to these varicosities, causing a rapid influx of calcium, whilst NA acts *via* the α₁ adrenoreceptor, a G-protein coupled receptor which sets into action second messenger pathways. This also leads to an intracellular Ca²⁺ increase but on an extended time scale, thus producing two phases of contraction; a rapid and slower phase, mediated by ATP and NA respectively. Membrane depolarisation following P2X activation additionally induces the activation of voltage-gated calcium channels, further increasing intracellular calcium content. The ultimate consequence of increased intracellular smooth muscle Ca²⁺ content, is the mobilisation of calmodulin (CaM), which modulates the activation of myosin light-chain kinase (MLCK). MLCK phosphorylates light chains in myosin heads, thereby increasing the ATPase activity of myosin, and providing the energy for the myosin-actin ratchet mechanism at the origin of muscle contraction.

2.5.3. Vasodilation: P2X4

In addition to the role of P2X1 in vasoconstriction, P2X receptors also play a part in the vasodilation process, through the action of P2X4. Vasodilation occurs when shear stress, exerted on the endothelial cells by blood flow, and hypoxia, a lack of sufficient oxygen, provoke the release of ATP, UDP and UTP (Paszkwiaik and Dardik, 2003; Ralevic and Dunn, 2015). The release of ATP can equally come from erythrocytes which also experience shear stress during blood flow (Bergfeld and Forrester, 1992). This activates P2Y (P2Y₁, P2Y₂, P2Y₆ and P2Y₄) and P2X4 receptors present on the endothelial cells, inducing an increase in intracellular Ca²⁺, which triggers the co-release of nitric oxide (NO), endothelium-derived hyperpolarizing factor (EDHF), and prostacyclin (PGI₂), all of which have vasodilatory effects (Burnstock and Ralevic, 2014). This vasodilation allows an increased blood flow, and therefore oxygen delivery, to the surrounding tissue, thus representing a mechanism to match oxygen supply with demand. The purinergic mechanisms behind vasodilation and vasoconstriction are summarised in Figure 9:

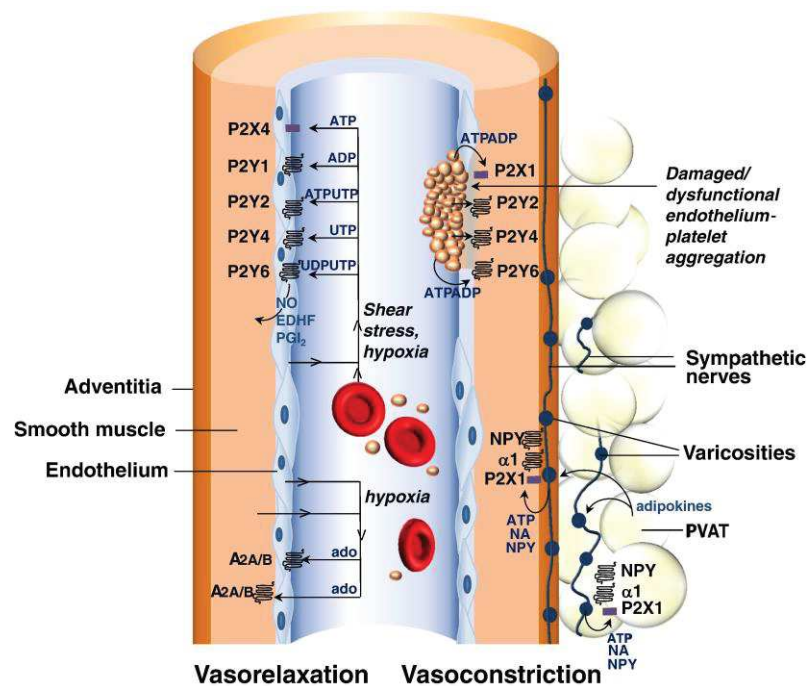


Figure 9. Purinergic receptor involvement in vasodilation and vasoconstriction.

Schematic representation of the purinergic receptor involvement in vasodilation (left, vasorelaxation) and vasoconstriction (right). **Vasodilation:** Shear stress and hypoxia results in the release of ATP, enzymatically converted to ADP, and release of UTP and UDP. These act as agonists at various P2 receptors, inducing an increase in intracellular Ca²⁺, triggering co-release of NO, EDHF and PGI₂, all of which have vasodilating effects. ATP can also be metabolised into adenosine, able to act on A2A/B receptors, also implicated in vasorelaxation, and present in endothelial cells and smooth muscle cells. **Vasoconstriction:** ATP and NA released from varicosities activate P2X1Rs and α-1 adrenoreceptors respectively in smooth muscle cells. Neuropeptide Y (NPY) and the NPY receptor may also be involved. At injury sites, platelets may also be a source of released ATP. Collectively, this results in an increase in intracellular Ca²⁺ in the smooth muscle cells, ultimately triggering vasoconstriction. Adipokines released from the perivascular adipose tissue (PVAT) surrounding blood vessels may modulate neurotransmission in these sympathetic perivascular regions. From (Ralevic and Dunn, 2015).

Originally thought only to involve P2Y receptors, there are several strong evidences for the presence of P2X4Rs in endothelial tissue which contribute to vasodilatory mechanisms. In human umbilical vein endothelial cells (HUVECs), knockdown of P2X4R expression using antisense oligonucleotides significantly reduced the ATP-provoked intracellular Ca^{2+} increase, whilst *P2RX4*^{-/-} mice exhibited a markedly reduced vasodilatory response: blood flow-provoked intracellular Ca^{2+} increase was impaired, and mice exhibited higher blood pressure, and smaller amounts of NO products in their urine than wild type mice (Yamamoto et al., 2006, 2000). *P2RX4* gene transfer by adenovirus could, however, rescue the flow-induced Ca^{2+} and NO increase, strongly indicating the implication of P2X4 in the vasodilatory response. Interestingly, in heterologous systems, laminar shear stress, such as that experienced as a result of blood flow, has also been shown to diminish desensitisation, presumably stabilising the open state of P2X4 (Kessler et al., 2011). P2X4Rs appear, therefore, likely to contribute to ATP-induced vasodilation, and the implication of TRPV1 has also been suggested, in addition to purinergic receptors (Mendoza et al., 2010).

2.5.4. Sensory functions: P2X4

Recently, a role for P2X4 in keratinocyte-derived mechanosensory transduction has been elucidated by the use of a mouse model combining optogenetically-controlled keratinocytes and P2X4 knockout in sensory neurons (Moehring et al., 2018). P2X4 has been shown as the most highly expressed P2X subtype on sensory neurons, with a broad expression pattern on both light touch and nociceptive neurons (Kobayashi et al., 2005). The study of Moehring *et al* elucidated that keratinocytes, skin cells present on the outermost epidermal layer, which are in close proximity to sensory nerve terminals, release ATP following mechanostimulation (Moehring et al., 2018). This released ATP acts upon P2X4 receptors present in sensory neurons, transmitting the signal of both innocuous and noxious touch to the spinal cord (Figure 10). The implication of P2X4 as the receptor for this mechano-induced ATP release was proven by the use of both pharmacological inhibition, and genetic ablation of P2X4R in a mouse model, which both resulted in a decrease in the response to both noxious and innocuous stimulation (Moehring et al., 2018). Equally, the use of ivermectin, a positive allosteric modulator of P2X4, decreased the thresholds of mechanical response, and increased the response to stimuli over this threshold.

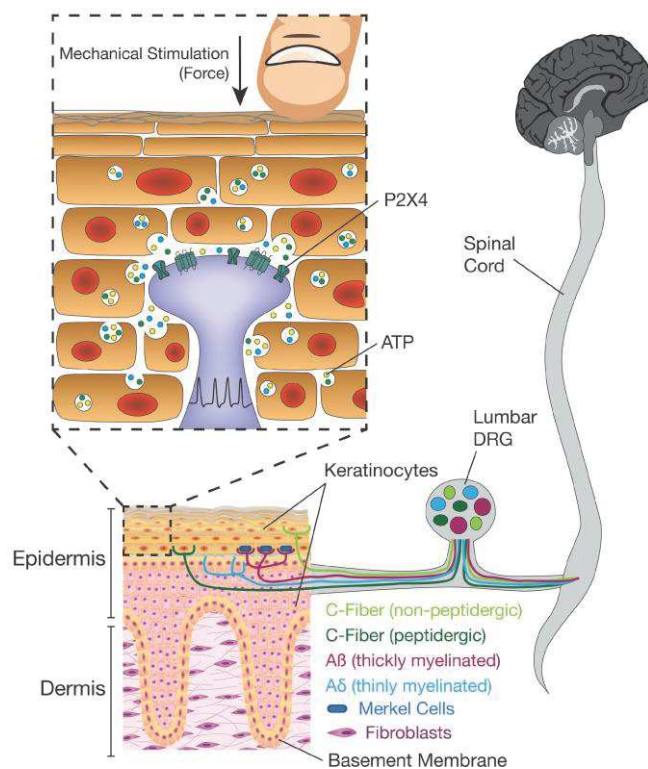


Figure 10. Implication of P2X4 in light touch and nociceptive signal transmission via keratinocytes.

Mechanical stimulation (through touch or noxious stimuli) induces keratinocytes to release ATP, which activates P2X4Rs on sensory neurons found within the epidermis, resulting in action potential firing in the neurons and downstream effects leading to touch perception. This is the case for several different nerve fibers: C, A β and A δ . From (Moehring et al., 2018)

2.5.4.1. Sensory functions in pathological states: P2X4 in neuropathic pain

Whilst P2X4 is implicated in sensory functions in physiological conditions, it is also involved in pathological sensory states, namely, in neuropathic pain. Neuropathic pain is defined as a state of chronic pain, resulting from damage to central or peripheral nerves, either from an acute injury or as a result of systemic disease, which causes a hyperexcitability of sensory neurons (Lemoine et al., 2012; Zhuo et al., 2011). P2X4 intervenes in this process through the brain-derived neurotrophic factor (BDNF) pathway: in response to nerve injury, P2X4R is upregulated in activated microglia of the spinal cord (Ulmann et al., 2008). These microglial P2X4Rs are activated by ATP release upon injury, and induce the release of BDNF, which, in turn binds to the tyrosine kinase receptor, TrkB, triggering the TrkB receptor signalling transduction cascade in post-synaptic neurones. This results in the downregulation of KCC2, a potassium/chloride symporter, the ultimate consequence of which is a build-up in the intracellular chloride concentration, which, upon activation of GABA_A and glycine receptors, produces an efflux of chloride ions, hyperpolarisation of the post-synaptic membrane, and neuronal hyperexcitability, which is at the origin of neuropathic pain (Lalisse et al., 2018; Tsuda et al., 2013; Zhuo et al., 2011).

A wealth of further pathophysiological roles exist for P2XRs, and in section three, we will encounter a few more examples within the specific context of P2X7Rs.

2.6. Structural features

Precluding the resolution of P2X crystal structures, a large amount of experimental data had succeeded in elucidating the key architectural features of P2X receptors. Whilst the stoichiometry of P2XRs remained unknown, several studies revealed vital details regarding the topology of individual subunits. Sequence analysis following the initial cloning of P2XRs suggested intracellular N- and C-termini, two putative transmembrane domains and a large hydrophilic, cysteine-rich ectodomain. Experiments probing the glycosylation profile of P2X2R confirmed the presence of this large extracellular domain, delineating the boundaries of the hydrophobic TM domains (Newbolt et al., 1998), and P2X2R constructs concatenated between the N- and C-termini demonstrated that these domains were indeed most likely located on the same side of the membrane: intracellularly (Newbolt et al., 1998; Torres et al., 1998). Cysteine scanning experiments in combination with sulfhydryl-reactive methanethiosulfonate (MTS) reagents determined pore-lining residues present in the TM2 domain, as well as the location of the channel “gate” – the most narrow section of the pore – as being between L338 and D349 (rP2X2 nomenclature) (Rassendren et al., 1997).

In terms of the multimeric organisation of P2XRs, several techniques permitted the elucidation of a trimeric assembly. Despite early observations that the ectodomain of P2X2 was able to form stable heteromeric assemblies in solution (Kim et al., 1997), pioneering biochemical cross-linking studies later provided strong evidence for the presence of P2X1 and P2X3 trimers (Nicke et al., 1998), whilst an alternative technique employing T336C mutant concatemers in conjunction with MTS blocking reagents also concluded that three subunits participated in P2X2 pore formation (Stoop et al., 1999). Later studies using microscopic techniques also alluded to a trimeric architecture; atomic force microscopy (AFM) studies produced images which appeared to resolve three distinct subunits (Barrera et al., 2005; Nakazawa et al., 2005), whilst FRET in conjunction with electron microscopy similarly indicated a trimeric structure and the associated dimensions (Young et al., 2008). Mio *et al* equally employed single particle analysis of electron microscopy data to visualise the trimeric organisation of P2X2, at >10 Å resolution (Mio et al., 2009, 2005). In terms of the ATP binding site, decisive proof of an intersubunit location had been provided by the use of cysteine mutants (K68C and F291C in P2X1), which formed trimers upon crosslinking by disulphide bridge formation, unless in the presence of ATP, which, lodged in its binding site, prevents the formation of such bridges (Marquez-Klaka et al., 2007).

Many of the structural details relating to P2XRs had, therefore, been resolved thanks to a combination of complementary techniques. All that was missing was high resolution structural determination to definitively support these conclusions. The resolution of the first P2XR in 2009, a truncated construct of zebrafish P2X4 (zfP2X4) was, therefore, a landmark feat within the field, and not only confirmed the global architecture of P2XRs, but also provided a platform upon which to base further study, and from which to re-interpret previously collected data within a more precise, structural context. Following this first *apo* closed state structure, the ATP-bound structure was resolved shortly after, and across the subsequent decade, seven structures of P2XRs have become available, of various subtypes and species. Here, we will consider just the principal, common features revealed by these structures, as they will be discussed in greater detail elsewhere: within section 3.4 and within chapter one.

2.6.1. Global architecture

In 2009 and 2012, the Gouaux group resolved the crystallographic structures of zfP2X4 in both the *apo*, closed and ATP-bound open states (Figure 11).

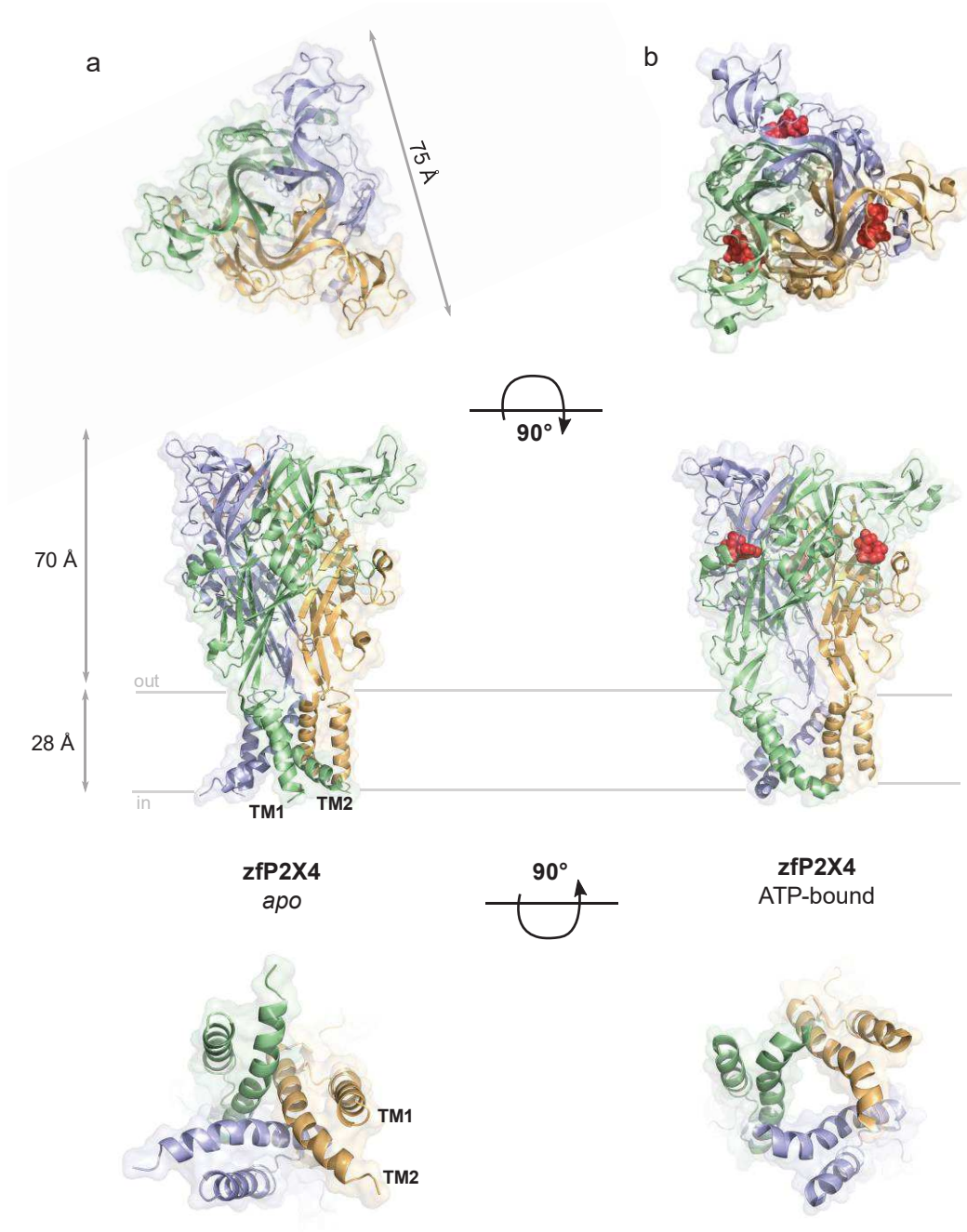


Figure 11. Crystallographic structures of zfP2X4.

View of the truncated zfP2X4 receptor in the *apo* closed state (a) and ATP-bound open state (b). ATP is shown in sphere representation (red), and zfP2X4 is shown in cartoon representation with surface partly transparent, each subunit is coloured differently. TM1 and TM2 are indicated, as is the position of the membrane bilayer. Upper panel: view along the 3-fold axis from the extracellular side. middle panel: lateral view along the membrane plane, lower panel: view along the 3-fold axis from the intracellular side. PDB: 4DW0 (closed) and 4DW1 (open). (Hattori and Gouaux, 2012; Kawate et al., 2009)

These structures revealed a chalice-like, trimeric assembly, with the extracellular domain protruding 70 Å proud of the membrane plane, and the transmembrane domains extending approximately 28 Å into the membrane. In the closed state, the transmembrane helices, TM1 and TM2, are placed about 45° from the membrane normal, and cross one another midway through the membrane. The ion conducting pore is defined by the association of three TM2 (Figure 11, lower panels). The extracellular domain, which when viewed from above is reminiscent of an equilateral triangle, measuring 75 Å, features extensive interactions between subunits, each one wrapped tightly around its neighbour (Figure 11a, upper panel). Kawate *et al* compare each individual monomer subunit to the shape of a leaping dolphin, with the fluke represented by the TM domains, the flippers, dorsal fin and head meanwhile, are present in the extracellular domain (Figure 12).

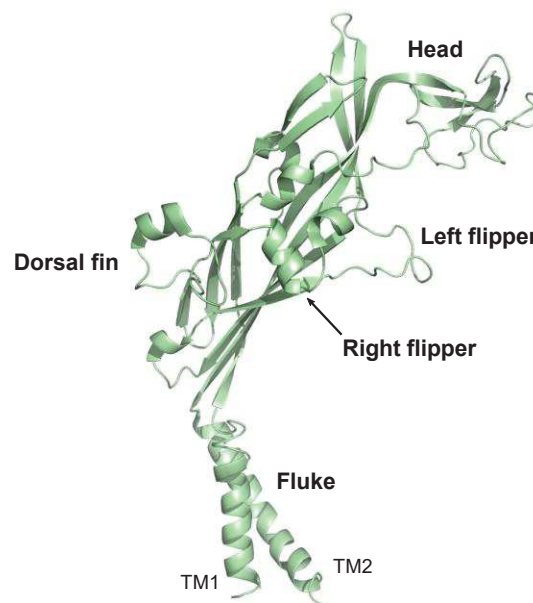


Figure 12. Individual monomer of zfp2X4.

Individual monomer subunit of zfp2X4 in the *apo* state, labelled according to the leaping dolphin analogy proposed by Kawate *et al*. PDB: 4DW0.

Resolution of zfp2X4 in an ATP-bound open state further shed light on the structural specificities of P2XRs, and provided insights as to the molecular movements which must take place during the transition from the closed to the open state. These structures, in combination with other experimental approaches including normal mode analysis (Du *et al.*, 2012), voltage clamp fluorometry (Lörinczi *et al.*, 2012) and metal bridge formation (Jiang *et al.*, 2012), have allowed a four-step mechanism to be proposed with regard to the structural changes induced upon ATP binding (Chataigneau *et al.*, 2013). The ATP binding site, localised in the extracellular domain (Figure 11b, upper and middle panels), forms an intersubunit “jaw”, which, upon ATP binding, undergoes a tightening movement, bringing the head domain in closer proximity to the dorsal fin. Closure of this jaw induces the upwards movement of the dorsal fin, in turn producing an outwards flexing motion of the β -sheets located in the lower body. These

β -sheets are directly coupled to the transmembrane helices, and their outwards flexing motion induces an iris-like rotation of TM1 and TM2 to open an ion permeable pore measuring approximately 5 Å (Figure 11b, lower panel).

2.6.2. Extracellular domain

The extracellular domain, aside from featuring a number of glycosylation points and disulphide bridges, contains the site of ATP fixation. Prior to the resolution of ATP-bound zP2X₄, numerous studies had probed the implications of various residues in ATP-binding, using a combination of mutagenesis and electrophysiology, targeting those extracellular residues which are highly conserved amongst P2X subtypes (Evans, 2010; Jiang et al., 2012; Marquez-Klaka et al., 2007). The ATP-bound zP2X₄ crystal structure confirmed much of this data and afforded valuable precisions into the exact spatial arrangement of the binding site, which, located between two subunits, involves domains originating from neighbouring monomers. Within this pocket, ATP adopts an unusual U-shaped conformation, allowing it to bind to a number of positively charged residues. Notably, the residue K70 interacts with oxygens on the α , β and γ phosphate groups, playing a crucial role in the binding process.

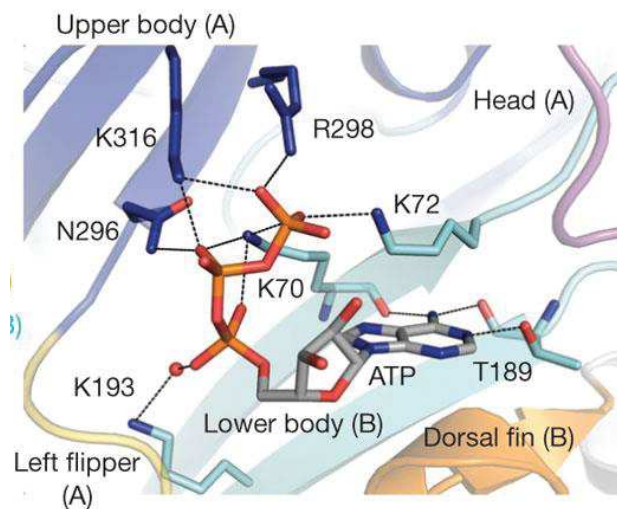


Figure 13. ATP binding site of zP2X₄.

ATP lodged in its binding site. The domains of each subunit involved in the formation of the binding site (A or B indicates different subunit monomers) are indicated. Black dashed lines indicate hydrogen bonding. From (Hattori and Gouaux, 2012).

2.6.3. Transmembrane helices and the gate

The transmembrane domain, as expected, comprises two helical domains, TM1 and TM2, the latter of these lining the conductive pore. In the closed state structure, the extra- and intracellular limits of the gates were defined as L340 and A347, with the centre of the gate, dictating the most constricted point of the pore, as A344. A number of previous studies, probing the accessibility of mutant cysteine residues to modification by MTS reagents or co-ordination to Ag⁺ and Cd²⁺, had alluded to this structural organisation albeit not in unified consensus (Kracun et al., 2010; Li et al., 2008; Rassendren et al., 1997).

In the open state, an additional feature became apparent: the presence of a “kink” in TM2, located around a flexible glycine residue at position G350, proposed to act as a hinge. The role of this glycine hinge in gating was later confirmed in rP2X2R (Habermacher et al., 2016).

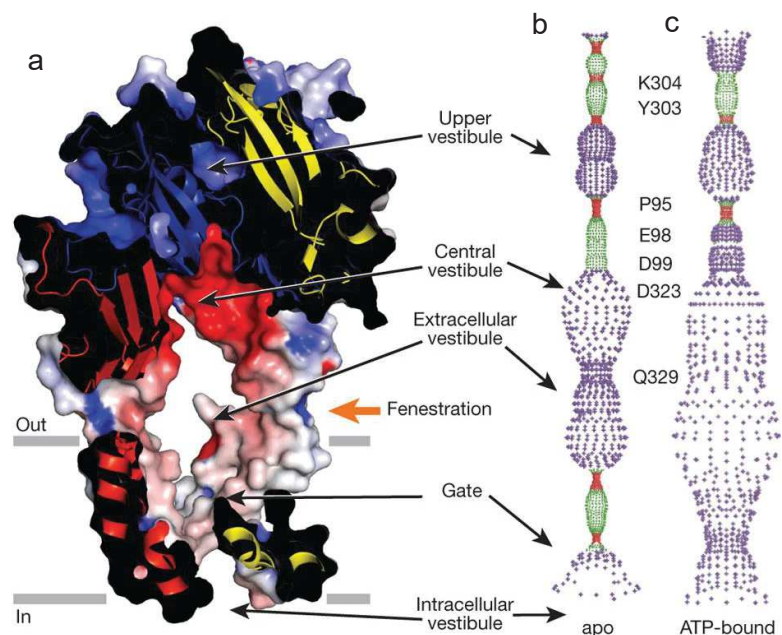
It is interesting to bring attention, here, to a limitation of these structures, in the form of large crevices located within the transmembrane domain. The presence of such intersubunit crevices was soon identified as a potential crystallisation artefact, and refined models proposed by a number of studies (Habermacher et al., 2016; Heymann et al., 2013). This will be discussed in further detail in the following chapters.

2.6.4. Ion conduction pathway

Following the resolution of the *apo*, closed state structure, two possible ion permeation pathways were identified. Three fenestrations located directly above the TM domains, measuring approximately 8 Å, were identified, through which lateral ion flow was proposed to occur, followed by conduction through the TM pore. Alternatively, an upper and central vestibule were identified, which, although in the closed structure appeared too narrow for ions to flow through, was proposed to undergo widening upon ATP-binding, which would allow ions to transit the channel the long of the three-fold symmetry axis. The resolution of the ATP-bound structure clarified these propositions, and confirmed that the upper vestibule was indeed too narrow to allow ion conduction. This, supported by studies using cysteine scanning and MTS reagent modification of residues located in the potential pathways (Samways et al., 2011), in addition to computational methods (Kawate et al., 2011), confirmed that the pathway of ions into the channel is *via* the lateral fenestrations.

Figure 14. Ion conduction pathway of P2XRs.

(a) 2 monomer units of the ATP-bound open state zfp2X4 structure shown in cartoon and surface representation, clipped to show the vestibules where ions may gather. The lateral fenestrations are indicated with an orange arrow. (b) Pore lining surfaces of the *apo* closed structure and (c) ATP-bound structure. Each colour indicates a different radius range from the pore centre (red: <1.15 Å, green: 1.15 – 2.3 Å, and purple: >2.3 Å). From (Hattori and Gouaux, 2012).



2.6.5. Intracellular domain: cytoplasmic cap

It was not until 2013, when the group of Gouaux resolved the crystal structure of hP2X3 in the *apo*, ATP-bound open and ATP-bound desensitised states, that we gained an insight into the structure of the intracellular domains of P2XRs. This structure revealed the presence of a so-called “cytoplasmic cap”, a highly intertwined structural motif present only in the open state of hP2X3Rs, presumably becoming disassembled in *apo* and desensitised states (Mansoor et al., 2016). The cap is formed by domain-swapping of the N- and C-termini of all three protomers: the C-terminal β -sheet of each monomer interacts with the N-terminal β -sheets of each of the remaining two monomers. This network of β -sheets is suggested to stabilise the open state structure, effectively locking it into place.

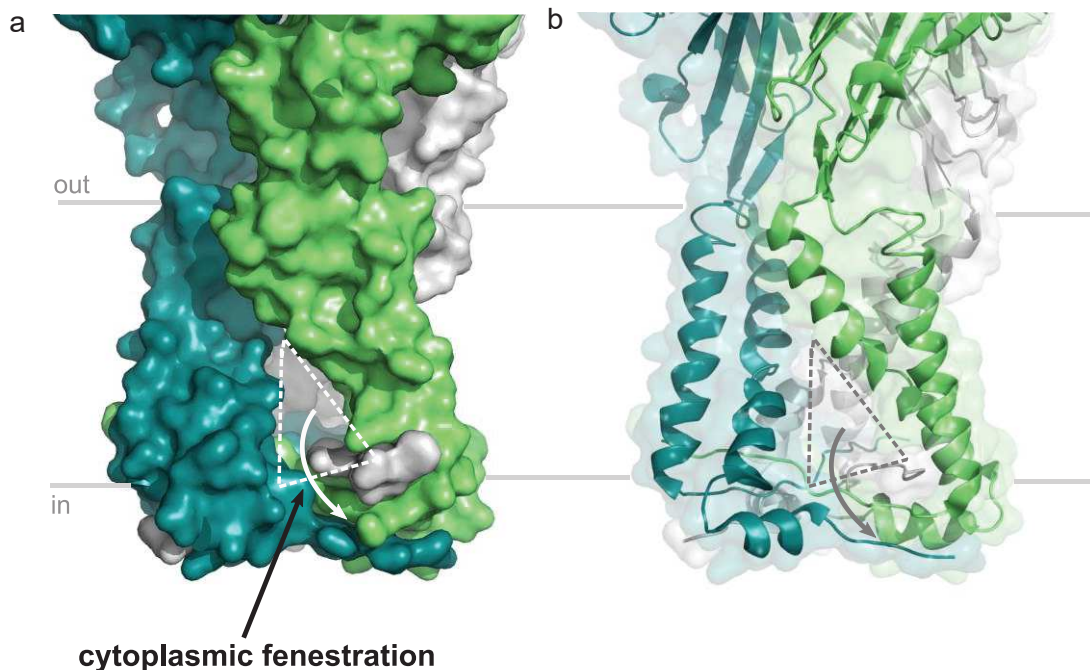


Figure 15. Crystallographic structure of ATP-bound hP2X3: TM domains and cytoplasmic cap.

Shown in (a) surface representation and (b) cartoon representation with transparent surface, each monomer coloured differently. The cytoplasmic fenestration is outlined as a triangle and the approximate ion egress pathway indicated by an arrow. PDB: 5SVK.

This structure also provides a further piece of the puzzle with regard to the ion permeation pathway. The channel orifice directly beneath the three-fold axis being too narrow to allow ion flux into the cytosol, the identification of three cytoplasmic fenestrations, triangular shaped exit points just above of the cytoplasmic cap, provides a feasible pathway through which ions may end their transit.

We gained even greater insight into the intracellular domains with the very recent cryo-EM resolution of rat P2X7R (rP2X7), which will be discussed in detail within section 3.

2.7. Allosteric conformational states

Ion channels are dynamic entities, able to experience a number of conformations. P2X receptors undergo a cycle of activation, fluctuating between several different allosteric conformational states, as outlined in Figure 16.

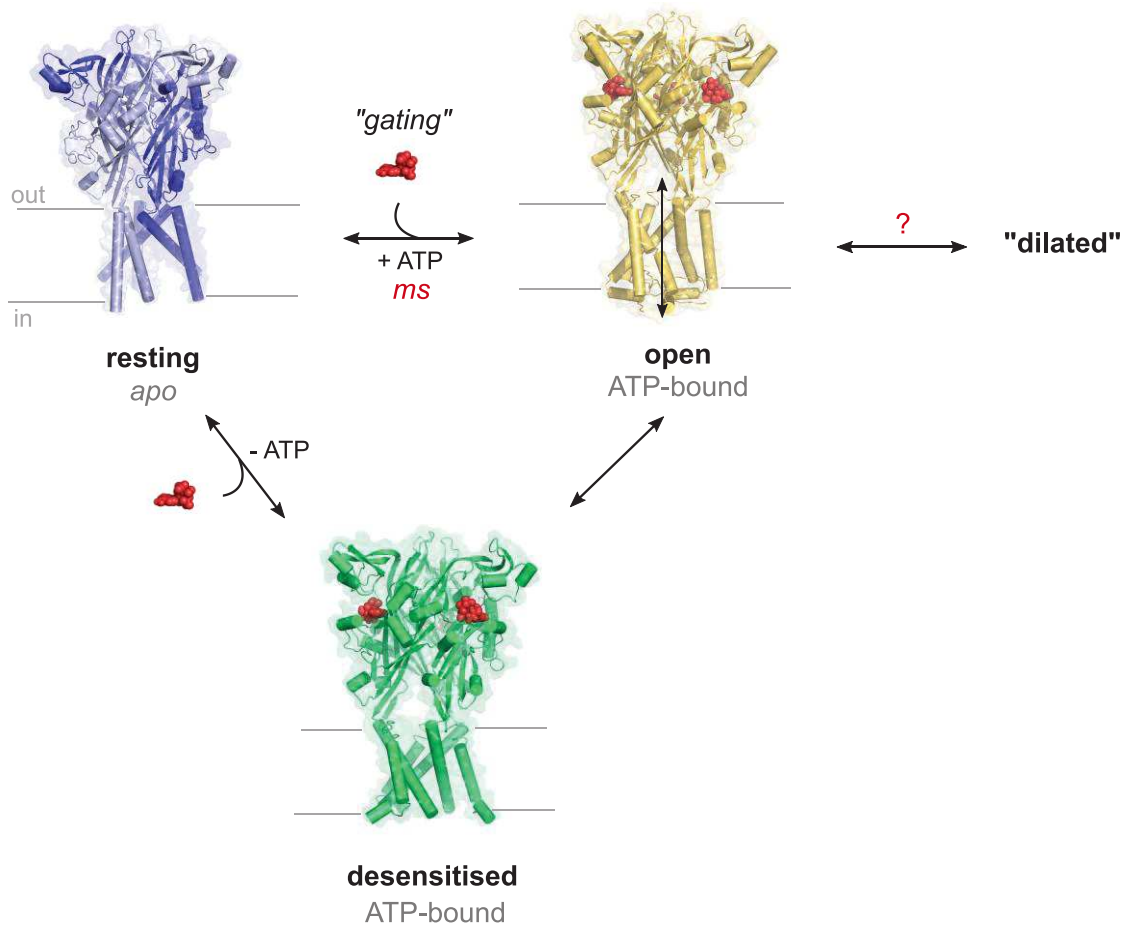


Figure 16. Principal allosteric conformational states of P2XRs.

Allosteric conformational states accessible to P2XRs: upon ATP binding, a transition occurs from the resting closed state to an open channel state. Certain subtypes may exhibit the desensitised state, whereby channel closure occurs despite the presence of bound ATP. Cycling between these states is dynamic. PDB: 5SVJ, 5SVL, 5SVK. (Mansoor et al., 2016)

2.7.1. Pore opening (*gating*)

For P2XRs, the transition from the resting, closed state to the agonist-bound open state, known as the process of *gating*, occurs upon binding of ATP. As we have seen in the above sections, the binding of ATP in its intersubunit binding pocket induces a cascade of structural changes across the globality of the protein, the outcome of which is a conformational change resulting

in the opening of a pore permeable to small inorganic cations such as Na⁺, Ca²⁺ and K⁺. This process occurs on the millisecond timescale, and is common amongst all P2XRs. Ding and Sachs' studies on P2X2Rs provided a number of valuable insights into the gating process, namely, that the three ATP binding sites act in a positive co-operative manner, with the association rate of incoming ATP molecules increased by the presence of each already-bound ATP (Ding and Sachs, 1999). This positive co-operativity is not only observed in an intra-receptor manner, but also between separate trimers: the mean open lifetime of channels increases when multiple channels are present (Ding and Sachs, 1999). Further precisions pertaining to the number of ATP molecules required to provoke the gating transition were uncovered by the use of concatemeric P2XRs carrying the mutation K69A (K69 being a key interaction point within the ATP binding site) either once, twice, or thrice, determining that two molecules of ATP were sufficient to induce pore opening (Stelmashenko et al., 2012).

The aforementioned single channel studies have also demonstrated the existence of several intermediate states, undocumented by the crystallographic structures. Single channel recordings revealed "flickering" behaviour, reflecting rapid conformational fluctuations between open and closed states in the presence of ATP, whilst rare glimpses of sub-conductance states were also observed (Ding and Sachs, 1999). An additional conformational state in the form of a "flipped" state, an intermediate, closed liganded state (Moffatt and Hume, 2007).

2.7.2. Desensitised state

A selection of P2XRs undergo *desensitisation*, that is, the closure of the channel despite the continued presence of bound ATP, thought to be of pertinence for neuromodulation and as a protection mechanism from neurotoxicity. This desensitisation differs according to the specific P2X subunit (illustrated in Figure 7), and studies using chimeric receptors (swapping domains in strongly desensitising P2X1R or P2X3R for those of weakly desensitising P2X2R), have shown the importance of the transmembrane domains in modulating the desensitisation profile (Werner et al., 1996).

The hP2X3 structure resolved in the desensitised state by Mansoor *et al* shed further light on this phenomenon, confirming the implication of the transmembrane domains in the transition. Namely, this concerns the formation of a 3₁₀-helix in the open state, which upon transition to the desensitised state recoils upwards to reform an α -helix, with concomitant deconstruction of the cytoplasmic cap (Mansoor et al., 2016).

2.7.3. “Dilated” state

For many years, the possibility of a second open state, whereby the P2X pore becomes progressively permeable to large organic cations, such as N-methyl-D-glucamine (NMDG⁺), and organic dyes, such as YO-PRO-1 and ethidium, was much discussed in the literature. This behaviour has been suggested for P2X₂, P2X₄ and P2X₇ receptors, as well as heteromeric assemblies P2X_{2/3} and P2X_{2/5} (Peverini et al., 2018). More recently, the existence of such a dilated P2X pore has been brought under intense scrutiny, with several studies providing strong evidence against such a phenomenon. This will not be discussed in detail at this point, as we shall explore the pore dilation theory further in section 3.4, as well as in chapter three.

3. P2X₇

Within this section, we will take an in-depth look at one particular P2X family member: P2X₇. P2X₇ is the least similar to the other family members in terms of amino acid sequence, largely due to its elongated C-terminus (North, 2002). This, in combination with several functional particularities, sets P2X₇ aside from the other P2X variants.

3.1. Historical aspect

The history of P2X₇ dates back to the 1970s, when Cockcroft and Gomperts first reported on the ATP-induced permeabilization of rat mast cells (Cockcroft and Gomperts, 1979). Following these initial observations, where the implication of a channel was suggested, but whose identity remained unknown, a number of studies were undertaken to characterise this unusual property: the use of fluorescent dyes of differing molecular weights allowed an upper size limit for permeating species to be approximated (Steinberg et al., 1987), and a variety of cell lines were probed with ATP stimulation to establish those possessing permeabilization behaviour. These cell lines initially included mouse fibroblasts, macrophages, Chinese hamster ovary cells (CHO), HeLa, melanoma cell lines and neuroblastoma cell lines (Steinberg and Silverstein, 1989). Upon the discovery of purinergic signalling, and the designation of specific classes of purinergic receptors (P₁, P₂, and within this latter group, P2X and P2Y), the macropore-forming ATP receptor was placed in a class of its own, the P2Z receptor (Burnstock, 2012, Burnstock, 1972; Burnstock and Kennedy, 1985; Gordon, 1986). It was not until the first cloning of this receptor from rat brain tissue in 1996 that a close proximity to the amino acid sequence of P2XRs was observed, and thus the P2Z receptor was re-classified as the seventh member of the P2X family, P2X₇ (Surprenant et al., 1996).

3.2. Localisation

P2X₇ is expressed in many cell types, particularly those of hematopoietic lineages such as mast cells, monocytes, macrophages, lymphocytes, as well as erythrocytes and epidermal

Langerhans cells (Collo et al., 1997; Illes et al., 2017; Skaper et al., 2009; Sluyter et al., 2004). P2X7 has additionally been found in bone-derived cells, such as osteoblasts and osteoclasts (Gartland, 2012; Gartland et al., 2001). In the CNS, P2X7Rs are highly present in immunocompetent cells, such as microglia and astrocytes. Their localisation within neurons, however, is a controversial topic, which remains unresolved in the literature, in part due to the lack of specific pharmacological tools and P2X7 antibodies with which to probe neuronal expression (Anderson and Nedergaard, 2006; Kaczmarek-Hajek et al., 2018). The recent development of P2X7-directed nanobodies has helped to shed light on this matter (Kaczmarek-Hajek et al., 2018).

In terms of localisation within the cell, P2X7R trafficking has been demonstrated to be dependent upon cell type (Robinson and Murrell-Lagnado, 2013), and the C-terminus of the receptor has been shown to be implicated in the control of trafficking from the endoplasmic reticulum to the cell membrane, as has glycosylation at several asparagine residues within the extracellular domain, specifically, N187 (Denlinger et al., 2003; Lenertz et al., 2010). Equally, the disulphide bond-forming cysteine residues in the ectodomain have been determined of vital importance for proper receptor trafficking.

Once at the plasma membrane, P2X7Rs have been found to associate with lipid raft fractions, microdomains within the membrane which are enriched in certain lipids, such as cholesterol, sphingolipids and saturated phospholipids, and which contribute to membrane asymmetry (Pike, 2004). Lipid raft association has been determined in heterologous expression systems (HEK293 cells), as well as in native tissues such as rat submandibular glands, peritoneal macrophages and mouse lung alveolar cells (Barth et al., 2008, 2007; García-Marcos et al., 2006b, 2006a; Gonnord et al., 2009). Lipid rafts and P2X7Rs will be discussed in greater detail within chapter three.

3.3. Structure

The very first P2X7 structures were resolved by X-ray crystallography, in the group of Kawate (Karasawa and Kawate, 2016). These structures, which featured a N- and C-terminally truncated panda P2X7 construct (pdP2X7) in the *apo*, resting state, as well as in complex with five non-competitive antagonists, confirmed the similarity of the global P2X7R architecture to the previously resolved P2X structures: trimeric, with each protomer conforming to the leaping dolphin model previously observed in zfP2X4 and hP2X3. Several differences were observed, however, regarding the presence of a novel drug binding pocket, which is discussed in section 3.5.2. Similarly, in 2017, the crystallographic structure of a truncated chicken P2X7 construct

(ckP2X7) was resolved in complex with competitive antagonist, TNP-ATP, again, giving insights into mechanisms of inhibition in P2X7Rs.

It was not until October 2019, in the final months of my PhD, that the cryo-EM structure of full length rP2X7 was resolved by the Mansoor group, giving the first complete view of P2X7R structure (McCarthy et al., 2019). For the first time, the three dimensional spatial arrangement of the elongated C-terminus could be visualised. In the study of P2X7 receptors, the resolution of such a full length structure is a landmark moment in the field, which for many years was preoccupied with questions regarding the organisation of this unusual intracellular domain. This structure therefore opens a wealth of new possibilities for the dissection of P2X7 receptor behaviour, as well as the opportunity to compliment previous functional data with new structural interpretations. In this section, we will consider the key structural features of P2X7, in the context of the new, cryo-EM structure.

3.3.1. Overall architecture

The overall architecture of rP2X7R is largely similar to the previously determined P2X crystallographic structures: a highly intertwined trimeric organisation comprised of two transmembrane helices, a large ectodomain, and a domain-swapped cytoplasmic cap. The unique elongated C-terminus hangs below this cap, in the form of an anchor-like ballast (Figure 17).

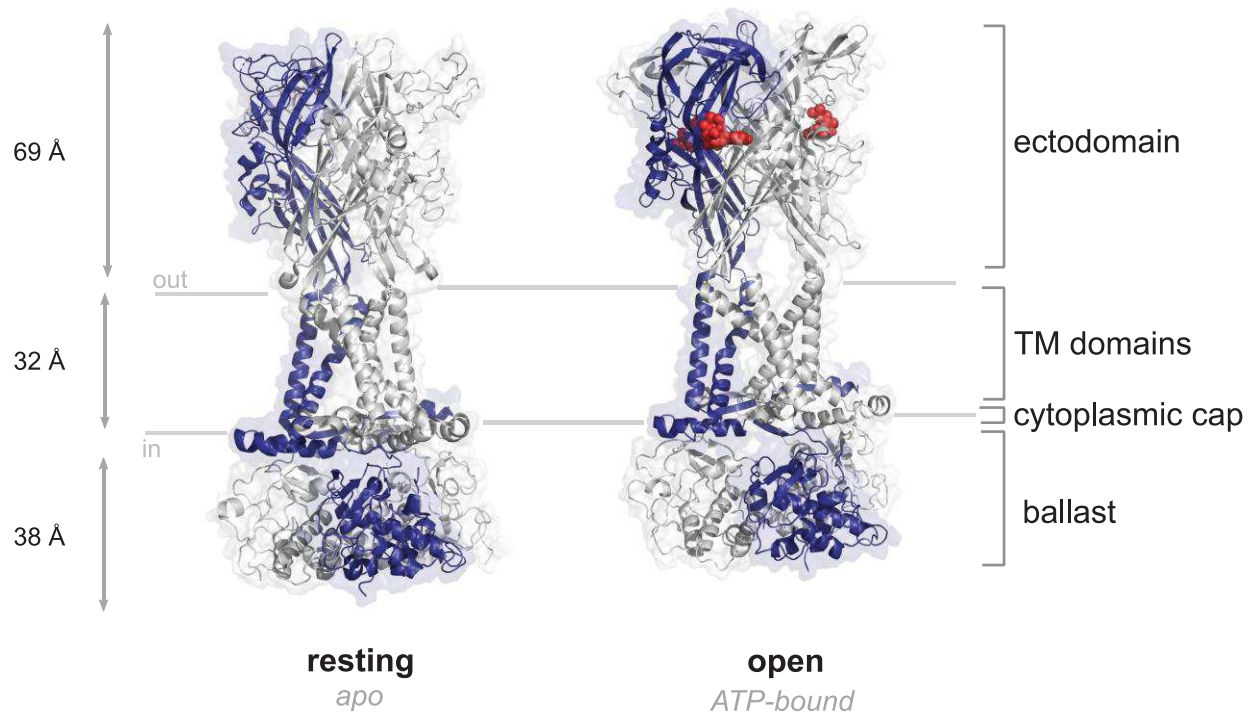


Figure 17. Cryo-EM structure of rP2X7R.

Key architectural features and dimensions are indicated. Structures are presented with each protomer coloured differently, and just one protomer coloured blue, to highlight the intertwining interactions between subunits. Left: in the resting, *apo* state, PDB: 6u9v. Right: in the ATP-bound open state, PDB: 6u9w.

3.3.2. The extracellular domain: ATP binding site

The first feature which reveals significant differences between rP2X7R and the other resolved P2X structures, is that of the ATP binding site within the ectodomain. The binding of ATP within this pocket is much the same as in the previously resolved structure, whilst the residues involved differ slightly, the U-shaped conformation is retained. However, a striking difference is present in terms of the solvent accessibility of the binding site. The *apo*, closed state structure features a narrow channel in proximity of the binding site, formed by the head and left flipper domains of the same protomer. This channel controls the solvent-accessibility of the binding pocket, and measures approximately 11 Å in the rP2X7R structure, compared with 17 Å for hP2X3R (Figure 18). The binding site is therefore much more shielded to solvent in the rP2X7 structure.

The authors propose that this difference in solvent accessibility may be at the origin of the markedly lower ATP sensitivity of P2X7 as compared to other P2X subtypes, rendering the time required for ATP to sample the correct conformation for entry and binding significantly greater.

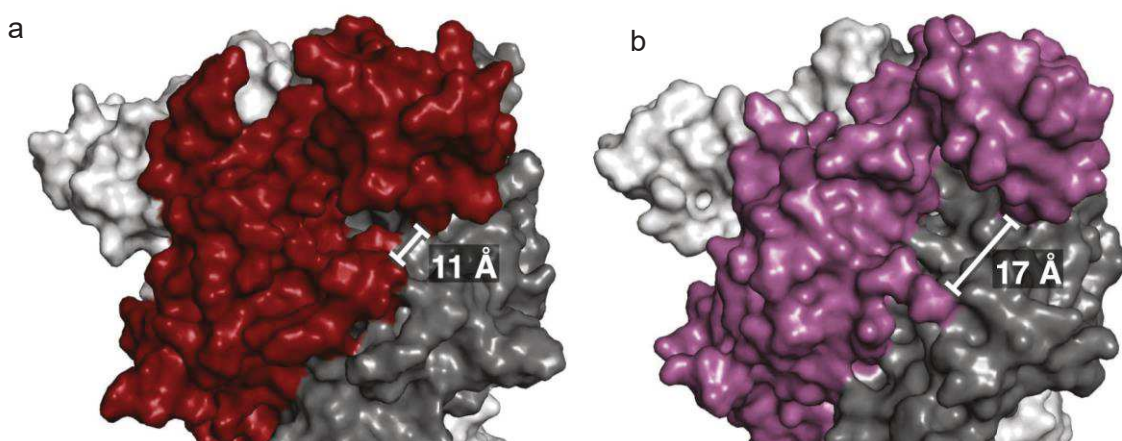


Figure 18. ATP binding site of rP2X7 as compared to hP2X3.

The extracellular domain viewed in surface representation featuring the ATP binding site, shielded by a channel formed between the head domain and left flipper of the same protomer (coloured), in (a) rP2X7, measuring 11 Å and (b) hP2X3, measuring 17 Å. From (McCarthy et al., 2019).

3.3.3. The TM domains

Consistent with other P2XRs, the pore is lined by the TM2 helix, with the gate located between S339 (extracellular side) and S342 (cytosolic side), consistent with previous electrophysiological data (Pippel et al., 2017). In the ATP-bound structure, S342 defines the

narrowest point in the pore, measuring approximately 2.5 Å in radius (Figure 19). This is analogous with hP2X3, whose structure reveals the narrowest point of the channel to be at the equivalent residue (Mansoor et al., 2016).

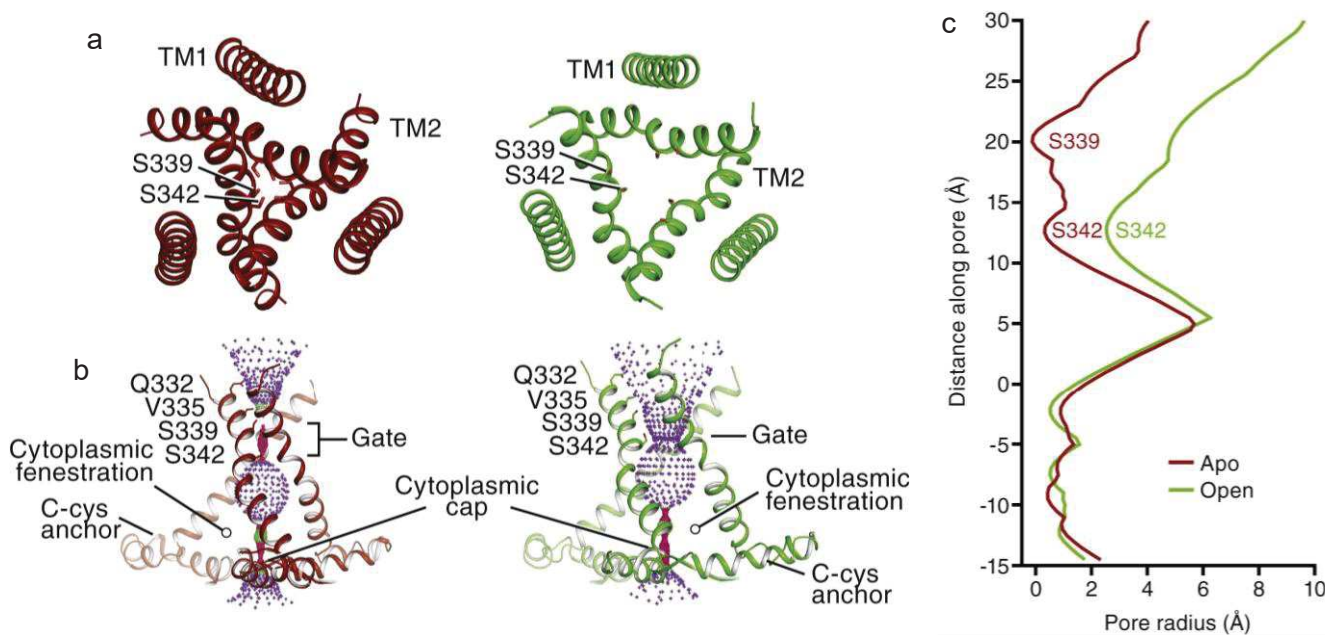


Figure 19. TM domains and pore of rP2X7R.

(a) View from above, along the three-fold symmetry axis, of the transmembrane domains and ion pore in the *apo* resting state (red, left) and the ATP-bound, open state (green, right), with key residues labelled. (b) Ion permeation pathway in the *apo* resting state (red, left) and the ATP-bound state (green, right), with distances indicated by different colours: <1.15 Å; green, between 1.15–2.30 Å; purple, >2.30 Å. Key residues and features are labelled, the N-terminus and ballast region have been removed for clarity. (c) Plot of pore radius as a function of distance along the pore axis for the *apo* state (red) versus the open state (green) of rP2X7. From (McCarthy et al., 2019).

The greatest diameter reached by the channel is determined at approximately 5 Å, just under the minimal effective diameter of 8.5 Å which was calculated for the human orthologue, by way of single channel recordings with permeating cations of increasing size (Riedel et al., 2007a).

3.3.4. The intracellular domains: cytoplasmic cap, Ccys anchor and the ballast region

The first glimpses of the P2X7 intracellular domains afforded by this structure reveal a number of interesting and unexpected structural features. The first of these concerns the cytoplasmic cap, a feature previously observed in the hP2X3 crystallographic structure, proposed to stabilise the open channel state. In rP2X7, this cytoplasmic cap is equally present. However, in stark contrast to hP2X3, whose cytoplasmic cap is disassembled in the closed state, rP2X7 features an intact cap in both the *apo* and ATP-bound states, making it a permanent structural scaffold. Within this cytoplasmic cap motif, is a sequence of 18 amino acids rich in cysteine

residues, named here the Ccys anchor, which is unique to P2X7. Within this region, at least four cysteine residues are palmitoylated, C362, C363, C374 and C377, as well as one serine, S360 and one N-terminal cysteine, C4 (Figure 20a and b). These palmitoyl groups extend into the membrane bilayer, effectively anchoring the cytoplasmic cap in place and restricting structural movements in these lower domains. This is thought to be at the origin of the lack of desensitisation at P2X7; the cytoplasmic cap, an open state stabilising motif, is locked into place *via* the Ccys anchor, preventing cap disassembly and desensitisation as observed in hP2X3.

Removal of the Ccys anchor, or indeed mutation of its palmitoylatable residues to alanine, which cannot undergo this post-translational modification, produces receptor constructs which almost completely desensitise during a prolonged ATP application, demonstrating that palmitoylation of this region is a critical determinant of the non-desensitising behaviour of P2X7. This is supported by previous work carried out with receptor constructs featuring deletions of this 18 amino acid region, which were shown to experience current desensitisation (Robinson et al., 2014). A study employing panda P2X7 receptor constructs (pdP2X7) of varying C-terminal lengths reconstituted into liposomes also shows the dependence of receptor activity on this cysteine rich region (Karasawa et al., 2017).

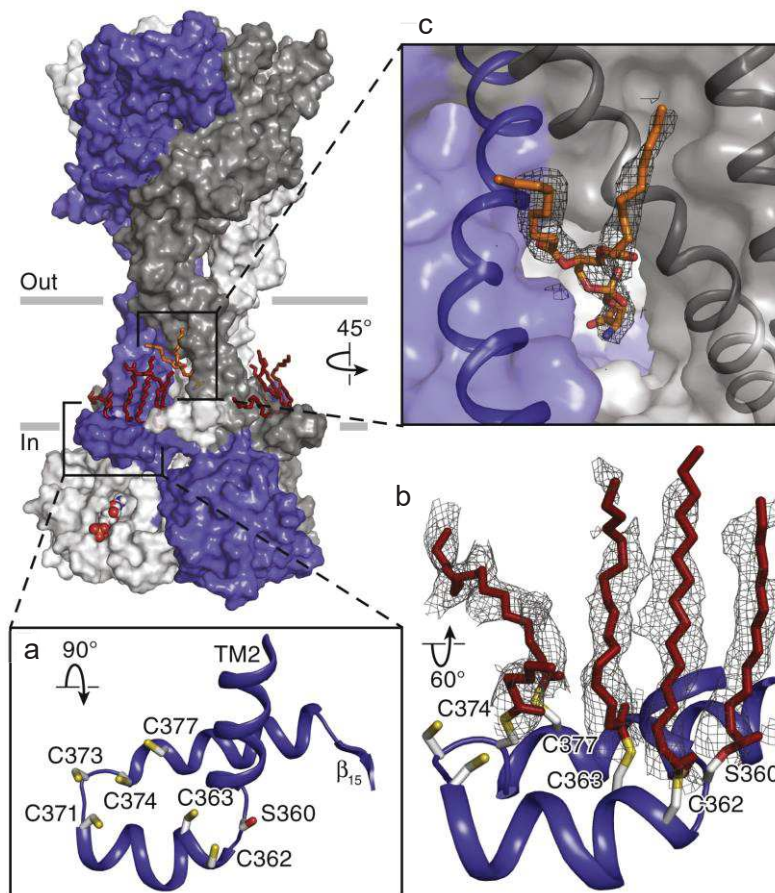


Figure 20. Ccys anchor and lipid binding site of rP2X7.

Structure of rP2X7 in surface representation with key features zoomed in for detail, (a) the Ccys region with sites of palmitoylation labelled, (b) Ccys region with the palmitoyl groups visible (c) the putative phospholipid binding site. From (McCarthy et al., 2019).

Another pertinent feature of this region is the resolution of a lipid molecule wedged between the transmembrane helices, just above the Ccys anchor. This feature is particularly interesting given the PS-flip which occurs following P2X7R activation (see section 3.4).

The final major discovery of this structure is the presence of the ballast, a uniquely folded domain hanging below the cytoplasmic cap, for which no homologous structure exists (Figure 21a). This ballast region comprises the final 200 residues of the C-terminus, and exhibits a globular structure, consisting of a number of β -sheet, α -helical, and loop regions. The first interesting feature of this ballast region involves a number of cysteine residues, which had previously been determined as important for proper receptor trafficking, and linked to palmitoylation (Gonnord et al., 2009). However, in the resolved structure, seven of these eight cysteines can be seen to be buried within the fold of the ballast, and involved in the complexation of a dinuclear zinc motif (Figure 21c).

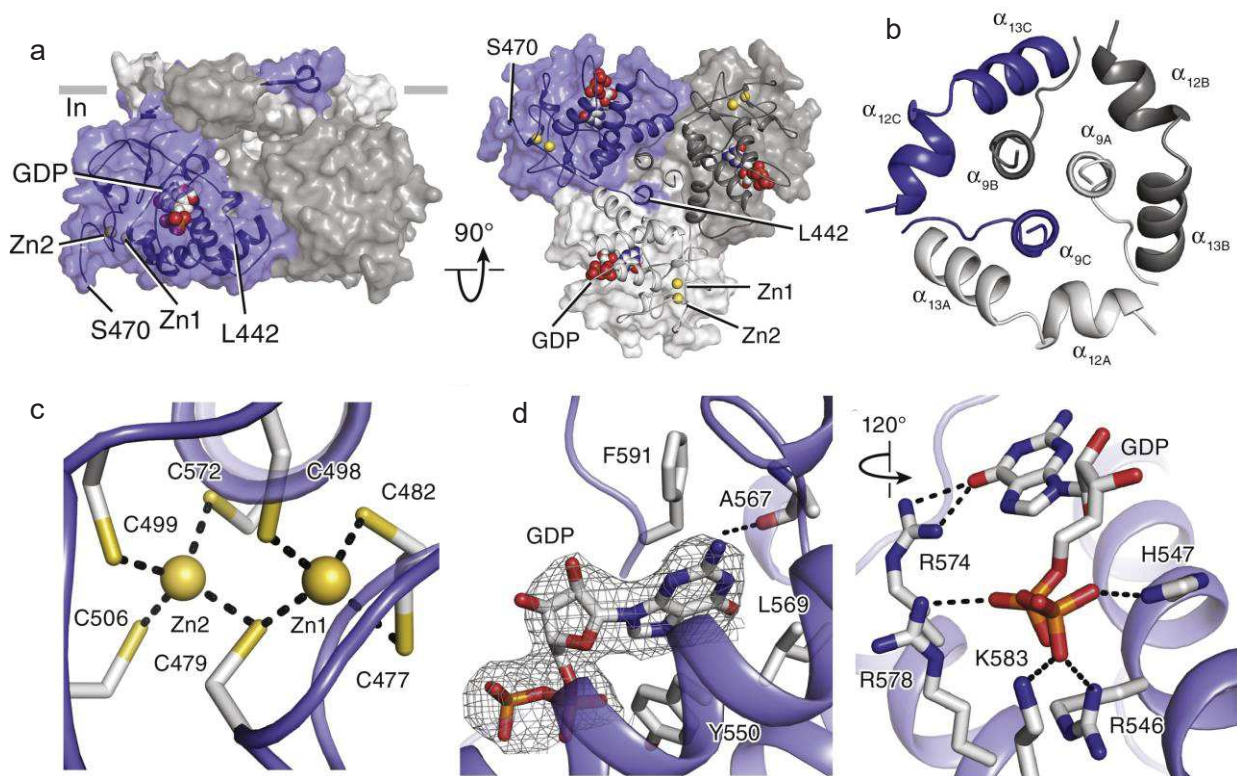


Figure 21. The rP2X7 ballast region.

(a) The ballast region viewed laterally, along the membrane plane (left) and along the three-fold axis from the intracellular side (right), in surface representation with one protomer highlighted in blue and in cartoon representation. GDP and Zn^{2+} are represented as spheres and indicated. (b) the cytoplasmic plug, formed from the association of three α_9 helices. (c) the Zn^{2+} dinuclear binding site and cysteines residues which are involved. (d) views of the GDP binding site, with those residues involved shown in stick representation and labelled. From (McCarthy et al., 2019)

A second binding motif was resolved within the ballast, in the form of a GDP binding pocket, where, despite having not been added exogenously during purification, GDP and its non-hydrolysable analogue GDP- γ -S were found to bind at particularly high affinity (40 nM). The physiological role of the ballast, its Zn²⁺ binding site as well as its GDP binding site, remain unknown, as upon its removal no changes to basic channel properties were observed by electrophysiology (McCarthy et al., 2019). These motifs will undoubtedly constitute the focus of future P2X7 research.

A final pertinent point resolved within the cytoplasmic cap pertains to the ion egress pathway. As observed in the crystallographic structure of hP2X3, ions are unlikely to exit the channel along the three-fold symmetry axis, due to dimensional restrictions. The rP2X7 structure features an additional limiting structural motif, the cytoplasmic “plug”, created by the association of three ballast-located helices (Figure 21b). This plug would prevent the flow of ions into the cytosol, thereby confirming the cytoplasmic fenestrations, as observed in the hP2X3 structure, as the more likely pathway for ion egress.

3.4. Function

In terms of function, P2X7, follows the common P2X model in that it is activated by extracellular ATP to open a non-selective cation permeable pore, typically allowing the permeation of Na⁺ and Ca²⁺ into the cell, and K⁺ efflux, with no permeability to anions (Kubick et al., 2012). The particularities of P2X7 are not only structural, as we have seen in the previous section, but also functional.

One of the principal functional features of P2X7 is the formation of the so-called cytolytic P2X7 macropore, whereby molecules of <900 Da have been observed to permeabilise the cell membrane following P2X7 activation. This is typically studied by monitoring the passage of large molecular weight cations, such as NMDG⁺, YO-PRO-1 or ethidium dyes into the cell upon P2X7 activation. Several explanations have been proposed regarding this macropore-related permeabilization, which are summarised in Figure 22. The first of these is that large molecular weight species transit through the P2X7 pore, as it becomes intrinsically dilated upon agonist stimulation. The second theory postulates that the P2X7 pore constitutes the permeation pathway for simple inorganic cations, whilst large molecules pass through a secondary, recruited annex channel. These scenarios are not mutually exclusive, and may also co-exist. Much debate exists in the literature on this subject, and we will return in greater detail to permeabilization and pore dilation in chapter three.

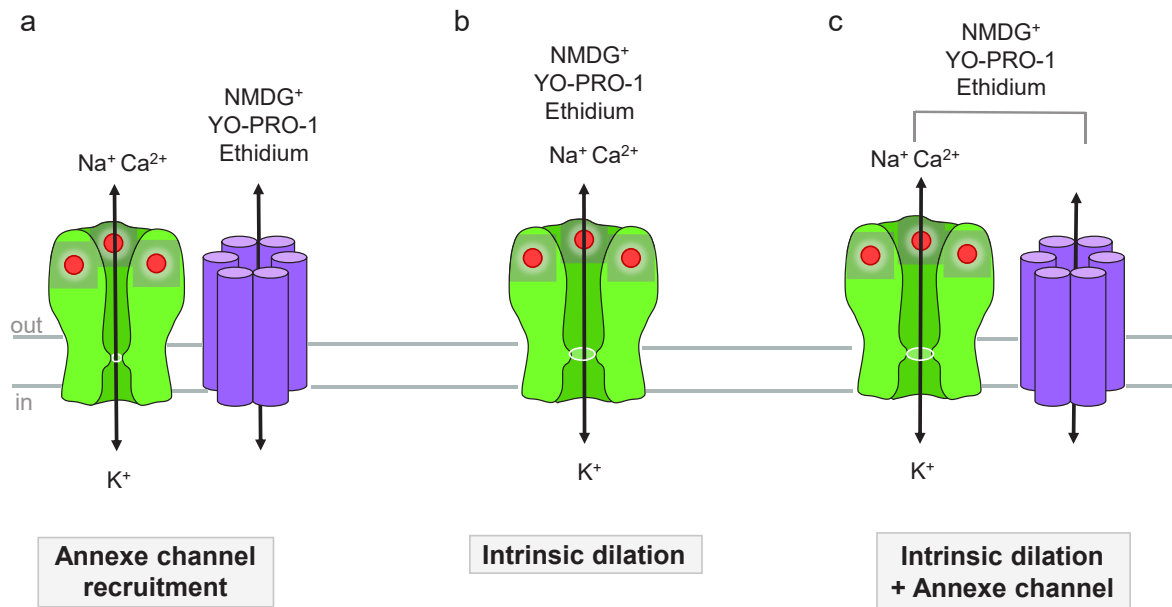


Figure 22. Possible pathways for P2X7 macropore-mediated large molecule permeabilisation.

(a) Scenario whereby small inorganic cations, linked to basic channel gating activity, pass through the P2X7 pore, whilst large molecules permeate the cell membrane *via* a recruited annexe channel. (b) Scenario whereby intrinsic pore dilation occurs and all permeating cations, small and of large molecular weight, pass through the P2X7 pore. (c) Scenario whereby the macropore identity is a combination of the scenarios outlined in (a) and (b).

The formation of this macropore is concomitant with dramatic, yet reversible, changes in cellular morphology in the form of membrane blebbing, and a host of other pseudoapoptotic markers, including actin filament disruption, mitochondrial depolarisation and swelling, and phosphatidylserine (PS) flip to the outer membrane bilayer (Mackenzie et al., 2005). In macrophages, the shed blebs have been found to contain caspase-1 and pro-inflammatory cytokine interleukin-1 β (Qu et al., 2007). This is, again, a unique characteristic to P2X7 activation.

Another unusual characteristic of P2X7 is its lack of desensitisation, in sharp contrast to other P2X family members. The structural reasons behind this we have seen in the previous section. In the place of desensitisation upon prolonged agonist stimulation, P2X7 exhibits a strikingly inverse behaviour, that of facilitation. Facilitation is a phenomenon unique to P2X7, whereby currents exhibit a marked increase upon repetitive or prolonged ATP-stimulation, shown in Figure 23. This phenomenon, with varying characteristics, has been shown in rat, mouse and human orthologues, in both recombinant and naïve systems and is known to be cholesterol-sensitive (Janks et al., 2018; Robinson et al., 2014).

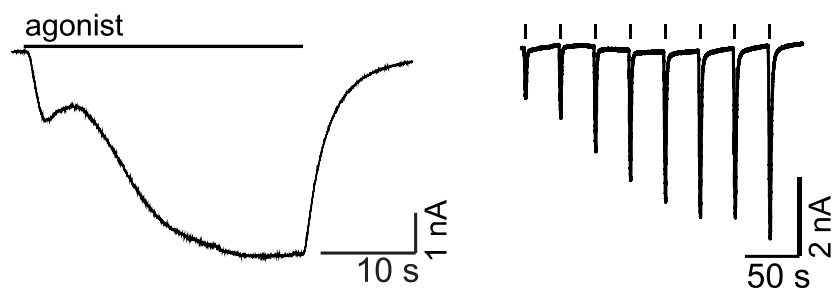


Figure 23. Sensitisation of P2X7.

Sensitisation of rP2X7 currents when stimulated with BzATP, either by a prolonged application (left) or repetitive applications (right).

These unusual P2X7 behaviours will be discussed in greater depth within chapter three.

3.4.1. Single channel level activity

Several single channel studies have been carried out on hP2X7Rs which have elucidated a number of functional details at the molecular level. A first study by Riedel *et al* probing hP2X7 in *Xenopus* oocytes observed two single channel conductance states; short openings of 9.5 pS and longer openings of 14.8 pS, with increasing probabilities of opening as ATP concentration reaches saturating levels (Riedel *et al.*, 2007a). Further work revealed that the unitary conductances observed are variable, and depend upon the permeating cation, exhibiting in general a decrease in conductance as the size of the permeating species increases (Figure 24, (Riedel *et al.*, 2007b)).

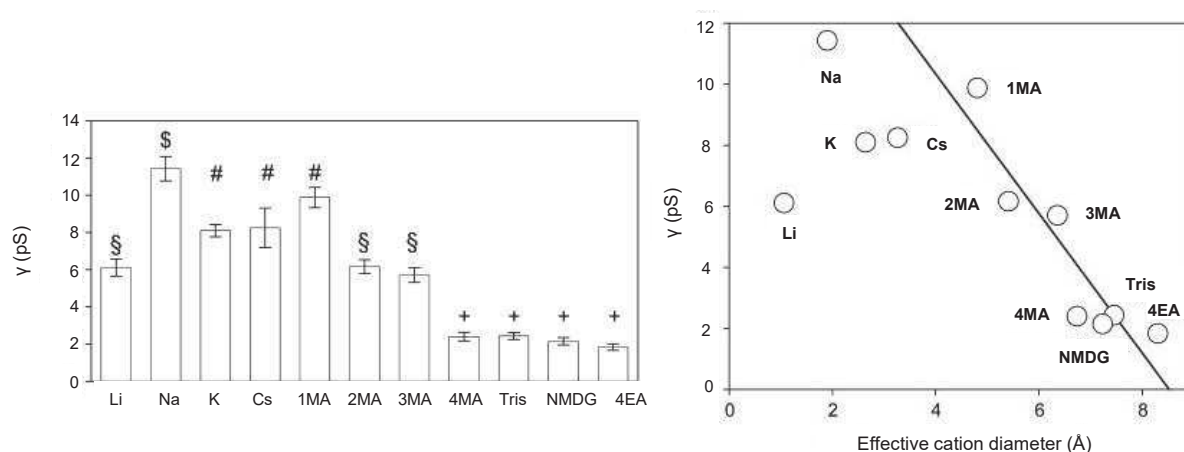


Figure 24. Permeating characteristics of hP2X7R at the single channel level.

(a) single-channel conductances (γ) recorded under asymmetric conditions (Cs^+ intrapipette solution) from outside-out *Xenopus* oocyte patches exposed to different extracellular cations. (b) Slope conductance (γ) of single hP2X7 channels versus the effective ionic diameter of each cation. 1MA = monomethylammonium, 2MA= diethylammonium, 3MA = trimethylammonium, 4MA = tetramethylammonium, Tris = tris-(hydroxymethyl)-aminomethane, NMDG = N-methyl-D-glucamine, 4EA =tetraethylammonium, all monovalent cations. From (Riedel *et al.*, 2007b).

Extrapolation of the linear regression fit in Figure 24b provided an approximation of the minimal effective diameter of the channel (i.e. where conductance is 0) of 8.5 Å. It was also shown that extracellular monovalent cations exert an influence over single channel properties. For example, replacement of external Na⁺ was shown to increase the mean open time of channels, resulting in an overall increased probability of opening (P_0). This was explained by the presence of an allosteric modulatory Na⁺ binding site, although the location of this binding site has not been fully investigated. Equally, the single channel kinetics of hP2X7R have been shown to be modulated by extracellular anions present in the bathing solution, with mean closed times decreasing in the order I⁻ > Cl⁻ > glutamate (Kubick et al., 2012).

Notably, none of these studies have observed an increase in unitary conductance over prolonged stimulation.

3.5. Pharmacology

In terms of pharmacology, P2X7R has several pharmacological features in common with the other P2X family members, as well as some particularities unique to this subtype.

3.5.1. Agonists

P2X7R is, as all members of the P2X family, activated by extracellular ATP. However, one of the defining features of P2X7 is that it requires particularly high concentrations of ATP for activation, in the mM range (Coddou et al., 2011b; Donnelly-Roberts et al., 2009; North, 2002). As such, the alternative ATP-derived agonist 2,3-O-(4-benzoylbenzoyl)-ATP (BzATP) is frequently used, as it allows activation of P2X7R in the low micromolar range. Although BzATP is often referred to as being “selective” for P2X7Rs, this is not actually the case, as BzATP is an agonist or partial agonist at a number of other P2X subtypes, and notably is most potent at P2X1R (Syed and Kennedy 2012). It is, however, P2X7R that exhibits the greatest difference between potency of ATP and its BzATP analogue. Other ATP analogues are also active at P2X7R: the thiol derivatives 2-meSATP and ATP γ S are partial agonists, whilst $\alpha\beta$ -MeATP and $\beta\gamma$ -MeATP are weak agonists (Coddou et al., 2011b; Donnelly-Roberts et al., 2009; Syed and Kennedy, 2012). The EC₅₀ values are highly dependent on the species in question, the facilitation state of the receptor, and the presence of modulators, such as divalent cations, but EC₅₀ values for ATP are approximately 2 – 4 mM, and for BzATP 10 μ M (Coddou et al., 2011b). Selected P2X7 ATP-analogue agonists are portrayed in Figure 25.

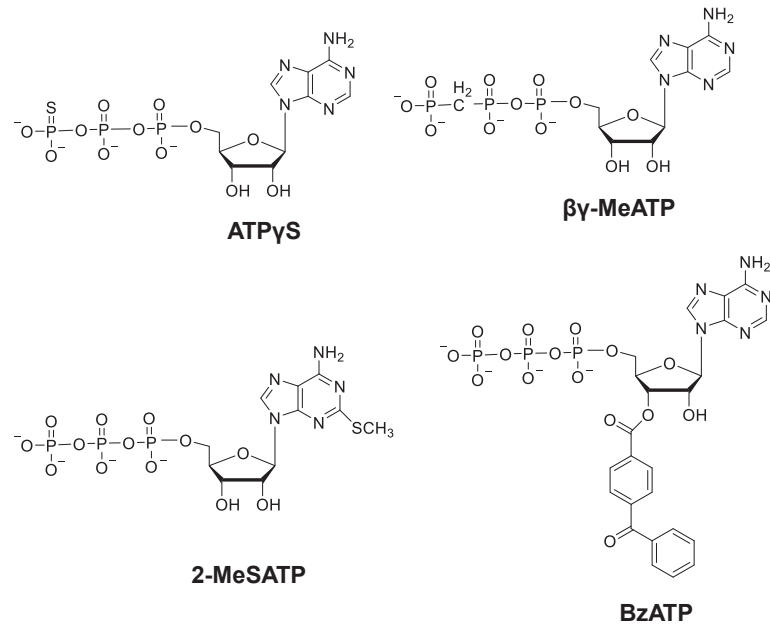


Figure 25. P2X7 agonists: ATP analogues.

Another interesting particularity of P2X7 is that it can also be activated by NAD⁺, a nucleotidic co-factor, *via* ADP-ribosylation. An ADP-ribose moiety is enzymatically transferred from NAD⁺ to R125, an arginine residue neighbouring the ATP-binding pocket. Long-lasting P2X7 activation results, although it remains unclear whether it is a direct agonistic action, or indeed whether it exerts a sensitising effect, rendering ATP a more efficient agonist (Di Virgilio et al., 2018a).

3.5.1.1. Non – nucleotide agonists

P2X7R is also interesting in that it can be activated by several non-nucleotide agonists. Although the precise molecular mechanisms of receptor activation by non-nucleotide agonists are not resolved, it is thought that these agents may in fact function by strongly sensitising the receptor to activation at ambient concentrations of ATP (Di Virgilio et al., 2017; Kanellopoulos and Delarasse, 2019). This is the case for the bactericidal peptide cathelicidin LL-37, which triggered Ca²⁺ influx and promoted ethidium dye uptake in P2X7-transfected HEK293 cells (Tomasinsig et al., 2008), and also for lipopolysaccharide (LPS), which acts from the cytosolic side. Another notable example is amyloid-β, which induces P2X7-dependent Ca²⁺ influx, ethidium dye uptake and cytotoxic markers in microglia cells (Sanz et al., 2009). However, in the absence of precise mechanistic details, it cannot be discounted that these agents act by provoking ATP release, which subsequently acts on the P2X7R.

3.5.2. Antagonists

In terms of antagonism, antagonists common to other P2X subtypes, such as suramin, PPADS and TNP-ATP are also active at P2X7R, albeit with lowered potency (Jarvis and Khakh, 2009). Brilliant Blue G inhibits P2X7Rs with a high degree of selectivity, and as such can be used as a distinguishing antagonist between P2X subtypes (Jiang et al., 2000). Calmidazolium has also been shown to act at P2X7R, in a reversible manner (Virginio et al., 1997) A covalent antagonist for P2X7 also exists, in the form of oxidised ATP (North and Jarvis, 2013).

Additionally, a number of synthetic antagonists have been produced, which exhibit high selectivity for P2X7, and as such have been employed in models of disease to probe their potential as therapeutic agents (Bartlett et al., 2014).

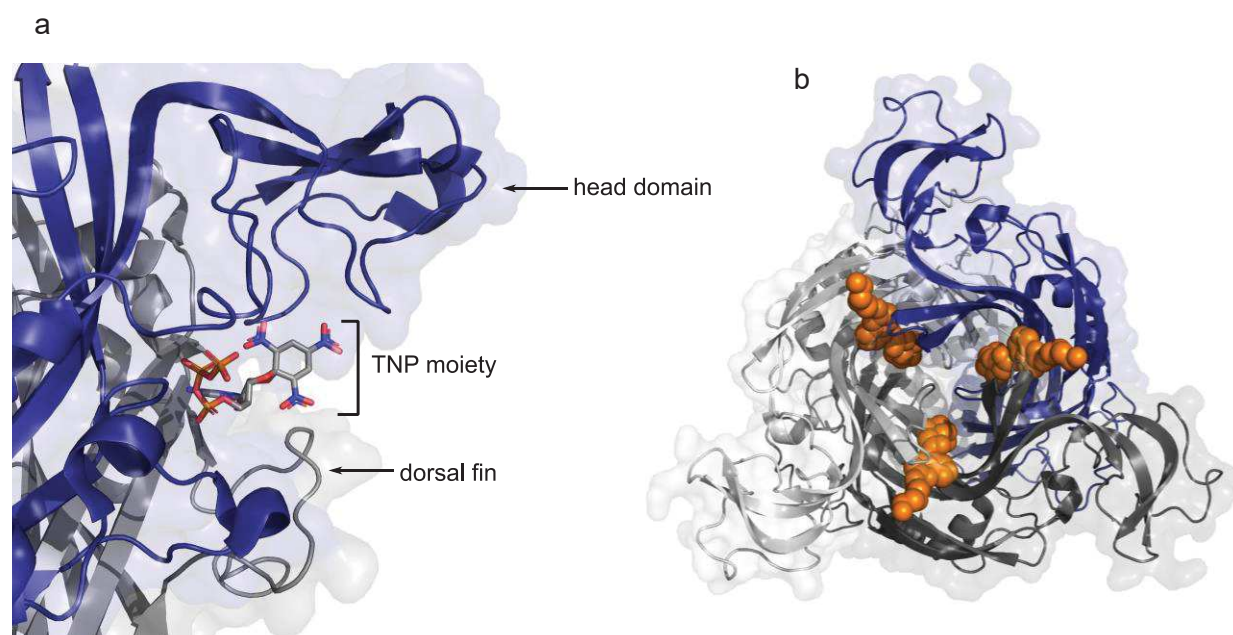


Figure 26. Non-competitive and competitive antagonists in complex with P2X7Rs.

(a) TNP-ATP in complex as a competitive antagonist with ckP2X7. The head domain and dorsal fin of adjacent subunits, which comprise the blocked binding jaw, are indicated. PDB: 5XW6 (b) Crystallographic structure of pdP2X7 in complex with non-competitive antagonist AZ10606120 (orange, sphere representation), bound in the P2X7-unique allosteric binding pocket. PDB: 5U1W.

For several synthetic antagonists, including AZ10606120, the resolution of non-competitive antagonist-bound pdP2X7 crystallographic structures allowed the identification of a novel antagonist binding site within the upper body domain, unique to P2X7R (Figure 26b). It was demonstrated that this cavity shrinks upon ATP-activation, and as such, presence of an antagonist blocked this movement, subsequently preventing channel opening (Karasawa and Kawate, 2016). Equally, crystallographic structures have also shed light on the molecular precisions regarding competitive antagonism at P2X7R, specifically, TNP-ATP, the structure of which was resolved in complex with chicken P2X7R (ckP2X7) (Figure 26a). This structure revealed that whilst TNP-ATP binds to the ATP binding pocket, it does so with an altered

conformation. This, and the added presence of the TNP moiety, means that the jaw binding mechanism required for channel opening following ATP binding is blocked and cannot take place, resulting in the formation of a liganded but closed channel state (Kasuya et al., 2017). A different binding conformation has been observed for TNP-ATP in complex with hP2X3, and it has been proposed that these differential conformations are at the origin of the vastly differing TNP-ATP potencies at these two variants (1000-fold greater potency hP2X3 compared to pdP2X7) (Pasqualetto et al., 2018).

It has been remarked that in several cases, antagonist efficacy is dependent on temperature, the bathing solution into which they are perfused, and the presence or not of supplementary proteins such as bovine serum albumin (Hibell et al., 2001).

3.5.3. Modulators

A number of modulators of P2X7 activity exist, which are summarised in Table 4. Of particular note are the divalent cations, which are often reduced in bathing solution for P2X7 electrophysiological studies, and cholesterol, which we will return to several times within this manuscript. It is also interesting to note the negative modulatory effect of extracellular Zn²⁺ and Cu²⁺, which, for other P2X family members, are positive allosteric modulators (Virginio et al., 1997).

	P2X1	P2X2	P2X3	P2X4	P2X5	P2X7
Agonists (EC₅₀ μM)						
ATP	0.07	1.2	0.5	10	10	100
2-meSATP	0.07	1.2	0.3	10	10	100
αβ-meATP	0.3	>300	0.8	>300	>300	>300
BzATP	0.003	0.75	0.08	7	>500	20
Antagonists (EC₅₀ μM)						
Suramin	1	10	3	>500	4	500
PPADS	1	1	1	>500	3	50
TNP-ATP	0.006	1	0.001	15	-	>30
IP ₅ I	0.003	>300	2.8	(+)	-	N.D
KN-62	-	-	-	-	-	0.3
Modulators (potentiation (+) or inhibition (-))						
Zn ²⁺	(-)	(+)	(+)	(+)	(+)	(-)
Cu ²⁺	N.D	(+)	N.D	(-)	N.D	(-)
Cd ²⁺	(-)	(+)	(-)	(+)	N.D	(-)
H ⁺	(-)	(+)	(-)	(-)	(-)	(-)
Ivermectin	N.D	none	none	(+)	N.D	(+)
Ethanol	N.D	(-)	(+)	(-)	N.D	N.D
Phosphoinositides	(+)	Desensitisation reduced	(+)	(+)	(+)	(+)

Table 4. Modulators of P2X7 activity.

A non-comprehensive list, according to chemical type. N.D = not described. Compiled from (Acuña-Castillo et al., 2007; Coddou et al., 2011b; Karasawa et al., 2017; Nakanishi et al., 2007; Norenberg et al. 2011; Robinson et al., 2014; Surprenant et al., 1996; Virginio et al., 1997)

3.5.4. Species differences

Although species differences with regard to P2X7 function do exist, such as the lower levels of dye uptake observed in hP2X7R as opposed to in rP2X7R (Rassendren et al., 1997) and various kinetic differences (Hibell et al., 2000), P2X7 function and the effects of P2X7 activation at a cellular level are largely retained between species. Some of the principal differences

between P2X7 orthologues is rather in their sensitivity to pharmacological agents, which can vary widely (Donnelly-Roberts et al., 2009; Rassendren et al., 1997; Surprenant et al., 1996).

3.6. Protein partners

P2X7 has been shown to have an extensive number of protein partners, interacting in both direct and non-direct manners, from both intra- and extracellular sides of the membrane (Kim et al., 2001; Kopp et al., 2019). In terms of direct interactions, over 50 partnerships have been reported, although the confirmation of such interactions in numerous independent studies and their physiological consequences remains poorly described (Kopp et al., 2019). The most interesting interactions in the context of this study are (i) those described between P2X7R and lipids and their metabolic enzymes and (ii) those described between P2X7R and other channels.

We have already seen that P2X7 has strong links with lipid components of the cell membrane, being partially located in lipid raft fractions, and its facilitation behaviour modulated by cholesterol (García-Marcos et al., 2006a; Gonnord et al., 2009; Robinson et al., 2014). The study of Karasawa *et al.* using reconstituted pdP2X7 constructs into proteoliposomes of varying composition has also demonstrated the strong dependence of P2X7R activity on lipidic composition, and in particular, a negative modulation of channel activity by cholesterol, thought to interact through the TM domains (Karasawa et al., 2017). In addition, links between P2X7 and several enzymes involved in lipid metabolism have been described: sphingomyelinase (Bianco et al., 2009), phospholipase D (Humphreys and Dubyak, 1996) and phospholipase A (Andrei et al., 2004; Costa-Junior et al., 2011; Garcia-Marcos et al., 2006) to name a few.

In addition to these lipid-based interactions, several examples exist of P2X7 interacting with other membrane-located channels, namely, Pannexin-1 and TMEM16F (also known as Anoctamin 6) (Iglesias et al., 2008; Ousingsawat et al., 2015; Pelegrin and Surprenant, 2006). These interactions will be evoked further within this manuscript.

It is also interesting to note that a number of studies, using co-immunoprecipitation experiments and Förster resonance energy transfer techniques (FRET), have determined a close physical and functional interaction between P2X4 and P2X7 (Guo et al., 2007; Pérez-Flores et al., 2015), although whether this is in the form of P2X4/7 remains debated (Nicke, 2008).

3.7. P2X7R variants

3.7.1. Splice variants

Alternative splicing is an important transcriptional mechanism, which, in modifying the structure of transcripts and thus the structure of the protein produced, vastly expands the repertoire of possible proteins from a relatively limited number of genes. A significant number of splice variants have been identified for P2X7, in both human (hP2X7) and rodent (mouse, mP2X7) orthologs.

Splice variant	Human	
	Structural	Functional
P2X7A	Full length form	
P2X7B	<ul style="list-style-type: none"> • ΔC232 	<ul style="list-style-type: none"> • No macropore activity • 5-fold lowered agonist sensitivity • Abundant in spleen, brain, lung tissue
P2X7C	<ul style="list-style-type: none"> • ΔC • Ext missing 	<ul style="list-style-type: none"> • ND
P2X7D	<ul style="list-style-type: none"> • ND 	<ul style="list-style-type: none"> • ND
P2X7E	<ul style="list-style-type: none"> • ΔC 	<ul style="list-style-type: none"> • ND
P2X7F	<ul style="list-style-type: none"> • Ext missing 	<ul style="list-style-type: none"> • ND
P2X7G	<ul style="list-style-type: none"> • ΔC • ΔTM1 	<ul style="list-style-type: none"> • Non functional
P2X7H	<ul style="list-style-type: none"> • ΔTM1 	<ul style="list-style-type: none"> • Non functional
P2X7I	<ul style="list-style-type: none"> • - 	<ul style="list-style-type: none"> • Null allele
P2X7J	<ul style="list-style-type: none"> • ΔC337 	<ul style="list-style-type: none"> • Non functional • Forms heteromers with P2X7A

Splice variant	Rodent	
	Structural	Functional
P2X7(a)	Dominant form	
P2X7(k)	<ul style="list-style-type: none"> • Alternative N-term • Alternative TM1 	<ul style="list-style-type: none"> • Increased macropore activity • Enhanced agonist sensitivity • Escapes knock-out in Glaxo^{-/-} mice • Sensitive to NAD partial agonism
P2X713b	<ul style="list-style-type: none"> • ΔC164 	<ul style="list-style-type: none"> • Reduced current amplitude • Dominant negative modulation when co-expressed with P2X7(a)
P2X713c	<ul style="list-style-type: none"> • ΔC175 	<ul style="list-style-type: none"> • Reduced current amplitude
P2X7 – v4	<ul style="list-style-type: none"> • ΔC-term • ΔTM2 • 153aa 	<ul style="list-style-type: none"> • Decreased macropore activity

Table 5. Summary of splice variants identified in human and rodent P2X7 genes.

Summary of the splice variants identified in P2X7 transcripts from (a) human and (b) rodent sources. ND = not described, Ext missing = part of the extracellular domain deleted. (Adinolfi et al., 2010; Cheewatrakoolpong et al., 2005; Feng et al., 2006; Kido et al., 2014; Masin et al., 2012; Nicke et al., 2009; Sluyter and Stokes, 2011; Xu et al., 2012)

Of these splice variants, P2X7B is particularly notable, as it had been determined as abundantly present in many tissues, in several cases in excess of the P2X7A variant (Cheewatrakoolpong et al., 2005). When expressed on its own in HEK293 cells, this variant causes an increase in intracellular ATP content, and stimulated cell growth, exhibiting basic channel activity but not macropore formation (Adinolfi et al., 2010). When co-expressed with P2X7A, heterotrimers were formed, exhibiting potentiated P2X7A-like characteristics. In rodents, the P2X7(k) variant is particularly expressed in the liver and in the spleen, and exhibits a heightened activity with respect to the P2X7(a) variant (Nicke et al., 2009).

3.7.2. Single Nucleotide Polymorphisms (SNPs)

In addition to the variation provided by alternative splicing, hP2X7 is highly polymorphic, with over 150 non-synonymous SNPs identified within the extracellular domain and the C-terminus (Di Virgilio et al., 2017). Selected SNPs have been functionally analysed, and the most common of those found in hP2X7R are presented in Figure 27.

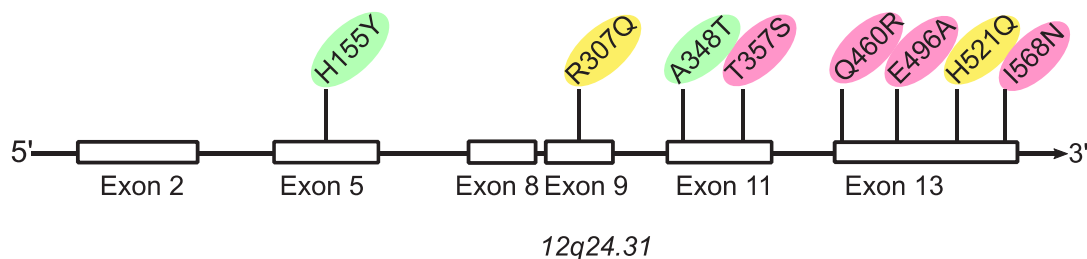


Figure 27. Coding exons of P2RX7.

Schematic representation of *P2RX7* gene, located on the 12q24.31 chromosome, with the approximate positions resulting in selected, common SNPs shown. Green indicates a gain-of-function mutation, yellow indicates neutral mutations and red indicates loss-of-function mutations.

H155Y and A348T mutations are particularly interesting to draw attention to, as these mutations correlate to the equivalent residues which are present in the rat ortholog (rP2X7), which exhibits a generally enhanced activity when compared to hP2X7. These two gain-of-function mutations, which affect the surface expression and single channel properties of the receptor, can therefore partially explain the difference in behaviour between these orthologs. In addition to functional aspects, many of these SNPs have been identified as being frequently present in pathological states, for example, affective disorders (H155Y, A348T, E496A, Q460R), post-mastectomy pain (H155Y, R270H), and osteoporosis (E496A, R307Q, I568N) to name a very select few (Roger et al., 2010; Soronen et al., 2011; Sun et al., 2013; Wiley et al., 2011).

Of note in rodent orthologs, is the mutant P451L, a mutation reducing the macropore formation of P2X7Rs, which is found naturally in C57BL/6 strain of mice, and is known to reduce pain

associated with mechanical allodynia (Adriouch et al., 2002; Sorge et al., 2012). Interestingly, the P2X7(k) splice variant was insensitive to this macropore-reducing mutation (Xu et al., 2012). The P2X7(a) variant, on the other hand, exhibited reduced macropore-associated dye uptake when carrying the P451L mutation (Xu et al., 2012).

A high degree of variation in structure and function of P2X7Rs is therefore present, in a cell-type and pathological state-dependent manner. The experiments described within this manuscript have been carried out using rP2X7(a), H155Y.

3.8. Physiological and pathophysiological roles

In this section we will briefly discuss the pleiotropic, and seemingly contradictory, roles of P2X7R in various systems, physiological and pathological.

3.8.1. P2X7 knock-out mouse models

Many of these roles have been deduced by the use of P2X7 knock-out mice, of which three different lines have been produced. The first of these was generated by GlaxoSmithKline, whereby the *P2RX7* gene is disrupted by insertion of a *lacZ* transgene into exon 1 (Sikora et al., 1999; Sim et al., 2004). This mouse line helped establish the role of P2X7R in inflammatory and neuropathic pain, amongst others (Chessell et al., 2005). However, this knockout line was found to express the P2X7(k) splice variant, which, by virtue of its alternate exon-1, escaped knock-out (Nicke et al., 2009).

A second knockout mouse line has been produced by Pfizer, whereby a portion of exon 13, encoding C506 to P532 (within the C-terminus) was replaced by a neomycin cassette (Solle et al., 2001). As seen previously with the Glaxo line, however, the presence of numerous splice variants renders this knockout inefficient with regard to those variants who exhibit a truncated C-terminus (Kaczmarek-Hájek et al., 2012; Masin et al., 2012). Indeed, several studies demonstrated the presence of a “P2X7-like” protein in this mouse line, by way of Western Blot and immunocytochemical assays (Marín-García et al., 2008; Sánchez-Nogueiro et al., 2005). Nevertheless, this knockout line has permitted to establish a role for P2X7 in cytokine production (Solle et al., 2001), bone formation (Ke et al., 2003), and the inflammatory response (Labasi et al., 2002).

Finally, an additional P2X7 knockout mouse line was established by Lexicon Genetics, by interference of exons 2 and 3 with a *lacZ* gene (Basso et al., 2009). This mouse line has allowed the elucidation of a role for P2X7 in affective disorders such as depression (Basso et al., 2009).

Whilst these knockout lines are highly valuable for delineating the role of P2X7 in pathological and physiological states, consideration must be given as to which isoforms of P2X7 are affected (or not) by knockout.

3.8.2. Physiological roles

3.8.2.1. Inflammation

The most well documented physiological role of P2X7R is as a key part of the inflammasome, specifically, the NLRP3 inflammasome, where it plays a central role in processing of IL-1 β . This process begins with two differing signals, firstly, the presence of pathogen associated molecular patterns (PAMPs), such as bacteria-derived lipopolysaccharides (LPS), activates toll-like receptor 4 (TLR4), which, *via* transcription factor NF- κ B, drives transcription of NLRP3 and pro-IL-1 β , the pre-cursor to pro-inflammatory cytokine interleukin 1- β . Meanwhile, the second signal takes place at P2X7Rs. Upon cell damage, eATP is present at high concentrations, sufficient to activate P2X7, therefore representing a damage associated molecular pattern (DAMP). Activation of P2X7R triggers the influx of Na⁺, Ca²⁺ and the efflux of K⁺ from the cell; it is this sharp decrease in potassium which triggers NLRP3 inflammasome activation. It has also been suggested that TWIK2 channels may contribute to this K⁺ efflux (Di et al., 2018; Kanellopoulos and Delarasse, 2019). The consequences of NLRP3 activation, is subsequent activation of caspase-1, the enzyme which cleaves pro-IL-1 β to mature IL-1 β , which is then released *via* secretory and exocytotic pathways. Recently, it has also been shown that caspase-1 cleaves Gasdermin D, a cytosolic protein, the N-terminus of which is then able to oligomerise, forming a pore in the cell membrane, ultimately leading to pyroptotic cell death (Ding et al., 2016). Several further roles of P2X7R in the inflammasome have also been suggested to occur *via* direct interaction: it has been reported that P2X7 may interact directly with NLRP3, following the observations of co-immunoprecipitation and co-localisation in mouse microglia and mouse peritoneal macrophages (Franceschini et al., 2015). In addition, P2X7R has been observed to be directly linked to NF- κ B activation, the first of the inflammatory response signals discussed above, likely through a direct, C-terminal interaction with myeloid differentiation primary response 88 (MyD88) (Liu et al., 2011).

There are several interesting points to note with regard to molecular characteristics of P2X7R function which become pertinent in an inflammatory context. Firstly, the ability of the P2X7 macropore to allow efflux of ATP has been demonstrated, raising the possibility that this represents an auto-amplification mechanism, which would reinforce and propagate the inflammatory effects of P2X7R to neighbouring cells (Pellegatti et al., 2005).

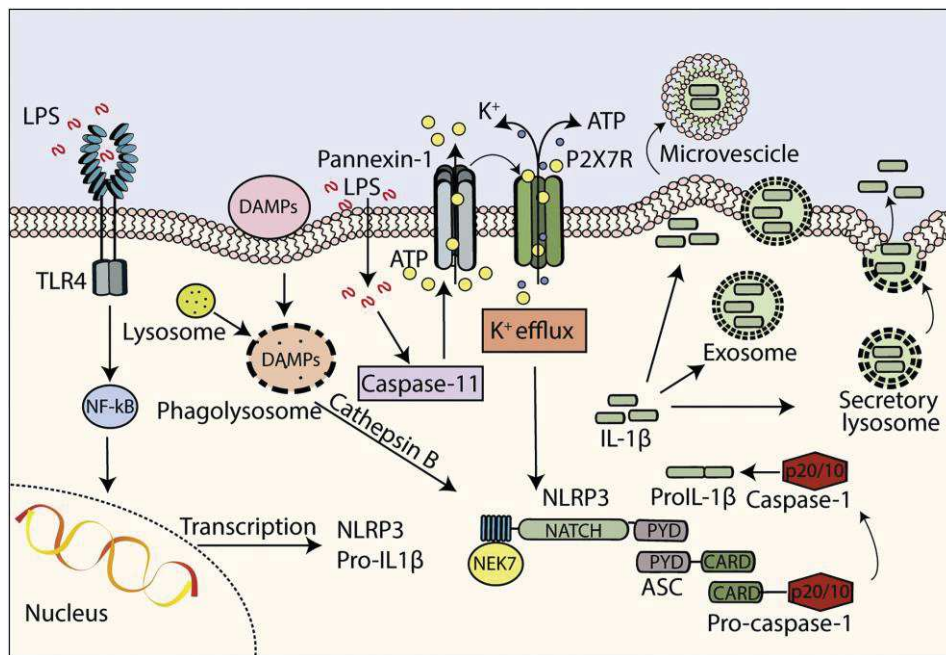


Figure 28. P2X7R in the NLRP3 inflammasome.
Schematic representation of the key steps within the NLRP3 inflammasome, involving P2X7. Taken from (Di Virgilio et al., 2017).

In mouse models, the sensitivity of P2X7R to NAD^+ may also represent an interesting molecular characteristic with implications for inflammation. In T cells, NAD^+ was shown to activate P2X7Rs by ADP ribosylation, at a position within the ATP-binding pocket, R125 (Adriouch et al., 2008; Seman et al., 2003). Increased NAD^+ levels have been shown at inflammatory sites, and in mouse T lymphocytes, NAD^+ activates P2X7R at micromolar concentrations, thus rendering P2X7R more sensitive to activation (Adriouch et al., 2007). Interestingly, the P2X7(k) variant, which was shown to be the most sensitive to ADP-ribosylation, is preferentially expressed in T lymphocytes (Rissiek et al., 2015). Equally, in mouse bone marrow-derived macrophages, LPS has been shown to sensitise P2X7R to ATP to the extent that pore formation is observed with concentrations of ATP in the nM range (Yang et al., 2015). This modulation is presumably *via* the putative LPS binding motif present in the C-terminus of P2X7R (Kopp et al., 2019). This PAMP therefore may also influence the P2X7-dependent component of the inflammation response, in addition to that of TLR4.

Inflammation is therefore a prime example of how molecular determinants of P2X7 behaviour influence its role within a physiological cellular network.

3.8.2.2. Cell life: proliferation

Contrary to its reputation as a cytolytic agent of cell death, P2X7R exhibits polar opposite behaviours, and in several contexts has a trophic effect, contributing to “cell life”, proliferation mechanisms.

This was first observed in human lymphoid cells, whereby basal stimulation of P2X7 was determined to enhance cell proliferation and allow growth in serum-free medium (Baricordi et

al., 1999, Baricordi et al. 1996), and has also been observed to induce proliferation in microglia (Monif et al., 2009). In HEK293 cells stably transfected with hP2X7R, tonic ATP-stimulation of P2X7Rs was shown to increase the mitochondrial potential, $\Delta\psi$, to increase the mitochondrial Ca^{2+} concentration and to stimulate ATP synthesis. This increase in cellular energy stores acts to confer a growth advantage to cells, which were shown to grow in serum-free medium. Conversely, if maximally stimulated with ATP, P2X7R caused a Ca^{2+} mitochondrial overload, dysfunction of the mitochondrial network and subsequent apoptosis. There exists, therefore, a subtle balance controlling the direction of P2X7R activity either towards “life” or “death” responses in the context of cellular energy metabolism, which is outlined in Figure 29. Further studies showed that this promotion of cell growth involves Nuclear Factor Of Activated T Cells 1 (NFATc1), and that P2X7B isoform, which does not exhibit the macropore-related cell death mechanisms, also exhibits this cell growth activity. This led to the interesting hypothesis that the cell-specific expression levels of P2X7A and P2X7B splice variants, which can also assemble to form heteromers, determine a dominant “cell life” or “cell death” activity of P2X7R (Adinolfi et al., 2010).

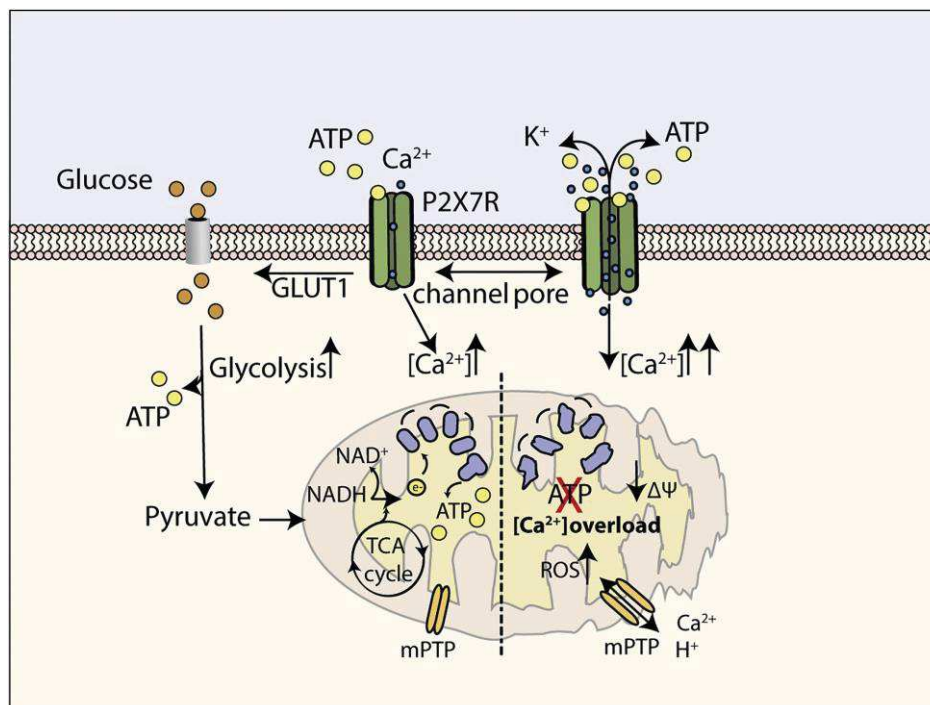


Figure 29. Implication of P2X7R in cellular energy metabolism mechanisms.

Basal activation of P2X7R increases mitochondrial potential and Ca^{2+} content, encouraging ATP synthesis and cell growth mechanisms. Sustained activation of P2X7R induces a mitochondrial Ca^{2+} overload, leading to mitochondrial breakdown and apoptosis. Taken from (Di Virgilio et al., 2017).

3.8.3. Cell death: apoptosis and necrosis

One of the primary characteristics of P2X7Rs is as the “cell death” receptor, and its role in the onset of apoptosis and necrosis has been known for a long period of time (Di Virgilio et al., 1998). The apoptotic pathway is the result of the inflammatory response (detailed in section 3.8.2.1), but the necrosis pathway remains poorly defined. In mouse thymocytes and

embryonic neuron progenitor cells (NPCs), Ca^{2+} independent pathways have been linked to P2X7R-induced necrosis, in the former case by sequential activation of factors leading to activation of the proteasome, and in the latter case, by mitochondrial membrane depolarisation (Kanellopoulos and Delarasse 2019).

3.8.4. Pathological roles

The implication of P2X7R in pathological states is astonishingly wide-ranging, with roles in many different classes of disease having been demonstrated in a vast number of studies. This includes neurodegenerative disorders (Alzheimer's, amyotrophic lateral sclerosis (ALS)), psychiatric disorders (schizophrenia, depression, mood disorders), coronary heart disease, lung disorders (asthma, chronic pulmonary obstruction, emphysema), inflammatory bowel diseases (Crohn's and ulcerative colitis), inflammatory skin disorders (dermatitis, psoriasis), musculoskeletal diseases (Duchenne muscular dystrophy, osteoporosis), as well as a number of cancers (Bhattacharya and Biber 2016; Burnstock and Knight, 2018; Geraghty et al., 2016; Neves et al., 2014; Woods et al., 2016). This list names just a select few of the pathologies in which P2X7R has been shown to have an implication; the therapeutic potential of this receptor becomes, therefore, very clear.

3.8.4.1. Neuropathic and inflammatory pain

Whilst P2X4R is well known for its role in neuropathic pain *via* the BDNF pathway, P2X7 has also been shown to be implicated in neuropathic and chronic inflammatory pain in a multitude of studies (Chessell et al., 2005; Grace et al., 2018; He et al., 2012; Honore et al., 2006; McGaraughty et al., 2007), in many cases as a result of its IL-1 β promoting behaviour (Donnelly-Roberts and Jarvis, 2007; Ferrari et al., 2006). One study, looking at various SNPs, has also functionally linked the pore forming ability of P2X7R to symptoms of mechanic allodynia and chronic inflammation in mouse and human models, finding that in women experiencing pain following mastectomy surgery (post mastectomy pain, PMP), those possessing alleles corresponding to hypofunctional SNPs of P2X7R (such as Y155H or R270H) reported less intense pain than those possessing the hyperfunctional equivalents. (Sorge et al., 2012).

3.8.4.2. Alzheimer's disease

Alzheimer's disease (AD) is a neurodegenerative disorder, characterised by the accumulation of extracellular amyloid- β peptides (A β), creating lesions, accompanied by a neuroinflammatory response (Querfurth and LaFerla, 2010). This disease is fatal, and symptoms include a progressive degradation of cognitive function and memory loss (Heppner

et al., 2015). Over the age of 85, there is a one in three chance of an AD diagnosis (Querfurth and LaFerla, 2010).

A role for P2X7 in AD has already been strongly suggested, by the observation that P2X7R expression is upregulated in mouse models of AD (McLarnon et al., 2006; Parvathenani et al., 2003). It has also been shown that in microglia, A β -triggered release of IL-1 β involves P2X7 (Rampe et al., 2004; Sanz et al., 2009).

Recently, a new role for P2X7 in AD has been established in the Delarasse group, who published a study using the Pfizer P2X knockout within an A β lesion-developing AD mouse model (Martin et al., 2019). This study demonstrated that the P2X7 knockout mice displayed less cognitive impairment, synapse dysfunction and memory loss compared to the wild type mice. These effects, however, were not produced by P2X7-mediated microglial activation and IL-1 β processing, but rather, by P2X7-modulated release of chemokines. The authors propose a coherent model whereby accumulation of A β peptides induces ATP release from glial cells, activating P2X7R, which leads to chemokine release from microglia and astrocytes (namely, CCL3, CCL4 and CCL5), which in turn causes damage to neurites, altered neuronal functions, and the recruitment of pathogenic T-cells (Martin et al., 2019).

3.9. Therapeutic outlook

At the time of writing, there are 10 studies listed on ClinicalTrials.gov (NIH) involving P2X7-targeted treatments, for conditions ranging from osteoporosis to major depressive disorder, as well as investigating the use of P2X7 as an accurate and effective biomarker for uterine cancer. However, thus far, therapeutic treatments targeting P2X7 with synthetic antagonists have proved to be rather disappointing. Di Virgilio *et al* postulate that this may be due to the fact that many of these antagonists are non-competitive, allosteric negative modulators, whose action may not be extreme enough at sites of inflammation, where ATP is present in extremely high concentration (Di Virgilio et al., 2017). Biological agents, such as the recently developed antibody BSCT, targeting a non-functional P2X7 (nfP2X7) involved in basal cell carcinoma, or nanobodies, small single-domain antibody fragments such as the P2X7-directed Dano1, which has been shown to prevent IL-1 β release in endotoxin-treated blood, may represent a more pertinent therapeutic avenue to explore. (Danquah et al., 2016; Koch-Nolte et al., 2019)

GENERAL THESIS OBJECTIVES

Within this introduction, we have seen that P2X7R is a highly complex and most interesting target of study, prone to display multifaceted responses to stimuli according to the conditions in which it is found; some of these responses are understood, and some not (yet). Endowed with the ability to enhance cell growth, or indeed to provoke cell death, P2X7 is a “Dr. Jekyll and Mr. Hyde” type character who exhibits several seemingly contradictory behaviours, none more so than this fine balance between cell life/death.

The objectives of this PhD focus on the elucidation of molecular-level P2X7 structural and functional details. Although widely studied in the literature, P2X7 remains one of the P2X family members with whom we are least familiar in terms of precise functional mechanisms. For this reason, I have undertaken three principal projects during this PhD, each of which is designed to explore the structure, function or indeed the structure/function relationships of P2X7 receptors, using different techniques and experimental approaches. A chapter is dedicated to each of these projects: chapter one focuses on the study of P2X7 from a structural biology viewpoint, chapter two will explore the use of optogenetics-based techniques to study P2X7Rs and finally, chapter three will investigate the molecular mechanisms behind P2X7 facilitation by way of single channel recordings, as well as probing the existence of a multi-protein complex mediating P2X7 activity, in particular, macropore formation.

CHAPTER ONE: TOWARDS A STRUCTURE OF P2X7 BY SINGLE PARTICLE CRYO ELECTRONMICROSCOPY

INTRODUCTION

In the study of biological systems, knowledge of the three-dimensional structures of the various actors involved in these systems is an important step in elucidating their inner workings. Structural determination of biological macromolecules in their many dynamic conformations gives us key insights into the molecular mechanisms by which they function and interact, and the combination of such structural data with other functional approaches represents a powerful means of achieving a comprehensive understanding of biological processes. Since the seminal works of Kendrew and Perutz, whose X-ray crystallographic resolution of the structures of myoglobin (Kendrew et al., 1958) and haemoglobin (Perutz et al., 1960), respectively, earned them the 1962 Nobel prize, the structural determination of complex proteins has grown in an exponential manner. Technological advances have aided this growth, and today a variety of structural determination techniques are available, X-Ray crystallography, cryo electronmicroscopy (cryoEM) and nuclear magnetic resonance spectroscopy (NMR) being amongst the most prominent, which cater for a variety of biological targets.

One group of biological targets for which structural determination presents a particular challenge is that of membrane proteins, including ion channels. Membrane proteins represent 20–30% of the proteomes of most organisms (Krogh et al., 2001); in the case of the human proteome this figure is estimated to be 27% (Almén et al., 2009). And yet, these numbers are not reflected in terms of structures deposited in the PDB. This is largely the result of difficulties experienced in the extraction and isolation of membrane proteins, which arise from their unique cellular environment. Embedded in a hydrophobic lipid membrane, but often featuring hydrophilic domains which reach out into intra- or extracellular space, the dual polarity of these proteins requires the use of detergents in order to maintain a stable structure. This can be challenging to achieve. In addition, their hydrophobic nature also means that membrane proteins are particularly prone to aggregation during the preparative process.

The preparation of protein samples for structural analysis requires a number of steps, and obtaining samples of high quality and in sufficient quantity frequently represents the bottleneck in the structural determination process. A combination of production, purification, reconstitution and structural determination approaches suited to each membrane protein target must be carefully selected, often by a “trial and error” approach. The overriding goal throughout the global structural determination processes, is for each step to be optimised in order to obtain

protein samples which are adequate for structural determination, whilst retaining to the fullest extent possible their native properties, in order to ensure that the resulting structures are of physiological relevance. Here will be briefly discussed the principal options in each step of structural determination for eukaryotic membrane proteins, specifically ion channels expressed at the cell surface membrane. A general workflow of the structural determination process is shown in Figure 30.

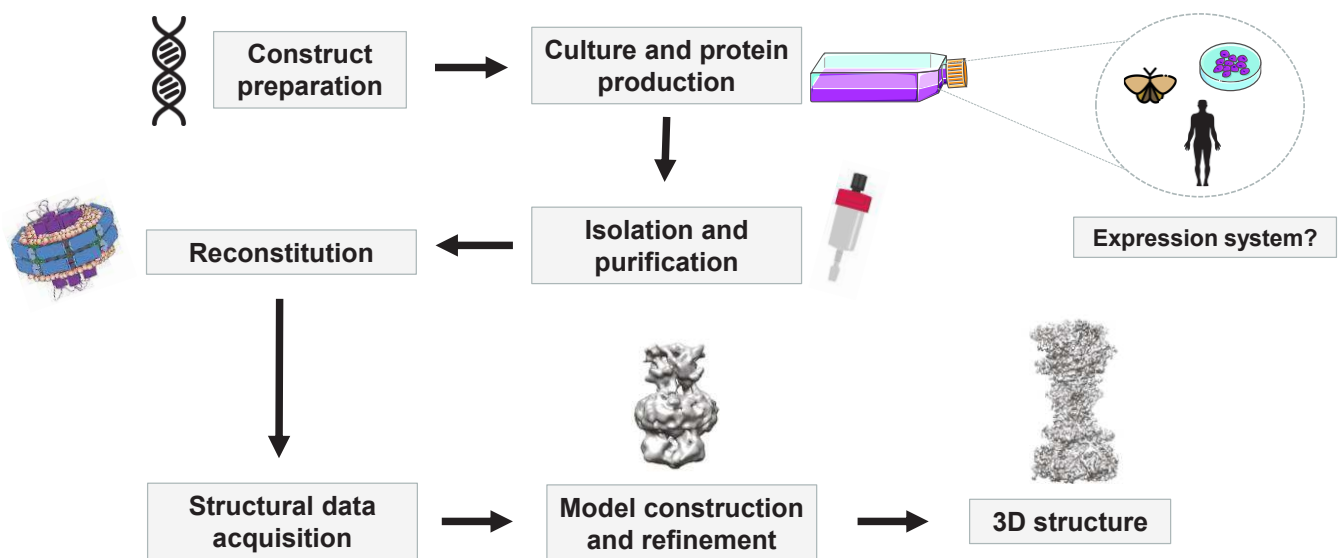


Figure 30. Overview of the principal steps of protein structure determination.

Images taken from Servier, PNG repo, GE Healthcare and McCarthy *et al.* (McCarthy *et al.*, 2019)

1. Methods of membrane protein production

Although some eukaryotic membrane protein structures have been solved using protein extracted from native tissues (e.g. Rhodopsin, (Palczewski *et al.*, 2000); ATP-synthase (Stock *et al.*, 1999), nicotinic acetylcholine receptor (O'Brien *et al.*, 1979), for the vast majority, recombinant expression in heterologous systems is a pre-requisite for obtaining the quantities required for structural studies.

The expression of membrane proteins *in vivo* is a highly complex process, requiring the synchronised orchestration of a number of cellular machineries: protein biosynthesis, processing of folding mechanisms, post translational modifications (PTM), trafficking and targeting to the cell membrane. The nature of each of these steps must be considered when choosing an appropriate host system to express the desired protein in its fully functional form, as well as the robustness of the system itself to withstand any perturbations which may originate from recombinant protein overexpression. In general, eukaryotic membrane proteins are more suited to eukaryotic expression systems (Tate, 2001). Three principal host systems of this type exist; yeast systems, insect cell systems and mammalian cell systems.

1.1. **Recombinant expression in yeast host system: *Pichia pastoris***

A number of yeast species can be used as recombinant expression systems. Of particular note for membrane proteins is *Pichia pastoris*. The *P. pastoris* system, a methylotrophic yeast, presents a number of advantages, namely “the handling simplicity of a unicellular microbe and the cellular sophistication of a eukaryotic organism”, as according to Bornert *et al.* (Bornert *et al.*, 2002). Rapid growth on inexpensive media renders this expression system cost-effective and relatively easy to establish. Stable expression of the target protein is achieved by integration of a *P. pastoris* vector, containing the desired protein gene, into the host genome. Of particular advantage is the nature of the AOX1 promotor utilised in this system, a strong, tightly regulated promotor induced by methanol (>1000 fold) and repressed by glucose or glycerol (Cereghino *et al.*, 2002). This promotor can therefore be used to generate an abundant expression of recombinant protein, whilst also allowing fine-tuning of expression levels, an advantage in the case of overexpression toxicity to the host organism. The yeast system lends itself to scale-up for protein production in bioreactors, where precise control over factors influential in protein expression (pH, temperature, aeration levels) is possible. This can achieve extremely high cell densities, up to 500 OD₆₀₀ units/mL (Cereghino *et al.*, 2002).

As a eukaryotic organism, *P. pastoris* possesses the necessary cellular machinery to carry out PTMs typically found in membrane proteins, such as phosphorylation, disulphide bridge formation, prenylation, and amino- and carboxy-terminal methylation to name a selection (Junge *et al.*, 2008). Whilst O- and N-glycosylation, a particularly important criteria for the folding and functional expression of membrane proteins (Imperiali and O’Connor, 1999), is possible in *P. pastoris*, it has been shown that the complex carbohydrate decoration found in higher eukaryotic organisms is absent from this system (Cereghino *et al.*, 2002). To combat this, genetically modified strains of *P. pastoris* capable of such complex modifications have been developed to produce “humanized” glycoproteins (Hamilton and Gerngross, 2007).

A further characteristic to take into account is the lipidic composition of the yeast membrane. In *P. pastoris*, the lipidic membrane composition varies significantly with respect to higher eukaryotic organisms, which can pose problem for the proper functioning of mammalian protein targets (Opekarová and Tanner, 2003). Of note is the low abundance of sterols, and absence of cholesterol, which is replaced by ergosterol in yeasts (Grillitsch *et al.*, 2014). Again, this problem may be circumvented by using genetically engineered *P. pastoris* strains capable of producing cholesterol to be employed for expression of mammalian sterol-sensitive proteins (Hirz *et al.*, 2013).

A final advantage of the yeast system is the ability to carry out functionality tests of heterologously expressed membrane proteins. This includes ligand binding assays, and of

particular pertinence to our field of interest, patch clamp electrophysiology studies have been carried out in *S. cerevisiae* yeast protoplasts expressing the plant potassium channel KAT1 (Bertl et al., 1995).

1.2. **Recombinant expression in insect cell systems: *Spodoptera frugiperda***

A second, commonly utilised expression system for eukaryotic membrane proteins is the insect cell/baculovirus system. A number of insect species may be used, but commonly encountered are Sf21 and their derivative Sf9 cells, originating from the fall army worm, *Spodoptera frugiperda*. This system takes advantage of the pathogenic insect-specific baculovirus, able to utilise the machinery of the host cell to produce a desired protein target. In brief, recombinant bacmid DNA containing the desired gene is transfected into insect cells, leading to the re-wiring of host gene expression to produce recombinant baculovirus particles. These virus particles are then used in insect cell infection, resulting in an expression of recombinant protein which can be harvested. Although several commercial systems exist to facilitate this preparation, it remains a lengthy, multi-step process, requiring expensive culture medium and fine-tuning of parameters such as cell density upon infection, and infectious viral titer for efficient protein production.

Nevertheless, the insect cell/baculovirus system is widely used due to a number of advantageous characteristics. Baculovirus DNA typically features strong polyhedrin or p10 promoters (Junge et al., 2008), well adapted for protein overexpression, and able to accommodate large recombinant inserts. Regarding PTMs, *S. frugiperda* cell lines possess the necessary machinery required for complex PTMs found in mammalian cell lines, such as palmitoylation, phosphorylation, acylation, amidation and O-glycosylation (Contreras-Gómez et al., 2014) (Junge et al., 2008). However, N-glycosylation, whilst possible in insect cells, does not offer the complexity present in their mammalian counterparts, resulting in recombinant proteins with non-native glycosylation patterns. As seen in yeast systems, genetic engineering has made possible insect cell lines which are capable of providing more authentic, mammalian-like N-glycosylation pathways in an attempt to overcome this drawback (Aumiller et al., 2012; Hollister and Jarvis, 2001)

With respect to the lipidic membrane composition, insect cell lines contain little cholesterol, and in general a small proportion of sterols compared to phospholipids (0.04), over 20 times lower than that found in higher eukaryotes (Gimpl et al., 1995; Opekarová and Tanner, 2003). There do exist, however, examples whereby addition of cholesterol contained within a methyl- β -cyclodextrin complex (MCD) to Sf9 culture medium has allowed the restoration of protein function otherwise absent in unmodified Sf9 membranes, presenting a potential solution to this issue (Gimpl et al., 1995).

For ion channels, insect cells also present the opportunity to assess channel functionality by patch clamp electrophysiology, in both whole cell and single channel configurations. A number of examples exist in the literature of such functionality tests for a variety of channels (Brock et al., 2001; Kunze et al., 1997; Phelps et al., 2010).

For eukaryotic membrane protein production, despite its high cost, the insect cell/baculovirus system remains widespread, and has previously been used to produce a variety of ion channel targets, amongst them P2X receptors (Hattori and Gouaux, 2012; Karasawa and Kawate, 2016; Kawate et al., 2009; Mansoor et al., 2016), ASIC (Gonzales et al., 2009; Jasti et al., 2007) and GluA2 receptor (Sobolevsky et al., 2009).

1.3. **Recombinant expression in mammalian cell systems**

The most effective expression systems for mammalian membrane proteins in terms of proximity to their native environments, are mammalian systems. Human embryonic kidney (HEK) and Chinese hamster ovary (CHO) cell lines in suspension cultures are the most widely used. These mammalian systems are able to provide all necessary PTMs and an authentic lipid environment, increasing the chances of producing a properly folded, fully functioning membrane protein. For application of this system to ion channels, HEK cells are offer a particularly attractive option, as they are routinely used for electrophysiological analysis, in whole cell and single channel configurations, in addition to other useful functional assays (Thomas and Smart, 2005).

Expression of recombinant proteins in mammalian cell lines is typically achieved by transfection. This can be done in either a transient or stable manner; transient transfection offers flexibility but variable expression rates, whereas stable transfection, although less flexible and more time consuming, can provide consistent, high expression rates, and is more suited to large scale protein production (Makrides, 1999; Pandey et al., 2016). Transient gene expression can also be achieved by infection with recombinant viruses, and recent development of the BacMam system, applying baculovirus technology to mammalian cell lines, provides the advantages of flexibility, reproducibility and high expression levels of the target protein in a mammalian host (Dukkipati et al., 2008).

The major drawbacks of mammalian systems are the high cost of culture medium and relatively slow growth rates. Nevertheless, a number of examples exist of structural determination of membrane proteins produced in recombinant mammalian systems, including the rat P2X7 receptor (Gruswitz et al., 2010; McCarthy et al., 2019; Penmatsa et al., 2013; Standfuss et al., 2007; Yoder and Gouaux, 2018)

2. Extraction, reconstitution and purification of membrane proteins

Once a satisfactory expression of the target membrane protein is achieved, extraction of this protein from the host membrane, purification and reconstitution into a form suitable for the desired structural determination technique must be carried out.

The precise pathway from extraction to reconstitution is highly dependent on i) the structural determination technique to be employed; NMR, single particle cryo electron microscopy (cryo-EM) and X-ray crystallography require vastly different protein reconstitutions, and ii) the membrane protein target and its biochemical behaviour.

2.1. Advance construct design

Prior to recombinant expression of a membrane protein by one of the systems discussed above, consideration of the eventual purification and reconstitution steps must be taken, in order to design a construct optimally adapted to the global structural determination strategy. Common protein modifications to facilitate structural determination are the use of fusion tags, point mutations to reduce heterogeneous PTMs and the truncation of constructs to reduce flexibility and disorder.

2.1.1. Use of fusion tags

The introduction of fusion tags to membrane protein targets is common practice. Affinity tags are usually fused to the protein of interest in order to aid subsequent purification steps and a number of such affinity tags are available, the most frequently used being the polyhistidine tag.

Fusion tags may also be introduced in the interest of high throughput screening, to assess expression levels, homogeneity and oligomerisation state of the membrane protein prior to structural determination. An example of this is the use of GFP for Fluorescence-Detected Size Exclusion Chromatography (FSEC), developed in the Gouaux group (Kawate and Gouaux, 2006).

An important consideration, particularly in the case of a construct where multiple tags may have been added, is the impact of these tags on the structure and function of the membrane protein. Although several factors can be optimised in an attempt to limit this impact, such as the length of the linker, and the position of N- or C-terminal, fusion tags remain a non-native addition with no physiological relevance. For this reason, tags are often cleaved following purification, which can be achieved by the introduction of a protease cleavage site within the linker (e.g. thrombin or TEV) (Pandey et al., 2016). In the absence of tag cleavage, functional studies should be carried out on these tagged constructs in order to assess their similarity to the native protein.

2.1.2. **Modifications of target protein**

A number of further modifications may be carried out to produce constructs adapted for reconstitution. These genetically introduced modifications are particularly widespread in crystallographic studies, in an attempt to facilitate crystallogenesis.

Glycosylation introduces a high degree of heterogeneity to membrane protein structures, due to the addition of long, flexible sugars at glycosylation sites. This heterogeneity poses problem for crystallogenesis, and as such, residues involved in N- and O-glycosylation are often replaced by point mutations, to an isosteric equivalent unable to participate in the glycosylation process.

Truncation at the C- and/or N-terminus of membrane proteins is also commonplace for X-ray crystallographic studies, as these domains are often highly flexible and disordered, thus preventing the formation of ordered crystal arrays (Stroud, 2011).

Evidently, serious caveats exist with regard to these modifications, given the role of glycosylation in processes such as expression, folding and trafficking, and the contribution of the C- and N-termini to protein conformation and function.

2.2. **Extraction and reconstitution of membrane proteins**

The extraction of membrane proteins and their reconstitution into a suitable form, maintaining native structure and function, is often considered the most challenging step of the structural determination process. The correct conditions are frequently determined by many rounds of trial and error, during a long period of optimisation.

Membrane proteins, embedded in their lipid bilayer, require the use of detergents for extraction and solubilisation. Of amphiphilic nature, detergents integrate the lipid bilayer, surrounding the transmembrane portions of the protein to form a hydrophobic “belt”, whilst ensuring aqueous solubility by their polar head groups. This results in the formation of a ternary complex: the membrane protein, a number of membrane-originating lipids and detergent (Figure 31).

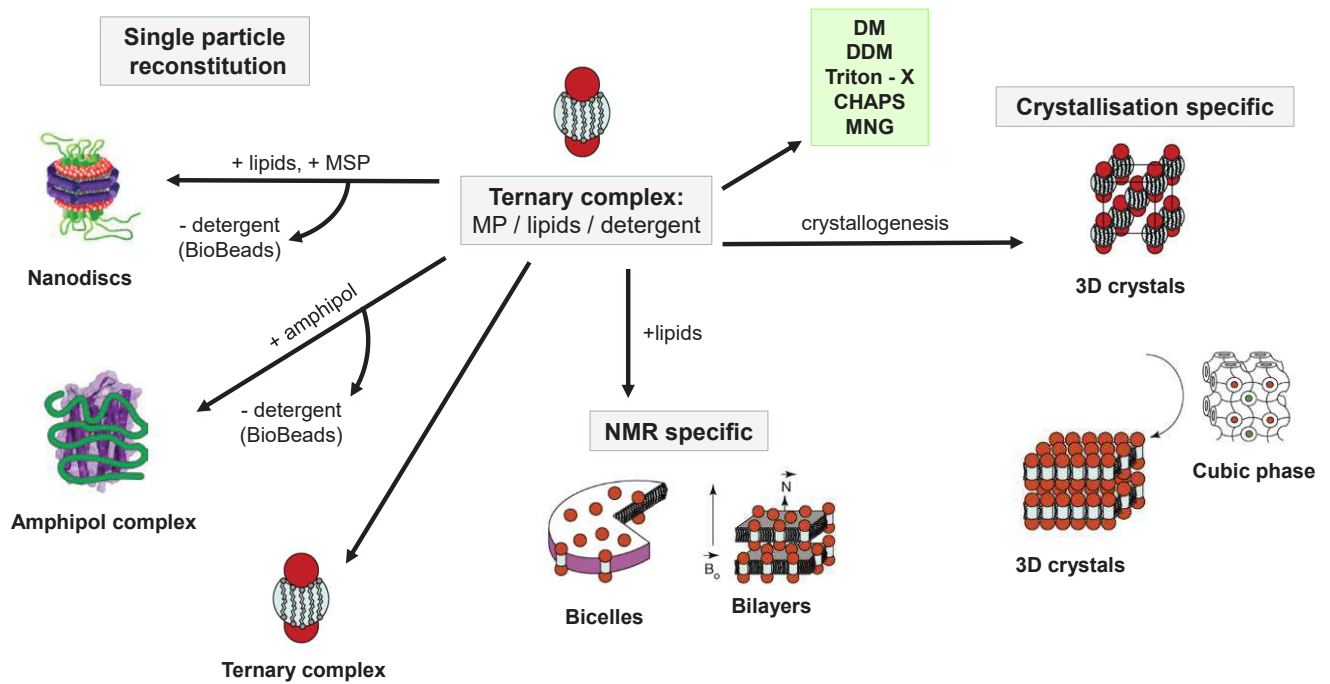


Figure 31. Non-exhaustive presentation of common reconstitution methods for structural determination.

From the common starting point of ternary lipid/membrane protein (MP)/detergent complexes, different strategies can be adopted. Some are technique-specific (crystallisation and NMR). Nanodiscs and amphipols may be used for single particle cryo-EM studies and NMR, whereas certain ternary MP/lipid/detergent complexes may be employed for single particle cryo-EM. A select few detergents often used in membrane protein solubilisation are noted (green box). Adapted from Lacapère *et al.*, Leitz *et al.*, and Mineev and Nadezhdin (Lacapère *et al.*, 2007; Leitz *et al.*, 2006; Mineev and Nadezhdin, 2016)

Whilst indispensable for handling membrane proteins, detergents must be chosen and used with care. The physicochemical properties of the detergent (charge, critical micelle concentration, three-dimensional form) are important parameters, and different membrane protein targets will require different combinations of these properties for successful solubilisation. If an unsuitable detergent is chosen, or indeed an unsuitable concentration is used, inefficient solubilisation will result from either i) aggregation of unprotected transmembrane domains or ii) dissociation of essential lipid molecules which may have implications for the protein structure.

This initial ternary complex is a common starting point from which the preparation of the sample in a technique-specific manner may be carried out. For crystallography, an ordered 3D crystal lattice is a strict requirement. Classic vapour diffusion methods can be used, or alternatively, the lipid cubic phase presents the opportunity for crystallisation in a more native-like lipid environment (Zha and Li, 2018). Reconstitution into single particle forms is principally used for cryo-EM studies, or in some instances NMR. Two particularly interesting possibilities are reconstitution into nanodiscs, or amphipols, both of which rely on the exchange of detergent molecules for more native-like components.

2.2.1. Nanodiscs

First developed by the Sligar group, nanodiscs are unique structures providing the possibility of precisely controlled, monodisperse reconstitution of membrane proteins into native-like lipid environments. These discs are formed by the spontaneous complexation of α -helical membrane spanning proteins (MSPs, derived from apolipoprotein A-1), which encapsulates an interior comprising lipids, designed to mimic the native phospholipid bilayer, and the membrane protein of interest (Denisov et al., 2004) (see Figure 31 for schematic representation). Precise control over the size, lipid content and homogeneity of samples can be achieved, and sterols such as cholesterol may also be incorporated. Many examples of nanodisc-encapsulated membrane protein structures exist, amongst them a number of ion channels, including TRPV1 (Autzen et al., 2018; Gao et al., 2016; Sierra-Valdez et al., 2018). Literature examples also exist of nanodiscs which retain native mammalian lipids, although these have not yet been used for structural purposes (Mak et al., 2017).

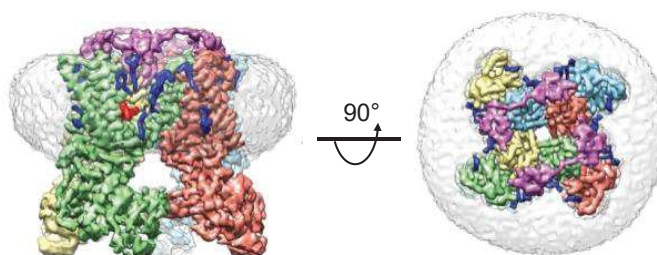


Figure 32. Three dimensional reconstructions of a TRPV1 channel nanodisc complex.

TRPV1 heteromers are visible in colour and electron density corresponding to the surrounding nanodisc is shown in grey. Taken from (Gao et al., 2016).

2.2.2. Amphipols

Amphipols are a relatively newly developed class of amphipathic polymers which are able to replace detergent molecules, and provide an environment better suited for retaining protein functionality, whilst ensuring good solubility of the protein complex (Popot et al., 2003). Amphipols have been shown to be effective for a number of ion channel examples (Baker et al., 2015; Huynh et al., 2014).

2.3. Purification of membrane proteins

Several methods of membrane protein purification exist, and purification steps may be carried out both prior to and following reconstitution. The most frequently encountered of these methods is purification by the use of affinity tags. Although several such affinity tags exist, the dominating method for membrane proteins is the polyhistidine tag. Comprising six or eight histidine residues, this tag gives the possibility of purification by immobilised metal affinity

chromatography (IMAC) (Young et al., 2012). IMAC works on the premise that histidine residues are tightly bound by resins containing metal ions such as Ni^{2+} and Co^{2+} , *via* co-ordination between the metal ion centre and a lone pair centred on a histidine nitrogen. Polyhis-tagged proteins can thus be retained, either on column or in batch, separated from unwanted contaminants, and eluted by competition with imidazole. TALON®, a novel Co^{2+} resin whose key feature is a strictly homogeneous co-ordination geometry, exhibits higher specificity than Ni^{2+} resins when binding to polyhis tags, thus reducing non-specific histidine binding and resulting in a more effective purification (Bornert et al., 2002). As such, it has become the resin of choice for IMAC purifications.

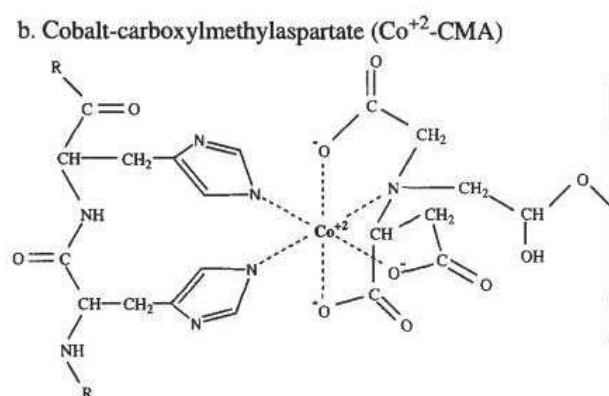


Figure 33. Co-ordination of histidine residues by a Co^{2+} -carboxymethylaspartate (CMA) resin.

Co-ordination of nitrogen lone pairs on histidine residues to Co^{2+} , which is held in an octahedral geometry within a CMA resin. These types of Co^{2+} exhibit high specificity and preferential binding to polyhistidine tags rather than non-specific adjacent histidine residues present in contaminating proteins. Figure from (Bornhorst and Falke, 2000).

A second purification technique commonly encountered in membrane protein sample preparation is Size Exclusion Chromatography (SEC). This method utilises a porous resin-packed column, which allows the separation of entities according to their hydrodynamic radius; small entities become trapped within pores, whilst larger entities are unretained and thus pass rapidly through the column. SEC is frequently used to assess the dispersity and oligomerisation state of membrane proteins once solubilised and reconstructed, in order to obtain monodisperse samples in the desired oligomeric state. In the case of reconstitution into, for example, nanodiscs, empty species can also be separated from protein-containing entities using SEC.

The chosen purification technique(s) must be compatible with the extraction method, and types of detergent used. A combination of several techniques is often required to obtain samples of sufficient purity for subsequent structural determination.

3. Structural determination of membrane proteins: principal methods

3.1. NMR spectroscopy

Application of multidimensional NMR spectroscopy, either in solution or solid state configuration, is a structural determination method which has been previously employed for a number of membrane protein targets (Hiller et al., 2008; Park et al., 2012; Teriete et al., 2007).

Analysis of a number of parameters (chemical shift, couplings, residual dipole couplings and nuclear overhauser effects) can offer information not only on the polypeptidic sequence, but also the nature of its three-dimensional organisation; torsion angles, interatomic distances and information on hydrogen bonding. A three-dimensional model can then be constructed, in compliance with these structural constraints.

One of the primary advantages of NMR study is that it is able to provide dynamic information, on conformational changes and ligand binding, all within a hydrated, lipid bilayer, mimicking the physiological environment of a membrane protein (Opella and Marassi, 2017). Reconstruction into micelles, bicelles and nanodiscs is possible for NMR studies (Liang and Tamm, 2016). However, structural determination by NMR is usually reserved for smaller proteins, with an upper limit of approximately 40 kDa (Kaptein and Wagner, 2015). This is due to the complex spectra resulting from large structures, which require extensive isotopic labelling strategies. This smaller size limit, however, represents a niche for structures which are commonly inaccessible *via* single particle cryo-EM and crystallography.

3.2. X-ray crystallography

X-ray crystallography has traditionally been the method of choice for protein structure determination, allowing an atomic level resolution when at its most effective. Using ordered three-dimensional crystal arrays of the protein of interest, incident X-rays are diffracted to produce an electron density map, from which a three-dimensional structure can be reconstructed. A wealth of protein structures have been resolved by X-ray crystallography, and it remains the most frequently employed technique for membrane proteins (Birch et al., 2018).

However, it is reliant on the production of high quality, ordered crystals for optimal diffraction, and crystallogenesis is frequently the bottleneck of this process, particularly for membrane proteins where finding the correct crystallisation conditions is usually considered an empirical procedure (McPherson and Gavira, 2013). A number of inherent disadvantages come with the use of crystals for structural determination. For one, these ordered arrays of protein molecules represent a sole protein conformation; dynamic information is lost, as is conformational variety, as samples are required to be as homogeneous as possible. Moreover, the crystal lattice environment in which the protein resides is far removed from its physiological surroundings, a

factor which may have implications for the conformation adopted by the protein. In addition to this, the formation of crystals is usually dependent on the use of detergents, which, again, have a limited similarity to the native membrane environment, although crystallisation techniques such as the lipidic cubic phase method present a solution to this (Zha and Li, 2018). Finally, as discussed in section 2.1.2, serious questions can be raised by the use of protein constructs heavily modified to give homogeneous samples for crystallogenesi – to what extent do these modifications alter the conformation adopted by the protein, and induce artefactual features?

3.3. **Single particle cryo-EM**

A complementary technique to X-ray crystallography is that of single particle cryo-EM, which has been steadily increasing in use thanks to the huge transformations it has undergone in recent years. Single molecules of the protein target are plunge frozen in liquid ethane to produce a thin layer of vitreous ice, in which these protein molecules are trapped in a number of random orientations. Two-dimensional projection images are produced by electron microscopy, and then grouped together to form clusters of particles in the same orientation, and averaged. These class averages are then used to construct a three-dimensional model of the target protein.

This variant of cryo-EM presents a number of advantages over crystallography, in that no crystals are required, and it is much less reliant on sample homogeneity; if a number of conformations are present, these can be identified and separated into different clusters. This characteristic also presents the attractive possibility of extracting dynamic information from samples regarding conformational changes (Fernandez-Leiro and Scheres, 2016). Cryo-EM is also compatible with reconstitution techniques such as nanodiscs and amphipols, providing a more native-like environment in which the protein is imaged. However, the technique suffers from poor signal:noise ratio, especially when detergents are employed. This produces a size limitation, whereby proteins of small molecular weight are very difficult to image. The smallest protein to date to be imaged by cryo-EM is haemoglobin (64 kDa) at a resolution of 3.2 Å.

Several recent technological advances have extended the possibilities of this technique, rendering it now equivalent to crystallography. Direct electron detectors have increased the sensitivity of data acquisition, and beam-induced motion, which previously caused blurry images, is now correctable thanks to newly developed tools. (Bai et al., 2015; Cheng, 2015; Murata and Wolf, 2018). In addition, recently developed powerful algorithms facilitate the image processing steps, making it possible to distinguish single particles with even minor conformational differences. These advances are at the origin of the cryo-EM revolution, which

is now seeing structures emerge at resolutions to rival crystallography. A number of ion channel examples exist at varying resolutions, amongst them TRPV1, Piezo 1, 5-HT_{3A} and P2X7 (Basak et al., 2018; Gao et al., 2016; Guo and MacKinnon, 2017; McCarthy et al., 2019).

3.4. Comparative analysis of the different methods

	X-ray crystallography	Cryo-EM	NMR
Quantity of protein	Several mg	<1 mg	Several mg
Crystals required?	Yes	No	No
Reconstitution	Detergents	Detergents, nanodiscs, amphipols possible	Detergents, nanodiscs, bicelles, bilayers possible
Size limitation	None	>100 kDa	<40 kDa
Resolution possible	Atomic	Near-atomic	NR

Table 6. Comparative table of the three major protein structural determination techniques.
NR = not relevant.

3.5. Global considerations

The key consideration to be kept in mind throughout the structural determination process is whether the chosen methodology is appropriate for gaining a structural insight into the protein in its physiological state. If the sample is prepared in such a way as to adopt a non-native conformation or present artefactual features, the resulting structure will be of limited physiological relevance. Ideally, conditions would be kept as close to those found physiologically, and tests showing that functionality remains closely comparable to that of the wild type are generally a good indicator of native-like structures. Equally, these three-dimensional structures should be interpreted in a critical manner, and as such they are often interpreted in combination with molecular modelling and biochemical experiments, which offer the opportunity for structural refinement.

4. Structural studies of P2X receptors

In the specific case of P2X receptors, a number of structures have been resolved over the past decade. These structures and the key insights they have provided are discussed below.

4.1. Structures obtained by X-ray crystallography

4.1.1. zfP2X4 *apo* resting state structure (2009)

The first insight into P2X receptor structure was provided in 2009, by the Gouaux group, who resolved the structure of zebrafish P2X4 (zfP2X4) in the *apo*, resting state (Kawate et al., 2009). This landmark structure allowed the confirmation of the global receptor architecture, as well as its trimeric organisation. Secondary structure motifs of the monomer were resolved, delineating a number of subdomains, the organisation of which can be compared to a leaping dolphin (Figure 34).

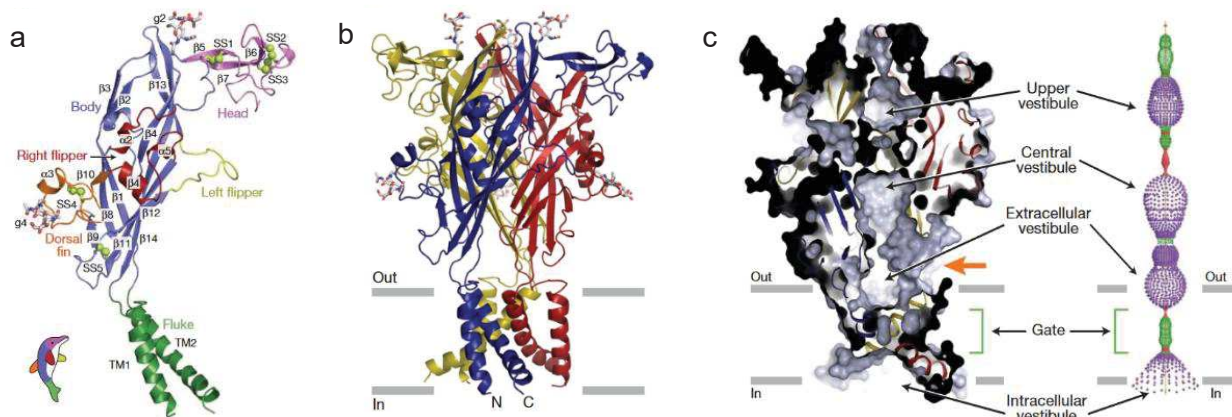


Figure 34. Structures of zfP2X4 solved by X-ray crystallography

(a) Structure of an individual zfP2X4 monomer unit in cartoon form next to a schematic leaping dolphin representation. (b) Structure of the trimeric form of zfP2X4 in the *apo* resting state (c) cross section of zfP2X4 trimer surface, next to a visual representation of pore lining surface calculations portraying the vestibule regions. The orange arrow indicates the lateral fenestration ion permeation pathway.

This structure also provided information on possible ion permeation pathways, identifying lateral fenestrations through which ion flow may be directed, as opposed to a simple model of ions entering from upper extracellular regions and flowing vertically down the long of the axis of symmetry.

Construct: $\Delta N27 \Delta C8$, point mutations N78K/N187R/C51F to eliminate two glycosylation sites and one disulphide bridge forming cysteine residue.

Reconstitution: detergent solubilised (DDM)

Functional properties: reduced expression levels, reduced peak current amplitudes, modified EC_{50} values.

Resolution: 3.1 Å

4.1.2. **zfP2X4 apo and ATP-bound open state structures (2012)**

Three years later, the Gouaux group resolved further structures of zfP2X4, this time at higher resolution, and in the ATP-bound open state as well as the *apo* resting state (Hattori and Gouaux, 2012). The resolution of ATP nestled in its interfacial binding site revealed that it adopts an unusual U-shaped conformation and confirmed precise interactions between key residues, many of which had been previously identified by mutagenesis scanning studies (Chataigneau et al., 2013). Comparison of these resting and open state structures also allowed a first insight into motions involved in gating on the molecular level; tightening of the ATP-binding jaw, flexing of the body β -sheets and an “iris-like” outwards rotation of the transmembrane domains to produce an open channel state.

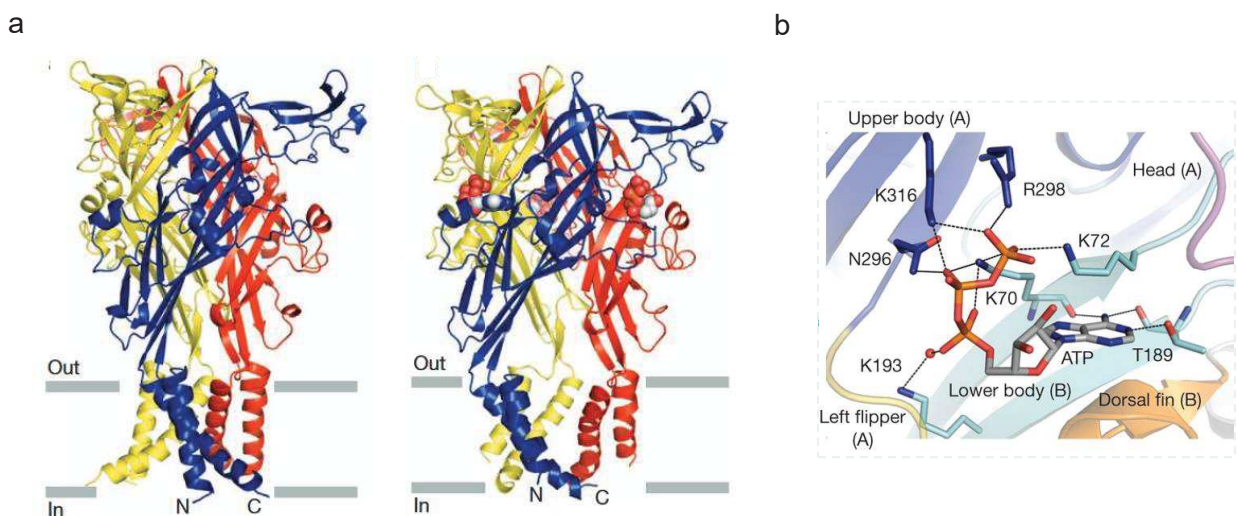


Figure 35. Crystallographic structures of zfP2X4

(a) Trimeric structures of zfP2X4 in the *apo* and ATP-bound states. (b) ATP-binding site with interacting residues labelled.

Construct: Δ N27/ Δ C24, point mutations N78K/N187R to eliminate two glycosylation sites.

Reconstitution: detergent solubilised (DDM)

Functional properties: ATP binding, similar gating properties (according to two electrode voltage clamp experiments)

Resolution: 2.8 – 2.9 Å

4.1.3. **amP2X**

The first structure of an invertebrate P2X receptor, amP2X of the Gulf Coast tick *Amblyomma maculatum* was determined in 2016 (Kasuya et al., 2016). Key structural details regarding two

divalent metal binding sites in the extracellular domains were revealed: site M1, a Zn^{2+} potentiation site, and M2, an Mg^{2+} site coupled with the ATP binding pocket which may contribute to regulation of ATP binding.

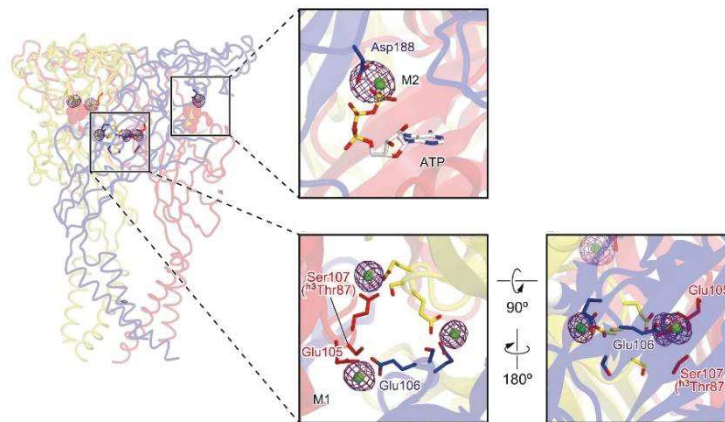


Figure 36. Crystallographic structure of amP2X highlighting M1 and M2 divalent metal binding sites. Divalent metal ion binding sites are shown in enlarged form, M2 site upper panel and M1 site lower panels. From (Kasuya et al., 2016).

Construct: $\Delta N23/\Delta C7$, point mutations N171K/C374L to eliminate one putative glycosylation site and one putative non-specific disulphide bridge forming site.

Reconstitution: detergent solubilised (DDM)

Functional properties: normal expression, gating properties not conserved

Resolution: 2.8 Å

4.1.4. hP2X3

The resolution of human P2X3 receptor (hP2X3R) in 2016, again by the Gouaux group, revealed for the first time the existence of the cytoplasmic cap, a structural motif in the intracellular domain serving to stabilise the open state. In addition to the structures of *apo*, open and competitive agonist-bound states, this work offered the first insight into the structure of the desensitised state (Mansoor et al., 2016).

Several differences present between hP2X3 and zfP2X4 were revealed, the most interesting of which being an unexpected transition of secondary structure in the TM2 domain, from an α -helix to a 3_{10} helix around the residues G333-V334-G335, producing an elongation of 4.4 Å. This reverts to its original α -helical form upon desensitisation. This structure has therefore provided the first glimpses into molecular motions involved in desensitisation.

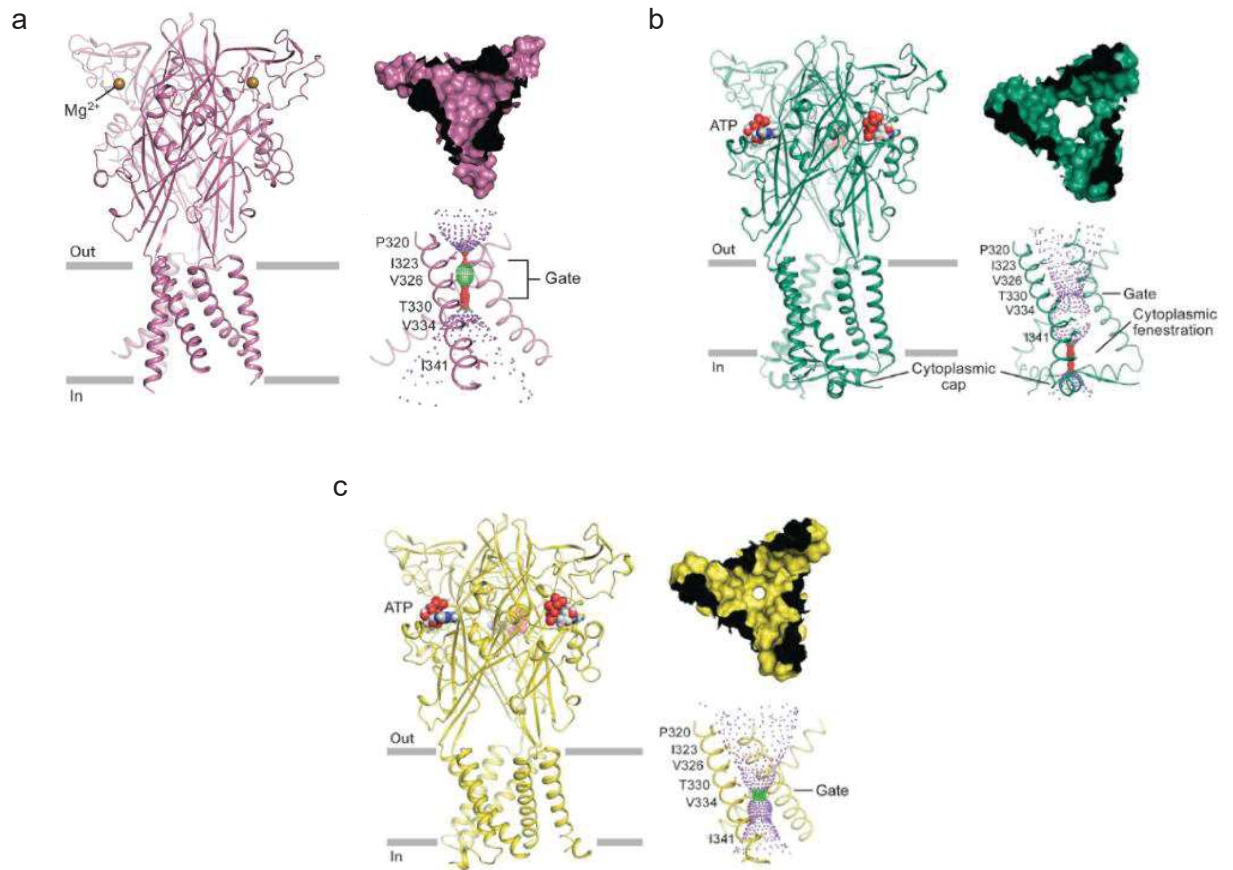


Figure 37. Structures of the (a) apo, (b) ATP-bound open and (c) ATP-bound desensitised states of hP2X3 receptor.

Construct: $\Delta N5 \Delta C33$, point mutations T13P/S15V/V16I to induce a slow desensitisation behaviour, used to resolve the open state structure.

Reconstitution: detergent solubilised (DDM)

Functional properties: wild type gating and ATP-affinity retained

Resolution: 2.77 – 2.98 Å

4.1.5. pdP2X7

The first example of a P2X7 subtype structure to be resolved was the structure of panda P2X7 receptor (pdP2X7) in the *apo* state as well as in complex with a number of antagonists. This structural work enabled the identification of an allosteric drug binding pocket and a potential corresponding mechanism of drug action at this site (Karasawa and Kawate, 2016).

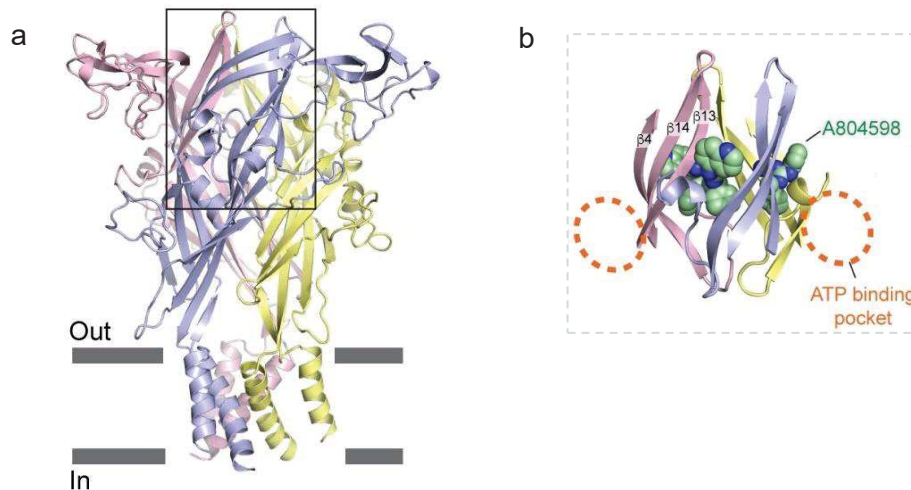


Figure 38. Crystallographic structures of pdP2X7

(a) Structure of pdP2X7 in the *apo* state with the allosteric site outlined in black. (b) Close-up image of the antagonist A804598 (shown as spheres) lodged in this allosteric binding site.

Construct: Δ N21 Δ C240, point mutations N241S/N284S/V35A/R125A/E174K to eliminate glycosylation sites and improve crystallisation behaviour.

Reconstitution: detergent solubilised (DDM)

Functional properties: reduced currents, modified EC_{50} , facilitation abolished

Resolution: 3.2 – 3.9 Å

4.1.6. ckP2X7

In quick succession, the structure of chicken P2X7 (ckP2X7) in complex with its competitive antagonist, TNP-ATP (Kasuya et al., 2017) was also resolved by X-ray crystallography. This structure allowed an insight into the mechanism of this antagonism, notably that the antagonist acts as a “wedge”, thus preventing complete activation of the receptor following ATP-binding. It should be noted, however, that the construct employed is electrophysiologically inactive.

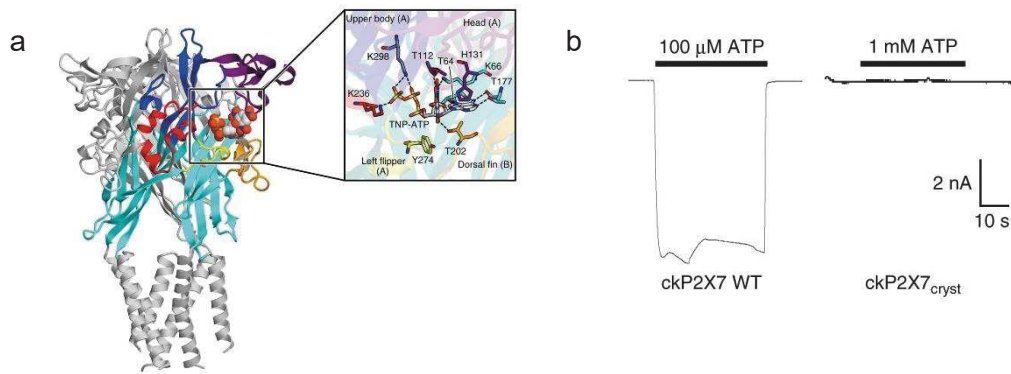


Figure 39. Structural studies of ckP2X7 in complex with TNP-ATP

(a) Crystallographic structure of ckP2X7 complexed with TNP-ATP (b) Whole cell electrophysiological recordings of WT ckP2X7 and the construct used in crystallographic studies.

Construct: $\Delta N27 \Delta C214$, point mutation N190 to eliminate a glycosylation point (replacement residue unspecified).

Reconstitution: detergent solubilised (DDM)

Functional properties: TNP-ATP binding retained; gating activity abolished

Resolution: 3.1 Å

4.2. Limitations of the crystallographic structures

The resolution of these P2X receptor structures are undoubtedly major breakthroughs, contributing to important advances in the field by providing insights into the molecular mechanisms behind P2X receptor activity. In addition, they have provided the structural basis for a wealth of biochemical and electrophysiological studies.

There remain, however, limitations to their use, largely based on the number of modifications that have been carried out to enable crystallogenes. A pertinent example of this is the presence of large crevices in the transmembrane region of the ATP-bound open zfP2X4 structure. Located within the phospholipid bilayer, these crevices are surprising as they would indicate a lack of intersubunit interactions, an unstable and thus unlikely scenario. Moreover, molecular dynamic simulations have shown that lipids would be able to diffuse *via* these crevices into the ion permeation pathway, an event incompatible with ion conduction in the open state (Heymann et al., 2013). Experimental approaches, one of which was carried out in our laboratory, have indicated that the intersubunit distances in the open state are in fact significantly smaller than observed in the crystallographic structure (Habermacher et al., 2016; Heymann et al., 2013). The fidelity of these crystallographic structures to the native receptor in its physiological state cannot, therefore, necessarily be considered as absolute.

For these reasons, and given the advantages outlined in section 3.3, the technique of cryo-EM may present a more judicious choice for P2X structure resolution.

4.3. Structures obtained by cryo-EM

Indeed, very recently, the first P2X structure by cryo-EM has been resolved, specifically that of rat P2X7 (rP2X7).

4.3.1. rP2X7

This structure is a landmark advance in P2X research, revealing for the first time the structural organisation of the enigmatic P2X7 C-terminus, comprising the cysteine rich region C-cys and the underlying Ballast, and demonstrating how palmitoylation of the C-cys region is at the origin of the non-desensitising behaviour of P2X7. This structure also showed the presence of several other unexpected interacting species; two cytoplasmic Zn^{2+} binding sites, a cytoplasmic GDP pocket, and a lipid binding site in the transmembrane region.

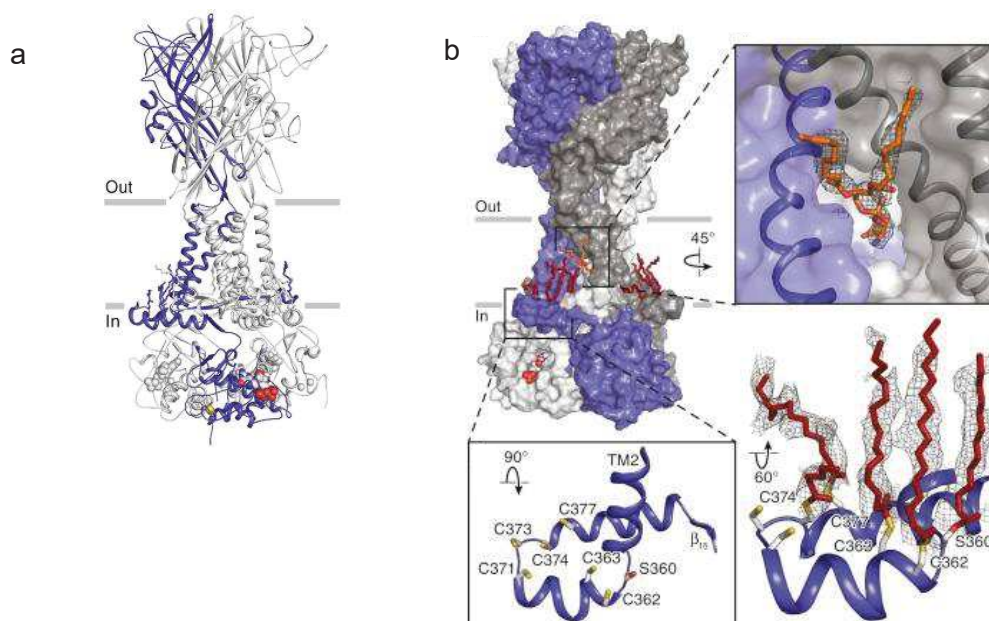


Figure 40. Cryo-EM structures of full length rP2X7

(a) Structure of trimeric rP2X7 shown in cartoon form, with GDP and Zn^{2+} visible in spherical representation. (b) Structure of trimeric rP2X7 shown as a surface representation, with the lipid binding site (upper insert) and the palmitoylated C-cys region (lower insert) in detail. (McCarthy et al., 2019)

Construct: full length, wild type

Reconstitution: detergent solubilised (DDM/cholseteryl hemmisuccinate)

Functional properties: wild type

Resolution: 2.9 – 3.3 Å

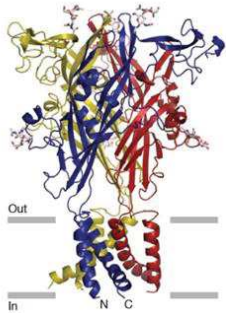
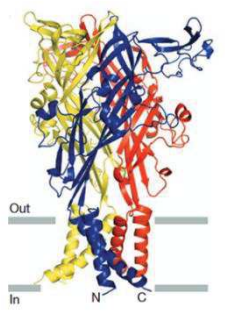
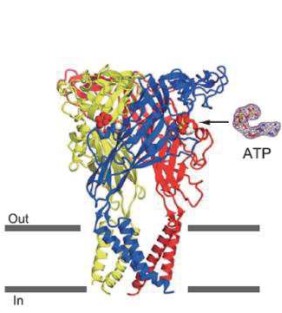
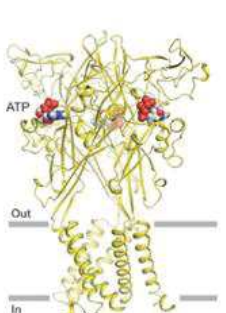
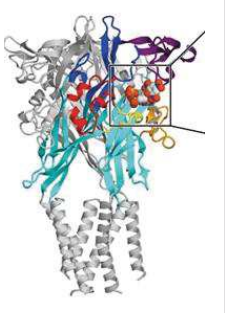
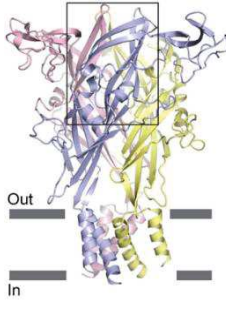
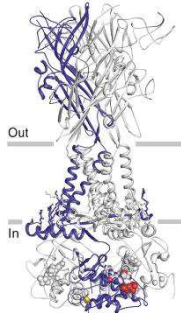
	zfP2X4 apo	zfP2X4 apo and ATP-bound	ampP2X	hP2X3	ckP2X7	pdP2X7	rP2X7
							
Construct	Δ N27 Δ C8 N78K/N187R/C51F to eliminate two glycosylation sites and one disulphide bridge forming cysteine residue.	Δ N27/ Δ C24 N78K/N187R to eliminate two glycosylation sites.	Δ N23/ Δ C7 N171QK/C374L to eliminate one putative glycosylation site and one putative non-specific disulphide bridge forming site.	Δ N5 Δ C33 T13P/S15V/V16I to induce a slow desensitisation behaviour, for open state structure resolution	Δ N27 Δ C214 N190 to eliminate a glycosylation site (replacement residue unspecified).	Δ N21 Δ C240 N241S/N284S/V35A/R125A/E174K to eliminate glycosylation sites and improve crystallisation behaviour.	Full length, wild type.
Expression	Sf9	Sf9	HEK293	HEK293	HEK293	Sf9	HEK293
Reconstitution	Detergent (DDM)	Detergent (DDM)	Detergent (DDM)	Detergent (DDM)	Detergent (DDM)	Detergent (Triton-X)	Detergent (DDM)/cholesteryl hemisuccinate tris
Functionality	<ul style="list-style-type: none"> Reduced expression levels Reduced peak current amplitudes Modified EC50 values. 	<ul style="list-style-type: none"> Similar gating properties to wild type ATP binding retained 	<ul style="list-style-type: none"> ATP binding retained Gating activity abolished 	<ul style="list-style-type: none"> Wild type gating retained ATP-affinity retained 	<ul style="list-style-type: none"> TNP-ATP binding retained Gating activity abolished 	<ul style="list-style-type: none"> Reduced currents Modified EC50 Facilitation abolished 	<ul style="list-style-type: none"> Wild type
Resolution (Å)	3.1	2.8–2.9	2.8	2.77–2.98	3.1	3.2–3.9	2.9–3.3
Key structural details	Confirmation of global architecture and precise identification of structural features	First resolution of the open state structure, identification of the ATP binding site.	Identification of two extracellular divalent metal binding sites	Identification of the cytoplasmic cap motif, resolution of the desensitised state, identification of an antagonist binding site	Resolution of antagonist TNP-ATP in its binding site	Identification of an allosteric drug binding pocket	First resolution of cytoplasmic domains, identification of the Ballast and C-cys anchor structural motifs

Table 7 Recapitulative table of all resolved P2X receptor structures.

(Hattori and Gouaux, 2012; Karasawa and Kawate, 2016; Kasuya et al., 2017, 2016; Kawate et al., 2009; Mansoor et al., 2016; McCarthy et al., 2019)

OBJECTIVES AND STRATEGY

1. Objectives

At the beginning of this project, the only P2X receptor structures available were those of truncated zfP2X4. No structure of P2X7 had been resolved, and the technique of cryo-EM had yet to be employed for P2X receptors. The initial objective was, therefore, to work towards the resolution of the full-length structure of human P2X7 (hP2X7) using the technique of cryo-EM. Given the implication of P2X7 in numerous human pathologies, the human orthologue was chosen for this project, in the knowledge that a structure of hP2X7 would be of particular value for exploitation in therapeutic research. We also aimed to use a reconstitution technique which would allow us to mimic the native membrane environment as much as possible: nanodiscs.

2. General strategy

The long-term strategy for this project comprises several steps:

- (i) **Construct generation:** addition of an octahistidine (8His) affinity tag to the N-terminus of hP2X7 in preparation for downstream purification, connected by a covalent, flexible linker sequence. If this 8His tag proves to be an effective means of purification, the linker sequence may be replaced by a cleavable sequence.

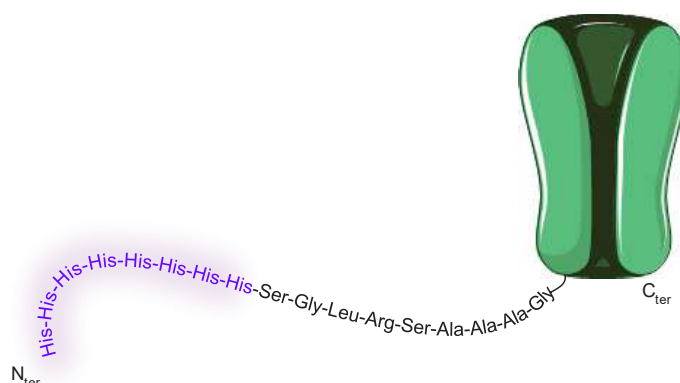


Figure 41. Schematic representation of the hP2X7-8His construct to be employed in these studies.

The N-terminally attached 8His affinity tag is shown (purple), followed by the linker sequence (black) to which hP2X7 (green) is attached.

- (ii) **Preparation of recombinant bacmid DNA:** subcloning of the hP2X7-8-His construct into the pFastBac vector and generation of recombinant bacmid DNA (utilisation of the commercial Bac-to-Bac system from Invitrogen).
- (iii) **Protein production using the baculovirus/Sf9 insect cell system:** carried out at the Baculovirus Platform (IGBMC, Illkirch Graffenstaden, France). We have chosen this expression system following its successful implementation in the resolution of previous

P2X structures. To be optimised is the exact bacmid clone employed, as well as the viral titer, which will be assessed by expression tests.

(iv) Isolation, purification and reconstitution of hP2X7-8His: membrane isolation using detergent is to be optimised, and purification is to be carried out *via* IMAC using Co²⁺ TALON® resin. Reconstitution into nanodiscs is also envisaged.

(v) Cryo-EM tests: monodispersity of trimeric P2X7 is to be verified by Dynamic Light Scattering (DLS), and eventually preliminary cryo-EM image tests are to be carried out.

EXPERIMENTAL SECTION

Molecular biology

For *S. frugiperda* expression, the generation of a DNA fragment containing the gene coding for octahis tagged hP2X7 (hP2X7-8His) was carried out by polymerase chain reaction (PCR) using the kit KAPA Robust 2G. This insert was then subcloned into i) pFastBac vector (Bac-to-Bac kit, Invitrogen) for bacmid preparation and ii) pcDNA3.1 (+) for electrophysiological experiments. Following subcloning, the DNA is dialysed, concentrated by SpeedVac, and the DNA pellet resolubilised in milliQ water before electroporation into electrocompetent DH5 α *E. coli* cells. These bacteria are cultured on ampicillin-containing solid agar-lysogeny broth (LB) medium overnight at 37°C, and resulting colonies re-cultured in solution in order to test the incorporation of the desired insert by restriction enzyme digestion screening. DNA was purified by the Nucleospin plasmid kit (Machery Nagel). Colonies with positive profiles were cultured on a larger scale and again purified by the Nucleospin plasmid kit. Sequences were verified by DNA sequencing (Eurofin Genomics). hP2X7-8His contained within pcDNA3.1(+) contains a 200bp insert between the promotor and start codon.

For *P. pastoris* expression, a DNA fragment containing the gene coding for hP2X7 is generated by PCR, using the Kapa HiFi HotStart kit, and sub-cloned into i) the vector pPIC9K MP4 (containing an in-frame linker and 10-histidine tag at the C-terminus of the gene of interest) and ii) the vector pPIC9K MP6 (containing an in-frame 10-histidine tag at the N-terminus of the gene of interest), both provided by R. Wagner (IMPreSs platform, ESBS, Illkirch Graffenstaden).

The non-tagged hP2X7 gene, as used for electrophysiological recordings, is contained within a pIRES vector, which features the same CMV promotor as pcDNA3.1(+).

For bacmid preparation, the Bac-to-Bac guide was followed. Briefly, the pFastBac vector containing the desired hP2X7-8-His construct is transformed by chemical transformation into DH10Bac *E. coli* and cultured on solid LB medium containing 50 μ g/mL kanamycin, 7 μ g/mL gentamicin, 10 μ g/mL tetracycline, 80 μ g/mL X-gal and 40 μ g/mL IPTG to select for transformants. After 48h, white colonies were selected and re-streaked on fresh plates. Once the white phenotype had been confirmed on this secondary solid culture, a 5 mL solution culture is started, overnight at 37°C, using the same antibiotic selection. Cells are resuspended in 15 mM Tris HCl pH 8.0, 10 mM EDTA, 100 μ g/mL RNaseA and lysed for 5 minutes upon addition of 200 mM NaOH and 1% SDS. 3 M potassium acetate pH 5.5 is then added and cells incubated for 5 minutes on ice to terminate the lysis. Bacmid DNA is precipitated by isopropanol, and left on ice for 30 minutes before centrifugation. After washing with 70 % ethanol, the bacmid DNA is resuspended in TES buffer. Verification that the desired insert has

been successfully transposed is carried out by PCR analysis of the T7 integration cassette. Bacmids exhibiting a band corresponding to the expected molecular weight of the insert-containing T7 integration cassette were then provided to the baculovirus platform (IGBMC, Illkirch Graffenstaden) and a stock was kept in 40% glycerol at -80°C for future use.

Expression tests: Sf9 membrane fraction isolation, SDS/native PAGE and Western Blot analysis

Sf9 cells are pelleted at 1000xg and gently washed with PBS/1 % glycerol, before resuspension in PBS containing 0.5 µg/mL leupeptin, 2 µg/mL aprotinin, 0.5 µg/mL pepstatin A and 0.5 mM phenylmethylsulfonyl fluoride (all Sigma Aldrich). For small scale expression tests, the totality of cells was directly used. For the large scale 2L Sf9 production, aliquots of cells were snap frozen in liquid nitrogen and stocked at -80°C for future use.

For isolation of membrane proteins, cells are broken by a series of sonications whilst on ice. After centrifugation at 2000 rpm, the membrane-containing supernatant is separated and re-centrifuged at 10,500 rpm at 4°C and the pellets, corresponding to the cell membrane fraction, are re-solubilised in either a DDM-based buffer, or, a Triton-X-100-based buffer, (referred to as Triton-X) according to the experiment, and left on vortex at 4°C overnight. The composition of the DDM-based buffer is: 40 mM DDM, 15 % glycerol in TBS (50 mM Tris pH 8.0, 150 mM NaCl) (according to the protocol of (Kawate et al., 2009)). The composition of the Triton-X-based buffer is: 2% Triton-X in PBS pH 7.4 (in agreement with the protocol of (Karasawa and Kawate, 2016)). All reagents were sourced from Sigma Aldrich.

For SDS PAGE analysis, the solubilised membrane fractions are then mixed with NuPage LDS sample buffer (Thermo Fischer), 70 mM DTT and boiled for 10 minutes. Samples are loaded onto 4-15% Mini Protean TGX precast gels (BioRad) and migrated in tris/glycine/SDS running buffer (BioRad) at 150 mV. Transfer onto nitrocellulose membrane using the TransBlot Turbo system (BioRad) and the membrane blocked in TPBS (PBS containing 1 % dried non-fat milk, 0.5 % BSA, 0.05 % Tween-20) for 30 minutes. The membrane is incubated overnight at 4°C with anti-polyhistidine antibody (produced in mouse) dilution 1:3000 in TPBS. After three washes with TPBS, the membrane is incubated with HRP-conjugated sheep@mouse antibody dilution 1:10,000 in TPBS for two hours at room temperature (both antibodies Sigma Aldrich). Three further washes with TPBS were carried out before revelation using Amersham ECL Prime Western Blotting Detection Reagent (GE Life Sciences). Chemiluminescence was measured using the Amersham Imager 600.

For native PAGE analysis, samples were mixed with 62.5 mM Tris-HCl pH 6.8, 40% glycerol, 0.01% bromophenol blue, loaded onto 4-15% Mini Protean TGX, and migrated in tris/glycine buffer (BioRad). Membrane transfer and revelation is carried out as described above.

RESULTS

1. Generation of hP2X7-8His constructs and functionality test

To verify that the addition of an 8His tag to the N-terminal of hP2X7 did not render the receptor non-functional, whole cell currents were recorded of the hP2X7 wild type (WT) receptor and the hP2X7-8His construct expressed in HEK293T cells. hP2X7-8His exhibited currents similar to that observed in the WT receptor, confirming that the presence of this tag does not prevent receptor function.

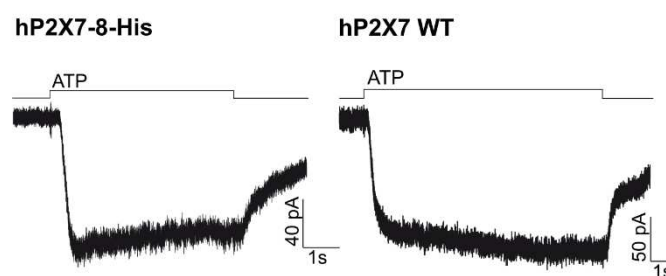


Figure 42. Whole cell electrophysiological traces of hP2X7-8His and hP2X7 WT.

Receptor constructs are expressed in HEK293T cells and the concentration of ATP used to evoke hP2X7 currents is 3mM.

2. Sf9/Baculovirus system expression tests

In the first instance, 9 bacmid clones were used for production of virus particles and Sf9 cell infection (transfection and infection carried out by the baculovirus platform, IGBMC). Small scale (1,5 mL) preparations of Sf9 cells infected by virus originating from these 9 clones were subsequently tested for expression of the desired hP2X7-8His protein, by isolating and solubilising the membranes in Triton-X based solubilisation buffer, followed by SDS-PAGE migration and Western Blot.

5 of the clones resulted in an expression, albeit very weak, determined by the presence of a band at 70 kDa, corresponding to the hP2X7-8His monomer.

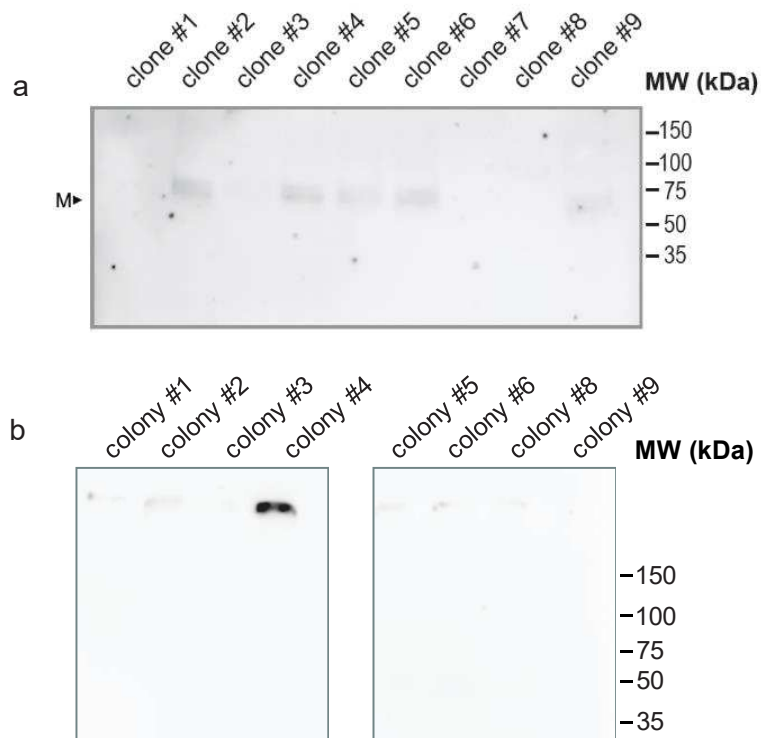


Figure 43. Western blots of (a) SDS-PAGE and (b) native electrophoresis gels of hP2X7-8His expressing Sf9 cells.

(a) Western Blot pertaining to SDS-PAGE analysis of Sf9 cells expressing hP2X7-8His, infected from bacmid clones #1- #9. The monomer is indicated by M and corresponds to a molecular weight of 70 kDa. (b) Western Blot relating to native PAGE analysis of the same Sf9 cells as in (a), at 5 days post membrane isolation. High molecular weight aggregates are visible above 150 kDa. Exposure times = 60 minutes.

To determine in which oligomeric form the hP2X7-8His has been isolated, a native PAGE analysis was carried out, at D+1 and D+5 from extraction, showing the weak presence of high molecular weight bands. This indicates that hP2X7-8His rapidly forms high molecular weight aggregates upon membrane extraction in Triton-X-based solubilisation buffer, which are difficult to disrupt even in denaturing conditions. The revelation of faint bands in the sample wells would indicate that aggregation prevents the passage of samples into the gel.

Following the confirmation of hP2X7-8His expression in Sf9 cells, the clone 4 was chosen, as this clone showed a consistent expression in both SDS and native PAGE assays. A second small scale assay was carried out, this time to determine whether viral titer has an influence on P2X7-8His expression levels. 3 viral titers of clone 4 were tested: 1, 5 and 10 Pfu per cell (plaque forming units). The western blot corresponding to this assay, as well as the total protein concentration of the solubilised membrane fraction as determined by Bradford assay is shown in Figure 44. A weak overall expression is again observed, despite the samples being concentrated x2 compared to the previous assay in an attempt to increase the signal. The viral

titer 10 Pfu seems to present the strongest expression of hP2X7-8His, however, a high proportion of high molecular weight aggregates, and to a lesser extent dimers, are observed.

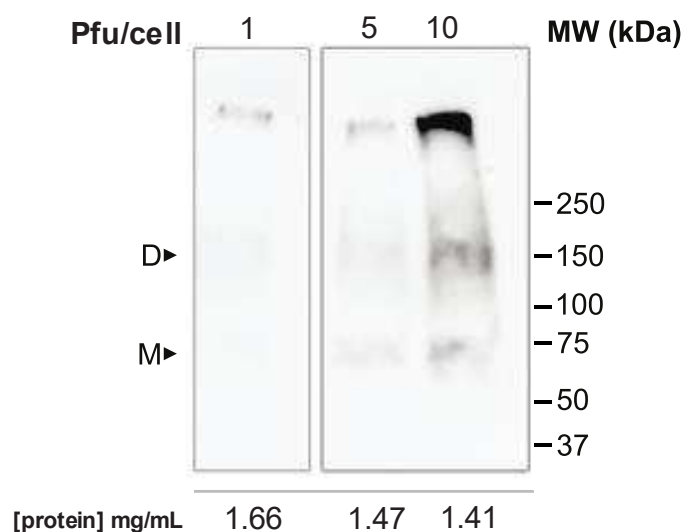


Figure 44. Western Blot of hP2X7-8His protein isolated from Sf9 membranes infected with a viral titer of 1, 5, or 10 Pfu.

Dimeric (D) and monomeric (M) weights are indicated, as is the total protein concentration of the membrane fraction, as determined by Bradford assay. Exposure time = 60 minutes.

Following this assay, a 2L production of the chosen hP2X7-8His clone, with infection carried out at 10 Pfu was generated (baculovirus platform, IGBMC), with a view to carrying out extraction tests in different conditions, using aliquots from the same expression batch. In previous structural studies of truncated P2X receptors, DDM-based or Triton-X based buffers have been employed for membrane protein solubilisation. Therefore, an initial test to compare these two detergents was carried out, using 100 mL of Sf9 culture. In parallel, a secondary assay was carried out in which these samples were either prepared for SDS PAGE under normal conditions, or, without boiling prior to loading. Heating of protein sample, especially in the case of membrane proteins, is known to be a potential cause of aggregation (Karginov and Agaphonov, 2016; Lee et al., 2005) and therefore this secondary assay was performed in order to determine whether aggregation such as that observed in Figure 44 occurs in fact during this preparative boiling step, and not during solubilisation.

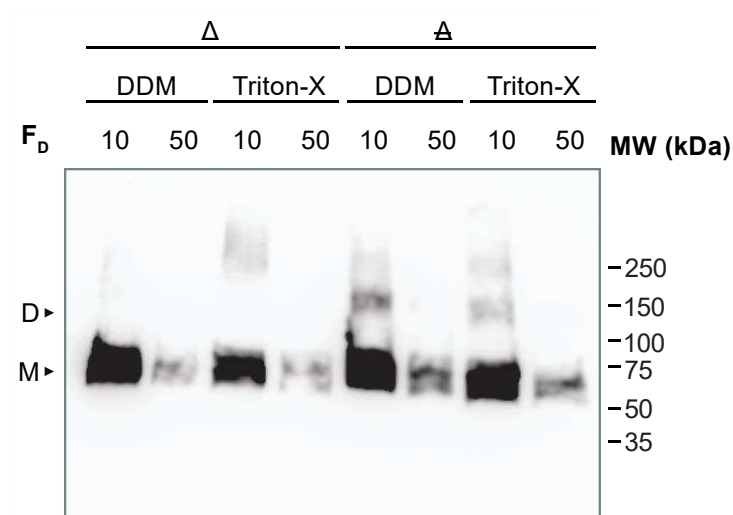


Figure 45. Western Blot of SDS-PAGE analysis of hP2X7-8His isolated from Sf9 membranes in different conditions.

Samples heated prior to loading onto SDS-PAGE gel are indicated by Δ, and those unheated are indicated by A. The detergent used for solubilisation is indicated, as is the factor of dilution (F_D) before gel loading. Exposure time = 120 s.

As can be observed in Figure 45, samples which are heated prior to loading contain fewer polymeric forms and high molecular weight aggregates resistant to denaturing conditions than sample which are heat-treated. Therefore, any aggregation observed is not due to the preparation of SDS-PAGE samples, but instead a feature resulting from the membrane extraction and solubilisation process. Concerning the two detergents tested, solubilisation with Triton-X appears to result in the presence of aggregates even in denaturing conditions (lane three, smeared band >250 kDa), which is not observed in DDM-based solubilisation buffer. In Figure 45, diluted samples have been loaded onto gel for greater clarity. DDM-based buffers may therefore present a more suitable choice for solubilisation of full length hP2X7, in contrast to the Triton-X solubilisation carried out in the purification of truncated pdP2X7.

3. *P. pastoris* expression tests

In parallel, the use of *P. pastoris* as an expression system for hP2X7 has been explored, as, to the best of our knowledge, purification of P2X receptors expressed in yeast expression systems has not yet been explored in the literature and may present an underexploited option. Vectors containing the gene for a C-terminal 10His tagged hP2X7, was transformed into *P. pastoris* and cultured on solid medium in the Wagner group (ESBS) for preliminary tests. From this solid culture, a “Yeastern” blot was carried out, to determine whether the construct is expressed. Whilst a generally low signal was observed, Yeastern blot indicated that this C-tagged construct is expressed in *P. pastoris* (Figure 46a). Subsequent Western Blot of the

membrane fraction of two selected colonies revealed the presence of two specific bands >170 kDa, which could correspond to the trimer (210 kDa) or indeed aggregates.

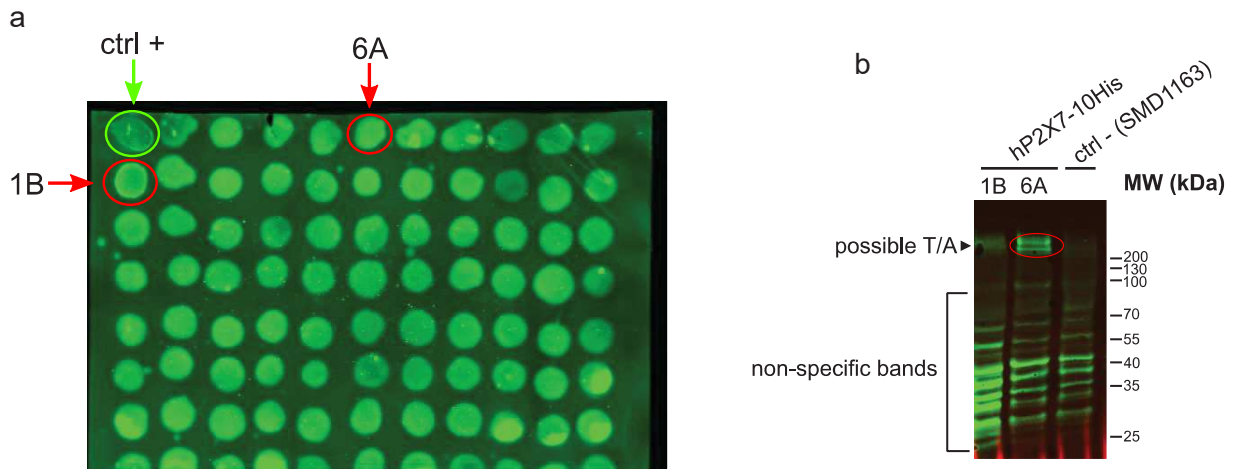


Figure 46. Expression tests of C_{term} 10His-tagged hP2X7 constructs in *P. pastoris*

(a) *P. pastoris* colonies transformed by C-terminally 10His-tagged hP2X7 (hP2X7-10His). Circled in green is a positive control, yeastern blot of a GPCR known to undergo robust recombinant expression in *P. pastoris*. All other spots represent hP2X7-10His colonies, and those colonies transferred to suspension medium for subsequent Western Blot analysis are circled in red. (b) Western Blot of the membrane fraction of *P. pastoris* colonies 6A and 1B, identified by yeastern blot. A negative control using the SMD1163 strain of *P. pastoris* is shown (far right), revealing the presence of non-specific bands. The colony 6A shows expression of bands which may correspond to a trimer, or, aggregate structures (circled in red). Carried out by Valérie Kugler, IMPReSs facility, ESBS.

DISCUSSION AND OUTLOOK

Aggregation has previously been noted as a problematic characteristic for wild-type P2X receptor purification, as for many membrane proteins. The Gouaux group have demonstrated that upon solubilisation in common detergents, including DDM, rP2X4 either dissociates into its monomeric form, or, upon cross-linking, forms high molecular weight aggregates. An example in the literature also shows that hP2X5 isolated in digitonin, although predominately present as a trimer, also exhibits a certain proportion of aggregates in native conditions (Duckwitz et al., 2006).

For P2X7, the truncated pdP2X7 structure resolved by Karasawa *et al* is apparently stable as a trimer in 2% Triton-X solubilisation buffer. In our brief assays, solubilisation of hP2X7-8-His with Triton-X resulted in the presence of aggregates in native conditions, as well as, to varying extents, in denaturing conditions. The presence of the C-cys anchor and the ballast, which are absent in the pdP2X7 structure, therefore likely have an important influence over the receptor's biochemical behaviour. Given the extensive secondary structure of the large ballast region with its numerous intersubunit interactions, disruption and unfolding of this domain during membrane isolation and solubilisation could feasibly result in aggregation behaviour so as to limit unfavourable solvent-protein interactions.

An additional consideration is that P2X7 has an extensive range of protein partners and lipid interactions (Kopp et al., 2019). These interactions, which serve a wide range of functional purposes, may also have structural importance, contributing to the stability of the global P2X7 architecture. Disruption of such interactions with detergent would therefore also represent a possible source of aggregation. Indeed, in the Mansoor group's recent study resolving the structure of rP2X7, HEK293 membranes expressing rP2X7 were solubilised in DDM-based buffer of the same composition as that described above, but with a supplement of 8 mM cholesteryl hemisuccinate tris salt (CHS). HEK293T membranes exhibit a cholesterol:phospholipid ratio of approximately 0.23 W/W (Dawaliby et al., 2016). The ratio of CHS:DDM employed by the Mansoor group is also equivalent to 0.23 W/W, thus mimicking the lipidic compositions of the HEK293 expression system. It may be therefore, that the addition of cholesterol, a known P2X7 modulator which interacts directly with the channel itself (Karasawa et al., 2017; Murrell-Lagnado, 2017; Robinson et al., 2014), allows for the structural maintenance of P2X7 throughout the solubilisation process.

Concerning the possibility of using yeast systems to express P2X7 for structural studies, the tests carried out with the Wagner group show that *P. pastoris* may be an option for large scale production of hP2X7-10His. Although these remain preliminary tests, the ease with which yeast systems can be handled offers the opportunity to test a number of expression and extraction

conditions in a rapid and efficient manner, and as such this initial demonstration of hP2X7-10His expression may present a good starting point for optimisation.

For the continuation of this project, a number of other detergents should be explored. DDM appears to be a good starting point, resulting in monomeric bands in denaturing conditions, but should be assessed for its propensity to solubilise intact trimers in native conditions. Taking inspiration from the Mansoor group, supplementing solubilisation buffer with CHS may also present an efficient means of solubilising native-like trimers for hP2X7. Considering that our choice of Sf9 expression system provides membranes with limited cholesterol content, introducing a cholesterol substitute such as CHS may be of particular importance. Use of the detergent CHAPS, which features a cholesterol-like motif, should also be explored, as well as the MNG class of amphiphilic detergents, which are reported to increase the stability of solubilised membrane proteins, thus reducing aggregation (Chae et al., 2010; Cho et al., 2015).

Despite the recent resolution of the structure of rP2X7, resolution of hP2X7 still merits research efforts given the considerable functional differences between these two orthologs. For example, they feature differing rates of facilitation, different single channel conductances as well as different pharmacological profiles (Donnelly-Roberts et al., 2009; Nörenberg et al., 2012; Rassendren et al., 1997; Roger et al., 2010a). It would therefore be interesting to explore whether there is a structural basis to these functional variations. Given the importance of lipid composition for the function of P2X7 (Karasawa et al., 2017), another interesting possibility to explore would be the use of reconstitution methods such as nanodiscs, discussed in section 2.2.1, which allow a more faithful reproduction of the native lipid environment. Native nanodiscs, incorporating endogeneous lipids of the HEK293 expression system have been described (Mak et al., 2017), and one example using the *E.Coli* bacterial expression system foregoes entirely the use of detergents to produce nanodiscs of a K⁺ channel directly from lysed cells (Dörr et al., 2014), although these techniques have been used for functional studies rather than structural. The use of such systems for P2X7 in combination with cryo-EM would offer the interesting possibility to gain an insight into P2X7 structure in its native environment. Resolution of a P2X7 structure in complex with one of its many protein partners is also a goal which could be realised using cryoEM techniques. This, in conjunction with the many cellular and biochemical approaches already employed to study such interactions, would provide precious insights into the role of P2X7 within multi-protein, complex biological systems.

CHAPTER TWO: USE OF PHOTOISOMERISABLE TOOLS TO PROBE STRUCTURE AND FUNCTION OF P2X7 RECEPTORS

INTRODUCTION

Aside from structural determination, there exist a plethora of techniques which may be employed to gain insight into biological processes at the molecular level. The difficulty comes in studying these biological interactions of interest in a precise manner, without perturbing the entirety of the wider system. Pharmacological methods, whilst of value and extensively used in neurobiology, suffer from a number of limitations. They rely on the diffusion of active compounds to the site of interest, which proves difficult to control both spatially and temporally, and often lack specificity for a unique target, as well as having limited reversibility. The use of light as an alternative stimulus offers the solution to many of these limitations. Light is a stimulus which can be applied with exquisite spatiotemporal control, can be used remotely and non-invasively, and depending on the wavelengths and intensities employed causes limited cell damage. In addition, as the majority of cell types are not intrinsically photosensitive, light can be considered as an orthogonal stimulus, the use of which does not risk triggering other, undesired biological processes. Since the dawn of channelrhodopsin-based optogenetics, a vast number of techniques employing light for the study of neurobiological systems have been developed. In the study of ion channels at the molecular level, as interests us, systems employing synthetic chemical photoswitches are widespread, and can be classed into two categories; one-component systems, as employed in **optopharmacology** and two-component systems, as employed in **optogenetic pharmacology**.

1. Photoswitches for ion channel studies

Chemical photoswitches are defined as molecules featuring a photochromic moiety capable of isomerisation upon the absorption of a photon, which is usually completely reversible (Mourot et al., 2013; Szymański et al., 2013). Applied to ion channels, the goal of their use is to achieve modulation or indeed total control of channel activity in a spatiotemporally precise manner. This can provide information concerning the downstream effects following activation of the channel in question, as well as conformational and mechanistic insights on the molecular level. A range of photochromic chemical groups have been used as the basis of biologically-targeted photoswitches; we will focus on the use of azobenzenes.

1.1. Azobenzene as a photoswitchable core motif

The most commonly employed photoswitchable motif in the study of biomolecules is the azobenzene moiety, which is able to access two geometrical isomers, and presents a number of advantages (Beharry and Woolley, 2011). In the dark at equilibrium, the *trans* (E) isomer is predominant (present at >99.99%), owing to its greater thermostability of 10-12 kcal/mol. Upon irradiation in the UV region (340 nm for unsubstituted azobenzene), isomerisation to the *cis* (Z) form is induced (Figure 47). Reversion to the *trans* form can either be achieved by irradiation in the visible region (450 nm), or by thermal relaxation, although the latter requires several days. Due to a certain level of overlap in the absorption spectra of the isomers, photostationary states exist whereby the *cis* isomer can be accessed at a maximum of 85%, and the *trans* isomer at 95%, although this can be modulated by the synthesis of substituted azobenzenes. One of the main advantages of this group is that isomerisation provokes significant changes in the geometry, length and polarity of the molecule. The *trans* isomer is planar, with a dipole moment of 0 Debye (D). Upon isomerisation to the *cis* isomer, the phenyl rings are twisted to 55° out of the plane of the N=N azo group, increasing the dipole moment to 3 D and reducing the end-to-end distance by approximately 3.5 Å (measured between the carbons at the *para* position on each phenyl ring). These drastic changes occur within a matter of picoseconds, which is superior to the timescale of most biological processes, a necessity when probing such events (Beharry and Woolley, 2011; Mourot et al., 2013; Renner and Moroder, 2006). In addition to these aforementioned advantages, azobenzenes are photochemically interesting in that they feature high quantum yields, reducing the intensity of irradiation required for efficient use, and are relatively resistant to photobleaching, meaning that they can be used in many cycles of isomerisation (Szymański et al., 2013).

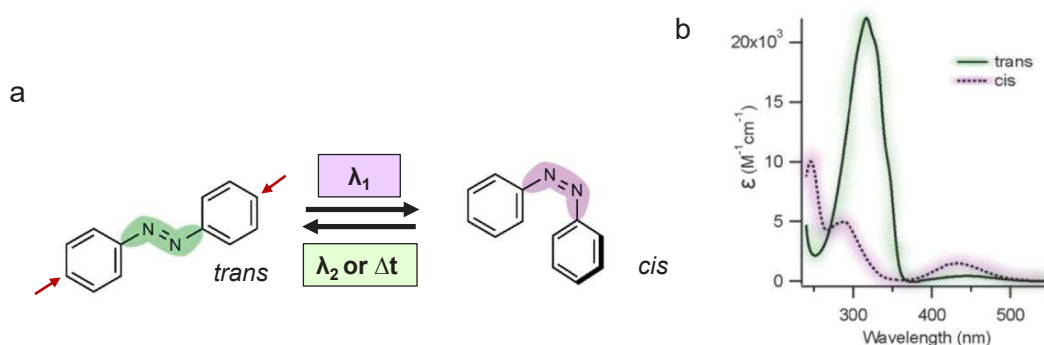


Figure 47. Azobenzene isomerisation.

(a) Isomerisation of an unsubstituted azobenzene from the *trans* (E) isomer to the *cis* (Z) isomer and reverse. The carbon atoms at position *para* to the azo group, from which end-to-end distances are calculated, are indicated with red arrows. (b) electronic absorption spectra of the two azobenzene isomers dissolved in ethanol, adapted from (Beharry and Woolley, 2011).

Chemical photoswitches featuring azobenzene as a core motif have been employed in a number of different strategies for the study of ion channels. These strategies can be broadly classed into two categories; one-components systems, as used in **optopharmacology** for channel control *via* a photochromic ligand, or two-component systems, as employed in **optogenetic pharmacology**, whereby channel control is achieved by the use of a photoisomerisable ligand in conjunction with genetic manipulation.

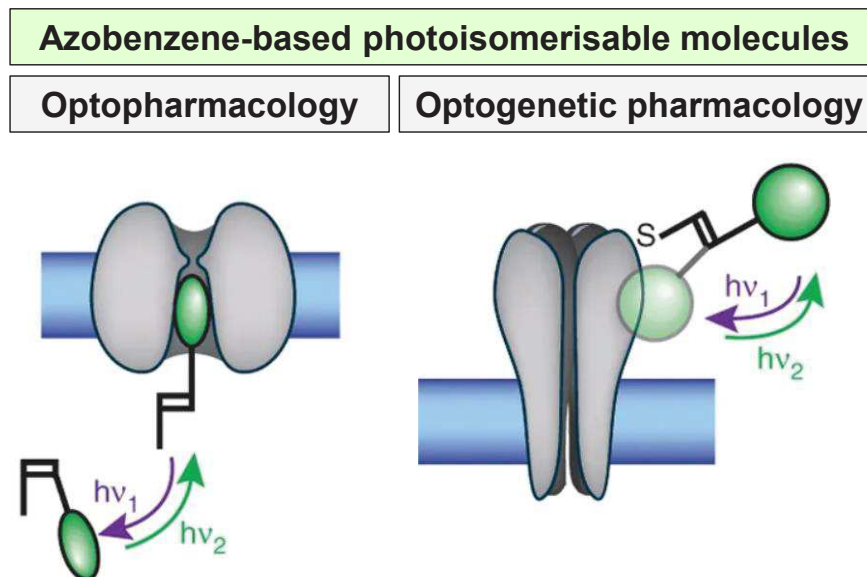


Figure 48. Schematic diagram describing the use of azobenzene for optopharmacology and optogenetic pharmacology.

Adapted from Kramer *et al* (Kramer *et al.*, 2013)

1.2. Optopharmacology

Optopharmacology broadly refers to the use of photo-activated compounds to modulate endogenous ion channel activity, and includes techniques such as the use of caged ligands and untethered chemical photoswitches (also known as photochromic ligands or PCLs). The azobenzene motif is particularly present in this latter class, and first came to use in the modulation of the acetylcholine receptor (Bartels *et al.*, 1971; Lester *et al.*, 1979). Since then, this principle has been applied to a range of ion channels, including GABA_A receptors (Stein *et al.*, 2012; Yue *et al.*, 2012), ionotropic Glutamate receptors (iGluR) (Volgraf *et al.*, 2007; Stawski *et al.*, 2012), and voltage-gated potassium channels (K_vs). The K_v family in particular has been the target of a wide range of PCLs of differing characteristics, employed *in vitro* as well as *in vivo*. The first such example utilised the photoswitch AAQ (Acrylamide Azobenzene Quaternary ammonium, Figure 49a) (Fortin *et al.*, 2008; Banghart *et al.*, 2009). This PCL acts by lodging the charged quaternary ammonium (QA) group in the intracellular tetraethylammonium binding site of K_v channels when in the *trans* configuration, thereby

blocking the channel and preventing K⁺ efflux. Irradiation at 380 nm evokes isomerisation to the *cis* isomer, thus resulting in the release of the channel block (Figure 49b and c).

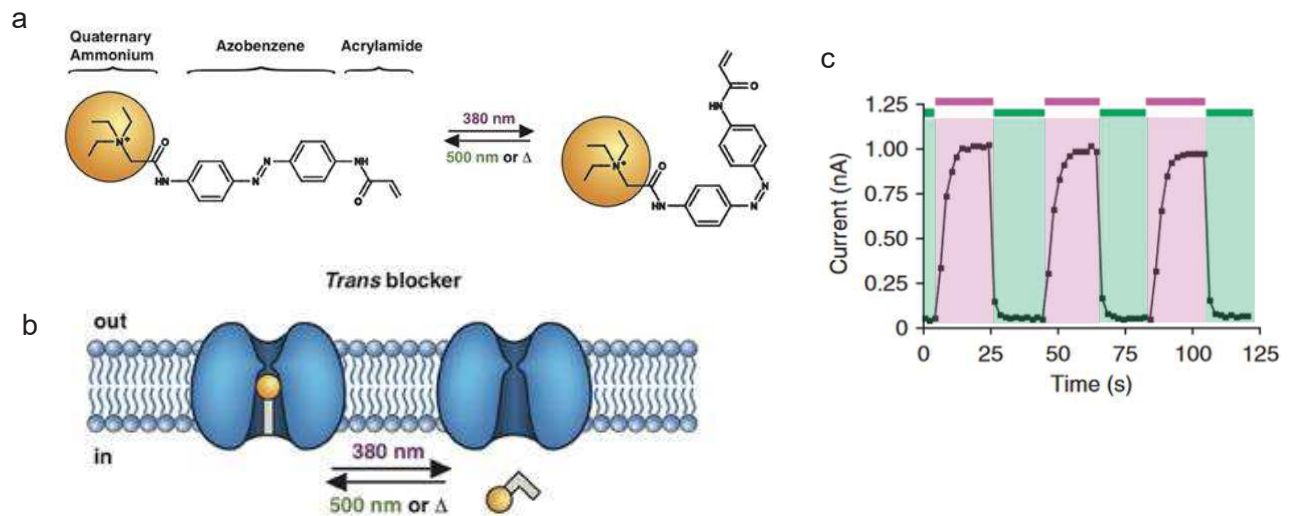


Figure 49. AAQ as a PCL targeting K_v channels.

(a) Chemical structure of the AAQ PCL as its *trans* (left) and *cis* (right) geometrical isomers. (b) Corresponding schematic diagram showing the mechanism of action of AAQ on K_v channels, where channel block is produced by the insertion of the quaternary ammonium moiety (shown as a yellow sphere), when AAQ is in its *trans* configuration, into a pocket of the channel. Upon UV irradiation and isomerisation to the *cis* geometrical isomer, this block is released. (c) Voltage-gated currents from Shaker channel-expressing HEK cells after AAQ treatment. Green regions represent irradiation at 500 nm and purple regions represent irradiation at 380 nm. Voltage-gated K⁺ currents were evoked by pulsing from -70 to +30 mV for 250 ms. (a) and (b) adapted from (Mourot et al., 2013) and (c) adapted from (Fortin et al., 2008).

Other variants based on the AAQ model have been synthesised, with optimised characteristics. For example, PhENAQ, which features a phenylethylamine group in place of the acrylamide, also functions as a K_v channel blocker, but this time in its less thermodynamically stable *cis* isomer (Mourot et al., 2011). Photoswitches whose “active” state is reached in the *cis* configuration, and which are therefore considered inert when in *trans*, can be seen as advantageous due to the fact that UV irradiation is only required when wishing to exert the photoswitch’s activity and not during inactive, resting periods. This therefore reduces the necessity of long and potentially damaging irradiations. The addition of the electrodonating aryl alkylamino group also presents the advantage of producing a “red-shift” phenomenon in the absorption spectra, enabling isomerisation to occur upon irradiation with blue light (480 nm), and therefore avoiding the use of UV wavelengths and their associated phototoxicity.

Although PCLs, as optically active molecules, benefit from the temporal and spatial precision of light, their use remains hampered by a lack of true specificity. AAQ, for example, acts on eight different subtypes of K_v channels (Mourot et al., 2013). This renders challenging the extraction of precise information on the molecular function of a particular channel, or indeed,

the implication of this channel in the function of a specific cellular subset. Few examples exist of systems featuring a heightened level of targeting, either to a specific cell type, or to a specific channel type. One example of a cell-targeting PCL is QAQ, developed between the Trauner et Kramer groups. QAQ, featuring two QA groups at the extremities of a central azobenzene core, is a membrane-impermeant *trans* blocker of K⁺, Na⁺ and Ca²⁺ voltage gated channels. This study takes advantage of other channels, namely TRPV1 and P2X7, for cell target specificity. TRPV1 and P2X7 have a common feature in that they exhibit enhanced large molecule permeabilities, and as such, are taken advantage of as molecular conduits to deliver QAQ to the cytosol, where it can be employed as a channel blocker for K⁺, Na⁺ and Ca²⁺ voltage gated channels. This original delivery strategy can either be employed by heterologously expressing these conduit channels in a desired cell type, or, by employing QAQ on cell types where endogenous expression of such channels is particularly high. This latter strategy has been demonstrated by using QAQ in co-application with capsaicin, a TRPV1 agonist, to selectively photosensitise mouse nociceptive neurons, where TRPV1 is particularly abundant.

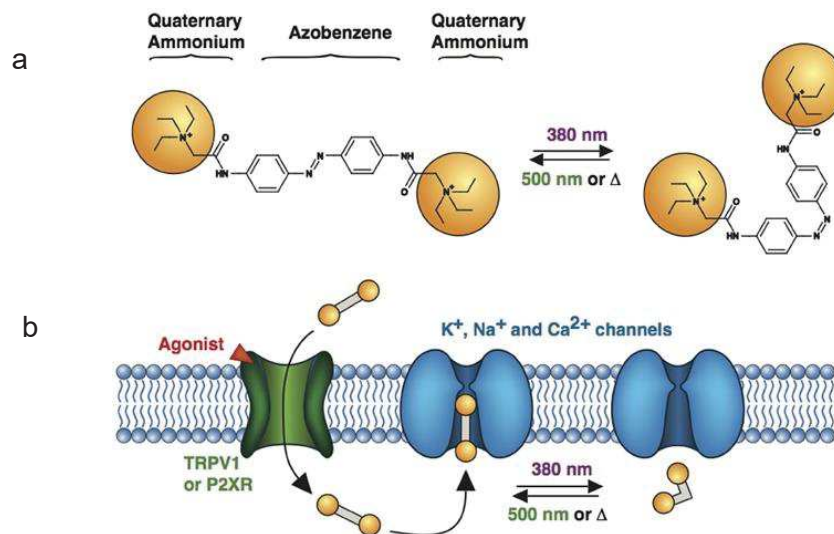


Figure 50. Cell-targeted QAQ strategy

(a) Chemical structure of the *trans* (left) and *cis* (right) geometrical isomers of QAQ. (b) Schematic representation of the QAQ system, whereby the photoswitch is delivered to the intracellular domains of selected cell types, through TRPV1 or P2X7 channels. Adapted from (Mourou et al., 2013).

Whilst the PCL strategy enables the study of endogenous channels, it largely retains the classical pharmacological drawback of low specificity. Efforts to counter this, such as that discussed above, require extensive optimisation and are not necessarily transferable to all ion channel, nor cell type, targets. Additionally, these PCL systems still rely on the principle of

diffusible ligands, which, due to the difficulty in controlling diffusion within a region of interest, can result in effective concentrations too weak to confer an efficient photosensitivity.

For these reasons, the use of optogenetic pharmacological methods, whereby the power and specificity of genetic manipulation is combined with the spatiotemporal control of photoswitchable ligands, can offer an attractive alternative strategy.

1.3. Optogenetic pharmacology

Optogenetic pharmacology describes the use of chemical photoswitches in conjunction with genetic modification to achieve photosensitivity of target receptors and ion channels in a precise and fully specific manner. These systems require the rational design, therefore, of two components: the photoswitch responsible for conferring light sensitivity and a genetically-introduced tethering point, typically a cysteine residue, to which this photoswitch will be covalently attached on the channel of interest. The underlying principle of this photoswitchable tethered ligand (PTL) technique, is that the photoswitch is covalently attached to a specific channel, at a specific, genetically-engineered point which is in spatial proximity to a site of ligand action, whether this be agonistic, antagonistic, allosterically modulating or a pore blocking site. Photoisomerisation of the PTL occurs in such a way as to present the ligand at its target site or indeed to withdraw it, thus modulating channel activity. The PTL must therefore comprise a tripartite structure: a moiety responsible for tethering to a genetically-introduced cysteine residue in the channel (typically a maleimide), the central photoisomerisable azobenzene group conferring light sensitivity, and an extremity featuring the desired ligand. The first example of a PTL system applied to an ion channel is that of so-called “SPARK” channels: synthetic photoisomerizable azobenzene-regulated K⁺ channels, specifically the *Drosophila* Shaker channel (Banghart et al., 2004; Chambers et al., 2006). Guided by structural data and previous cysteine scanning experiments, the exact position of the genetically-introduced cysteine tether point and the chemical structure of the photoswitch (MAQ, Figure 51a) were designed in such a way that when in the *trans* isomeric form, the PTL is of sufficient length to present the QA moiety to a pore-lining TEA binding site, thus creating a block to K⁺ efflux, whilst upon UV-induced photoisomerisation to the *cis* configuration, the PTL effectively shortens, releasing this blocking effect. This was demonstrated in *X. laevis* oocytes transfected with the mutant Shaker channel and incubated with MAQ, as well as in cultured hippocampal neurons, where exposure to UV light silenced spontaneous action potential firing (Figure 51c and d). PTL strategies have since been extended to mammalian K⁺ channels (Fortin et al., 2011; Sandoz et al., 2012), as well as to a number of ligand-gated ion channels, including nAChRs (agonistic and antagonist PTLs) (Tochitsky et al., 2012), all 6

GABA_A receptor isoforms (Lin et al., 2015), and iGluRs (Gorostiza et al., 2007; Janovjak et al., 2010; Numano et al., 2009; Szobota et al., 2007; Volgraf et al., 2006).

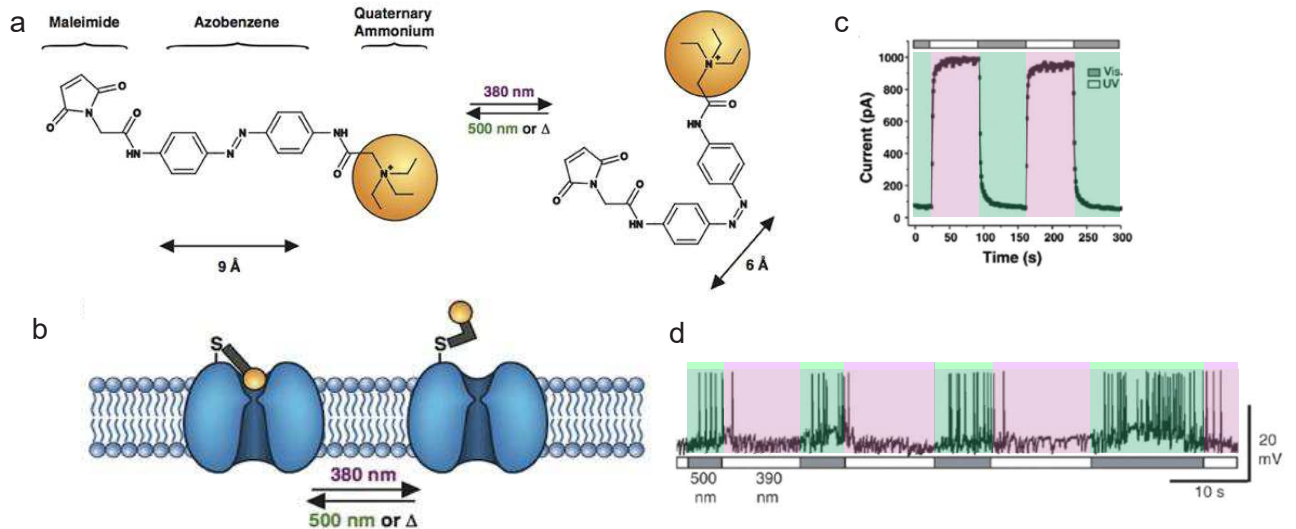


Figure 51. Example of the MAQ PTL system as applied to Shaker K⁺ channels

(a) Chemical structure of the MAQ PTL in its *trans* isomeric form (left) and *cis* isomeric form (right). (b) Schematic diagram demonstrating the mode of function for the MAQ photoswitch as applied to *Drosophila* Shaker K⁺ channels. (c) Currents recorded from an outside-out patch of mutant Shaker-expressing oocyte treated with MAQ, held at -90 mV, with alternating visible (500 nm) and UV (380 nm) light irradiations. Currents were elicited by 100 ms steps to -20 mV at 1 Hz. (d) Trace showing the silencing of spontaneous action potential (AP) firing in a mutant Shaker channel-expressing hippocampal pyramidal neuron treated with MAQ and irradiated at 390 nm, and subsequent resumption of AP firing when irradiated at 500 nm. (a) and (b) taken from (Mourot et al., 2013) and (c) and (d) adapted from (Banghart et al., 2004).

A number of these examples have also been applied *in vivo*: iGluR PTL systems have been employed to study neuronal circuitry in zebrafish larvae (Szobota et al., 2007) as well as to counteract inherited blindness in rodent models (Caporale et al., 2011), whilst the GABA_A PTL system of Lin *et al* has been applied to control sensory responses in mice (Lin et al., 2015).

The high degree of specificity achieved by this technique, however, comes with the drawbacks of genetic manipulation: in *ex-* or *in vivo* studies, over-expression of the mutant channels required for the PTL strategy may be inefficient, non-uniform, and even disruptive to the normal physiological functioning of the tissues involved (Allen et al., 2015), whilst for *in vitro* molecular-level experiments, care should be taken in considering whether the presence of the cysteine mutation and use of a PTL for channel manipulation furnish physiologically relevant molecular information. These concerns have been addressed in part in the literature by the example of a hybrid approach using targeted covalent photoswitches (TCPs), whereby the photoswitch features an electrophilic group for covalent tethering to endogenous lysine residues present in a specific channel target to which it is guided by affinity labelling (Izquierdo-Serra et al., 2016).

In this example, endogenous WT GluK1 kainate receptors are specifically targeted by the presence of glutamate on one extremity of the photoswitch, allowing control of channel activity in mouse dorsal root ganglia.

The opto(genetic) pharmacological techniques described above, although requiring a careful design and optimisation, offer the possibility to study neurobiological systems and the individual receptor channels involved in heightened spatiotemporal precision and selectivity. For this reason, several new technologies inspired by these principles have been developed for the study of P2X receptors.

2. Optogenetic pharmacological tools for P2X receptors

Despite the significant advances provided by the structural determination of P2X receptors in a number of their allosteric states, these structures do not allow a comprehensive understanding of their different functionalities and the molecular mechanisms behind them. Whilst comparison of structures in different allosteric states may give insights as to the molecular motions involved in the transitions between such states, they remain fixed, non-dynamic “snapshots” and as such cannot be considered to convey a full picture. As we have discussed in chapter one, there are also a number of inherent limitations to the interpretation of these structures. Other complementary approaches are therefore required to gain a full understanding of P2X receptor structure and function. As P2X receptors suffer from a lack of specific, pharmacological tools, the use of optogenetic-based techniques and photoisomerisable molecules presents an attractive alternative.

Two such optogenetic tools have been developed for use with P2X receptors in our laboratory: the **optogating** system (Lemoine et al., 2013) and the **optotweezers** method (Habermacher et al., 2016). A similar technique to this latter method has also been published by the North group, in the context of P2X2, P2X3, P2X2/3 and ASIC channels (Browne et al., 2014). These techniques have been developed with a dual purpose in mind. Not only does the specific, optical modulation of P2X receptors provide the opportunity to delineate their roles in physiological and pathophysiological states, but the use of photoisomerisable tools also allows for a precise structural and mechanistic exploration of P2X receptors at the molecular level. Both of these strategies have been put into practice using the rP2X2-3T receptor; a mutant receptor with properties similar to the wild type, carrying three mutations to convert endogenous, extracellularly located cysteine residues, which are not engaged in disulphide bridges, to isosteric threonine.

2.1. Optogating: MEA-TMA

The first of these strategies employs a photoswitch inspired by the structure of MAQ, named MEA-TMA (Figure 52). Similar to PTLs, this molecule features three key components: a central azobenzene moiety responsible for photoisomerisation, flanked on one extremity by an electrophilic maleimide group to which covalent tethering to a genetically engineered cysteine residue in the channel of interest is possible by a non-reversible 1,4-Michael addition. At the other extremity is a positively charged quaternary ammonium group, which promotes labelling efficiency.

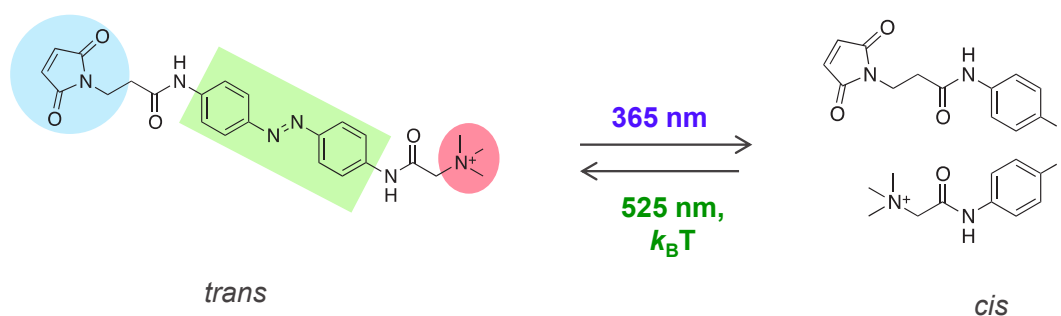


Figure 52. Chemical structure and isomerisation of MEA-TMA.

Highlighted in blue is the maleimide tethering group, in green the azobenzene moiety and in red the cationic quaternary ammonium group.

Contrary to the PTL strategies discussed above, this technique allows optical manipulation of P2X₂ not by the insertion and withdrawal of a specific ligand from its binding site, but by targeted manipulation of the transmembrane domains, regions which have been shown to be of critical importance to the gating process (Jiang et al., 2001; Li et al., 2008; Rassendren et al., 1997). Tethering the photoswitch to different TM positions imparts either *cis* or *trans*-opening characteristics, producing a P2X channel which is fully controllable by light, in total absence of ATP (Figure 53a and b). This strategy has been named optogating. In addition, when bound to the channel, MEA-TMA exhibits bistable behaviour, meaning that it remains in its last tuned state for a period of time even when irradiation is ceased. This is a particularly attractive characteristic of the system, as it circumvents the need for long and potentially harmful irradiations.

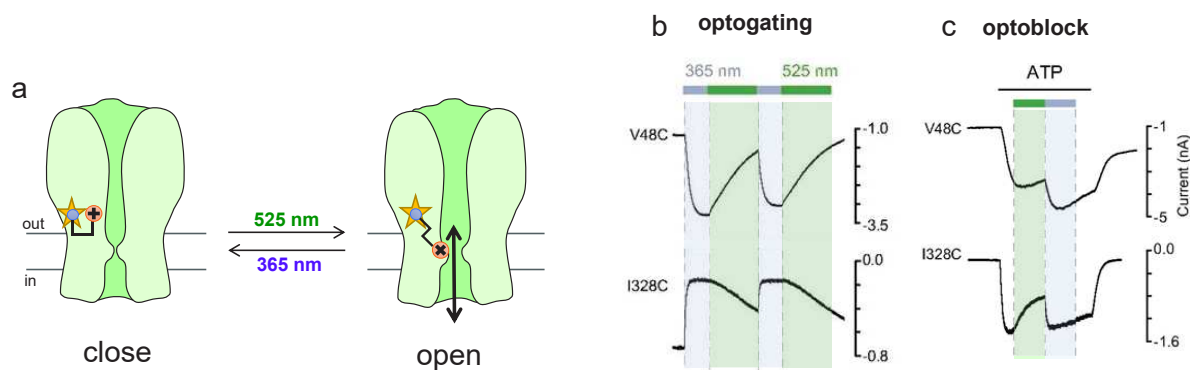


Figure 53. MEA-TMA optogating and optoblock(a)

(a) Schematic representation of the supposed mechanism of MEA-TMA optogating, in this case for a *trans*-opener. The mutated cysteine tethering residue is represented as a yellow star. Upon isomerisation to the *trans* isomer, disruption of the TM helices causes the opening of a pore through which ion conduction occurs. Comparison of (b) optogating and (c) optoblock behaviour for two P2X2 cysteine mutants expressed in HEK293T cells treated with MEA-TMA. V48C is a *cis*-opener and a *trans* blocker, whilst I328C is a *trans*-opener and a *trans* blocker. Adapted from (Lemoine et al., 2013)

In parallel, a secondary light-modulated behaviour is observed using MEA-TMA, operating through an independent mechanism. This phenomenon, named the optoblock, occurs in the presence of ATP, whereby MEA-TMA acts as a modulator of the open channel. Depending on the tethering position, the inwards current is blocked either by irradiation with UV or visible light, producing *trans*- and *cis*-blockers (Figure 53c). Upon isomerisation, the MEA-TMA photoswitch is likely placed in line of the ion permeation pathway, thus presenting a steric and/or electrostatic block to conduction.

Although the precise molecular mechanism of optogating is not fully resolved, previous work has indicated that it is likely due to the disruption of inter and/or intrasubunit interactions between the TM helices, which in turn invokes an opening of the channel. In terms of stoichiometry, the attachment of three MEA-TMA molecules is required for optogating, whilst the optoblock is observable with the attachment of just one molecule, but is amplified by the presence of a second and third (thesis work of *Dr. Chloé Habermacher* and *Dr. Juline Beudez*).

Whilst the properties of optogated P2X2 channels remain largely similar to those of the wild-type, some differences are observed, namely a 5-fold reduced Ca^{2+} permeability, and lengthened gating kinetics compared to those observed with endogenous ATP responses. In addition, photoinduced openings remain stable thanks to the bistable nature of bound MEA-TMA, contrary to wild-type P2X2 which desensitises over the course of ATP-evoked openings.

2.2. Optotweezers: MAM

The second strategy retains this concept of channel manipulation from within the transmembrane regions, this time using an original “optotweezers” device. Previous work has shown the utility of these photoisomerisable crosslinkers for probing of peptidic and DNA secondary structures (Beharry and Woolley, 2011), and application to P2X2R demonstrates the possibility to extend this manner of structural and functional exploration to ion channels. The photoswitch employed is named MAM, to reflect its structure comprising a central azobenzene moiety, linked by spacer arms on each side to maleimide groups (Figure 54a). The presence of two maleimides enables tethering of the photoswitch on both sides, creating a sort of molecular tweezers, the extremities of which can be brought closer together or farther apart upon isomerisation of the central azobenzene with different wavelengths of light.

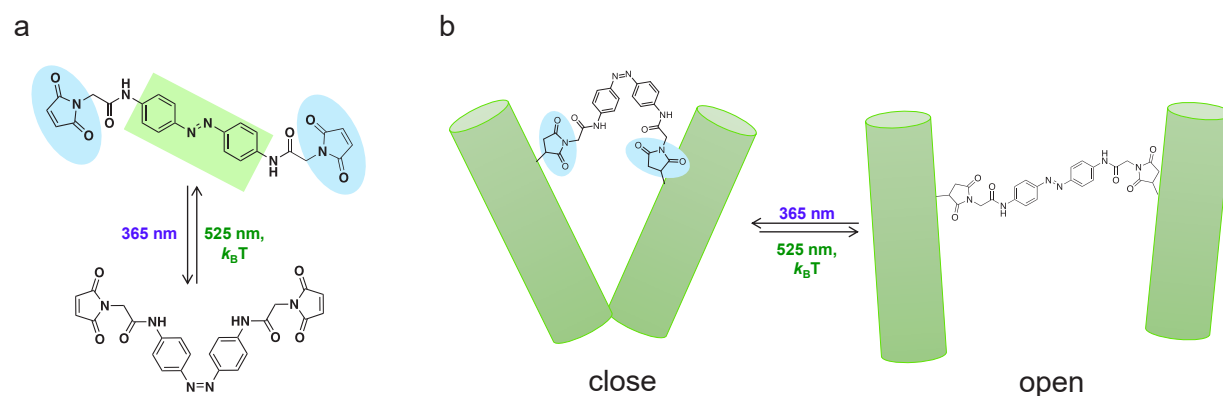


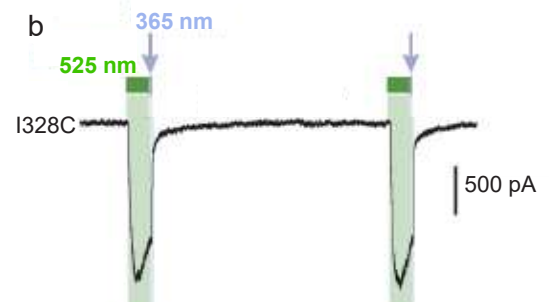
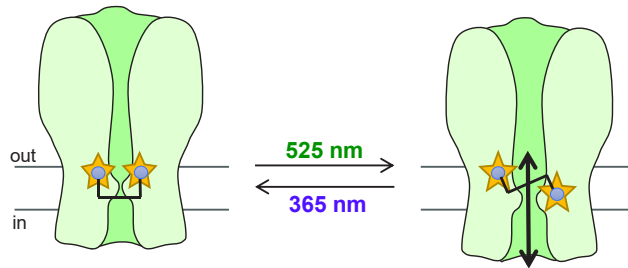
Figure 54. MAM photoswitch and the optotweezers strategy.

(a) Chemical structure of MAM and its *trans* (upper) and *cis* (lower) geometrical isomers. (b) Schematic representation of MAM once bound to cysteine attachment points on the channel, whereby toggling between geometrical isomers brings extremities, and thus attachment points on the protein, closer together or farther apart.

When MAM is bound to genetically-introduced cysteine residues in the TM domains, the movements induced by toggling between *trans* and *cis* configurations are in turn transmitted to the protein, bringing tethering residues either closer together or farther apart (Figure 54b). This strategy uses the photoisomerisation movement of MAM to manipulate natural gating elements that are already present in the channel to induce an opening or closing of the ionic pore. In P2X2R, two such gating motions have been illustrated by the optotweezers strategy and subsequently exploited to photoregulate channel activity. The first is a horizontally based gating movement, corresponding to a lateral expansion of the distance between the outer ends of the TM2 helices, probed using receptors carrying one cysteine mutation per subunit. The second is a vertically based gating motion, which corresponds to a hinge-like bending movement, bringing closer together the inner and outer ends of TM2 helices in adjacent

subunits. This motion is probed using mutant receptors carrying two cysteine mutations per subunit, allowing a crosslinking between the upper and lower ends of adjacent TM2 helices. The positions producing the most robust light-gated currents were I328C and I328C/S345C for horizontal and vertical cross-linking respectively.

a Horizontal motions – single cysteine mutants



c Vertical motions – double cysteine mutants

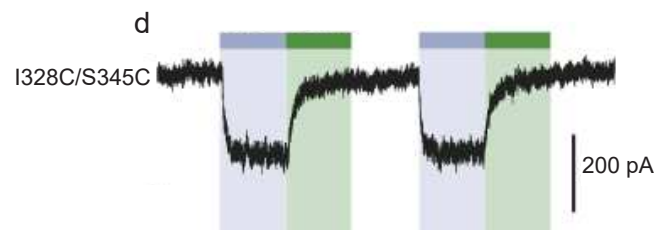
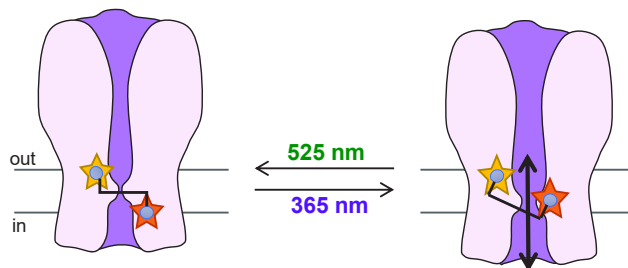


Figure 55. Optotweezers strategy as applied to P2X2 receptors.

(a) Schematic representation of MAM used to probe gating motions *via* horizontal cross-linking, resulting in channel opening in the *trans* configuration. Yellow stars represent a single cysteine mutation. (b) Representative trace of the horizontally MAM cross-linked single mutant I328C channel opening and closing in response to light when expressed in HEK293T cells (c) Schematic representation of MAM used to probe gating motions *via* vertical cross-linking, resulting in channel opening in the *cis* configuration. Yellow and orange stars represent different cysteine mutations. (d) Representative trace of the vertically MAM cross-linked double mutant I328C/S345C channel opening and closing in response to light when expressed in HEK293T cells. (b) and (d) are adapted from (Habermacher et al., 2016)

Regarding the physiological pertinence of this light-induced gating, key biophysical properties were assessed and found to be largely similar to that of ATP-gating. Activation kinetics were close to that of the wild-type, and for the horizontally crosslink experiments, a rapid inactivation of channel activity occurred once irradiation was ceased, reminiscent of the desensitisation undergone by wild-type P2X2 channels. Permeabilities remained broadly similar, with the exception of a slight decrease in the Ca^{2+} permeability (1.5-fold) (Habermacher et al., 2016). These biophysical similarities indicate therefore that the optotweezers strategy appears to produce light-induced openings closer to those produced by ATP than the optogating method. The fact that several cysteine mutations produced cross-linked receptors (assessed by SDS-PAGE), but not photoregulated currents would suggest that only positions where physiological gating elements are at play can be manipulated by MAM, and that the openings produced are therefore not the result of forced, non-natural motions (Harkat et al., 2017).

The optotweezers strategy therefore presents a complementary approach to optogating, not only allowing the specific optical control of channel opening and closing, but also the opportunity to probe precise molecular movements and distances involved in allosteric conformational state transitions. This has been demonstrated in two publications, one of which focuses on the molecular movements behind the gating process mentioned above (Habermacher et al., 2016), and the second of which dissects the controversial permeation of large organic cations through the P2X2 pore (Harkat et al., 2017).

The former study has also employed MAM as a molecular ruler, taking advantage of the defined end-to-end lengths in the channel-bound MAM *trans* and *cis* geometries to measure distances between particular residues. This approach, which combined crosslinking experiments and molecular dynamics simulations, allowed a refinement of the crystallographic zfP2X4 structure, demonstrating that the large intersubunit crevices observed (encountered in chapter one, section 4.2), are likely artefactual.

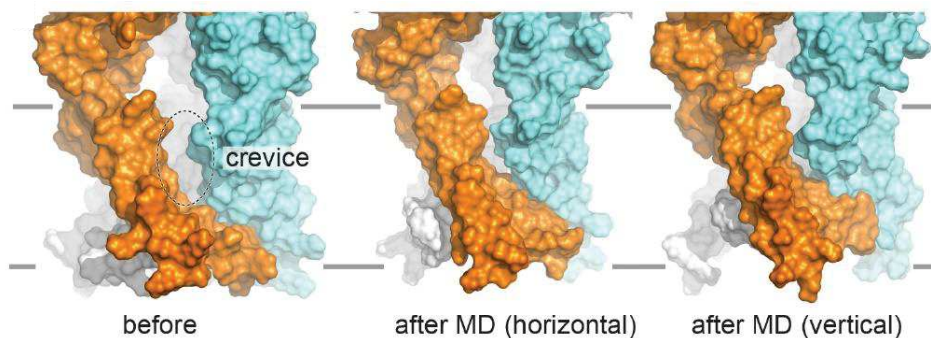


Figure 56. Refinement of the zfP2X4 crystallographic structure

A combination of molecular dynamics and horizontal and vertical crosslinking experiments with MAM enables the refinement of intersubunit distances observed in the crystallographic zfP2X4 structure, resulting in the disappearance of the TM-level crevices. From (Habermacher et al., 2016).

OBJECTIVES AND STRATEGIES

The demonstration of how these optogenetics-based methods allow not only optical control of P2X2 channels but also elucidation of molecular-level structural and mechanistic details raises the interesting possibility of application to study P2X structure and function in other subtypes and in other contexts. One of the key strengths of these methods is that, unlike classic PTL and PCL strategies, there is no channel-specific ligand involved. The targeting of the TM domains as opposed to a specific binding pocket means that these techniques should, in theory, be extendable to other P2X subtypes, and even to other ion channels. The global goal of the projects described in this chapter, therefore, was to install these new optical technologies for use with P2X7 receptors. Given the unusual structural distinctions of the P2X7 subtype, no structure of which was yet available during this project, in conjunction with its unique functional particularities and wide-ranging pathophysiological roles, the scope for an optically modulated P2X7 channel is unparalleled.

1. Optogating of P2X7

The first subsection of this project concerns the extension of the optogating method to P2X7. Following its initial development for use with the rat P2X2 subtype (rP2X2), application of optogating to other P2X subtypes was explored (unpublished work by *Dr. Damien Lemoine*). The *trans*-opener I328C, located within the TM2 domain, had previously been shown as a position which activates the channel when bound to sulfhydryl-reactive cationic MTSET reagent (Rassendren et al., 1997). This position exhibited the most stable and robust optogating, and sequence alignment of the TM2 region of all P2X subtypes shows that this isoleucine residue is conserved amongst the rat subtype variants (Figure 57).

		TM2
rP2X1	329	IPTMTTIGSGIGIFGVATVLCDDLLL
rP2X2	328	IPTIINLATALTSIGVGSFLCDWILL
rP2X3	319	IPTIISSVAAFTSVGVGTVLCDIILL
rP2X4	333	IPTMINVGSGGLALLGVATVLCDVIVL
rP2X5	334	IPTVINIGSGLALMGAGAFFCDLVLI
rP2X6	327	IPTAITVGTGAAWLGMVTFLCDLLL
rP2X7	331	IQLVVYIGSTLSYFGLATVCIDLIIN

Figure 57. Sequence alignment of the TM2 domain regions of rat P2X subtypes 1-7
Conserved isoleucine residue, corresponding to I328 in P2X2, is highlighted in yellow.

Robust optogating was achieved for all homomeric P2X subtypes by tethering at the equivalent position to I328, with the exception of rP2X7 (Figure 58).

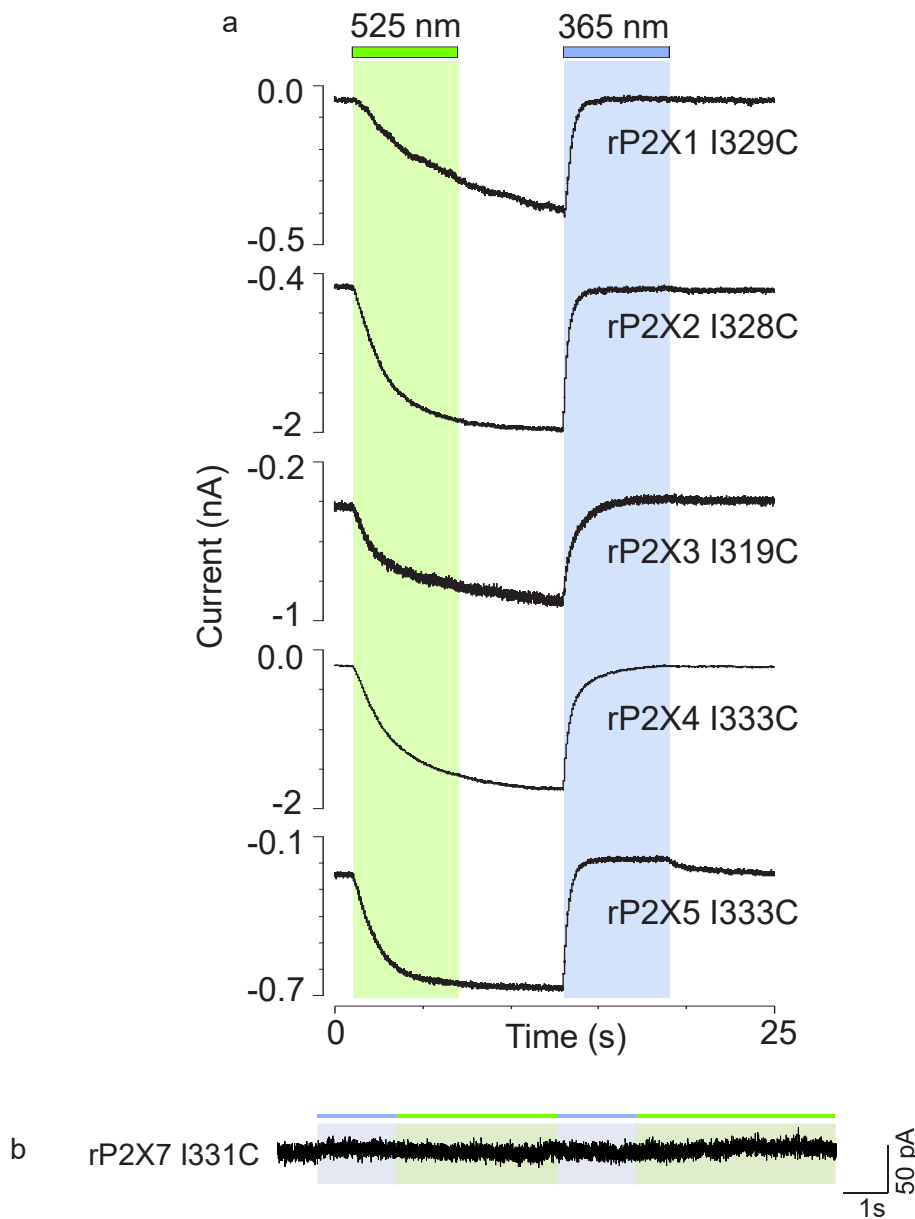


Figure 58. Extension of optogating to other homomeric P2X subtypes

(a) Robust light-controlled openings are possible when tethering to a cysteine introduced in place of the conserved isoleucine position (equivalent to I328C in P2X2). Work of *Dr. Damien Lemoine*. (b) No light-gated openings are observed for MEA-TMA treated I331C mutant (equivalent to I328C in rP2X2R).

Given the fact that P2X7 is the least similar in terms of sequence, structure, and arguably also behavioural features, it is perhaps not surprising that tethering at this position, despite its success for other P2X subtypes, is not optimal for P2X7. The goals of this part of the project were therefore the following:

- (i) Extend the optogating technology to P2X7 receptors, by looking into other, potentially more effective tethering positions.

- (ii) Extend the optoblock strategy for the modulation of P2X7 channel activity and explore how this may be exploited to probe P2X7 structure and function.

2. Extension of optotweezers strategy to P2X7

Having been developed for use with the P2X2 subtype, the optotweezers strategy has not been employed to study other P2X variants. The primary goal in this part of the project was, therefore, to extend the use of MAM optotweezers as a technique for light control of P2X7. The secondary goal of this project, was to explore whether the motions involved in P2X7 gating, to be revealed using the optotweezers, are similar to those already determined to be involved in P2X2 gating.

The thesis work of *Dr. Laurie Peverini* included the development of a range of MAMs of variable length (MAM-1 – MAM-5), as well as MAMs featuring biphenyl groups to provide a greater extent of rigidity (MAMBP1, MAMBP2), shown in Figure 59. This provides a number of options to test with P2X7, in the event that MAM-3 (which was employed in the previous P2X2 example), is not suitable for light control of P2X7.

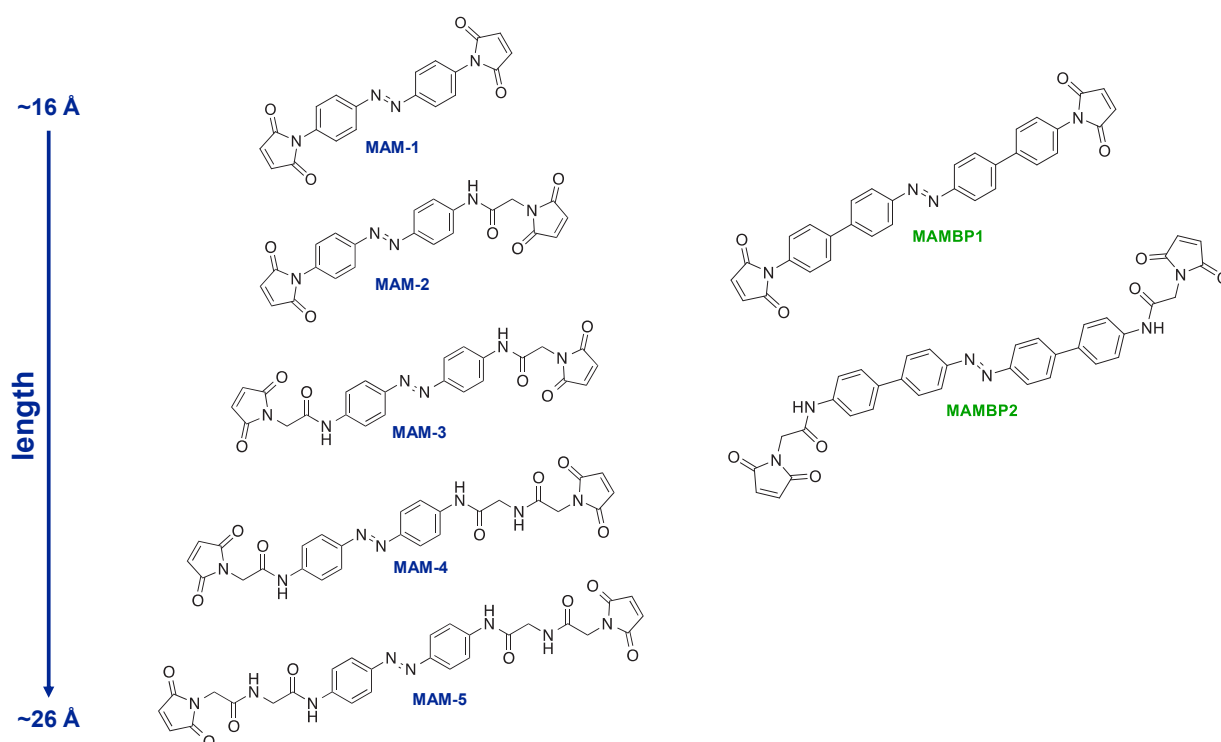


Figure 59. Range of MAMs of differing lengths and rigidities available for use.

Left, blue: range of MAMs with increasing lengths. Right, green: Biphenyl MAM variants of greater rigidity.

The projects described in this chapter were explored before the resolution of the rP2X7 structure and therefore were guided by the structures available at the time, zfP2X4.

3. Apparatus: irradiation-coupled patch clamp electrophysiology

In order to measure light-evoked P2X activity, an adapted patch clamp electrophysiology apparatus, whereby the set-up is coupled to LEDs, is employed. This system allows for irradiations at the required wavelengths of light in conjunction with electrophysiological recordings (Figure 60).

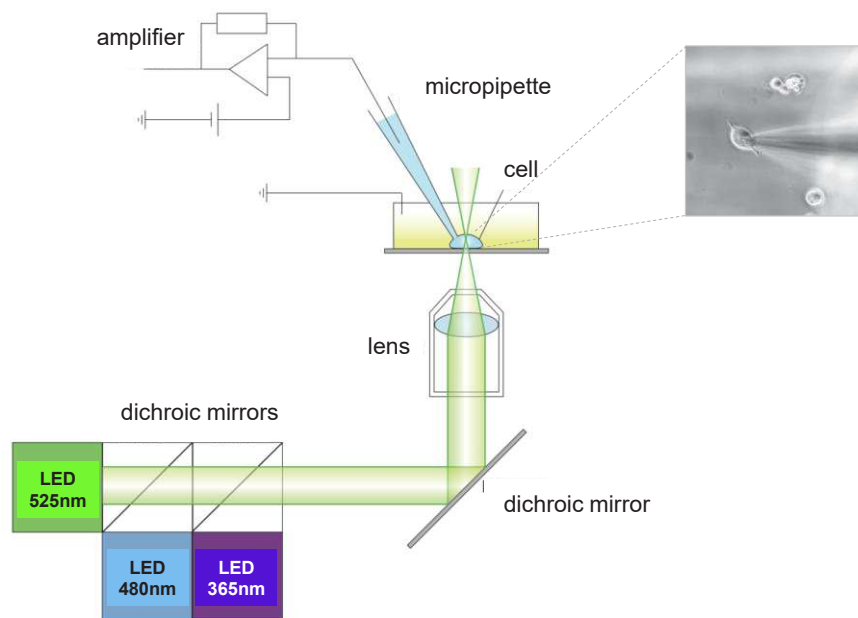


Figure 60. LED-coupled patch clamp electrophysiology apparatus.

EXPERIMENTAL SECTION

Cell culture

HEK293T cells (ATCC) were cultured in Dulbecco's modified Eagle's medium, supplemented with 10% foetal bovine serum, 1x GlutaMax, 100 units/mL penicillin and 100 µg/mL streptomycin (Gibco Life Technologies). Trypsin-treated cells were seeded onto 9-12mm glass coverslips (VWR) in 35mm dishes, pre-treated with poly-L-lysine (Sigma Aldrich). Cells were incubated at 37 °C and in presence of 5% CO₂.

Transfections

Transfections were carried out using the calcium phosphate precipitation method. The cDNA encoding rat P2X7 (rP2X7) constructs and enhanced Green Fluorescent Protein construct (eGFP) were contained within pcDNA3.1(+) plasmids (Invitrogen). For electrophysiological experiments, cDNA of rP2X7 constructs (1µg) was co-transfected with that of eGFP (0.3µg) in order to identify by fluorescence those cells which had undergone efficient transfection. Cells were used for electrophysiological experiments within 24 – 48 hours after transfection.

Patch clamp electrophysiology

Patch pipettes were pulled from borosilicate glass capillaries (Harvard Apparatus) to yield resistances of 3–5 MΩ. Cells were continuously bathed in normal extracellular solution (NES), containing 140 mM NaCl, 2.8 KCl, 2 mM CaCl₂, 2 mM MgCl₂, 10 mM glucose, 10 mM HEPES and adjusted to pH 7.32 – 7.33 with NaOH. Intracellular solution contained 140 mM KCl, 5 mM EGTA, mM MgCl₂, 10 mM HEPES, 10 mM glucose, adjusted to pH 7.32 – 7.33 with NaOH. All solutions used were maintained at approximately 300 mOsm. For recordings involving an ATP-evoked response, a solution of 1 mM or 5 mM ATP as indicated (disodium salt hydrate, Sigma Aldrich) in NES was employed, pH adjusted to 7.32 – 7.33 with NaOH. For inhibitors, solutions at a concentration of 20 µM (TA), 100 µM (DIDs) and 1 µM (AZ106) respectively in NES were used, again adjusted to pH 7.32 – 7.33 with NaOH if necessary.

Solutions were applied using a perfusion system comprising three capillaries placed above the cell of interest, which are displaced in order to bathe the cell in the desired solution. This is controlled computationally by a Werner Fast Step SF77B system, which ensures displacement of the perfusion capillaries in 5 – 10 ms. Cells were voltage clamped at -60 mV using the EPC10 amplifier (HEKA) and recordings carried out using PATCHMASTER (HEKA) software. Irradiation of cells was carried out using collimated LEDs directly coupled to the microscope

(Prizmatix). A UHP-Mic-LED-525 and a UHP-Mic-LED-365 were used, providing an output of 525 nm and 365 nm respectively, and the measured wavelength output intensities were 0.36 mW/mm² (for 525 nm) and 2.4 mW/mm² (for 365 nm). The switching on and off of the LEDs is controlled by TTL signals generated by the EPC10 amplifier.

Photoswitch labelling

For **MEA-TMA** labelling, cells were incubated for five minutes in a solution containing 200 µM MEA-TMA in NES containing ATP at a concentration of 125 – 300 µM depending on the mutant construct studied. This co-incubation with ATP is based on a protocol previously described, to increase accessibility of pore-located cysteine residues (Li et al., 2008).

For **MAM** labelling, cells were incubated for 20 minutes in a solution of NES containing 10 µM MAM and ATP at a concentration of 30, 125, or 300 µM (initial exploration of incubation conditions). MAMs were solubilised in DMSO and aliquoted into stock solutions, which upon use were diluted to ensure a final concentration of ≤ 1% DMSO.

Analysis

For electrophysiological data analysis, FitMaster (HEKA Electronics v2x73x1) and Igor Pro (WaveMetrics, v6.32A) were used. Experiments were repeated several times, over at least two independent transfections. For sequence alignments, Clustal Omega (*via* UniProt) was used. Figures showing the rP2X7 cryo-EM structure were created with Pymol software, using structures of accession numbers 6U9W and 6U9V.

RESULTS

1. Use of MEA-TMA photoswitch: optogating and optoblock of rP2X7

1.1. Optogating for light-controlled P2X7 activity

Guided by the previous work on optogating of the other rP2X homologs, we have chosen to target the upper TM2 region as a point from which to tether the photoswitch MEA-TMA, selecting eight residues surrounding I331, the equivalent residue to I328 in rP2X2R (Figure 61a and b).

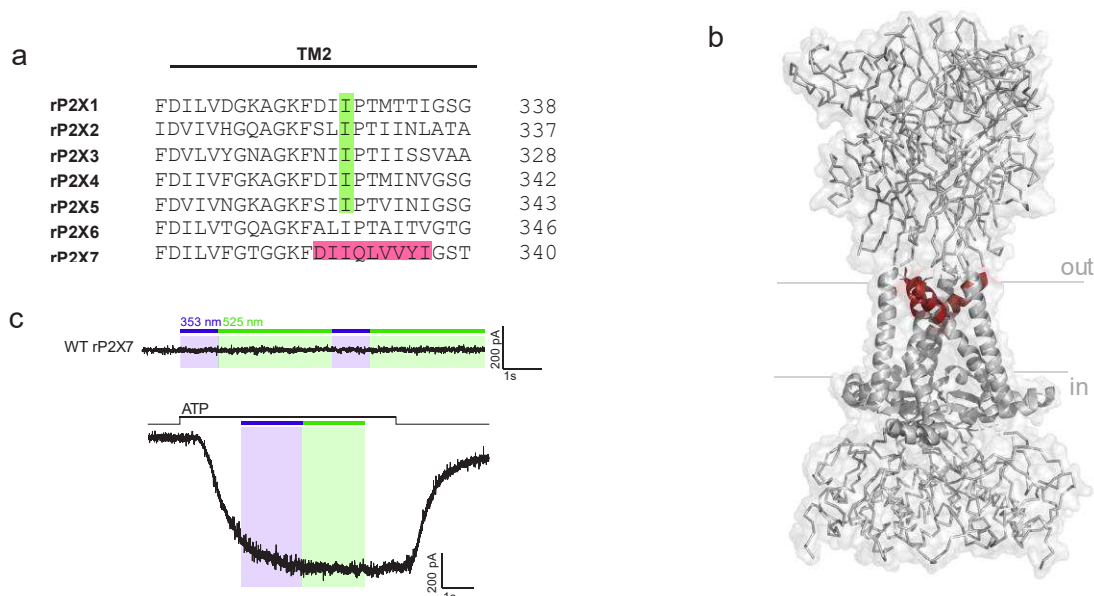


Figure 61. Strategy for rP2X7R optogating.

(a) Alignment of all rat P2X receptor subtypes (by Clustal Omega) with the conserved isoleucine residue used as a tethering point for optogating in Figure 58 highlighted in green. Residues of rP2X7 selected for mutation to cysteine to be screened for optogating activity are highlighted in red. (b) Structure of rP2X7 with the selected residues for cysteine mutation coloured in red, at the extracellular extremity of TM2. The TM regions are shown in cartoon representation, whilst the extracellular domain, cytoplasmic cap and ballast regions are shown in ribbon representation. (c) Representative whole cell electrophysiological trace from an rP2X7-expressing HEK293T cell treated with MEA-TMA. Upper: no light-gated currents are observed in the absence of ATP. Lower: No modulation of the ATP-response (1 mM) by UV and visible irradiation is observed.

For the rP2X2 receptor, a construct carrying three cysteine-to-threonine mutations was employed, in order to remove free endogenous cysteines (those not engaged in disulphide bridges) with which MEA-TMA may react. rP2X7 contains a large number of free cysteines, which have important implications for proper receptor expression and function (Gonnord et al., 2009; Kopp et al., 2019), and it is therefore desirable to limit genetic interference with regard to these residues. Consequently, we carried out an initial control whereby WT rP2X7R-expressing HEK293T cells were incubated with MEA-TMA and irradiated in the absence and presence of ATP to verify that MEA-TMA does not have an effect on the WT receptor. No optogating was observed, nor was an optoblock influence of irradiation on the ATP-response

(Figure 61c). This suggests that MEA-TMA does not tether to endogenous cysteines within rP2X7R, or, if indeed tethered, it exerts no effects on channel activity. We therefore created the series of cysteine mutants on this WT background.

Of the eight cysteine mutants tested, only one exhibited traces of optogating behaviour: V335C is a very weak *cis*-opener, showing UV light-gated openings of 0.76 ± 0.31 pA/pF, albeit not systematically (four out of seven cells). Although a comprehensive optimisation of incubation conditions at each position individually was not carried out, no other cysteine mutant exhibited light gated currents.

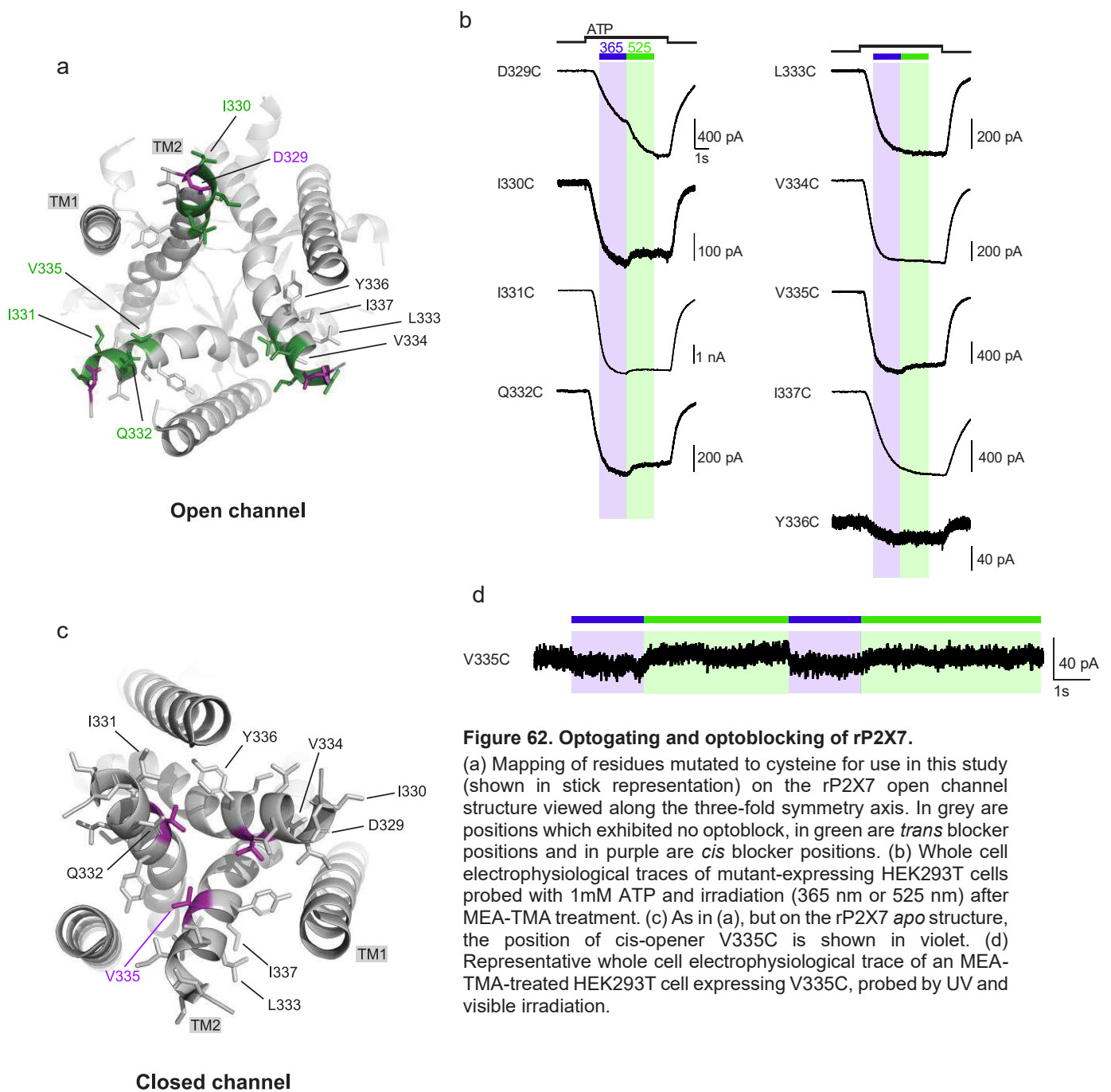


Figure 62. Optogating and optoblocking of rP2X7.

(a) Mapping of residues mutated to cysteine for use in this study (shown in stick representation) on the rP2X7 open channel structure viewed along the three-fold symmetry axis. In grey are positions which exhibited no optoblock, in green are *trans* blocker positions and in purple are *cis* blocker positions. (b) Whole cell electrophysiological traces of mutant-expressing HEK293T cells probed with 1mM ATP and irradiation (365 nm or 525 nm) after MEA-TMA treatment. (c) As in (a), but on the rP2X7 apo structure, the position of *cis*-opener V335C is shown in violet. (d) Representative whole cell electrophysiological trace of an MEA-TMA-treated HEK293T cell expressing V335C, probed by UV and visible irradiation.

In rP2X2R, *cis*-openers are mainly located at positions between TM1 and TM2 helices of the same subunit (Lemoine et al., 2013). Interestingly, in the closed state, V335 of rP2X7R is located in proximity to the TM1 domain of an adjacent subunit. Although it is difficult to imagine MEA-TMA disrupting intrasubunit TM2-TM1 interactions, it is possible that it is rather the intersubunit TM1 and TM2 interactions which are compromised by isomerisation of MEA-TMA to the *cis* configuration in rP2X7.

Following these negative optogating results, the modulation of MEA-TMA on ATP-evoked currents in the form of the optoblock was tested (Figure 62a and b). Several positions exhibited a modulation of the ATP response, although, as for V335C optogating, results were not reproducible in every cell. For Y336C, ATP-induced currents were of small magnitude, which rendered the interpretation of possible optoblock effects difficult. This is, however, at odds with the levels of functionality described in the literature for this mutant, where it is reported that Y336C exhibits activity similar to the rP2X7 wild type (Kim et al., 2001), which suggests that the conditions used for this mutant were perhaps not optimal. This same mutant in hP2X7 has a right-shifted ATP dose-response curve, and therefore we may need to repeat these experiments using elevated concentrations of ATP. Three mutants, L333C, V334C and I337C, systematically exhibited robust ATP currents which were unaffected by UV and visible irradiation, indicating that MEA-TMA is likely unable to tether at these positions. Previous work has shown that in hP2X7R, these residues, are also unmodified by MTSEA⁺, a small and positively charged sulfhydryl-reactive reagent (Pippel et al., 2017). Equally, in rP2X2, MEA-TMA does not exhibit a significant effect at the equivalent positions (Lemoine et al., 2013). Inspection of the location of these residues in the rP2X7 structure shows that in both the closed and open state, side chains are facing away from the ion pore and towards the lipid bilayer (Figure 62a and c). These observations are therefore consistent with the theory that MEA-TMA, a positively charged reagent of greater molecular weight than MTSEA⁺, is unable to access and label these residues. Again in contrast to rP2X2 optoblocking, whereby more internally located residues were *cis*-blockers and externally located pore facing residues were *trans* blockers, the majority of positions tested in rP2X7R, even those more internally located, are *trans*-blockers, with the exception of D329C, the most externally located residue, which exhibits a strong *cis*-blocking effect. This trend, as well as the difficulties encountered in engineering an optogated rP2X7R, underline the subtle differences that must exist between the pore architectures of these two subtypes.

The near-total absence of optogating observed in other mutants, but proof of cysteine accessibility to MEA-TMA by the presence of the optoblock, suggests that the use of these single upper TM2 cysteine mutants is likely not a viable technique for light control of rP2X7. As such, we decided not to carry out a comprehensive optimisation of the incubation

conditions, as the lack of initial promising results suggests that robust optogating would not be achievable even upon optimisation of the MEA-TMA labelling efficiency.

1.2. Use of a TM cavity-bordering tyrosine-to-serine mutation to enable P2X7 optogating

1.2.1. Background

In the context of thesis work carried out by *Dr. Juline Beudez* on the mechanism of MEA-TMA action, a P2X7 receptor carrying the double mutation I331C/Y343S was shown to be controllable by optogating (Figure 63 and Figure 64a). This work concluded that MEA-TMA is likely placed within the hydrophobic transmembrane cavities when in the *trans* configuration, disturbing interactions between the TM2 helices and resulting in an opening of the channel. Conversely to P2X2, which features a serine at the equivalent position, in the P2X7 receptor a tyrosine is present at position 343, bordering the transmembrane hydrophobic crevasses. This tyrosine is conserved amongst P2X7 orthologs (Figure 63b).

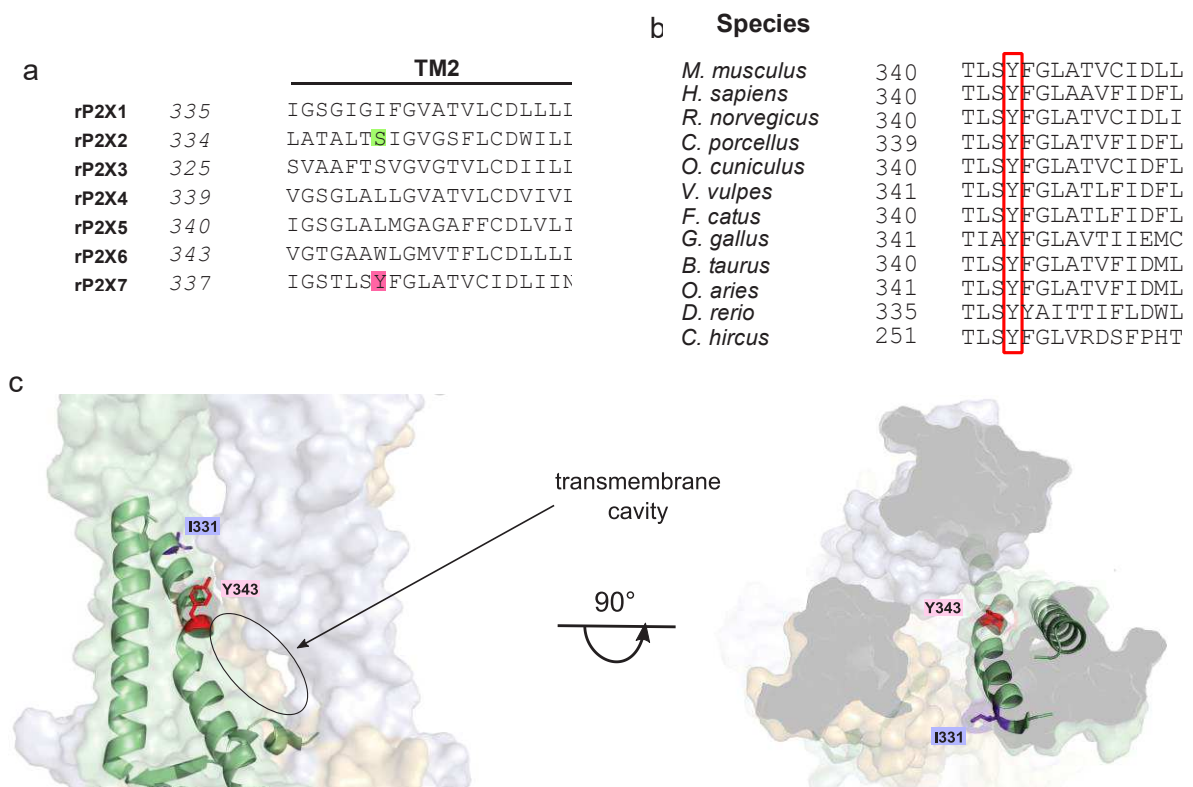


Figure 63. I331C/Y343S P2X7 mutant.

(a) Sequence alignment (via Clustal Omega) of the TM2 domain of all rat P2X subtypes. Highlighted in red is the tyrosine residue present at position 343 in rP2X7, and highlighted in green is the serine residue present in the equivalent position in rP2X2 receptor. (b) Sequence alignment (via Clustal Omega) showing the conserved TM tyrosine residue in the P2X7 receptor of various different species. (c) Lateral (left) and top-down along the 3-fold symmetry axis (right) view of rP2X7 receptor, with I331 residue (blue) and Y343 residue (red) sidechains shown in stick representation. The surface of all three subunits is shown, whilst only one protomer in cartoon representation is shown for clarity.

The presence of this tyrosine residue, which presents a bulky, aromatic side chain, likely prevents the placement of MEA-TMA between the TM helices, thus preventing optogating from taking place. When replaced by a serine, MEA-TMA would be able to slide efficiently into position to effect channel opening.

The use of this mutant receptor for light-controlled P2X7 channel activity was therefore further explored in the context of the current project.

1.2.2. Characterisation of P2X7 I331C/Y343S mutant optogating

The robustness of optogating using this I331C/Y343S mutant was assessed by recording light-gated currents from MEA-TMA treated cells, and comparing the current density to that produced by stimulation with a saturating concentration of ATP (1mM). As shown in Figure 64b, a current density of -3.15 ± 1.27 pA/pF was determined for optogated currents, whilst the corresponding ATP-gated currents from the same cells exhibited a current density of -13.6 ± 3.88 pA/pF. Currents produced by optogating represent on average only 20.7% of the corresponding ATP-evoked response.

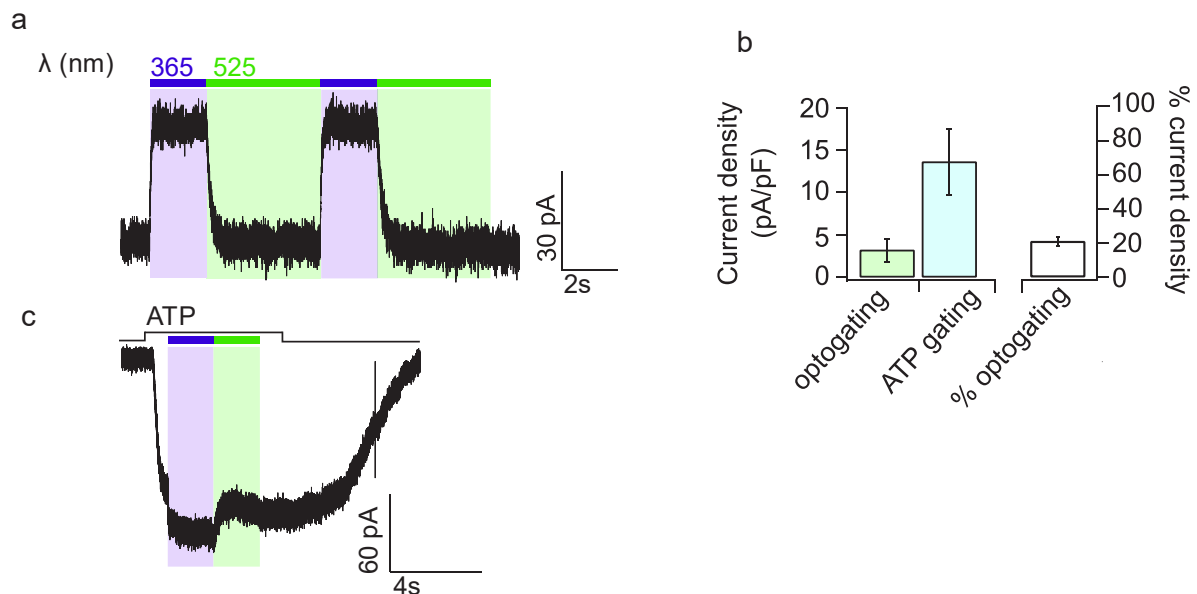


Figure 64. Optogating of rP2X7 mutant I331C/Y343S.

(a) Representative whole cell electrophysiological trace of light-gated currents produced by MEA-TMA treated I331C/Y343S rP2X7 mutant expressed in HEK293T cells, showing channel opening upon irradiation in the visible region and isomerisation to the *trans* isomer, and channel closing upon irradiation in the UV region and isomerisation to the *cis* configuration. (b) Histograms showing the inwards current density resulting from optogating and ATP-evoked gating (left, green and blue respectively) and the optogated current density as a percentage of the ATP-evoked current density produced in the same cell (right, white). (n=5) (c) Representative whole cell electrophysiological trace of MEA-TMA treated I331C/Y343S mutant, showing modulation of the ATP-evoked current (1 mM) by irradiation. This mutant exhibits *trans*-blocking behaviour, which is released upon UV irradiation.

In accordance with the single I331C mutant, *trans*-blocking behaviour was also observed for the I331C/Y343S double mutant, whereby ATP-induced currents were blocked by irradiation at 525 nm, when MEA-TMA is in the *trans* configuration. This block is released upon UV-induced isomerisation to the *cis* geometrical isomer (Figure 64c).

In an attempt to increase the magnitude of optogating, which is five-fold less than an endogenous saturating ATP response, we trialled the use of methyl- β -cyclodextrin (MCD), a cholesterol chelating agent, in conjunction with MEA-TMA treatment. Cholesterol, as an inhibitor of P2X7 present in the surrounding plasma membrane, can be chelated and depleted by the use of MCD, causing a dramatic increase in the magnitude of ATP-evoked currents (see chapter three for further details on this topic). We therefore considered whether removing cholesterol inhibition would equally provoke an increase in the magnitude of optogated currents. A number of incubation conditions were tested, with 5 mM MCD being applied either before, after or concomitantly to MEA-TMA treatment, for durations ranging from fifteen minutes to one hour. However, this two-reagent incubation rendered cells fragile and electrophysiological experiments virtually impossible due to instable patches. Only one exploitable patch which exhibited light-gated currents was obtained, from a 15-minute 5mM MCD incubation at 37°C prior to MEA-TMA treatment, and the current density resulting from optogating was -4.06 pA/pF, comparable to the average current density obtained with cells not having undergone cholesterol depletion. The use of MCD as a strategy to enhance optogated currents is not, therefore, effective.

Following this, optogating was explored in the presence of P2X7 inhibitors, the aim of this being to probe whether light-induced opening of rP2X7 I331C/Y343S mimics that which occurs physiologically. If movements induced by optogating are close to those which occur upon ATP-activation, no channel activity should be detected in the presence of inhibitors. For these tests, we employed inhibitors of varying nature (Figure 65a): AZ10606120 (AZ), a synthetic allosteric inhibitor with almost complete selectivity for P2X7 over other subtypes, which binds to an intersubunit hydrophobic pocket (Karasawa and Kawate, 2016); 4,4'-Diisothiocyano-2,2'-stilbenedisulfonic acid (DIDS), a known P2X7 and P2X2 inhibitor, as well as a broad-spectrum inhibitor of chloride channels, and finally tannic acid (TA). Tannic acid is a non-specific chloride channel inhibitor, and is employed in this context as an inhibitor of TMEM16s, a chloride channel protein partner of P2X7 which, when inhibited, transmits this inhibition to P2X7R (see chapter three for further discussion on this subject).

Optogated currents were observed in the presence of AZ, DIDS and TA (Figure 65b), suggesting that optogating of the I331C/Y343S mutant relies on “local” movements, and not

global motions taking place across the entirety of the receptor structure, which would be otherwise impeded by these inhibitors.

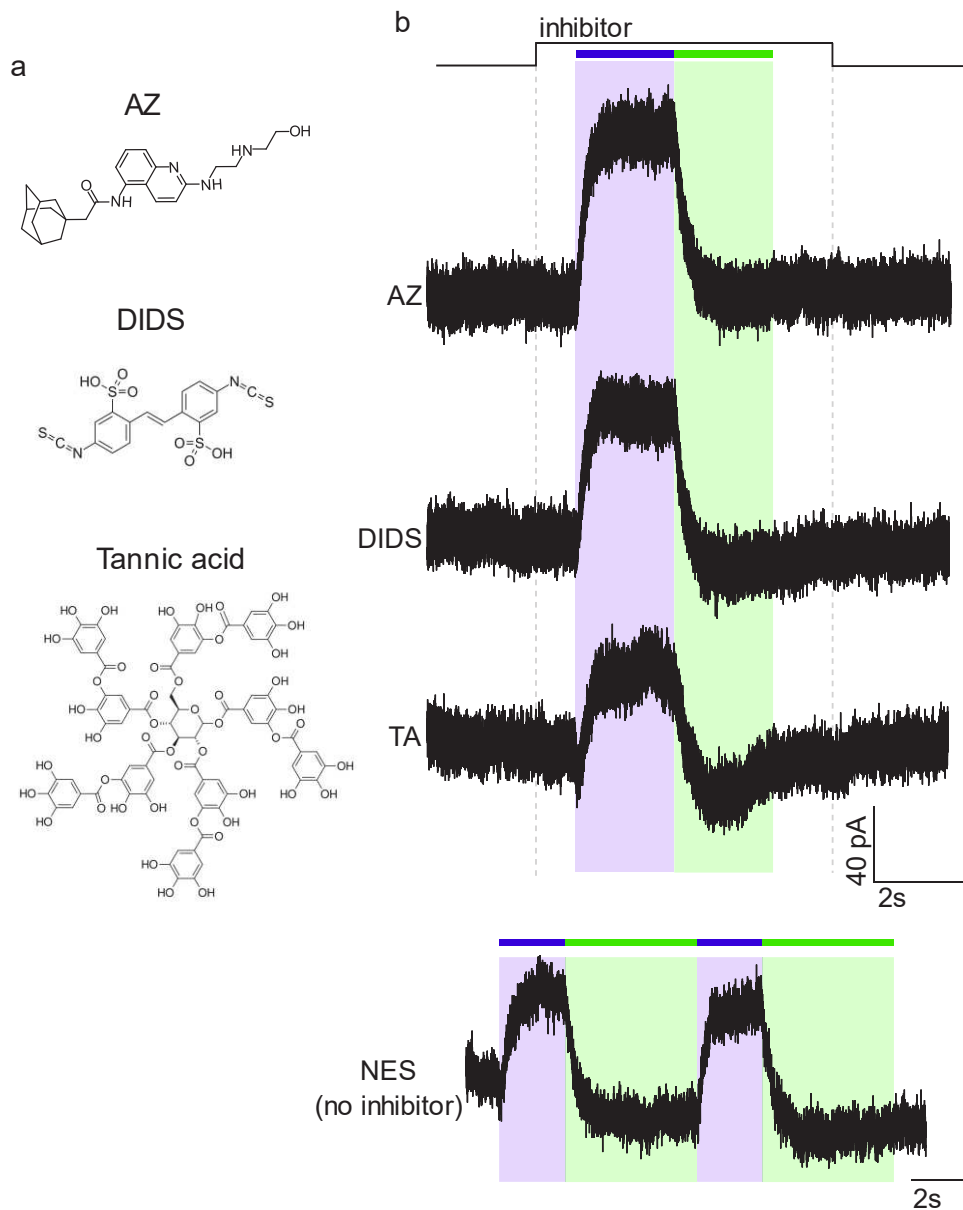


Figure 65. Optogating of I331C/Y343S P2X7 mutant in the presence of inhibitors.

(a) Chemical structures of various inhibitors of P2X7 activity. (b) Representative traces of whole cell electrophysiological recordings from I331C/Y343S P2X7 mutant-expressing HEK293T cells, treated with MEA-TMA. Upper: Irradiation in the UV and visible regions is carried out during a 6s-perfusion of the inhibitor compound. Lower: Irradiations are carried out in NES, in the absence of inhibitor. Concentrations of inhibitor are as follows: AZ 1 μ M, DIDS 100 μ M, TA 20 μ M.

These combined results demonstrate that the optogating strategy for P2X7 proves complicated. Of the single TM2 cysteine mutants, only one position, V335C, results in minute optogated currents. Whilst the double mutant I331C/Y343C exhibits optogating, light-induced current density remains only 20% that of the equivalent ATP-induced current density, and more

importantly, these light-induced openings have been shown to be likely non-physiological due to their persistence in the presence of P2X7 inhibitors. These factors therefore led us to the conclusion that it would be more interesting to focus on the second objective of this project, that is to exploit the optoblock character of MEA-TMA as a modulator of endogenous ATP-invoked P2X7 activity.

1.3. Use of optoblocking to investigate P2X7 facilitation behaviour.

Of the positions enabling optoblocking of rP2X7R, one showed particularly striking modulation of the ATP-evoked current: the *cis*-blocker D329C. This residue is the most extracellularly located of those tested, and is placed at the very beginning of the TM2 helices. Such a strong modulation may seem surprising for a residue at the extremities of the pore-lining helical domains, but when viewed laterally mapped onto the structure of rP2X7, it can be seen that D329 is in close proximity to the lateral fenestrations (Figure 66). These lateral fenestrations constitute the first portion of the ion permeation pathway, through which ions flow and are subsequently able to transit down the axis of the channel. It is therefore possible that, when in the *cis* geometrical configuration, MEA-TMA is able to modulate the ATP current by presenting a physical and/or electrostatic block across the lateral fenestration ion entry point.

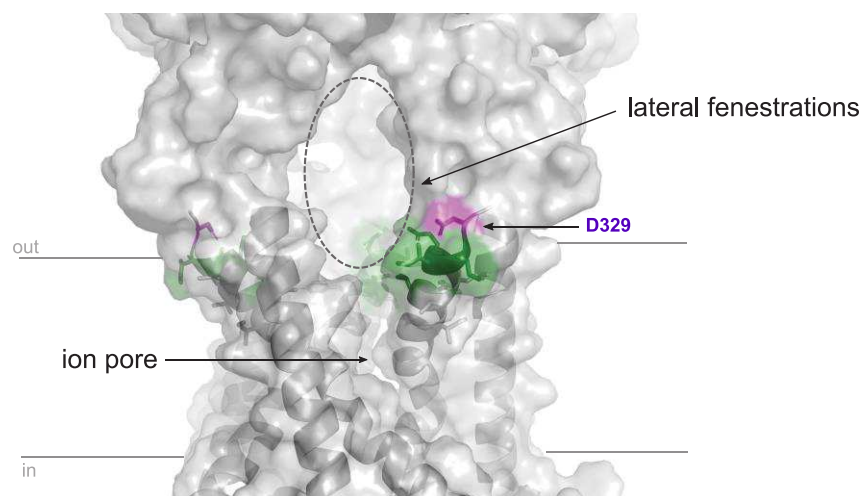


Figure 66. Lateral view of optoblocking residues on rP2X7R.

Structure of rP2X7 with cysteine mutants created for this project shown in stick representation, and coloured according to optoblock behaviour; grey indicates no detectable optoblock, green indicates a *trans* blocker and purple indicates a *cis* blocker. One of the lateral fenestrations is circled in grey dashed lines and indicated, and the ion pore is indicated.

Given the striking optoblock modulation of the D329C mutant, we questioned whether this may be utilised as a tool to investigate P2X7 function. During this PhD, as will be described in further detail in chapter three, we have been particularly interested in the phenomenon of facilitation.

The D329C mutant retains facilitation behaviour (Figure 67), and as such presents an interesting opportunity to probe this process using the optoblock tool. During the initial screening described above, we remarked that the *cis*-block profile of D329C changed with each subsequent application of ATP, coinciding with facilitation of ATP-evoked currents.

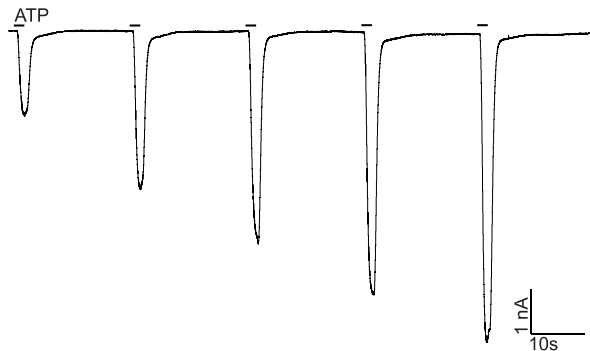


Figure 67. Facilitation profile of D329C mutant. Repetitive 2s applications of 5 mM ATP reveal a facilitation in the D329C receptor response, much like the WT.

We therefore devised a protocol whereby ATP was applied in conjunction with irradiation in the visible region (to “unblock” currents) and in the UV region (to “reblock” currents), shown in Figure 68. An initial brief irradiation in the UV region was carried out to commence the protocol with “blocked” receptors. This produced an ATP-evoked current comprising two components, which we named “ I_1 ”, the blocked current, and “ I_2 ”, the block-released current. Over the course of the protocol, these two components evolved in a differing manner; I_1 gradually increased in magnitude, reminiscent of a classic facilitation profile, whereas I_2 gradually decreased (Figure 68b).

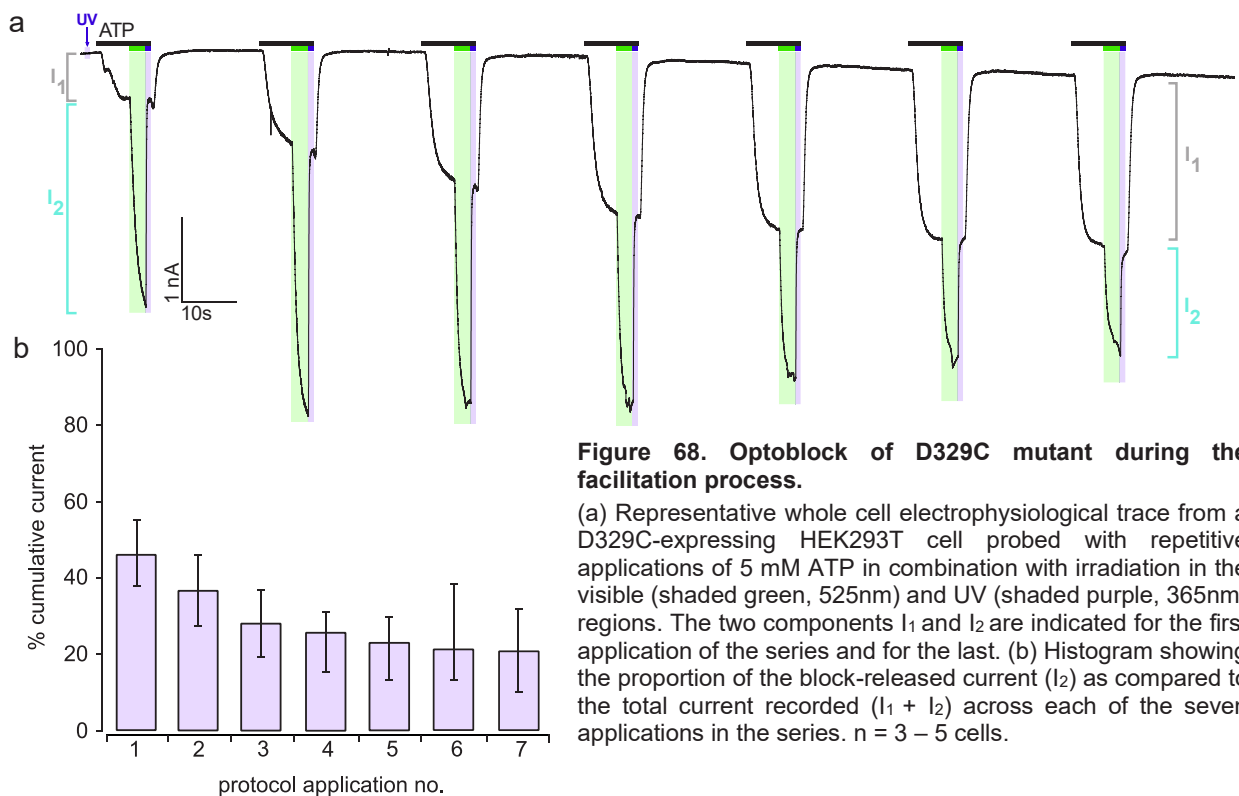


Figure 68. Optoblock of D329C mutant during the facilitation process.

(a) Representative whole cell electrophysiological trace from a D329C-expressing HEK293T cell probed with repetitive applications of 5 mM ATP in combination with irradiation in the visible (shaded green, 525nm) and UV (shaded purple, 365nm) regions. The two components I_1 and I_2 are indicated for the first application of the series and for the last. (b) Histogram showing the proportion of the block-released current (I_2) as compared to the total current recorded ($I_1 + I_2$) across each of the seven applications in the series. $n = 3 - 5$ cells.

These results reveal that two populations of rP2X7 are involved in the facilitation process, which evolve in different manners over the course of facilitation.

2. Use of MAMs: optotweezers strategy applied to P2X7

The second strategy explored in the context of light controlling rP2X7 was the utilisation of MAMs. Prior to the resolution of the rP2X7 cryo-EM structure, biochemical studies had shown the P2X7 pore to be permeable to nanometer size dyes (Browne et al., 2014), in contrast to rP2X2, whose pore diameter has been approximated to 11 - 14 Å (Eickhorst et al., 2002). We therefore decided in the first instance to probe the use of the optotweezers strategy by using MAM-4, as this variant features a second glycine group on one side of the central azobenzene, rendering it longer than the MAM-3 variant employed for rP2X2. However, during this initial phase of exploration, controls carried out on the WT rP2X7 receptor revealed sporadic visible *trans*-photoregulation of the receptor when treated with MAM-4, albeit of weak magnitude (Figure 69a, upper).

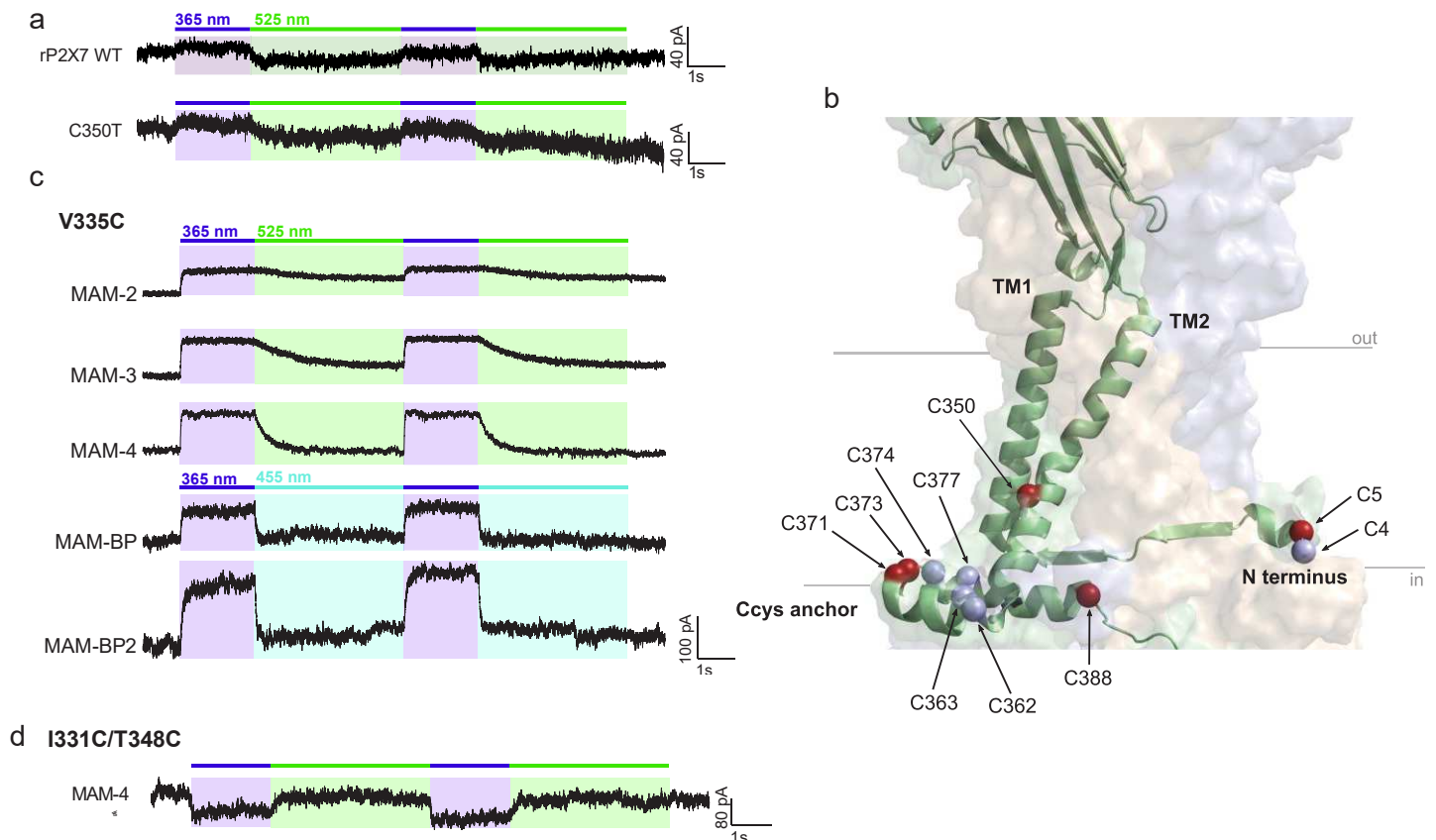


Figure 69. Photoregulation of rP2X7 by MAMs.

(a) Electrophysiological traces in whole cell configuration taken from HEK-293T cells expressing rP2X7 WT or C350T mutant, following MAM-4 treatment. (b) Structure of rP2X7R with free cysteine residues present in the N-terminus, TM2 domain and early C-terminus (Ccys anchor) in sphere representation. Coloured in blue are those cysteines shown to be palmitoylated in the cryo-EM structure, and in red those cysteines which are not palmitoylated. For clarity only one protomer is shown in cartoon representation, and the ballast region is not shown. (c) Electrophysiological traces in whole cell configuration taken from HEK-293T cells expressing V335C mutant, following MAMs treatment. (d) Electrophysiological trace of double mutant I331C/T348C after MAM-4 incubation, exhibiting *cis*-photoregulation.

In contrast to MEA-TMA, the MAM photoswitches do not feature a charged moiety, and as such have an increased hydrophobicity. It is therefore feasible that they are able to pass through the hydrophobic lipid bilayer, and access free cysteines which are found deeper within the pore and in the early cytosolic domains. rP2X7R contains 18 free cysteine residues, located in the N-terminus, TM2 domain and predominantly in the C-terminus. During this project, the structure of rP2X7 had not yet been resolved, and as such the precise spatial organisation of the cysteine residues within the N- and C-terminus was not yet available. We hypothesised that the cysteine residue C350, at the very end of the TM2 domain, was a probable candidate for endogenous MAM-4 tethering. In light of the now-resolved rP2X7 structure, the thiol side chain can be seen to point outwards towards the lipid bilayer, confirming the possibility that MAM-4 may attach at this point, following diffusion through the bilayer.

In addition, the presence of a lower TM2 cysteine is conserved among P2X subtype variants, and is one of the three cysteines residues mutated to threonine in the rP2X2-3T construction. We therefore created a threonine mutant C350T, and re-tested for photoregulation following MAM-4 treatment. Unfortunately, this construct also exhibited photoregulation, with 45.5% of cells patched exhibiting weak openings in the visible region of approximately -1 pA/pF. The residue C350 may still be involved in MAM-4 tethering, but given that mutating this position to threonine does not eliminate endogenous photoregulation, it is clearly not the sole residue to be involved. Although these openings are of very small amplitude, we cannot be sure of the exact cysteine positions involved in endogenous MAM-4 tethering.

Out of curiosity, we decided to carry out preliminary tests of MAM on genetically introduced cysteine mutants, without carrying out an extensive optimisation. We targeted the position V335C which had previously been the only position of those tested which proved susceptible to light-manipulation in the optogating project. This position exhibited photoregulation with a number of the MAMs (Figure 69c), although, similar to what is observed with WT and C350T mutant, the results were inconsistent and varied from cell to cell, even within the same incubation. Similar to the WT, channel opening is observed when each of the MAMs is in the *trans* configuration, however, the amplitude of these openings is greater than that observed with the WT and C350T controls, which suggests that openings are indeed produced by tethering to the desired V335C residue. We also briefly tested the mutant I331C/T348C with MAM-4 (Figure 69d), the equivalent to the I328C/S342C mutant used to probe vertical gating motions in rP2X2. In line with the results observed in rP2X2, channel opening occurred following UV irradiation and isomerisation to the *cis*-isomer, which would suggest the presence of a vertical shortening during the gating process. As with the single mutant, V335C, channel opening was not observed in all cells tested (approximately only 30%), and sporadic *trans*-openings were also recorded. Despite the glimpses of photoregulation observed in these

preliminary tests, due to the uncertainty over tethering position, we cannot exploit nor interpret these results any further. This, in addition to the small magnitude of photoregulation as compared to ATP currents, and the inconsistencies encountered surrounding labelling, led us to leave to one side the use of optotweezers as applied to rP2X7.

DISCUSSION AND OUTLOOK

1. MEA-TMA optogating and optoblock strategies

The use of the MEA-TMA photoswitch on rP2X7R presented mixed results. Regarding the optogating strategy, we have not managed to tailor the use of optogating for light-controlled activity of rP2X7. This may be due to a number of reasons. Firstly, it has been shown in the thesis works of *Dr. Chloe Habermacher* and *Dr. Juline Beudez*, by the use of concameters endowed with varying numbers of I328C mutations, that rP2X2 requires tethering of MEA-TMA on all three subunits to effect robust optogating. Equally, the optoblock phenomenon, whilst visible with only one tethered MEA-TMA molecule, is augmented as the number of tethered photoswitches increases. As we are able to observe optoblocking of the ATP response by MEA-TMA tethered at a variety of positions on rP2X7R, we can confirm that labelling does indeed occur, however, the extent of this labelling has not been determined. It could be speculated that, D329C, the most externally-located position, is the most easily accessible for labelling, thus explaining the striking optoblocking effect which is observed at this position but not elsewhere on the TM2-located cysteine mutants. However, the external location of this residue may also be the reason as to why optogating cannot be achieved; MEA-TMA tethered at this position is likely too external to the TM domains, and therefore unable to influence those gating elements located within. Those positions located more internally to the pore may present more effective options; indeed, V335C exhibits a light-induced *trans* opening, albeit of very weak magnitude. Whilst an optimisation of the labelling conditions could be carried out, in the event that not all three V335C cysteines are labelled by MEA-TMA, we are somewhat limited in the sense that incubations of over five minutes render the cells extremely fragile and electrophysiological recordings very difficult to carry out. The concentration of ATP with which to incubate was briefly tested, but, again, we are somewhat limited by the fact that rP2X7 receptors sensitise upon prolonged ATP exposure, causing a massive influx of cations into the cell, which eventually results in cell membrane blebbing and cell death. In addition, it has previously been shown that G345C, a pore-lining residue located much deeper within the channel, is dramatically covalently modified by MTS-Rhodamine when in the open state (Browne et al., 2013). This is a nanometer-sized MTS dye, larger than MEA-TMA, which renders less likely the theory that inefficient labelling is the origin of the absence of optogating at this position, although it is possible that precise side-chain orientation may have an influence.

The difficulties encountered in optogating rP2X7 underline the presence of structural differences between this subtype and the other members of the P2X family, which all exhibit robust optogated currents (Figure 58). There may be several structural elements behind this,

one of which being the bulky tyrosine residue located near the hydrophobic crevasses, Y343. The use of the I331C/Y343S mutant initially presented a potential solution, and explanation, to the difficulties encountered in the first stages of this project. As discussed in section 1.2.1, whilst the molecular mechanism behind optogating is not clearly resolved, previous work has indicated that it is likely due to the sliding of MEA-TMA in its *trans* configuration into the hydrophobic crevasses, disrupting interactions between TM helices and resulting in a channel opening. The presence of a tyrosine bordering these crevasses may represent a steric hindrance, preventing therefore the mode of action of MEA-TMA, at least when tethered at the I331C position. Equally, the presence of TM-bordering palmitoyl groups, revealed by the recently resolved rP2X7 structure, may also represent a possible source of steric hindrance impacting on MEA-TMA action.

We may speculate as to what other structural elements, in addition to steric hindrance from Y343 and palmitoyl groups, are behind the difficulties of optogating rP2X7R. One possibility is the TM-bordering cytoplasmic cap. The presence of a cytoplasmic cap has also been shown in the crystallographic structure of hP2X3 in the open state (Mansoor et al., 2016). Conversely to rP2X7, however, the cap is not observed in the *apo* structure, where these regions are presumably too flexible and disordered to be resolved. The cryo-EM structures of rP2X7R, on the other hand, demonstrate that the cytoplasmic cap is intact in both the *apo* and ATP-bound open state. We could speculate that the presence of this cap, which deeply intertwines the three subunits, reinforces the intersubunit interactions, rendering the disruption of these interactions and thus robust opening of the channel by MEA-TMA, particularly difficult.

Further to the actual implementation of rP2X7 optogating, it should be considered whether these light-gated currents are of physiological relevance, and use. Whilst optogating was observed in the I331C/Y343S mutant, it was of small magnitude, and of limited physiological similarity given the lack of inhibition by various compounds which have been shown to inhibit wild type, ATP-evoked P2X7 currents. This implies that the molecular motions by which optogating occurs do not imitate those which take place in physiological conditions upon binding of the endogenous agonist ATP, which would be prevented from occurring in the presence of these antagonists. Moreover, it has been demonstrated that for rP2X2, the calcium permeability of optogated openings is reduced 5-fold as compared to the wild type receptor (Lemoine et al., 2013). As a number of P2X7 physio- and pathophysiological behaviours involve Ca²⁺ mediated signalling pathways downstream of P2X7 (Adinolfi et al., 2009; Díaz-Hernandez et al., 2008; Gómez-Villafuertes et al., 2009; Yip et al., 2009), a similarly reduced calcium permeability in the case of P2X7 would render difficult the use of optogating as a means of probing its role in certain systems.

The optoblock, on the other hand, has proved to be of interest for probing rP2X7 function, specifically the facilitation phenomenon. The differential evolution of the two components, blocked I_1 and block-released I_2 , is indicative of the involvement of two different populations of rP2X7 receptors. The nature of these populations, however, remains to be identified. The notion of duality is one which is recurrent in the literature concerning P2X7, and many hypotheses may be made as to the nature of these two populations.

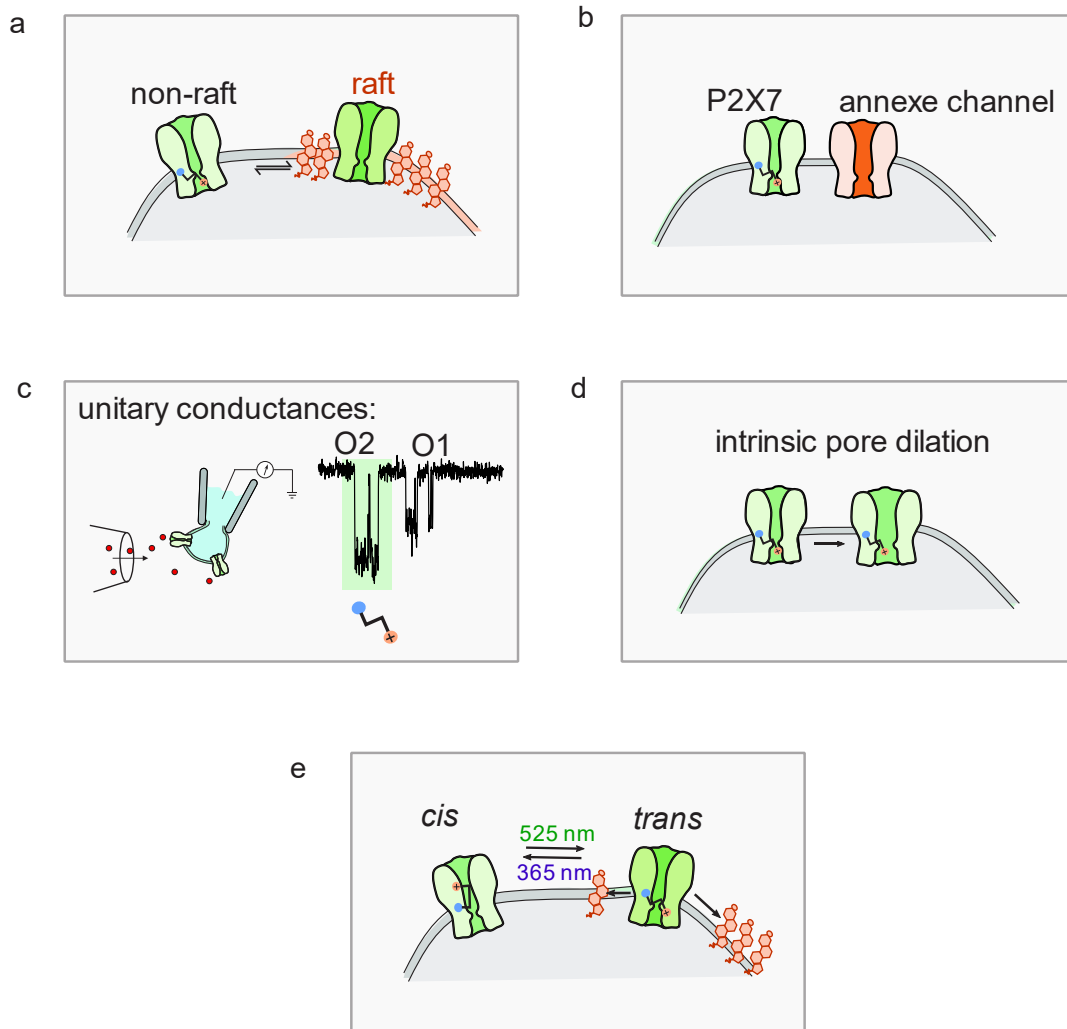


Figure 70. Hypotheses concerning the nature of the optoblock during facilitation.

(a) Scenario whereby P2X7Rs located in raft (dark green) and non-raft (pale green) domains are differentially labelled by MEA-TMA, and the equilibrium of these populations shifts during facilitation. (b) Scenario whereby the augmentation in current observed would be due to the recruitment of a non-labelled annex channel (orange). (c) Scenario whereby the unitary conductances of P2X7 are differentially modulated by the optoblock, and evolve differentially during the course of facilitation. (d) Scenario whereby an intrinsic dilation of the pore of a labelled P2X7R increases the current observed, and results in a decreased effect of the optoblock. (e) Scenario whereby the optoblock is in fact an 'apparent' current block, released by MEA-TMA entering into the membrane in the *trans* configuration and displacing cholesterol from its inhibitory TM position.

From a molecular viewpoint, hP2X7 exhibits two populations of unitary conductance, revealed by single channel recordings (Riedel et al., 2007). rP2X7 equally exhibits two distinct unitary conductance states, which we name O1 and O2, which is treated at length in chapter three. It would be particularly interesting to probe whether the optoblock affects just one or indeed both

of these conductances. It could be speculated that the optoblock selectively affects just one of the conductance states, and that these two species O1 and O2 therefore represent the two populations delineated by the optoblock in whole cell recordings, evolving in differing manners over the course of facilitation (Figure 70c). Such single channel experiments would also provide a more general opportunity to probe the precise mechanism of the optoblock on a molecular level, by observing the differences in ATP-induced single channel openings with irradiation in the UV and visible light regions.

This duality also exists in terms of membrane localisation. Dual populations of P2X7 receptors have been determined, in lipid raft and non-raft fractions (Barth et al., 2007; García-Marcos et al., 2006a). In HEK cells, the distribution of hP2X7 receptors in raft and non-raft fractions has been determined as 50% for each (Gonnord et al., 2009). Could these two populations revealed by MEA-TMA be due to differential labelling between raft and non-raft P2X7Rs, the distribution of which changes throughout the process of facilitation? Cholesterol, a known inhibitor of P2X7 and modulator of facilitation, is present at elevated concentrations in lipid rafts, and has been proposed to bind to the TM domain of P2X7 (Karasawa et al., 2017). It could be suggested that the presence of cholesterol around the TM domain results in conformational changes to the receptor, which in turn affects the efficiency of MEA-TMA labelling. We could speculate that raft-located populations of P2X7 are poorly labelled, whilst non-raft populations undergo effective labelling. Changes in the distribution of P2X7 within raft and non-raft domains during facilitation, specifically a shift of the equilibrium towards non-raft domains, would be consistent with the results obtained. This could occur whereby non-labelled, raft-located P2X7 receptors become more active upon removal from the cholesterol-rich raft environment, thereby adding to the I_1 current, without contributing to the I_2 block-released current, as they are unlabelled by MEA-TMA. This would explain the increase in current observed, coinciding with a decrease in the proportion of the optoblock. This remains, of course, speculative, and further experiments are required to test this hypothesis. MCD, which disrupts lipid rafts by chelating cholesterol, could be employed to influence the equilibrium of raft – non-raft localised P2X7Rs, however, previous work on the I331C/Y343S mutant (section 1.2) revealed that incubations of MCD and MEA-TMA combined rendered electrophysiological experiments complicated. One alternative could be to sensitise P2X7Rs using a long or repeated application of ATP, and then to carry out MEA-TMA treatment.

On the same premise as the above scenario, our results could also be explained by the recruitment of a secondary, annexed channel, which would contribute to the P2X7 current observed, but not undergo MEA-TMA labelling (Figure 70b). A wealth of protein partners have been proposed to associate with P2X7 (Kopp et al., 2019), amongst them the ion channels

TMEM16F and Pannexin-1. However, for the moment none have been demonstrated to contribute directly to BzATP or ATP currents.

The concept of intrinsic P2X7 pore dilation is equally one which evokes two populations of P2X7; one possessing a pore permeable to small cations and the second possessing a dilated pore, permeable to molecules of higher molecular weight, constituting the enigmatic P2X7 macropore. This concept, which is discussed elsewhere in this manuscript in detail, remains controversial in the literature, and as yet no structure of a dilated pore has been resolved. However, the slow progressive dilation of the P2X pore could fit these results, whereby the proportion of current blocked by MEA-TMA becomes progressively smaller as the diameter of the pore, and thus quantity of ions transiting through, increases dramatically.

A final hypothesis may be evoked to explain the results of the optoblock (Figure 70e). This possibility pertains to the fact that in several cells, like that shown in Figure 68a, the cumulative current obtained upon irradiation in the visible regions remains relatively stable throughout the series of applications. Although we did not have enough data to be able to analyse this for statistical significance, it raises an interesting possibility: MEA-TMA in the *trans* configuration is highly hydrophobic, and could easily be imagined to enter the membrane. As cholesterol is thought to interact with the TM domains of P2X7 (Karasawa et al., 2017), one could imagine that MEA-TMA enters the membrane, perturbing the interaction of cholesterol and the TM domains, effectively removing cholesterol inhibition and resulting in a fully facilitated current. This scenario, therefore, would not involve an actual physical block to ion flow, but rather, an apparent block whereby the block-released condition is in fact the physical displacement of neighbouring cholesterol by MEA-TMA. The two populations observed, therefore, relate to receptors surrounded by cholesterol, and those where cholesterol has been 'chased' away by MEA-TMA.

2. MAM optotweezers strategy

The use of MAM has proved complicated to implement for rP2X7 during the course of this project. The currents observed with MAM-2, MAM-3, MAM-4, MAM-BP and MAM-BP2 are of relatively small magnitude compared to currents evoked by ATP. In addition, and of most importance, the photoregulation of the rP2X7 WT receptor after MAM-4 treatment casts uncertainties on the precise tethering location of the MAMs with regard to the many endogenous juxtatransmembrane cysteine residues. As mentioned previously, at the time of this project, the structures of rP2X7 were not yet available, and as such the spatial organisation of this juxtatransmembrane region was not clearly defined. In light of the recently resolved structure, it can be remarked that a vast number of endogenous tethering possibilities exist. Although the ballast domain contains eight cysteine residues, they are unlikely to be implicated due to the fact that they are buried, mostly involved in Zn^{2+} complexation, and would also require MAM-4, a hydrophobic reagent, to enter the cytosol to reach these positions. According to molecular dynamics simulations (unpublished work of *Dr. Nicolas Calimet*, Cecchini group, University of Strasbourg), the S-S distance of MAM-4 in the thermodynamically stable *trans* isomer ranges from $\sim 15 - 30 \text{ \AA}$, with maximum probability corresponding to a length of 25 \AA . This is therefore consistent with the distances observed in the cryo-EM structure between a number of both intra- and intersubunit endogenous cysteine residues. Figure 71a shows that the distances between our targeted C350 residue and several nearby unpalmitoylated cysteines fall well within this range.

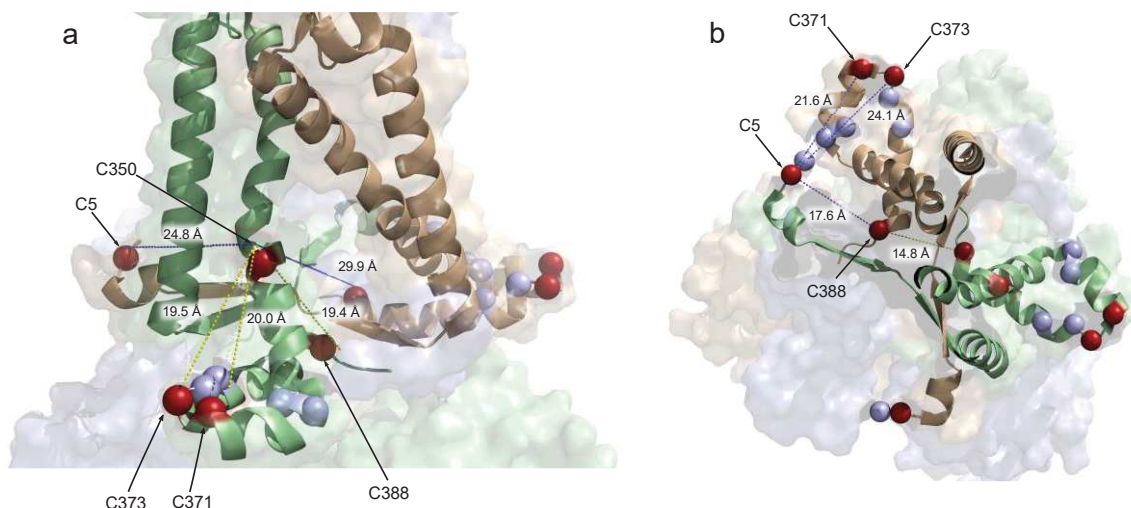


Figure 71. Possible sites of MAM tethering to endogenous cysteine residues in rP2X7

(a) Sideways view of rP2X7 focussed on the TM domains and early cytoplasmic region (N-terminus and Ccys anchor). Cysteine residues are shown in sphere representation; palmitoylated cysteines as according to the cryo-EM structure are coloured light blue and non-palmitoylated cysteine residues are coloured in red. Distances between C350 and other cysteines are displayed; yellow dashed lines indicate intrasubunit distances and blue dashed lines indicated intersubunit distances. For clarity, only two protomers are shown in cartoon representation. (b) As in (a), but from a top-down view point, along the 3-fold axis. Here, distances from C388 and C5 to other cysteine residues are shown.

Although the C350T mutation did not negate endogenous photoregulation by MAM-4, it cannot be discounted that MAM-4 may tether from C350 to one of these possible positions, and that the photoregulation observed in the WT originates from MAM-4 tethering at a number of different cysteine pairs. Shown in Figure 71b are the distances between several pairs of cysteine residues which could also be feasibly involved in MAM-4 endogenous tethering. C5 and C388 in particular exhibit several possibilities. To the best of my knowledge precise roles of C388 and C5 have not been reported in the literature. C5A mutation has recently been shown to respond to BzATP and exhibit a fractional calcium current similar to that of the WT (Liang et al., 2019), whilst C388A mutation has been shown to possess a cell surface expression profile similar to that of WT rP2X7 (Gonnord et al., 2009). Therefore, the mutation of these residues to threonine could be explored, and, if found to affect receptor functionality to a minimal extent, may present an effective choice of background onto which we could introduce the desired TM cysteine mutations for MAM tethering, similar to the rP2X2-3T background previously employed (Habermacher et al., 2016). However, given the roles of other cysteine residues present in the Ccys anchor in rP2X7 function, it would not be judicious to carry out threonine mutations at these positions.

In Figure 71 only the non-palmitoylated residues as shown in the cryo-EM structure have been taken into consideration as possible endogenous tethering points (coloured in red). However, it must be remembered that palmitoylation is a reversible process (Bijlmakers and Marsh, 2003), and discrepancies are found in the literature concerning the exact cysteines involved in palmitoylation (Gonnord et al., 2009; McCarthy et al., 2019). Therefore, it cannot be excluded that these residues (coloured in light blue) may also be involved in endogenous MAM tethering. The tailoring of MAM-4 for use with rP2X7 therefore proves to be extremely complicated, and not a viable strategy to achieve robust, rigorously controlled photoregulation of the receptor. Additionally, facilitation, a distinguishing hallmark feature of P2X7 channel activity, was not retained in the photoinduced openings shown in Figure 69c. This is therefore a major difference between ATP-gated and light-gated channel openings, and arguably renders inutile the use of the optotweezers strategy as a means to intrinsically control P2X7 channel activity in a close-to-physiological manner. The lack of clarity surrounding the tethering of MAM-4 to endogenous cysteines also renders unreliable any information which could be gleaned on the molecular movements involved in rP2X7 gating. Although the entire series of MAMs available was not tested against the WT, we decided that in light of the small current magnitudes, and inconsistencies encountered with respect to MAM labelling, we would not pursue any further the application of the optotweezers to rP2X7.

CONCLUSION

Considering together the optogating and optotweezers methods, neither has proved an effective means of light-controlling rP2X7 activity, in a way that would be of use in understanding the role of the receptor in wider biological systems, whether that be its role in a signalling cascade, or indeed its role in a specific cellular subset. The more interesting application of these tools, then, is not in the outright control of rP2X7 activity, but rather in the probing and modulation of ATP-evoked activity.

The use of MAM as a probe of rP2X7 gating motions has proven difficult given the tethering of the molecule to the WT receptor. However, it has been demonstrated that MEA-TMA and the optoblock provides the opportunity to probe P2X7 behaviour, here delineating two populations involved in facilitation. These results provide the initial basis from which chapter three, which focuses in detail on this unique characteristic, is developed. Due to time restrictions, the further experiments evoked within this discussion have not yet been carried out, but remain an interesting prospect to explore in the future. Future use of the optoblock could also be envisaged to probe other aspects of rP2X7 behaviour, for example, to investigate the pathway by which the passage of larger molecules, such as NMDG⁺, occurs across the P2X7 pore, or indeed, to investigate the intrinsic contribution of the channel to macropore formation, by measuring the incorporation of fluorescent dyes such as YO-PRO-1 or ethidium upon blocked or block-released conditions.

CHAPTER THREE: STUDIES ON THE PHENOMENA OF FACILITATION AND MACROPORE FORMATION IN P2X7 RECEPTORS

INTRODUCTION

The work described in this chapter constitutes the main focus of my PhD work. In light of the results obtained in chapter two, whereby the optoblock tool revealed the presence of two populations involved in the facilitation phenomenon, we decided to study further this enigmatic property which is unique to P2X7 receptors. In addition to facilitation, P2X7 receptors possess a second, highly curious property. This is the phenomenon of permeabilisation, whereby P2X7 activation renders the membrane permeable to species of high molecular weight *via* a “macropore”, the identity of which remains elusive. In this chapter, we aim to explore these processes and to consider the eventual participation of a secondary membrane protein, TMEM16 chloride channels.

In order to present this study in the most effective way, an introduction will first be provided to its context, discussing in turn (i) the facilitation phenomenon, (ii) the P2X7 macropore and permeabilisation phenomenon, and finally (iii) the TMEM16 family of ion channel/scramblases, a role for which may exist in these two processes.

1. Facilitation phenomenon of P2X7 receptors

1.1. Context

The facilitation of P2X7 receptors is one of the defining, hallmark features of P2X7 (Figure 72). It is characterised by a gradual increase in agonist-evoked currents, upon repetitive or prolonged application, accompanied by a 2.5-fold leftwards shift in the EC₅₀ value (rP2X7, (Roger et al., 2008)).

The time course of facilitation is concomitant to a number of cellular alterations, including phosphatidylserine translocation, mitochondrial swelling, loss of mitochondrial membrane potential, and membrane blebbing, which, although reversible, can lead to cell death (Adinolfi et al., 2009; Mackenzie et al., 2005; Pfeiffer et al., 2004; Verhoef et al., 2003).

This facilitation property is unique to P2X7 amongst the other P2X family members, which do not experience this significant increase in currents, but rather a current run-down, due to the process of desensitisation. Whilst facilitation has been observed in voltage-gated Ca²⁺ channels following repetitive stimulating pulses (Dai et al., 2009; Lee et al., 2000), to the best

of my knowledge, no other LGIC has been shown to possess this property in response to agonist application.

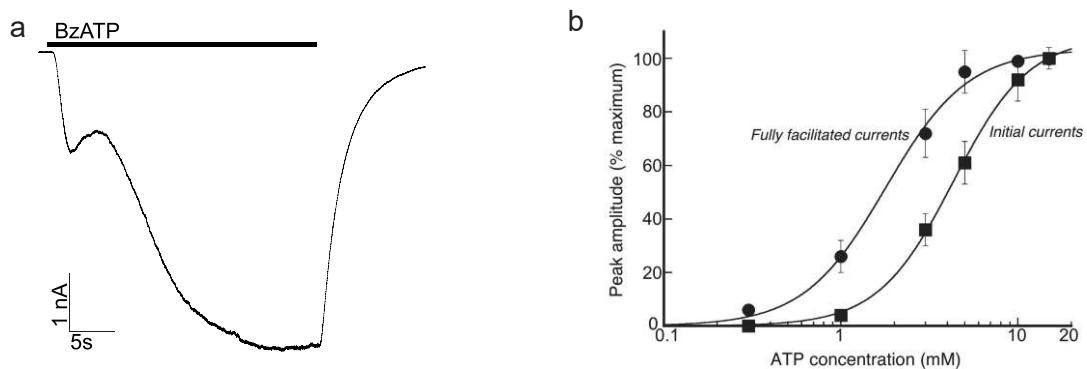


Figure 72. Characteristics of facilitation in rP2X7.

a) Electrophysiological recording from rP2X7-expressing HEK293T cells stimulated with 30s BzATP at -60 mV. (b) Taken from (Roger et al., 2008). Dose response curves for rP2X7 constructed from the initial current and fully facilitated currents, whereby the leftwards shift of EC_{50} can be observed.

A number of studies have revealed important details surrounding the facilitation phenomenon, however, this perplexing characteristic of P2X7 receptors remains rather understudied in the literature, at least in comparison to other facets of P2X function, such as macropore formation and desensitisation. Here will be discussed the most pertinent discoveries with regard to P2X7 facilitation thus far.

1.2. Modulation by cholesterol

Cholesterol has a varying effect across the family of P2X subtype variants (Murrell-Lagnado, 2017). P2X1 is highly sensitive to cholesterol, exhibiting an activity reduction of 90% upon treatment with cholesterol-depleting agent methyl- β -cyclodextrin (MCD), whilst P2X2, P2X3 and P2X4 have been shown to exhibit little cholesterol sensitivity (Allsopp et al., 2010). The influence of cholesterol on the activity of P2X1, has been indicated to occur not *via* a direct effect on channel gating itself, but rather an effect on the raft-associated actin cytoskeleton (Lalo et al., 2011). In contrast, cholesterol has been shown not only to strongly inhibit P2X7 current amplitudes, but also to modulate the facilitation phenomenon.

1.2.1. Cholesterol: a P2X7 inhibitor

Cholesterol exerts a striking modulatory effect on P2X7 receptors, which has been demonstrated primarily by the use of MCD. This cyclodextrin is particularly versatile, and when “empty” can incorporate membrane cholesterol, effectively depleting it from the cell membrane, or indeed can be “pre-loaded” with cholesterol, and used as a vehicle by which to deliver and

enrich the cell membrane with cholesterol. This action is the result of the intrinsic conical shape of cyclodextrins, featuring a hydrophobic cavity, where cholesterol may reside, and a hydrophilic exterior thanks to the presence of hydroxyl groups, which confers solubility to the cyclodextrin-cholesterol complex.

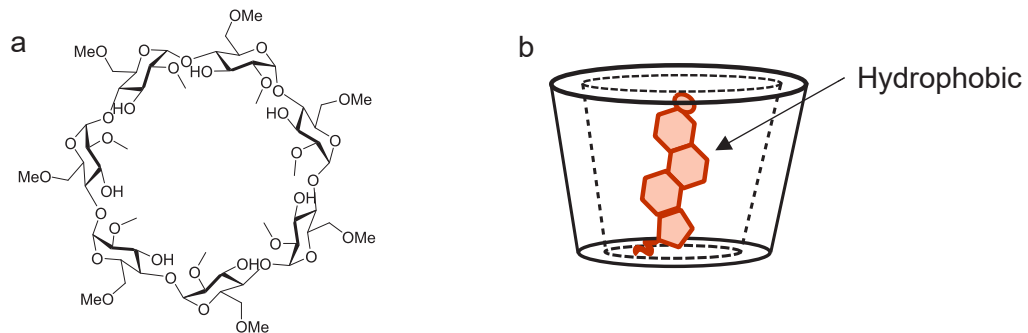


Figure 73. Methyl-beta-cyclodextrin (MCD) and its cholesterol chelating action

(a) Chemical structure of methyl- β -cyclodextrin (MCD) (b) Schematic representation of cholesterol (orange) residing within the hydrophobic cavity of MCD.

Work carried out by Robinson *et al* has employed MCD to explore the modulatory effect of cholesterol on facilitation in both rodent and human P2X7Rs. This study demonstrated that cholesterol depletion had a potentiatory effect on P2X7 current amplitude, as well as facilitation. Following treatment with MCD, currents recorded were of significantly larger amplitude, and remained relatively constant, reminiscent of a fully facilitated state (Robinson *et al.*, 2014). This effect was not the result of an increased surface expression following MCD exposure, nor was it linked to a perturbatory effect on the actin cytoskeleton, as observed in P2X1. This therefore was the indication that cholesterol exerts its effect on properties of the P2X7 channel itself. Notably, cholesterol depletion also resulted in an upregulation of ethidium dye uptake, indicative of a modulatory effect for cholesterol also with regard to permeabilisation.

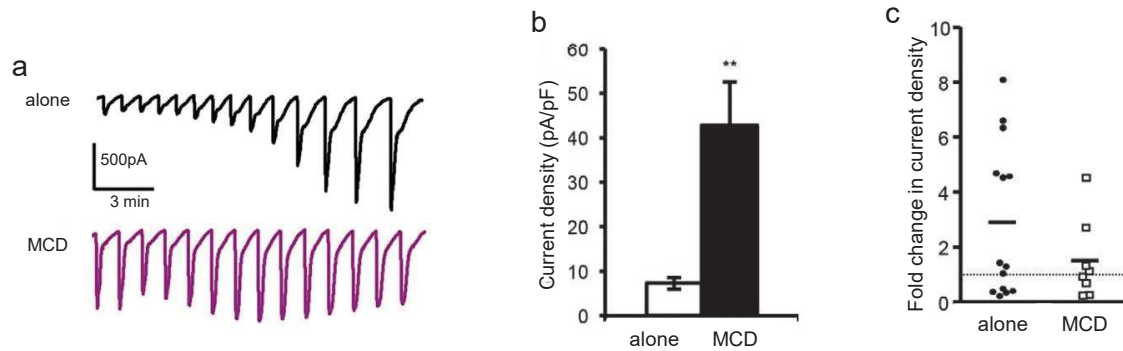


Figure 74. Modulation of facilitation and initial currents of hP2X7 by cholesterol depletion with MCD.

Taken from (Robinson et al., 2014). (a) Whole cell electrophysiological traces of HEK293 cells expressing hP2X7, either in standard conditions (labelled alone, black) or following MCD treatment (5 mM, labelled MCD, purple) upon BzATP stimulation (300 μ M). (b) Histogram showing the difference in current density upon the first agonist stimulation, with and without MCD treatment. (c) Representation of the fold-difference from first to last agonist application (>10), with or without MCD treatment. The solid line represents the mean, and dotted line is at 1.

Considering the potential molecular determinants behind this modulation of P2X7, Robinson *et al* identified four cholesterol recognition amino acid consensus (CRAC) motifs in the proximal C-terminus, several tyrosine residues within which were shown to have a cumulative effect on MCD sensitivity. This would argue in favour of cholesterol binding to the P2X7 itself, as opposed to modulating channel activity indirectly through some intermediate. In support of this, YO-PRO-1 uptake observed in liposomes containing reconstituted, truncated pdP2X7 receptors, was shown to be negatively correlated to the percentage content of cholesterol (Karasawa et al., 2017). This is further evidence that cholesterol is acting upon the P2X7 channel itself, and, given the truncation of this construct at both termini ($\Delta 1-21/\Delta 360-600$), probably on the TM domains.

1.2.2. P2X7 in cholesterol-rich lipid raft environments

Given the strong modulation of P2X7 channel properties by cholesterol, in particular its facilitation profile, it is interesting to consider the lipidic environments in which P2X7 is found, and whether cholesterol constitutes a key component. One such environment is of particular pertinence, that of lipid rafts. The plasma membrane is a heterogeneous and fluctuating environment, and lipid rafts are dynamic microdomains within the membrane, enriched in cholesterol, sphingolipids and glycerophospholipids. These regions are resistant to detergents (and are also known as detergent resistant membranes, DRMs) and can be found within the upper fractions of a sucrose gradient, exhibiting a low buoyant density, hence the name “rafts” (Lingwood and Simons, 2010; Pike, 2004). Several protein markers are associated with these microdomains, such as caveolin-1, which is present in special types of rafts called caveolae. As is the case for P2X1 – 4 receptors, P2X7 has also been found to associate with lipid rafts (Murrell-Lagnado, 2017). This has been demonstrated in both heterologous systems such as

HEK cells (Gonnord et al., 2009), as well as native receptors in mouse peritoneal macrophages (Gonnord et al., 2009), rat submandibular glands (García-Marcos et al., 2006a, 2006b) and mouse lung alveolar epithelial cells (Barth et al., 2007). In our system of study, HEK293 cells, mP2X7R was found to localise in equal proportions between raft and non-raft fractions (Gonnord et al., 2009).

Two hypotheses have been put forward as to how P2X7 may target to such lipid rafts, the first *via* an interaction with caveolin-1, which has been shown to co-immunoprecipitate with P2X7 in mouse lung epithelial cells (Barth et al., 2008; Weinhold et al., 2010), and secondly by palmitoylation of the P2X7 C-terminus (Gonnord et al., 2009). The direct interaction of TM proteins with raft-associated lipids is a known process named “wetting”, and facilitates their integration into raft regions (Lingwood and Simons, 2010).

The presence of P2X7 in lipid rafts is of particular interest owing to the wealth of lipid signalling pathways that are activated following P2X7 activation. These pathways are complex, and vary according to cell type, but various studies have shown that P2X7 activation is able in turn to initiate the activation of sphingomyelinases (SMases) (Bianco et al., 2009; García-Marcos et al., 2006a), phospholipase A2 (PLA₂) (Andrei et al., 2004; García-Marcos et al., 2006a) and *de novo* synthesis of ceramide (Lépine et al., 2006; Raymond and Stunff, 2006). Ceramide, produced either *de novo* or indeed by SMase hydrolysis of sphingolipids, has been shown to selectively displace cholesterol present in lipid rafts (Megha and London, 2004). In this way, a positive feedback loop can be imagined, whereby the disruption of lipid rafts upon P2X7 activation displaces raft-located receptors to less cholesterol-rich membrane environments, thereby increasing the activity of these receptors. Moreover, the activity of PLA₂ mobilises arachidonic acid, which has been shown to potentiate P2X7-induced Ca²⁺ influx in both native and recombinant systems (Alloisio et al., 2006), as well as lysophosphatidylcholine, which has been demonstrated to increase P2X7 agonist potency in recombinant and native systems (Michel and Fonfria, 2007).

Modulation of P2X7 activity by lipids and their signalling pathways is complex, and it is likely that the composition of the lipid environment represents a means of regulating P2X7 activity, which may vary between cell types and even dynamically within a cell. The precise pathways linking this lipid modulation to the facilitation phenomenon remain unclear, but are of interest owing to the possibility that this could represent an under-exploited therapeutic target. For example, Majeed syndrome, an autoinflammatory disease, is provoked by downregulatory mutations in *LPIN2*, the gene coding for lipin-2, an enzyme implicated in lipid metabolism. Strong evidence using macrophages taken from *Lpin2*^{-/-} mice, suggests that lipin-2 regulates the level of cholesterol, and therefore P2X7 activity. In the absence of this enzyme, P2X7

activity is disinhibited, and its activity sharply increased, resulting in an overstimulation of the inflammasome (Lordén et al., 2017).

1.3. Modulation by the Ccys anchor

The cysteine-rich region (also known as Ccys or Ccys anchor) is an 18-amino acid long motif located immediately after the TM2 domain, which contains 6 cysteine residues and is highly conserved between P2X7 orthologs. Before resolution of the cryo-EM structure in 2019, this domain had already been identified as an important contributor to P2X7 receptor function, and in particular to the facilitation behaviour. Constructs whereby various sections of this cysteine rich domain have been deleted have been studied. Deletion of C372 – V389 resulted in a construct with a 2-fold left shifted EC_{50} , which exhibited instantaneous currents similar to the WT, but with no observable facilitation, and a slight desensitisation in repetitive responses (Jiang et al., 2005; Roger et al., 2010a). Another study found that deletion of C358 – C375 in rP2X7 produced receptors unable to sensitise but which exhibited slightly, but not significantly, larger initial responses to BzATP (Yan et al., 2008). Meanwhile, deletion of C362 – C379 in hP2X7R resulted in a receptor exhibiting the same levels of surface expression as the wild type, but whose ATP-evoked currents were shown to be reduced by approximately 75%, and of rapidly desensitising nature (Robinson et al., 2014). The Ccys region is therefore involved in determining the facilitation or indeed opposing desensitisation profiles, but chimeric receptors of P2X1 and P2X2 carrying this Ccys motif failed to show an increase in current in response to prolonged ATP application, indicating that the Ccys anchor alone cannot induce facilitation (Allsopp & Evans, 2015).

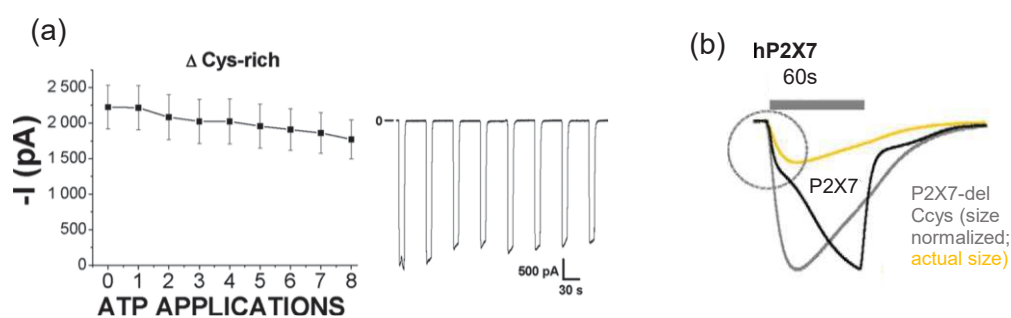


Figure 75. Characteristics of P2X7 receptors lacking the Ccys region.

(a) Analysis and representative whole cell trace of HEK293 cells expressing an rP2X7 construct lacking the Ccys region (C372 – V389), showing no facilitation behaviour with repetitive applications of 5 mM ATP. (b) Whole cell recording of HEK293 cells expressing hP2X7 and an hP2X7 construct lacking the Ccys region (C362 – 379), stimulated by 1 mM ATP.

The recently resolved cryo-EM structure of rP2X7 has shed further light on the role of this domain. The palmitoylation of a number of residues in the juxtatransmembrane regions,

including those within the Ccys domain, visibly serve to anchor the receptor tightly to the plasma membrane, into which the aliphatic chains of these palmitoyl groups extend and integrate. This is supported by the use of mutant rP2X7 constructs, featuring either a deletion of the Ccys region, or indeed, mutations of all palmitoylatable residues to alanine, an amino acid which cannot undergo this PTM. Both constructs exhibit a large desensitisation of ATP-induced currents, demonstrating that this motif modulates P2X7 channel behaviour, namely by preventing desensitisation.

The study of Karasawa *et al* provides a link between the work carried out on palmitoylation of the Ccys anchor and modulation of the P2X7 receptor by cholesterol. Using truncated pdP2X7 reconstituted into liposomes, they demonstrated that re-introduction of the cysteine rich region to this truncated construct could re-instate sensitivity to MCD, restoring dye uptake in the presence of MCD. This was attributed to the presence of palmitoylated residues, in particular C362, C363, C370.

Facilitation can therefore only occur when these Ccys anchor motifs are in place.

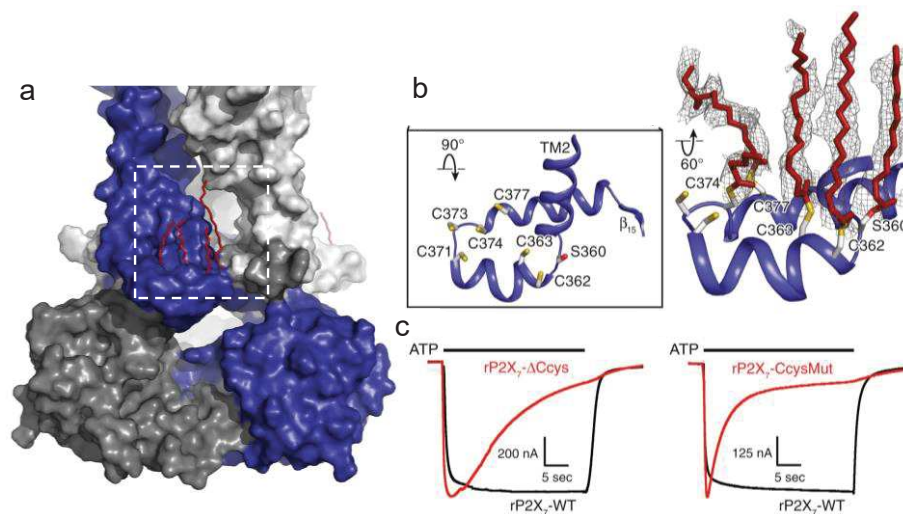


Figure 76. Location of Ccys anchor and behaviour of Ccys mutants.

(a) Cryo-EM structure of rP2X7 shown in surface representation, with the Ccys anchor region outlined in white dashed lines, and palmitoyl groups shown in red stick representation. (b) Zooms of the Ccys anchor region and the palmitoylatable residues indicated. (c) Whole cell electrophysiological recordings in *Xenopus* oocytes, comparing ATP responses of rP2X7 WT and Ccys mutant receptors, showing that either deletion of the Ccys region, or indeed the mutation of palmitoylated residues to alanine, induce a desensitising behaviour of the receptor. From (McCarthy *et al.*, 2019).

1.4. Modulation by Calmodulin

Two studies by Roger *et al* have demonstrated that Ca^{2+} plays a role in the facilitation process, *via* the intermediate of calmodulin (CaM), a calcium-sensing protein with wide-ranging physiological roles. The first of these studies determined two components to rP2X7 facilitation

in HEK293 cells; a Ca^{2+} -independent component and a second, Ca^{2+} -dependent component (Roger et al., 2008). The Ca^{2+} -independent process was determined to constitute 100% of the total facilitation at depolarising membrane potentials (+60 mV, zero calcium influx), and just 25 – 30% of the total facilitation at hyperpolarised potentials of -60 mV, as shown by the use of Ca^{2+} chelating compounds such as EGTA/BAPTA (Figure 77b), and the substitution of Ca^{2+} by Ba^{2+} in the bathing solution. This Ca^{2+} -independent process had faster kinetics than the Ca^{2+} -dependent components, reaching full facilitation more quickly. It was also suggested that this component is responsible for the leftwards shift in the ATP EC_{50} value following facilitation.

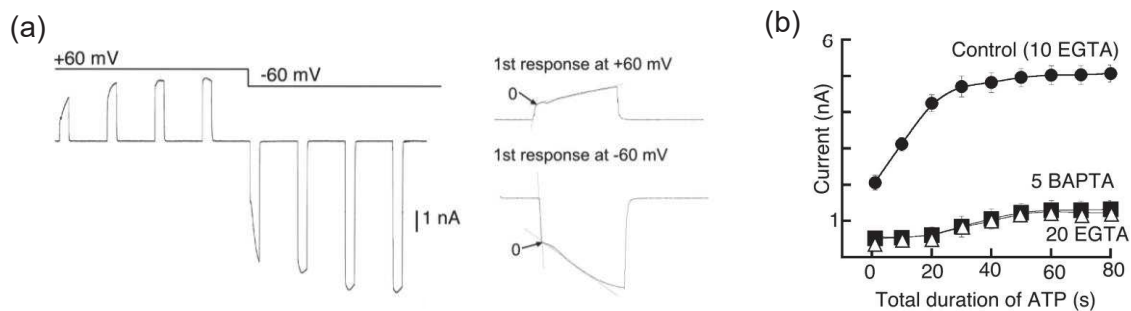


Figure 77. Calcium-dependent and -independent facilitation of rP2X7.

Taken from (Roger et al., 2008), (a) Whole cell electrophysiological recordings from rP2X7-expressing HEK293 cells stimulated with 10s repetitive applications of 5 mM ATP, at +60 mV and then -60 mV holding potential. (b) Evolution of current at -60 mV with respect to total duration of ATP application, with different composition of intracellular Ca^{2+} chelating buffers.

Concerning the Ca^{2+} -dependent component, it was demonstrated that this component is modulated *via* CaM, which is able to bind to the ballast domain in the C-terminus of rP2X7 by way of a 1-5-16 CaM binding motif. Mutation of two residues within this binding motif, I541T/S552C, abolished Ca^{2+} dependence, leaving only the Ca^{2+} -independent component present. Co-immunoprecipitation experiments revealed that CaM is constitutively bound to rP2X7 in the absence of ATP-stimulation, but that dynamic binding of CaM occurs upon rP2X7 stimulation, to significantly increase the amount of CaM protein associated with rP2X7 (Roger et al., 2008).

1.5. Species differences concerning facilitation

The second study by Roger *et al* looks further into the Ca^{2+} dependent component of facilitation, this time in the context of species differences between the rP2X7 and hP2X7 facilitation phenotypes. Facilitation occurs in hP2X7, although with much slower kinetics and smaller current amplitudes than in the rat equivalent (Figure 78). hP2X7 was found to exhibit only the Ca^{2+} -independent facilitation component, although, the Ca^{2+} CaM modulated

component could be installed in hP2X7R by recreating the 1-5-16 binding motif found in rP2X7R (Roger et al., 2010a). This mutant receptor was also found to bind to CaM by co-immunoprecipitation experiments, conversely to the WT hP2X7R.

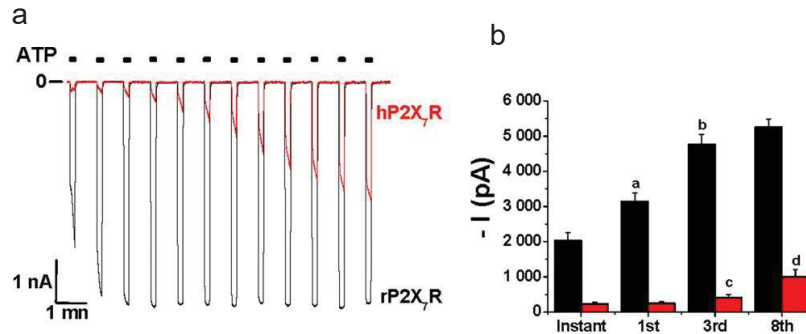


Figure 78. Difference in facilitation profile for rP2X7 and hP2X7 receptors.

Taken from (Roger et al., 2010a). (a) Whole cell electrophysiological recordings of HEK293 cells expressing either rP2X7R (black) or hP2X7R (red) stimulated by 5 mM ATP at -60 mV holding potential. (b) Histogram representation of the increase response following facilitation for hP2X7 (red) and rP2X7 (black).

1.6. Role of the N-terminus

The previously discussed zones of modulation are all found in the C-terminus, within the ballast region or within the 18-cysteine rich Ccys anchor. However, the N-terminus, although less documented, has also been shown to exert an influence over the facilitation profile of P2X7. The juxtamembrane N-terminal region was shown to exert an influence over the facilitation behaviour of hP2X7, by way of two residues; N16, present within a protein kinase C phosphorylation consensus sequence in the cytoplasmic cap, and S23, located at the very tip of the inner TM1 helix. These residues, when mutated to their equivalent residues in hP2X2 (that is, N16P and S23N), produce receptors exhibiting no facilitation. Equally, in rP2X7 receptors expressed in *Xenopus* oocytes, T15E, T15K and T15W mutants were unable to undergo facilitation (Robinson et al., 2014). The process of facilitation, therefore, relies on several intracellular features, and not solely the C-terminus.

1.7. General comments

The work discussed in this section highlights that the phenomenon of facilitation is complex, with modulation originating from a number of different sources, acting on different regions of the receptor. Whilst these studies have shed light on facilitation behaviour, the phenomenon remains unexplored on the molecular level, and a biophysical characterisation of P2X7 receptors in the facilitated state has thus far not been carried out.

2. The P2X7 macropore

A second, equally enigmatic characteristic possessed by P2X7 is the formation of a so-called macropore (or “pore formation”), rendering the membrane permeable to species of large molecular weight. This trait is not unique to P2X7; P2X2 and P2X4 have also been determined as permeable to organic cations and fluorescent dyes of high molecular weight (Khakh et al., 1999). However, this phenomenon is arguably of most interest in the context of the P2X7 subtype for several reasons. Firstly, the P2X7 subtype has been shown to permeabilise the cell to compounds of up to 900 Da, much greater in size than what has been observed with P2X2, P2X2/3 and P2X4. Unlike in these other subtypes, P2X7-induced permeabilisation is irreversible, and coincides with cell membrane blebbing and eventual cell death (Mackenzie et al., 2005; Virginio et al., 1999). Additionally, a role for the P2X7 macropore has also been evoked in P2X7-related pathophysiologies, thus rendering this phenomenon of potential interest from a therapeutic viewpoint (Di Virgilio et al., 2018b).

2.1. Brief historical context

The concept of macropore formation dates back to the discovery of the P2Z “cytolytic” pore (see also general introduction). Extracellular ATP had previously been observed to induce a concentration-dependent membrane permeabilisation effect, leading to the efflux of metabolites in rat mast cells (Cockcroft and Gomperts, 1979). In a variety of cell lines, this permeabilisation was observed with regard to a number of large molecules, including the dyes 6-carboxyfluorescein (376 Da), lucifer yellow (430 Da), fura-2 (636 Da) and indo-1 (645 Da) (Greenberg et al., 1988; Steinberg et al., 1987). Following the discovery of purinergic signalling (Burnstock et al., 1970) and P2 receptors (Burnstock and Kennedy, 1985), the entity behind this permeabilisation phenomenon was named the P2Z receptor (Abbracchio and Burnstock, 1994; Gordon, 1986). It was not until the first cloning of P2X7 from rat brain cells that the close homology link to P2X receptors was identified, and P2Z receptors reclassified as the seventh member of the P2X family (Surprenant et al., 1996). Since then, there has been a vast amount of literature published regarding the molecular mechanism behind macropore formation, which is often conflicting between different cell types. In general, two principal hypotheses have been evoked as to the identity of the macropore, which are not mutually exclusive (*cf.* Figure 22). The first is that macropore formation is the result of a slow, progressive dilation of the P2X pore to accommodate the passage of large organic molecules such as NMDG⁺ and dyes such as YO-PRO-1, whilst the second calls upon the contribution of a secondary, annexe channel(s) as the conduit(s) for such large molecular weight species. This will be discussed in more detail in section 2.3, but first, we shall consider the

methodologies employed to study this phenomenon, as these too have proved to be controversial.

2.2. Methodologies to study macropore formation and their caveats

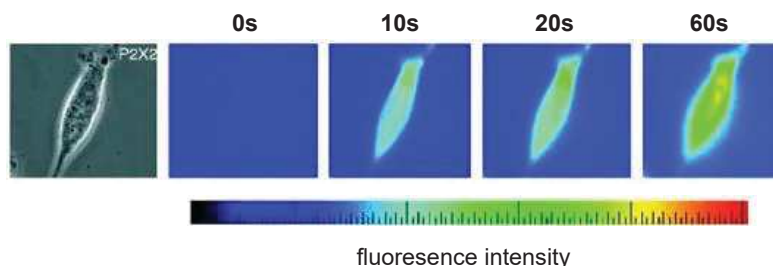
The permeability of P2X7 to large molecules and the formation of the macropore have typically been studied using two different methodologies.

The first of these is by way of electrophysiological recordings, observing the entry of large, organic cations and the changes in reversal potential of these species (E_{rev}) during extended receptor stimulation. One of the primary arguments for a progressive pore dilation mechanism was born from the observation that P2X receptors exhibited a progressively increasing permeability to larger, organic cations, such as NMDG⁺ or Tris⁺ (Surprenant et al., 1996; Virginio et al., 1999). This was typically demonstrated by a shift in the NMDG⁺ E_{rev} values from negative values to less negative values following ATP-activation. However, Li *et al* have determined that this shift in E_{rev} values is most likely artefactual, and the result of drastic changes in ionic concentrations during the prolonged ATP activation (Li et al., 2015). In brief, prolonged ATP activation of P2X2 in bi-ionic conditions results in the depletion of internal Na⁺ (from 140 mM to 20 mM), accompanied by an internal accumulation of NMDG⁺ (to over 200 mM). These changes in ion concentration are also influenced by parameters such as cell size, resistance access and the density of channels expressed at the membrane surface. As the equation of Goldman Hodgkin Katz, which is used to determine E_{rev} values, is dependent on ionic concentrations as well as ionic permeabilities, the drastic concentration changes observed in bi-ionic conditions renders the values calculated non-representative. For P2X7 receptors, this effect will be even more prevalent, due to the increase in the open probability of the channel upon removal of extracellular Na⁺ (Riedel et al., 2007a). It was demonstrated that under symmetrical ionic conditions (i.e. NMDG⁺_{out}/NMDG⁺_{in}), whereby drastic changes in ionic concentration did not occur, P2X2 receptors are permeable to NMDG⁺ on the same millisecond time scale as observed with Na⁺ (Harkat et al., 2017; Li et al., 2015). In light of this work, care must therefore be taken when interpreting results originating from electrophysiological experiments using bi-ionic solutions.

The second of these methodologies is the incorporation of fluorescent dyes into the cell upon P2X7 activation. This is typically achieved by use of fluorescent DNA markers, such as YO-PRO-1, ethidium or propidium dyes, which become fluorescent upon binding to DNA following entry into the cell. This may also be achieved by loading cells with a certain dye, and measuring its efflux.

Figure 79. Incorporation of YO-PRO-1 into HEK293 cells expressing rP2X2.

Taken from (Virginio et al., 1999). Incorporation YO-PRO-1 into rP2X2-expressing HEK293 cells upon 60s stimulation with ATP.



This technique has been employed to show a gradual formation of the macropore, with fluorescence appearing on the second time scale. Potential caveats of this method exist, however, again in the context of the pore dilation theory, where this gradual incorporation was previously attributed to a gradual increase in pore diameter. However, care must be taken with regard to this interpretation, as the fact that slower kinetics are observed during dye uptake may simply be due to the fact that the read-out signal of this technique develops more slowly. This, in combination with conformational and orientational factors which may influence the rate of large molecule permeation into the cell differentially to that of small inorganic cations, may not, therefore, necessarily be indicative of a gradual progression to increased pore size.

2.3. Classic theories behind macropore formation

2.3.1. Intrinsic P2X7 permeation

The pore dilation theory has long been under consideration as a possible mechanism behind P2X7-evoked large molecule permeability. This was largely due to the previously-described gradual changes in E_{rev} value, but work using alternative techniques, such as the atomic force microscopy (AFM) study of Shinozaki *et al* on P2X4, has also supported this theory.

Figure 80 shows time lapse AFM images obtained during this study, indicating conformational changes which seem to correlate to an ATP-induced dilation of pore diameter.

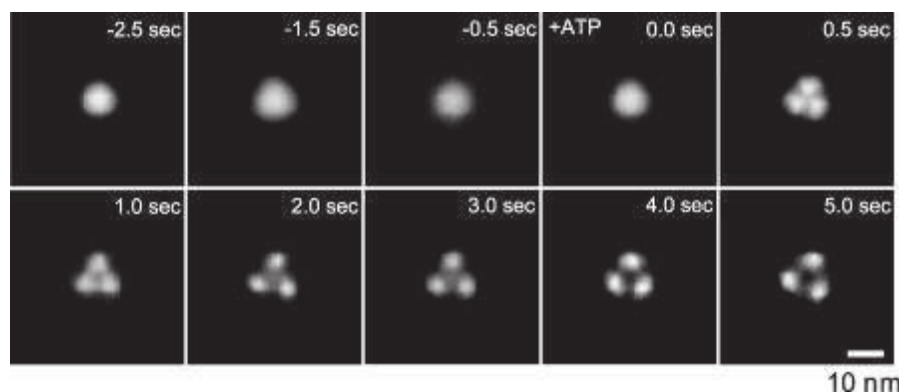


Figure 80. Fast-scanning AFM images of P2X4 receptor.

Time lapse images showing structural changes in P2X4 receptor following activation with ATP. From (Shinozaki et al., 2009).

In recent times, a number of challenges arguing against this theory have gained in traction. The primary study behind this is that of the Swartz group, discussed previously, who in 2015 published evidence demonstrating that the progressive shifts in E_{rev} values of large organic cations, interpreted as a progressive dilation of the P2X pore, were in fact artefactually induced as a result of changes in ionic concentration during electrophysiological recordings (Li et al., 2015). In line with this conclusion, work carried out in our laboratory on the pore dilation of P2X2 receptors has determined that an NMDG⁺ permeable pore is opened within milliseconds of ATP activation, on the same time course as Na⁺ permeation (Harkat et al., 2017). Equally, single channel studies of hP2X7, in *Xenopus* oocytes as well as in human B lymphocytes, have determined no changes to single channel conductance, nor reversal potential over the course of ATP application (Markwardt et al., 1997; Riedel et al., 2007, 2007). Also of note, is that no class averages portraying a pore-dilated state were observed during the cryo-EM study of rP2X7 (McCarthy et al., 2019). These works combined have therefore put into question the existence of an intrinsic, progressive pore dilation and its involvement in the macropore phenomenon.

It remains, however, a possibility that the P2X7 pore itself represents the macropore, but that it is rapidly, rather than progressively, permeable to large molecular weight species upon ATP activation. Previous work, using MTS-dye reagents and cysteine mutations within the P2X7 pore, has shown that nanometer sized dyes are able to directly pass through the pore (Browne et al., 2013). Reconstruction of truncated pdP2X7 into liposomes (where P2X7 is the only protein present, therefore) has shown that the pore itself is capable of YO-PRO-1 uptake, and that the efficiency of this uptake is highly sensitive to the lipidic environment (Karasawa et al., 2017). The latter study therefore revives the possibility that P2X7 may itself be the conduit of large molecular weight dyes, and may be modulated according to the surrounding lipids. However, as the cryo-EM structures suggest the open channel diameter to be ~5 Å, it is difficult to imagine that the passage of YO-PRO-1, whose minimal cross-section measures ~7 Å, in a robust and efficient manner takes place solely *via* the channel itself. Moreover, the passage of much larger molecules, such as TOTO-1 (795 Da) as has been described upon P2X7 activation, seems incompatible with this model (Cankurtaran-Sayar et al., 2009; Janks et al., 2019).

2.3.2. Recruitment of an annexe channel

The second hypothesis relating to the identity of the P2X7 macropore, is that macropore formation requires the recruitment of a secondary, accessory channel. Much data exists in the literature with regard to this hypothesis and much variation between cell types has been

observed. Several observations, however, have indicated the involvement of accessory proteins in the formation of the macropore. For example, no YO-PRO-1 dye uptake is observed upon ATP-stimulation of rP2X7-expressing *Xenopus* oocytes (Klapperstück et al., 2000; Petrou et al., 1997), which would suggest that a secondary channel is required for this activity. However, some studies have indeed observed uptake of YO-PRO-1 in *Xenopus* oocytes, rendering the literature conflicted on this point (Marques-da-Silva et al., 2011). Some other cell types, such as human B lymphocytes, have exhibited P2X7 channel activity, without observation of macropore formation and the associated dye efflux (Löhn et al., 2001). Other studies show differential effects of various conditions on the P2X7 channel activity and macropore activity, which would suggest that these two processes do not originate from a sole and unique protein. For example, colchicine, which disturbs the microtubule organisation within the cell, inhibited YO-PRO-1 uptake in both HEK293 cells and macrophages, without affecting current amplitudes (Marques-da-Silva et al., 2011). Equally, calmidazolium at the rat P2X7 receptor inhibits channel activity, but has no effect on YO-PRO-1 dye uptake (Virginio et al., 1997). Another interesting observation which suggests the involvement of an accessory protein, is the significantly different temperature sensitivities of ion channel activity, and macropore related dye uptake. Whilst channel activity and permeation of small inorganic cations is not affected by temperature variations, the uptake of Lucifer yellow was drastically impaired when temperatures were reduced from 37°C to 20°C (Nuttall and Dubyak, 1994; Steinberg et al., 1987).

In addition, there exist a number of P2X7 construct variants which exhibit differing effects on channel activity and dye uptake. Numerous examples of this exist within the extended C-terminus region. Deletion of 418 C-terminal amino acids produces a construct which is not different to the WT in terms of channel gating, but which exhibits reduced YO-PRO-1 uptake in HEK293 cells (Surprenant et al., 1996). Equally, removal of the 18 amino acid-long cysteine rich motif was shown to have no effect on YO-PRO-1 uptake, but to prevent the passage of NMDG⁺ (Jiang et al., 2005). Point mutations with differential effects also exist, such as the P451L mutation, which is a non-synonymous single nucleotide polymorphism (SNP) found in mouse P2X7R and known to be associated with reduced pain sensitivity (Sorge et al., 2012). This mutation has been found to reduce YO-PRO-1 uptake, whilst not affecting currents in HEK293 cells (Xu et al., 2012; Young et al., 2006). Interestingly, this reduction in dye uptake was no longer observed when the mutation was introduced into the P2X7k splice variant background. These differences would also support the hypothesis that a secondary annex channel is behind macropore formation, accounting for the differential effects of these variations on channel activity and large molecular weight dye uptake.

Finally, as P2X7 receptors have been determined to be poorly permeable to anionic chloride ions (Browne et al., 2013), the passage of an anionic dye through the P2X7 pore is also met with scepticism. In addition, the discrepancies between cationic dye and anionic dye permeation suggest that the P2X7 pore cannot represent a unified pathway, and even that cationic and anionic dyes may require two different accessory proteins to permeabilise the cell membrane. This is discussed further in section 2.5.

2.4. **Pannexin-1 as a possible annexe channel**

Initially, the most likely candidate for this annexe channel was pannexin-1 (PANX1), from the pannexin family of hemichannels. These are voltage-gated hemichannels, widely expressed in many different tissues, and permeable to small molecules (Barbe et al., 2006). In HEK293 cells, it was shown that when co-expressed, recombinant rP2X7 and PANX1 co-immunoprecipitate (Pelegriin and Surprenant, 2006). Additionally, siRNA knock-down, as well as carbenoxolone inhibition of endogenous PANX1 in HEK293, J774 and human lung macrophages significantly reduced P2X7-induced ethidium dye uptake, without altering current amplitude (Pelegriin and Surprenant, 2006). Whilst this data appears to identify the macropore-forming channel, subsequent works were in disagreement, and did not observe a dependency on PANX1 for macropore activity (Alberto et al., 2013; Hanley et al., 2012; Janks et al., 2019; Qu et al., 2011).

2.5. **Permeating species and characterisation**

It has been demonstrated that large molecular weight dyes of both cationic and anionic natures can permeate cells following P2X7 activation. As observed by Ugur and Ugur, the data in the literature show a tendency for permeabilities to differ when P2X7R is expressed in recombinant systems compared to P2X7R found endogenously (Ugur and Ugur, 2019), with recombinant systems primarily, but not exclusively, permeable to cationic species.

As mentioned previously, there are a number of discrepancies which suggest that there may be distinct, separate pathways for cations and anions. When ethidium and Lucifer yellow uptake was monitored in RAW264 macrophages, a sub-population of cells within the same sample was observed to only take up ethidium, whereas the majority of cells showed uptake of both dyes (Cankurtaran-Sayar et al., 2009). This could be indicative of separate uptake pathways for cationic and anionic dyes, which are differentially activated upon P2X7 activation. Schachter *et al* observed uptake of both ethidium and Lucifer yellow in macrophages, but only uptake of ethidium in HEK293 cells (Schachter et al., 2008). Additionally, different temperature sensitivities were observed for uptake of cationic vs. anionic dyes, pointing towards two separate uptake mechanisms being at play.

A non-comprehensive summary of species shown to pass the P2X7-induced macropore are portrayed in Figure 81.

2.6. General remarks

Despite a wealth of work carried out to understand the origin of the P2X7 macropore, the identity of physiological permeating species, and the implications for the macropore in cellular processes and pathologies, there remain many uncertainties with regard to this phenomenon. This is mostly the result of vast discrepancies between different studies and different cell types. In light of these differences, it should be kept in mind that perhaps a single, common mechanism behind the macropore does not exist, and instead, macropore formation, and its precise permeation characteristics, is modulatable according to the accessory protein partners within a particular cell type, as well as its membrane lipidic composition.

Cations			Anions			Neutral	
Species	MW (Da)	Charge	Species	MW (Da)	Charge	Species	MW (Da)
Na	23	1	D-glutamate	133	-	Doxorubicin	543
K	39	1+	L-glutamate	147	-		
Ca	40	2+	FITC	387	-		
Tetramethylammonium	74	+	Lucifer yellow	430	2-		
Tris ⁺	121	+	Fura-2	636	5-		
Spermidine	145	3+	Indo-1	645	5-		
NMDG	195	+					
Ethidium	314	+					
YO-PRO-1	375	2+					
Propidium	415	2+					
YOYO-1	763	4+					
TOTO-1	795	4+					

Figure 81. Identity of various species known to pass the P2X7 macropore.

(Browne et al., 2013; Cankurtaran-Sayar et al., 2009; Di Virgilio et al., 2018b; Duan et al., 2003; Faria et al., 2017; Fellin et al., 2006; Greenberg et al., 1988; Munerati et al., 1994; Schachter et al., 2008; Steinberg et al., 1987)

3. **TMEM16 channels : a possible P2X7 complex with implications for facilitation and macropore formation ?**

Recently, the suggestion that a family of calcium-activated chloride channels (CaCCs) may be involved in P2X7 activity, and more specifically, the formation of the macropore, has been made in several literature studies. Specifically, the involvement of TMEM16F, a member of the TMEM family of membrane proteins (also known as anoctamins) has been proposed in microglial cells, human and mouse macrophages, as well as HEK293 cells (Janks et al., 2019, 2018; Ousingsawat et al., 2015). This family of CaCCs, for which ten subtypes exist (TMEM16A, B, C, D, E, F, G, H, J and K), have diverse functionalities. Originally thought to be a family of chloride channels, it has been demonstrated that whilst TMEM16A and B act primarily as anionic, chloride permeable ion channels (Caputo et al., 2008; Schroeder et al., 2008), other members of the family exhibit lipid scramblase activity and even non-selective cation permeability (Alvadia et al., 2019; Di Zanni et al., 2018; Suzuki et al., 2013; Yang et al., 2012).

TMEM16F in particular has been well characterised as a lipid scramblase, a class of enzymes which disrupt the asymmetry of the plasma membrane by facilitating the movement of lipids between both leaflets of the membrane bilayer. (Alvadia et al., 2019; Schreiber et al., 2018). In terms of ion channel activity, TMEM16F has been shown to be preferentially permeable to cations rather than anions, and to be non-selective in this cationic permeability, producing Na⁺, Cs⁺, NMDG⁺ and TEA⁺-carried currents (Yang et al., 2012). Noise analysis of electrophysiological experiments also permitted to identify TMEM16F as a small conductance Ca²⁺-activated non-selective cation channel (SCAN), with a sub-picosiemens single channel conductance. Recently, the structure of murine TMEM16F has been resolved by cryo-EM, revealing a dimeric organisation featuring a subunit cavity in each monomer: membrane accessible aqueous vestibules which could facilitate the passage of polar lipid head groups across the hydrophobic core of the membrane (Figure 82). Although the precise mechanism of lipid scrambling remains unclear, these structures leave several possibilities open. It remains to be determined, therefore, whether scramblase and ion channel activity occur through the same pore (Alvadia et al., 2019; Feng et al., 2019).

Three principal papers describe a possible role for TMEM16F in modulation of P2X7 activity. The first of these, published by Ousingsawat *et al*, suggested the existence of a functional link between TMEM16F and P2X7 in a number of cell types (Ousingsawat et al., 2015). In *Xenopus* oocytes, siRNA knockdown of TMEM16F reduced recombinantly expressed hP2X7 currents by 45%, as did treatment with niflumic acid (NFA) and tannic acid (TA), non-selective chloride channel blockers.

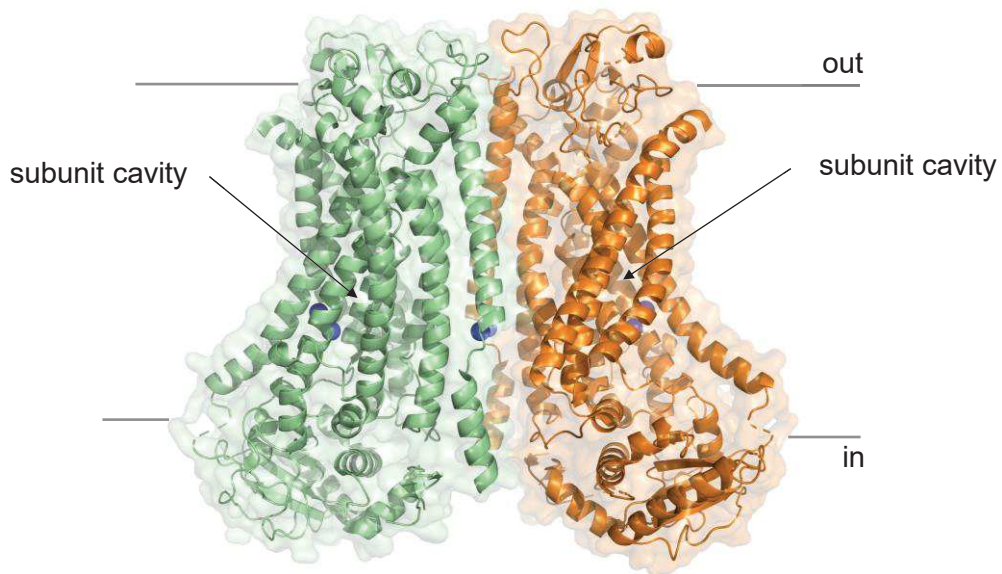


Figure 82. Cryo-EM structure of mTMEM16F.

Structure of mTMEM16F as resolved by cryo-EM in complex with Ca²⁺ (blue spheres). Each monomer is coloured differently, in cartoon representation and surface. The approximative positions of the subunit cavities are indicated. PDB: 6QP6. (Alvadia et al., 2019)

This was equally observed in HEK293 cells, where siRNA knockdown and pharmacological inhibition with TA reduced BzATP induced currents. In HEK293 cells, overexpressed P2X7 and TMEM16F could also be co-immunoprecipitated, indicating a close physical interaction. Regarding macropore formation, in HEK293 cells, YO-PRO-1 uptake was only weakly attenuated by siRNA knockdown of TMEM16F, but strongly inhibited by use of broad-spectrum chloride channel inhibitors. Single human THP-1 macrophages, on the other hand, exhibited inhibition of both YO-PRO-1 and fluorescein uptake when treated with siRNA to knock down endogenous TMEM16F expression. Finally, in mouse TMEM16^{-/-} macrophages, no BzATP evoked currents were observed, indicating that, in this particular cell type at least, TMEM16F appears to be fundamental for P2X7 activity. A model concerning the joint role of P2X7 and TMEM16F in macrophages was proposed (Figure 83).

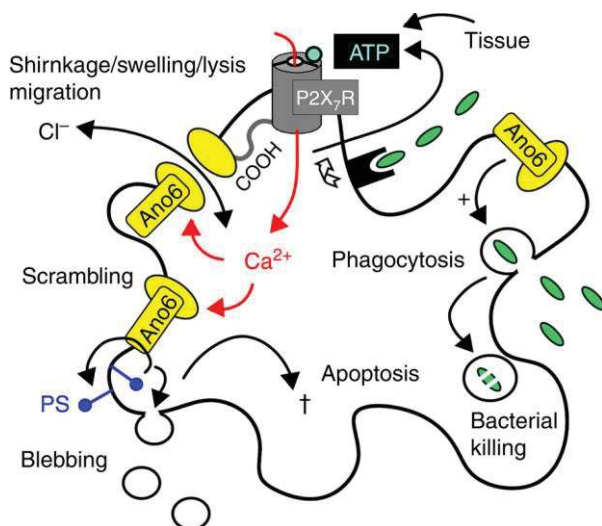


Figure 83. Possible P2X7/TMEM16F interaction mechanisms.

Model regarding the roles of TMEM16F (Anoctamin 6, Ano6) in macrophages. ATP activates P2X7R, triggering an influx of Ca²⁺, which activates TMEM16F. This has several consequences: activation of chloride currents, phospholipid scrambling, leading to plasma membrane blebbing and apoptosis. Activation of TMEM16F also supports the migration of macrophages, enhancing the opportunities for phagocytosis.

From (Ousingsawat et al., 2015).

Janks *et al* expanded on this work, studying a possible interaction in monocyte-derived human macrophages. In this cell line, YO-PRO-1 and YOYO-1 cationic uptake was observed, but unlike in THP-1 macrophages, no anionic dyes, such as Lucifer yellow and fluorescein, permeated in response to ATP stimulation. Use of general chloride channel blockers, such as TA, DIDS, NPPB and A01 inhibited the uptake of YO-PRO-1, and this dye uptake was also found to be dependent on PLA₂ activity, but not on intracellular Ca²⁺. However, again contrary to THP-1 macrophages, siRNA knockdown of TMEM16F had no effect on YO-PRO-1 uptake. TMEM16F does not thus appear to be implicated in macropore formation in monocyte-derived human macrophages. However, the inhibition observed by chloride channel blockers suggests that another chloride channel may be involved. Interestingly, TA also had an effect on ATP-induced currents, and these effects were different depending on whether the inhibitor was applied pre- or post-facilitation. Significant inhibition was observed when TA was applied following total facilitation, whilst TA applied before facilitation had taken place prevented the development of facilitation with subsequent ATP application (Figure 84).

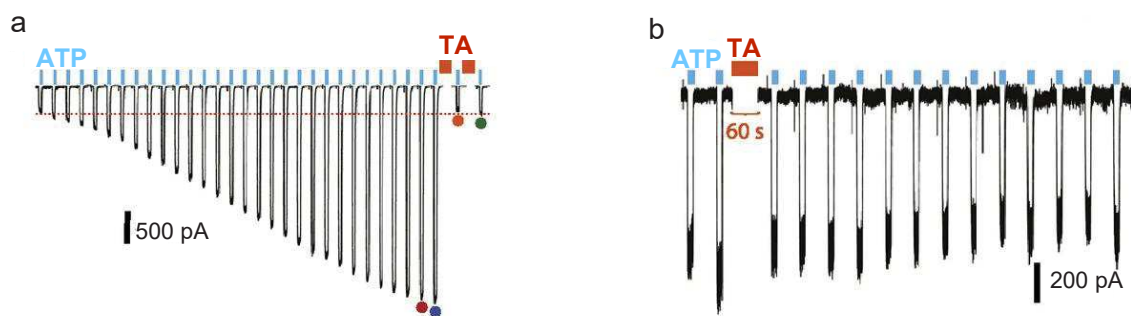


Figure 84. Effects of TA on facilitation of P2X7 currents in human macrophages.

(a) TA (20 μ M) applied after full ATP-facilitation (2 mM) of P2X7 currents sharply inhibits current amplitude. (b) TA applied before facilitation has occurred “blocks” the process and maintains currents at similar amplitudes following subsequent ATP stimulation. From (Janks *et al.*, 2019)

The third example investigating a link between TMEM16F and P2X7 was published by the same group, this time focussing on human microglial cells. Similarly to the previous macrophage study, only cationic dyes were taken up in microglia, in a Ca²⁺-independent manner, with the exception of the larger molecular weight YOYO-1, which could not permeate at all. YO-PRO-1 uptake was blocked by chloride channel blockers TA and DIDS, whereas these inhibitors had no effect on ATP-evoked currents, nor on facilitation (Figure 85). Dye uptake and channel gating therefore seem to be dissociated and independent processes in human microglia.

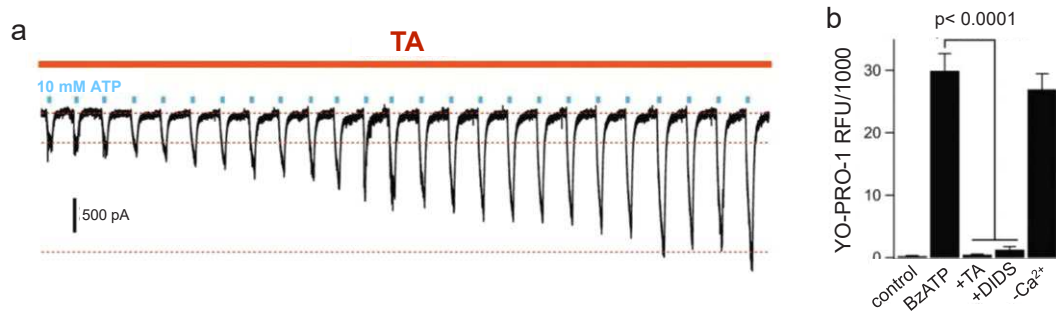


Figure 85. Effect of chloride channel blockers on P2X7 currents and YO-PRO-1 uptake in microglia.

(a) TA (20 μ M) has no effect on ATP (10 mM) evoked current facilitation in human microglia. (b) YO-PRO-1 dye uptake is inhibited by TA and DIDS but not dependent on calcium.

Whilst there is evidence for involvement of TMEM16s in P2X7 channel activity, major differences exist between the conclusions of these three studies. The identity of the P2X7 macropore remains to be definitively determined, and it should be kept in mind that the macropore may have a fluctuating identity according to cell type.

OBJECTIVES

As discussed above, the phenomena of facilitation and macropore formation represent some of the hallmark characteristics of P2X7R. However, many questions remain as to the mechanisms behind these processes, especially from a molecular point of view.

Facilitation has been characterised by whole cell electrophysiological recordings, but this provides an averaged view of the process, merging currents from the globality of P2X7Rs expressed at the cell surface membrane. As we have seen in chapter two, facilitation involves two populations of P2X7 receptors, differences between which cannot be resolved *via* the whole cell technique. How are “facilitated” P2X7 receptors characterised on the molecular level? Does cholesterol influence these molecular characteristics? And what are the precise differences between these facilitated receptors, and naïve P2X7Rs?

Considering the potential mechanisms behind these two phenomena, a number of possibilities could feasibly represent common pathways for both processes. An intrinsically dilating pore, although seemingly unlikely given previous work in the literature, could represent a pathway for large organic dyes, whilst also explaining the progressively increasing currents of facilitation. Progressive recruitment of an annex channel, which would act as the conduit for high molecular weight dyes as well as contributing to the facilitated P2X7 currents would also present a possible scenario. Whilst previous work in the literature has already considered whether macropore formation and P2X7 channel gating may share a common pathway, the relationship between the process of facilitation and pore formation has been much less explored. Thus the question is raised – to what extent, if any, are these two processes linked?

Finally, the connections between facilitation, macropore formation and a possible involvement of TMEM16 channels also remain unclear. Untangling these factors remains a challenge, due to the lack of specific pharmacological tools with which to do so, as well as a high variability between cell types.

This considered, three objectives were identified for the project covered in this chapter. They were the following:

- (i) To characterise the sensitised state on the molecular level by way of single channel recordings in the outside-out configuration.

- (ii) To investigate whether the permeabilisation phenomenon associated with the P2X7 macropore occurs *via* the same mechanism as facilitation, or, whether two different pathways are involved in our system of study (rP2X7, HEK293T cells)

- (iii) To probe further the possibility of a P2X7-TMEM16 complex and its potential role in these phenomena.

EXPERIMENTAL SECTION

Cell culture and transfection

HEK293T cells (ATCC) were cultured in Dulbecco's modified Eagle's medium, supplemented with 10% fetal bovine serum, 1x GlutaMax, 100 units/mL penicillin and 100 µg/mL streptomycin (Gibco Life Technologies). For HEK293T TMEM16F-null cells, this medium was further supplemented with 1 µg/mL puromycin dihydrochloride (Gibco Life Technologies). Trypsin-treated cells were seeded onto 9-12mm glass coverslips (VWR) in 35mm dishes for patch-clamp and fluorescence experiments, or in 100 mm dishes for biochemical experiments, in both cases pre-treated with poly-L-lysine (Sigma Aldrich). Cells were incubated at 37 °C and in presence of 5% CO₂.

Transfections were carried out using the calcium phosphate precipitation method. The cDNA encoding rat P2X7 (rP2X7) constructs and enhanced Green Fluorescent Protein construct (eGFP) were contained within pcDNA3.1(+) plasmids (Invitrogen). rTMEM16F cDNA was contained within a pCMV6 vector featuring a c-myc tag (OriGene). For whole cell patch clamp experiments, cells were co-transfected with the rP2X7 constructs (0.5–0.8 µg) and an eGFP (0.3µg) which allowed to identify cells having undergone efficient transfection. For single channel experiments, the quantity of rP2X7 construct DNA transfected was reduced to 0.01–0.08 µg. Cells were washed one day after transfection with PBS solution, and the medium replaced with fresh. For biochemical experiments, each 100 mm dish was transfected with cDNA encoding rP2X7R either alone (10 µg) or co-transfected with cDNA encoding rTMEM16F construct (5 µg of each). For fluorescence measurements, cells were transfected with 2 µg rP2X7 construct either alone or co-transfected with 1 or 2 µg rTMEM16F.

Molecular biology

Point mutation P451L was introduced into the rP2X7 WT background using KAPA HiFi HotStart mutagenesis kit (Cliniscience). The mutation was then verified by sequencing (Eurofin Genomics). CRISPR Cas9 method was carried out as previously described (Le et al., 2019; Ran et al., 2013). The oligonucleotide encoding the sgRNA sequence (5'-AATAGTACTCACAACTCCG-3'), which targets exon 2 of TMEME16F, containing BbsI overhangs was cloned into BbsI sites in pSpCas9(BB)-2A-Puro (Addgene plasmid ID:48139). The plasmid obtained was transfected into HEK293T using the calcium phosphate precipitation

method. After 48h of transfection, 1 µg/mL puromycin was applied to select cells for 72h–96h, with medium change every 24h. Then, transfected cells were serial-diluted in 96-well plates to select for single-cell colonies. After 14–21 days, the single-cell colonies were expanded and screened for the absence of hTMEME16F. Verification was carried out by sequencing and Western Blot.

Patch-clamp electrophysiology

Whole-cell recordings were carried out 24h–48h after transfection, and single-channel recordings 24h after transfection. Patch pipettes were pulled from borosilicate glass capillaries (Harvard Apparatus) to yield resistances of 3–5 MΩ for whole-cell recordings, and 15–20 MΩ for single-channel recordings. For single-channel recordings, pipettes were coated with Sylgard 184 (Dow Corning Co.) and fire polished before use. pH was verified for all solutions used, and if necessary, adjusted carefully using NaOH to pH 7.32–7.33. All solutions were maintained at approximately 300 mOsm.

Cells were voltage-clamped to -60 mV (whole cell) or -120mV (outside out) using the EPC10 amplifier (HEKA), and data were recorded with PATCHMASTER software. Data were sampled at 10 kHz and low-pass filtered at 2.9 kHz. Applications of agonist and/or inhibitor were carried out by perfusion, using three capillary tubes placed directly over the cell/patch of interest. These capillaries are displaced using the SF-77B Perfusion Fast Step system (Warner), ensuring solution exchange within 5–10 ms. For whole-cell recordings, Normal Extracellular Solution (NES) contained 140 mM NaCl, 2.8 mM KCl, 1 mM CaCl₂, 0.1 mM MgCl₂, 10 mM HEPES, 10 mM Glucose, pH 7.32-7.33. Patch pipettes contained 140 mM KCl, 5 mM MgCl₂, 5 mM EGTA, 10 mM Hepes, adjusted to pH 7.3 with NaOH. For single-channel recordings, NES contained 147 mM NaCl, 2 mM KCl, 1 mM CaCl₂, 0.1 mM MgCl₂, 10 mM HEPES, 10 mM Glucose adjusted to pH 7.3 with NaOH. Intracellular solution contained 147 mM NaF, 10 mM Hepes and 10 mM EGTA, adjusted to pH 7.3.

All agonist/inhibitor reagents were solubilised in NES. 2'(3')-O-(4-Benzoylbenzoyl) adenosine 5'-triphosphate (BzATP) (triethylammonium salt, Sigma Aldrich) was used as P2X7 agonist at a concentration of 10 µM. TMEM16 inhibitors used were the following: tannic acid (TA) 20 µM, flufenamic acid (FFA) 100 µM, 9-anthracene-carboxylic acid (9-AC) 1 mM. Specific P2X7 antagonist AZ10606120 (dihydrochloride salt, Tocris) was used at a concentration of 1 µM. MTS-Rhodamine was used at a concentration of 3 µM, and prepared immediately prior to the

experiment. Owing to the facilitation effect produced by prolonged agonist exposure, only one cell was patched per coverslip, to ensure that receptors studied are indeed “naïve” upon the first agonist stimulation. For cells and patches treated by methyl- β -cyclodextrin (MCD), coverslips were incubated with 50 μ L of 15 mM MCD (Sigma Aldrich) for 15 minutes at 37°C. For patches having undergone facilitation treatment, perfusion of BzATP (10 μ M) was carried out for 30s whilst in the cell attached configuration, before piercing of the membrane and excising of the patch to the outside out configuration, in which recordings were carried out.

Co-immunoprecipitation and western blotting

HEK293T and 16F-null cells, either untransfected or transfected with rP2X7-c-myc and rTMEM16F-c-myc (ratio 1:1) were lysed by incubation with gentle agitation for 80 minutes at 4°C with lysis buffer containing 200 mM Hepes, 100 mM NaCl, 1% Triton-X, 5 mM EDTA, Pierce Protease Inhibitor Tablets (Thermo Fischer). After 10 minutes of centrifugation at 14,000 rpm the supernatant was collected. Input samples were collected at this stage. For co-immunoprecipitations, Protein G Sepharose Fast Flow resin was employed (GE Life Sciences). After an initial pre-clearing process (see manufacturer’s instructions), 3 μ g anti-TMEM16F rabbit antibody was added to the cell lysate and left under gentle agitation for 2 hours at 4°C. Protein G Sepharose Fast Flow resin was then added and left under gentle agitation for 1h at 4°C. Following this, the resin was washed three times with washing buffer containing 200 mM Hepes, 500 mM NaCl, 1% Triton-X, 5 mM EDTA, Pierce Protease Inhibitor Tablets (Thermo Fischer), and a final time with lysis buffer. The resin was then resuspended in NuPage LDS Sample Buffer x1 (Thermo Fischer) and 70 mM DTT, and boiled for 10 minutes. The supernatant was loaded onto NuPage Novex Bis-Tris 4–12 % gel (Thermo Fischer) and migrated in MOPS buffer. Transfer onto nitrocellulose membrane was carried out using the TransBlot Turbo system (BioRad) and the membrane blocked for 30 minutes in TPBS (PBS supplemented by 1 % dried non-fat milk, 0.5 % BSA, 0.05 % Tween-20). The membrane was incubated overnight at 4°C with TPBS containing either anti-c-myc mouse antibody, dilution 1:2,500 (Invitrogen, Thermo Fischer, reference MA1-980) or anti- β -actin mouse antibody, dilution 1:5,000 (Sigma Aldrich, reference A5441). Three washes with TPBS were carried out, before a second incubation in TPBS containing HRP-conjugated sheep anti-mouse antibody, dilution 1:10,000 (GE Life Sciences, reference NA9310) for 2 hours at room temperature. Three further washes with TPBS were carried out before revelation using Amersham ECL Prime Western Blotting Detection Reagent (GE Life Sciences). Chemiluminescence was measured using the Amersham Imager 600.

Fluorescence video microscopy

Fluorescence measurements were carried out using a Leica FW4000 and 40x objective (Platform of Quantitative Imagery, Faculté de Pharmacie, Université de Strasbourg). Acquisition of fluorescence images is carried out at an interval of every 5 seconds using the software MetaMorph (Molecular Devices). The experiment is divided into two acquisition periods; an initial acquisition of 10 minutes where cells are incubated in NES/YO-PRO-1 solution where YO-PRO is at a concentration of 10 μM (iodide salt, Thermo Fischer). The solution is then gently exchanged for a NES/YO-PRO-1 solution containing BzATP and/or inhibitors for a second acquisition period of 15 minutes. This second solution is prepared immediately prior to application, and concentrations used are the same as those used for electrophysiology. MCD treatment was carried out as for electrophysiology.

Data analysis

For electrophysiological data analysis, FitMaster (HEKA Electronics v2x73x1) and Igor Pro (WaveMetrics, v6.32A) were used. Experiments were repeated several times, over at least two independent transfections. The extent of facilitation is determined by calculating the fold difference between the 8th agonist-evoked current and initial agonist-evoked current in a series of 8 repeated applications. The current density is calculated as the pA/pF of the 8th agonist-evoked current in a series of 8 repeated applications. For single channel data analysis, TAC and TACFit (Bruxton) were used. Data were re-filtered offline to give a final f_c of 100 Hz. In these conditions, the dead time (T_d) was equal to 1.8 ms, and consequently events faster than ~ 2 ms were not observed. Single-channel current amplitudes were determined by all points histograms fitted to Gaussian distributions, using maximum likelihood methods:

$$f(I) = \sum_{i=1}^n \frac{a_i}{\sigma_i \sqrt{2\pi}} \exp \left[-\frac{(I - A_i)^2}{2\sigma_i^2} \right]$$

Where $f(I)$ is the total probability density of a given amplitude value I , A_i is the i^{th} channel amplitude, σ_i is the standard deviation of the i^{th} channel amplitude, and a_i is the fraction of the data represented by the i^{th} amplitude. Conductance was determined by dividing current amplitudes by the holding potential (-120 mV).

For mean open time analysis, only patches featuring 3 or fewer channels were analysed, and analysis of stacked events resulting from simultaneous channel openings was less than 5 % of the total events analysed. Detection of events was carried out by using 50 % of the single-channel current amplitude as the detection threshold. Dwell time histograms were fitted by the minimum number of exponential functions according to the following equation:

$$f(t) = \sum_{i=1}^n a_i / \tau_i \exp(-t/\tau_i)$$

where t is the time, τ_i is the time constant, and a_i is the relative area (the sum of all areas is equal to 1). The mean open time for a selected state is given by:

$$\tau_{state} = \sum a_i \tau_i$$

For fluorescence experiment analysis, Fiji and Igor Pro were used.

Statistical analysis

Data are reported as mean values \pm SEM. Experiments were repeated several times after, at least, two independent transfections. For statistical analyses, GraphPad Prism software (v8.0.2) was used. The normality of data distribution was tested before selection of an appropriate test of statistical significance and $P < 0.05$ was considered as significant difference. For electrophysiological data, two-tailed unpaired Student's t -tests were used for statistical analysis. For fluorescence measurements, one-way Kruskal-Wallis analysis of variance (ANOVA) test or Mann-Whitney test was employed, as indicated.

Nota bene:

My contributions to this project are the design of research (with *Dr. Thomas Grutter*) and the totality of electrophysiological experiments. Fluorescence data was acquired and analysed by *Adeline Martz* and *Fanny Gautherat*; CRISPR/Cas9 and co-immunoprecipitation experiments were realised by *Adeline Martz*.

RESULTS

1. Molecular characterisation of the rP2X7 facilitated state.

In response to the first objective of this study, we were interested in the molecular characteristics of facilitation. Although well documented in the literature by way of whole cell electrophysiological experiments, a study of this process on the molecular level has never been carried out. With this study, we therefore aimed to carry out a single channel-level biophysical characterisation of rP2X7R in the facilitated state, and reasoned that such a characterisation would also provide information as to the mechanisms through which this state is accessed.

For this study, given that rP2X7 is inhibited by divalent cations (Virginio et al., 1997), we decided to use an adapted extracellular solution (NES), containing reduced levels of Mg^{2+} and Ca^{2+} , below their IC_{50} values. Whilst recordings with very low divalent cation concentration have been previously used in the literature (Klapperstück et al., 2000), we found that in our conditions, total removal of Mg^{2+} and Ca^{2+} resulted in spontaneous inwards currents when recording patches from untransfected HEK293T cells in the outside-out configuration. These currents were not observable in whole cell conditions, but are in accordance with a study demonstrating that low divalent cation conditions activated TRPM7 channels in HEK293 cells (Nörenberg et al., 2016). For these reasons, we decided to use BzATP, an ATP analogue which is more potent to P2X7Rs (Surprenant et al., 1996). BzATP can be used at much smaller concentrations to stimulate P2X7 activity (μM range), which limits ATP-chelation of divalent cations in the bath solution and also circumvents the risk of activating endogenous P2Y channels present in HEK293 cells (Thomas and Smart, 2005).

We devised a protocol whereby single channel recordings in the outside out configuration were carried out in both naïve patches, containing rP2X7Rs which had never been stimulated by BzATP, and patches containing pre-facilitated rP2X7Rs, having been stimulated by BzATP for 30 seconds prior to recording. This pre-facilitation was carried out by perfusion in the cell-attached configuration, before membrane piercing and cytosol dialysis, in order to retain any cellular components and pathways which may be required for facilitation to occur (Figure 86a). The 30 second prolonged application protocol induced a strong current facilitation (4.2-fold \pm 0.5, $n = 3$, Figure 86c) when probed in whole cell recordings, which was similar to that obtained with eight short repetitive BzATP applications (3.4-fold \pm 0.4, $n = 10$), as has been previously observed in the literature (Robinson et al., 2014).

In rP2X7-expressing, naïve HEK293T excised membrane patches, barely visible events were observed when data were filtered at a corner frequency (f_c) of 1 kHz, however, once filtering

was increased to 100 kHz, channel openings and closings could be clearly resolved (Figure 86c).

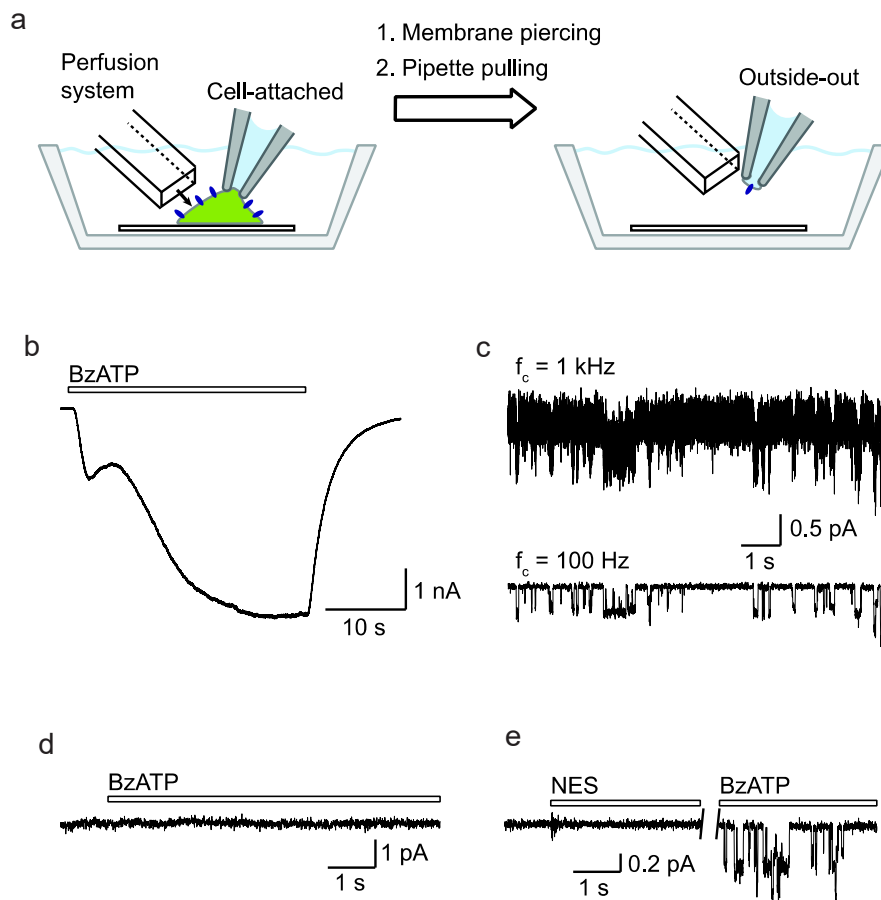


Figure 86. Probing facilitation of rP2X7R with single channel recordings.

(a) Schematic representation of the protocol to record outside-out single channel currents from rP2X7-expressing HEK293T cells in the facilitated state. BzATP (10 μM) perfusion is carried out for 30s whilst in the cell attached configuration, then the membrane is pierced and pipette gently extracted to excise a small patch of membrane from which single channel recordings are taken. (b) Representative whole cell recording of an rP2X7-expressing HEK293T cell demonstrating the facilitation of rP2X7 which occurs following this 30s BzATP perfusion. (c) In rP2X7-expressing HEK293T excised membrane patches, BzATP-induced single channel openings are barely visible when filtered at a corner frequency of 1 kHz (upper), but become clear when this filtering is increased to 100 kHz (lower). (d) BzATP in reduced divalent cation NES elicits no channel openings in untransfected HEK293T cells. (e) In rP2X7-expressing HEK293T membrane patches, channel activity is only observed when BzATP is applied.

Control experiments in untransfected HEK293T membrane patches, as well as rP2X7-transfected patches confirmed that these events did indeed originate from P2X7 channel openings and closings, and not from endogenous channel activity induced by low levels of divalent cations (Figure 86d and e).

In control, naïve patches, we observed two, discrete unitary current conductances, which we refer to as O1 and O2. These conductances are not the result of multiple, stacked events, but distinct conductance states, reflecting a dual gating mechanism. This is in close agreement to a previous study, which observed two conductance states, a short-lived state and a long-lived

state, from hP2X7-expressing oocyte membrane patches when stimulated with ATP (Riedel et al., 2007). We observed both O1 and O2 in the majority of patches (5/6), with the exception of one patch which showed only O2 conductances. All points histogram analysis allowed to determine the unitary conductances of O1 and O2 as 1.89 ± 0.26 pS and 3.39 ± 0.44 pS respectively (Figure 87a and b).

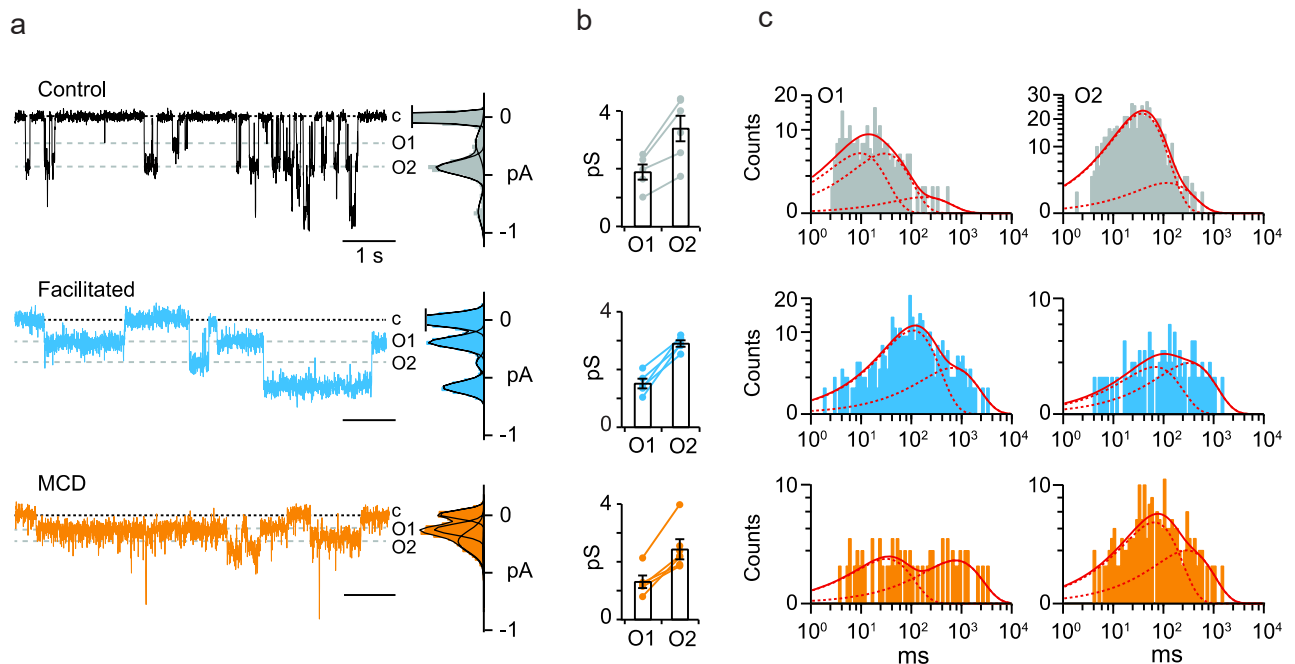


Figure 87. BzATP-evoked current facilitation results in a cholesterol-dependent increase of single channel open probability.

(a) Representative single channel currents elicited by BzATP (10 μM) from outside out patches of rP2X7-expressing HEK293T cells. Cells were either untreated, naïve (control, black), prefacilitated with a 30s perfusion of BzATP (facilitated, blue) or treated with MCD (15 mM) for 15 minutes (MCD, orange) prior to membrane excision. Data were recorded at -120 mV. Conductance states O1 and O2 are indicated with dashed lines. Corresponding all points histograms are shown to the right of the trace. Distributions were fit by the sum of Gaussians, where Gaussians centered at 0 indicate closed channels, labelled c. (b) Summary of corresponding unitary conductances. Linking lines indicate data points that originate from the same outside-out patches (n = 6 patches for control, 5 for facilitated and 7 for MCD-treated conditions). Bars represent mean ± SEM. (c) Corresponding open dwell-time histograms fitted by the sum (solid red line) of several exponential functions (dashed red lines). For control patches (grey histograms), $\tau_1 = 9.6$ ms, relative area, $a_1 = 0.49$; $\tau_2 = 29$ ms, $a_2 = 0.48$; $\tau_3 = 180$ ms, $a_3 = 0.03$; mean open time, $\tau_{O1} = 24$ ms for O1, and $\tau_1 = 38$ ms, $a_1 = 0.92$; $\tau_2 = 119$ ms, $a_2 = 0.08$; $\tau_{O2} = 44$ ms for O2. For facilitated (blue histograms), $\tau_1 = 108$ ms, $a_1 = 0.77$; $\tau_2 = 654$ ms, $a_2 = 0.23$; $\tau_{O1} = 234$ ms for O1 and $\tau_1 = 68$ ms, $a_1 = 0.46$; $\tau_2 = 332$ ms, $a_2 = 0.54$; $\tau_{O2} = 211$ ms for O2. For MCD-treated patches (orange histograms), $\tau_1 = 32$ ms, $a_1 = 0.52$; $\tau_2 = 752$ ms, $a_2 = 0.48$; $\tau_{O1} = 378$ ms, for O1 and $\tau_1 = 66$ ms, $a_1 = 0.70$; $\tau_2 = 294$ ms, $a_2 = 0.30$; $\tau_{O2} = 134$ ms for O2.

Analysis of open and closed time histograms fitted with multiple exponentials revealed a mean open time for O1 (τ_{O1}) of 24 ms and a mean open time for O2 (τ_{O2}) of 44 ms, whilst mean closed time (τ_c) was determined as 185 ms.

We then undertook experiments to determine these same characteristics in pre-facilitated patches. Here also, we found that two discrete unitary conductances were present, and that the values of these conductance states were similar to those found in control, untreated patches. However, we observed a dramatic increase in the mean open times of both O1 (~10-

fold) and O2 (~5-fold), (Figure 87c and summarised in Figure 88a). The mean closed time also increased slightly (~1.5-fold). As a result, the open channel probability (NP_o) for both conductance states combined also increased by ~2.9-fold, from 0.17 to 0.47, shown in Figure 88c. Of note is that this fold increase is in the same range as that which we observed in whole cell recordings, using either a prolonged or repetitive agonist application (4.2 and 3.5-fold respectively). These results therefore demonstrate that in HEK293T cells, a large increase in the open probability is at the origin of BzATP-evoked facilitation.

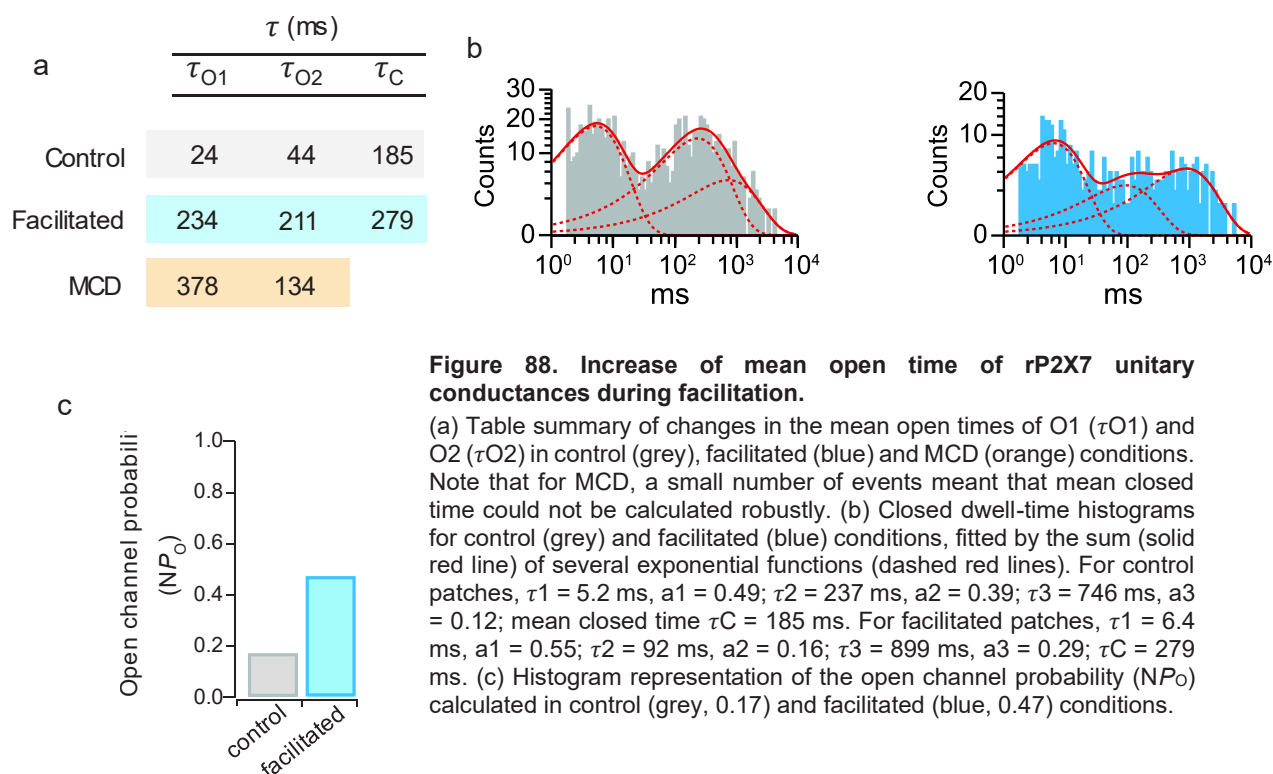
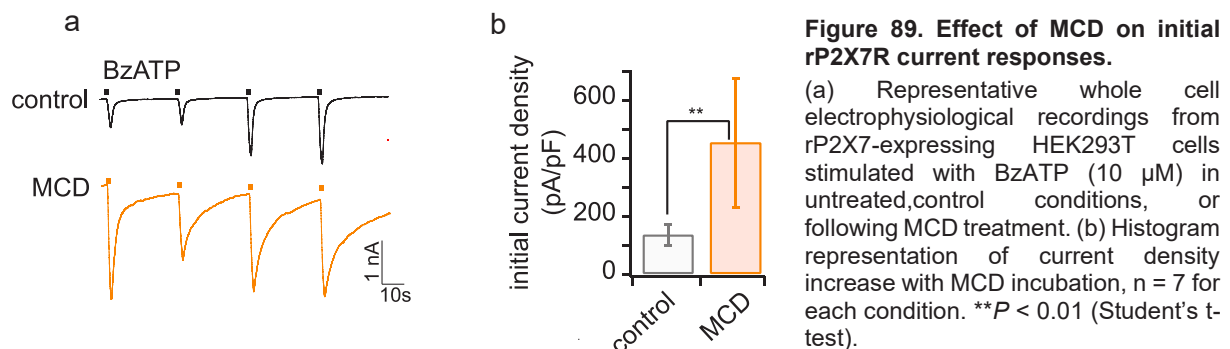


Figure 88. Increase of mean open time of rP2X7 unitary conductances during facilitation.

(a) Table summary of changes in the mean open times of O1 (τ_{O1}) and O2 (τ_{O2}) in control (grey), facilitated (blue) and MCD (orange) conditions. Note that for MCD, a small number of events meant that mean closed time could not be calculated robustly. (b) Closed dwell-time histograms for control (grey) and facilitated (blue) conditions, fitted by the sum (solid red line) of several exponential functions (dashed red lines). For control patches, $\tau_1 = 5.2$ ms, $a_1 = 0.49$; $\tau_2 = 237$ ms, $a_2 = 0.39$; $\tau_3 = 746$ ms, $a_3 = 0.12$; mean closed time $\tau_C = 185$ ms. For facilitated patches, $\tau_1 = 6.4$ ms, $a_1 = 0.55$; $\tau_2 = 92$ ms, $a_2 = 0.16$; $\tau_3 = 899$ ms, $a_3 = 0.29$; $\tau_C = 279$ ms. (c) Histogram representation of the open channel probability (NP_o) calculated in control (grey, 0.17) and facilitated (blue, 0.47) conditions.

Following this, we decided to investigate further the molecular basis of facilitation, in particular, the role of cholesterol. Cholesterol has been shown to modulate the process of facilitation, with cells depleted in cholesterol by methyl- β -cyclodextrin (MCD) exhibiting dramatically enhanced initial currents, and little increase with repeated agonist applications, as if already in a facilitated state (Robinson et al., 2014). We therefore decided to carry out these same single channel recordings, this time from patches in which the membrane cholesterol had been acutely depleted by MCD (15 mM, 15 minutes incubation at 37°C). These incubation conditions have previously been shown in the literature to reduce membrane cholesterol by a small but significant amount (Robinson et al., 2014). We first verified that MCD treatment resulted in the expected modulation of current using whole cell recordings, where we found that the first response to agonist in MCD treated cells was indeed of a significantly greater magnitude than that in untreated control cells (137 ± 36 pA/pF for control cells as opposed to 454 ± 220 pA/pF

in MCD treated cells, $n = 7$, Figure 89). Although we did not quantify kinetic parameters, we observed lengthened deactivation kinetics in these cholesterol depleted patches.



Single channel recordings revealed that this cholesterol-depleting treatment enhanced the mean open times of both conductance states O1 and O2 as compared to control patches (~16-fold for O1 and ~3-fold for O2, Figure 87 and Figure 88a). As for pre-facilitated patches, the absolute values of both conductances did not vary significantly from control conditions, as shown in Figure 87b. MCD treatment therefore recapitulates BzATP-induced facilitation, presumably by the dissociation of cholesterol from the receptor.

For MCD-treated patches, we were unable to robustly determine a mean closed time, due to too few events. There are two reasons for this, firstly, MCD-treated patches exhibited a greater level of instability and were more challenging to patch than in control conditions, likely due to heightened fluidity in the cholesterol-depleted membrane which may influence the quality of the seal as well as noise. We therefore obtained less analysable data for this condition. Secondly, given the increase in activity, channels remained open for longer, and so fewer closed events were detected within the analysable patches.

These results taken together show that the facilitated state of rP2X7 is characterised by a heightened probability of opening, and indicate that this increase in NP_O is likely produced as a result of a membrane reorganisation, which induces the dissociation of cholesterol from rP2X7R.

1.1. Mathematical kinetic modelling (*Dr. Thomas Grutter*)

To describe this electrophysiological data quantitatively, we adopted a linear kinetic scheme, as has been previously used to describe P2X2 receptors (Ding and Sachs, 1999). The model describes two discrete conductance states, O1 and O2, directly linked to a common closed channel state. Our data set contained too few experimental events to be able to perform fitting procedures, so instead the rate constants were varied until a realistic set of constants were

found, which mimicked closely single channel and whole cell currents (Pearson's $r \geq 0.950$). By decreasing the transition rates between open and closed states, simulated single channel current behaviour, as well as whole cell kinetics and current facilitation could closely reproduce experimental observations (Pearson's $r \geq 0.989$). This model therefore suggests that cholesterol acts to stabilise closed channel states and/or destabilises open channel states and that its removal favours the stabilisation of open channel states.

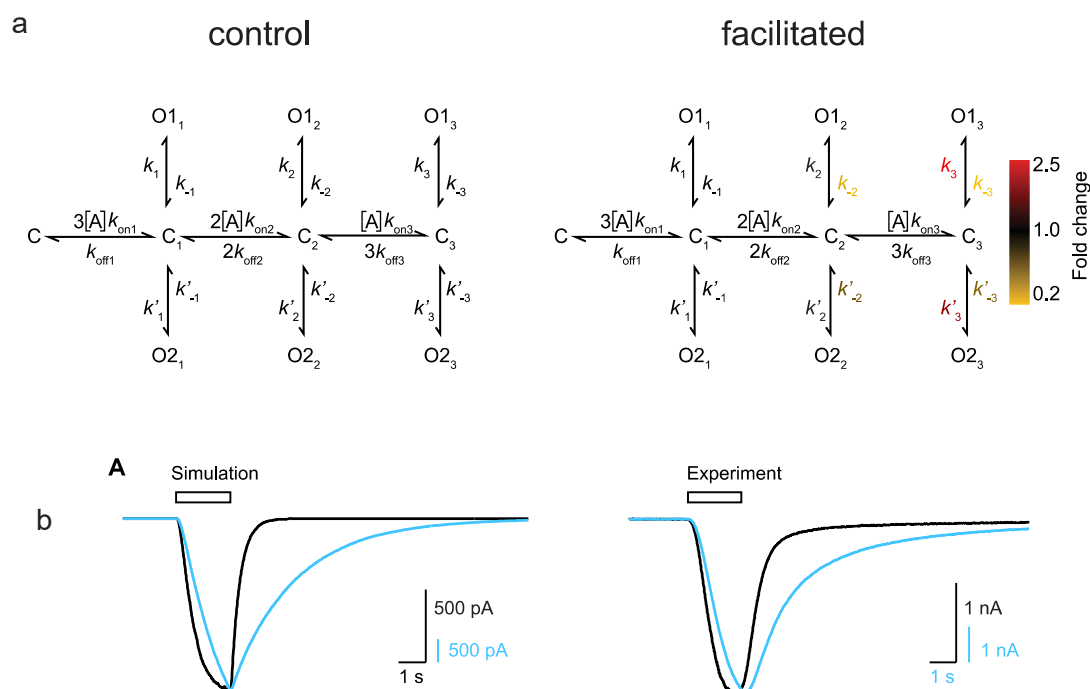


Figure 90. Kinetic modelling of single channel and whole cell currents.

(a) Kinetic schemes used for modelling electrophysiological data in control (left) and facilitated (right) conditions. Fold change of rate constants in facilitated conditions as compared to control are displayed according to colour coding. C = closed channel state, O1 = open channel in the O1 state, O2 = open channel in the O2 state. Numerical values are available in Annexe 1. (b) Left: normalised, simulated whole cell currents (50,000 channels active in simulations), evoked by BzATP 10 μ M in control conditions (black) and facilitated conditions (blue). Right: normalised experimental whole cell currents (averaged from 3 experimental traces) evoked by the first (black) and eighth (blue) application of 10 μ M BzATP in rP2X7-expressing HEK293T cells.

1.2. Probing the pore diameter of the facilitated state.

As part of this project to characterise the facilitated state of rP2X7, in parallel to our single channel study, we carried out preliminary tests probing the diameter of the pore in both naïve and facilitated P2X7Rs. To do so, we employed pore-lining cysteine mutants and MTS-Rhodamine (MTSR), a sulfhydryl-reactive reagent of large molecular weight and nanometer dimensions (696 Da, 0.9 x 1.4 x 1.65 nm). This reagent has previously been used in the literature as part of a study probing the size of the open rP2X7 pore, where it was found to covalently modify the position G345C, producing a block of the ATP-evoked current. We reasoned that if transition to the facilitated state provokes a change in diameter (*cf.* pore dilation) or a change in receptor conformation, certain positions may undergo MTSR modifications of differing nature in naïve and facilitated conditions. As depletion of cholesterol is known to reproduce facilitated-like whole cell currents (Robinson et al., 2014), and to recapitulate BzATP-facilitated single channel conductances (this study), we decided to use MCD to acutely deplete the cell membrane of cholesterol, and to test the nature of MTSR modification in both untreated and MCD-treated cells. We chose just two mutants on which to carry out initial tests, G345C, for which the modification and current blocking effect has already been described in ATP-facilitated cells (Browne et al., 2013), and S339C, shown in Figure 91. Both of these residues are pore-lining, and in hP2X7 define the channel gate (Pippel et al., 2017).

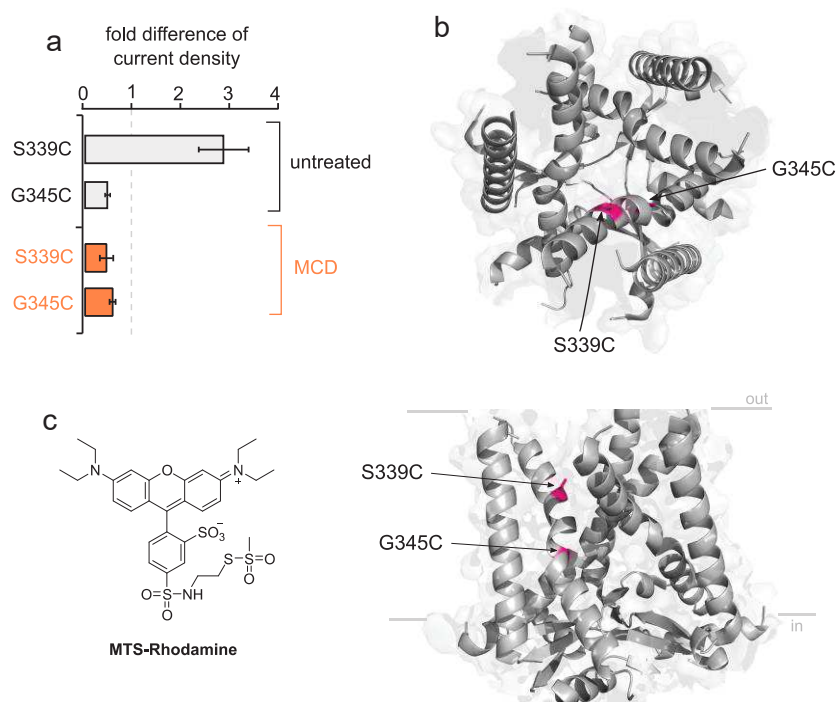


Figure 91. MTSR modification of rP2X7 cysteine mutants in the naïve and facilitated state.

(a) Summary of the fold difference in BzATP-evoked current upon application of MTSR reagent (reversible inhibition components subtracted), of S339C and G345C mutants in untreated (black) “naïve” conditions, and MCD-treated (15 mM, 15 minutes, 37°C, orange) cholesterol depleted conditions. (b) View of the position of G345 and S339 (highlighted in pink) from above the 3-fold axis (upper panel) or laterally along the membrane (lower panel). (c) Chemical structure of MTSR.

As observed in the literature (Browne et al., 2013), MTSR provoked a block of the open current in the WT receptor, but this block was fully reversible upon washout and re-application of agonist. We found that at position G345C, MTSR (3 μ M) provoked a covalent, non-reversible inhibition of currents in both MCD-treated and naïve, unfacilitated conditions (57.2%, n=3 and 47.5%, n=6 for MCD-treated and untreated cells respectively, Figure 91a). This is in close agreement with Browne *et al*, who facilitated G345C-expressing HEK293T cells before co-application of MTSR, and in these conditions found inhibition to be 59%. On the other hand, S339C mutant produced very different profiles upon MTSR application (Figure 92). In untreated cells, we observed a large potentiation of the BzATP current upon MTSR addition, resulting in a 2.85-fold increase in current, which did not return to the baseline upon washout, indicating that MTSR modification at S339C may result in a channel which subsequently remains constitutively open. We also observed this non-return to baseline levels in MCD-treated cells. However, in these cholesterol-depleted cells we did not observe this potentiation, but instead a slight reduction in current upon MTSR application (43.2% inhibition, n=3).

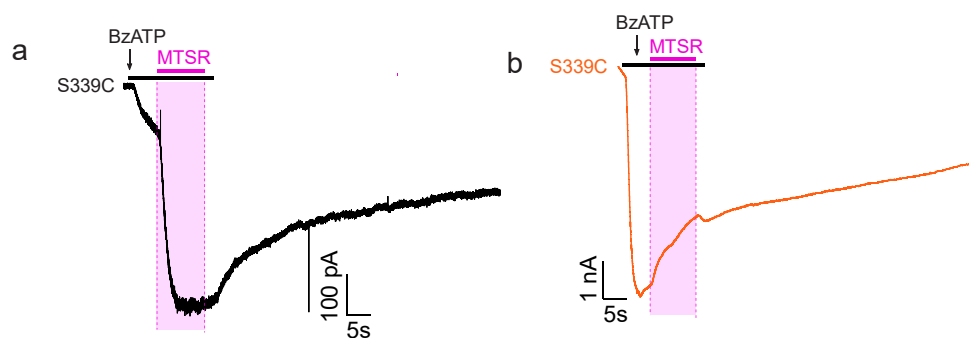


Figure 92. Differing MTSR modifications of native and MCD-treated S339C mutant receptors.

Representative whole cell trace of S339C rP2X7 expressed in HEK293T cells firstly stimulated with BzATP (10 μ M, 6s) followed by co-application of MTSR (3 μ M, 8s), followed by 2s of BzATP alone and 60s of washout, in (a) naïve, untreated conditions (black) and (b) MCD-treated conditions (orange). Note that as for previous experiments, only one cell per coverslip is probed.

The fact that MTSR induces such opposing effects in untreated and MCD cholesterol-depleted cells, may indicate that the S339C position experiences some kind of spatial reorientation under cholesterol-depleted, facilitated-like conditions, rendering MTSR unable to induce the same potentiation under these conditions.

Whilst these results are interesting, and suggest a that a conformational change may accompany the increase in open channel probability observed *via* single channel recordings, we have a small data set for MCD-treated conditions, as these cells proved difficult to patch for the duration of the protocol given the large currents produced by cholesterol depleted conditions, especially for S339C mutant where currents did not return to baseline conditions upon washout. It should also be noted that interpretation of such cysteine scanning experiments should be cautious, as use of MTS reagents can create complex effects on the molecular level, of which we only obtain a global, averaged view in whole cell recordings. At

S339C position in hP2X7, for example, application of MTSEA⁺ causes a diminution of unitary currents, but simultaneously causes a dramatic increase in the probability of opening, which translates to an overall apparent increase of currents in whole cell recordings (Pippel et al., 2017). Care must be taken, therefore, not to over-interpret such results. Nevertheless, it would be interesting to carry out a more comprehensive cysteine scanning study, with a greater number and variation of cysteine mutants, to probe which positions within the pore may be susceptible to conformational changes. In addition, it could be envisaged to use the 30s BzATP facilitation protocol in the place of MCD treatment, as this condition typically provokes a facilitation of receptors but without the difficulties relating to patch and gigaseal quality, which can render it complicated to obtain analysable traces from MCD-treated cells.

2. Studies on a possible rP2X7/TMEM16s complex and its implication in facilitation and macropore formation.

The second section of this project investigates the role of TMEM16 channels in rP2X7 activity, in terms of channel gating, facilitation behaviour, and macropore formation.

2.1. Probing the regulation of channel gating by an rP2X7/TMEM16 protein complex.

Following characterisation of rP2X7 currents at the single-channel level in both naïve and facilitated states, we questioned whether endogenously present TMEM16 channels could have a regulatory effect on these unitary currents, in light of their suggested involvement in P2X7 activity discussed previously (Chapter three introduction, section 3). We reasoned that if a strong interaction is present between these channels, they will remain in complex even upon membrane excision to the outside-out configuration. As such, rP2X7R unitary currents would be allosterically sensitive to modulators acting on the endogenous channel. To investigate this possible interaction, we decided to use several non-selective CaCC inhibitors (shown in figure Figure 93): tannic acid (TA), flufenamic acid (FFA) and 9-anthracene-carboxylic acid (9-AC), which have been previously shown to modulate members of the TMEM16 family when expressed in recombinant systems, specifically, TMEM16A (Liu et al., 2015; Namkung et al., 2010), TMEM16B (Cherian et al., 2015; Namkung et al., 2010) and TMEM16F (Ousingsawat et al., 2015).

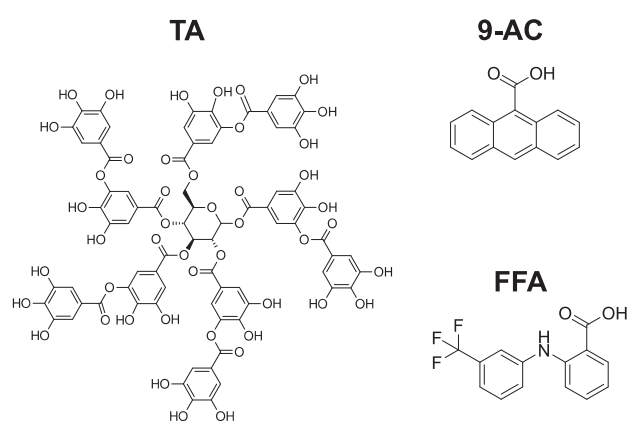


Figure 93. CaCC inhibitors employed in this study.

Chemical structures of CaCC inhibitors employed in this study. Left: tannic acid (TA), used at 20 μ M; Right upper: 9-anthracene carboxylic acid (9-AC), used at 1 mM; Right lower: flufenamic acid (FFA), used at 100 μ M.

Shown in Figure 94a and b, co-application of BzATP and TA (20 μ M) to outside-out patches from rP2X7-expressing HEK293T cells completely, but reversibly, inhibited BzATP-evoked single channel currents, as did co-application with FFA (100 μ M), 9-AC (1 mM) or the selective P2X7 inhibitor, AZ (1 μ M). These results indicate that one or several members of the TMEM16s

allosterically regulate rP2X7R single channel activity, suggesting the presence of a stable, rP2X7/TMEM16 protein complex.

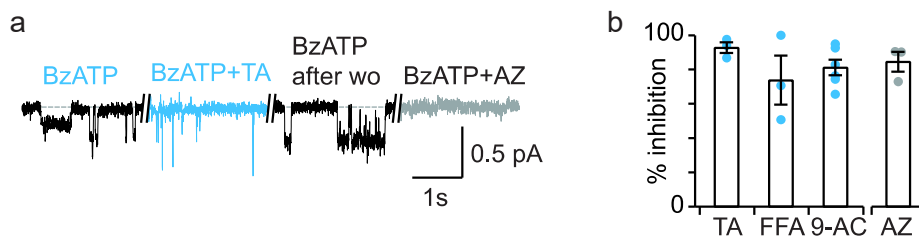


Figure 94. Effects of CaCC inhibitors on rP2X7 single channel and whole cell currents.

(a) Representative single channel recording in the outside-out configuration of rP2X7-expressing HEK293T cells. Currents elicited by BzATP (10 μ M, -120 mV, f_c = 100 Hz) are inhibited by TA (20 μ M) and AZ (1 μ M). (b) % inhibition of single channel currents calculated for CaCC inhibitors and P2X7 inhibitor AZ (TA, n=3, FFA, n=3 and 9-AC, n=6).

As these compounds have poor selectivity, we have considered whether they may act on rP2X7R itself. TA and FFA have previously been reported in the literature to not exert a direct, inhibitory effect on P2X7 (Janks et al., 2018; Ma et al., 2009; Ousingisawat et al., 2015). Nevertheless, with our collaborator *Dr. Eric Boué-Grabot (Université de Bordeaux)*, we decided to test the effects of these inhibitors on BzATP-elicited currents in rP2X7-expressing Axolotl (*A. mexicanum*) oocytes, which are reported to be void of endogenous CaCCs, at least electrophysiologically (Wozniak et al., 2018; Schroeder et al., 2008). These experiments demonstrated that FFA and 9-AC had no inhibitory effect on BzATP-evoked currents in CaCC-void Axolotl oocytes expressing rP2X7 (Figure 95). However, this was not the case for TA, application of which resulted in an inhibition of BzATP current. We cannot confirm, therefore, that TA does not act by directly inhibiting rP2X7 activity. However, this remains unclear, as the previous study of Janks *et al* demonstrated that TA has no effect on ATP-evoked P2X7 currents in human microglia (Figure 85, (Janks et al., 2018)). We therefore remain cautious with our interpretation of results from TA inhibition. Despite the uncertainty surrounding the mechanism of TA inhibition, by demonstrating that FFA and 9-AC do not directly act on the rP2X7R, these results reinforce our previous conclusion of an allosteric regulation and a likely protein complex between TMEM16 channels and rP2X7R.

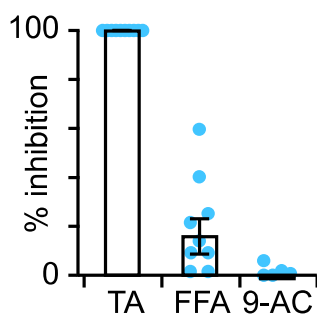


Figure 95. Effects of CaCC inhibitors on BzATP-elicited currents in rP2X7-expressing Axolotl oocytes. (Dr. Eric Boué-Grabot).

Percentage inhibition of BzATP-induced currents (10 μ M) in rP2X7-transfected Axolotl oocytes following 60s perfusion of inhibitors TA (20 μ M), FFA (100 μ M) or 9AC (1 mM). Inhibition is calculated by carrying out four sequential applications of BzATP, followed by inhibitor perfusion and re-stimulation with four sequential BzATP applications. The current density of the fourth BzATP application before inhibitor application is compared with the first BzATP application following inhibitor perfusion. TA treatment results in total inhibition, whilst FFA and 9AC do not exhibit a significant inhibition of currents.

We then decided to test these same inhibitor compounds in whole cell recordings to probe whether or not TMEM16s are involved in the BzATP-evoked facilitation process of rP2X7. We devised a protocol whereby receptors were pre-facilitated by four short agonist applications, then perfused with the inhibitor of interest for 60s, followed by a second series of four short agonist stimulations, in order to observe the effects of these inhibitors on facilitated rP2X7Rs (Figure 96).

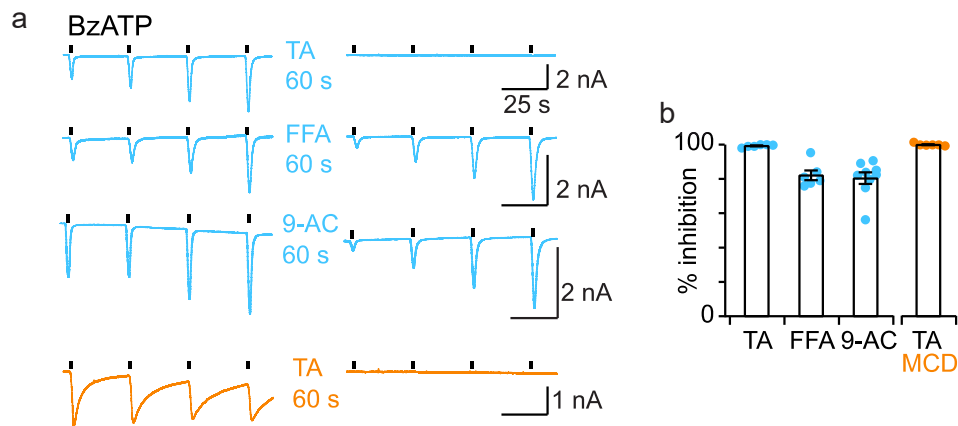


Figure 96. Effects of CaCC inhibitors on BzATP-evoked whole cell rP2X7 currents.

(a) Whole-cell rP2X7R currents (-60 mV) evoked by sequential application of 10 μ M BzATP before (i.e. current facilitation) and after 60-s perfusion of TMEM16 inhibitors (applied alone) in control cells (blue traces) or MCD-treated cells (orange traces). (b) Summary of whole-cell P2X7 current inhibition after current facilitation (blue, TA, n = 6 cells; FFA, n = 6; 1 mM 9-AC, n = 9) or MCD treatment (orange, TA, n = 6). Inhibition is calculated by comparing the current density of the fourth BzATP application before inhibitor application with the first BzATP application following inhibitor perfusion.

We found that all compounds inhibited facilitated rP2X7 currents, albeit to differing extents. FFA and 9-AC produced a strong inhibition of currents, 82.2 ± 2.9 % and 80.5 ± 3.4 % respectively, which were fully reversible upon washout. TA produced total inhibition of currents, which was non-reversible, even after prolonged washout, and was observed in cells pre-facilitated with BzATP (Figure 96a, first trace, blue) or with MCD treatment (Figure 96a, fourth trace, orange). This irreversible abolition of currents by TA highlights that it is likely acting *via* an alternative mechanism to FFA and 9-AC, as demonstrated by the results from Axolotl oocytes. We further investigated the action of TA by employing different experimental protocols: a repetitive co-application of BzATP and TA, and a repetitive application of BzATP using KCl intrapipette solution supplemented with TA, allowing 5 minutes before recording to allow dialysis to take place and TA to effectively diffuse into the cell (Figure 97b).

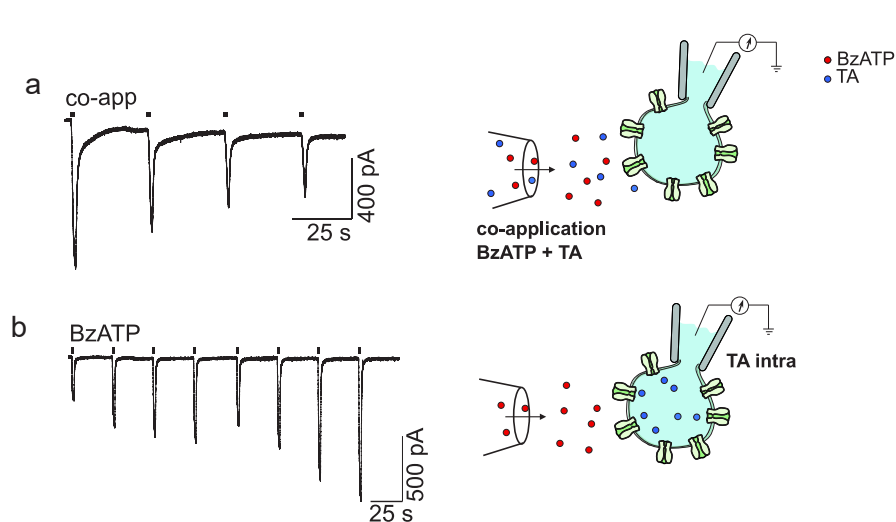


Figure 97. Probing TA inhibition of rP2X7 whole cell currents.

(a) Left: representative whole cell recording from rP2X7-expressing HEK293T cell stimulated by a co-application of BzATP (10 μ M) and TA (20 μ M). Right: schematic representation of the co-application experimental set-up. (b) Left: representative whole cell recording from rP2X7-expressing HEK293T stimulated by BzATP (10 μ M) using intracellular solution of standard composition supplemented with TA (20 μ M). Right: schematic representation of the TA intrapipette experimental set-up.

We found that when co-applied with BzATP, TA also produces a pronounced inhibition of the whole cell currents, as expected given the observed inhibition of unitary conductances (Figure 97a, 65.1 ± 7.9 % over 4 co-applications, $n=8$). This result, taken together with the total inhibition observed after the 60s inhibitor perfusion protocol (Figure 96), demonstrates that TA inhibits rP2X7 BzATP-induced currents when rP2X7R is in the both the open and closed state. Repetitive stimulation of cells containing TA within the intrapipette solution, on the other hand, had no inhibitory effect on rP2X7 currents, thus indicating that TA exerts its effect from an extracellularly-facing component and not through inhibition of some cytosolic pathway. How TA inhibits rP2X7R currents remains unresolved; TA is known to inhibit CaCCs, but as we cannot be sure of the extent to which it inhibits directly rP2X7, we remain cautious when interpreting results obtained with TA.

2.2. Probing the role of rP2X7/TMEM16 protein complex in macropore formation.

Having probed the role of an rP2X7/TMEM16 complex on rP2X7 channel gating, we then questioned whether such a complex may have implications for macropore formation and dye uptake. To investigate this, we monitored uptake of YO-PRO-1 into rP2X7-transfected HEK293T cells upon BzATP stimulation. We devised a dye-uptake protocol featuring two acquisition periods: an initial period of 10 minutes in which the cells are bathed in NES containing YO-PRO-1 (10 μ M) to monitor basal YO-PRO-1 uptake, and a second acquisition period of 15 minutes, during which the cells are bathed in a solution of NES, YO-PRO-1 and BzATP to stimulate rP2X7 activation and dye uptake.

This dye uptake assay (work of *Adeline Martz* and *Fanny Gautherat*) demonstrated that, similar to channel gating, these inhibitors had differing effects on macropore formation. Control conditions showed a significant uptake of YO-PRO-1 upon BzATP application, and interestingly, a heightened basal level of YO-PRO-1 uptake as compared to non-transfected (NT) cells (Figure 98a).

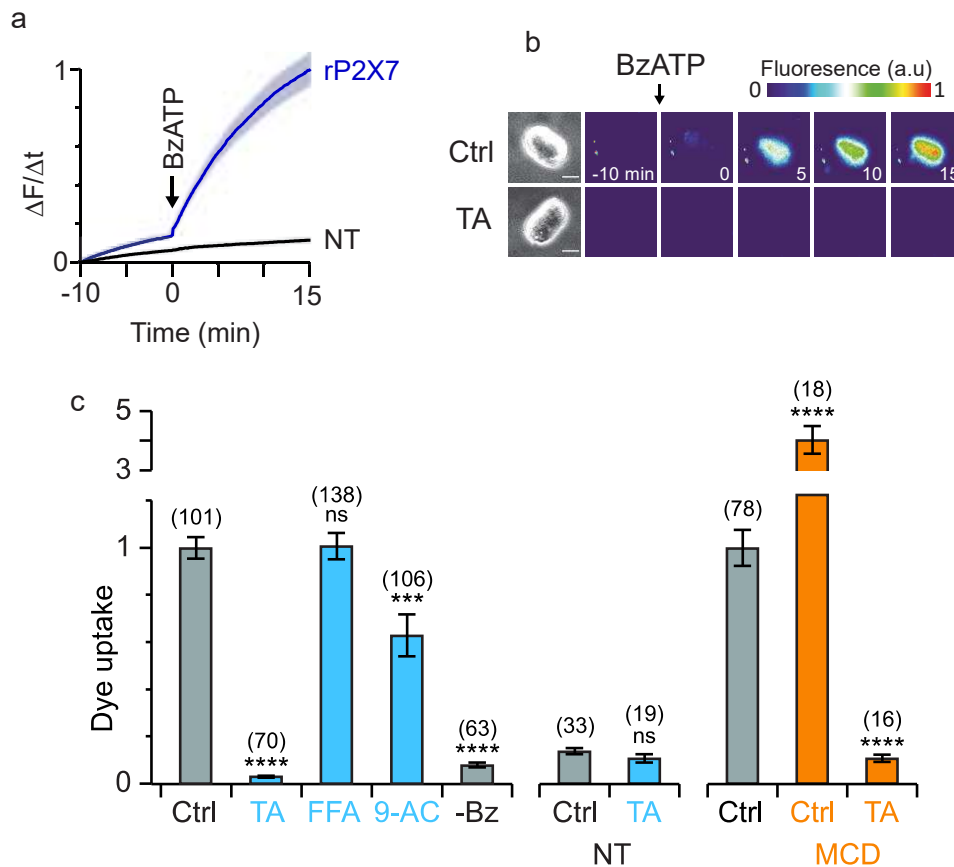


Figure 98. rP2X7-induced dye uptake and its regulation by CaCC inhibitors.

(a) Rate of YO-PRO-1 dye uptake in rP2X7-expressing HEK293T cells (n=78 cells) or non-transfected (NT) HEK293T cells (n=25). BzATP application is indicated by an arrow. Solid lines represent the mean \pm SEM (shaded area). (b) Time series images of YO-PRO-1 uptake in rP2X7-expressing HEK293T cells in absence (Ctrl) or presence (TA) of tannic acid. (c) Summary of YO-PRO-1 dye uptake in different conditions, normalised to rP2X7 transfected HEK293T cells stimulated with BzATP (10 μ M) in the absence of any inhibitor (far left, grey). Number of cells is indicated in brackets, and statistical significance is with respect to the appropriate control condition: *** $P < 0.0003$; **** $P < 0.0001$; ns not significant. Analysis performed by Kruskal-Wallis test or Mann-Whitney test in the case of NT data. Work of *Adeline Martz* and *Fanny Gautherat*.

The BzATP-induced dye uptake was inhibited strongly by TA (97 % inhibition, Figure 98b), and to a lesser, but still statistically significant extent by 9-AC (37.3 %). FFA, on the other hand, surprisingly had no effect on YO-PRO-1 dye uptake (Figure 98c), which is in sharp contrast to the inhibition of channel gating observed by electrophysiology. Previous work has shown that FFA can serve to discriminate between TMEM16 family members, inhibiting strongly TMEM16A, but not TMEM16F (Yang et al., 2012). These results combined with our previous electrophysiological findings therefore suggest two things: firstly, that TMEM16F may be

required for rP2X7-mediated dye uptake, and secondly, that only a small proportion of those complexes responsible for BzATP evoked currents participate in macropore formation and dye uptake.

We also decided to probe macropore formation when rP2X7Rs are in the facilitated state. To do so, we pre-treated cells with MCD before applying the dye uptake protocol. As expected, and in line with previously published observations for rP2X7 and other orthologs (Karasawa et al., 2017; Robinson et al., 2014), YO-PRO-1 dye uptake is sharply increased in cholesterol-depleted cells, indicating that rP2X7 macropore formation is also mediated by cholesterol. We then tested the effect of TA on dye uptake and, as expected, found a significant decrease in YO-PRO-1 incorporation (Figure 98c, far right). We did not test other inhibitors on MCD-treated cells, but given the uncertainty surrounding the mode of action of TA, we plan to repeat these experiments with FFA and 9-AC, in order to conclude definitively whether TMEM16s regulate rP2X7-dependent dye uptake in the facilitated state or not.

2.3. Contribution of TMEM16F subtype to rP2X7 activity.

In light of the results we have obtained using pharmacological inhibition of TMEM16s, as well as the previous work of Ousingsawat *et al*, we suspected that TMEM16F channels may represent all, or part of, the conduit for dye permeation in HEK293T cells. RT-PCR analysis in the literature has shown that mRNA coding for all TMEM16 family members, with the exception of TMEM16G and TMEM16J, is found in HEK293 cells, and that gene expression of TMEM16F is ~4 orders of magnitude greater than that of TMEM16A or B (Banerjee et al., 2017). TMEM16F protein expression was also detected by Western blot. This supports the possibility that endogenous TMEM16F channels may be implicated in rP2X7-mediated dye uptake. Due to the pharmacological promiscuity of known CaCC inhibitors, not only within the CaCC family but also with regard to other channels, we decided to apply the CRISPR-Cas9 method, in order to genetically mute TMEM16F expression, generating a TMEM16F-deficient HEK293T cell line, which we will refer to as 16F-null (realised by *Adeline Martz*). Verification by Western blot demonstrated that TMEM16F was indeed no longer expressed in this 16F-null cell line, compared to WT HEK293T cells.

In this 16F-null cell line, we expressed rP2X7 and, using the same protocol as described previously, measured the BzATP-induced uptake of YO-PRO-1 (*Adeline Martz*). In 16F-null cells, we observed a significant reduction in YO-PRO-1 uptake, of $35 \pm 4\%$ (Figure 99a). We then decided to re-transfect 16F-null cells with rTMEM16F (cDNA ratio 0.5:1 rTMEM16:rP2X7), to see whether full dye uptake can be restored by re-expression of TMEM16F. Whilst we did observe a slight increase in dye uptake, this was not significant compared to 16F-null cells transfected solely with rP2X7, suggesting that these expression conditions are perhaps not

optimal. Attempts to increase the ratio of transfected DNA resulted in fragilised cells, from which fluorescence acquisitions could not be reliably analysed.

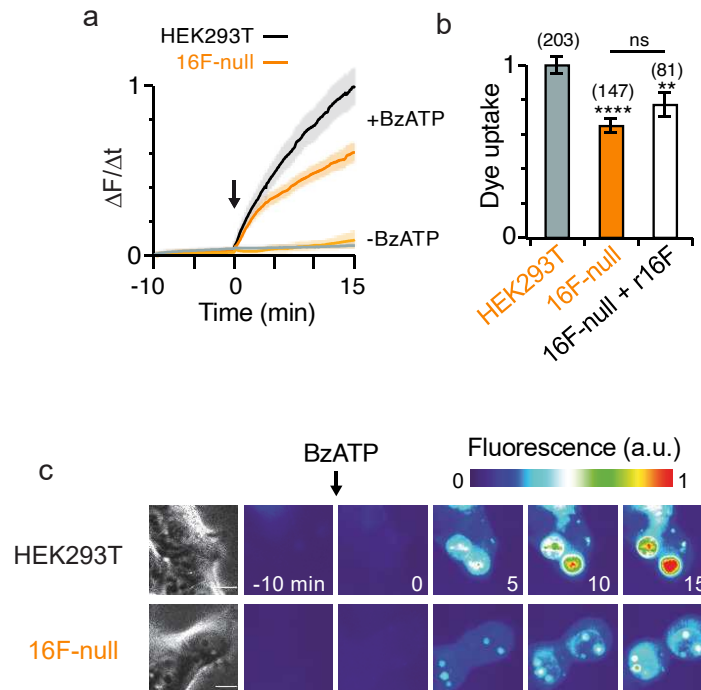


Figure 99. Dye uptake in rP2X7-expressing 16F-null cells.

(a) Rate of fluorescence due to YO-PRO-1 dye uptake in rP2X7-expressing HEK293T cells (black) or 16F-null cells (orange) upon BzATP stimulation (indicated by black arrow, 10 μ M). (b) Histogram summary of YO-PRO-1 dye uptake in 16F-null cells expressing either rP2X7 alone (16F-null, orange) or expressing rP2X7 and rTMEM16F (16F-null + r16F). *n* is indicated in brackets, and was acquired over 6 transfections. Shown is the specific dye uptake, obtained by subtracting the residual dye uptake in the absence of BzATP, normalised to dye uptake obtained in rP2X7-expressing HEK293T cells. **** $P < 0.0001$; ** $P < 0.001$, ns = not significant. Statistical analysis was carried out by a Kruskal Wallis test with Dunn's comparison. (c) Time series fluorescence images of YO-PRO-1 dye uptake in HEK293T cells and 16F-null cells expressing rP2X7 upon activation with BzATP (10 μ M).

We then tested the BzATP-induced dye uptake of this 16F-null cell line in the presence of CaCC inhibitors. As observed in HEK293T cells, co-application of TA strongly inhibited dye uptake in 16F-null cells, whilst FFA did not affect uptake. However, 9-AC no longer inhibited YO-PRO-1 uptake in this 16F-null cell line (Figure 100a), suggesting that 9-AC inhibits specifically TMEM16F in HEK293T cells as opposed to other TMEM16 subtypes. Taken together, these results demonstrate that endogenous TMEM16F channels contribute to rP2X7-mediated macropore formation, albeit in a minor way. Our data also show that there is a remaining contribution to dye uptake, which must originate from channels which are insensitive to FFA and 9-AC.

To support the suggestion that a rP2X7/TMEM16F complex is at play, we carried out co-immunoprecipitation pull-down assays in HEK293T cells overexpressing both rP2X7 and rTMEM16F, both tagged at the C-terminus with a c-myc tag (*Adeline Martz*). In line with the work of Ousingsawat *et al*, the presence of rTMEM16F-c-myc specifically co-immunoprecipitated rP2X7-c-myc, indicating that a physical association occurs between rP2X7 and rTMEM16F (Figure 100b). The two bands observed by Western blot (Figure 100b, left panel) are most likely due to different glycosylated forms. However, when solely rP2X7 is recombinantly expressed, we were unable to observe this co-immunoprecipitation. This is likely due to the fact that endogenous rP2X7/TMEM16F complexes are too few in number and thus under the detection limit of this technique.

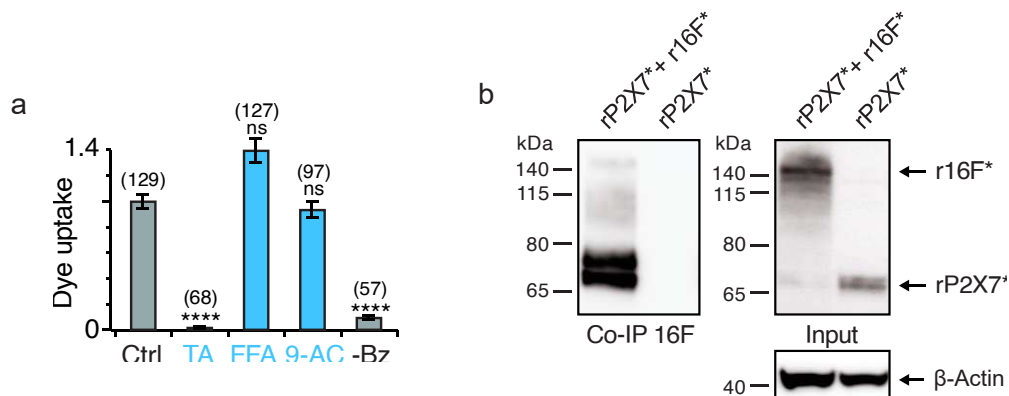


Figure 100. A possible rP2X7/TMEM16F complex with implications for dye uptake.

(a) Summary of YO-PRO-1 dye uptake in rP2X7-expressing 16F-null cells when stimulated with BzATP in the absence (ctrl) or presence of inhibitor (as indicated). -Bz indicates the control conditions, whereby no BzATP is added (basal uptake). Statistical significance was calculated by a Kruskal Wallis test with Dunn's comparison. **** $P < 0.0001$; ns = not significant. Number of cells is shown in bracket, and data is shown as averages \pm SEM. (b) Left : Western blot showing co-immunoprecipitation of rP2X7-cmyc (rP2X7*) and rTMEM16F-cmyc (r16F*), co-immunoprecipitation was performed with anti-TMEM16F antibody. In rP2X7*/r16F* co-transfected cells, two bands corresponding to glycosylated variants of rP2X7* are observed at approximately 70 kDa. The band corresponding to r16F* is visible as a faint, smeared band at approximately 105 kDa. Right : Western blot of total cell lysate, performed with anti-cmyc antibody. In rP2X7*/r16F* co-transfected cells, rP2X7* is present as a very faint band at 70 kDa, and r16F* as a faint, smeared band at approx 105 kDa. The intense band at 140 kDa is likely aggregates. In rP2X7* transfected cells, only the band corresponding to rP2X7* is observed. Work of *Adeline Martz*.

2.4. Contribution of TMEM16F to rP2X7 channel gating.

After investigating the contribution of TMEM16F to macropore formation, we then considered whether TMEM16F may have implications for channel gating properties, including the process of facilitation. We therefore decided to characterise both whole cell and unitary rP2X7 currents in this 16F-null cell line for comparison with HEK293T cells. Whole cell currents obtained from rP2X7 expressed in 16F-null cells exhibited no significant differences to that expressed in HEK293T WT cells (Figure 101d and e). Current density reached after eight short, repetitive applications of BzATP remained similar, at 214 ± 57 pA/pF in 16F-null cells as opposed to 235 ± 29 pA/pF in HEK293T cells. In addition, the extent of facilitation, which was calculated by the fold difference in current measured over eight consecutive BzATP applications, did not change

in a statistically significant manner (2.67-fold increase in 16F-null cells as opposed to 3.36-fold increase in HEK293T cells, n=10 – 15 cells). From the global, averaged perspective that whole cell recordings allow, channel gating properties do not appear to vary whether TMEM16F is endogenously present or not.

However, when probed on the molecular level using outside-out single channel recordings, two interesting differences were apparent. Firstly, in seven out of the nine total patches analysed, we only observed the O1 conductance state. The remaining two patches also exhibited the O1 conductance state, as well as unitary currents of higher magnitude than those which correspond to the O2 conductance state as observed in HEK293T cells. We named these higher conductances HC, but as they occurred only very occasionally, we could not attribute them definitively.

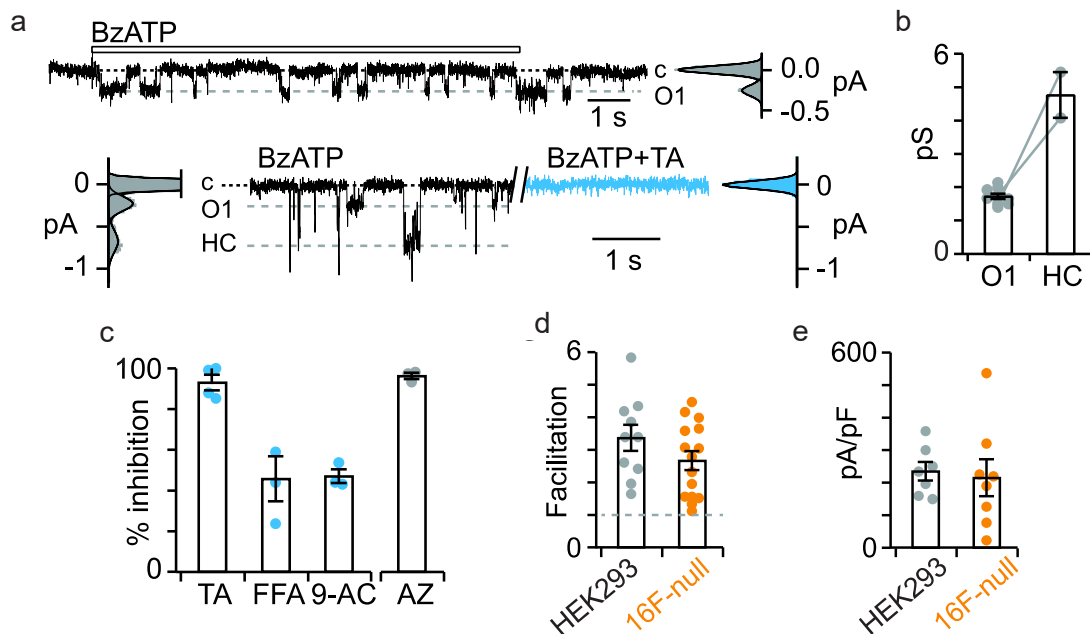


Figure 101. Channel gating properties of rP2X7 in TMEM16F-void cells.

(a) Representative outside-out single channel recordings of rP2X7-expressing 16F-null patches (recorded at -120 mV, $f_c = 100$ Hz, BzATP 10 μ M). Upper panel: representative trace exhibiting uniquely the O1 conductance state and the corresponding all points histogram shown to the right. Lower panel: representative trace exhibiting both the O1 and HC conductance states, and inhibition of these unitary conductances when BzATP is co-applied with TA (20 μ M). Corresponding all points histograms are shown to the left (BzATP application) or to the right (BzATP/TA co-application). (b) Summary of corresponding unitary conductances found in 16F-null cells. Points originating from the same patch are linked with a line, n=9 patches. (c) Summary of percentage inhibition of single channel currents when BzATP is co-applied with the respective CaCC inhibitor (TA n=4, FFA n=3 and 9-AC n=3 patches). P2X7 inhibitor AZ is also shown for comparison (n=3 patches). (d) Histogram representation of the extent of facilitation of rP2X7 expressed in both HEK293T (n=10 cells) and 16F-null cells (n=15 cells) (e) Histogram representation of current density of the eighth consecutive BzATP-evoked response in rP2X7-expressing HEK293T (n=7 cells) or 16F-null cells (n=8 cells).

Given the “loss” of the O2 conductance state in these 16F-null cells, we were surprised that the current density observed in whole cell recordings was not reduced. We therefore decided to analyse the open and closed time histograms of events detected in these outside-out recordings, and found that the mean open time of channels in the 16F-null cell line was

increased as compared to the HEK293T cell line; $rP2X7 NP_o$ was determined as 0.32 in 16F-null cells, compared to 0.17 when expressed in HEK293T cells. This increase in NP_o may therefore account for the unchanged current density observed in whole cell which is observed, despite the disappearance of the O_2 conductance state.

We then decided to investigate the effects of CaCC inhibitors on rP2X7 currents in the 16F-null cell line, to see whether inhibition of channel gating is retained. In outside out patches, inhibition of BzATP currents was observed with all inhibitors, although for FFA and 9-AC percentage inhibition was lower than that observed in HEK293T cells ($45.7 \pm 11.1\%$ for FFA and $47.0 \pm 3.4\%$ for 9-AC, compared to $73.8 \pm 14.3\%$ and $81.1 \pm 4.6\%$ in HEK293T cells respectively).

Whole cell facilitated currents of rP2X7-expressing 16F-null cells were also strongly inhibited by TA, FFA and 9-AC. As in HEK293T cells, TA completely and irreversibly abolished BzATP currents, whilst FFA and 9-AC inhibited to a slightly lower extent ($83.6 \pm 6.3\%$ and $82.7 \pm 7.2\%$ respectively), and in a reversible manner.

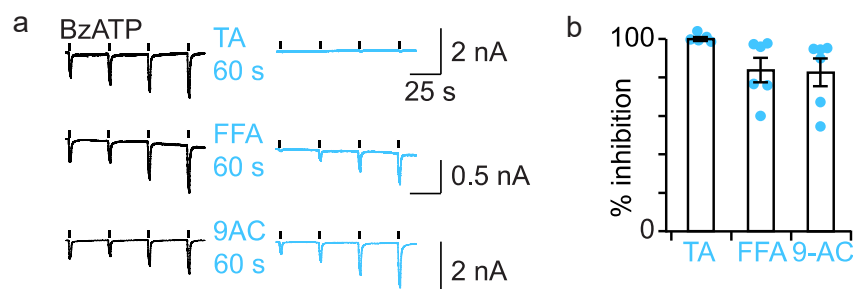


Figure 102. Effects of CaCC inhibitors on whole cell rP2X7 currents in 16F-null cells.

(a) Representative whole cell currents in rP2X7-expressing 16F-null cells, obtained by sequential stimulation with BzATp ($10 \mu\text{M}$), before (left, black) and after (right, blue) 60s perfusion with the respective inhibitor. (b) Summary of percentage inhibition of facilitated rP2X7 currents with CaCC inhibitors. Inhibition is calculated by comparing the current density of the fourth BzATP application before inhibitor application with the first BzATP application following inhibitor perfusion.

These data combined indicate that TMEM16F does have indeed an influence on rP2X7 channel gating properties at the microscopic level, but that channel gating properties at the whole cell level are largely conserved even in the absence of TMEM16F.

2.5. Study of P451L mutant to probe the link between facilitation and macropore formation.

After obtaining evidence for an rP2X7/TMEM16F complex implicated in both channel gating and macropore formation, we decided to consider whether the process of facilitation and macropore formation are linked by a common pathway. As discussed in the introduction to this chapter, basic channel gating has largely been demonstrated to be decoupled from macropore formation, however, few examples exist whereby facilitation and macropore activity are

considered together. We, and other studies (Robinson et al., 2014), remark that facilitation and macropore formation are both modulated by cholesterol, and previous work using a C-terminally truncated rP2X7 construct has observed that whilst channel gating properties remain highly similar, macropore formation is not observed, and nor is facilitation of currents upon repetitive agonist application (Surprenant et al., 1996).

We therefore thought it interesting to investigate whether it is possible to delineate facilitation from macropore formation by way of a point mutation. If such a point mutation were to have significant effects on one of these behaviours, without significantly impacting the other, this would provide evidence to suggest that facilitation and macropore formation do not originate from a common mechanistic pathway. We decided to use the P451L mutant construct, which has been identified as a non-synonymous SNP found in mouse P2X7R, associated with reduced pain sensitivity (Sorge et al., 2012). This mutant has previously been shown to exhibit impaired dye uptake activity (Adriouch et al., 2002; Xu et al., 2012; Young et al., 2006), although surface expression remained comparable to that of the WT in both rat and mouse orthologs (Adriouch et al., 2002; Young et al., 2006). In the mouse rP2X7 construct carrying this P451L mutation, facilitation of currents was observed and found to be comparable to that of the WT, but this was not fully quantified and tested for significance (Young et al., 2006).

In our conditions, rP2X7 carrying P451L mutation exhibited robust channel gating, and after eight consecutive applications of BzATP, the observed current densities were 246 ± 61.2 pA/pF and 189 ± 32.3 pA/pF in the WT and P451L mutant respectively, which was not significantly different when tested statistically (Student's *t*-test, $n = 10 - 14$ cells). Equally, channel gating on the single channel level was found to be very similar to the WT receptor, with two conductances corresponding to O1 and O2 present (Figure 103c, O1 = 1.70 ± 0.11 pS; O2 = 3.39 ± 0.37 pS, $n = 4$ patches). Only one patch exhibited uniquely the O1 conductance.

We observed a robust facilitation in the P451L mutant, resulting in a 2.27-fold difference compared to 3.36 in the wild type (Figure 103a and b). Nevertheless, this slight reduction (32.5%) in the extent of facilitation did prove to be statistically significant ($P=0.018$). The impact of the P451L mutation on dye uptake was, however, more pronounced, with a reduction of $68.7 \pm 9\%$ observed incorporation of YO-PRO-1, as shown in Figure 103d and e (realised by *Fanny Gautherat*). Although both processes studied appear to be affected by the mutation P451L, the effects on facilitation are much milder when compared to the severe impairment of dye uptake which we observed. This suggests that facilitation and the P2X7 macropore likely do not occur through a common mechanistic pathway, as if this were the case, we would expect to see a more consistent impact of the mutation towards the two processes.

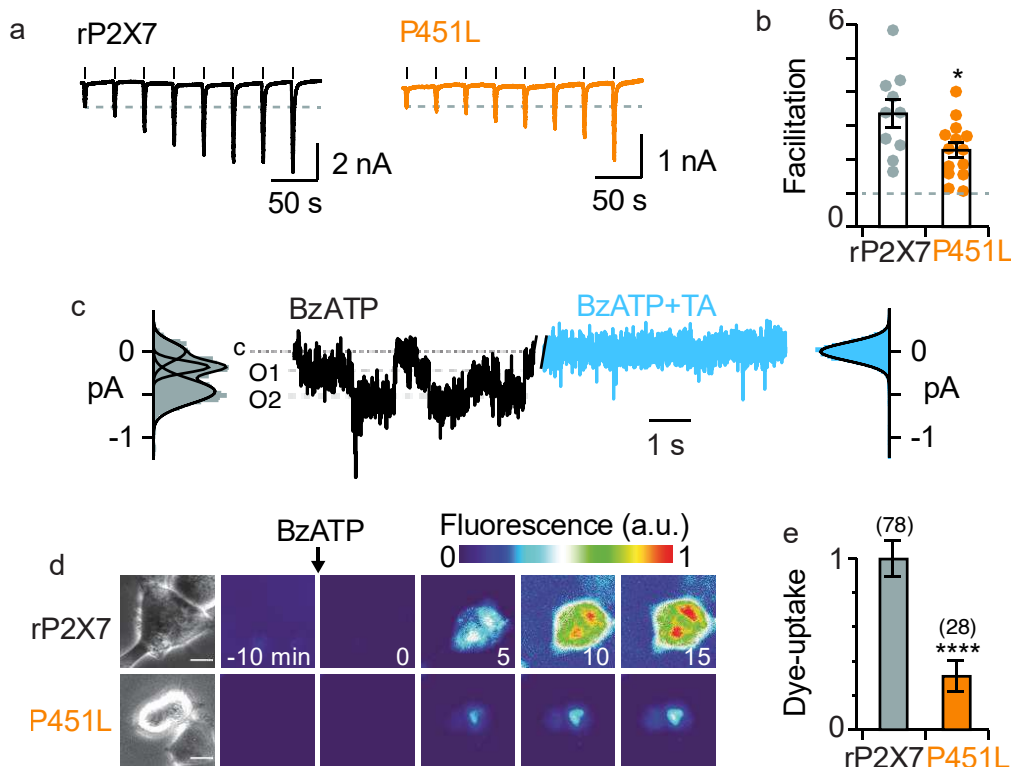


Figure 103. Characterisation of facilitation and macropore formation in P451L mutant.

(a) Representative whole cell electrophysiological traces of HEK293T cells expressing either rP2X7 WT (black, left) or P451L mutant receptors (right, orange), stimulated eight times with BzATP (10 μM). (b) Summary of the extent of facilitation observed in either WT or P451L mutant (calculated by comparison of the eighth response to the first). $P=0.0187$ by Student's *t*-test, $n=10$ for WT and $n=14$ for P451L mutant. (c) Single-channel currents elicited by 10 μM BzATP in the absence (black trace) or presence of 20 μM TA (blue trace) from an outside-out patch of HEK293T cells transfected with the P451L mutant. Corresponding all points histograms of currents are shown to the side of the traces. (d) Time series fluorescence images of YO-PRO-1 dye uptake in HEK293T cells heterologously expressing rP2X7R WT or P451L mutant receptors. On the left are shown the corresponding microphotographs under transmitted light (scale bar, 10 μm). (e) Summary of corresponding BzATP-induced YO-PRO-1 dye uptake for rP2X7R (black, from 12 transfections) and P451L mutant (orange, from 5 transfections). Shown is the specific dye-uptake subtracted by residual uptake recorded in the absence of BzATP. Statistical analysis was performed using Mann-Whitney test. **** $P < 0.0001$. Number of cells analysed is indicated in brackets. Dye uptake is the work of Fanny Gautherat.

Having determined that TMEM16F contributes to rP2X7-evoked dye uptake, and obtaining strong evidence that this contribution is in the form of an rP2X7/TMEM16F complex, the question can also be raised as to whether the reduced dye uptake observed with the P451L mutant may be the result of impaired rP2X7/TMEM16F complex formation. Interestingly, the P451L mutation has also been shown to reduce phosphatidylserine (PS) exposure at the membrane surface, a key marker of scramblase activity (Sorge et al., 2012). At present, we have only tested the effect of the CaCC inhibitor TA on single channel P451L currents, and found that sensitivity to this inhibitor is retained. However, once again due to the uncertainty surrounding the mode of inhibition of TA on rP2X7 activity, this P451L mutant should be tested

with FFA and 9-AC, in single channel recordings as well as dye uptake assays, to probe more definitively whether the mutation affects the ability of an rP2X7/TMEM16F complex to form.

2.6. A molecular model supporting rP2X7/TMEM16F complex formation.

Finally, we collaborated with *Dr. Antoine Taly (IPBC, Paris)*, to explore whether the physical association of rP2X7 and TMEM16F in a complex can be supported by molecular modelling experiments. Using the recently resolved cryo-EM structures of rP2X7 and mTMEM16F, docking experiments using Monte-carlo methods were carried out to produce two models, one with rP2X7 in the closed state and one featuring the ATP-bound open state. These models reveal a potential association between the ballast of one rP2X7 subunit and the cytoplasmic domain of one mTMEM16F monomer. These models therefore support the possibility of a close physical association between rP2X7 and TMEM16F in complex.

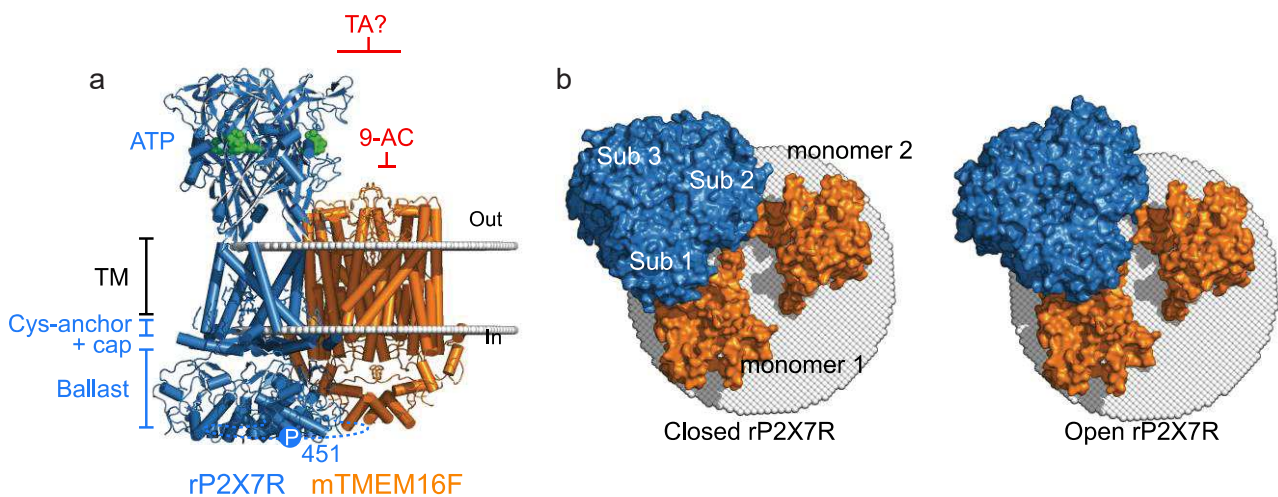


Figure 104. Molecular model of rP2X7 and mTMEM16F in complex.

(a) Lateral view of rP2X7/mTMEM16F complex modelled by docking experiments, carried out *a priori*, except for their position in the membrane plane. rP2X7 is shown in blue (PDB: 6U9V) and Ca²⁺-bound mTMEM16F in orange (PDB/ 6QPC). In this complex it can be determined that 9-AC acts to inhibit the TMEM16F component, whilst TA may inhibit both members of the complex. FFA inhibits neither. (b) Bottom-up views from the cytoplasmic surface of the models in the closed (left) and open (right) rP2X7 states. P2X7 subunits as well as TMEM16F monomers are indicated. Work of *Dr. Antoine Taly*.

DISCUSSION AND OUTLOOK

During this project, we have been able to investigate further the processes of facilitation and macropore formation. One of the principal findings is that both of these hallmark P2X7 phenomena are reliant on rP2X7/TMEM16 protein complexes, which form a “hub”, exerting considerable influence over all aspects of P2X7 activity.

Our single channel study on the facilitated state of rP2X7Rs suggests that the dramatic increase of currents observed upon prolonged ATP stimulation originates from a considerable increase in the rP2X7 NP_o , which in turn is dependent on the depletion of cholesterol from the membrane. The cellular mechanism through which cholesterol is depleted upon prolonged rP2X7 activity remains to be fully determined, although as we have seen in chapter two, rP2X7 activation has influence over several lipid metabolic pathways with potential consequences for lipid raft domains, where cholesterol is abundant. As approximately half of the rP2X7Rs expressed in HEK293 cells are found in lipid rafts, the depletion of cholesterol from these raft environments and the accompanying increase in rP2X7 open probability represents a very possible source of the dramatic current increases observed upon receptor facilitation. Given that rP2X7 activation has been shown to upregulate ceramide production (Lépine et al., 2006; Raymond and Stunff, 2006), and ceramide has been shown to selectively displace cholesterol from lipid raft domains (Megha and London, 2004), a focused study into the relationships between rP2X7, ceramide and rP2X7-bound cholesterol as a possible facilitation pathway would shed light as to how this facilitated, cholesterol-depleted state is accessed. Another interesting study to mention at this point is one in which single-particle tracking photoactivated localisation microscopy (sptPALM) has shown that ATP regulates the mobility of P2X7Rs at the cell membrane, including those which are found within nanoclusters similar to lipid rafts (Shrivastava et al., 2013). This represents another means as to how the activity of rP2X7 may be regulated by changes in its surrounding lipidic environment brought on by ATP application.

Our study suggests that cholesterol maintains the rP2X7/TMEM16 complex in a low channel activity state, and that, upon prolonged or repetitive channel activation and subsequent dissociation of cholesterol, switching of the channel into a higher activity state occurs. Precisely how cholesterol is associated with rP2X7/TMEM16 complexes, however, remains to be investigated. The study of Karasawa *et al* using truncated pdP2X7 receptors reconstituted into liposomes of varying lipidic composition has suggested a direct association of cholesterol and rP2X7, most likely through binding to the TM domains (Karasawa et al., 2017), and at least two CRAC motifs have also been identified in the sequence of P2X7 within the C-terminal regions (Kopp et al., 2019). Several residues within the TM domains have also been shown to modulate receptor sensitisation (Jindrichova et al., 2015), and may merit further investigation

in the context of cholesterol interactions. Whether cholesterol also binds to TMEM16 components of the complex remains to be determined. One possibility is that, in addition to rP2X7 sensitivity to cholesterol, TMEM16F, and other TMEM channels which may be involved in complex formation, are themselves regulated directly by cholesterol. Recent studies indicate that MCD treatment stabilises TMEM16A activity, with a putative cholesterol-binding motif identified in the fifth transmembrane domain (De Jesús-Pérez et al., 2018). An alternative scenario would be that rP2X7 is the only cholesterol-sensitive component of the rP2X7/TMEM16 complex, and that upregulation of P2X7 following cholesterol dissociation is in turn transmitted *via* cross-talk mechanisms to an upregulation of TMEM16 activity. Mutagenesis scanning studies of the residues comprising these putative cholesterol binding sites and their effects on facilitation behaviour should be carried out to gain a more precise understanding of the mode of action of cholesterol at rP2X7/TMEM16 complexes.

Our single channel data have also confirmed similarities between the rat and human P2X7 orthologs on the molecular level, in that the presence of two conductance states appears to be a common feature between these species. Our observations are also consistent with those of Riedel *et al* in that the absolute values of unitary conductances do not change over the course of ATP stimulation (Riedel et al., 2007). No significant difference in unitary conductance was observed between naïve patches or those having undergone BzATP induced facilitation prior to membrane excision. This observation therefore goes against the argument for a pore dilation mechanism being at play, as if the diameter of the P2X7 pore were to change dramatically during the transition to the facilitated state, we would expect to see some alterations in the magnitude of unitary conductances, whereas this is not the case.

We believe that the conductance states O1 and O2 originate from the rP2X7 channel itself, rather than the outwardly-rectifying TMEM16 channels, for which activity is expected to be minimal at the holding potential of -120 mV (Adomaviciene et al., 2013; Alvadia et al., 2019; Yang et al., 2012). The experiments carried out in Axolotl oocytes provide evidence that FFA and 9-AC do not act directly on the rP2X7 channel. Therefore, the pharmacological inhibition by these P2X7-inactive CaCC inhibitors, of rP2X7 currents observed at the single channel level, suggests that rP2X7 is closely associated with TMEM16 channels. Whilst we do not know the precise mechanisms behind how the complex may function, these results suggest that a sort of synergistic relationship exists, whereby inhibition of one component of the complex results in a transmitted inhibition of the complex as a whole, in a pharmacological cross-talk mechanism. This possibility is supported by the results of the co-immunoprecipitation experiments, which indicate a close physical association between rP2X7 and rTMEM16F (Figure 100), and molecular modelling experiments which confirm that such a physical association would be energetically feasible.

During this project, we have chosen to focus on the possibility of a rP2X7/TMEM16F complex, in light of the previously discussed work of Ousingsawat *et al* suggesting that this TMEM subtype may be implicated in P2X7 activity. CRISPR/Cas-9 knock-out of TMEM16F confirms that TMEM16F does indeed exert an influence over several rP2X7 behaviours, one of these being the unitary conductances. In 16F-null cells, the absence of O₂, along with the sporadic appearance of a higher conductance state HC, and the increase in mean open time suggests that TMEM16F has a “shaping” influence over unitary currents. The specificities of how this occurs have not yet been investigated, but an influence over the unitary currents of channels by protein partners and auxiliary subunits acting as “molecular switches” with regard to unitary conductances has been documented in the literature (Kaulin *et al.*, 2009; Wakamori *et al.*, 1999). If TMEM16F is present in a tight molecular complex with rP2X7, our data suggests that it cannot be the sole TMEM16 variant to be involved. Given that rP2X7 unitary currents are inhibited by TMEM16F-inactive FFA, and that sensitivity to CaCC inhibitors is retained in 16F-null cells, our data suggests that TMEM16F may associate with other, FFA-sensitive TMEM16 subunit variants within the complex, for example in the form of heteromers. This ability of TMEM16 channels to assemble in a heteromeric manner has been previously been demonstrated, notably between TMEM16F and TMEM16B subtypes (Henkel *et al.*, 2015). Another possibility to account for our observation that sensitivity to CaCC inhibitors is retained in 16F-null cells, is that gene regulatory networks may exist concerning the expression of TMEM16s, which would be set into action upon deletion of TMEM16F, resulting in altered expression levels of other TMEM16s in order to compensate for this deletion. This could be probed by RT-PCR analysis and comparison between HEK293T and 16F-null cell lines. A particularly interesting possibility to further investigate would be the expression profile of TMEM16E, as this subtype is the closest to TMEM16F within the phylogenetic tree and, like TMEM16F, has been shown to exhibit scramblase activity (Di Zanni *et al.*, 2018; Milenkovic *et al.*, 2010). In this way we can imagine a wider, combinatorial approach to rP2X7/TMEM16 complexes, whereby in different cell types, according to the expression profile of TMEM16s, the specific characteristics of the rP2X7/TMEM16 complexes are altered. This may also account for the variations observed in dye uptake between cell types.

Aside from the implications of TMEM16s for rP2X7 channel gating activity, our results indicate that TMEM16s also have strong implications for macropore formation and dye uptake activity. Firstly, our results demonstrate that in HEK293T cells, rP2X7 mediated dye uptake requires additional proteins. In HEK293T WT cells, FFA showed no inhibitory effects on dye uptake (Figure 98). Compared to the electrophysiological results, where FFA inhibits approximately 82% of P2X7 currents, this leads us to conclude that only a minority of rP2X7-embedded complexes are involved in dye uptake (those which are insensitive to FFA). If this were not the

case, we would expect to see the same levels of FFA inhibition in both YO-PRO-1 incorporation and channel gating. In 16F-null cells, dye uptake is reduced by 35 – 40 %, confirming that TMEM16F is implicated in dye uptake. Interestingly, 9-AC inhibits dye uptake in HEK293T cells by 37%, and this inhibition disappears upon knock-out of TMEM16F in 16F-null cells. These results suggest that in HEK293T cells, 9-AC acts by inhibiting TMEM16F.

In light of these results in 16F-null cells, the remaining contribution to dye uptake has been demonstrated to be insensitive to inhibition by FFA or 9-AC (Figure 99). This therefore raises two possibilities of components which may be behind the remaining dye uptake. Firstly, as we have shown in *Axolotl* oocytes that rP2X7 is not affected by FFA or 9-AC, the pharmacological profile of dye uptake in 16F-null cells is consistent with an intrinsic dye uptake of rP2X7. This scenario would be consistent with the study of Karasawa *et al* who determined that YO-PRO-1 dye uptake is an intrinsic property of pdP2X7 truncated receptors reconstructed into liposomes, therefore requiring no additional proteins. However, the recent cryo-EM structure of rP2X7 shows an open state pore diameter of approximately 5Å, and no class average images showing a dilated pore were identified. The minimal cross section of YO-PRO-1, 7Å, exceeds the diameter of the open pore resolved in this structure, suggesting that direct passage of YO-PRO-1 likely occurs at very reduced rates, as has been suggested to be the case for rP2X2Rs (Harkat *et al.*, 2017). Considering the larger dyes for which P2X7-dependent cell permeabilization has been recorded, such as YOYO-1 (763 Da) and TOTO-1 (894 Da) (Figure 81), direct permeation through the P2X7 pore would be most unlikely. For YO-PRO-1 however, this permeation pathway remains a possibility. It would be interesting to probe this possibility further, using an experimental design allowing to selectively block the P2X7 pore, thereby allowing to delineate whether this remaining component of YO-PRO-1 uptake is direct permeation through the P2X7 pore. This could be envisaged with, for example, bulky MTS reagents in conjunction with cysteine mutations in order to block the P2X7 pore, or indeed point mutations within the P2X7 pore to introduce bulky residues within the channel. The latter would be a particularly interesting possibility if a mutation were identified which allowed small inorganic cations to pass as usual, lessening perturbation to channel activity and subsequent downstream pathways, but impacted upon permeation of larger dyes.

The second possibility for this remaining dye uptake component is, as mentioned earlier, that TMEM16 subtypes other than TMEM16F may be involved in dye uptake. Following the pharmacological profile of dye uptake in 16F-null cells, these TMEM16s would be insensitive to FFA and 9-AC. An interesting consideration to discuss at this point is that TMEM16F is primarily a lipid scramblase, effecting the passage of lipids between bilayer leaflets. Recently, it has been shown that a fungal TMEM16 homologue is able to scramble polyethylene glycol-conjugated lipids of very high molecular weight (up to 5000 Da) (Malvezzi *et al.*, 2018), which

would lend credibility to the possibility that the scramblase activity of TMEM16F confers the ability to transport large molecular weight dyes across the cell membrane. In this scenario, the rP2X7/TMEM16 complexes involved in dye permeation would feature exclusively TMEM16 variants possessing scrambling activities.

In order to test the possible involvement of further TMEM16 variants, a number of future experiments can be envisaged. Firstly, it would be interesting to recombinantly express TMEM16 variants in the Axolotl system, to test directly which subtypes are sensitive, or not, to FFA and 9-AC inhibition. This would identify TMEM16s whose implication in a dye-incorporating rP2X7 complex would be consistent with the pharmacological profile observed in the 16F-null cells. We also plan to carry out further, specific CRISPR/Cas-9 knock-outs of individual TMEM16 channels from HEK293T. Previous work in the literature has found mRNA of all TMEM16 variants, with the exception of TMEM16J, to be endogenously expressed in HEK293 cells (Banerjee et al., 2017). The experiments in Axolotl oocytes would therefore be judicious to guide us in the decision of which TMEM16s to target in the CRISPR/Cas-9 knockout assay.

Regarding our efforts to delineate macropore formation and facilitation, through the P451L mutant, our data suggest that these two phenomena likely do not share a common pathway. The fact that our 16F-null cell lines exhibits reduced dye uptake but unchanged facilitation behaviour also provides evidence that these two pathways are not one and the same. It would be interesting to probe further this P451L mutant which exerts such a dramatic effect on dye uptake. One possibility, which would be supported by the molecular docking experiments, is that P451L is a key residue involved in the formation of a physical association between rP2X7 and TMEM16s. Unfortunately, the region containing P451 is unresolved in the cryo-EM structure, so we are unable to uncover through the model exactly which positions within TMEM16F may be in interaction with P451 in rP2X7. However, approximate regions of possible interaction can be identified in this model, not only in the cytosolic regions, which may contain the interaction site of P451, but also in the extracellular domain. These regions should therefore be the object of future mutagenesis scanning experiments which may be able to identify more precisely residues which are indispensable for complex formation. We also plan to continue this part of the project by testing the inhibition of FFA and 9-AC on channel gating and dye uptake of P451L mutant, to determine whether sensitivity to CaCC inhibitors, and thus existence of a rP2X7/TMEM16 complex, is fully retained.

CONCLUSION

To conclude this section, through this study we have been able to shed light on the facilitation phenomenon from a molecular point of view, which, up until now had remained unexplored. Whilst the pathway through which rP2X7Rs transition to the facilitated state remains to be precisely identified and thoroughly characterised, we confirm the likely involvement of cholesterol and the effects of this on the molecular level.

This study has also allowed us to obtain strong evidence for a rP2X7/TMEM16 complex with numerous implications for both channel gating and macropore formation. More specifically, we have been able to identify that in HEK293T cells, TMEM16F is (one of) the TMEM16 family member(s) to be involved in macropore formation. We propose that the P2X7/TMEM16 complex constitutes a hub, which may be assembled in a combinatorial manner according to the cell type and levels of TMEM16 subtype expression. This kind of assembly would represent a regulatory platform, from which the pleiotropic effects resulting from ATP activation of P2X7 could be mediated, in physiological and pathological states. Activation of the hub would trigger a co-ordinated hive of activity, including not only channel gating processes, such as Ca^{2+} , Na^{+} and K^{+} flux, and facilitation upon prolonged agonist exposure, but also macropore formation and downstream signalling pathways resulting in membrane blebbing, interleukin release and phospholipid scrambling (Di Virgilio et al., 2018b). The existence of such a regulating hub is therefore also particularly interesting from a therapeutic viewpoint; P2X7-related diseases may occur following the dysregulation of hub activity. This study now opens a number of new prospects regarding future research into the intimate association of P2X7 and TMEM16 channels, which will hopefully untangle further mechanistic details.

GENERAL CONCLUSIONS

Within this PhD, three principal projects have been undertaken, with the global aim of furthering the comprehension of P2X7R structure and function.

The first of these projects aimed to work towards the resolution of a P2X7R cryo-EM structure. We rapidly encountered difficulties regarding the aggregation of P2X7R during the extraction and purification process. The recently resolved cryo-EM structure of rP2X7 has overcome these difficulties, and we may speculate that this is by way of including cholesterol, with which P2X7R has been shown to closely interact (Karasawa et al., 2017; Robinson et al., 2014). The inclusion of cholesterol during purification may act, therefore, to stabilize the protein, and future structural resolutions could be envisaged following this protocol. This would be particularly interesting in the case of structures featuring P2X7R in complex with a protein partner.

The second of these projects focused on the use of two original photochemical tools for the study of P2X7R, MEA-TMA and MAM. The application of these tools to P2X7R for robust photocontrol of channel activity proved difficult, underlining the differences between P2X7 and the other P2X family members, for which, photocontrol was readily adaptable. In the case of MAM, tethering to endogenous cysteines and inconsistent photoregulated activity largely hampered the use of this strategy as a means to light-control receptors, and to elucidate information relating to structural movements. In the case of MEA-TMA, optogating was not observed, unless steric hindrance from residue Y343 was removed, in which case weak light-gated openings could be observed. Light-induced channel activity persisted even in the presence of inhibitors, indicating that the molecular motions behind these openings are likely the result of local rearrangements and not, therefore, identical to the global, physiological movements involved in ATP-gating. However, in the context of a photochemical tool with which to probe P2X7 activity, MEA-TMA proved to be of interest. In this case, we applied this tool to the study of the facilitation process, and were able to show that two populations are involved in this phenomenon. Although the precise nature of these two populations remains to be determined, several possibilities have been evoked and merit further study.

In the last chapter of this manuscript, we studied this facilitation phenomenon further. Single channel recordings afforded a molecular-level characterisation of this process, and we determined that facilitated currents result from an increase in the open probability of channels, likely as a result of the dissociation of cholesterol. We also investigated the possibility of a P2X7/TMEM16 complex. We found strong evidence for the existence of such a complex, between P2X7R and the TMEM16F subtype in particular, although it is highly likely that this is

not the only TMEM16 subtype involved. This complex has implications not only on macropore formation, probed by dye uptake assays, but also on channel gating, as observed at the single channel level.

The work in particular of this last chapter suggests that a thorough understanding of the molecular mechanisms of P2X7R, therefore, requires not only an isolated consideration of the P2X7R protein itself, but a wider consideration of P2X7 within the networks in which it resides, whether this be the lipidic bilayer and its components, or indeed protein partnerships. This PhD work has hopefully contributed a basis to study several of these P2X7-containing networks further.

BIBLIOGRAPHY

- Abbracchio, M.P., Burnstock, G., 1994. Purinoceptors: Are there families of P2X and P2Y purinoceptors? *Pharmacol. Ther.* 64, 445–475. [https://doi.org/10.1016/0163-7258\(94\)00048-4](https://doi.org/10.1016/0163-7258(94)00048-4)
- Acuña-Castillo, C., Coddou, C., Bull, P., Brito, J., Huidobro-Toro, J.P., 2007. Differential role of extracellular histidines in copper, zinc, magnesium and proton modulation of the P2X7 purinergic receptor. *J. Neurochem.* 101, 17–26. <https://doi.org/10.1111/j.1471-4159.2006.04343.x>
- Adinolfi, E., Callegari, M.G., Cirillo, M., Pinton, P., Giorgi, C., Cavagna, D., Rizzuto, R., Virgilio, F.D., 2009. Expression of the P2X7 Receptor Increases the Ca²⁺ Content of the Endoplasmic Reticulum, Activates NFATc1, and Protects from Apoptosis. *J. Biol. Chem.* 284, 10120–10128. <https://doi.org/10.1074/jbc.M805805200>
- Adinolfi, E., Cirillo, M., Woltersdorf, R., Falzoni, S., Chiozzi, P., Pellegatti, P., Callegari, M.G., Sandonà, D., Markwardt, F., Schmalzing, G., Di Virgilio, F., 2010. Trophic activity of a naturally occurring truncated isoform of the P2X7 receptor. *FASEB J.* 24, 3393–3404. <https://doi.org/10.1096/fj.09-153601>
- Adomaviciene, A., Smith, K.J., Garnett, H., Tammaro, P., 2013. Putative pore-loops of TMEM16/anoctamin channels affect channel density in cell membranes. *J. Physiol.* 591, 3487–3505. <https://doi.org/10.1113/jphysiol.2013.251660>
- Adriouch, S., Bannas, P., Schwarz, N., Fliegert, R., Guse, A.H., Seman, M., Haag, F., Koch-Nolte, F., 2008. ADP-ribosylation at R125 gates the P2X7 ion channel by presenting a covalent ligand to its nucleotide binding site. *FASEB J. Off. Publ. Fed. Am. Soc. Exp. Biol.* 22, 861–869. <https://doi.org/10.1096/fj.07-9294com>
- Adriouch, S., Dox, C., Welge, V., Seman, M., Koch-Nolte, F., Haag, F., 2002. Cutting edge: a natural P451L mutation in the cytoplasmic domain impairs the function of the mouse P2X7 receptor. *J. Immunol. Baltim. Md* 1950 169, 4108–4112. <https://doi.org/10.4049/jimmunol.169.8.4108>
- Adriouch, S., Hubert, S., Pechberty, S., Koch-Nolte, F., Haag, F., Seman, M., 2007. NAD⁺ released during inflammation participates in T cell homeostasis by inducing ART2-mediated death of naive T cells in vivo. *J. Immunol. Baltim. Md* 1950 179, 186–194. <https://doi.org/10.4049/jimmunol.179.1.186>
- Alberto, A.V.P., Faria, R.X., Couto, C.G.C., Ferreira, L.G.B., Souza, C. a. M., Teixeira, P.C.N., Fróes, M.M., Alves, L.A., 2013. Is pannexin the pore associated with the P2X7

- receptor? *Naunyn. Schmiedebergs Arch. Pharmacol.* 386, 775–787. <https://doi.org/10.1007/s00210-013-0868-x>
- Alexander, S.P., Peters, J.A., Kelly, E., Marrion, N.V., Faccenda, E., Harding, S.D., Pawson, A.J., Sharman, J.L., Southan, C., Davies, J.A., 2017. THE CONCISE GUIDE TO PHARMACOLOGY 2017/18: Ligand-gated ion channels. *Br. J. Pharmacol.* 174, S130–S159. <https://doi.org/10.1111/bph.13879>
- Allen, B.D., Singer, A.C., Boyden, E.S., 2015. Principles of designing interpretable optogenetic behavior experiments. *Learn. Mem.* 22, 232–238. <https://doi.org/10.1101/lm.038026.114>
- Alloisio, S., Aiello, R., Ferroni, S., Nobile, M., 2006. Potentiation of Native and Recombinant P2X7-Mediated Calcium Signaling by Arachidonic Acid in Cultured Cortical Astrocytes and Human Embryonic Kidney 293 Cells. *Mol. Pharmacol.* 69, 1975–1983. <https://doi.org/10.1124/mol.105.020164>
- Allsopp, R.C., Evans, R.J., 2015. Contribution of the Juxtatransmembrane Intracellular Regions to the Time Course and Permeation of ATP-gated P2X7 Receptor Ion Channels. *J. Biol. Chem.* 290, 14556–14566. <https://doi.org/10.1074/jbc.M115.642033>
- Allsopp, R.C., Lalo, U., Evans, R.J., 2010. Lipid raft association and cholesterol sensitivity of P2X1-4 receptors for ATP: chimeras and point mutants identify intracellular amino-terminal residues involved in lipid regulation of P2X1 receptors. *J. Biol. Chem.* 285, 32770–32777. <https://doi.org/10.1074/jbc.M110.148940>
- Almén, M.S., Nordström, K.J., Fredriksson, R., Schiöth, H.B., 2009. Mapping the human membrane proteome: a majority of the human membrane proteins can be classified according to function and evolutionary origin. *BMC Biol.* 7, 50. <https://doi.org/10.1186/1741-7007-7-50>
- Alvadia, C., Lim, N.K., Clerico Mosina, V., Oostergetel, G.T., Dutzler, R., Paulino, C., 2019. Cryo-EM structures and functional characterization of the murine lipid scramblase TMEM16F. *eLife* 8, e44365. <https://doi.org/10.7554/eLife.44365>
- Anderson, C.M., Nedergaard, M., 2006. Emerging challenges of assigning P2X7 receptor function and immunoreactivity in neurons. *Trends Neurosci.* 29, 257–262. <https://doi.org/10.1016/j.tins.2006.03.003>
- Andrei, C., Margiocco, P., Poggi, A., Lotti, L.V., Torrisi, M.R., Rubartelli, A., 2004. Phospholipases C and A2 control lysosome-mediated IL-1 β secretion: Implications for inflammatory processes. *Proc. Natl. Acad. Sci.* 101, 9745–9750. <https://doi.org/10.1073/pnas.0308558101>

- Armstrong, N., Sun, Y., Chen, G.Q., Gouaux, E., 1998. Structure of a glutamate-receptor ligand-binding core in complex with kainate. *Nature* 395, 913–917. <https://doi.org/10.1038/27692>
- Aumiller, J.J., Mabashi-Asazuma, H., Hillar, A., Shi, X., Jarvis, D.L., 2012. A new glycoengineered insect cell line with an inducibly mammalianized protein N-glycosylation pathway. *Glycobiology* 22, 417–428. <https://doi.org/10.1093/glycob/cwr160>
- Autzen, H.E., Myasnikov, A.G., Campbell, M.G., Asarnow, D., Julius, D., Cheng, Y., 2018. Structure of the human TRPM4 ion channel in a lipid nanodisc. *Science* 359, 228–232. <https://doi.org/10.1126/science.aar4510>
- Bai, X., McMullan, G., Scheres, S.H.W., 2015. How cryo-EM is revolutionizing structural biology. *Trends Biochem. Sci.* 40, 49–57. <https://doi.org/10.1016/j.tibs.2014.10.005>
- Baker, M.R., Fan, G., Serysheva, I.I., 2015. Single-particle cryo-EM of the ryanodine receptor channel in an aqueous environment. *Eur. J. Transl. Myol.* 25, 35–48. <https://doi.org/10.4081/ejtm.2015.4803>
- Banerjee, J., Leung, C.-T., Li, A., Peterson-Yantorno, K., Ouyang, H., Stamer, W.D., Civan, M.M., 2017. Regulatory Roles of Anoctamin-6 in Human Trabecular Meshwork Cells. *Invest. Ophthalmol. Vis. Sci.* 58, 492–501. <https://doi.org/10.1167/iovs.16-20188>
- Banghart, M., Borges, K., Isacoff, E., Trauner, D., Kramer, R.H., 2004. Light-activated ion channels for remote control of neuronal firing. *Nat. Neurosci.* 7, 1381–1386. <https://doi.org/10.1038/nn1356>
- Banghart, M.R., Mouro, A., Fortin, D.L., Yao, J.Z., Kramer, R.H., Trauner, D., 2009. Photochromic blockers of voltage-gated potassium channels. *Angew. Chem. Int. Ed Engl.* 48, 9097–9101. <https://doi.org/10.1002/anie.200904504>
- Barbe, M.T., Monyer, H., Bruzzone, R., 2006. Cell-Cell Communication Beyond Connexins: The Pannexin Channels. *Physiology*. <https://doi.org/10.1152/physiol.00048.2005>
- Baricordi, O.R., Ferrari, D., Melchiorri, L., Chiozzi, P., Hanau, S., Chiari, E., Rubini, M., Di Virgilio, F., 1996. An ATP-activated channel is involved in mitogenic stimulation of human T lymphocytes. *Blood* 87, 682–690. <https://doi.org/10.1182/blood.V87.2.682.bloodjournal872682>
- Baricordi, O.R., Melchiorri, L., Adinolfi, E., Falzoni, S., Chiozzi, P., Buell, G., Virgilio, F.D., 1999. Increased Proliferation Rate of Lymphoid Cells Transfected with the P2X7 ATP Receptor. *J. Biol. Chem.* 274, 33206–33208. <https://doi.org/10.1074/jbc.274.47.33206>

- Barrera, N.P., Ormond, S.J., Henderson, R.M., Murrell-Lagnado, R.D., Edwardson, J.M., 2005. Atomic Force Microscopy Imaging Demonstrates that P2X2 Receptors Are Trimers but That P2X6 Receptor Subunits Do Not Oligomerize. *J. Biol. Chem.* 280, 10759–10765. <https://doi.org/10.1074/jbc.M412265200>
- Bartels, E., Wassermann, N.H., Erlanger, B.F., 1971. Photochromic Activators of the Acetylcholine Receptor. *Proc. Natl. Acad. Sci. U. S. A.* 68, 1820–1823.
- Barth, K., Weinhold, K., Guenther, A., Linge, A., Gereke, M., Kasper, M., 2008. Characterization of the molecular interaction between caveolin-1 and the P2X receptors 4 and 7 in E10 mouse lung alveolar epithelial cells. *Int. J. Biochem. Cell Biol.* 40, 2230–2239. <https://doi.org/10.1016/j.biocel.2008.03.001>
- Barth, K., Weinhold, K., Guenther, A., Young, M.T., Schnittler, H., Kasper, M., 2007. Caveolin-1 influences P2X7 receptor expression and localization in mouse lung alveolar epithelial cells. *FEBS J.* 274, 3021–3033. <https://doi.org/10.1111/j.1742-4658.2007.05830.x>
- Bartlett, R., Stokes, L., Sluyter, R., 2014. The P2X7 receptor channel: recent developments and the use of P2X7 antagonists in models of disease. *Pharmacol. Rev.* 66, 638–675. <https://doi.org/10.1124/pr.113.008003>
- Basak, S., Gicheru, Y., Samanta, A., Molugu, S.K., Huang, W., Fuente, M. la de, Hughes, T., Taylor, D.J., Nieman, M.T., Moiseenkova-Bell, V., Chakrapani, S., 2018. Cryo-EM structure of 5-HT 3A receptor in its resting conformation. *Nat. Commun.* 9, 1–10. <https://doi.org/10.1038/s41467-018-02997-4>
- Basso, A.M., Bratcher, N.A., Harris, R.R., Jarvis, M.F., Decker, M.W., Rueter, L.E., 2009. Behavioral profile of P2X7 receptor knockout mice in animal models of depression and anxiety: Relevance for neuropsychiatric disorders. *Behav. Brain Res.* 198, 83–90. <https://doi.org/10.1016/j.bbr.2008.10.018>
- Beharry, A.A., Woolley, G.A., 2011. Azobenzene photoswitches for biomolecules. *Chem. Soc. Rev.* 40, 4422–4437. <https://doi.org/10.1039/c1cs15023e>
- Bennett, M.R., 2001. *History of the Synapse*. CRC Press.
- Bergfeld, G.R., Forrester, T., 1992. Release of ATP from human erythrocytes in response to a brief period of hypoxia and hypercapnia. *Cardiovasc. Res.* 26, 40–47. <https://doi.org/10.1093/cvr/26.1.40>
- Bertl, A., Anderson, J.A., Slayman, C.L., Gaber, R.F., 1995. Use of *Saccharomyces cerevisiae* for patch-clamp analysis of heterologous membrane proteins: characterization of Kat1, an inward-rectifying K⁺ channel from *Arabidopsis thaliana*, and comparison with

- endogeneous yeast channels and carriers. *Proc. Natl. Acad. Sci. U. S. A.* 92, 2701–2705.
- Bhattacharya, A., Biber, K., 2016. The microglial ATP-gated ion channel P2X7 as a CNS drug target. *Glia* 64, 1772–1787. <https://doi.org/10.1002/glia.23001>
- Bianco, F., Perrotta, C., Novellino, L., Francolini, M., Riganti, L., Menna, E., Saglietti, L., Schuchman, E.H., Furlan, R., Clementi, E., Matteoli, M., Verderio, C., 2009. Acid sphingomyelinase activity triggers microparticle release from glial cells. *EMBO J.* 28, 1043–1054. <https://doi.org/10.1038/emboj.2009.45>
- Bijlmakers, M.-J., Marsh, M., 2003. The on–off story of protein palmitoylation. *Trends Cell Biol.* 13, 32–42. [https://doi.org/10.1016/S0962-8924\(02\)00008-9](https://doi.org/10.1016/S0962-8924(02)00008-9)
- Birch, J., Axford, D., Foadi, J., Meyer, A., Eckhardt, A., Thielmann, Y., Moraes, I., 2018. The fine art of integral membrane protein crystallisation. *Methods, Recombinant Membrane Protein Methods* 147, 150–162. <https://doi.org/10.1016/j.ymeth.2018.05.014>
- Bo, X., Jiang, L.-H., Wilson, H.L., Kim, M., Burnstock, G., Surprenant, A., North, R.A., 2003. Pharmacological and biophysical properties of the human P2X5 receptor. *Mol. Pharmacol.* 63, 1407–1416. <https://doi.org/10.1124/mol.63.6.1407>
- Bornert, O., Alkhalfioui, F., Logez, C., Wagner, R., 2002. Overexpression of Membrane Proteins Using *Pichia pastoris*. *Curr. Protoc. Protein Sci.* 29, 29.2.1-29.2.24. <https://doi.org/10.1002/0471140864.ps2902s67>
- Bornhorst, J.A., Falke, J.J., 2000. [16] Purification of Proteins Using Polyhistidine Affinity Tags. *Methods Enzymol.* 326, 245–254.
- Brake, A.J., Wagenbach, M.J., Julius, D., 1994. New structural motif for ligand-gated ion channels defined by an ionotropic ATP receptor. *Nature* 371, 519–523. <https://doi.org/10.1038/371519a0>
- Brock, M.W., Lebaric, Z.N., Neumeister, H., DeTomaso, A., Gilly, W.F., 2001. Temperature-Dependent Expression of a Squid Kv1 Channel in Sf9 Cells and Functional Comparison with the Native Delayed Rectifier. *J. Membr. Biol.* 180, 147–161. <https://doi.org/10.1007/s002320010066>
- Browne, L.E., Compan, V., Bragg, L., North, R.A., 2013. P2X7 Receptor Channels Allow Direct Permeation of Nanometer-Sized Dyes. *J. Neurosci.* 33, 3557–3566. <https://doi.org/10.1523/JNEUROSCI.2235-12.2013>

- Browne, L.E., Nunes, J.P.M., Sim, J.A., Chudasama, V., Bragg, L., Caddick, S., North, R.A., 2014. Optical control of trimeric P2X receptors and acid-sensing ion channels. *Proc. Natl. Acad. Sci.* 111, 521–526. <https://doi.org/10.1073/pnas.1318582111>
- Buell, G., Lewis, C., Collo, G., North, R.A., Surprenant, A., 1996. An antagonist-insensitive P2X receptor expressed in epithelia and brain. *EMBO J.* 15, 55–62.
- Burnstock, G., 2018. Purine and purinergic receptors: *Brain Neurosci. Adv.* <https://doi.org/10.1177/2398212818817494>
- Burnstock, G., 2012. Discovery of purinergic signalling, the initial resistance and current explosion of interest. *Br. J. Pharmacol.* 167, 238–255. <https://doi.org/10.1111/j.1476-5381.2012.02008.x>
- Burnstock, G., 2008. Purinergic signalling and disorders of the central nervous system. *Nat. Rev. Drug Discov.* 7, 575–590. <https://doi.org/10.1038/nrd2605>
- Burnstock, G., 1972. Purinergic nerves. *Pharmacol. Rev.* 24, 509–581.
- Burnstock, G., Campbell, G., Satchell, D., Smythe, A., 1970. Evidence that adenosine triphosphate or a related nucleotide is the transmitter substance released by non-adrenergic inhibitory nerves in the gut. *Br. J. Pharmacol.* 40, 668–688.
- Burnstock, G., Kennedy, C., 1985. Is there a basis for distinguishing two types of P2-purinoceptor? *Gen. Pharmacol. Vasc. Syst.* 16, 433–440. [https://doi.org/10.1016/0306-3623\(85\)90001-1](https://doi.org/10.1016/0306-3623(85)90001-1)
- Burnstock, G., Knight, G.E., 2018. The potential of P2X7 receptors as a therapeutic target, including inflammation and tumour progression. *Purinergic Signal.* 14, 1–18. <https://doi.org/10.1007/s11302-017-9593-0>
- Burnstock, G., Ralevic, V., 2014. Purinergic Signaling and Blood Vessels in Health and Disease. *Pharmacol. Rev.* 66, 102–192. <https://doi.org/10.1124/pr.113.008029>
- Burnstock, G., Verkhatsky, A., 2009. Evolutionary origins of the purinergic signalling system. *Acta Physiol.* 195, 415–447. <https://doi.org/10.1111/j.1748-1716.2009.01957.x>
- Burnstock, G.A., 1978. A basis for distinguishing two types of purinergic receptor. *Cell Membr. Recept. Drugs Horm. Multidiscip. Approach* 107–118.

- Cankurtaran-Sayar, S., Sayar, K., Ugur, M., 2009. P2X7 receptor activates multiple selective dye-permeation pathways in RAW 264.7 and human embryonic kidney 293 cells. *Mol. Pharmacol.* 76, 1323–1332. <https://doi.org/10.1124/mol.109.059923>
- Caporale, N., Kolstad, K.D., Lee, T., Tochitsky, I., Dalkara, D., Trauner, D., Kramer, R., Dan, Y., Isacoff, E.Y., Flannery, J.G., 2011. LiGluR Restores Visual Responses in Rodent Models of Inherited Blindness. *Mol. Ther.* 19, 1212–1219. <https://doi.org/10.1038/mt.2011.103>
- Caputo, A., Caci, E., Ferrera, L., Pedemonte, N., Barsanti, C., Sondo, E., Pfeffer, U., Ravazzolo, R., Zegarra-Moran, O., Galletta, L.J.V., 2008. TMEM16A, a membrane protein associated with calcium-dependent chloride channel activity. *Science* 322, 590–594. <https://doi.org/10.1126/science.1163518>
- Cereghino, G.P.L., Cereghino, J.L., Ilgen, C., Cregg, J.M., 2002. Production of recombinant proteins in fermenter cultures of the yeast *Pichia pastoris*. *Curr. Opin. Biotechnol.* 13, 329–332. [https://doi.org/10.1016/S0958-1669\(02\)00330-0](https://doi.org/10.1016/S0958-1669(02)00330-0)
- Chae, P.S., Rasmussen, S.G.F., Rana, R., Gotfryd, K., Chandra, R., Goren, M.A., Kruse, A.C., Nurva, S., Loland, C.J., Pierre, Y., Drew, D., Popot, J.-L., Picot, D., Fox, B.G., Guan, L., Gether, U., Byrne, B., Kobilka, B., Gellman, S.H., 2010. Maltose-neopentyl glycol (MNG) amphiphiles for solubilization, stabilization and crystallization of membrane proteins. *Nat. Methods* 7, 1003–1008. <https://doi.org/10.1038/nmeth.1526>
- Chambers, J.J., Banghart, M.R., Trauner, D., Kramer, R.H., 2006. Light-Induced Depolarization of Neurons Using a Modified Shaker K⁺ Channel and a Molecular Photoswitch. *J. Neurophysiol.* 96, 2792–2796. <https://doi.org/10.1152/jn.00318.2006>
- Changeux, J.P., Kasai, M., Lee, C.Y., 1970. Use of a snake venom toxin to characterize the cholinergic receptor protein. *Proc. Natl. Acad. Sci. U. S. A.* 67, 1241–1247. <https://doi.org/10.1073/pnas.67.3.1241>
- Chataigneau, T., Lemoine, D., Grutter, T., 2013. Exploring the ATP-binding site of P2X receptors. *Front. Cell. Neurosci.* 7. <https://doi.org/10.3389/fncel.2013.00273>
- Cheewatrakoolpong, B., Gilchrest, H., Anthes, J.C., Greenfeder, S., 2005. Identification and characterization of splice variants of the human P2X7 ATP channel. *Biochem. Biophys. Res. Commun.* 332, 17–27. <https://doi.org/10.1016/j.bbrc.2005.04.087>
- Chen, C.C., Akopian, A.N., Sivilotti, L., Colquhoun, D., Burnstock, G., Wood, J.N., 1995. A P2X purinoceptor expressed by a subset of sensory neurons. *Nature* 377, 428–431. <https://doi.org/10.1038/377428a0>

- Cheng, Y., 2015. Single-Particle Cryo-EM at Crystallographic Resolution. *Cell* 161, 450–457. <https://doi.org/10.1016/j.cell.2015.03.049>
- Cherian, O.L., Menini, A., Boccaccio, A., 2015. Multiple effects of anthracene-9-carboxylic acid on the TMEM16B/anoctamin2 calcium-activated chloride channel. *Biochim. Biophys. Acta* 1848, 1005–1013. <https://doi.org/10.1016/j.bbamem.2015.01.009>
- Chessell, I.P., Hatcher, J.P., Bountra, C., Michel, A.D., Hughes, J.P., Green, P., Egerton, J., Murfin, M., Richardson, J., Peck, W.L., Grahames, C.B.A., Casula, M.A., Yiangou, Y., Birch, R., Anand, P., Buell, G.N., 2005. Disruption of the P2X7 purinoceptor gene abolishes chronic inflammatory and neuropathic pain. *Pain* 114, 386–396. <https://doi.org/10.1016/j.pain.2005.01.002>
- Cho, K.H., Husri, M., Amin, A., Gotfryd, K., Lee, H.J., Go, J., Kim, J.W., Loland, C.J., Guan, L., Byrne, B., Chae, P.S., 2015. Maltose neopentyl glycol-3 (MNG-3) analogues for membrane protein study. *Analyst* 140, 3157–3163. <https://doi.org/10.1039/C5AN00240K>
- Cockayne, D.A., Dunn, P.M., Zhong, Y., Rong, W., Hamilton, S.G., Knight, G.E., Ruan, H.-Z., Ma, B., Yip, P., Nunn, P., McMahon, S.B., Burnstock, G., Ford, A.P.D.W., 2005. P2X2 knockout mice and P2X2/P2X3 double knockout mice reveal a role for the P2X2 receptor subunit in mediating multiple sensory effects of ATP. *J. Physiol.* 567, 621–639. <https://doi.org/10.1113/jphysiol.2005.088435>
- Cockcroft, S., Gomperts, B.D., 1979. ATP induces nucleotide permeability in rat mast cells. *Nature* 279, 541–542. <https://doi.org/10.1038/279541a0>
- Coddou, C., Stojilkovic, S.S., Huidobro-Toro, J.P., 2011a. Allosteric modulation of ATP-gated P2X receptor channels. *Rev. Neurosci.* 22, 335–354. <https://doi.org/10.1515/RNS.2011.014>
- Coddou, C., Yan, Z., Obsil, T., Huidobro-Toro, J.P., Stojilkovic, S.S., 2011b. Activation and Regulation of Purinergic P2X Receptor Channels. *Pharmacol. Rev.* 63, 641–683. <https://doi.org/10.1124/pr.110.003129>
- Colgan, S.P., Eltzschig, H.K., Eckle, T., Thompson, L.F., 2006. Physiological roles for ecto-5'-nucleotidase (CD73). *Purinergic Signal.* 2, 351–360. <https://doi.org/10.1007/s11302-005-5302-5>
- Collo, G., Neidhart, S., Kawashima, E., Kosco-Vilbois, M., North, R.A., Buell, G., 1997. Tissue distribution of the P2X7 receptor. *Neuropharmacology* 36, 1277–1283. [https://doi.org/10.1016/S0028-3908\(97\)00140-8](https://doi.org/10.1016/S0028-3908(97)00140-8)

- Collo, G., North, R.A., Kawashima, E., Merlo-Pich, E., Neidhart, S., Surprenant, A., Buell, G., 1996. Cloning OF P2X5 and P2X6 receptors and the distribution and properties of an extended family of ATP-gated ion channels. *J. Neurosci. Off. J. Soc. Neurosci.* 16, 2495–2507.
- Contreras-Gómez, A., Sánchez-Mirón, A., García-Camacho, F., Molina-Grima, E., Chisti, Y., 2014. Protein production using the baculovirus-insect cell expression system. *Biotechnol. Prog.* 30, 1–18. <https://doi.org/10.1002/btpr.1842>
- Costa-Junior, H.M., Sarmiento Vieira, F., Coutinho-Silva, R., 2011. C terminus of the P2X7 receptor: treasure hunting. *Purinergic Signal.* 7, 7–19. <https://doi.org/10.1007/s11302-011-9215-1>
- Dai, S., Hall, D.D., Hell, J.W., 2009. Supramolecular Assemblies and Localized Regulation of Voltage-Gated Ion Channels. *Physiol. Rev.* 89, 411–452. <https://doi.org/10.1152/physrev.00029.2007>
- Danquah, W., Meyer-Schwesinger, C., Rissiek, B., Pinto, C., Serracant-Prat, A., Amadi, M., Iacenda, D., Knop, J.-H., Hammel, A., Bergmann, P., Schwarz, N., Assunção, J., Rothier, W., Haag, F., Tolosa, E., Bannas, P., Boué-Grabot, E., Magnus, T., Laeremans, T., Stortelers, C., Koch-Nolte, F., 2016. Nanobodies that block gating of the P2X7 ion channel ameliorate inflammation. *Sci. Transl. Med.* 8, 366ra162. <https://doi.org/10.1126/scitranslmed.aaf8463>
- Dawaliby, R., Trubbia, C., Delporte, C., Noyon, C., Ruyschaert, J.-M., Antwerpen, P.V., Govaerts, C., 2016. Phosphatidylethanolamine Is a Key Regulator of Membrane Fluidity in Eukaryotic Cells. *J. Biol. Chem.* 291, 3658–3667. <https://doi.org/10.1074/jbc.M115.706523>
- De Jesús-Pérez, J.J., Cruz-Rangel, S., Espino-Saldaña, Á.E., Martínez-Torres, A., Qu, Z., Hartzell, H.C., Corral-Fernandez, N.E., Pérez-Cornejo, P., Arreola, J., 2018. Phosphatidylinositol 4,5-bisphosphate, cholesterol, and fatty acids modulate the calcium-activated chloride channel TMEM16A (ANO1). *Biochim. Biophys. Acta Mol. Cell Biol. Lipids* 1863, 299–312. <https://doi.org/10.1016/j.bbalip.2017.12.009>
- Denisov, I.G., Grinkova, Y.V., Lazarides, A.A., Sligar, S.G., 2004. Directed Self-Assembly of Monodisperse Phospholipid Bilayer Nanodiscs with Controlled Size. *J. Am. Chem. Soc.* 126, 3477–3487. <https://doi.org/10.1021/ja0393574>
- Denlinger, L.C., Sommer, J.A., Parker, K., Gudipaty, L., Fiset, P.L., Watters, J.W., Proctor, R.A., Dubyak, G.R., Bertics, P.J., 2003. Mutation of a Dibasic Amino Acid Motif Within the C Terminus of the P2X7 Nucleotide Receptor Results in Trafficking Defects and Impaired Function. *J. Immunol.* 171, 1304–1311. <https://doi.org/10.4049/jimmunol.171.3.1304>

- Di, A., Xiong, S., Ye, Z., Malireddi, R.K.S., Kometani, S., Zhong, M., Mittal, M., Hong, Z., Kanneganti, T.-D., Rehman, J., Malik, A.B., 2018. The TWIK2 Potassium Efflux Channel in Macrophages Mediates NLRP3 Inflammasome-Induced Inflammation. *Immunity* 49, 56-65.e4. <https://doi.org/10.1016/j.immuni.2018.04.032>
- Di Virgilio, F., Chiozzi, P., Falzoni, S., Ferrari, D., Sanz, J.M., Venketaraman, V., Baricordi, O.R., 1998. Cytolytic P2X purinoceptors. *Cell Death Differ.* 5, 191–199. <https://doi.org/10.1038/sj.cdd.4400341>
- Di Virgilio, F., Dal Ben, D., Sarti, A.C., Giuliani, A.L., Falzoni, S., 2017. The P2X7 Receptor in Infection and Inflammation. *Immunity* 47, 15–31. <https://doi.org/10.1016/j.immuni.2017.06.020>
- Di Virgilio, F., Giuliani, A.L., Vultaggio-Poma, V., Falzoni, S., Sarti, A.C., 2018a. Non-nucleotide Agonists Triggering P2X7 Receptor Activation and Pore Formation. *Front. Pharmacol.* 9. <https://doi.org/10.3389/fphar.2018.00039>
- Di Virgilio, F., Schmalzing, G., Markwardt, F., 2018b. The Elusive P2X7 Macropore. *Trends Cell Biol.* 28, 392–404. <https://doi.org/10.1016/j.tcb.2018.01.005>
- Di Zanni, E., Gradogna, A., Scholz-Starke, J., Boccaccio, A., 2018. Gain of function of TMEM16E/ANO5 scrambling activity caused by a mutation associated with gnathodiaphyseal dysplasia. *Cell. Mol. Life Sci.* 75, 1657–1670. <https://doi.org/10.1007/s00018-017-2704-9>
- Díaz-Hernandez, M., Puerto, A. del, Díaz-Hernandez, J.I., Diez-Zaera, M., Lucas, J.J., Garrido, J.J., Miras-Portugal, M.T., 2008. Inhibition of the ATP-gated P2X7 receptor promotes axonal growth and branching in cultured hippocampal neurons. *J. Cell Sci.* 121, 3717–3728. <https://doi.org/10.1242/jcs.034082>
- Ding, J., Wang, K., Liu, W., She, Y., Sun, Q., Shi, J., Sun, H., Wang, D.-C., Shao, F., 2016. Pore-forming activity and structural autoinhibition of the gasdermin family. *Nature* 535, 111–116. <https://doi.org/10.1038/nature18590>
- Ding, S., Sachs, F., 1999. Single channel properties of P2X2 purinoceptors. *J. Gen. Physiol.* 113, 695–720. <https://doi.org/10.1085/jgp.113.5.695>
- Donnelly-Roberts, D.L., Jarvis, M.F., 2007. Discovery of P2X7 receptor-selective antagonists offers new insights into P2X7 receptor function and indicates a role in chronic pain states. *Br. J. Pharmacol.* 151, 571–579. <https://doi.org/10.1038/sj.bjp.0707265>
- Donnelly-Roberts, D.L., Namovic, M.T., Han, P., Jarvis, M.F., 2009. Mammalian P2X7 receptor pharmacology: comparison of recombinant mouse, rat and human P2X7 receptors. *Br. J. Pharmacol.* 157, 1203–1214. <https://doi.org/10.1111/j.1476-5381.2009.00233.x>

- Dörr, J.M., Koorengel, M.C., Schäfer, M., Prokofyev, A.V., Scheidelaar, S., van der Crujzen, E.A.W., Dafforn, T.R., Baldus, M., Killian, J.A., 2014. Detergent-free isolation, characterization, and functional reconstitution of a tetrameric K⁺ channel: the power of native nanodiscs. *Proc. Natl. Acad. Sci. U. S. A.* 111, 18607–18612. <https://doi.org/10.1073/pnas.1416205112>
- Doyle, D.A., Cabral, J.M., Pfuetzner, R.A., Kuo, A., Gulbis, J.M., Cohen, S.L., Chait, B.T., MacKinnon, R., 1998. The Structure of the Potassium Channel: Molecular Basis of K⁺ Conduction and Selectivity. *Science* 280, 69–77. <https://doi.org/10.1126/science.280.5360.69>
- Drury, A.N., Szent-Györgyi, A., 1929. The physiological activity of adenine compounds with especial reference to their action upon the mammalian heart. *J. Physiol.* 68, 213–237. <https://doi.org/10.1113/jphysiol.1929.sp002608>
- Du, J., Dong, H., Zhou, H.-X., 2012. Gating mechanism of a P2X₄ receptor developed from normal mode analysis and molecular dynamics simulations. *Proc. Natl. Acad. Sci.* 109, 4140–4145. <https://doi.org/10.1073/pnas.1119546109>
- Duan, S., Anderson, C.M., Keung, E.C., Chen, Yongmei, Chen, Yiren, Swanson, R.A., 2003. P2X₇ Receptor-Mediated Release of Excitatory Amino Acids from Astrocytes. *J. Neurosci.* 23, 1320–1328. <https://doi.org/10.1523/JNEUROSCI.23-04-01320.2003>
- Duckwitz, W., Hausmann, R., Aschrafi, A., Schmalzing, G., 2006. P2X₅ Subunit Assembly Requires Scaffolding by the Second Transmembrane Domain and a Conserved Aspartate. *J. Biol. Chem.* 281, 39561–39572. <https://doi.org/10.1074/jbc.M606113200>
- Dukkipati, A., Park, H.H., Waghray, D., Fischer, S., Garcia, K.C., 2008. BacMam System for High-Level Expression of Recombinant Soluble and Membrane Glycoproteins for Structural Studies. *Protein Expr. Purif.* 62, 160–170. <https://doi.org/10.1016/j.pep.2008.08.004>
- Egan, T.M., Khakh, B.S., 2004. Contribution of calcium ions to P2X channel responses. *J. Neurosci. Off. J. Soc. Neurosci.* 24, 3413–3420. <https://doi.org/10.1523/JNEUROSCI.5429-03.2004>
- Eickhorst, A.N., Berson, A., Cockayne, D., Lester, H.A., Khakh, B.S., 2002. Control of P2X₂ channel permeability by the cytosolic domain. *J. Gen. Physiol.* 120, 119–131. <https://doi.org/10.1085/jgp.20028535>
- Eltzschig, H.K., Eckle, T., Mager, A., Küper, N., Karcher, C., Weissmüller, T., Boengler, K., Schulz, R., Robson, S.C., Colgan, S.P., 2006. ATP release from activated neutrophils occurs via connexin 43 and modulates adenosine-dependent endothelial cell function. *Circ. Res.* 99, 1100–1108. <https://doi.org/10.1161/01.RES.0000250174.31269.70>

- Evans, R.J., 2010. Structural interpretation of P2X receptor mutagenesis studies on drug action. *Br. J. Pharmacol.* 161, 961–971. <https://doi.org/10.1111/j.1476-5381.2010.00728.x>
- Faria, R.X., Freitas, H.R., Reis, R.A.M., 2017. P2X7 receptor large pore signaling in avian Müller glial cells. *J. Bioenerg. Biomembr.* 49, 215–229. <https://doi.org/10.1007/s10863-017-9717-9>
- Fellin, T., Pozzan, T., Carmignoto, G., 2006. Purinergic receptors mediate two distinct glutamate release pathways in hippocampal astrocytes. *J. Biol. Chem.* 281, 4274–4284. <https://doi.org/10.1074/jbc.M510679200>
- Feng, S., Dang, S., Han, T.W., Ye, W., Jin, P., Cheng, T., Li, J., Jan, Y.N., Jan, L.Y., Cheng, Y., 2019. Cryo-EM Studies of TMEM16F Calcium-Activated Ion Channel Suggest Features Important for Lipid Scrambling. *Cell Rep.* 28, 567-579.e4. <https://doi.org/10.1016/j.celrep.2019.06.023>
- Feng, Y.-H., Li, X., Wang, L., Zhou, L., Gorodeski, G.I., 2006. A Truncated P2X7 Receptor Variant (P2X7-j) Endogenously Expressed in Cervical Cancer Cells Antagonizes the Full-length P2X7 Receptor through Hetero-oligomerization. *J. Biol. Chem.* 281, 17228–17237. <https://doi.org/10.1074/jbc.M602999200>
- Fernandez-Leiro, R., Scheres, S.H.W., 2016. Unravelling biological macromolecules with cryo-electron microscopy. *Nature* 537, 339–346. <https://doi.org/10.1038/nature19948>
- Ferrari, D., Pizzirani, C., Adinolfi, E., Lemoli, R.M., Curti, A., Idzko, M., Panther, E., Virgilio, F.D., 2006. The P2X7 Receptor: A Key Player in IL-1 Processing and Release. *J. Immunol.* 176, 3877–3883. <https://doi.org/10.4049/jimmunol.176.7.3877>
- Fields, R.D., Burnstock, G., 2006. Purinergic signalling in neuron–glia interactions. *Nat. Rev. Neurosci.* 7, 423–436. <https://doi.org/10.1038/nrn1928>
- Fortin, D.L., Banghart, M.R., Dunn, T.W., Borges, K., Wagenaar, D.A., Gaudry, Q., Karakossian, M.H., Otis, T.S., Kristan, W.B., Trauner, D., Kramer, R.H., 2008. Photochemical control of endogenous ion channels and cellular excitability. *Nat. Methods* 5, 331–338. <https://doi.org/10.1038/nmeth.1187>
- Fortin, D.L., Dunn, T.W., Fedorchak, A., Allen, D., Montpetit, R., Banghart, M.R., Trauner, D., Adelman, J.P., Kramer, R.H., 2011. Optogenetic photochemical control of designer K⁺ channels in mammalian neurons. *J. Neurophysiol.* 106, 488–496. <https://doi.org/10.1152/jn.00251.2011>
- Fountain, S.J., 2013. Primitive ATP-activated P2X receptors: discovery, function and pharmacology. *Front. Cell. Neurosci.* 7. <https://doi.org/10.3389/fncel.2013.00247>

- Franceschini, A., Capece, M., Chiozzi, P., Falzoni, S., Sanz, J.M., Sarti, A.C., Bonora, M., Pinton, P., Virgilio, F.D., 2015. The P2X7 receptor directly interacts with the NLRP3 inflammasome scaffold protein. *FASEB J.* 29, 2450–2461. <https://doi.org/10.1096/fj.14-268714>
- Gao, Y., Cao, E., Julius, D., Cheng, Y., 2016. TRPV1 structures in nanodiscs reveal mechanisms of ligand and lipid action. *Nature* 534, 347–351. <https://doi.org/10.1038/nature17964>
- García-Marcos, M., Pérez-Andrés, E., Tandel, S., Fontanils, U., Kumps, A., Kabré, E., Gómez-Muñoz, A., Marino, A., Dehaye, J.-P., Pochet, S., 2006a. Coupling of two pools of P2X7 receptors to distinct intracellular signaling pathways in rat submandibular gland. *J. Lipid Res.* 47, 705–714. <https://doi.org/10.1194/jlr.M500408-JLR200>
- García-Marcos, M., Pochet, S., Marino, A., Dehaye, J.-P., 2006. P2X7 and phospholipid signalling: The search of the “missing link” in epithelial cells. *Cell. Signal.* 18, 2098–2104. <https://doi.org/10.1016/j.cellsig.2006.05.008>
- García-Marcos, M., Pochet, S., Tandel, S., Fontanils, U., Astigarraga, E., Fernández-González, J.A., Kumps, A., Marino, A., Dehaye, J.-P., 2006b. Characterization and comparison of raft-like membranes isolated by two different methods from rat submandibular gland cells. *Biochim. Biophys. Acta* 1758, 796–806. <https://doi.org/10.1016/j.bbamem.2006.05.008>
- Gartland, A., 2012. P2X receptors in bone. *Wiley Interdiscip. Rev. Membr. Transp. Signal.* 1, 221–227. <https://doi.org/10.1002/wmts.26>
- Gartland, A., Hipskind, R.A., Gallagher, J.A., Bowler, W.B., 2001. Expression of a P2X7 receptor by a subpopulation of human osteoblasts. *J. Bone Miner. Res. Off. J. Am. Soc. Bone Miner. Res.* 16, 846–856. <https://doi.org/10.1359/jbmr.2001.16.5.846>
- Geraghty, N.J., Watson, D., Adhikary, S.R., Sluyter, R., 2016. P2X7 receptor in skin biology and diseases. *World J. Dermatol.* 5, 72–83. <https://doi.org/10.5314/wjd.v5.i2.72>
- Gimpl, G., Klein, U., Reilaender, H., Fahrenholz, F., 1995. Expression of the Human Oxytocin Receptor in Baculovirus-Infected Insect Cells: High-Affinity Binding Is Induced by a Cholesterol-Cyclodextrin Complex. *Biochemistry* 34, 13794–13801. <https://doi.org/10.1021/bi00042a010>
- Gómez-Villafuertes, R., Puerto, A. del, Díaz-Hernández, M., Bustillo, D., Díaz-Hernández, J.I., Huerta, P.G., Artalejo, A.R., Garrido, J.J., Miras-Portugal, M.T., 2009. Ca²⁺/calmodulin-dependent kinase II signalling cascade mediates P2X7 receptor-dependent inhibition of neurite outgrowth in neuroblastoma cells. *FEBS J.* 276, 5307–5325. <https://doi.org/10.1111/j.1742-4658.2009.07228.x>

- Gonnord, P., Delarasse, C., Auger, R., Benihoud, K., Prigent, M., Cuif, M.H., Lamaze, C., Kanellopoulos, J.M., 2009. Palmitoylation of the P2X7 receptor, an ATP-gated channel, controls its expression and association with lipid rafts. *FASEB J. Off. Publ. Fed. Am. Soc. Exp. Biol.* 23, 795–805. <https://doi.org/10.1096/fj.08-114637>
- Gonzales, E.B., Kawate, T., Gouaux, E., 2009. Pore architecture and ion sites in acid sensing ion channels and P2X receptors. *Nature* 460, 599–604. <https://doi.org/10.1038/nature08218>
- Gordon, G.R.J., Baimoukhametova, D.V., Hewitt, S.A., Rajapaksha, W.R.A.K.J.S., Fisher, T.E., Bains, J.S., 2005. Norepinephrine triggers release of glial ATP to increase postsynaptic efficacy. *Nat. Neurosci.* 8, 1078–1086. <https://doi.org/10.1038/nn1498>
- Gordon, G.R.J., Iremonger, K.J., Kantevari, S., Ellis-Davies, G.C.R., MacVicar, B.A., Bains, J.S., 2009. Astrocyte-mediated distributed plasticity at hypothalamic glutamate synapses. *Neuron* 64, 391–403. <https://doi.org/10.1016/j.neuron.2009.10.021>
- Gordon, J.L., 1986. Extracellular ATP: effects, sources and fate. *Biochem. J.* 233, 309–319. <https://doi.org/10.1042/bj2330309>
- Gorostiza, P., Volgraf, M., Numano, R., Szobota, S., Trauner, D., Isacoff, E.Y., 2007. Mechanisms of photoswitch conjugation and light activation of an ionotropic glutamate receptor. *Proc. Natl. Acad. Sci.* 104, 10865–10870. <https://doi.org/10.1073/pnas.0701274104>
- Grace, P.M., Strand, K.A., Galer, E.L., Rice, K.C., Maier, S.F., Watkins, L.R., 2018. Protraction of neuropathic pain by morphine is mediated by spinal damage associated molecular patterns (DAMPs) in male rats. *Brain. Behav. Immun., Danger-associated molecular patterns in health and disease* 72, 45–50. <https://doi.org/10.1016/j.bbi.2017.08.018>
- Greenberg, S., Di Virgilio, F., Steinberg, T.H., Silverstein, S.C., 1988. Extracellular nucleotides mediate Ca²⁺ fluxes in J774 macrophages by two distinct mechanisms. *J. Biol. Chem.* 263, 10337–10343.
- Grillitsch, K., Tarazona, P., Klug, L., Wriessnegger, T., Zellnig, G., Leitner, E., Feussner, I., Daum, G., 2014. Isolation and characterization of the plasma membrane from the yeast *Pichia pastoris*. *Biochim. Biophys. Acta* 1838, 1889–1897. <https://doi.org/10.1016/j.bbamem.2014.03.012>
- Gruswitz, F., Chaudhary, S., Ho, J.D., Schlessinger, A., Pezeshki, B., Ho, C.-M., Sali, A., Westhoff, C.M., Stroud, R.M., 2010. Function of human Rh based on structure of RhCG at 2.1 Å. *Proc. Natl. Acad. Sci. U. S. A.* 107, 9638–9643. <https://doi.org/10.1073/pnas.1003587107>

- Guo, C., Masin, M., Qureshi, O.S., Murrell-Lagnado, R.D., 2007. Evidence for functional P2X4/P2X7 heteromeric receptors. *Mol. Pharmacol.* 72, 1447–1456. <https://doi.org/10.1124/mol.107.035980>
- Guo, Y.R., MacKinnon, R., 2017. Structure-based membrane dome mechanism for Piezo mechanosensitivity. *eLife* 6, e33660. <https://doi.org/10.7554/eLife.33660>
- Habermacher, C., Martz, A., Calimet, N., Lemoine, D., Peverini, L., Specht, A., Cecchini, M., Grutter, T., 2016. Photo-switchable tweezers illuminate pore-opening motions of an ATP-gated P2X ion channel. *eLife* 5, e11050. <https://doi.org/10.7554/eLife.11050>
- Hamill, O.P., Marty, A., Neher, E., Sakmann, B., Sigworth, F.J., 1981. Improved patch-clamp techniques for high-resolution current recording from cells and cell-free membrane patches. *Pflüg. Arch.* 391, 85–100. <https://doi.org/10.1007/BF00656997>
- Hamilton, S.R., Gerngross, T.U., 2007. Glycosylation engineering in yeast: the advent of fully humanized yeast. *Curr. Opin. Biotechnol., Expression technologies / Tissue and cell engineering* 18, 387–392. <https://doi.org/10.1016/j.copbio.2007.09.001>
- Hanley, P.J., Kronlage, M., Kirschning, C., del Rey, A., Di Virgilio, F., Leipziger, J., Chessell, I.P., Sargin, S., Filippov, M.A., Lindemann, O., Mohr, S., Königs, V., Schillers, H., Bähler, M., Schwab, A., 2012. Transient P2X7 receptor activation triggers macrophage death independent of Toll-like receptors 2 and 4, caspase-1, and pannexin-1 proteins. *J. Biol. Chem.* 287, 10650–10663. <https://doi.org/10.1074/jbc.M111.332676>
- Harkat, M., Peverini, L., Cerdan, A.H., Dunning, K., Beudez, J., Martz, A., Calimet, N., Specht, A., Cecchini, M., Chataigneau, T., Grutter, T., 2017. On the permeation of large organic cations through the pore of ATP-gated P2X receptors. *Proc. Natl. Acad. Sci. U. S. A.* 114, E3786–E3795. <https://doi.org/10.1073/pnas.1701379114>
- Hattori, M., Gouaux, E., 2012. Molecular mechanism of ATP binding and ion channel activation in P2X receptors. *Nature* 485, 207–212. <https://doi.org/10.1038/nature11010>
- He, W.-J., Cui, J., Du, L., Zhao, Y.-D., Burnstock, G., Zhou, H.-D., Ruan, H.-Z., 2012. Spinal P2X7 receptor mediates microglia activation-induced neuropathic pain in the sciatic nerve injury rat model. *Behav. Brain Res.* 226, 163–170. <https://doi.org/10.1016/j.bbr.2011.09.015>
- Henkel, B., Drose, D.R., Ackels, T., Oberland, S., Spehr, M., Neuhaus, E.M., 2015. Co-expression of Anoctamins in Cilia of Olfactory Sensory Neurons. *Chem. Senses* 40, 73–87. <https://doi.org/10.1093/chemse/bju061>
- Heppner, F.L., Ransohoff, R.M., Becher, B., 2015. Immune attack: the role of inflammation in Alzheimer disease. *Nat. Rev. Neurosci.* 16, 358–372. <https://doi.org/10.1038/nrn3880>

- Heymann, G., Dai, J., Li, M., Silberberg, S.D., Zhou, H.-X., Swartz, K.J., 2013. Inter- and intrasubunit interactions between transmembrane helices in the open state of P2X receptor channels. *Proc. Natl. Acad. Sci.* 110, E4045–E4054. <https://doi.org/10.1073/pnas.1311071110>
- Hibell, A.D., Kidd, E.J., Chessell, I.P., Humphrey, P.P.A., Michel, A.D., 2000. Apparent species differences in the kinetic properties of P2X7 receptors. *Br. J. Pharmacol.* 130, 167–173. <https://doi.org/10.1038/sj.bjp.0703302>
- Hibell, A.D., Thompson, K.M., Xing, M., Humphrey, P.P., Michel, A.D., 2001. Complexities of measuring antagonist potency at P2X(7) receptor orthologs. *J. Pharmacol. Exp. Ther.* 296, 947–957.
- Hiller, S., Garces, R.G., Malia, T.J., Orekhov, V.Y., Colombini, M., Wagner, G., 2008. Solution structure of the integral human membrane protein VDAC-1 in detergent micelles. *Science* 321, 1206–1210. <https://doi.org/10.1126/science.1161302>
- Hirz, M., Richter, G., Leitner, E., Wriessnegger, T., Pichler, H., 2013. A novel cholesterol-producing *Pichia pastoris* strain is an ideal host for functional expression of human Na,K-ATPase $\alpha 3\beta 1$ isoform. *Appl. Microbiol. Biotechnol.* 97, 9465–9478. <https://doi.org/10.1007/s00253-013-5156-7>
- Hodgkin, A.L., Huxley, A.F., Katz, B., 1952. Measurement of current-voltage relations in the membrane of the giant axon of *Loligo*. *J. Physiol.* 116, 424–448. <https://doi.org/10.1113/jphysiol.1952.sp004716>
- Hollister, J.R., Jarvis, D.L., 2001. Engineering lepidopteran insect cells for sialoglycoprotein production by genetic transformation with mammalian beta 1,4-galactosyltransferase and alpha 2,6-sialyltransferase genes. *Glycobiology* 11, 1–9. <https://doi.org/10.1093/glycob/11.1.1>
- Holton, P., 1959. The liberation of adenosine triphosphate on antidromic stimulation of sensory nerves. *J. Physiol.* 145, 494–504.
- Honore, P., Donnelly-Roberts, D., Namovic, M.T., Hsieh, G., Zhu, C.Z., Mikusa, J.P., Hernandez, G., Zhong, C., Gauvin, D.M., Chandran, P., Harris, R., Medrano, A.P., Carroll, W., Marsh, K., Sullivan, J.P., Faltynek, C.R., Jarvis, M.F., 2006. A-740003 [N-(1-[(Cyanoimino)(5-quinolinylamino) methyl]amino)-2,2-dimethylpropyl)-2-(3,4-dimethoxyphenyl)acetamide], a Novel and Selective P2X7 Receptor Antagonist, Dose-Dependently Reduces Neuropathic Pain in the Rat. *J. Pharmacol. Exp. Ther.* 319, 1376–1385. <https://doi.org/10.1124/jpet.106.111559>
- Humphreys, B.D., Dubyak, G.R., 1996. Induction of the P2z/P2X7 nucleotide receptor and associated phospholipase D activity by lipopolysaccharide and IFN-gamma in the human THP-1 monocytic cell line. *J. Immunol.* 157, 5627–5637.

- Huynh, K.W., Cohen, M.R., Moiseenkova-Bell, V.Y., 2014. Application of amphipols for structure-functional analysis of TRP channels. *J. Membr. Biol.* 247, 843–851. <https://doi.org/10.1007/s00232-014-9684-6>
- Iglesias, R., Locovei, S., Roque, A., Alberto, A.P., Dahl, G., Spray, D.C., Scemes, E., 2008. P2X7 receptor-Pannexin1 complex: pharmacology and signaling. *Am. J. Physiol.-Cell Physiol.* 295, C752–C760. <https://doi.org/10.1152/ajpcell.00228.2008>
- Illes, P., Khan, T.M., Rubini, P., 2017. Neuronal P2X7 Receptors Revisited: Do They Really Exist? *J. Neurosci.* 37, 7049–7062. <https://doi.org/10.1523/JNEUROSCI.3103-16.2017>
- Imperiali, B., O'Connor, S.E., 1999. Effect of N-linked glycosylation on glycopeptide and glycoprotein structure. *Curr. Opin. Chem. Biol.* 3, 643–649. [https://doi.org/10.1016/S1367-5931\(99\)00021-6](https://doi.org/10.1016/S1367-5931(99)00021-6)
- Izquierdo-Serra, M., Bautista-Barrufet, A., Trapero, A., Garrido-Charles, A., Díaz-Tahoces, A., Camarero, N., Pittolo, S., Valbuena, S., Pérez-Jiménez, A., Gay, M., García-Moll, A., Rodríguez-Esrich, C., Lerma, J., de la Villa, P., Fernández, E., Pericàs, M.À., Llebaria, A., Gorostiza, P., 2016. Optical control of endogenous receptors and cellular excitability using targeted covalent photoswitches. *Nat. Commun.* 7, 12221. <https://doi.org/10.1038/ncomms12221>
- Janks, L., Sharma, C.V.R., Egan, T.M., 2018. A central role for P2X7 receptors in human microglia. *J. Neuroinflammation* 15, 325. <https://doi.org/10.1186/s12974-018-1353-8>
- Janks, L., Sprague, R.S., Egan, T.M., 2019. ATP-Gated P2X7 Receptors Require Chloride Channels To Promote Inflammation in Human Macrophages. *J. Immunol.* 202, 883–898. <https://doi.org/10.4049/jimmunol.1801101>
- Janovjak, H., Szobota, S., Wyart, C., Trauner, D., Isacoff, E.Y., 2010. A light-gated, potassium-selective glutamate receptor for the optical inhibition of neuronal firing. *Nat. Neurosci.* 13, 1027–1032. <https://doi.org/10.1038/nn.2589>
- Jarvis, M.F., Khakh, B.S., 2009. ATP-gated P2X cation-channels. *Neuropharmacology, Ligand-Gated Ion Channels* 56, 208–215. <https://doi.org/10.1016/j.neuropharm.2008.06.067>
- Jasti, J., Furukawa, H., Gonzales, E.B., Gouaux, E., 2007. Structure of acid-sensing ion channel 1 at 1.9 Å resolution and low pH. *Nature* 449, 316–323. <https://doi.org/10.1038/nature06163>
- Jiang, L.-H., Mackenzie, A.B., North, R.A., Surprenant, A., 2000. Brilliant Blue G Selectively Blocks ATP-Gated Rat P2X7 Receptors. *Mol. Pharmacol.* 58, 82–88. <https://doi.org/10.1124/mol.58.1.82>

- Jiang, L.-H., Rassendren, F., Mackenzie, A., Zhang, Y.-H., Surprenant, A., North, R.A., 2005. N-methyl-d-glucamine and propidium dyes utilize different permeation pathways at rat P2X7 receptors. *Am. J. Physiol.-Cell Physiol.* 289, C1295–C1302. <https://doi.org/10.1152/ajpcell.00253.2005>
- Jiang, L.-H., Rassendren, F., Spelta, V., Surprenant, A., North, R.A., 2001. Amino Acid Residues Involved in Gating Identified in the First Membrane-spanning Domain of the Rat P2X2 Receptor. *J. Biol. Chem.* 276, 14902–14908. <https://doi.org/10.1074/jbc.M011327200>
- Jiang, R., Taly, A., Lemoine, D., Martz, A., Cunrath, O., Grutter, T., 2012. Tightening of the ATP-binding sites induces the opening of P2X receptor channels. *EMBO J.* 31, 2134–2143. <https://doi.org/10.1038/emboj.2012.75>
- Jindrichova, M., Bhattacharya, A., Rupert, M., Skopek, P., Obsil, T., Zemkova, H., 2015. Functional characterization of mutants in the transmembrane domains of the rat P2X7 receptor that regulate pore conductivity and agonist sensitivity. *J. Neurochem.* 133, 815–827. <https://doi.org/10.1111/jnc.13078>
- Junge, F., Schneider, B., Reckel, S., Schwarz, D., Dötsch, V., Bernhard, F., 2008. Large-scale production of functional membrane proteins. *Cell. Mol. Life Sci. CMLS* 65, 1729–1755. <https://doi.org/10.1007/s00018-008-8067-5>
- Kaczmarek-Hájek, K., Lörinczi, É., Hausmann, R., Nicke, A., 2012. Molecular and functional properties of P2X receptors—recent progress and persisting challenges. *Purinergic Signal.* 8, 375–417. <https://doi.org/10.1007/s11302-012-9314-7>
- Kaczmarek-Hajek, K., Zhang, J., Kopp, R., Grosche, A., Rissiek, B., Saul, A., Bruzzone, S., Engel, T., Jooss, T., Krautloher, A., Schuster, S., Magnus, T., Stadelmann, C., Sirko, S., Koch-Nolte, F., Eulenburg, V., Nicke, A., 2018. Re-evaluation of neuronal P2X7 expression using novel mouse models and a P2X7-specific nanobody. *eLife* 7, e36217. <https://doi.org/10.7554/eLife.36217>
- Kaebisch, C., Schipper, D., Babczyk, P., Tobiasch, E., 2015. The role of purinergic receptors in stem cell differentiation. *Comput. Struct. Biotechnol. J.* 13, 75–84. <https://doi.org/10.1016/j.csbj.2014.11.003>
- Kanellopoulos, J.M., Delarasse, C., 2019. Pleiotropic Roles of P2X7 in the Central Nervous System. *Front. Cell. Neurosci.* 13, 401–401. <https://doi.org/10.3389/fncel.2019.00401>
- Kaptein, R., Wagner, G., 2015. NMR studies of membrane proteins. *J. Biomol. NMR* 61, 181–184. <https://doi.org/10.1007/s10858-015-9918-7>

- Karasawa, A., Kawate, T., 2016. Structural basis for subtype-specific inhibition of the P2X7 receptor. *eLife* 5, e22153. <https://doi.org/10.7554/eLife.22153>
- Karasawa, A., Michalski, K., Mikhelzon, P., Kawate, T., 2017. The P2X7 receptor forms a dye-permeable pore independent of its intracellular domain but dependent on membrane lipid composition. *eLife* 6. <https://doi.org/10.7554/eLife.31186>
- Karginov, A., Agaphonov, M., 2016. A simple enrichment procedure improves detection of membrane proteins by immunoblotting. *BioTechniques* 61, 260–261. <https://doi.org/10.2144/000114474>
- Kasuya, G., Fujiwara, Y., Takemoto, M., Dohmae, N., Nakada-Nakura, Y., Ishitani, R., Hattori, M., Nureki, O., 2016. Structural Insights into Divalent Cation Modulations of ATP-Gated P2X Receptor Channels. *Cell Rep.* 14, 932–944. <https://doi.org/10.1016/j.celrep.2015.12.087>
- Kasuya, G., Yamaura, T., Ma, X.-B., Nakamura, R., Takemoto, M., Nagumo, H., Tanaka, E., Dohmae, N., Nakane, T., Yu, Y., Ishitani, R., Matsuzaki, O., Hattori, M., Nureki, O., 2017. Structural insights into the competitive inhibition of the ATP-gated P2X receptor channel. *Nat. Commun.* 8, 1–10. <https://doi.org/10.1038/s41467-017-00887-9>
- Kaulin, Y.A., De Santiago-Castillo, J.A., Rocha, C.A., Nadal, M.S., Rudy, B., Covarrubias, M., 2009. The Dipeptidyl-Peptidase-Like Protein DPP6 Determines the Unitary Conductance of Neuronal Kv4.2 Channels. *J. Neurosci.* 29, 3242–3251. <https://doi.org/10.1523/JNEUROSCI.4767-08.2009>
- Kawate, T., Gouaux, E., 2006. Fluorescence-Detection Size-Exclusion Chromatography for Precrystallization Screening of Integral Membrane Proteins. *Structure* 14, 673–681. <https://doi.org/10.1016/j.str.2006.01.013>
- Kawate, T., Michel, J.C., Birdsong, W.T., Gouaux, E., 2009. Crystal structure of the ATP-gated P2X4 ion channel in the closed state. *Nature* 460, 592–598. <https://doi.org/10.1038/nature08198>
- Kawate, T., Robertson, J.L., Li, M., Silberberg, S.D., Swartz, K.J., 2011. Ion access pathway to the transmembrane pore in P2X receptor channels. *J. Gen. Physiol.* 137, 579–590. <https://doi.org/10.1085/jgp.201010593>
- Ke, H.Z., Qi, H., Weidema, A.F., Zhang, Q., Panupinthu, N., Crawford, D.T., Grasser, W.A., Paralkar, V.M., Li, M., Audoly, L.P., Gabel, C.A., Jee, W.S.S., Dixon, S.J., Sims, S.M., Thompson, D.D., 2003. Deletion of the P2X7 nucleotide receptor reveals its regulatory roles in bone formation and resorption. *Mol. Endocrinol. Baltim. Md* 17, 1356–1367. <https://doi.org/10.1210/me.2003-0021>

- Kendrew, J.C., Bodo, G., Dintzis, H.M., Parrish, R.G., Wyckoff, H., Phillips, D.C., 1958. A Three-Dimensional Model of the Myoglobin Molecule Obtained by X-Ray Analysis. *Nature* 181, 662–666. <https://doi.org/10.1038/181662a0>
- Kessler, S., Clauss, W.G., Fronius, M., 2011. Laminar shear stress modulates the activity of heterologously expressed P2X4 receptors. *Biochim. Biophys. Acta BBA - Biomembr.* 1808, 2488–2495. <https://doi.org/10.1016/j.bbamem.2011.07.010>
- Khakh, B.S., Bao, X.R., Labarca, C., Lester, H.A., 1999. Neuronal P2X transmitter-gated cation channels change their ion selectivity in seconds. *Nat. Neurosci.* 2, 322–330. <https://doi.org/10.1038/7233>
- Khakh, B.S., North, R.A., 2012. Neuromodulation by extracellular ATP and P2X receptors in the CNS. *Neuron* 76, 51–69. <https://doi.org/10.1016/j.neuron.2012.09.024>
- Kido, Y., Kawahara, C., Terai, Y., Ohishi, A., Kobayashi, S., Hayakawa, M., Kamatsuka, Y., Nishida, K., Nagasawa, K., 2014. Regulation of activity of P2X7 receptor by its splice variants in cultured mouse astrocytes. *Glia* 62, 440–451. <https://doi.org/10.1002/glia.22615>
- Kim, J.-B., 2014. Channelopathies. *Korean J. Pediatr.* 57, 1–18. <https://doi.org/10.3345/kjp.2014.57.1.1>
- Kim, M., Jiang, L.-H., Wilson, H.L., North, R.A., Surprenant, A., 2001. Proteomic and functional evidence for a P2X7 receptor signalling complex. *EMBO J.* 20, 6347–6358. <https://doi.org/10.1093/emboj/20.22.6347>
- Kim, M., Yoo, O.J., Choe, S., 1997. Molecular assembly of the extracellular domain of P2X2, an ATP-gated ion channel. *Biochem. Biophys. Res. Commun.* 240, 618–622. <https://doi.org/10.1006/bbrc.1997.7713>
- Klapperstück, M., Büttner, C., Böhm, T., Schmalzing, G., Markwardt, F., 2000. Characteristics of P2X7 receptors from human B lymphocytes expressed in *Xenopus* oocytes. *Biochim. Biophys. Acta* 1467, 444–456. [https://doi.org/10.1016/s0005-2736\(00\)00245-5](https://doi.org/10.1016/s0005-2736(00)00245-5)
- Kobayashi, K., Fukuoka, T., Yamanaka, H., Dai, Y., Obata, K., Tokunaga, A., Noguchi, K., 2005. Differential expression patterns of mRNAs for P2X receptor subunits in neurochemically characterized dorsal root ganglion neurons in the rat. *J. Comp. Neurol.* 481, 377–390. <https://doi.org/10.1002/cne.20393>
- Koch-Nolte, F., Eichhoff, A., Pinto-Espinoza, C., Schwarz, N., Schäfer, T., Menzel, S., Haag, F., Demeules, M., Gondé, H., Adriouch, S., 2019. Novel biologics targeting the P2X7 ion channel. *Curr. Opin. Pharmacol., Cancer Immunomodulation* 47, 110–118. <https://doi.org/10.1016/j.coph.2019.03.001>

- Kopp, R., Krautloher, A., Ramírez-Fernández, A., Nicke, A., 2019. P2X7 Interactions and Signaling – Making Head or Tail of It. *Front. Mol. Neurosci.* 12. <https://doi.org/10.3389/fnmol.2019.00183>
- Kracun, S., Chaptal, V., Abramson, J., Khakh, B.S., 2010. Gated Access to the Pore of a P2X Receptor STRUCTURAL IMPLICATIONS FOR CLOSED-OPEN TRANSITIONS. *J. Biol. Chem.* 285, 10110–10121. <https://doi.org/10.1074/jbc.M109.089185>
- Kramer, R.H., Mouro, A., Adesnik, H., 2013. Optogenetic pharmacology for control of native neuronal signaling proteins. *Nat. Neurosci.* 16, 816–823. <https://doi.org/10.1038/nn.3424>
- Krogh, A., Larsson, B., von Heijne, G., Sonnhammer, E.L.L., 2001. Predicting transmembrane protein topology with a hidden markov model: application to complete genomes¹¹Edited by F. Cohen. *J. Mol. Biol.* 305, 567–580. <https://doi.org/10.1006/jmbi.2000.4315>
- Kubick, C., Schmalzing, G., Markwardt, F., 2012. The Effect of Anions on the Human P2X7 Receptor. *Biophys. J.* 102, 337a. <https://doi.org/10.1016/j.bpj.2011.11.1848>
- Kunze, D.L., Sinkins, W.G., Vaca, L., Schilling, W.P., 1997. Properties of single *Drosophila* Trpl channels expressed in Sf9 insect cells. *Am. J. Physiol.* 272, C27-34. <https://doi.org/10.1152/ajpcell.1997.272.1.C27>
- Labasi, J.M., Petrushova, N., Donovan, C., McCurdy, S., Lira, P., Payette, M.M., Brissette, W., Wicks, J.R., Audoly, L., Gabel, C.A., 2002. Absence of the P2X7 receptor alters leukocyte function and attenuates an inflammatory response. *J. Immunol. Baltim. Md 1950* 168, 6436–6445. <https://doi.org/10.4049/jimmunol.168.12.6436>
- Lacapère, J.-J., Pebay-Peyroula, E., Neumann, J.-M., Etchebest, C., 2007. Determining membrane protein structures: still a challenge! *Trends Biochem. Sci.* 32, 259–270. <https://doi.org/10.1016/j.tibs.2007.04.001>
- Lalisse, S., Hua, J., Lenoir, M., Linck, N., Rassendren, F., Ulmann, L., 2018. Sensory neuronal P2RX4 receptors controls BDNF signaling in inflammatory pain. *Sci. Rep.* 8, 1–12. <https://doi.org/10.1038/s41598-018-19301-5>
- Lalo, U., Roberts, J.A., Evans, R.J., 2011. Identification of human P2X1 receptor-interacting proteins reveals a role of the cytoskeleton in receptor regulation. *J. Biol. Chem.* 286, 30591–30599. <https://doi.org/10.1074/jbc.M111.253153>
- Lazarowski, E.R., Sesma, J.I., Seminario-Vidal, L., Kreda, S.M., 2011. Molecular mechanisms of purine and pyrimidine nucleotide release. *Adv. Pharmacol. San Diego Calif* 61, 221–261. <https://doi.org/10.1016/B978-0-12-385526-8.00008-4>

- Lê, K.-T., Babinski, K., Séguéla, P., 1998. Central P2X4 and P2X6 Channel Subunits Coassemble into a Novel Heteromeric ATP Receptor. *J. Neurosci.* 18, 7152–7159. <https://doi.org/10.1523/JNEUROSCI.18-18-07152.1998>
- Lê, K.T., Babinski, K., Séguéla, P., 1998. Central P2X4 and P2X6 channel subunits coassemble into a novel heteromeric ATP receptor. *J. Neurosci. Off. J. Soc. Neurosci.* 18, 7152–7159.
- Lê, K.T., Paquet, M., Nouel, D., Babinski, K., Séguéla, P., 1997. Primary structure and expression of a naturally truncated human P2X ATP receptor subunit from brain and immune system. *FEBS Lett.* 418, 195–199. [https://doi.org/10.1016/s0014-5793\(97\)01380-x](https://doi.org/10.1016/s0014-5793(97)01380-x)
- Le, T., Le, S.C., Yang, H., 2019. Drosophila Subdued is a moonlighting transmembrane protein 16 (TMEM16) that transports ions and phospholipids. *J. Biol. Chem.* jbc.AC118.006530. <https://doi.org/10.1074/jbc.AC118.006530>
- Lee, A., Scheuer, T., Catterall, W.A., 2000. Ca²⁺/Calmodulin-Dependent Facilitation and Inactivation of P/Q-Type Ca²⁺ Channels. *J. Neurosci.* 20, 6830–6838. <https://doi.org/10.1523/JNEUROSCI.20-18-06830.2000>
- Lee, Y.-N., Chen, L.-K., Ma, H.-C., Yang, H.-H., Li, H.-P., Lo, S.-Y., 2005. Thermal aggregation of SARS-CoV membrane protein. *J. Virol. Methods* 129, 152–161. <https://doi.org/10.1016/j.jviromet.2005.05.022>
- Leitz, A.J., Bayburt, T.H., Barnakov, A.N., Springer, B.A., Sligar, S.G., 2006. Functional reconstitution of β 2-adrenergic receptors utilizing self-assembling Nanodisc technology. *BioTechniques* 40, 601–612. <https://doi.org/10.2144/000112169>
- Lemoine, D., Habermacher, C., Martz, A., Méry, P.-F., Bouquier, N., Diverchy, F., Taly, A., Rassendren, F., Specht, A., Grutter, T., 2013. Optical control of an ion channel gate. *Proc. Natl. Acad. Sci.* 110, 20813–20818. <https://doi.org/10.1073/pnas.1318715110>
- Lemoine, D., Jiang, R., Taly, A., Chataigneau, T., Specht, A., Grutter, T., 2012. Ligand-Gated Ion Channels: New Insights into Neurological Disorders and Ligand Recognition. *Chem. Rev.* 112, 6285–6318. <https://doi.org/10.1021/cr3000829>
- Lenertz, L.Y., Wang, Z., Guadarrama, A., Hill, L.M., Gavala, M.L., Bertics, P.J., 2010. Mutation of Putative N-linked Glycosylation Sites on the Human Nucleotide Receptor P2X7 Reveals a Key Residue Important for Receptor Function. *Biochemistry* 49, 4611–4619. <https://doi.org/10.1021/bi902083n>
- Lépine, S., Le Stunff, H., Lakatos, B., Sulpice, J.C., Giraud, F., 2006. ATP-induced apoptosis of thymocytes is mediated by activation of P2X7 receptor and involves de novo

- ceramide synthesis and mitochondria. *Biochim. Biophys. Acta BBA - Mol. Cell Biol. Lipids* 1761, 73–82. <https://doi.org/10.1016/j.bbaliip.2005.10.001>
- Lester, H.A., Krouse, M.E., Nass, M.M., Wassermann, N.H., Erlanger, B.F., 1979. Light-activated drug confirms a mechanism of ion channel blockade. *Nature* 280, 509–510. <https://doi.org/10.1038/280509a0>
- Lewis, C., Neidhart, S., Holy, C., North, R.A., Buell, G., Surprenant, A., 1995a. Coexpression of P2X2 and P2X3 receptor subunits can account for ATP-gated currents in sensory neurons. *Nature* 377, 432–435. <https://doi.org/10.1038/377432a0>
- Lewis, C., Neidhart, S., Holy, C., North, R.A., Buell, G., Surprenant, A., 1995b. Coexpression of P2X2 and P2X3 receptor subunits can account for ATP-gated currents in sensory neurons. *Nature* 377, 432–435. <https://doi.org/10.1038/377432a0>
- Li, M., Chang, T.-H., Silberberg, S.D., Swartz, K.J., 2008. Gating the pore of P2X receptor channels. *Nat. Neurosci.* 11, 883–887. <https://doi.org/10.1038/nn.2151>
- Li, M., Toombes, G.E.S., Silberberg, S.D., Swartz, K.J., 2015. Physical basis of apparent pore dilation of ATP-activated P2X receptor channels. *Nat. Neurosci.* 18, 1577–1583. <https://doi.org/10.1038/nn.4120>
- Liang, B., Tamm, L.K., 2016. NMR as a tool to investigate the structure, dynamics and function of membrane proteins. *Nat. Struct. Mol. Biol.* 23, 468–474. <https://doi.org/10.1038/nsmb.3226>
- Liang, X., Samways, D.S.K., Cox, J., Egan, T.M., 2019. Ca²⁺ flux through splice variants of the ATP-gated ionotropic receptor P2X7 is regulated by its cytoplasmic N terminus. *J. Biol. Chem.* 294, 12521–12533. <https://doi.org/10.1074/jbc.RA119.009666>
- Lin, W.-C., Tsai, M.-C., Davenport, C.M., Smith, C.M., Veit, J., Wilson, N.M., Adesnik, H., Kramer, R.H., 2015. A Comprehensive Optogenetic Pharmacology Toolkit for In Vivo Control of GABA(A) Receptors and Synaptic Inhibition. *Neuron* 88, 879–891. <https://doi.org/10.1016/j.neuron.2015.10.026>
- Lingwood, D., Simons, K., 2010. Lipid rafts as a membrane-organizing principle. *Science* 327, 46–50. <https://doi.org/10.1126/science.1174621>
- Liu, Y., Xiao, Y., Li, Z., 2011. P2X7 receptor positively regulates MyD88-dependent NF- κ B activation. *Cytokine* 55, 229–236. <https://doi.org/10.1016/j.cyto.2011.05.003>

- Liu, Y., Zhang, Huiran, Huang, D., Qi, J., Xu, J., Gao, H., Du, X., Gamper, N., Zhang, Hailin, 2015. Characterization of the effects of Cl⁻ channel modulators on TMEM16A and bestrophin-1 Ca²⁺ activated Cl⁻ channels. *Pflugers Arch.* 467, 1417–1430. <https://doi.org/10.1007/s00424-014-1572-5>
- Löhn, M., Klapperstück, M., Riemann, D., Markwardt, F., 2001. Sodium block and depolarization diminish P2Z-dependent Ca²⁺-entry in human B lymphocytes. *Cell Calcium* 29, 395–408. <https://doi.org/10.1054/ceca.2001.0202>
- Lordén, G., Sanjuán-García, I., de Pablo, N., Meana, C., Alvarez-Miguel, I., Pérez-García, M.T., Pelegrín, P., Balsinde, J., Balboa, M.A., 2017. Lipin-2 regulates NLRP3 inflammasome by affecting P2X7 receptor activation. *J. Exp. Med.* 214, 511–528. <https://doi.org/10.1084/jem.20161452>
- Lörinczi, É., Bhargava, Y., Marino, S.F., Taly, A., Kaczmarek-Hájek, K., Barrantes-Freer, A., Dutertre, S., Grutter, T., Rettinger, J., Nicke, A., 2012. Involvement of the cysteine-rich head domain in activation and desensitization of the P2X1 receptor. *Proc. Natl. Acad. Sci.* 109, 11396–11401. <https://doi.org/10.1073/pnas.1118759109>
- Ma, W., Hui, H., Pelegrin, P., Surprenant, A., 2009. Pharmacological Characterization of Pannexin-1 Currents Expressed in Mammalian Cells. *J. Pharmacol. Exp. Ther.* 328, 409–418. <https://doi.org/10.1124/jpet.108.146365>
- Mackenzie, A.B., Young, M.T., Adinolfi, E., Surprenant, A., 2005. Pseudoapoptosis induced by brief activation of ATP-gated P2X7 receptors. *J. Biol. Chem.* 280, 33968–33976. <https://doi.org/10.1074/jbc.M502705200>
- Maehle, A.-H., 2004. “Receptive Substances”: John Newport Langley (1852–1925) and his Path to a Receptor Theory of Drug Action. *Med. Hist.* 48, 153–174.
- Mak, S., Sun, R., Schmalenberg, M., Peters, C., Lippa, P.B., 2017. Express incorporation of membrane proteins from various human cell types into phospholipid bilayer nanodiscs. *Biochem. J.* 474, 1361–1371. <https://doi.org/10.1042/BCJ20161110>
- Makrides, S.C., 1999. Components of vectors for gene transfer and expression in mammalian cells. *Protein Expr. Purif.* 17, 183–202. <https://doi.org/10.1006/prep.1999.1137>
- Malvezzi, M., Andra, K.K., Pandey, K., Lee, B.-C., Falzone, M.E., Brown, A., Iqbal, R., Menon, A.K., Accardi, A., 2018. Out-of-the-groove transport of lipids by TMEM16 and GPCR scramblases. *Proc. Natl. Acad. Sci.* 115, E7033. <https://doi.org/10.1073/pnas.1806721115>

- Mansoor, S.E., Lü, W., Oosterheert, W., Shekhar, M., Tajkhorshid, E., Gouaux, E., 2016. X-ray structures define human P2X3 receptor gating cycle and antagonist action. *Nature* 538, 66–71. <https://doi.org/10.1038/nature19367>
- Marín-García, P., Sánchez-Nogueiro, J., Gómez-Villafuertes, R., León, D., Miras-Portugal, M.T., 2008. Synaptic terminals from mice midbrain exhibit functional P2X7 receptor. *Neuroscience* 151, 361–373. <https://doi.org/10.1016/j.neuroscience.2007.10.038>
- Markwardt, F., Löhn, M., Böhm, T., Klapperstück, M., 1997. Purinoceptor-operated cationic channels in human B lymphocytes. *J. Physiol.* 498, 143–151. <https://doi.org/10.1113/jphysiol.1997.sp021847>
- Marques-da-Silva, C., Chaves, M.M., Castro, N.G., Coutinho-Silva, R., Guimaraes, M.Z.P., 2011. Colchicine inhibits cationic dye uptake induced by ATP in P2X2 and P2X7 receptor-expressing cells: implications for its therapeutic action. *Br. J. Pharmacol.* 163, 912–926. <https://doi.org/10.1111/j.1476-5381.2011.01254.x>
- Marquez-Klaka, B., Rettinger, J., Bhargava, Y., Eisele, T., Nicke, A., 2007. Identification of an intersubunit cross-link between substituted cysteine residues located in the putative ATP binding site of the P2X1 receptor. *J. Neurosci. Off. J. Soc. Neurosci.* 27, 1456–1466. <https://doi.org/10.1523/JNEUROSCI.3105-06.2007>
- Martin, E., Amar, M., Dalle, C., Youssef, I., Boucher, C., Duigou, C.L., Brückner, M., Prigent, A., Sazdovitch, V., Halle, A., Kanellopoulos, J.M., Fontaine, B., Delatour, B., Delarasse, C., 2019. New role of P2X7 receptor in an Alzheimer's disease mouse model. *Mol. Psychiatry* 24, 108–125. <https://doi.org/10.1038/s41380-018-0108-3>
- Masin, M., Young, C., Lim, K., Barnes, S.J., Xu, X.J., Marschall, V., Brutkowski, W., Mooney, E.R., Gorecki, D.C., Murrell-Lagnado, R., 2012. Expression, assembly and function of novel C-terminal truncated variants of the mouse P2X7 receptor: re-evaluation of P2X7 knockouts. *Br. J. Pharmacol.* 165, 978–993. <https://doi.org/10.1111/j.1476-5381.2011.01624.x>
- McCarthy, A.E., Yoshioka, C., Mansoor, S.E., 2019. Full-Length P2X7 Structures Reveal How Palmitoylation Prevents Channel Desensitization. *Cell* 179, 659-670.e13. <https://doi.org/10.1016/j.cell.2019.09.017>
- McGaraughty, S., Chu, K.L., Namovic, M.T., Donnelly-Roberts, D.L., Harris, R.R., Zhang, X.-F., Shieh, C.-C., Wismer, C.T., Zhu, C.Z., Gauvin, D.M., Fabiyi, A.C., Honore, P., Gregg, R.J., Kort, M.E., Nelson, D.W., Carroll, W.A., Marsh, K., Faltynek, C.R., Jarvis, M.F., 2007. P2X7-related modulation of pathological nociception in rats. *Neuroscience* 146, 1817–1828. <https://doi.org/10.1016/j.neuroscience.2007.03.035>
- McLarnon, J.G., Ryu, J.K., Walker, D.G., Choi, H.B., 2006. Upregulated Expression of Purinergic P2X7 Receptor in Alzheimer Disease and Amyloid- β Peptide-Treated

- Microglia and in Peptide-Injected Rat Hippocampus. *J. Neuropathol. Exp. Neurol.* 65, 1090–1097. <https://doi.org/10.1097/01.jnen.0000240470.97295.d3>
- McPherson, A., Gavira, J.A., 2013. Introduction to protein crystallization. *Acta Crystallogr. Sect. F Struct. Biol. Commun.* 70, 2–20. <https://doi.org/10.1107/S2053230X13033141>
- Megha, London, E., 2004. Ceramide Selectively Displaces Cholesterol from Ordered Lipid Domains (Rafts) IMPLICATIONS FOR LIPID RAFT STRUCTURE AND FUNCTION. *J. Biol. Chem.* 279, 9997–10004. <https://doi.org/10.1074/jbc.M309992200>
- Mendoza, S.A., Fang, J., Gutterman, D.D., Wilcox, D.A., Bubolz, A.H., Li, R., Suzuki, M., Zhang, D.X., 2010. TRPV4-mediated endothelial Ca²⁺ influx and vasodilation in response to shear stress. *Am. J. Physiol. Heart Circ. Physiol.* 298, H466-476. <https://doi.org/10.1152/ajpheart.00854.2009>
- Michel, A.D., Fonfria, E., 2007. Agonist potency at P2X7 receptors is modulated by structurally diverse lipids. *Br. J. Pharmacol.* 152, 523–537. <https://doi.org/10.1038/sj.bjp.0707417>
- Milenkovic, V.M., Brockmann, M., Stöhr, H., Weber, B.H., Strauss, O., 2010. Evolution and functional divergence of the anoctamin family of membrane proteins. *BMC Evol. Biol.* 10, 319. <https://doi.org/10.1186/1471-2148-10-319>
- Mineev, K.S., Nadezhdin, K.D., 2016. Membrane mimetics for solution NMR studies of membrane proteins. *Nanotechnol. Rev.* 6, 15–32. <https://doi.org/10.1515/ntrev-2016-0074>
- Mio, K., Kubo, Y., Ogura, T., Yamamoto, T., Sato, C., 2005. Visualization of the trimeric P2X2 receptor with a crown-capped extracellular domain. *Biochem. Biophys. Res. Commun.* 337, 998–1005. <https://doi.org/10.1016/j.bbrc.2005.09.141>
- Mio, K., Ogura, T., Yamamoto, T., Hiroaki, Y., Fujiyoshi, Y., Kubo, Y., Sato, C., 2009. Reconstruction of the P2X2 Receptor Reveals a Vase-Shaped Structure with Lateral Tunnels above the Membrane. *Structure* 17, 266–275. <https://doi.org/10.1016/j.str.2008.12.007>
- Moehring, F., Cowie, A.M., Menzel, A.D., Weyer, A.D., Grzybowski, M., Arzua, T., Geurts, A.M., Palygin, O., Stucky, C.L., 2018. Keratinocytes mediate innocuous and noxious touch via ATP-P2X4 signaling. *eLife* 7, e31684. <https://doi.org/10.7554/eLife.31684>
- Moffatt, L., Hume, R.I., 2007. Responses of Rat P2X2 Receptors to Ultrashort Pulses of ATP Provide Insights into ATP Binding and Channel Gating. *J. Gen. Physiol.* 130, 183–201. <https://doi.org/10.1085/jgp.200709779>

- Monif, M., Reid, C.A., Powell, K.L., Smart, M.L., Williams, D.A., 2009. The P2X7 Receptor Drives Microglial Activation and Proliferation: A Trophic Role for P2X7R Pore. *J. Neurosci.* 29, 3781–3791. <https://doi.org/10.1523/JNEUROSCI.5512-08.2009>
- Montana, V., Malarkey, E.B., Verderio, C., Matteoli, M., Parpura, V., 2006. Vesicular transmitter release from astrocytes. *Glia* 54, 700–715. <https://doi.org/10.1002/glia.20367>
- Mourof, A., Kienzler, M.A., Banghart, M.R., Fehrentz, T., Huber, F.M.E., Stein, M., Kramer, R.H., Trauner, D., 2011. Tuning Photochromic Ion Channel Blockers. *ACS Chem. Neurosci.* 2, 536–543. <https://doi.org/10.1021/cn200037p>
- Mourof, A., Tochitsky, I., Kramer, R.H., 2013. Light at the end of the channel: optical manipulation of intrinsic neuronal excitability with chemical photoswitches. *Front. Mol. Neurosci.* 6. <https://doi.org/10.3389/fnmol.2013.00005>
- Munerati, M., Cortesi, R., Ferrari, D., Di Virgilio, F., Nastruzzi, C., 1994. Macrophages loaded with doxorubicin by ATP-mediated permeabilization: potential carriers for antitumor therapy. *Biochim. Biophys. Acta* 1224, 269–276. [https://doi.org/10.1016/0167-4889\(94\)90200-3](https://doi.org/10.1016/0167-4889(94)90200-3)
- Murata, K., Wolf, M., 2018. Cryo-electron microscopy for structural analysis of dynamic biological macromolecules. *Biochim. Biophys. Acta BBA - Gen. Subj., Biophysical Exploration of Dynamical Ordering of Biomolecular Systems* 1862, 324–334. <https://doi.org/10.1016/j.bbagen.2017.07.020>
- Murrell-Lagnado, R.D., 2017. Regulation of P2X Purinergic Receptor Signaling by Cholesterol. *Curr. Top. Membr.* 80, 211–232. <https://doi.org/10.1016/bs.ctm.2017.05.004>
- Nakanishi, M., Mori, T., Nishikawa, K., Sawada, M., Kuno, M., Asada, A., 2007. The effects of general anesthetics on P2X7 and P2Y receptors in a rat microglial cell line. *Anesth. Analg.* 104, 1136–1144, tables of contents. <https://doi.org/10.1213/01.ane.0000260615.12553.4e>
- Nakazawa, K., Yamakoshi, Y., Tsuchiya, T., Ohno, Y., 2005. Purification and aqueous phase atomic force microscopic observation of recombinant P2X2 receptor. *Eur. J. Pharmacol.* 518, 107–110. <https://doi.org/10.1016/j.ejphar.2005.06.018>
- Namkung, W., Thiagarajah, J.R., Phuan, P.-W., Verkman, A.S., 2010. Inhibition of Ca²⁺-activated Cl⁻ channels by gallotannins as a possible molecular basis for health benefits of red wine and green tea. *FASEB J. Off. Publ. Fed. Am. Soc. Exp. Biol.* 24, 4178–4186. <https://doi.org/10.1096/fj.10-160648>

- Neher, E., Sakmann, B., 1976. Single-channel currents recorded from membrane of denervated frog muscle fibres. *Nature* 260, 799–802. <https://doi.org/10.1038/260799a0>
- Neves, A.R., Castelo-Branco, M.T.L., Figliuolo, V.R., Bernardazzi, C., Buongusto, F., Yoshimoto, A., Nanini, H.F., Coutinho, C.M.L.M., Carneiro, A.J.V., Coutinho-Silva, R., de Souza, H.S.P., 2014. Overexpression of ATP-activated P2X7 receptors in the intestinal mucosa is implicated in the pathogenesis of Crohn's disease. *Inflamm. Bowel Dis.* 20, 444–457. <https://doi.org/10.1097/01.MIB.0000441201.10454.06>
- Newbolt, A., Stoop, R., Virginio, C., Surprenant, A., North, R.A., Buell, G., Rassendren, F., 1998. Membrane Topology of an ATP-gated Ion Channel (P2X Receptor). *J. Biol. Chem.* 273, 15177–15182. <https://doi.org/10.1074/jbc.273.24.15177>
- Nicke, A., 2008. Homotrimeric complexes are the dominant assembly state of native P2X7 subunits. *Biochem. Biophys. Res. Commun.* 377, 803–808. <https://doi.org/10.1016/j.bbrc.2008.10.042>
- Nicke, A., Bäumer, H.G., Rettinger, J., Eichele, A., Lambrecht, G., Mutschler, E., Schmalzing, G., 1998. P2X1 and P2X3 receptors form stable trimers: a novel structural motif of ligand-gated ion channels. *EMBO J.* 17, 3016–3028. <https://doi.org/10.1093/emboj/17.11.3016>
- Nicke, A., Kuan, Y.-H., Masin, M., Rettinger, J., Marquez-Klaka, B., Bender, O., Górecki, D.C., Murrell-Lagnado, R.D., Soto, F., 2009. A functional P2X7 splice variant with an alternative transmembrane domain 1 escapes gene inactivation in P2X7 knock-out mice. *J. Biol. Chem.* 284, 25813–25822. <https://doi.org/10.1074/jbc.M109.033134>
- Nörenberg, W., Hempel, C., Urban, N., Sobottka, H., Illes, P., Schaefer, M., 2011. Clemastine Potentiates the Human P2X7 Receptor by Sensitizing It to Lower ATP Concentrations. *J. Biol. Chem.* 286, 11067–11081. <https://doi.org/10.1074/jbc.M110.198879>
- Nörenberg, W., Plötz, T., Sobottka, H., Chubanov, V., Mittermeier, L., Kalwa, H., Aigner, A., Schaefer, M., 2016. TRPM7 is a molecular substrate of ATP-evoked P2X7-like currents in tumor cells. *J. Gen. Physiol.* 147, 467–483. <https://doi.org/10.1085/jgp.201611595>
- Nörenberg, W., Sobottka, H., Hempel, C., Plötz, T., Fischer, W., Schmalzing, G., Schaefer, M., 2012. Positive allosteric modulation by ivermectin of human but not murine P2X7 receptors. *Br. J. Pharmacol.* 167, 48–66. <https://doi.org/10.1111/j.1476-5381.2012.01987.x>
- North, R.A., 2002. Molecular physiology of P2X receptors. *Physiol. Rev.* 82, 1013–1067. <https://doi.org/10.1152/physrev.00015.2002>

- North, R.A., Jarvis, M.F., 2013. P2X Receptors as Drug Targets. *Mol. Pharmacol.* 83, 759–769. <https://doi.org/10.1124/mol.112.083758>
- Numano, R., Szobota, S., Lau, A.Y., Gorostiza, P., Volgraf, M., Roux, B., Trauner, D., Isacoff, E.Y., 2009. Nanosculpting reversed wavelength sensitivity into a photoswitchable iGluR. *Proc. Natl. Acad. Sci.* 106, 6814–6819. <https://doi.org/10.1073/pnas.0811899106>
- Nuttle, L.C., Dubyak, G.R., 1994. Differential activation of cation channels and non-selective pores by macrophage P2z purinergic receptors expressed in *Xenopus* oocytes. *J. Biol. Chem.* 269, 13988–13996.
- O'Brien, R.D., Sumikawa, K., Gibson, R.E., 1979. The Nicotinic Acetylcholine Receptor from Torpedo Electroplax, in: Tuček, S. (Ed.), *Progress in Brain Research, The Cholinergic Synapse*. Elsevier, pp. 279–291. [https://doi.org/10.1016/S0079-6123\(08\)64640-3](https://doi.org/10.1016/S0079-6123(08)64640-3)
- Opekarová, M., Tanner, W., 2003. Specific lipid requirements of membrane proteins—a putative bottleneck in heterologous expression. *Biochim. Biophys. Acta BBA - Biomembr., Overexpression of Integral Membrane Proteins* 1610, 11–22. [https://doi.org/10.1016/S0005-2736\(02\)00708-3](https://doi.org/10.1016/S0005-2736(02)00708-3)
- Opella, S.J., Marassi, F.M., 2017. Applications of NMR to membrane proteins. *Arch. Biochem. Biophys.* 628, 92–101. <https://doi.org/10.1016/j.abb.2017.05.011>
- Ousingsawat, J., Wanitchakool, P., Kmit, A., Romao, A.M., Jantarajit, W., Schreiber, R., Kunzelmann, K., 2015. Anoctamin 6 mediates effects essential for innate immunity downstream of P2X7 receptors in macrophages. *Nat. Commun.* 6, 6245. <https://doi.org/10.1038/ncomms7245>
- Palczewski, K., Kumasaka, T., Hori, T., Behnke, C.A., Motoshima, H., Fox, B.A., Trong, I.L., Teller, D.C., Okada, T., Stenkamp, R.E., Yamamoto, M., Miyano, M., 2000. Crystal Structure of Rhodopsin: A G Protein-Coupled Receptor. *Science* 289, 739–745. <https://doi.org/10.1126/science.289.5480.739>
- Pandey, A., Shin, K., Patterson, R.E., Liu, X.-Q., Rainey, J.K., 2016. Current strategies for protein production and purification enabling membrane protein structural biology. *Biochem. Cell Biol. Biochim. Biol. Cell.* 94, 507–527. <https://doi.org/10.1139/bcb-2015-0143>
- Park, S.H., Das, B.B., Casagrande, F., Tian, Y., Nothnagel, H.J., Chu, M., Kiefer, H., Maier, K., Angelis, A.A.D., Marassi, F.M., Opella, S.J., 2012. Structure of the chemokine receptor CXCR1 in phospholipid bilayers. *Nature* 491, 779–783. <https://doi.org/10.1038/nature11580>

- Parvathenani, L.K., Tertyshnikova, S., Greco, C.R., Roberts, S.B., Robertson, B., Posmantur, R., 2003. P2X7 mediates superoxide production in primary microglia and is up-regulated in a transgenic mouse model of Alzheimer's disease. *J. Biol. Chem.* 278, 13309–13317. <https://doi.org/10.1074/jbc.M209478200>
- Pasqualetto, G., Brancale, A., Young, M.T., 2018. The Molecular Determinants of Small-Molecule Ligand Binding at P2X Receptors. *Front. Pharmacol.* 9. <https://doi.org/10.3389/fphar.2018.00058>
- Paszkwowiak, J.J., Dardik, A., 2003. Arterial wall shear stress: observations from the bench to the bedside. *Vasc. Endovascular Surg.* 37, 47–57. <https://doi.org/10.1177/153857440303700107>
- Pelegriin, P., Surprenant, A., 2006. Pannexin-1 mediates large pore formation and interleukin-1 β release by the ATP-gated P2X7 receptor. *EMBO J.* 25, 5071–5082. <https://doi.org/10.1038/sj.emboj.7601378>
- Pellegatti, P., Falzoni, S., Pinton, P., Rizzuto, R., Di Virgilio, F., 2005. A Novel Recombinant Plasma Membrane-targeted Luciferase Reveals a New Pathway for ATP Secretion. *Mol. Biol. Cell* 16, 3659–3665. <https://doi.org/10.1091/mbc.e05-03-0222>
- Penmatsa, A., Wang, K.H., Gouaux, E., 2013. X-ray structure of dopamine transporter elucidates antidepressant mechanism. *Nature* 503, 85–90. <https://doi.org/10.1038/nature12533>
- Pérez-Flores, G., Lévesque, S.A., Pacheco, J., Vaca, L., Lacroix, S., Pérez-Cornejo, P., Arreola, J., 2015. The P2X7/P2X4 interaction shapes the purinergic response in murine macrophages. *Biochem. Biophys. Res. Commun.* 467, 484–490. <https://doi.org/10.1016/j.bbrc.2015.10.025>
- Perutz, M.F., Rossmann, M.G., Cullis, A.F., Muirhead, H., Will, G., North, A.C.T., 1960. Structure of Hæmoglobin: A Three-Dimensional Fourier Synthesis at 5.5-Å. Resolution, Obtained by X-Ray Analysis. *Nature* 185, 416–422. <https://doi.org/10.1038/185416a0>
- Petrou, S., Ugur, M., Drummond, R.M., Singer, J.J., Walsh, J.V., 1997. P2X7 purinoceptor expression in *Xenopus* oocytes is not sufficient to produce a pore-forming P2Z-like phenotype. *FEBS Lett.* 411, 339–345. [https://doi.org/10.1016/S0014-5793\(97\)00700-X](https://doi.org/10.1016/S0014-5793(97)00700-X)
- Peveerini, L., Beudez, J., Dunning, K., Chataigneau, T., Grutter, T., 2018. New Insights Into Permeation of Large Cations Through ATP-Gated P2X Receptors. *Front. Mol. Neurosci.* 11. <https://doi.org/10.3389/fnmol.2018.00265>

- Pfeiffer, Z.A., Aga, M., Prabhu, U., Watters, J.J., Hall, D.J., Bertics, P.J., 2004. The nucleotide receptor P2X7 mediates actin reorganization and membrane blebbing in RAW 264.7 macrophages via p38 MAP kinase and Rho. *J. Leukoc. Biol.* 75, 1173–1182. <https://doi.org/10.1189/jlb.1203648>
- Phelps, C.B., Wang, R.R., Choo, S.S., Gaudet, R., 2010. Differential Regulation of TRPV1, TRPV3, and TRPV4 Sensitivity through a Conserved Binding Site on the Ankyrin Repeat Domain. *J. Biol. Chem.* 285, 731–740. <https://doi.org/10.1074/jbc.M109.052548>
- Pike, L.J., 2004. Lipid rafts: heterogeneity on the high seas. *Biochem. J.* 378, 281–292. <https://doi.org/10.1042/BJ20031672>
- Pippel, A., Stolz, M., Woltersdorf, R., Kless, A., Schmalzing, G., Markwardt, F., 2017. Localization of the gate and selectivity filter of the full-length P2X7 receptor. *Proc. Natl. Acad. Sci. U. S. A.* 114, E2156–E2165. <https://doi.org/10.1073/pnas.1610414114>
- Popot, J.-L., Berry, E.A., Charvolin, D., Creuzenet, C., Ebel, C., Engelman, D.M., Flötenmeyer, M., Giusti, F., Gohon, Y., Hong, Q., Lakey, J.H., Leonard, K., Shuman, H.A., Timmins, P., Warschawski, D.E., Zito, F., Zoonens, M., Pucci, B., Tribet, C., 2003. Amphipols: polymeric surfactants for membrane biology research. *Cell. Mol. Life Sci. CMLS* 60, 1559–1574. <https://doi.org/10.1007/s00018-003-3169-6>
- Pouget, J.-T., Toulme, E., Martinez, A., Choquet, D., Hosy, E., Boué-Grabot, E., 2014. ATP P2X receptors downregulate AMPA receptor trafficking and postsynaptic efficacy in hippocampal neurons. *Neuron* 83, 417–430. <https://doi.org/10.1016/j.neuron.2014.06.005>
- Qu, Y., Franchi, L., Nunez, G., Dubyak, G.R., 2007. Nonclassical IL-1 β Secretion Stimulated by P2X7 Receptors Is Dependent on Inflammasome Activation and Correlated with Exosome Release in Murine Macrophages. *J. Immunol.* 179, 1913–1925. <https://doi.org/10.4049/jimmunol.179.3.1913>
- Qu, Y., Misaghi, S., Newton, K., Gilmour, L.L., Louie, S., Cupp, J.E., Dubyak, G.R., Hackos, D., Dixit, V.M., 2011. Pannexin-1 Is Required for ATP Release during Apoptosis but Not for Inflammasome Activation. *J. Immunol.* 186, 6553–6561. <https://doi.org/10.4049/jimmunol.1100478>
- Querfurth, H.W., LaFerla, F.M., 2010. Alzheimer's disease. *N. Engl. J. Med.* 362, 329–344. <https://doi.org/10.1056/NEJMra0909142>
- Ralevic, V., 2012. P2X receptors in the cardiovascular system. *Wiley Interdiscip. Rev. Membr. Transp. Signal.* 1, 663–674. <https://doi.org/10.1002/wmts.58>

- Ralevic, V., Dunn, W.R., 2015. Purinergic transmission in blood vessels. *Auton. Neurosci., Purinergic signalling and the autonomic nervous system* 191, 48–66. <https://doi.org/10.1016/j.autneu.2015.04.007>
- Rampe, D., Wang, L., Ringheim, G.E., 2004. P2X7 receptor modulation of β -amyloid- and LPS-induced cytokine secretion from human macrophages and microglia. *J. Neuroimmunol., Neuroimmune Circuits and Infectious Disease: Proceedings of the 9th Conference of the Society for Neuroimmune Pharmacology* 147, 56–61. <https://doi.org/10.1016/j.jneuroim.2003.10.014>
- Ran, F.A., Hsu, P.D., Wright, J., Agarwala, V., Scott, D.A., Zhang, F., 2013. Genome engineering using the CRISPR-Cas9 system. *Nat. Protoc.* 8, 2281–2308. <https://doi.org/10.1038/nprot.2013.143>
- Rassendren, F., Buell, G., Newbolt, A., North, R.A., Surprenant, A., 1997. Identification of amino acid residues contributing to the pore of a P2X receptor. *EMBO J.* 16, 3446–3454. <https://doi.org/10.1093/emboj/16.12.3446>
- Rassendren, François, Buell, G.N., Virginio, C., Collo, G., North, R.A., Surprenant, A., 1997. The Permeabilizing ATP Receptor, P2X7 CLONING AND EXPRESSION OF A HUMAN cDNA. *J. Biol. Chem.* 272, 5482–5486. <https://doi.org/10.1074/jbc.272.9.5482>
- Raymond, M.-N., Stunff, H.L., 2006. Involvement of de novo ceramide biosynthesis in macrophage death induced by activation of ATP-sensitive P2X7 receptor. *FEBS Lett.* 580, 131–136. <https://doi.org/10.1016/j.febslet.2005.11.066>
- Renner, C., Moroder, L., 2006. Azobenzene as Conformational Switch in Model Peptides. *ChemBioChem* 7, 868–878. <https://doi.org/10.1002/cbic.200500531>
- Riedel, T., Lozinsky, I., Schmalzing, G., Markwardt, F., 2007a. Kinetics of P2X7 receptor-operated single channels currents. *Biophys. J.* 92, 2377–2391. <https://doi.org/10.1529/biophysj.106.091413>
- Riedel, T., Schmalzing, G., Markwardt, F., 2007b. Influence of Extracellular Monovalent Cations on Pore and Gating Properties of P2X7 Receptor-Operated Single-Channel Currents. *Biophys. J.* 93, 846–858. <https://doi.org/10.1529/biophysj.106.103614>
- Rissiek, B., Haag, F., Boyer, O., Koch-Nolte, F., Adriouch, S., 2015. ADP-ribosylation of P2X7: a matter of life and death for regulatory T cells and natural killer T cells. *Curr. Top. Microbiol. Immunol.* 384, 107–126. https://doi.org/10.1007/82_2014_420
- Robinson, L.E., Murrell-Lagnado, R.D., 2013. The trafficking and targeting of P2X receptors. *Front. Cell. Neurosci.* 7, 233. <https://doi.org/10.3389/fncel.2013.00233>

- Robinson, L.E., Shridar, M., Smith, P., Murrell-Lagnado, R.D., 2014. Plasma membrane cholesterol as a regulator of human and rodent P2X7 receptor activation and sensitization. *J. Biol. Chem.* 289, 31983–31994. <https://doi.org/10.1074/jbc.M114.574699>
- Roger, S., Gillet, L., Baroja-Mazo, A., Surprenant, A., Pelegrin, P., 2010a. C-terminal Calmodulin-binding Motif Differentially Controls Human and Rat P2X7 Receptor Current Facilitation. *J. Biol. Chem.* 285, 17514–17524. <https://doi.org/10.1074/jbc.M109.053082>
- Roger, S., Mei, Z.-Z., Baldwin, J.M., Dong, L., Bradley, H., Baldwin, S.A., Surprenant, A., Jiang, L.-H., 2010b. Single nucleotide polymorphisms that were identified in affective mood disorders affect ATP-activated P2X7 receptor functions. *J. Psychiatr. Res.* 44, 347–355. <https://doi.org/10.1016/j.jpsychires.2009.10.005>
- Roger, S., Pelegrin, P., Surprenant, A., 2008. Facilitation of P2X7 receptor currents and membrane blebbing via constitutive and dynamic calmodulin binding. *J. Neurosci. Off. J. Soc. Neurosci.* 28, 6393–6401. <https://doi.org/10.1523/JNEUROSCI.0696-08.2008>
- Ruppelt, A., Ma, W., Borchardt, K., Silberberg, S.D., Soto, F., 2001. Genomic structure, developmental distribution and functional properties of the chicken P2X(5) receptor. *J. Neurochem.* 77, 1256–1265. <https://doi.org/10.1046/j.1471-4159.2001.00348.x>
- Samways, D.S.K., Khakh, B.S., Dutertre, S., Egan, T.M., 2011. Preferential use of unobstructed lateral portals as the access route to the pore of human ATP-gated ion channels (P2X receptors). *Proc. Natl. Acad. Sci.* 108, 13800–13805. <https://doi.org/10.1073/pnas.1017550108>
- Samways, D.S.K., Li, Z., Egan, T.M., 2014. Principles and properties of ion flow in P2X receptors. *Front. Cell. Neurosci.* 8. <https://doi.org/10.3389/fncel.2014.00006>
- Sánchez-Nogueiro, J., Marín-García, P., Miras-Portugal, M.T., 2005. Characterization of a functional P2X(7)-like receptor in cerebellar granule neurons from P2X(7) knockout mice. *FEBS Lett.* 579, 3783–3788. <https://doi.org/10.1016/j.febslet.2005.05.073>
- Sandoz, G., Levitz, J., Kramer, R.H., Isacoff, E.Y., 2012. Optical Control of Endogenous Proteins with a Photoswitchable Conditional Subunit Reveals a Role for TREK1 in GABAB Signaling. *Neuron* 74, 1005–1014. <https://doi.org/10.1016/j.neuron.2012.04.026>
- Sanz, J.M., Chiozzi, P., Ferrari, D., Colaianna, M., Idzko, M., Falzoni, S., Fellin, R., Trabace, L., Di Virgilio, F., 2009. Activation of microglia by amyloid {beta} requires P2X7 receptor expression. *J. Immunol. Baltim. Md* 1950 182, 4378–4385. <https://doi.org/10.4049/jimmunol.0803612>

- Saul, A., Hausmann, R., Kless, A., Nicke, A., 2013. Heteromeric assembly of P2X subunits. *Front. Cell. Neurosci.* 7. <https://doi.org/10.3389/fncel.2013.00250>
- Schachter, J., Motta, A.P., Zamorano, A. de S., Silva-Souza, H.A. da, Guimarães, M.Z.P., Persechini, P.M., 2008. ATP-induced P2X7-associated uptake of large molecules involves distinct mechanisms for cations and anions in macrophages. *J. Cell Sci.* 121, 3261–3270. <https://doi.org/10.1242/jcs.029991>
- Schreiber, R., Ousingsawat, J., Wanitchakool, P., Sirianant, L., Benedetto, R., Reiss, K., Kunzelmann, K., 2018. Regulation of TMEM16A/ANO1 and TMEM16F/ANO6 ion currents and phospholipid scrambling by Ca²⁺ and plasma membrane lipid. *J. Physiol.* 596, 217–229. <https://doi.org/10.1113/JP275175>
- Schroeder, B.C., Cheng, T., Jan, Y.N., Jan, L.Y., 2008. Expression Cloning of TMEM16A as a Calcium-Activated Chloride Channel Subunit. *Cell* 134, 1019–1029. <https://doi.org/10.1016/j.cell.2008.09.003>
- Seman, M., Adriouch, S., Scheuplein, F., Krebs, C., Freese, D., Glowacki, G., Deterre, P., Haag, F., Koch-Nolte, F., 2003. NAD-induced T cell death: ADP-ribosylation of cell surface proteins by ART2 activates the cytolytic P2X7 purinoceptor. *Immunity* 19, 571–582. [https://doi.org/10.1016/s1074-7613\(03\)00266-8](https://doi.org/10.1016/s1074-7613(03)00266-8)
- Shinozaki, Y., Sumitomo, K., Tsuda, M., Koizumi, S., Inoue, K., Torimitsu, K., 2009. Direct Observation of ATP-Induced Conformational Changes in Single P2X4 Receptors. *PLoS Biol.* 7. <https://doi.org/10.1371/journal.pbio.1000103>
- Shrivastava, A.N., Rodriguez, P.C., Triller, A., Renner, M., 2013. Dynamic micro-organization of P2X7 receptors revealed by PALM based single particle tracking. *Front. Cell. Neurosci.* 7. <https://doi.org/10.3389/fncel.2013.00232>
- Sierra-Valdez, F., Azumaya, C.M., Romero, L.O., Nakagawa, T., Cordero-Morales, J.F., 2018. Structure–function analyses of the ion channel TRPC3 reveal that its cytoplasmic domain allosterically modulates channel gating. *J. Biol. Chem.* 293, 16102–16114. <https://doi.org/10.1074/jbc.RA118.005066>
- Sigworth, F.J., Neher, E., 1980. Single Na⁺ channel currents observed in cultured rat muscle cells. *Nature* 287, 447–449. <https://doi.org/10.1038/287447a0>
- Sikora, A., Liu, J., Brosnan, C., Buell, G., Chessel, I., Bloom, B.R., 1999. Cutting Edge: Purinergic Signaling Regulates Radical-Mediated Bacterial Killing Mechanisms in Macrophages Through a P2X7-Independent Mechanism. *J. Immunol.* 163, 558–561.

- Sim, J.A., Young, M.T., Sung, H.-Y., North, R.A., Surprenant, A., 2004. Reanalysis of P2X7 Receptor Expression in Rodent Brain. *J. Neurosci.* 24, 6307–6314. <https://doi.org/10.1523/JNEUROSCI.1469-04.2004>
- Skaper, S.D., Debetto, P., Giusti, P., 2009. The P2X7 purinergic receptor: from physiology to neurological disorders. *FASEB J.* 24, 337–345. <https://doi.org/10.1096/fj.09-138883>
- Sluyter, R., Shemon, A.N., Barden, J.A., Wiley, J.S., 2004. Extracellular ATP Increases Cation Fluxes in Human Erythrocytes by Activation of the P2X7 Receptor. *J. Biol. Chem.* 279, 44749–44755. <https://doi.org/10.1074/jbc.M405631200>
- Sluyter, R., Stokes, L., 2011. Significance of P2X7 receptor variants to human health and disease. *Recent Pat. DNA Gene Seq.* 5, 41–54. <https://doi.org/10.2174/187221511794839219>
- Sobolevsky, A.I., Rosconi, M.P., Gouaux, E., 2009. X-ray structure, symmetry and mechanism of an AMPA-subtype glutamate receptor. *Nature* 462, 745–756. <https://doi.org/10.1038/nature08624>
- Solle, M., Labasi, J., Perregaux, D.G., Stam, E., Petrushova, N., Koller, B.H., Griffiths, R.J., Gabel, C.A., 2001. Altered cytokine production in mice lacking P2X(7) receptors. *J. Biol. Chem.* 276, 125–132. <https://doi.org/10.1074/jbc.M006781200>
- Sorge, R.E., Trang, T., Dorfman, R., Smith, S.B., Beggs, S., Ritchie, J., Austin, J.-S., Zaykin, D.V., Meulen, H.V., Costigan, M., Herbert, T.A., Yarkoni-Abitbul, M., Tichauer, D., Livneh, J., Gershon, E., Zheng, M., Tan, K., John, S.L., Slade, G.D., Jordan, J., Woolf, C.J., Peltz, G., Maixner, W., Diatchenko, L., Seltzer, Z., Salter, M.W., Mogil, J.S., 2012. Genetically determined P2X7 receptor pore formation regulates variability in chronic pain sensitivity. *Nat. Med.* 18, 595–599. <https://doi.org/10.1038/nm.2710>
- Soronen, P., Mantere, O., Melartin, T., Suominen, K., Vuorilehto, M., Rytsälä, H., Arvilommi, P., Holma, I., Holma, M., Jylhä, P., Valtonen, H.M., Haukka, J., Isometsä, E., Paunio, T., 2011. P2RX7 gene is associated consistently with mood disorders and predicts clinical outcome in three clinical cohorts. *Am. J. Med. Genet. Part B Neuropsychiatr. Genet. Off. Publ. Int. Soc. Psychiatr. Genet.* 156B, 435–447. <https://doi.org/10.1002/ajmg.b.31179>
- Soto, F., Garcia-Guzman, M., Gomez-Hernandez, J.M., Hollmann, M., Karschin, C., Stühmer, W., 1996. P2X4: an ATP-activated ionotropic receptor cloned from rat brain. *Proc. Natl. Acad. Sci. U. S. A.* 93, 3684–3688. <https://doi.org/10.1073/pnas.93.8.3684>
- Standfuss, J., Xie, G., Edwards, P.C., Burghammer, M., Oprian, D.D., Schertler, G.F.X., 2007. Crystal structure of a thermally stable rhodopsin mutant. *J. Mol. Biol.* 372, 1179–1188. <https://doi.org/10.1016/j.jmb.2007.03.007>

- Stawski, P., Sumser, M., Trauner, D., 2012. A Photochromic Agonist of AMPA Receptors. *Angew. Chem. Int. Ed.* 51, 5748–5751. <https://doi.org/10.1002/anie.201109265>
- Stein, M., Middendorp, S.J., Carta, V., Pejo, E., Raines, D.E., Forman, S.A., Sigel, E., Trauner, D., 2012. Azo-Propofols: Photochromic Potentiators of GABAA Receptors. *Angew. Chem. Int. Ed.* 51, 10500–10504. <https://doi.org/10.1002/anie.201205475>
- Steinberg, T.H., Newman, A.S., Swanson, J.A., Silverstein, S.C., 1987. ATP₄- permeabilizes the plasma membrane of mouse macrophages to fluorescent dyes. *J. Biol. Chem.* 262, 8884–8888.
- Steinberg, T.H., Silverstein, S.C., 1989. Chapter 3 ATP Permeabilization of the Plasma Membrane, in: Tartakoff, A.M. (Ed.), *Methods in Cell Biology*. Academic Press, pp. 45–61. [https://doi.org/10.1016/S0091-679X\(08\)61601-5](https://doi.org/10.1016/S0091-679X(08)61601-5)
- Stelmashenko, O., Lalo, U., Yang, Y., Bragg, L., North, R.A., Compan, V., 2012. Activation of Trimeric P2X₂ Receptors by Fewer than Three ATP Molecules. *Mol. Pharmacol.* 82, 760–766. <https://doi.org/10.1124/mol.112.080903>
- Stock, D., Leslie, A.G.W., Walker, J.E., 1999. Molecular Architecture of the Rotary Motor in ATP Synthase. *Science* 286, 1700. <https://doi.org/10.1126/science.286.5445.1700>
- Stoop, R., Thomas, S., Rassendren, F., Kawashima, E., Buell, G., Surprenant, A., North, R.A., 1999. Contribution of individual subunits to the multimeric P2X₂ receptor: estimates based on methanethiosulfonate block at T336C. *Mol. Pharmacol.* 56, 973–981. <https://doi.org/10.1124/mol.56.5.973>
- Stroud, R.M., 2011. New tools in membrane protein determination. *F1000 Biol. Rep.* 3. <https://doi.org/10.3410/B3-8>
- Sun, C., Heid, M.E., Keyel, P.A., Salter, R.D., 2013. The second transmembrane domain of P2X₇ contributes to dilated pore formation. *PloS One* 8, e61886. <https://doi.org/10.1371/journal.pone.0061886>
- Surprenant, A., Rassendren, F., Kawashima, E., North, R.A., Buell, G., 1996. The Cytolytic P_{2Z} Receptor for Extracellular ATP Identified as a P_{2X} Receptor (P2X₇). *Science* 272, 735. <https://doi.org/10.1126/science.272.5262.735>
- Suzuki, J., Fujii, T., Imao, T., Ishihara, K., Kuba, H., Nagata, S., 2013. Calcium-dependent Phospholipid Scramblase Activity of TMEM16 Protein Family Members. *J. Biol. Chem.* 288, 13305–13316. <https://doi.org/10.1074/jbc.M113.457937>

- Syed, N., Kennedy, C., 2012. Pharmacology of P2X receptors. *Wiley Interdiscip. Rev. Membr. Transp. Signal.* 1, 16–30. <https://doi.org/10.1002/wmts.1>
- Szobota, S., Gorostiza, P., Del Bene, F., Wyart, C., Fortin, D.L., Kolstad, K.D., Tulyathan, O., Volgraf, M., Numano, R., Aaron, H.L., Scott, E.K., Kramer, R.H., Flannery, J., Baier, H., Trauner, D., Isacoff, E.Y., 2007. Remote Control of Neuronal Activity with a Light-Gated Glutamate Receptor. *Neuron* 54, 535–545. <https://doi.org/10.1016/j.neuron.2007.05.010>
- Szymański, W., Beierle, J.M., Kistemaker, H.A.V., Velema, W.A., Feringa, B.L., 2013. Reversible Photocontrol of Biological Systems by the Incorporation of Molecular Photoswitches. *Chem. Rev.* 113, 6114–6178. <https://doi.org/10.1021/cr300179f>
- Tanaka, K., Choi, J., Cao, Y., Stacey, G., 2014. Extracellular ATP acts as a damage-associated molecular pattern (DAMP) signal in plants. *Front. Plant Sci.* 5, 446. <https://doi.org/10.3389/fpls.2014.00446>
- Tate, C.G., 2001. Overexpression of mammalian integral membrane proteins for structural studies. *FEBS Lett., Structure, Dynamics and Function of Proteins in Biological Membranes* 504, 94–98. [https://doi.org/10.1016/S0014-5793\(01\)02711-9](https://doi.org/10.1016/S0014-5793(01)02711-9)
- Teriete, P., Franzin, C.M., Choi, J., Marassi, F.M., 2007. Structure of the Na,K-ATPase Regulatory Protein FXYD1 in Micelles. *Biochemistry* 46, 6774–6783. <https://doi.org/10.1021/bi700391b>
- Thimm, D., Knospe, M., Abdelrahman, A., Moutinho, M., Alsdorf, B.B.A., von Kügelgen, I., Schiedel, A.C., Müller, C.E., 2013. Characterization of new G protein-coupled adenine receptors in mouse and hamster. *Purinergic Signal.* 9, 415–426. <https://doi.org/10.1007/s11302-013-9360-9>
- Thimm, D., Schiedel, A.C., Peti-Peterdi, J., Kishore, B.K., Müller, C.E., 2015. The nucleobase adenine as a signalling molecule in the kidney. *Acta Physiol. Oxf. Engl.* 213, 808–818. <https://doi.org/10.1111/apha.12452>
- Thomas, P., Smart, T.G., 2005. HEK293 cell line: A vehicle for the expression of recombinant proteins. *J. Pharmacol. Toxicol. Methods, Electrophysiological Methods in Neuropharmacology* 51, 187–200. <https://doi.org/10.1016/j.vascn.2004.08.014>
- Tochitsky, I., Banghart, M.R., Mouro, A., Yao, J.Z., Gaub, B., Kramer, R.H., Trauner, D., 2012. Optochemical control of genetically engineered neuronal nicotinic acetylcholine receptors. *Nat. Chem.* 4, 105–111. <https://doi.org/10.1038/nchem.1234>
- Tomasinsig, L., Pizzirani, C., Skerlavaj, B., Pellegatti, P., Gulinelli, S., Tossi, A., Di Virgilio, F., Zanetti, M., 2008. The human cathelicidin LL-37 modulates the activities of the P2X7

- receptor in a structure-dependent manner. *J. Biol. Chem.* 283, 30471–30481. <https://doi.org/10.1074/jbc.M802185200>
- Torres, G.E., Egan, T.M., Voigt, M.M., 1999. Hetero-oligomeric assembly of P2X receptor subunits. Specificities exist with regard to possible partners. *J. Biol. Chem.* 274, 6653–6659. <https://doi.org/10.1074/jbc.274.10.6653>
- Torres, G.E., Egan, T.M., Voigt, M.M., 1998. Topological analysis of the ATP-gated ionotropic [correction of ionotropic] P2X2 receptor subunit. *FEBS Lett.* 425, 19–23. [https://doi.org/10.1016/s0014-5793\(98\)00179-3](https://doi.org/10.1016/s0014-5793(98)00179-3)
- Trautmann, A., 2009. Extracellular ATP in the immune system: more than just a “danger signal.” *Sci. Signal.* 2, pe6. <https://doi.org/10.1126/scisignal.256pe6>
- Traynelis, S.F., Wollmuth, L.P., McBain, C.J., Menniti, F.S., Vance, K.M., Ogden, K.K., Hansen, K.B., Yuan, H., Myers, S.J., Dingledine, R., 2010. Glutamate receptor ion channels: structure, regulation, and function. *Pharmacol. Rev.* 62, 405–496. <https://doi.org/10.1124/pr.109.002451>
- Tsuda, M., Masuda, T., Tozaki-Saitoh, H., Inoue, K., 2013. P2X4 receptors and neuropathic pain. *Front. Cell. Neurosci.* 7. <https://doi.org/10.3389/fncel.2013.00191>
- Ugur, M., Ugur, Ö., 2019. A Mechanism-Based Approach to P2X7 Receptor Action. *Mol. Pharmacol.* 95, 442–450. <https://doi.org/10.1124/mol.118.115022>
- Ulmann, L., Hatcher, J.P., Hughes, J.P., Chaumont, S., Green, P.J., Conquet, F., Buell, G.N., Reeve, A.J., Chessell, I.P., Rassendren, F., 2008. Up-Regulation of P2X4 Receptors in Spinal Microglia after Peripheral Nerve Injury Mediates BDNF Release and Neuropathic Pain. *J. Neurosci.* 28, 11263–11268. <https://doi.org/10.1523/JNEUROSCI.2308-08.2008>
- Valera, S., Hussy, N., Evans, R.J., Adami, N., North, R.A., Surprenant, A., Buell, G., 1994. A new class of ligand-gated ion channel defined by P2X receptor for extracellular ATP. *Nature* 371, 516–519. <https://doi.org/10.1038/371516a0>
- Vavra, V., Bhattacharya, A., Zemkova, H., 2011. Facilitation of glutamate and GABA release by P2X receptor activation in supraoptic neurons from freshly isolated rat brain slices. *Neuroscience* 188, 1–12. <https://doi.org/10.1016/j.neuroscience.2011.04.067>
- Verhoef, P.A., Estacion, M., Schilling, W., Dubyak, G.R., 2003. P2X7 Receptor-Dependent Blebbing and the Activation of Rho-Effector Kinases, Caspases, and IL-1 β Release. *J. Immunol.* 170, 5728–5738. <https://doi.org/10.4049/jimmunol.170.11.5728>

- Virginio, C., Church, D., North, R.A., Surprenant, A., 1997. Effects of divalent cations, protons and calmidazolium at the rat P2X7 receptor. *Neuropharmacology* 36, 1285–1294. [https://doi.org/10.1016/s0028-3908\(97\)00141-x](https://doi.org/10.1016/s0028-3908(97)00141-x)
- Virginio, C., MacKenzie, A., Rassendren, F.A., North, R.A., Surprenant, A., 1999. Pore dilation of neuronal P2X receptor channels. *Nat. Neurosci.* 2, 315–321. <https://doi.org/10.1038/7225>
- Volgraf, M., Gorostiza, P., Numano, R., Kramer, R.H., Isacoff, E.Y., Trauner, D., 2006. Allosteric control of an ionotropic glutamate receptor with an optical switch. *Nat. Chem. Biol.* 2, 47–52. <https://doi.org/10.1038/nchembio756>
- Volgraf, M., Gorostiza, P., Szobota, S., Helix, M.R., Isacoff, E.Y., Trauner, D., 2007. Reversibly Caged Glutamate: A Photochromic Agonist of Ionotropic Glutamate Receptors. *J. Am. Chem. Soc.* 129, 260–261. <https://doi.org/10.1021/ja067269o>
- Wakamori, M., Mikala, G., Mori, Y., 1999. Auxiliary subunits operate as a molecular switch in determining gating behaviour of the unitary N-type Ca²⁺ channel current in *Xenopus* oocytes. *J. Physiol.* 517, 659–672. <https://doi.org/10.1111/j.1469-7793.1999.0659s.x>
- Weinhold, K., Krause-Buchholz, U., Rödel, G., Kasper, M., Barth, K., 2010. Interaction and interrelation of P2X7 and P2X4 receptor complexes in mouse lung epithelial cells. *Cell. Mol. Life Sci. CMLS* 67, 2631–2642. <https://doi.org/10.1007/s00018-010-0355-1>
- Werner, P., Seward, E.P., Buell, G.N., North, R.A., 1996. Domains of P2X receptors involved in desensitization. *Proc. Natl. Acad. Sci. U. S. A.* 93, 15485–15490.
- Wiley, J.S., Sluyter, R., Gu, B.J., Stokes, L., Fuller, S.J., 2011. The human P2X7 receptor and its role in innate immunity. *Tissue Antigens* 78, 321–332. <https://doi.org/10.1111/j.1399-0039.2011.01780.x>
- Woods, L.T., Ajit, D., Camden, J.M., Erb, L., Weisman, G.A., 2016. Purinergic receptors as potential therapeutic targets in Alzheimer's disease. *Neuropharmacology* 104, 169–179. <https://doi.org/10.1016/j.neuropharm.2015.10.031>
- Wozniak, K.L., Phelps, W.A., Tembo, M., Lee, M.T., Carlson, A.E., 2018. The TMEM16A Channel Mediates the fast polyspermy block in *Xenopus Laevis*. *bioRxiv* 270629. <https://doi.org/10.1101/270629>
- Xu, X.J., Boumechache, M., Robinson, L.E., Marschall, V., Gorecki, D.C., Masin, M., Murrell-Lagnado, R.D., 2012. Splice variants of the P2X7 receptor reveal differential agonist dependence and functional coupling with pannexin-1. *J. Cell Sci.* 125, 3776–3789. <https://doi.org/10.1242/jcs.099374>

- Yamamoto, K., Korenaga, R., Kamiya, A., Qi, Z., Sokabe, M., Ando, J., 2000. P2X4 receptors mediate ATP-induced calcium influx in human vascular endothelial cells. *Am. J. Physiol.-Heart Circ. Physiol.* 279, H285–H292. <https://doi.org/10.1152/ajpheart.2000.279.1.H285>
- Yamamoto, K., Sokabe, T., Matsumoto, T., Yoshimura, K., Shibata, M., Ohura, N., Fukuda, T., Sato, T., Sekine, K., Kato, S., Isshiki, M., Fujita, T., Kobayashi, M., Kawamura, K., Masuda, H., Kamiya, A., Ando, J., 2006. Impaired flow-dependent control of vascular tone and remodeling in P2X4-deficient mice. *Nat. Med.* 12, 133–137. <https://doi.org/10.1038/nm1338>
- Yan, Z., Li, S., Liang, Z., Tomić, M., Stojilkovic, S.S., 2008. The P2X7 Receptor Channel Pore Dilates under Physiological Ion Conditions. *J. Gen. Physiol.* 132, 563–573. <https://doi.org/10.1085/jgp.200810059>
- Yang, D., He, Y., Muñoz-Planillo, R., Liu, Q., Núñez, G., 2015. Caspase-11 Requires the Pannexin-1 Channel and the Purinergic P2X7 Pore to Mediate Pyroptosis and Endotoxic Shock. *Immunity* 43, 923–932. <https://doi.org/10.1016/j.immuni.2015.10.009>
- Yang, H., Kim, A., David, T., Palmer, D., Jin, T., Tien, J., Huang, F., Cheng, T., Coughlin, S.R., Jan, Y.N., Jan, L.Y., 2012. TMEM16F Forms a Ca²⁺-Activated Cation Channel Required for Lipid Scrambling in Platelets during Blood Coagulation. *Cell* 151, 111–122. <https://doi.org/10.1016/j.cell.2012.07.036>
- Yip, L., Woehrle, T., Corriden, R., Hirsh, M., Chen, Y., Inoue, Y., Ferrari, V., Insel, P.A., Junger, W.G., 2009. Autocrine regulation of T-cell activation by ATP release and P2X7 receptors. *FASEB J.* 23, 1685–1693. <https://doi.org/10.1096/fj.08-126458>
- Yoder, N., Gouaux, E., 2018. Divalent cation and chloride ion sites of chicken acid sensing ion channel 1a elucidated by x-ray crystallography. *PLOS ONE* 13, e0202134. <https://doi.org/10.1371/journal.pone.0202134>
- Young, C.L., Britton, Z.T., Robinson, A.S., 2012. Recombinant protein expression and purification: A comprehensive review of affinity tags and microbial applications. *Biotechnol. J.* 7, 620–634. <https://doi.org/10.1002/biot.201100155>
- Young, M.T., Fisher, J.A., Fountain, S.J., Ford, R.C., North, R.A., Khakh, B.S., 2008. Molecular Shape, Architecture, and Size of P2X4 Receptors Determined Using Fluorescence Resonance Energy Transfer and Electron Microscopy. *J. Biol. Chem.* 283, 26241–26251. <https://doi.org/10.1074/jbc.M804458200>
- Young, M.T., Pelegrin, P., Surprenant, A., 2006. Identification of Thr283 as a key determinant of P2X7 receptor function. *Br. J. Pharmacol.* 149, 261–268. <https://doi.org/10.1038/sj.bjp.0706880>

Yue, L., Pawlowski, M., Dellal, S.S., Xie, A., Feng, F., Otis, T.S., Bruzik, K.S., Qian, H., Pepperberg, D.R., 2012. Robust photoregulation of GABA A receptors by allosteric modulation with a propofol analogue. *Nat. Commun.* 3, 1–12. <https://doi.org/10.1038/ncomms2094>

Zha, J., Li, D., 2018. Lipid Cubic Phase for Membrane Protein X-ray Crystallography, in: Wang, H., Li, G. (Eds.), *Membrane Biophysics: New Insights and Methods*. Springer, Singapore, pp. 175–220. https://doi.org/10.1007/978-981-10-6823-2_7

Zhuo, M., Wu, G., Wu, L.-J., 2011. Neuronal and microglial mechanisms of neuropathic pain. *Mol. Brain* 4, 31. <https://doi.org/10.1186/1756-6606-4-31>

Zimmermann, H., 2006. Ectonucleotidases in the nervous system. *Novartis Found. Symp.* 276, 113–128; discussion 128-130, 233–237, 275–281.

ANNEXES

ANNEXE 1: Rate and dissociation constants obtained from simulations.

Rate and dissociation constants	Control	After current facilitation
k_1 (s ⁻¹)	1	1
k_{-1} (s ⁻¹)	104	104
k'_1 (s ⁻¹)	1	1
k'_{-1} (s ⁻¹)	3000	3000
k_2 (s ⁻¹)	0.4	0.4
k_{-2} (s ⁻¹)	34	9.3
k'_2 (s ⁻¹)	0.4	0.4
k'_{-2} (s ⁻¹)	26	14
k_3 (s ⁻¹)	200	500
k_{-3} (s ⁻¹)	8.4	1.6
k'_3 (s ⁻¹)	50	100
k'_{-3} (s ⁻¹)	5.5	2.8
k_{on1} (M ⁻¹ × s ⁻¹)	5×10^4	5×10^4
k_{off1} (s ⁻¹)	3	3
K_{D1} (μM)	60	60
k_{on2} (M ⁻¹ × s ⁻¹)	2.5×10^5	2.5×10^5
k_{off2} (s ⁻¹)	66.66	66.66
K_{D2} (μM)	266.6	266.6
k_{on3} (M ⁻¹ × s ⁻¹)	5×10^6	5×10^6
k_{off3} (s ⁻¹)	66.66	66.66
K_{D3} (μM)	13.3	13.3

$$K_D = k_{off}/k_{on}$$

ANNEXE 2: Publications.

Participation in:

- 1.) Harkat, M.*; Peverini, L.*; Cerdan, A.H., **Dunning, K.**, Beudez, J., Martz, A., Calimet, N., Specht, A., Cecchini, M., Chataigneau, T., Grutter, T., 2017. On the permeation of large organic cations through the pore of ATP-gated P2X receptors. Proc. Natl. Acad. Sci. U. S. A. 114, E3786–E3795

(In this publication, I participated in the biochemical cell-surface crosslinking and Western Blot experiments.)

- 2.) Peverini, L., Beudez, J., **Dunning, K.**, Chataigneau, T., Grutter, T., 2018. New Insights Into Permeation of Large Cations Through ATP-Gated P2X Receptors. Front. Mol. Neurosci. 11.
- 3.) Habermacher, C., **Dunning, K.**, Chataigneau, T., Grutter, T., 2016. Molecular Structure and Function of P2X Receptors. Neuropharm. 104, 18 – 30.



On the permeation of large organic cations through the pore of ATP-gated P2X receptors

Mahboubi Harkat^{a,b,1}, Laurie Peverini^{a,b,1}, Adrien H. Cerdan^{b,c}, Kate Dunning^{a,b}, Juline Beudez^{a,b}, Adeline Martz^{a,b}, Nicolas Calimet^{b,c}, Alexandre Specht^{a,b}, Marco Cecchini^{b,c}, Thierry Chataigneau^{a,b}, and Thomas Grutter^{a,b,2}

^aLaboratoire de Conception et Application de Molécules Bioactives, Équipe de Chimie et Neurobiologie Moléculaire, Faculté de Pharmacie, Centre National de la Recherche Scientifique (CNRS), UMR 7199, F-67400 Illkirch, France; ^bUniversité de Strasbourg, F-67000 Strasbourg, France; and ^cLaboratoire d'Ingénierie des Fonctions Moléculaires, Institut de Science et d'Ingénierie Supramoléculaires (ISIS), UMR 7006, CNRS, F-67000 Strasbourg, France

Edited by Christopher Miller, Howard Hughes Medical Institute, Brandeis University, Waltham, MA, and approved March 31, 2017 (received for review January 25, 2017)

Pore dilation is thought to be a hallmark of purinergic P2X receptors. The most commonly held view of this unusual process posits that under prolonged ATP exposure the ion pore expands in a striking manner from an initial small-cation conductive state to a dilated state, which allows the passage of larger synthetic cations, such as *N*-methyl-D-glucamine (NMDG⁺). However, this mechanism is controversial, and the identity of the natural large permeating cations remains elusive. Here, we provide evidence that, contrary to the time-dependent pore dilation model, ATP binding opens an NMDG⁺-permeable channel within milliseconds, with a conductance that remains stable over time. We show that the time course of NMDG⁺ permeability superimposes that of Na⁺ and demonstrate that the molecular motions leading to the permeation of NMDG⁺ are very similar to those that drive Na⁺ flow. We found, however, that NMDG⁺ “percolates” 10 times slower than Na⁺ in the open state, likely due to a conformational and orientational selection of permeating molecules. We further uncover that several P2X receptors, including those able to desensitize, are permeable not only to NMDG⁺ but also to spermidine, a large natural cation involved in ion channel modulation, revealing a previously unrecognized P2X-mediated signaling. Altogether, our data do not support a time-dependent dilation of the pore on its own but rather reveal that the open pore of P2X receptors is wide enough to allow the permeation of large organic cations, including natural ones. This permeation mechanism has considerable physiological significance.

pore dilation | purinergic receptor | photoswitches | YO-PRO uptake | spermidine

P2X receptors are nonselective cation channels activated by adenosine 5'-triphosphate (ATP). They are integral membrane proteins and form a family of trimeric receptors composed of seven subunits (P2X1–P2X7) that are involved in a wide range of physiological and pathological processes, including pain sensation, hearing protection, taste, modulation of neurotransmitter release, hypertension, inflammation, and neuropathic pain (1–5). P2X receptors have, therefore, attracted attention as promising therapeutic targets (5, 6). Supported by recent X-ray structures (7–11), a functional receptor is composed of three subunits that assemble in the cell membrane as a homo- or heterotrimer to form a central transmembrane pore (12, 13). Each subunit comprises two transmembrane helices, named TM1 and TM2, which are linked by an extracellular domain, where the ATP-binding sites are nestled. In response to a short application of ATP, the pore rapidly opens on the millisecond timescale—a process known as gating—to a state that is selective to small inorganic cations, such as Na⁺, K⁺, and Ca²⁺ ions. The flow of these cations is estimated to occur at relatively high conduction rates, from 6 to 20 × 10⁶ ions per second at a given driving force amplitude (14–16). This rapidly affects the ion balance of the cell and consequently initiates signal transduction. This open state is sometimes referred to as I₁ state (2).

A remarkable feature of P2X receptors is that a longer ATP application causes a striking time-dependent pore dilation of the channel. This process, named pore dilation, is observed only for selected subtypes, notably homomeric P2X2, P2X4, and P2X7 and heteromeric receptors P2X2/3 and P2X2/5 (17–21). Different possible mechanisms have been proposed to explain pore dilation (22, 23), but the most prevailing one posits that the open pore of the initial I₁ state progressively dilates for several seconds to form an enlarged pore, denoted I₂ state, that is permeable to large organic cations such as *N*-methyl-D-glucamine (NMDG⁺) or fluorescent dyes such as ethidium bromide and YO-PRO-1, a carbocyanine DNA binding dye (2). As these cations are larger than small inorganic ions, they are believed to be impermeable to the I₁ state. This belief has been supported by many biophysical studies, including atomic force microscopy (AFM), patch-clamp electrophysiology, fluorescent dye uptakes, and real-time conformational change measurements (17, 18, 24–31). However, the molecular mechanism of pore expansion is still unclear.

Very recently, a study has challenged the pore dilation paradigm (32). The study suggests that the slow transition toward the I₂ state is not caused by a progressive change in the permeability ratio of NMDG⁺ relative to Na⁺, which is usually determined by measuring the hallmark shift in equilibrium potentials by patch-clamp electrophysiology under bi-ionic conditions but rather by a dramatic, unappreciated change of the concentrations of these ions inside the cell. Moreover, this study showed that NMDG⁺ permeability is rapidly activated and can be inhibited when a

Significance

Unlike many ion channels whose pore conductances remain relatively stable over time, it is thought that prolonged ATP applications to P2X receptors cause a striking increase over time in the permeability of large molecules, a process dubbed pore dilation. However, this mechanism remains poorly understood and highly controversial. Here, we use different methods spanning single-channel recordings, photochemistry, molecular biology, and computations to show that contrary to longstanding view, rapid activation by ATP allows the stable passage of large cations through the P2X pore. We further discover that spermidine, a large natural cation known to modulate other ion channels, is able to transit through many P2X receptors, including those thought to be nondilating. Our data thus reveal an unacknowledged P2X-mediated signaling.

Author contributions: A.S., M.C., and T.G. designed research; M.H., L.P., A.H.C., K.D., J.B., A.M., N.C., A.S., M.C., and T.C. performed research; M.H., L.P., A.H.C., K.D., J.B., A.M., N.C., A.S., M.C., T.C., and T.G. analyzed data; and T.G. wrote the paper.

The authors declare no conflict of interest.

This article is a PNAS Direct Submission.

¹M.H. and L.P. contributed equally to this work.

²To whom correspondence should be addressed. Email: grutter@unistra.fr.

This article contains supporting information online at www.pnas.org/lookup/suppl/doi:10.1073/pnas.1701379114/-DCSupplemental.

pore-lining cysteine residue is reacted with methanethiosulfonate (MTS) reagents, suggesting that the open state of P2X receptors exhibits measurable and stable permeability to large cations. In line with this work, pore dilation has never been observed at the single-channel level (16, 33), and no crystal structure of a dilated state has been reported to date, making the study of this peculiar state particularly difficult. Finally, the physiological relevance of P2X pore dilation remains unclear, especially due to the unknown identity of the natural molecules that permeate through the dilated state. A recent work has, however, shown that genetically determined P2X7 dilated pore formation regulates variability in chronic pain sensitivity (34). The study revealed that in women having undergone a mastectomy there is a genetic association between lower pain intensity and the hypofunctional His270 (rs7958311) allele of *P2RX7* gene, suggesting that selectively targeting P2X pore formation may be a new strategy for individualizing the treatment of chronic pain. The concept of pore dilation of P2X receptors has remained a matter of controversy for almost 20 years, and as such, understanding of this molecular mechanism with new approaches represents a challenging and pertinent issue.

In this paper, we discover the molecular mechanism of permeation of large organic cations in P2X receptors. Contrary to the prevailing assumptions, we provide evidence by single-channel recordings that the pore does not undergo a time-dependent dilation upon opening but rather enters rapidly, in response to ATP binding, a state that allows the stable passage of large organic cations. In addition, we designed and used photo-switchable cross-linkers of different lengths to probe conformational changes of engineered cysteine-substituted P2X2 receptors that are associated with NMDG⁺ and YO-PRO-1 permeability. We demonstrate that the molecular motions leading to the permeation of these large organic cations are very similar to those that drive Na⁺ flow. We

further reveal by molecular dynamics (MD) simulations a complex mechanism for NMDG⁺ permeation, which involves both a conformational and orientational selection of the permeating molecules. Finally, we uncover that desensitizing P2X receptors have the capacity to transiently conduct NMDG⁺ ions in response to ATP binding and identify spermidine as a natural large molecule able to permeate selected human P2X pores. Our results underscore a previously unappreciated P2X signaling.

Results

ATP Gates a Pore That Is Immediately Permeable to NMDG⁺. In a recent study carried out in P2X2 receptors, it has been shown that ATP rapidly gates macroscopic currents in symmetric NMDG⁺ solutions (32). To determine whether this occurs at the level of the single channel, we used the outside-out configuration of the patch-clamp technique that enables fast solution exchange at the cell membrane on the millisecond time scale. We used symmetric NMDG⁺ solutions, in which NMDG⁺ is present in both the external (outside) and internal (inside the pipette) solutions (NMDG⁺_{out}/NMDG⁺_{in}) and thus represents the only carrier of cationic currents. To increase seal resistance and patch stability, fluoride ions (F⁻) were used as internal counterions to NMDG⁺ cations (*Materials and Methods*). We transiently transfected human embryonic kidney (HEK-293) cells with plasmids encoding the rat P2X2-3T, which is a cysteine-less mutated receptor that retains wild-type P2X2 functionality (35) but displays increased single-channel conductance (36). In a first series of experiments, we used excised outside-out patches that contained multiple channels and observed robust inward NMDG⁺ currents that developed rapidly following fast perfusion of 3 μM ATP, while holding the voltage to -120 mV (activation time constant $\tau_{\text{NMDG}^+} = 203 \pm 47$ ms, $n = 9$ patches; Fig. 1A, *Left* and Fig. S1A and B). NMDG⁺ currents remained constant during the 6-s time

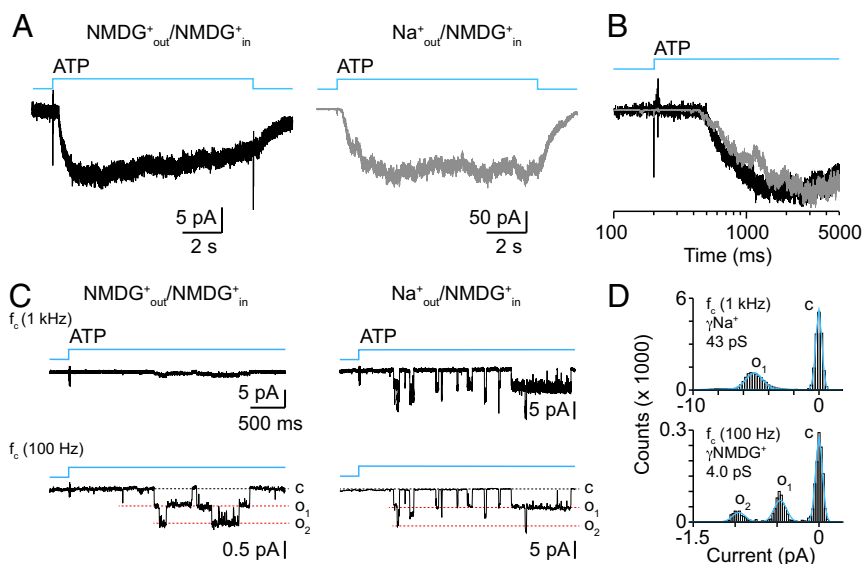


Fig. 1. Rapid ATP activation of P2X2-3T receptors induces instantaneous and stable permeation of NMDG⁺. (A) Fast application of ATP (3 μM, blue traces) to a multiple channel-containing outside-out patch from HEK-293 cells expressing the P2X2-3T receptor evokes rapid NMDG⁺ (*Left*) and Na⁺ (*Right*) currents recorded at -120 mV. The patch was first bathed in extracellular NMDG⁺ solution (NMDG⁺_{out}/NMDG⁺_{in}, *Left*) and then rapidly exchanged to extracellular Na⁺ solution (Na⁺_{out}/NMDG⁺_{in}, *Right*). Note the difference in current scale. (B) Superposition of normalized NMDG⁺ (black trace) and Na⁺ (gray trace) currents shown in A in logarithmic timescale. (C) Single-channel recordings from an outside-out patch recorded at -120 mV of currents elicited by 1 μM ATP, first in NMDG⁺_{out}/NMDG⁺_{in} solution (*Left*) and then in Na⁺_{out}/NMDG⁺_{in} solution (*Right*). Data were sampled at 10 kHz and filtered at a final corner frequency (f_c) of 1 kHz (*Top* traces) or 100 Hz (*Bottom* traces). Channel openings (o) are downward deflections indicated by the red dashed lines. Baseline currents, which correspond to closed channels (c), are indicated by the black dashed lines. (D) All-points amplitude histograms of single-channel Na⁺ (*Top*, f_c = 1 kHz) and NMDG⁺ (*Bottom*, f_c = 100 Hz) obtained from the patch shown in C. Distributions were fit by a sum of four Gaussians for Na⁺ currents and three Gaussians for NMDG⁺ currents (blue lines). Gaussians centered at 0 pA represent closed channels. For this patch, the mean unitary conductance of Na⁺ currents in Na⁺_{out}/NMDG⁺_{in} is 43 pS, whereas that of NMDG⁺ currents in NMDG⁺_{out}/NMDG⁺_{in} is 4.0 pS.

application. Increasing ATP concentration consistently decreased activation time constants ($\tau_{\text{NMDG}^+} = 36 \pm 4$ ms, $n = 10$ patches at 10 μM ; Fig. S1B). Consistent with a recent study (32), these data show that ATP rapidly gates an NMDG⁺ conductance, which remains stable over time.

We next compared these NMDG⁺ currents to those carried by Na⁺ at the same potential, by rapidly exchanging (less than 1 s) external NMDG⁺ for Na⁺ (i.e., Na⁺_{out}/NMDG⁺_{in}), and then challenging again the same patch with 3 μM ATP. Robust inward Na⁺ currents were recorded that were larger than NMDG⁺ currents ($I_{\text{NMDG}^+}/I_{\text{Na}^+} = 9.7 \pm 1.7\%$, $n = 9$ patches; Fig. 1A, Right). This enhancement is expected, as the electrochemical driving force is in favor of Na⁺ influx in Na⁺_{out}/NMDG⁺_{in} solution. Comparison of normalized ATP-gated Na⁺ currents to ATP-gated NMDG⁺ currents revealed similar onsets of inward currents (Fig. 1B), quantified by similar activation rates ($\tau_{\text{Na}^+} = 235 \pm 74$ ms at 3 μM ATP, $n = 9$; Fig. S1A and B). Increasing ATP concentration also consistently decreased activation time constants ($\tau_{\text{Na}^+} = 27 \pm 4$ ms at 10 μM , $n = 10$ patches; Fig. S1B), with no substantial change of the ratio $I_{\text{NMDG}^+}/I_{\text{Na}^+}$ (11.4 \pm 0.6%, $n = 9$). These results indicate that the ATP-gated P2X2 open pore is simultaneously permeable to both Na⁺ and NMDG⁺. The similarity of the activation rates determined in both solutions at a given ATP concentration suggests similar gating kinetics and that the difference in the current ratio must be due to different rates of permeation of these ions.

To determine NMDG⁺ permeation rates, we measured unitary conductance of NMDG⁺ current from outside-out patches that contained single channels, using the same protocols as described for patches that contained multiple channels. In NMDG⁺_{out}/NMDG⁺_{in}, barely visible single openings and closings were detected following 1 μM ATP application, whereas robust single-channel currents were recorded in Na⁺_{out}/NMDG⁺_{in} (Fig. 1C, Top) with a mean conductance of 44 ± 8 pS ($n = 7$ patches, data filtered at 1 kHz). However, when the same recordings were further filtered at a much lower bandwidth (100 Hz; Materials and Methods), discernable unitary currents were then resolved in symmetric NMDG⁺ solution (Fig. 1C, Bottom). These small unitary currents were always recorded in patches that responded to ATP in Na⁺_{out} (16 out of 24 examined patches; the remaining 8 patches were unresponsive to ATP and no unitary NMDG⁺ currents were detected), and they were not observed in the absence of ATP (Fig. S1D). All-points histogram analysis revealed that the mean conductance of these unitary currents was 3.3 ± 0.6 pS (mean amplitude of 0.40 ± 0.04 pA, $n = 6$ patches), which represented 7.5% of the unitary Na⁺ currents, a value that was close to that of the ratio $I_{\text{NMDG}^+}/I_{\text{Na}^+}$ determined from multi-channel currents (Fig. 1D and Fig. S1C). Increasing ATP concentration to 10 or 30 μM did not change the ratio of the mean conductance of NMDG⁺ relative to Na⁺, suggesting that a near saturating concentration of ATP does not increase NMDG⁺ conductance (Fig. S1C). Compared with recordings carried out in symmetric Na⁺ solution (43 ± 6 pS, $n = 4$ patches at 1 μM ATP; Fig. S1E), the unitary conductance of NMDG⁺ currents was about 13 times lower than that of Na⁺ currents. From these values, we conclude that NMDG⁺ ions flow through the ATP-gated open pore at extremely low rates ($\sim 2.5 \times 10^6$ NMDG⁺ ions per second per channel at -120 mV with 132.6 mM NMDG⁺) compared with Na⁺ ($\sim 32 \times 10^6$ Na⁺ ions per second per channel at -120 mV with 132.6 mM Na⁺). Given the fact that NMDG⁺ can rapidly transit through the ATP-gated receptor channel, our data demonstrate that the open pore is wide enough to allow its passage on the millisecond time scale.

Molecular Motions Underlying NMDG⁺ Permeation Are Similar to Those Underlying Na⁺ Permeation. We next sought to determine the molecular motions that drive permeation of NMDG⁺. We used our recent “opto-tweezers” strategy, which enabled us to

probe the gating mechanism of P2X2 receptors by using light to open and close the pore (36). This strategy entails the use of a synthetic semirigid azobenzene cross-linker, 4,4'-bis(maleimido-glycine) azobenzene, called MAM (named hereafter MAM-3), which is covalently tethered between a pair of engineered cysteine-substituted residues located at an appropriate distance apart. Light stimulation at specific wavelengths can then be used to force parts of the protein to come closer together or move farther apart due to isomerization of the azobenzene between defined *trans* and *cis* configurations (Fig. 2A and B). These light-driven motions provide a faithful readout of the molecular movements induced by ATP (36, 37).

We focused on the region of the pore that is particularly effective for manipulating molecular motions by light—that is, around residues I328 and S345, which can be cross-linked horizontally or vertically relative to the membrane plane by MAM-3 (36) (Fig. 2C). To increase the chance of trapping any incremental change of the pore diameter, we synthesized two shorter, more rigid photo-switchable cross-linkers, named MAM-1 (also known as BMA) (37) and MAM-2, in which the cysteine-reactive maleimides are either directly attached to both extremities of the azobenzene core (MAM-1) or indirectly at one of the two extremities by a glycine unit (MAM-2) (Fig. 2A and Figs. S2–S4). As a result, the two end-to-end maleimides are incrementally separated by 2 Å between any two consecutive MAMs in their *trans* configuration (Fig. S5). The end-to-end distance distributions in the *cis* configuration were significantly broader and more difficult to interpret. We produced 13 single and double cysteine mutants in the P2X2–3T background that were expressed in HEK-293 cells and individually treated with each photo-switchable cross-linker, giving rise to 42 different combinations, including controls on the P2X2–3T (Fig. 2E). Effects of light on receptor activity were then assayed using whole-cell patch-clamp recordings on 365-nm (80 ms or 2 s, 17.7 mW/mm²), 530-nm (2 or 4 s, 13.3 mW/mm²), or 455-nm (2 s, 39.5 mW/mm²) illumination cycles to elicit photocurrents in symmetric NMDG⁺ solutions. These currents were normalized to those carried by Na⁺ ($I_{\text{NMDG}^+}/I_{\text{Na}^+}$), following the rapid exchange of cells to an Na⁺_{out}/NMDG⁺_{in} solution.

The screening revealed four important findings. First, all mutants responded to ATP and were permeable to NMDG⁺ when ATP was used as an agonist, with $I_{\text{NMDG}^+}/I_{\text{Na}^+}$ ratios that were similar to those recorded in outside-out patches (between 4% and 15%; Fig. 2E, Fig. S6A, and Table S1). In control experiments, no light-gated currents were observed with P2X2–3T incubated with any MAM (Fig. 2E and Fig. S6B). Second, only a few of the cysteine mutants (7 combinations out of 39) showed reliable light-induced NMDG⁺ currents, with a $I_{\text{NMDG}^+}/I_{\text{Na}^+}$ ratio > 5 (mean $9 \pm 3\%$) that was close to that of ATP controls (Fig. 2E). Indeed, most of the cysteine mutants responded to light following incubation with MAMs (27/39), but control experiments revealed that many of the light-gated currents originating from double mutants (12/19) had activation profiles that were similar to those of one of their single-mutant counterparts (asterisk-labeled boxes in Fig. 2E). In addition, two other combinations—I332C/F346C incubated with MAM-2 or MAM-3—which displayed the highest $I_{\text{NMDG}^+}/I_{\text{Na}^+}$ ratios, were discarded because MAM treatment appeared to dramatically reduce light-gated Na⁺ currents, which, in turn, may introduce uncertainty regarding ratio measurements (Fig. 2D and E).

Third, two phenotypes were observed in light-induced NMDG⁺ currents: Horizontally cross-linked single mutants (I328C treated with MAM-2 or MAM-3, and I332C treated with MAM-1) were activated in the *trans* configuration of the azobenzene, leading to an NMDG⁺ permeability, whereas vertically cross-linked double mutants (I328C/S345C treated with any MAMs, and I332C/S345C treated with MAM-2) were activated in the *cis* configuration (Fig. 2D and E). Conversely, backward isomerization of the

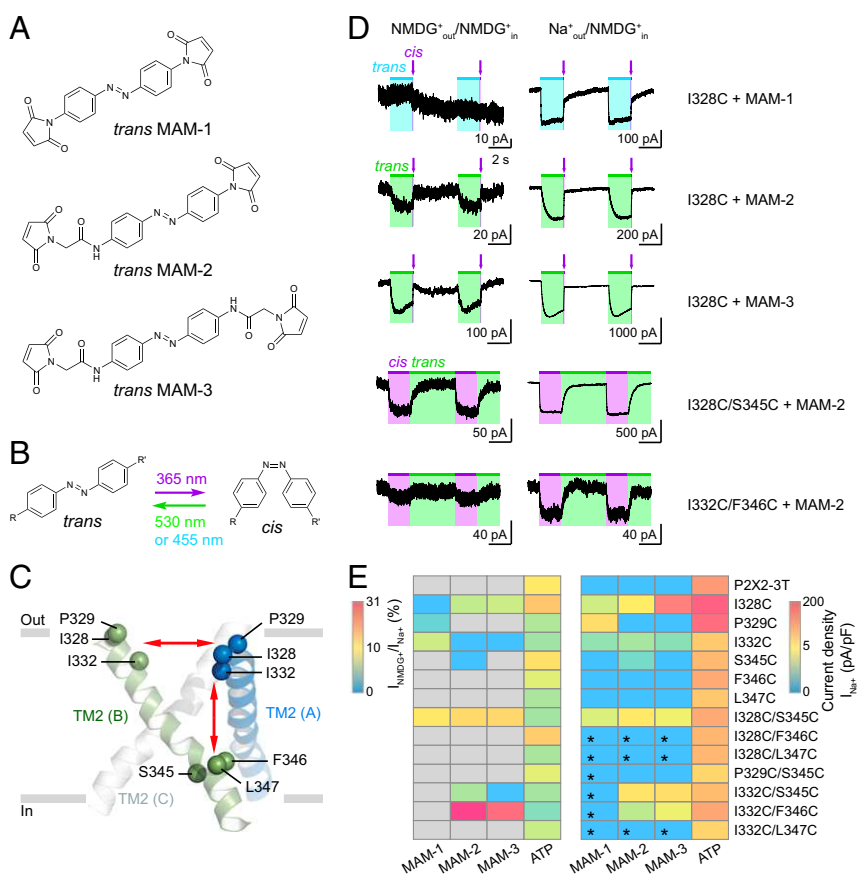


Fig. 2. NMDG⁺ permeation operates with similar molecular motions to Na⁺ permeation. (A) Chemical structures of MAMs in the *trans* state. (B) *Cis*–*trans* isomerization of the azobenzene induced by the indicated wavelengths of light. The backward *cis*–*trans* isomerization is induced by irradiation at 455 nm for MAM-1 or 530 nm for MAM-2 and MAM-3. (C) Side view of the three transmembrane TM2 helices of the hP2X3 ATP-bound X-ray structure [Protein Data Bank (PDB) ID code 5SVK] (10) shown in ribbons and color-coded by subunit. Residues selected for cysteine substitution are indicated by spheres on monomers A and B, and for clarity, they were converted to equivalent rP2X2 numbering. Double red arrows indicate possible horizontal and vertical MAMs cross-linking, relative to the membrane plane, between engineered cysteines. (D) Macroscopic light-gated currents recorded at –60 mV from HEK-293 cells expressing the indicated mutants treated with the indicated MAMs. Cells were first bathed in extracellular NMDG⁺ solution (NMDG⁺_{out}/NMDG⁺_{in}, *Left*), which was then rapidly exchanged for extracellular Na⁺ solution (Na⁺_{out}/NMDG⁺_{in}, *Right*). Illumination was carried out, as indicated, at 365 nm (violet bars) and 455 nm (blue bars) or 530 nm (green bars) to elicit the *cis* and *trans* states of the azobenzene, respectively. Short illuminations (80 ms) are indicated by violet arrows. For MAM-treated single mutants, cells were briefly preirradiated at 365 nm (80 ms) before recordings. (E) Heat map of NMDG⁺ currents normalized to Na⁺ currents (*Left*) and of Na⁺ currents density (*Right*) recorded in indicated conditions. All light-gated currents recorded for single mutants were induced by the *trans* configuration, whereas all light-gated currents recorded for double mutants were elicited by the *cis* configuration, except those indicated by asterisks, which responded to the *trans* configuration, similarly to their single mutant counterparts [I328C, P329C, or I332C]. Gray boxes indicate that $I_{\text{NMDG}^+}/I_{\text{Na}^+}$ cannot be determined. In controls, 30 μM ATP, applied on untreated cells, elicited responses that range between 32% and 92% of the maximal response (see Table S2) (for each box, $n = 4$ –7 cells).

azobenzene from *trans* to *cis*, in the case of horizontally cross-linked mutants, or *cis* to *trans* configuration, for vertically cross-linked mutants, closed the pore, and an additional illumination cycle revealed full reversibility of the light-gated NMDG⁺ currents. Supported by intersubunit cross-linking (Fig. S6C), these data demonstrate that the opening of the NMDG⁺-permeable pore involves two molecular motions: (i) a specific vertical shortening of the distance between extracellular and intracellular ends of adjacent TM2 helices, and (ii) an outward separation of the extracellular ends from two adjacent TM2 helices.

Fourth, a clear correlation between light-gated NMDG⁺ and Na⁺ currents was observed, whereby Na⁺ currents were always observed in the case of NMDG⁺ currents, and inversely, no light-gated NMDG⁺ currents were recorded when no light-gated Na⁺ currents were recorded, indicating that the molecular mechanism underlying NMDG⁺ permeation is very similar to that underlying Na⁺ permeation.

Unlike our previous work (36), we found substantial NMDG⁺ permeability in mutant I328C cross-linked horizontally with MAM-3.

The reason for this discrepancy is unknown, but given that NMDG⁺ permeability had been obtained by measuring E_{rev} from bi-ionic experiments (36), it remains possible that its permeability was underestimated, further stressing the need to use symmetric solutions to measure direct permeation events.

Occurrence of Partially Open States. The correlation between light-gated NMDG⁺ and Na⁺ currents was, however, not perfect. The results revealed that in 3 out of 11 combinations that displayed sizeable light-gated Na⁺ currents (current density > 3 pA/pF), no or very small light-gated NMDG⁺ currents were recorded ($I_{\text{NMDG}^+}/I_{\text{Na}^+}$ were equal or close to zero; Fig. 2E). These data were observed in both vertical (I332C/S345C treated with MAM-3) and horizontal (I328C and P329C treated with MAM-1) cross-linking. Of note, increasing the length of the “tweezers” in the horizontal I328C cross-linking from MAM-1 to MAM-2 to MAM-3 increased the ratio $I_{\text{NMDG}^+}/I_{\text{Na}^+}$ from 0% to ~7% (Fig. 2D). Likewise, decreasing the length of the tweezers in the vertical I332C/S345C cross-linking from MAM-3 to MAM-2 also increased the ratio

$I_{\text{NMDG}^+}/I_{\text{Na}^+}$ from $\sim 0.2\%$ to $\sim 6\%$. Although we cannot rule out the hypothesis that the presence of MAM is specifically interfering with the bulkier NMDG⁺, these data suggest the existence of partially, Na⁺-selective open states that are not permeable to NMDG⁺.

Light-Induced Motions Gate Dye Uptake in Physiological Conditions.

To further confirm data obtained by patch-clamp electrophysiology, we measured YO-PRO-1 dye uptake in physiological conditions, where Na⁺ replaced NMDG⁺. We focused on the pair I328C and S345C treated with MAM-2, which gave both the highest $I_{\text{NMDG}^+}/I_{\text{Na}^+}$ ratio and the most robust light-gated Na⁺ current density. Robust dye uptake following a pulse of 5 s of light at 365 nm was observed for the double mutant I328C/S345C (Fig. 3 *A* and *C*). These uptakes were light-dependent and were similar to those induced by 30 μM ATP on the P2X2–3T background (Fig. 3 *A* and *B*). In contrast, no dye uptake was observed in cells expressing the single mutant I328C or S345C incubated with MAM-2 that were illuminated at 530 nm, following a brief preirradiation at 365 nm before YO-PRO-1 application to reset the azobenzene in the *cis* state (Fig. 3 *D* and *E*). Although these fluorescence data were in agreement with patch-clamp data, the lack of YO-PRO-1 intake for I328C seemed to be in contrast to the recorded NMDG⁺ permeability. However, a careful analysis showed a rapid inactivation of light-gated currents during and after irradiation of cells expressing the I328C mutant treated with MAM-2, whereas stable light-gated currents were recorded for the double mutant I328C/S345C incubated with the same photo-cross-linker (Fig. S7). The transient light-gated activation of the single mutant likely prevents substantial accumulation of YO-PRO-1 into cells, a hypothesis that readily explains the apparent lack of dye uptake. All together, these results provide evidence that YO-PRO-1 uptake induced by the *cis* configuration of MAM-2 tethered to the I328C/S345C double mutant occurs in physiological conditions.

MD Simulations of NMDG⁺ Permeation. To obtain insights into the permeation mechanism of large organic cations in P2X receptors, NMDG⁺ conductance was explored by all-atom MD. For this purpose, an atomistic model of the open state of zP2X4 equilibrated with three MAM-2 vertically cross-linked between I336C and N353C (i.e., equivalent to I328C and S345C in rP2X2) was simulated in the presence of a membrane potential generated by a constant electric field (*Materials and Methods*). To capture NMDG⁺ permeation events on the simulation time scale (i.e., < 50 ns), the ion channel devoid of the extracellular domain was simulated in the presence of a large membrane potential (up to -2 V) in the absence of MAM and with harmonic restraints on the backbone atoms to preserve its open-pore conformation. The MD results show that our open-state model of zP2X4 is permeable to NMDG⁺ (Fig. 4 and *Movie S1*) with a permeation rate of $7 \times 10^7 \text{ s}^{-1}$, which is approximately one order of magnitude lower than that simulated in the presence of Na⁺ (*Table S1*). Of note, these results closely match the ratio measured from single-channel recordings, although the absolute values obtained from modeling were largely higher than those determined experimentally. This is likely due to the non-physiological value of the electrochemical driving force that was used in MD. These simulations reveal that the difference in permeability observed for Na⁺ versus NMDG⁺ is due to a more complex permeation mechanism for the latter, which involves a selection for permeation based on both the molecular conformation and the orientation of the organic cation relative to the pore axis. In fact, by monitoring the end-to-end distance and the orientation of NMDG⁺ along a series of successful permeation events sampled by MD, we found that to be able to cross the constriction point, the organic cation must adopt a fully extended conformation ($d > 7.5 \text{ \AA}$) and have the charged nitrogen atom

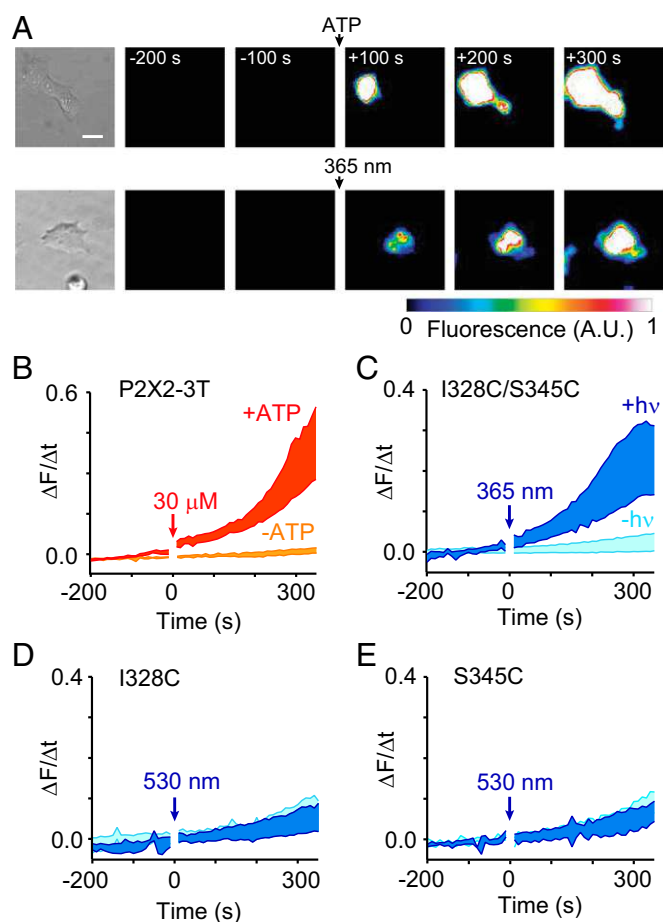


Fig. 3. Structural changes of TM2 helices induce cellular dye uptake in physiological conditions. (*A*) Selected time series of YO-PRO-1 dye uptake in HEK-293 cells expressing the P2X2–3T receptor (*Upper*) and double mutant I328C/S345C treated with MAM-2 (*Lower*). Fluorescence (in arbitrary units) was acquired before and during ATP (30 μM) or light (365 nm for 5 s) activation that started at 0 s as indicated. On the left are shown the corresponding microphotographs under transmitted light. (Scale bar, 20 μm .) (*B*) Corresponding rate of YO-PRO-1 dye uptake in cells ($n = 15$ cells) expressing the P2X2–3T receptor in the absence (orange) or presence (red) of ATP. The arrow indicates the time at which ATP was applied. (*C*) Corresponding rate of dye uptake in cells expressing the double mutant I328C/S345C treated with MAM-2 in the absence (light blue) or presence (dark blue) of irradiation at 365 nm ($n = 18$ cells). The arrow indicates the time at which cells were briefly irradiated. (*D*) Same protocol as in *C* for cells expressing the single mutant I328C treated with MAM-2, except that irradiation occurred at 530 nm ($n = 12$ cells). (*E*) Same protocol as in *D* for cells expressing the single mutant S345C treated with MAM-2 ($n = 18$ –21 cells). For *D* and *E*, cells were briefly preirradiated at 365 nm for 2 s just before YO-PRO-1 application. Shaded areas denote mean \pm SEM.

facing downward along the electrochemical gradient ($\theta < -50^\circ$) (Fig. 4). In addition, the simulations indicated that before populating a permeable conformation, the flexible NMDG⁺ needs to sample several conformations and orientations, which significantly hinders its permeability, consistent with low unitary conductance of single-channel NMDG⁺ currents. Hence, the simulation results confirm that the open-channel state elicited by MAM is permeable to NMDG⁺ and provide an atomistic picture of the permeation mechanism.

Permeation of YO-PRO-1 was also investigated by MD; however, in sharp contrast to results obtained for NMDG⁺, no permeation event was sampled under similar simulation conditions (see *Table S1*).

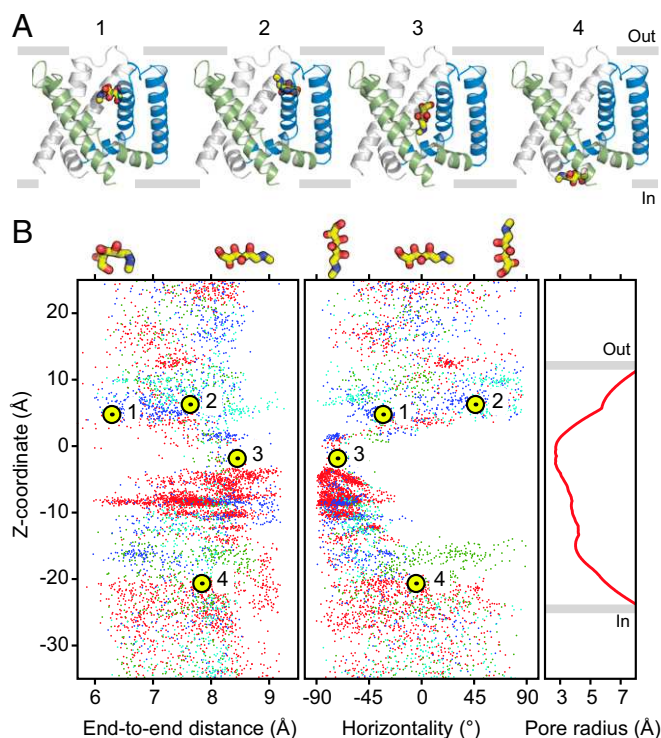


Fig. 4. Mechanism of NMDG⁺ permeation revealed by MD simulations. (A) Snapshots at different simulation times. (B) End-to-end distance of NMDG⁺ (Left) and angle formed by the longitudinal axis of NMDG⁺ cation with the axis parallel to the membrane plane (Middle) are displayed per frame of the simulation for all permeant molecules. Data were collected from four different NMDG⁺ concentration and membrane potential simulation setups: 1 M at -1 V (red dots), 0.15 M at -1 V (green), 0.15 M at -1.5 V (blue), and 0.15 M at -2 V (cyan). Molecular snapshots of NMDG⁺ conformations and orientations corresponding to extreme values for these two observables are shown on top. Indicated numbered dots in yellow are snapshots from A. HOLE profile of the zfP2X4 open-state model after 50 ns of equilibration (Right). The simulation results indicate that the ion pore of the ATP-bound state is sufficiently wide to allow for the passage of large organic cations.

Selected Homomeric P2X Receptors Conduct Large Natural Molecules in Response to ATP. Our data reveal that the permeability to large cations develops within milliseconds upon ATP application, with the same time course as permeability to small cations. We thus asked whether this process is also true for other P2X members, especially for the fast-desensitizing P2X1 and P2X3 receptors, which were presumed to be “nondilating.” To this end, we recorded ATP-gated currents in HEK cells transfected with rat P2X1, P2X3, P2X4, P2X5, P2X7, and human P2X2 and P2X3 receptors in symmetric NMDG⁺ solutions (Fig. 5A and Fig. S8). We observed fast and robust NMDG⁺ currents for all these P2X receptors, except for P2X1, which for unknown reasons was not functional in symmetric NMDG⁺ solution (no ATP-gated current was observed in the control solution Na⁺_{out}/NMDG⁺_{in}). Importantly, we provide evidence that NMDG⁺ can permeate the rat and human P2X3 receptors, demonstrating that these desensitizing P2X receptors do indeed carry the ability to rapidly enter a state that is wide enough to allow the passage of large molecules.

Finally, having shown that rapid activation of P2X receptors allows permeation of NMDG⁺, we sought to determine which natural compounds can transit through the pore. We focused on positively charged compounds that share a similar size to NMDG⁺. We selected spermidine, which is a natural polyamine known to modulate many ion channels (38), and produced symmetric spermidine solutions (Materials and Methods). We observed robust inward spermidine whole-cell currents following rapid application of

ATP in cells expressing the human P2X2 and P2X3 receptors while the membrane was held at -60 mV (Fig. 5B). Of note, MD simulations show that the ATP-bound, zfP2X4 open state is also permeable to spermidine (Movie S2). In addition, the simulations indicate that its permeation rate ($5 \times 10^8 \text{ s}^{-1}$) is sevenfold faster than that of NMDG⁺ under the same membrane potential. The symmetrical structure of spermidine in addition to the presence of positive charges at the extremities make both the conformational and orientational barriers for permeation almost vanish, thus drastically enhancing its permeability relative to NMDG⁺ despite their similar size. These data therefore uncover a previously unappreciated P2X signaling in which large molecules can rapidly permeate through the pore in response to ATP binding.

Discussion

In this article we uncover the molecular mechanism underlying the permeability of P2X receptors to large organic cations and identify an important natural ion channel modulator able to flow through the ATP-gated pore. Our data tackle the pore dilation paradigm, which has remained for nearly 20 years one of the most enigmatic features of ionotropic purinergic receptors (19, 20). Until recently, the dogma concerning pore dilation was that the channel undergoes a progressive expansion, over time reaching a diameter wide enough to allow permeation of large cations, such as NMDG⁺ and YO-PRO-1. However, a recent study challenged this model by elegantly demonstrating that P2X channels rapidly develop an

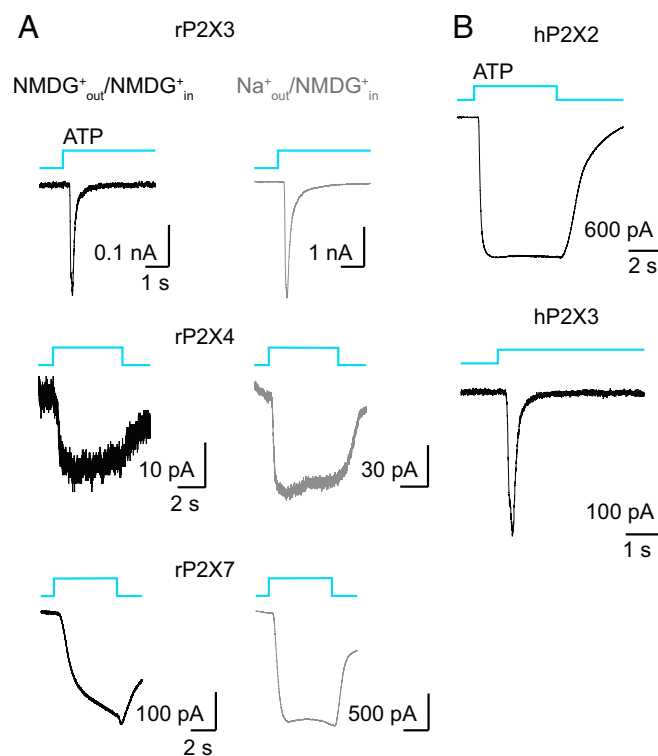


Fig. 5. P2X receptors are permeable to natural organic cations. (A) Macroscopic ATP-gated currents recorded at -60 mV from HEK-293 cells expressing the indicated rat P2X receptors. Recordings were first made in symmetric NMDG⁺_{out}/NMDG⁺_{in} solution (black traces) and then in Na⁺_{out}/NMDG⁺_{in} (gray traces) solution. ATP concentration was 30 μM for rP2X3 and rP2X4 and 300 μM for rP2X7 receptors. For rP2X3 receptors, ATP applications were spaced at least by 3 min. (B) Macroscopic ATP-gated currents recorded in symmetric spermidine solution at -60 mV from HEK-293 cells expressing the indicated human P2X receptors. ATP concentration was 30 μM. Spermidine current density was as follows: hP2X2, $43 \pm 4 \text{ pA/pF}$ ($n = 5$ cells); hP2X3, $6 \pm 2 \text{ pA/pF}$ ($n = 7$ cells). For all traces, ATP application lasted 5 s.

NMDG⁺ current upon ATP binding and lack the slow phase of pore dilation (32). Our results are consistent with this work, and taken together, these two studies firmly establish that, in striking contrast to earlier beliefs, the open state that is reached in milliseconds following ATP binding is also permeable to large molecules. This important finding raises considerable questions concerning the previously predominant view that suggested that the initial I₁ open state is only selective to small cations, such as Na⁺, K⁺, and Ca²⁺. The immediate implication of our results is that the structure of the open pore of the ATP-bound state must be sufficiently wide to accommodate large molecules. From the X-ray structures of the ATP-bound zfp2X4 receptor (8) and very recently the ATP-bound human P2X3 (hP2X3) receptor (10), this seems to be the case, as the minimal cross-section of an extended NMDG⁺ (6 Å × 6 Å × 12.5 Å) is less than the diameter of the open pore (~7 Å for zfp2X4 and 6.4 Å for hP2X3). However, reliable NMDG⁺ permeation by MD simulations cannot be made on the zfp2X4 X-ray structure because the pore systematically collapses within a few nanoseconds (<5) of equilibration (36), likely due to the lack of the intracellular domain that was removed for crystallization purposes (8). By using an improved model of the open state of zfp2X4 (36), which was equilibrated by 50-ns MD in a physiological environment and stabilized by three vertically cross-linked MAM-2 molecules, we provide clear evidence that both NMDG⁺ and the natural cation spermidine may flow through the ion pore of the ATP-bound state. We found, however, that the flow of NMDG⁺ was significantly lower than that of Na⁺, as the former needs to “snake” through the permeating pathway in a fully linear conformation, with the positively charged nitrogen head group pointing downward along the electrochemical gradient. The conformational confinement to this extended form, along with specific orientational constraints in the narrowest region of the pore, introduces significant barriers that hinder cation permeability, thus revealing a complex mechanism for NMDG⁺ permeation. These molecular requirements therefore cause a decrease in the overall rate of NMDG⁺ flow. This conclusion is fully consistent with the low unitary conductance of single-channel NMDG⁺ currents that we (present study) and others (16, 33, 39) have measured for P2X2 and P2X7 receptors.

In contrast to NMDG⁺, we were unable to sample permeation events for YO-PRO-1 in MD simulations. Because the minimal cross-section of the dye (7 Å × 8 Å × 19 Å) reaches the outer limits of the open pore (~7 Å), it is possible that YO-PRO-1 needs to sample more conformations and orientations before a successful permeation can occur, a process that would take considerably more time. As a result, the flux of this fluorescent dye would be extremely low, likely below that of NMDG⁺. Such a molecular sampling-limited step may help to explain the apparent delayed entry of fluorescent dyes that were typically used for monitoring dye uptake through P2X receptors.

An important finding of this study is that the molecular motions driving NMDG⁺ conductance are very similar to those that lead to Na⁺ flow. By using our recently reported opto-tweezers approach (36), we tested the ability of three photo-switchable cross-linkers of different lengths to optically control NMDG⁺ permeability of 13 cysteine mutants. We observed reliable NMDG⁺ permeation with only 7 out of the 39 tested combinations and found a clear correlation between light-gated NMDG⁺ currents and light-gated Na⁺ currents. The specificity of cross-linked residues and the size dependence of the MAMs strengthen the conclusion that the used tweezers do not induce disorder in the protein but rather can be used as mechanical actuators to justly monitor naturally relevant motions. We identified two molecular motions that lead to permeation of large organic cations: a horizontal outward separation of the extracellular ends of TM2 helices and a vertical motion, in which the N and C termini of TM2 helices from adjacent subunits come closer together or change their orientations relative to one another, most

likely through a change of the helical structure. Importantly, such similar molecular motions were also identified during channel gating (36), suggesting that ATP binding drives the rapid opening of a pore that is simultaneously selective to both small and large cations. As we do not have evidence for a time-dependent increase of the permeability of large cations, our data thus support the conclusion that pore dilation is not an intrinsic property of the channel itself. However, we do not rule out the possibility that pore dilation does exist, but if this were the case, it must require a regulatory element that is external to the P2X pore and that would be lost in our experimental conditions.

One intriguing feature of the mechanism revealed by the opto-tweezers approach is that it raises the possibility to open the channel in a state that is not fully open. We found that an insufficient horizontal outward separation or inappropriate vertical motions of two adjacent TM2 helices failed to open NMDG⁺ conductance but not Na⁺ conductance, suggesting that the pore is partially open. A further variation, by only a few Å, of adjacent helices induced an NMDG⁺ permeation in addition to the Na⁺ flow, thus allowing the pore to become fully opened. The physiological relevance of these partially open states remains unclear, but they might be related to dynamic changes of other biophysical properties of P2X receptors, such as ATP potency and rectification, as reported previously (40, 41). Another possibility would be that these partially open states might correspond to the actual I₁ state. However, we do not favor this hypothesis because we provide no evidence that ATP binding naturally drives the opening of the channel in partially open states that are only selective to small cations.

Finally, we have identified spermidine as a natural cation able to permeate through the ATP-gated open state. Polyamines are well-known to modulate the activity of many ion channels, including synaptic ligand-gated ion channels (38). Importantly, we show that even desensitizing receptors, such as hP2X3, which have been considered thus far as nondilating pores, are able to briefly activate their pores in an open state, allowing for a transient flow of spermidine. This finding has considerable physiological significance because it discloses an unsuspected role of polyamines in P2X signaling and more generally because it raises the possibility that activation of P2X receptors may allow for the exchange of other physiological molecules between cells, such as amino acids. Notably, a recent study exploited the large-pore property of P2X receptors to deliver small membrane-impermeable drugs to diseased retina cells (42). We thus propose that besides the critical role of the permeation of inorganic cations, the passage of small-sized metabolites, like spermidine, through the ATP-gated open P2X pore may contribute to alternative physiological responses. These findings open up new horizons in P2X signaling.

Materials and Methods

Chemical Synthesis. All chemicals were purchased from Sigma-Aldrich, Fluka, Across, or Alfa Aesar in analytical grade. An Agilent LC-MS RRLC 1200SL/ESI QToF 6520 was used for ESI analysis. ¹H NMR and ¹³C NMR were run at 400 and 100 MHz, respectively, on an Avance^{III} 400 NMR spectrometer from Bruker. Coupling constants (*J*) are quoted in Hz and chemical shifts (δ) are given in parts per million (ppm) using the residue solvent peaks as reference relative to tetramethylsilane (TMS).

For MAM-1 synthesis, 498 mg (2.348 mmol) of (*E*)-4,4'-(diazene-1,2-diyl)dianiline and 462.3 mg (4.715 mmol, 2 eq) of maleic anhydride were mixed in 20 mL of anhydrous THF and left 1 h at 4 °C. The resulting product was centrifuged (4 min, 8,000 g), and the precipitate was resolubilized in 20 mL of anhydrous THF. Then, 0.5 mL (5.324 mmol, 2.3 eq) of acetic anhydride and 50.2 mg of sodium acetate were added. The mixture was heated under microwave conditions (20 min, 110 °C). Distilled water was added (100 mL), and after centrifugation (10 min, 8,000 g), the precipitate was resolubilized in 100 mL of methanol and an orange solid was obtained by slowly adding cold water. After filtration, purification was carried out by Flash-column chromatography (silica) with dichloromethane and ethyl acetate (gradient 100:0 \geq 95:5). After evaporation of the solvent, the pure MAM-1 was obtained as a bright orange solid (36% yield): NMR ¹H (CDCl₃): δ (ppm), 8.01 (4H, d, *J* = 8.8 Hz), 7.55 (4H, d, *J* = 8.8 Hz), and

6.88 (4H, s); NMR ^{13}C (CDCl_3): δ (ppm), 169.16, 151.23, 134.42, 133.72, 126.22, and 123.70; and (ESI-HMRS):(m/z , $[\text{M}+\text{H}]^+$), calculated for $\text{C}_{20}\text{H}_{13}\text{N}_4\text{O}_4^+$, 373.0859; found, 373.0932.

For synthesis of intermediate 1, 398 mg (1.875 mmol) of (*E*)-4,4'-(diazene-1,2-diyl)dianiline and 726.8 mg (4.7 mmol, 2.5 eq) of 2-(2,5-dioxo-2,5-dihydro-1H-pyrrol-1-yl)acetic acid were solubilized in a mixture of anhydrous DMF/acetonitrile. We then added 1.108 g (4.7 mmol, 2.5 eq) of HATU and 0.65 mL of anhydrous triethylamine (4.7 mmol, 2.5 eq). The mixture was agitated at room temperature for 20 h. After extraction (NaHCO_3 , 3 \times ethyl acetate), the crude product was washed with acetone. The supernatant was purified by flash-column chromatography (silica) with ethyl acetate and heptane (60:40). An orange product was obtained (compound 1, 51% yield): NMR ^1H (acetone- d_6): δ (ppm), 9.66 (1H, s), 7.78 (2H, d, $J = 9.3$ Hz), 7.76 (2H, d, $J = 9.3$ Hz), 7.71 (2H, d, $J = 8.9$ Hz), 7.01 (2H, s), 6.78 (2H, d, $J = 8.9$ Hz), and 4.41 (2H, s); NMR ^{13}C (DMSO- d_6): δ (ppm), 170.64, 165.11, 152.47, 139.70, 138.55, 136.20, 134.95, 128.15, 125.90, 123.50, 122.23, 118.86, 112.85, 112.52, 68.49, 55.81, 32.08, and 29.58.

For synthesis of MAM-2, 200 mg (0.5725 mmol) of intermediate 1 was mixed with 112.3 mg (1.145 mmol, 2 eq) of maleic anhydride and heated under microwave conditions (110 $^\circ\text{C}$, 90 min) in acetone. The obtained precipitate was filtered and resuspended in acetone and then heated 5 min at 60 $^\circ\text{C}$ with 0.12 mL of triethylamine (0.8588 mmol, 1.5 eq). We then added 0.54 mL of acetic anhydride (5.725 mmol, 10 eq) with a catalytic amount of manganese acetate (III), and the mixture was heated under microwave conditions (90 min, 110 $^\circ\text{C}$). After addition of water and filtration, 46.1 mg of MAM-2 was obtained (19% yield): NMR ^1H (DMSO- d_6): δ (ppm), 10.66 (1H, s), 7.97 (2H, d, $J = 8.8$ Hz), 7.92 (2H, d, $J = 8.8$ Hz), 7.79 (2H, d, $J = 8.8$ Hz), 7.58 (2H, d, $J = 8.8$ Hz), 7.23 (2H, s), 7.16 (2H, s), and 4.34 (2H, s); NMR ^{13}C (acetone- d_6): δ (ppm), 171.30, 170.38, 166.17, 152.11, 149.51, 142.76, 135.71, 135.60, 135.25, 127.78, 124.83, 123.80, 120.53, and 41.46; (ESI-HMRS):(m/z , $[\text{M}+\text{H}]^+$), 429.1073 calculated for $\text{C}_{22}\text{H}_{15}\text{N}_5\text{O}_5^+$; found, 429.1069.

The synthesis of MAM-3 was carried out as previously described (36).

Molecular Biology. Cysteine mutations were introduced into a rP2X2 receptor background in which Cys9, Cys348, and Cys430 were mutated to threonine (P2X2-3T) (35) using KAPA HiFi HotStart PCR kit (Cliniscience). All mutations were confirmed by DNA sequencing (GATC-Biotech). All P2X encoding genes were subcloned in pcDNA3.1 vector, except that encoding hP2X2, which was subcloned in the vector pCMV6-AC-mGFP (OriGene). hP2X2 contains mGFP at its C terminus.

Expression in Cultured Cells. HEK-293 and TSA-201 cells were cultured and transiently transfected using phosphate calcium procedure with the pcDNA3.1(+) vectors (0.05–0.1 μg for single channel recordings, 0.3 μg for whole-cell recordings, and 10 μg for cell surface cross-linking) and a vector encoding a green fluorescent protein (0.3 μg), as previously described (43).

Patch-Clamp Electrophysiology. Single-channel recordings using outside-out configuration were carried out using HEK-293 cells at room temperature 24 h after transfection. Recording pipettes pulled from borosilicate glass (Harvard Apparatus) were coated with Sylgard 184 (Dow Corning Co.) and fire polished to yield resistances of 10–20 M Ω (Sutter model p-97). The holding potential was -120 mV. The extracellular solution contained 132.6 mM NaCl or NMDG (Sigma), 0.3 mM CaCl_2 , 0.25 mM MgCl_2 , 10 mM Hepes, pH 7.3, adjusted with NaOH (for NaCl solution) or HCl solution (for NMDG solution). The intracellular solution contained either 132.6 mM NMDG, 9.46 mM Hepes, and 10 mM EDTA, adjusted to pH 7.3, first approximately with a 5% HF solution, then more precisely with 0.5% HF with Polypropylene (PP) pipettes (Dominique Dutscher) or 132.6 mM NaF, 9.46 mM Hepes, and 10 mM EDTA, adjusted to pH 7.3 with NaOH. Osmolarity was adjusted to 290–310 mOsmol $\cdot\text{kg}^{-1}$ with glucose. Data were acquired with a patch-clamp amplifier (HEKA EPC 10) using PATCHMASTER software (HEKA Co.), sampled at 4–10 kHz, and low-pass filtered at 2.9 kHz. For offline analysis, data were refiltered to give a cascaded filter corner frequency (f_c) of either 1 kHz or 100 Hz. For data analyses, FitMaster (HEKA Electronics, v2 \times 73.2) and IGOR PRO (WaveMetrics, v6.37A) softwares were used. Channel events were detected by using TAC software (Bruyton Co.), and conductance levels were measured by all-points amplitude histograms fitted to Gaussian distributions. Fitting procedures to access the time constant were based on the single-exponential decay equation function, $I_t = I_0 + A \exp(-t/\tau)$, where I_t is the instantaneous current; I_0 and A are the residual current and maximal amplitude, respectively; t is the time in seconds; and τ is the time constant in seconds.

Whole-cell recordings were performed 24–48 h after transfection in HEK-293 cells. Normal external solution (NES) contained 140 mM NaCl, 2.8 mM KCl, 2 mM CaCl_2 , 2 mM MgCl_2 , 10 mM glucose, 10 mM Hepes, adjusted to

pH 7.3 with NaOH. Normal internal solution (NIS) contained 140 mM KCl, 5 mM MgCl_2 , 5 mM EGTA, 10 mM Hepes, adjusted to pH 7.3 with NaOH. For MAMs incubation, cells were incubated before recordings at room temperature with, respectively, MAM-1 (10 μM for 5 min, 1% final concentration of DMSO in NES), MAM-2 (10 μM for 10 min, 1% DMSO in NES), and MAM-3 (3 μM for 20 min, 1% DMSO in NES) and 3 μM ATP. After treatment, cells were washed out with NES. Patch pipettes contained 140 mM NMDG, 10 mM Hepes, and 10 mM EDTA, pH adjusted with HCl to 7.3. To measure NMDG $^+$ permeation, extracellular solution contained 140 mM NMDG and 10 mM Hepes, pH 7.3. The solution was then exchanged to NaCl solution containing 140 mM NaCl and 10 mM Hepes, pH 7.3. For control experiments, these solutions were supplemented with 30 μM ATP. For spermidine permeation experiments, whole-cell recordings were performed 24–48 h after transfection. Patch pipettes contained 33 mM spermidine, 10 mM Hepes, and 10 mM EDTA, pH adjusted to 7.3 with HCl. The extracellular solution contained 33 mM spermidine and 10 mM Hepes, pH 7.3, supplemented with 30 μM ATP. Osmolarity of all these solutions was adjusted as described above. Current density was obtained by dividing the current by the cell membrane capacitance.

Cell-Surface Cross-Linking. Cross-linking of cell-surface receptors was performed as follows. TSA-201 cells in dishes were transfected with pcDNA3.1(+) vectors containing the mutant constructs. After 24 h or 48 h, cells in dishes were washed with ice-cold PBS that contained 154 mM NaCl, 2.68 mM KCl, 4.2 mM Na_2HPO_4 , 1.47 mM KH_2PO_4 , pH 7.0, supplemented with 1 mM MgCl_2 and 0.4 mM CaCl_2 . Then, cells were incubated under gentle agitation with 50 μM photo-switchable cross-linker in the presence of 3 μM ATP in ice-cold PBS, for 20 min (MAM-3) or 15 min (MAM-1, MAM-2). Quenching of unreacted MAM solution was carried out by a 10-min incubation with 10 mM *N*-acetyl-L-cysteine methyl ester (Sigma-Aldrich), in ice-cold PBS, pH 8.0. Dishes were rapidly washed with PBS and incubated with a thiol-cleavable, membrane-impermeant reagent sulfo-succinimidyl-2-(biotinamido)ethyl-1,3-dithiopropionate (Sulfo-NHS-SS-Biotin; ThermoFisher Scientific) in PBS at pH 8.0 for 30 min under gentle agitation. Unreacted Sulfo-NHS-SS-Biotin was quenched by incubation with 20 mM Tris(hydroxymethyl)aminomethane (Biosolve Chemicals) in ice-cold PBS, pH 8.0, for 10 min. Cells were solubilized in lysis buffer, and the supernatant was incubated overnight with neutravidin-agarose beads (ThermoFisher Scientific) as previously described (43). Protein samples were separated on 4–15% SDS/PAGE gels in Tris/Glycine/SDS running buffer (Bio-Rad). Samples were transferred to a nitrocellulose membrane as described (43), which was then incubated in TPBS (PBS supplemented with 1% nonfat dry milk, 0.5% BSA, and 0.05% Tween 20) to block the membrane. The membrane was incubated in TPBS buffer overnight at 4 $^\circ\text{C}$ with mouse anti-c-Myc antibody (ThermoFisher Scientific) diluted at 1:2,500. After three washes with TPBS, the blot was incubated with peroxidase-conjugated sheep anti-mouse antibody for 2 h (dilution 1:10,000; GE Healthcare life Sciences) at room temperature and washed a further three times with TPBS and developed using Amersham ECL Prime Western blotting detection reagent (Dominique Dutscher).

Fluorescence Measurements. Fluorescence was measured using an Olympus IX73 (Olympus LUCPlanFLN 20 \times /0.45 PH1) with ProgRes MF-cool camera. Images were captured at 0.5 Hz. For each experiment, YO-PRO-1 (ThermoFisher) fluorescence was measured from three single cells per field with excitation at 455 nm (ET-EGFP filter, Chroma). For the double-mutant I328C/S345C, cells were first incubated with 10 μM MAM-2 in the presence of 3 μM ATP for 10 min and washed with NES buffer. Then, cells were incubated with 10 μM YO-PRO-1 (4-[(3-methyl-1,3-benzoxazol-2(3H)-ylidene)methyl]-1-[3-(trimethylammonio)propyl]quinolinium diiodide) in NES, and following 10 min of incubation, cells were irradiated at 365 nm for 5 s. For single-mutant I328C and S345C, the same protocol was carried out, except that activation was achieved by 530 nm irradiation and that cells were briefly preirradiated at 365 nm before YO-PRO-1 incubation to reset the azobenzene in the *cis* state. In control experiments with the P2X2-3T, the incorporation of 10 μM YO-PRO-1 was measured in response to 30 μM ATP.

Molecular Modeling. The end-to-end distances for the free MAM-1 and MAM-2 molecules in solution (\sim 10,000 atoms with water molecules) were obtained from all-atom MD simulations performed with ACEMD (44). Eight 100 ns-long unrestrained MD simulations were computed in the NVT ensemble at 310 K for the *cis* and *trans* configurations and for the R/R, S/R, R/S, and S/S stereoisomers. The mean distances between the S–S atoms were computed by averaging over the four stereoisomers for a total of $n = 200,000$ per *cis* or *trans* configuration. Normalized probability distributions of the S–S distance were obtained by clustering all distance values using a bin width of 0.5 Å . The permeation mechanism of Na^+ ,

NMDG⁺, YO-PRO-1²⁺, and spermidine³⁺ in P2X was explored by all-atom MD simulations starting from a relaxed open-state model of zP2X4 stabilized by three vertical MAM-2 photo-switchable cross-linkers fused at the positions I336C/N353C in cis configuration. The latter model (~138,000 atoms) was produced following the procedure described previously (36), with a few differences: (i) Three MAM-2 (instead of MAM-3) cross-linkers were fused to zP2X4 with the glycine unit placed downward near N353C; (ii) the 2-ns equilibration MD was followed by a production of 50 ns with no positional restraints; (iii) in addition to the distance restraints mimicking the internal TM1/TM2 Cd²⁺ binding site (45), the symmetry of the P2X trimer was loosely controlled by using the "Symmetry Restraints" command in NAMD with force constants of 0.25 and 1.0 kcal·mol⁻¹·Å⁻² for the extracellular and the transmembrane domains, respectively; and (iv) the side chain of L351 involved in the new TM2-TM2 interface was simulated using four non-interacting copies (46) together with the R/R, R/S, S/R, and S/S stereoisomers of MAM-2.

For the MD simulations of cation permeation, two modifications were introduced in the resulting model of the P2X open state. First, the MAM-2 linkers were removed (while keeping the mutated residues into cysteines) to mimic the physiological conditions. Second, the extracellular domain of the receptor was deleted to reduce the size of the system and to enhance the sampling of permeation events on the simulation timescale. This modification was done by introducing a peptide bond between D59 and F333 at the top of the transmembrane domain. The resulting structure was energy-minimized for 5,000 steps with NAMD 2.11 (47) using the CHARMM force-field version 36 (48). NMDG⁺, YO-PRO-1²⁺, and spermidine³⁺ parameters were obtained from the CHARMM general force field (49). During all simulations, harmonic restraints (5 kcal·mol⁻¹·Å⁻²) on the backbone atoms of the protein were applied to preserve the configuration of the transmembrane domain as in the MAM2-equilibrated model. The receptor was then embedded into a pre-equilibrated 1-palmitoyl-2-oleoyl-sn-glycero-3-phosphocholine (POPC) lipid bilayer, solvated with TIP3P water molecules and NaCl at 0.15 M or 1 M concentration using VMD (50). To study permeation of large organic cations, Na⁺ ions were replaced by NMDG⁺, YO-PRO-1²⁺, or spermidine³⁺ (51). All simulations were performed with periodic boundary conditions and Particle Mesh Ewald long-range electrostatics. The system (~90,000 atoms) was minimized during 5,000 steps, briefly thermalized (600ps) to 300K, and equili-

brated for 2 ns in the NPT ensemble at 1 atm pressure. Production runs were performed in NVT ensemble imposing a membrane potential to increase the ion permeation probability on the simulation timescale. The membrane potential V_m was generated by introducing a constant electric field E_z on all atoms along the z axis perpendicular to the membrane plane (52), $E_z = V_m/L_z$, where L_z is the size of the simulated system in the z direction. The membrane potential was set to the following voltages: -2, -1.5, and -1 V. Analysis of ion permeation was done using Tcl scripting in VMD, whereas the pore profiles were computed by the program HOLE (53). The End-to-End distance of permeant NMDG⁺ was computed at each simulation step as the distance between the two terminal carbons. To compute the horizontality, we selected a vector from the center of mass of the molecule to the terminal carbon linked to the nitrogen, and then the complement of the polar angle was computed. The z coordinate of the center of mass of permeant NMDG⁺ was plotted as a function of the two previous observables.

Data Analysis. All experiments were performed at least four times from at least two transfections, and values are presented as mean ± SEM. For modeling, values of distribution of *cis* and *trans* configurations are presented as mean ± SE. The number of cells or patches used for the experiments is provided in the text or corresponding figure legends.

ACKNOWLEDGMENTS. We thank Professor Hongbo Zhao and Dr. François Rassendren for providing human P2X2 and human P2X3 receptors, respectively; and Dr. Frederic Bolze and Romain Vauchelles for imaging advising. This work was supported by Agence Nationale de la Recherche Grant ANR-14-CE11-0004-01 (to T.G.), the Ministère de la Recherche, and the Fondation Pierre et Jeanne Spiegel. Financial support from the International Center for Frontier Research in Chemistry (icFRC) and the Agence Nationale de la Recherche through the LabEx project Chemistry of Complex Systems (ANR-10-LABX-0026 CSC; to M.C.) is gratefully acknowledged. This work was granted access to the High Performance Computing resources of the Centre de Calcul Recherche et Technologie/Centre Informatique National de l'Enseignement Supérieur/Institut du Développement et des Ressources en Informatique Scientifique under the allocation 2016-[076644] made by the Grand Equipement National de Calcul Intensif.

- Idzko M, Ferrari D, Eltzschig HK (2014) Nucleotide signalling during inflammation. *Nature* 509:310–317.
- Khakh BS, North RA (2012) Neuromodulation by extracellular ATP and P2X receptors in the CNS. *Neuron* 76:51–69.
- Wirkner K, Sperlagh B, Illes P (2007) P2X3 receptor involvement in pain states. *Mol Neurobiol* 36:165–183.
- Yan D, et al. (2013) Mutation of the ATP-gated P2X(2) receptor leads to progressive hearing loss and increased susceptibility to noise. *Proc Natl Acad Sci USA* 110:2228–2233.
- Pijacka W, et al. (2016) Purinergic receptors in the carotid body as a new drug target for controlling hypertension. *Nat Med* 22:1151–1159.
- North RA, Jarvis MF (2013) P2X receptors as drug targets. *Mol Pharmacol* 83:759–769.
- Kawate T, Michel JC, Birdsong WT, Gouaux E (2009) Crystal structure of the ATP-gated P2X(4) ion channel in the closed state. *Nature* 460:592–598.
- Hattori M, Gouaux E (2012) Molecular mechanism of ATP binding and ion channel activation in P2X receptors. *Nature* 485:207–212.
- Kasuya G, et al. (2016) Structural insights into divalent cation modulations of ATP-gated P2X receptor channels. *Cell Reports* 14:932–944.
- Mansoor SE, et al. (2016) X-ray structures define human P2X(3) receptor gating cycle and antagonist action. *Nature* 538:66–71.
- Karasawa A, Kawate T (2016) Structural basis for subtype-specific inhibition of the P2X7 receptor. *eLife* 5:5.
- Browne LE, Jiang LH, North RA (2010) New structure enlivens interest in P2X receptors. *Trends Pharmacol Sci* 31:229–237.
- Habermacher C, Dunning K, Chataigneau T, Grutter T (2016) Molecular structure and function of P2X receptors. *Neuropharmacology* 104:18–30.
- Ding S, Sachs F (1999) Single channel properties of P2X2 purinoceptors. *J Gen Physiol* 113:695–720.
- Evans RJ (1996) Single channel properties of ATP-gated cation channels (P2X receptors) heterologously expressed in Chinese hamster ovary cells. *Neurosci Lett* 212:212–214.
- Riedel T, Schmalzing G, Markwardt F (2007) Influence of extracellular monovalent cations on pore and gating properties of P2X7 receptor-operated single-channel currents. *Biophys J* 93:846–858.
- Virginio C, MacKenzie A, Rassendren FA, North RA, Surprenant A (1999) Pore dilation of neuronal P2X receptor channels. *Nat Neurosci* 2:315–321.
- Khakh BS, Bao XR, Labarca C, Lester HA (1999) Neuronal P2X transmitter-gated cation channels change their ion selectivity in seconds. *Nat Neurosci* 2:322–330.
- Rokic MB, Stojilkovic SS (2013) Two open states of P2X receptor channels. *Front Cell Neurosci* 7:215.
- Wei L, Casey E, Li D, Jiang LH (2016) ATP-induced P2X receptor-dependent large pore formation: How much do we know? *Front Pharmacol* 7:5.
- Compan V, et al. (2012) P2X2 and P2X5 subunits define a new heteromeric receptor with P2X7-like properties. *J Neurosci* 32:4284–4296.
- Jiang LH, et al. (2005) N-methyl-D-glucamine and propidium dyes utilize different permeation pathways at rat P2X(7) receptors. *Am J Physiol Cell Physiol* 289:C1295–C1302.
- Pelegri P, Surprenant A (2006) Pannexin-1 mediates large pore formation and interleukin-1beta release by the ATP-gated P2X7 receptor. *EMBO J* 25:5071–5082.
- Eickhorst AN, Berson A, Cockayne D, Lester HA, Khakh BS (2002) Control of P2X(2) channel permeability by the cytosolic domain. *J Gen Physiol* 120:119–131.
- Fisher JA, Girdler G, Khakh BS (2004) Time-resolved measurement of state-specific P2X2 ion channel cytosolic gating motions. *J Neurosci* 24:10475–10487.
- Khakh BS, Egan TM (2005) Contribution of transmembrane regions to ATP-gated P2X2 channel permeability dynamics. *J Biol Chem* 280:6118–6129.
- Chaumont S, Khakh BS (2008) Patch-clamp coordinated spectroscopy shows P2X2 receptor permeability dynamics require cytosolic domain rearrangements but not Panx-1 channels. *Proc Natl Acad Sci USA* 105:12063–12068.
- Yan Z, Li S, Liang Z, Tomić M, Stojilkovic SS (2008) The P2X7 receptor channel pore dilates under physiological ion conditions. *J Gen Physiol* 132:563–573.
- Shinozaki Y, et al. (2009) Direct observation of ATP-induced conformational changes in single P2X(4) receptors. *PLoS Biol* 7:e1000103.
- Khadra A, et al. (2012) Gating properties of the P2X2a and P2X2b receptor channels: Experiments and mathematical modeling. *J Gen Physiol* 139:333–348.
- Browne LE, Compan V, Bragg L, North RA (2013) P2X7 receptor channels allow direct permeation of nanometer-sized dyes. *J Neurosci* 33:3557–3566.
- Li M, Toombes GE, Silberberg SD, Swartz KJ (2015) Physical basis of apparent pore dilation of ATP-activated P2X receptor channels. *Nat Neurosci* 18:1577–1583.
- Ding S, Sachs F (1999) Ion permeation and block of P2X(2) purinoceptors: Single channel recordings. *J Membr Biol* 172:215–223.
- Sorge RE, et al. (2012) Genetically determined P2X7 receptor pore formation regulates variability in chronic pain sensitivity. *Nat Med* 18:595–599.
- Li M, Chang TH, Silberberg SD, Swartz KJ (2008) Gating the pore of P2X receptor channels. *Nat Neurosci* 11:883–887.
- Habermacher C, et al. (2016) Photo-switchable tweezers illuminate pore-opening motions of an ATP-gated P2X ion channel. *eLife* 5:e11050.
- Browne LE, et al. (2014) Optical control of trimeric P2X receptors and acid-sensing ion channels. *Proc Natl Acad Sci USA* 111:521–526.
- Guerra GP, Rubin MA, Mello CF (2016) Modulation of learning and memory by natural polyamines. *Pharmacol Res* 112:99–118.
- Pippel A, et al. (2017) Localization of the gate and selectivity filter of the full-length P2X7 receptor. *Proc Natl Acad Sci USA* 114:E2156–E2165.
- Clyne JD, Brown TC, Hume RI (2003) Expression level dependent changes in the properties of P2X2 receptors. *Neuropharmacology* 44:403–412.

41. Fujiwara Y, Kubo Y (2004) Density-dependent changes of the pore properties of the P2X2 receptor channel. *J Physiol* 558:31–43.
42. Tochitsky I, et al. (2016) How azobenzene photoswitches restore visual responses to the blind retina. *Neuron* 92:100–113.
43. Jiang R, et al. (2010) A putative extracellular salt bridge at the subunit interface contributes to the ion channel function of the ATP-gated P2X2 receptor. *J Biol Chem* 285:15805–15815.
44. Harvey MJ, Giupponi G, Fabritiis GD (2009) ACEMD: Accelerating biomolecular dynamics in the microsecond time scale. *J Chem Theory Comput* 5:1632–1639.
45. Heymann G, et al. (2013) Inter- and intrasubunit interactions between transmembrane helices in the open state of P2X receptor channels. *Proc Natl Acad Sci USA* 110:E4045–E4054.
46. Roitberg A, Elber R (1991) Modeling side chains in peptides and proteins: Application of locally enhanced sampling and simulated annealing methods to find minimum energy conformations. *J Chem Phys* 95:9277–9287.
47. Phillips JC, et al. (2005) Scalable molecular dynamics with NAMD. *J Comput Chem* 26:1781–1802.
48. Best RB, et al. (2012) Optimization of the additive CHARMM all-atom protein force field targeting improved sampling of the backbone ϕ , ψ and side-chain $\chi(1)$ and $\chi(2)$ dihedral angles. *J Chem Theory Comput* 8:3257–3273.
49. Vanommeslaeghe K, et al. (2010) CHARMM general force field: A force field for drug-like molecules compatible with the CHARMM all-atom additive biological force fields. *J Comput Chem* 31:671–690.
50. Humphrey W, Dalke A, Schulten K (1996) VMD: Visual molecular dynamics. *J Mol Graph* 14:27–38.
51. Onasch F, et al. (1984) The interactions between nucleic acids and polyamines. III. Microscopic protonation constants of spermidine. *Biophys Chem* 19:245–253.
52. Roux B (2008) The membrane potential and its representation by a constant electric field in computer simulations. *Biophys J* 95:4205–4216.
53. Smart OS, Neduvellil JG, Wang X, Wallace BA, Sansom MS (1996) HOLE: A program for the analysis of the pore dimensions of ion channel structural models. *J Mol Graph* 14:354–360, 376.



New Insights Into Permeation of Large Cations Through ATP-Gated P2X Receptors

Laurie Peverini, Juline Beudez, Kate Dunning, Thierry Chataigneau and Thomas Grutter*

CNRS, CAMB UMR 7199, Équipe de Chimie et Neurobiologie Moléculaire, Université de Strasbourg, Strasbourg, France

The permeability of large cations through the P2X pore has remained arguably the most controversial and complicated topic in P2X-related research, with the emergence of conflicting studies on the existence, mechanism and physiological relevance of a so-called “dilated” state. Due to the important role of several “dilating” P2X subtypes in numerous diseases, a clear and detailed understanding of this phenomenon represents a research priority. Recent advances, however, have challenged the existence of a progressive, ATP-induced pore dilation, by demonstrating that this phenomenon is an artifact of the method employed. Here, we discuss briefly the history of this controversial and enigmatic dilated state, from its initial discovery to its recent reconsideration. We will discuss the literature in which mechanistic pathways to a large cation-permeable state are proposed, as well as important advances in the methodology employed to study this elusive state. Considering recent literature, we will also open the discussion as to whether an intrinsically dilating P2X pore exists, as well as the physiological relevance of such a large cation-permeable pore and its potential use as therapeutic pathway.

OPEN ACCESS

Edited by:

Joe Lynch,
The University of Queensland,
Australia

Reviewed by:

Toshi Kawate,
Cornell University, United States
Elsa Fabbretti,
University of Trieste, Italy

*Correspondence:

Thomas Grutter
grutter@unistra.fr

Received: 29 May 2018

Accepted: 13 July 2018

Published: 31 July 2018

Citation:

Peverini L, Beudez J, Dunning K,
Chataigneau T and Grutter T
(2018) New Insights Into Permeation
of Large Cations Through ATP-Gated
P2X Receptors.
Front. Mol. Neurosci. 11:265.
doi: 10.3389/fnmol.2018.00265

Keywords: LGICs, P2X receptors, dilation, spermidine, ion permeation

INTRODUCTION

For most ion channels, ion selectivity remains stable over time once the pore has opened, allowing small metal ions, such as Na⁺, K⁺ and Ca²⁺ to flow across the cell membrane. However, a few channels, namely TRPV1 (Chung et al., 2008), TRPV2 (Nabissi et al., 2013; Zubcevic et al., 2018), TRPA1 (Banke et al., 2010), acid-sensing ion channels (ASICs; Lingueglia et al., 1997; de Weille et al., 1998) and ATP-gated P2X receptors (Khakh and Lester, 1999; Virginio et al., 1999a) exhibit a striking increase in their permeability to larger cations, such as fluorescent dyes or synthetic organic molecules. This phenomenon was initially thought to occur through a time-dependent change of their ion selectivity upon repeated stimulation, a process known as “pore dilation.” However, recent advances have challenged the idea of a slow dynamic change in ion selectivity (Puopolo et al., 2013; Li et al., 2015). In the case of P2X receptors, for which this phenomenon was first described several decades ago, pore dilation has failed to be unanimously accepted due to the increasing emergence of conflicting studies, and alternative mechanisms have been tentatively suggested (Jiang et al., 2005; Rokic and Stojilkovic, 2013; Wei et al., 2016). Given the importance of these ligand-gated ion channels in various physiological and pathological processes, including inflammation and neuropathic pain (Khakh and Alan North, 2006; Abbracchio et al., 2009; Khakh and North, 2012; Lemoine et al., 2012; Bernier et al., 2017),

a clear and detailed understanding of this unusual process at the molecular level is of utmost importance.

First cloned in 1994 (Brake et al., 1994; Valera et al., 1994), the family of P2X receptors is comprised of seven different subunit subtypes (P2X1-P2X7). A functional receptor is composed of three subunits, which are assembled as homo- or heterotrimers (Saul et al., 2013). Each subtype monomer shares a common architecture: two transmembrane domains (named TM1 and TM2) linked by a large, multi-glycosylated and disulfide bridge-containing extracellular domain, and intracellular C- and N-termini (Kawate et al., 2009; **Figure 1**). There are three ATP-binding sites which are found within the extracellular domain, positioned in cavities at the interface of adjacent subunits (Chataigneau et al., 2013; Habermacher et al., 2016a). In response to ATP binding, P2X receptors cycle between a number of different allosteric conformational states for which X-ray structures are now available (Kawate et al., 2009; Hattori and Gouaux, 2012; Mansoor et al., 2016; **Figure 1**). Initial ATP binding to the resting, closed channel state triggers a conformational change, resulting in the displacement of all six transmembrane helices and subsequent opening of the transmembrane pore (Li et al., 2008; Kracun et al., 2010). This transition (termed “gating”) usually takes place on the millisecond time scale and allows the small metal cations Na^+ , K^+ and Ca^{2+} to pass through the open pore (sometimes called I_1 state) according to their electrochemical gradient (North, 2002). Sustained application of ATP then leads to the inactivation of the pore (with the exception of P2X7), a process called desensitization, in which ion flux is terminated despite the fact that ATP remains bound to the receptor. ATP dissociation from these states reverts the pore to the initial closed state, from which the receptor is able to undergo further gating cycles upon re-activation (**Figure 1**).

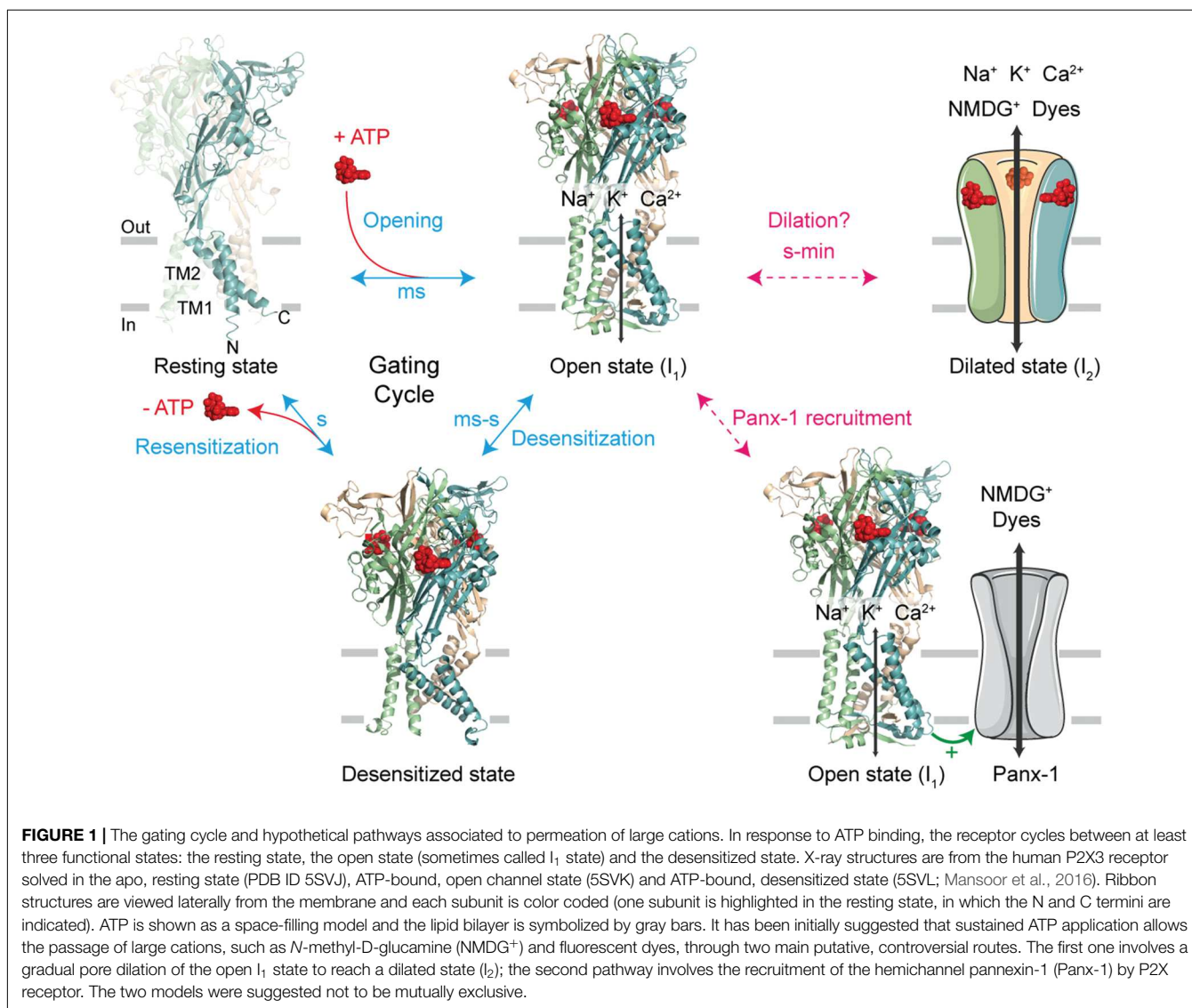
To account for the gradual increase of permeability to larger cations, several mechanistic pathways linked to the P2X gating cycle have been proposed (Jiang et al., 2005; Rokic and Stojilkovic, 2013; Wei et al., 2016). For one of these routes, a putative dilated state (called I_2 state) corresponding to a progressive pore expansion of the open I_1 state following sustained ATP application has been suggested (Khakh and Lester, 1999; Virginio et al., 1999a; **Figure 1**). However, recent studies have seriously challenged this pore dilation hypothesis, by demonstrating that this phenomenon is rather an artifact of the method used to measure ion permeability change. In this review, we will discuss briefly the historical emergence of the controversial dilated state in the P2X family, as well as the recent important advances in the methodology employed that have led to the reconsideration of pore dilation. Finally, we will open the discussion to new physiological and therapeutic perspectives.

BRIEF HISTORY OF THE INCREASE OF PERMEABILITY

The ability of ATP to permeabilize membranes from different cells, such as mast cells, macrophages and transformed

fibroblasts, was first discovered in the late 70s by demonstrating that the membrane permeability of cells gradually increases with increasing concentrations of ATP (Cockcroft and Gomperts, 1979). Besides small inorganic cations, larger organic molecules, such as carboxyfluorescein (376 Da), ethidium bromide (394 Da), lucifer yellow (444 Da) and fura-2 (636 Da) were also shown to be able to cross membranes following ATP application. However, solutes of higher molecular weight, such as Trypan Blue (872 Da), Evans Blue (961 Da) and inulin (more than 5000 Da) did not permeate the membrane (Steinberg et al., 1987; Steinberg and Silverstein, 1989), suggesting that molecules exceeding a certain radius cannot pass. At this point in time, the protein responsible for this behavior was unknown, and additionally, the observed “pore formation” features largely varied according to the cellular subtypes studied (Heppel et al., 1985).

Following these observations, and the discovery of ATP-activated purinergic receptors (P2X and P2Y; Burnstock, 1990), the passage of such large molecules across cell membranes was attributed to the fact that those cell types, in particular immune cells, express an unusual P2 receptor with an apparently non-selective pore. This was initially classified as the P2Z receptor: the “pore-forming” protein was thus named (Gordon, 1986; Abbracchio and Burnstock, 1994). P2Z receptors were then extensively studied for their ability to allow the permeation of large organic molecules into macrophages through a “macropore” (Nuttall and Dubyak, 1994), leading to cytolysis (Di Virgilio, 1995). The link with a putative P2X-related mechanism arose from the identification of the close proximity between P2Z receptor and P2X family receptor sequences. This similarity led to the re-classification of P2Z as the P2X7 receptor subtype (Surprenant et al., 1996). A few years later, two seminal articles reported that other P2X subtypes, the P2X2 and P2X4, also exhibit a striking increase in the permeability of large cations following several seconds of ATP application (Khakh et al., 1999; Virginio et al., 1999b). The concept of P2X “pore dilation” was born and multiple research groups have since confirmed and extended the concept to homomeric and heteromeric receptors (e.g., P2X2/3 and P2X2/5) expressed either in recombinant systems or in native tissues (Khakh et al., 1999; Virginio et al., 1999b; Yan et al., 2008; Compan et al., 2012; Browne et al., 2013). However, certain P2X subtypes, namely P2X1 and P2X3 which are fast desensitizing receptors, were classified as “non-dilating” channels as there was no evidence for an apparent increase in the permeability to large cations. Moreover, distinctive behaviors have been observed for P2X7 receptor splice variants, of which there are nine in humans, classified from P2X7B to P2X7J, and four in rodents (P2X7B, P2X7C, P2X7D and P2X7K); P2X7A is the full-length common P2X7 subunit (Rassendren et al., 1997; Cheewatrakoolpong et al., 2005; Sluyter, 2017). Some of these variants show an altered permeability for large cations. For instance, P2X7B, a variant bearing a largely truncated C terminus, is considered “non-dilating” (Cheewatrakoolpong et al., 2005; Adinolfi et al., 2010). On the contrary, P2X7K, which features a modified TM1 sequence as well as a more lipophilic N terminus, has been shown to be



constitutively and immediately dilated (Nicke et al., 2009; Xu et al., 2012).

METHODS AND INTERPRETATIONS LEADING TO THE CONTROVERTED DILATED STATE

Two main experimental approaches have been used to monitor the apparent gradual increase in large cation permeability. In the first approach, the cellular uptake of fluorescent dyes, such as YO-PRO-1 or ethidium bromide, is observed as a function of time. Dye uptake usually develops several seconds after ATP application. As these cationic dyes become fluorescent when bound to DNA, this method is a simple and direct read-out of the passage of large molecules following P2X activation. Studies involving cysteine reactive compounds, such as methanethiosulfonate (MTS) reagents, have also shown the

ability of larger sized molecules to pass into the cell (Browne et al., 2013). This method has been employed for P2X2, P2X4 and P2X7 receptors (Khakh et al., 1999; Virginio et al., 1999a,b; Yan et al., 2008).

In the second approach, the permeability of large cations is measured by patch-clamp electrophysiology (Khakh et al., 1999; Virginio et al., 1999b). In this indirect method, reversal potentials (E_{rev}) are measured in bi-ionic solutions, where *N*-methyl-D-glucamine (NMDG⁺), a synthetic large organic cation, is the sole permeating ion present outside the cell (NMDG⁺_{out}) and Na⁺ is the sole permeating cation present inside the cell (Na⁺_{in}). According to the Goldman-Hodgkin-Katz voltage equation, a shift in E_{rev} signals a change in membrane permeability to one or both cations provided the concentrations of ions on either side of the membrane remain unchanged. The gradual and positive shifts in E_{rev} measured during long applications of ATP have been interpreted as a time-dependent change in the relative permeability of NMDG⁺ relative to Na⁺ (P_{NMDG^+}/P_{Na^+}). At the

beginning of extracellular ATP application, the agonist opens a pore that is initially more permeable to Na^+ than NMDG^+ , but during sustained activation of the channel, E_{rev} shifts towards less negative values that signify a dramatic increase in the permeability to NMDG^+ (Khakh et al., 1999; Virginio et al., 1999b). This method has been extensively employed to probe shifts in E_{rev} for many P2X receptors, such as P2X2, P2X2/3, P2X2/5, P2X4 and P2X7 (Khakh et al., 1999; Virginio et al., 1999a,b; Compan et al., 2012).

The fact that shifts of E_{rev} and dye uptake occur on the same time scale has led to the belief that a common mechanism would be at work. Two main hypotheses have then emerged (Figure 1). One hypothesis involves the recruitment of an auxiliary protein by P2X receptors. This protein is pannexin-1 (Panx-1), a hemichannel that is responsible for the passage of larger molecules. This hypothesis is supported by the observation that P2X permeability to large cations is inhibited when inhibitors of Panx-1 are applied (Pelegriin and Surprenant, 2006). In addition, colchicine, a drug that disrupts the cytoskeleton, has been shown to affect YO-PRO-1 uptake into cells transfected with P2X2 or P2X7 subtypes, but not the permeability for small cations. This would indicate that these two types of permeability result from different pathways (Marques-da-Silva et al., 2011).

On the other hand, a second hypothesis postulates the existence of an intrinsic “pore dilation” mechanism, whereby the P2X pore itself undergoes a slow conformational change. This would lead to a physical expansion in the diameter of the P2X ion pore from the I_1 state to the putative I_2 dilated state, allowing the passage of larger molecules. This “pore dilation” mechanism has been extensively studied by site-directed mutagenesis, patch-clamp electrophysiology, fluorescent dye uptake and use of chemical reagents (Khakh et al., 1999; Virginio et al., 1999a,b; Eickhorst et al., 2002; Khakh and Egan, 2005; Browne et al., 2013). Moreover, it has been shown that cells which do not express Panx-1 nonetheless exhibit “dilating” properties and, in agreement with this hypothesis, overexpression or inhibition of Panx-1 by carbenoxolone does not affect dilation of P2X2 receptors expressed in HEK-293 cells (Chaumont and Khakh, 2008; Yan et al., 2008).

As evidence has been found both in support of and against each hypothetical pathway, the question has been raised as to whether these two distinct mechanisms may in fact co-exist (Jiang et al., 2005; Cankurtaran-Sayar et al., 2009). One mechanism would be dedicated to NMDG^+ permeability and the other to larger molecules such as YO-PRO-1 and even occasionally the permeation of organic anions (Browne et al., 2013). Moreover, interactions with other proteins may play a role. For instance, cytoskeletal proteins have been described as important for pore dilation in P2X7 receptor subtype (Kim et al., 2001; Gu et al., 2009). In addition, characterization of the apparent “pore dilation” has been shown to be dependent on cell types used for experiments as well as expression levels of receptors (Fujiwara and Kubo, 2004). Of greatest importance is the fact that dynamic changes of unitary conductance following prolonged ATP application have never been observed at the single channel level (Ding and Sachs, 1999; Riedel et al., 2007b),

thus bringing into question the reality of an intrinsic “pore dilation”.

CHANGING THE PARADIGM

In 2015, the team of K. Swartz offered an alternative explanation of the change in E_{rev} measured in bi-ionic $\text{NMDG}^+_{\text{out}}/\text{Na}^+_{\text{in}}$ solutions (Li et al., 2015). The authors elegantly demonstrate in the P2X2 receptor that shifts in E_{rev} , although very real, are not caused by a time-dependent change in channel permeability, but rather by a dramatic and unappreciated change of the intracellular ion concentrations, which may vary by more than 100 mM throughout the course of the experiment. Combining electrophysiology and mathematical modeling, the authors were able to convincingly demonstrate that prolonged ATP activation leads to a depletion of intracellular Na^+ , from 140 mM to around 20 mM, and accumulation of NMDG^+ , from 0 mM to over 200 mM. They further showed that physical parameters such as channel densities, pore conductance, cell volume, and access resistance (R_{access}) between the cell and the pipette electrode, may directly change ion concentrations inside the cell following sustained exposure to ATP. Because of these changes, the Goldman-Hodgkin-Katz voltage equation cannot be used to reliably determine the relative permeability of ions. This study therefore proved that the time-dependent shift in the E_{rev} measured in bi-ionic solutions is an artifact of the method employed, and that extreme caution must be taken when measuring permeability changes during whole-cell patch-clamp recordings.

This outstanding article seriously challenges the pore dilation paradigm which held true for almost two decades. However, it is important to emphasize that the study did not question the ability of NMDG^+ to permeate through the activated P2X pore, as initially suggested by the seminal articles (Khakh et al., 1999; Virginio et al., 1999b), but that this NMDG^+ permeation occurs soon after ATP activation. As a direct proof of this assumption, Li et al. (2015) showed that whole-cell currents carried by NMDG^+ using symmetrical solutions (whereby both intracellular and extracellular solutions contain NMDG^+) developed immediately following ATP application. These observations indicate that a gradual pore dilation mechanism is not necessary to account for NMDG^+ permeation.

A NEW MECHANISTIC POINT OF VIEW

The publication of Li et al. (2015) opens an appealing hypothesis: the dimensions of the pore itself may be directly adequate for the direct passage of NMDG^+ following several milliseconds of ATP application. From a mechanistic point of view, the I_1 state would represent the most parsimonious hypothesis, provided the diameter of the narrowest part of its open pore is sufficiently wide to allow the passage of such large molecules. We have investigated this possibility by combining single-channel recordings, molecular modeling and

the use of photo-switchable tweezers (Harkat et al., 2017), a recently developed technology that allows identification of the molecular motions involved in channel activation (Habermacher et al., 2016b). By covalently tethering synthetic azobenzene cross-linkers to a pair of selected engineered cysteine residues, these “molecular tweezers” are capable of pulling or pushing on gating elements once azobenzene isomerization is triggered by light irradiation. To provide a read-out of the large cation permeation, we used symmetric NMDG⁺ solutions, where NMDG⁺ was the sole permeating ion. A rapid solution exchange of the extracellular solutions from an NMDG⁺-containing to a Na⁺-containing solution allowed direct comparison of molecular motions involved in pore opening and permeation of NMDG⁺ and Na⁺. We screened several positions near a flexible region of TM2 in the P2X2 receptor, as well as a region of the pore surrounding a kink that was previously identified in channel gating (Habermacher et al., 2016b; Mansoor et al., 2016). Firstly, we identified two types of molecular motions involved in the permeation of large cations: a horizontal expansion of the upper end of TM2 helices and a vertical flexing of the extremities of two adjacent TM2 helices. Surprisingly, we observed no NMDG⁺ permeation for mutants bearing no permeability to Na⁺, suggesting that none of the molecular motions that we monitored can produce a pathway dedicated exclusively to NMDG⁺ permeation. Secondly, for the motions that allowed the passage of both NMDG⁺ and Na⁺, the ratio of the current $I_{\text{NMDG}^+}/I_{\text{Na}^+}$ was around 10%, suggesting that NMDG⁺ follows the same pathway as Na⁺ across the P2X pore but is not able to permeate as easily.

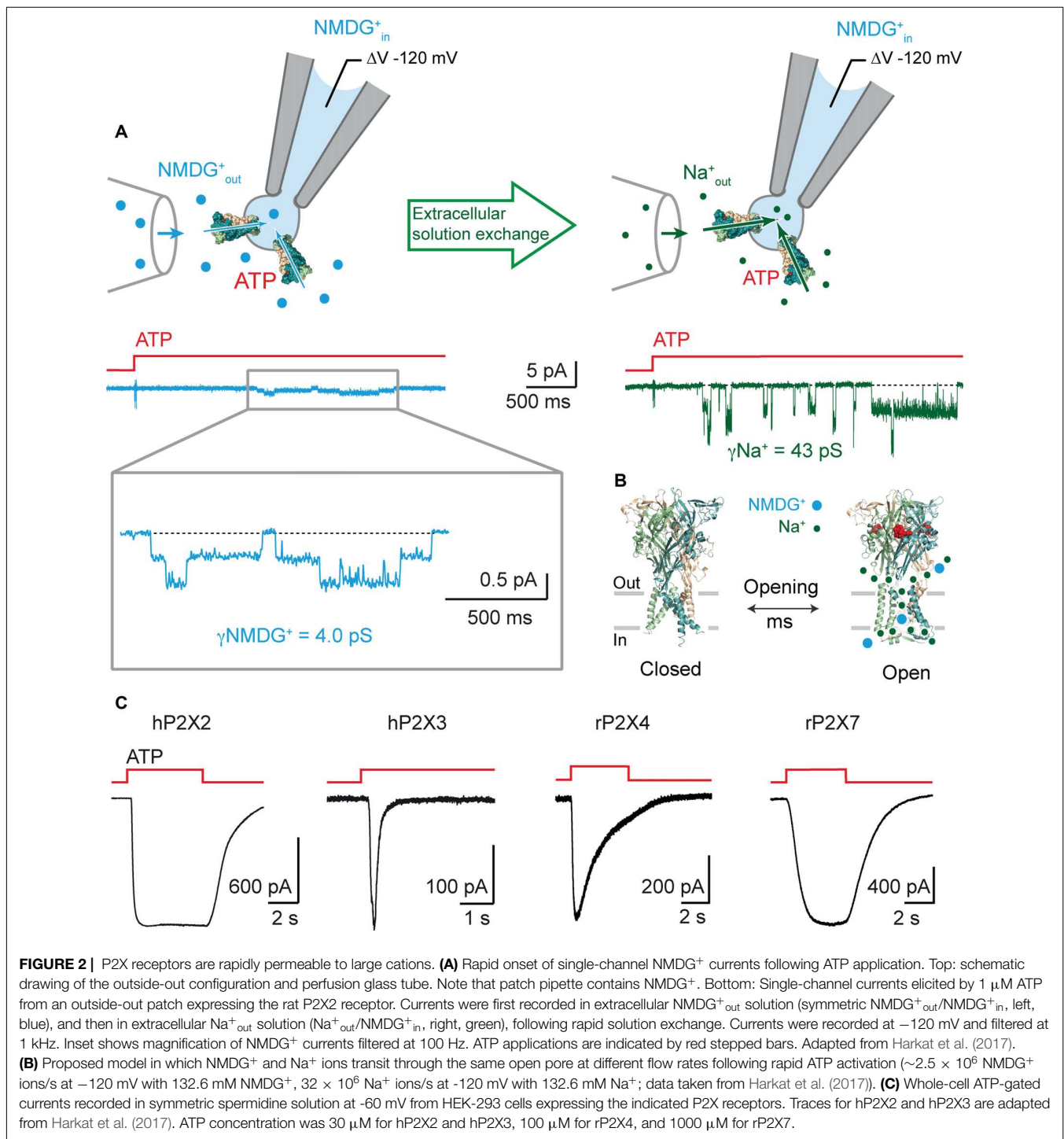
To further support this observation, we recorded ATP-induced single-channel currents from outside-out patches using symmetrical NMDG⁺ solutions (Figure 2A). We not only showed that P2X2 receptors are NMDG⁺-permeable channels, activated on the millisecond timescale, with kinetics similar to those observed when Na⁺ is the primary permeating ion, but we also established the first measurements of the unitary conductance of NMDG⁺ currents (around four pS for several ATP concentrations). This is approximately 10 times lower than that of Na⁺ currents. We further confirmed these experimental data by molecular dynamic simulations carried out on a model of ATP-bound P2X receptors. These computations represent a step forwards in the understanding of the molecular mechanism of NMDG⁺ permeation, which is the result of a conformational and orientational selection process (Harkat et al., 2017). We further validated our methodology by measuring YO-PRO-1 uptake in cells expressing engineered receptors, to discount the presence of possible artifacts caused by the use of non-physiological media for electrophysiological recordings. For the mutants exhibiting light-induced motions leading to a “desensitizing-like” phenotype, we were not able to show fluorescence uptake, but for those associated with a stable opening induced by light, YO-PRO-1 was successfully incorporated into cells, suggesting that desensitization may hinder dye accumulation into cells. However, no YO-PRO-1 uptake was observed during molecular dynamic simulations, which brings back the possibility of two distinct mechanisms for YO-PRO-1 and NMDG⁺ uptake.

Alternatively, this could be the result of a limitation of the method used, as it is possible that the sampling time for computations may not have been sufficient to observe the passage of low-conductance YO-PRO-1. Altogether, our data support that the open I₁ state likely represents the main route for both small and large cations (Figure 2B).

In agreement with data obtained from P2X2 receptors, two recent reports carried out on P2X7 receptors further support an instantaneous permeation of large cations upon ATP activation (Karasawa et al., 2017; Pippel et al., 2017). In the first study, a rigorous and thorough analysis of single-channel currents demonstrate that the unitary conductance of the human P2X7 channel remains stable over time following prolonged ATP application (up to 30 min; Riedel et al., 2007a,b; Pippel et al., 2017). Interestingly, the authors even showed that chemical modification of engineered cysteine side chains with charged MTS reagents increased dramatically the open probability of the channel, with no sign of apparent pore dilation (Pippel et al., 2017). In the second study, the biophysical properties of the “macropore” feature of P2X7 channel have been scrutinized in a synthetic system, in which the functionality of the P2X7 protein has been monitored in the absence of other protein cellular components (Karasawa et al., 2017). To do so, a purified, yet truncated, version of the giant panda P2X7 receptor (pdP2X7-ΔNC) was reconstituted into manufactured liposomes. To distinguish channel activity (I₁ state) from “macropore” formation (I₂ state), proteoliposomes encapsulated either Fluo-4, a Ca²⁺-sensing fluorescent probe, or DNA, to which binding of YO-PRO-1 enhances dye fluorescence emission. The authors elegantly and convincingly showed that pdP2X7-ΔNC was not only permeable to YO-PRO-1, but also to Ca²⁺ with the same apparent kinetics, suggesting a common pathway for both small and large cations (Karasawa et al., 2017). Therefore, in a reconstituted system, the purified P2X7 receptor is able to form an intrinsic and immediate dye-permeable pore with no apparent time-lag, a finding that is apparently not compatible with the slow and progressive process of pore dilation.

IS THE CONCEPT OF PORE DILATION DEAD?

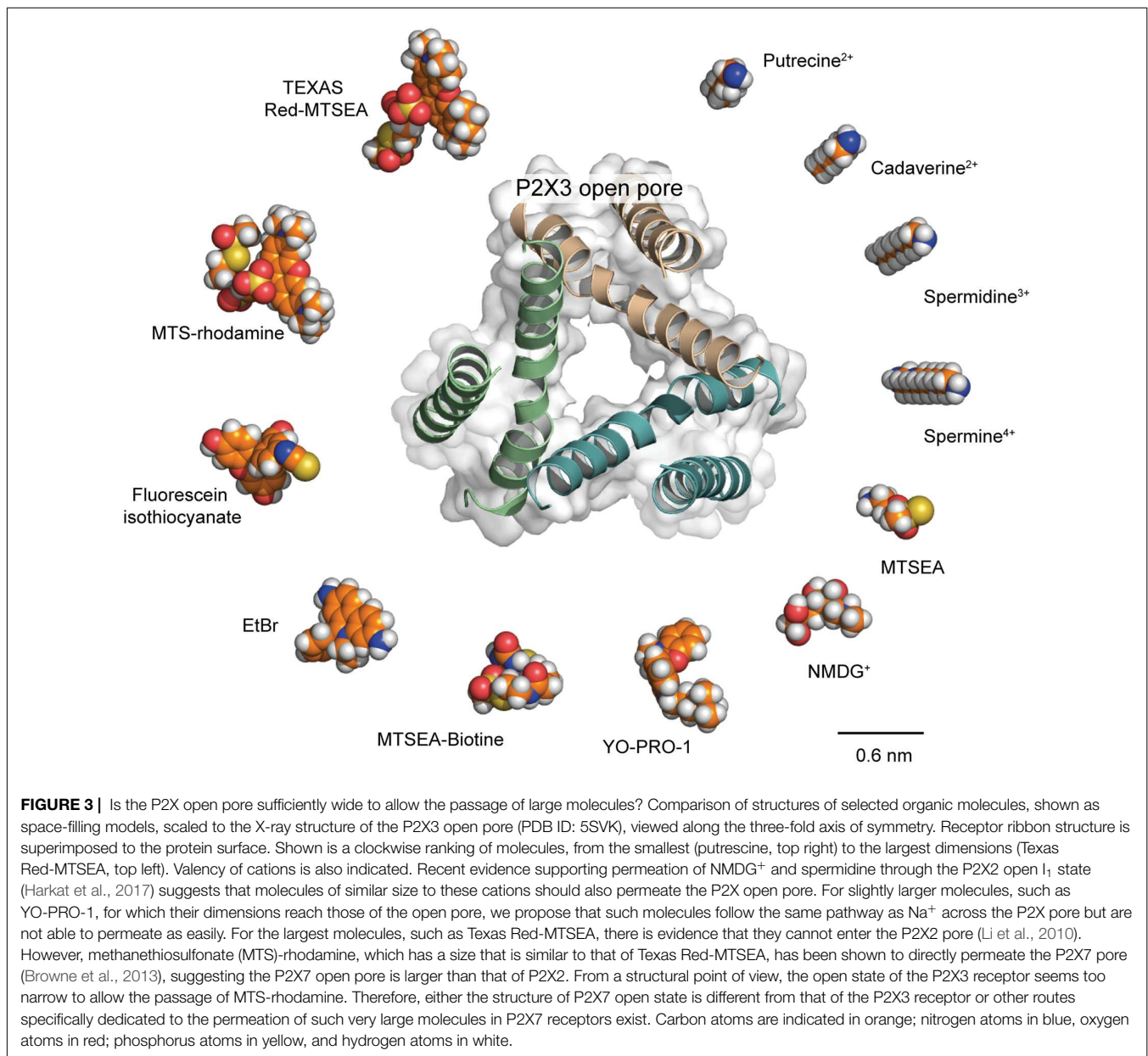
As stated above, recent data now support the hypothesis that the open I₁ state would be sufficiently wide to allow the passage of relatively large molecules, without the need for an ATP-induced pore dilation. However, comparison of the structure of the largest permeating molecules with recent X-ray structures of the ATP-bound, open state casts doubt on the fact that the open I₁ state truly represents the sole ion pathway (Figure 3). This is particularly true for P2X7 receptors, for which MTS-rhodamine, a nanometer-sized dye, was shown to penetrate the open channel and block at a cysteine-substituted residue located deeply in the pore (Browne et al., 2013), whereas the structure of the open pore derived from the human P2X3 receptor (the structure of P2X7 open pore is not yet determined) appears to be too narrow to accommodate such a molecule. Interestingly, molecules of similar size, such as Texas Red-MTSEA, cannot



enter the P2X2 pore (Li et al., 2015) suggesting that the P2X7 receptor, when activated by ATP, can reach a diameter that is larger than that of the P2X2 receptor (Figure 3). Other routes specifically dedicated to the permeation of such very large molecules may also exist. As stated above, Panx-1 is a candidate, as close proximity between Panx-1 and P2X7 channels has been established in human and mouse macrophages cells (Pelegrin and Surprenant, 2006). Alternatively, there is still a possibility

that P2X7 receptors do indeed dilate under certain conditions that remain to be determined.

A finding which may reconcile P2X7 (and perhaps other P2X subtypes) with the concept of “pore dilation” comes from recent studies that emphasize the importance of the lipid composition of the membrane for the passage of large cations through the P2X pore. Although lipids, such as phosphoinositides (Bernier et al., 2008a,b) and cholesterol (Murrell-Lagnado, 2017),



seem to be important for the regulation of allosteric states of P2X receptors, this factor has been underestimated in “dilation” studies thus far. However, Kawate and co-workers (Karasawa et al., 2017) have very recently demonstrated in reconstituted liposomes that sphingomyelin and phosphatidylglycerol-containing membranes facilitate pdP2X7-ΔNC-dependent dye uptake, whereas the presence of cholesterol rather inhibits this process. It is thus conceivable that the lipid composition may have a direct impact on the physical diameter of the P2X7 open channel state that would allow the passage of very large molecules (up to 900 Da). Alternatively, a conformational plasticity in the selectivity filter of the P2X pore may allow the passage of large molecules, as very recently shown on TRPV2 ion channel (Zubcevic et al., 2018). Although appealing, these hypotheses

need convincing evidence; in particular the structure of the P2X7 open channel state (and also other P2X subtypes) solved in a lipid bilayer will certainly advance this issue.

PHYSIOPATHOLOGICAL ROLE OF LARGE CATION PERMEATION

Now that there is no doubt that P2X receptors are permeable to large cations, is there any link between this feature and pathological states? Evidence exists indicating a possible link at least involving the P2X7 receptor, which is arguably of most therapeutic interest due to its implication in a large variety of diseases. Expressed in a range of immune and microglial

TABLE 1 | Polyamine modulation of ion channels and ligand-gated ion channels.

Ion channel/ligand-gated ion channel	Nature of the interaction with polyamines	Observations suggesting a possible implication of P2X receptors
AMPA receptors	Voltage-dependent block by intracellular polyamines (Bowie et al., 1998)	Co-localization Synaptic scaling Synaptic depression Functional interactions (Pougnnet et al., 2014)
Kainate receptors	Voltage-dependent block by intracellular polyamines (Perrais et al., 2010)	Co-expression of kainate receptors and P2X receptors in some populations of neurons (Lucifora et al., 2006)
NMDA receptors	Potentiation by extracellular polyamines, existence of a polyamine binding site (Han et al., 2008; Mony et al., 2011)	Modulation of NMDA-dependent plasticity (Boué-Grabot and Pankratov, 2017)
Nicotinic receptors	Binding site for polyamine-derived toxins (Bixel et al., 2001)	Interaction between nicotinic receptors and P2X receptors: cross inhibition (Khakh et al., 2005)
Inward rectifier K ⁺ (Kir) channels	Voltage-dependent blockage by intracellular polyamines Existence of a polyamine binding site (Kurata et al., 2006)	<i>To be determined</i>
ASICs	Potentiation by spermine (Babini et al., 2002)	Functional interaction between P2X receptors and ASICs (Birdsong et al., 2010; Stephan et al., 2018)
TRPV1 receptors	Polyamines can act as ligands and are able to pass through TRPV1 (Ahern et al., 2006)	Cross-talk between TRPV1 and P2X receptors (Stanchev et al., 2009)

cells, P2X7 receptors are widely involved in the immune and inflammatory response, notably in the nervous system. Several recent reviews extensively cover the involvement of P2X7 receptors in pathological immune-related conditions, such as neuropathic pain, Alzheimer's disease, Huntington's disease and multiple sclerosis to name but a few (De Marchi et al., 2016; Di Virgilio et al., 2017; Savio et al., 2018). A first possible link may involve the ability of Panx-1 channels to allow entry of large cations into the cell, as it has been demonstrated that an increase in extracellular ATP induces the clustering of Panx-1 with P2X7 receptors, leading to their internalization (Boyce et al., 2015). An impairment of this internalization mechanism could contribute to the over-activity of P2X-mediated signaling that may lead to pathophysiological states, such as neuropathic pain (Swayne and Boyce, 2017). Another possible link may involve the P2X7 protein itself. An association between nerve-induced pain behavior (mechanical allodynia) and the P451L mutation found in the mouse *P2rx7* gene has been identified. This mutation impaired "pore formation" by affecting the entry of YO-PRO-1 and ethidium bromide in HEK-293 cells and calcein dye into macrophages, but interestingly the mutation did not affect Ca²⁺ entry (Adriouch et al., 2002; Young et al., 2006; Sorge et al., 2012). Mice in which P2X7 receptors have impaired pore formation as a result of this mutation showed less allodynia than mice with the pore-forming receptors. Moreover, in two independent human chronic pain cohorts, it has been shown that human mutations affecting the amino acid sequence of P2X7 receptor modify the chronic pain sensitivity (Sorge et al., 2012). For instance, in the cohort experiencing post-mastectomy chronic pain, the H155Y single nucleotide polymorphism, which leads to hyperfunctional P2X7 receptors, was associated with an increased pain sensitivity. In contrast, mastectomized women with the hypofunctional

mutation R270H of P2X7 receptor, experienced reduced chronic pain (Sorge et al., 2012). These correlations thus clearly suggest that the level of pore activity is related to pathological states and indicate that P2X7 receptors are vital targets for the treatment of diseases such as neuropathic pain. Differences in Na⁺, K⁺ and Ca²⁺ ion flux may trigger such pathological responses, but permeation of large, pathologically relevant cations may also be involved. These large molecules remain to be identified.

NEW DIRECTIONS CONCERNING THE P2X PERMEATION OF LARGE CATIONS: THE CASE OF POLYAMINES

What is the physiological implication of P2X permeability to large cations? To answer to this question, it is first important to consider whether this unusual large cation permeation feature is shared by all members of the P2X family. Before 2017, a striking observation was that fast-desensitizing receptors, namely P2X1 and P2X3 receptors, were apparently unable to allow the entry of larger cations through the pore. By using symmetric solutions, we have provided evidence that P2X3 receptors are actually permeable to NMDG⁺, suggesting that these receptors should be reconsidered as channels permeable to large cations (Harkat et al., 2017). However, NMDG⁺ is a synthetic molecule, and we sought rather to establish the permeability of large, naturally occurring cations through the P2X pore. We have very recently found that spermidine permeates through the human P2X2 and P2X3 receptor ion channels (Harkat et al., 2017). Now we have extended this permeation to the rat P2X4 and P2X7 receptors, suggesting permeation of spermidine may be a common feature

shared by many, if not all members of the P2X family (Figure 2C).

Spermidine is a natural, ubiquitously distributed polyamine that is vital for the cell (Guerra et al., 2016; Madeo et al., 2018). It is formed intracellularly and is involved in several important cellular functions, such as growth, division and proliferation. Spermidine is also recognized as an allosteric modulator of many ion channels, including ionotropic glutamate receptors, nicotinic acetylcholine receptor, potassium channels, ASICs and TRPV1 channels (Table 1). For some of these channels, spermidine must exit the cell through dedicated pathways to reach the targeted extracellular sites. One of these such pathways may be the vesicular polyamine transporter (VPAT) that stores polyamines in secretory vesicles in astrocytes and mast cells (Hiasa et al., 2014; Takeuchi et al., 2017). As we provide evidence that spermidine permeates through the open pore of P2X receptors (Figure 2C), we propose that P2X receptors may represent an alternative polyamine pathway that is under the control of ATP. Given the importance of spermidine for the function of several other ion channels, as well as the known interactions of P2X receptors with such channels (Khakh et al., 2005; Stanchev et al., 2009; Pougnet et al., 2014; Boué-Grabot and Pankratov, 2017; Stephan et al., 2018), the question is now raised as to what extent can P2X receptors be the physiological mediator of spermidine transit.

By discovering spermidine permeation through P2X receptors, our results uncover a possible overlooked P2X signaling pathway that may be extended to other natural large molecules. Earlier work provided strong evidence that P2X7 receptors are sites of release of important molecules, such as ATP and excitatory amino acids (Duan et al., 2003; Pellegatti et al., 2005; Suadicani et al., 2006; Di Virgilio et al., 2018). It now remains to determine whether these signaling molecules are physically able to cross directly through the P2X7 open pore. Identification of the mechanisms involved will undoubtedly advance the biology of P2X receptors and their role in pathological states.

COULD P2X RECEPTORS ACT AS A PATHWAY FOR THERAPEUTIC APPLICATIONS?

P2X receptors can act as a pathway for the entry of large molecules into cells—to what extent can this property be exploited for therapeutic applications? Two examples of P2X receptors being used as pathways for the passage of azobenzene-based molecules have been published by the team of R. Kramer. The first example is related to the control of nociception, by manipulation of neurons involved in pain signaling via voltage-gated ion channels (Mourot et al., 2012). This was carried out by the incorporation of QAQ, an azobenzene-based photoswitch bearing two quaternary ammonium moieties, into cells through the P2X pore. Control of nociception is based on the activation/deactivation process of local voltage-gated ion channels (calcium, potassium, sodium), which is provided by the geometrical switching between *trans* and *cis* isomers of

QAQ. The route responsible for the entry of QAQ, which is otherwise a membrane-impermeable molecule, can be TRPV1 or alternatively P2X7 receptors (Mourot et al., 2012). In 2016, they further developed this concept of P2X-mediated membrane passage in order to resurrect light-sensitivity of retinal ganglion cells of degenerated retina in blind mice. They employed the same methodology: a charged photoswitchable molecule based on an azobenzene moiety is applied to cells and permeates the membrane via P2X receptors. This molecule is then able to act on voltage-gated ion channels, restoring the responsiveness of retinal-ganglion cells to light (Tochitsky et al., 2016).

As stated above, the presence and implication of P2X7 in many diseases could inspire new approaches, whereby the permeability of the receptor to large cations may be utilized to therapeutic effect, in the delivery of biological effectors to P2X7-expressing cells. Equally, P2X7 has been found in over-expressed levels in several types of cancers, such as chronic B lymphocytic leukemia (De Marchi et al., 2016) and thyroid papillary cancer (Solini et al., 2008). One could envisage the exploitation of these high expression levels in conjunction with the permeability of P2X7 to large molecules, to deliver anti-cancer drugs through the P2X7 pathway.

CONCLUSION

For some time now, there has been much controversy surrounding the passage of large cations through the P2X pore, and a clear explanation on the mechanism of this particular permeation pathway has remained highly elusive. However, recent advances in experimental technique allow a more just study of large cation permeation. Equally, new information showing the highly sensitive nature of P2X7 function to lipid membrane composition, which can vary between cellular types, may be considered in future studies probing the permeability of P2X7 to large cations.

New important features of P2X receptor permeability are now being brought to light. First, it is important to reconsider the structure of the open state, which exhibits an immediate extended permeability, and to consider more closely the critical role of the membrane lipid environment in order to fully understand the functionality of these proteins. Secondly, their physiological importance must also be reconsidered, with the new information that they are able to allow the passage of important physiological modulators. A final interesting point is to look further into the potential application of P2X receptors as pathway for drug delivery.

AUTHOR CONTRIBUTIONS

LP, KD, TC and TG wrote the manuscript. JB made the figures.

FUNDING

This work was supported by the Agence Nationale de la Recherche (grant no. ANR-14-CE11-0004-01) and the Ministère de la Recherche.

REFERENCES

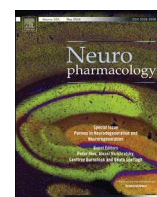
- Abbracchio, M. P., and Burnstock, G. (1994). Purinoceptors: are there families of P2X and P2Y purinoceptors? *Pharmacol. Ther.* 64, 445–475. doi: 10.1016/0163-7258(94)00048-4
- Abbracchio, M. P., Burnstock, G., Verkhratsky, A., and Zimmermann, H. (2009). Purinergic signalling in the nervous system: an overview. *Trends Neurosci.* 32, 19–29. doi: 10.1016/j.tins.2008.10.001
- Adinolfi, E., Cirillo, M., Woltersdorf, R., Falzoni, S., Chiozzi, P., Pellegatti, P., et al. (2010). Trophic activity of a naturally occurring truncated isoform of the P2X7 receptor. *FASEB J.* 24, 3393–3404. doi: 10.1096/fj.09-153601
- Adriouch, S., Dox, C., Welge, V., Seman, M., Koch-Nolte, F., and Haag, F. (2002). Cutting edge: a natural P451L mutation in the cytoplasmic domain impairs the function of the mouse P2X7 receptor. *J. Immunol.* 169, 4108–4112. doi: 10.4049/jimmunol.169.8.4108
- Ahern, G. P., Wang, X., and Miyares, R. L. (2006). Polyamines are potent ligands for the capsaicin receptor TRPV1. *J. Biol. Chem.* 281, 8991–8995. doi: 10.1074/jbc.M513429200
- Babini, E., Paukert, M., Geisler, H.-S., and Grunder, S. (2002). Alternative splicing and interaction with di- and polyvalent cations control the dynamic range of acid-sensing ion channel 1 (ASIC1). *J. Biol. Chem.* 277, 41597–41603. doi: 10.1074/jbc.M205877200
- Banke, T. G., Chaplan, S. R., and Wickenden, A. D. (2010). Dynamic changes in the TRPA1 selectivity filter lead to progressive but reversible pore dilation. *Am. J. Physiol. Cell Physiol.* 298, C1457–C1468. doi: 10.1152/ajpcell.00489.2009
- Bernier, L.-P., Ase, A. R., Chevallier, S., Blais, D., Zhao, Q., Boué-Grabot, E., et al. (2008a). Phosphoinositides regulate P2X₄ ATP-gated channels through direct interactions. *J. Neurosci.* 28, 12938–12945. doi: 10.1523/JNEUROSCI.3038-08.2008
- Bernier, L.-P., Ase, A. R., Tong, X., Hamel, E., Blais, D., Zhao, Q., et al. (2008b). Direct modulation of P2X₁ receptor-channels by the lipid phosphatidylinositol 4,5-bisphosphate. *Mol. Pharmacol.* 74, 785–792. doi: 10.1124/mol.108.047019
- Bernier, L.-P., Ase, A. R., and Séguéla, P. (2017). P2X receptor channels in chronic pain pathways. *Br. J. Pharmacol.* 175, 2219–2230. doi: 10.1111/bph.13957
- Birdsong, W. T., Fierro, L., Williams, F. G., Spelta, V., Naves, L. A., Knowles, M., et al. (2010). Sensing muscle ischemia: coincident detection of acid and ATP via interplay of two ion channels. *Neuron* 68, 739–749. doi: 10.1016/j.neuron.2010.09.029
- Bixel, M. G., Weise, C., Bolognesi, M. L., Rosini, M., Briery, M. J., Mellor, I. R., et al. (2001). Location of the polyamine binding site in the vestibule of the nicotinic acetylcholine receptor ion channel. *J. Biol. Chem.* 276, 6151–6160. doi: 10.1074/jbc.M008467200
- Boué-Grabot, E., and Pankratov, Y. (2017). Modulation of central synapses by astrocyte-released ATP and postsynaptic P2X receptors. *Neural Plast.* 2017:9454275. doi: 10.1155/2017/9454275
- Bowie, D., Lange, G. D., and Mayer, M. L. (1998). Activity-dependent modulation of glutamate receptors by polyamines. *J. Neurosci.* 18, 8175–8185. doi: 10.1523/JNEUROSCI.18-20-08175.1998
- Boyce, A. K. J., Kim, M. S., Wicki-Stordeur, L. E., and Swayne, L. A. (2015). ATP stimulates pannexin 1 internalization to endosomal compartments. *Biochem. J.* 470, 319–330. doi: 10.1042/bj20141551
- Brake, A. J., Wagenbach, M. J., and Julius, D. (1994). New structural motif for ligand-gated ion channels defined by an ionotropic ATP receptor. *Nature* 371, 519–523. doi: 10.1038/371519a0
- Browne, L. E., Compan, V., Bragg, L., and North, R. A. (2013). P2X7 receptor channels allow direct permeation of nanometer-sized dyes. *J. Neurosci.* 33, 3557–3566. doi: 10.1523/JNEUROSCI.2235-12.2013
- Burnstock, G. (1990). Overview. Purinergic mechanisms. *Ann. N Y Acad. Sci.* 603, 1–17; discussion 18. doi: 10.1111/j.1749-6632.1990.tb37657.x
- Cankurtaran-Sayar, S., Sayar, K., and Ugur, M. (2009). P2X7 receptor activates multiple selective dye-permeation pathways in RAW 264.7 and human embryonic kidney 293 cells. *Mol. Pharmacol.* 76, 1323–1332. doi: 10.1124/mol.109.059923
- Chataigneau, T., Lemoine, D., and Grutter, T. (2013). Exploring the ATP-binding site of P2X receptors. *Front. Cell. Neurosci.* 7:273. doi: 10.3389/fncel.2013.00273
- Chaumont, S., and Khakh, B. S. (2008). Patch-clamp coordinated spectroscopy shows P2X2 receptor permeability dynamics require cytosolic domain rearrangements but not Panx-1 channels. *Proc. Natl. Acad. Sci. U S A* 105, 12063–12068. doi: 10.1073/pnas.0803008105
- Cheewatrakoolpong, B., Gilchrist, H., Anthes, J. C., and Greenfeder, S. (2005). Identification and characterization of splice variants of the human P2X₇ ATP channel. *Biochem. Biophys. Res. Commun.* 332, 17–27. doi: 10.1016/j.bbrc.2005.04.087
- Chung, M.-K., Güler, A. D., and Caterina, M. J. (2008). TRPV1 shows dynamic ionic selectivity during agonist stimulation. *Nat. Neurosci.* 11, 555–564. doi: 10.1038/nn.2102
- Cockcroft, S., and Gomperts, B. D. (1979). ATP induces nucleotide permeability in rat mast cells. *Nature* 279, 541–542. doi: 10.1038/279541a0
- Compan, V., Ulmann, L., Stelmashenko, O., Chemin, J., Chaumont, S., and Rassendren, F. (2012). P2X2 and P2X5 subunits define a new heteromeric receptor with P2X7-like properties. *J. Neurosci.* 32, 4284–4296. doi: 10.1523/JNEUROSCI.6332-11.2012
- De Marchi, E., Orioli, E., Dal Ben, D., and Adinolfi, E. (2016). P2X7 receptor as a therapeutic target. *Adv. Protein Chem. Struct. Biol.* 104, 39–79. doi: 10.1016/bs.apcsb.2015.11.004
- de Weille, J. R., Bassilana, F., Lazdunski, M., and Waldmann, R. (1998). Identification, functional expression and chromosomal localisation of a sustained human proton-gated cation channel. *FEBS Lett.* 433, 257–260. doi: 10.1016/s0014-5793(98)00916-8
- Di Virgilio, F. (1995). The P2Z purinoceptor: an intriguing role in immunity, inflammation and cell death. *Immunol. Today* 16, 524–528. doi: 10.1016/0167-5699(95)80045-x
- Di Virgilio, F., Dal Ben, D., Sarti, A. C., Giuliani, A. L., and Falzoni, S. (2017). The P2X7 receptor in infection and inflammation. *Immunity* 47, 15–31. doi: 10.1016/j.immuni.2017.06.020
- Di Virgilio, F., Sarti, A. C., and Grassi, F. (2018). Modulation of innate and adaptive immunity by P2X ion channels. *Curr. Opin. Immunol.* 52, 51–59. doi: 10.1016/j.coi.2018.03.026
- Ding, S., and Sachs, F. (1999). Single channel properties of P2X₂ purinoceptors. *J. Gen. Physiol.* 113, 695–720. doi: 10.1085/jgp.113.5.695
- Duan, K., Yu, X., Zhang, C., and Zhou, Z. (2003). Control of secretion by temporal patterns of action potentials in adrenal chromaffin cells. *J. Neurosci.* 23, 11235–11243. doi: 10.1523/JNEUROSCI.23-35-11235.2003
- Eickhorst, A. N., Berson, A., Cockayne, D., Lester, H. A., and Khakh, B. S. (2002). Control of P2X₂ channel permeability by the cytosolic domain. *J. Gen. Physiol.* 120, 119–131. doi: 10.1085/jgp.20028535
- Fujiwara, Y., and Kubo, Y. (2004). Density-dependent changes of the pore properties of the P2X₂ receptor channel. *J. Physiol.* 558, 31–43. doi: 10.1113/jphysiol.2004.064568
- Gordon, J. L. (1986). Extracellular ATP: effects, sources and fate. *Biochem. J.* 233, 309–319. doi: 10.1042/bj2330309
- Gu, B. J., Rathsam, C., Stokes, L., McGeachie, A. B., and Wiley, J. S. (2009). Extracellular ATP dissociates nonmuscle myosin from P2X₇ complex: this dissociation regulates P2X₇ pore formation. *Am. J. Physiol. Cell Physiol.* 297, C430–C439. doi: 10.1152/ajpcell.00079.2009
- Guerra, G. P., Rubin, M. A., and Mello, C. F. (2016). Modulation of learning and memory by natural polyamines. *Pharmacol. Res.* 112, 99–118. doi: 10.1016/j.phrs.2016.03.023
- Habermacher, C., Dunning, K., Chataigneau, T., and Grutter, T. (2016a). Molecular structure and function of P2X receptors. *Neuropharmacology* 104, 18–30. doi: 10.1016/j.neuropharm.2015.07.032
- Habermacher, C., Martz, A., Calimet, N., Lemoine, D., Peaverini, L., Specht, A., et al. (2016b). Photo-switchable tweezers illuminate pore-opening motions of an ATP-gated P2X ion channel. *ELife* 5:e11050. doi: 10.7554/eLife.11050
- Han, X., Tomitori, H., Mizuno, S., Higashi, K., Füll, C., Fukiwake, T., et al. (2008). Binding of spermine and ifenprodil to a purified, soluble regulatory domain of the N-methyl-D-aspartate receptor. *J. Neurochem.* 107, 1566–1577. doi: 10.1111/j.1471-4159.2008.05729.x
- Harkat, M., Peaverini, L., Cerdan, A. H., Dunning, K., Beudez, J., Martz, A., et al. (2017). On the permeation of large organic cations through the pore of ATP-gated P2X receptors. *Proc. Natl. Acad. Sci. U S A* 114, E3786–E3795. doi: 10.1016/j.bpj.2016.11.22514
- Hattori, M., and Gouaux, E. (2012). Molecular mechanism of ATP binding and ion channel activation in P2X receptors. *Nature* 485, 207–212. doi: 10.1038/nature11010

- Heppel, L. A., Weisman, G. A., and Friedberg, I. (1985). Permeabilization of transformed cells in culture by external ATP. *J. Membr. Biol.* 86, 189–196. doi: 10.1007/bf01870597
- Hiasa, M., Miyaji, T., Haruna, Y., Takeuchi, T., Harada, Y., Moriyama, S., et al. (2014). Identification of a mammalian vesicular polyamine transporter. *Sci. Rep.* 4:6836. doi: 10.1038/srep06836
- Jiang, L.-H., Rassendren, F., Mackenzie, A., Zhang, Y. H., Surprenant, A., and North, R. A. (2005). N-methyl-D-glucamine and propidium dyes utilize different permeation pathways at rat P2X₇ receptors. *Am. J. Physiol. Cell Physiol.* 289, C1295–C1302. doi: 10.1152/ajpcell.00253.2005
- Karasawa, A., Michalski, K., Mikhelzon, P., and Kawate, T. (2017). The P2X₇ receptor forms a dye-permeable pore independent of its intracellular domain but dependent on membrane lipid composition. *Elife* 6:e31186. doi: 10.7554/eLife.31186
- Kawate, T., Michel, J. C., Birdsong, W. T., and Gouaux, E. (2009). Crystal structure of the ATP-gated P2X₄ ion channel in the closed state. *Nature* 460, 592–598. doi: 10.1038/nature08198
- Khakh, B. S., and Alan North, R. (2006). P2X receptors as cell-surface ATP sensors in health and disease. *Nature* 442, 527–532. doi: 10.1038/nature04886
- Khakh, B. S., and Egan, T. M. (2005). Contribution of transmembrane regions to ATP-gated P2X₂ channel permeability dynamics. *J. Biol. Chem.* 280, 6118–6129. doi: 10.1074/jbc.M411324200
- Khakh, B. S., Bao, X. R., Labarca, C., and Lester, H. A. (1999). Neuronal P2X transmitter-gated cation channels change their ion selectivity in seconds. *Nat. Neurosci.* 2, 322–330. doi: 10.1038/7233
- Khakh, B. S., Fisher, J. A., Nashmi, R., Bowser, D. N., and Lester, H. A. (2005). An angstrom scale interaction between plasma membrane ATP-gated P2X₂ and $\alpha_4\beta_2$ nicotinic channels measured with fluorescence resonance energy transfer and total internal reflection fluorescence microscopy. *J. Neurosci.* 25, 6911–6920. doi: 10.1523/JNEUROSCI.0561-05.2005
- Khakh, B. S., and Lester, H. A. (1999). Dynamic selectivity filters in ion channels. *Neuron* 23, 653–658. doi: 10.1016/s0896-6273(01)80025-8
- Khakh, B. S., and North, R. A. (2012). Neuromodulation by extracellular ATP and P2X receptors in the CNS. *Neuron* 76, 51–69. doi: 10.1016/j.neuron.2012.09.024
- Kim, M., Jiang, L. H., Wilson, H. L., North, R. A., and Surprenant, A. (2001). Proteomic and functional evidence for a P2X₇ receptor signalling complex. *EMBO J.* 20, 6347–6358. doi: 10.1093/emboj/20.22.6347
- Kracun, S., Chaptal, V., Abramson, J., and Khakh, B. S. (2010). Gated access to the pore of a P2X receptor: structural implications for closed-open transitions. *J. Biol. Chem.* 285, 10110–10121. doi: 10.1074/jbc.M109.089185
- Kurata, H. T., Marton, L. J., and Nichols, C. G. (2006). The polyamine binding site in inward rectifier K⁺ channels. *J. Gen. Physiol.* 127, 467–480. doi: 10.1085/jgp.200509467
- Lemoine, D., Jiang, R., Taly, A., Chataigneau, T., Specht, A., and Grutter, T. (2012). Ligand-gated ion channels: new insights into neurological disorders and ligand recognition. *Chem. Rev.* 112, 6285–6318. doi: 10.1021/cr3000829
- Li, M., Chang, T.-H., Silberberg, S. D., and Swartz, K. J. (2008). Gating the pore of P2X receptor channels. *Nat. Neurosci.* 11, 883–887. doi: 10.1038/nn.2151
- Li, M., Kawate, T., Silberberg, S. D., and Swartz, K. J. (2010). Pore-opening mechanism in trimeric P2X receptor channels. *Nat. Commun.* 1:44. doi: 10.1038/ncomms1048
- Li, M., Toombes, G. E. S., Silberberg, S. D., and Swartz, K. J. (2015). Physical basis of apparent pore dilation of ATP-activated P2X receptor channels. *Nat. Neurosci.* 18, 1577–1583. doi: 10.1038/nn.4120
- Lingueglia, E., de Weille, J. R., Bassilana, F., Heurteaux, C., Sakai, H., Waldmann, R., et al. (1997). A modulatory subunit of acid sensing ion channels in brain and dorsal root ganglion cells. *J. Biol. Chem.* 272, 29778–29783. doi: 10.1074/jbc.272.47.29778
- Lucifora, S., Willcockson, H. H., Lu, C.-R., Darstein, M., Phend, K. D., Valtchanoff, J. G., et al. (2006). Presynaptic low- and high-affinity kainate receptors in nociceptive spinal afferents. *Pain* 120, 97–105. doi: 10.1016/j.pain.2005.10.018
- Madeo, F., Eisenberg, T., Pietrocola, F., and Kroemer, G. (2018). Spermidine in health and disease. *Science* 359:eaan2788. doi: 10.1126/science.aan2788
- Mansoor, S. E., Lü, W., Oosterheert, W., Shekhar, M., Tajkhorshid, E., and Gouaux, E. (2016). X-ray structures define human P2X₃ receptor gating cycle and antagonist action. *Nature* 538, 66–71. doi: 10.1038/nature19367
- Marques-da-Silva, C., Chaves, M., Castro, N., Coutinho-Silva, R., and Guimaraes, M. (2011). Colchicine inhibits cationic dye uptake induced by ATP in P2X₂ and P2X₇ receptor-expressing cells: implications for its therapeutic action. *Br. J. Pharmacol.* 163, 912–926. doi: 10.1111/j.1476-5381.2011.01254.x
- Mony, L., Zhu, S., Carvalho, S., and Paoletti, P. (2011). Molecular basis of positive allosteric modulation of GluN2B NMDA receptors by polyamines. *EMBO J.* 30, 3134–3146. doi: 10.1038/emboj.2011.203
- Mouro, A., Fehrentz, T., Le Feuvre, Y., Smith, C. M., Herold, C., Dalkara, D., et al. (2012). Rapid optical control of nociception with an ion-channel photoswitch. *Nat. Methods* 9, 396–402. doi: 10.1038/nmeth.1897
- Murrell-Lagnado, R. D. (2017). Regulation of P2X purinergic receptor signaling by cholesterol. *Curr. Top. Membr.* 80, 211–232. doi: 10.1016/bs.ctm.2017.05.004
- Nabissi, M., Morelli, M. B., Santoni, M., and Santoni, G. (2013). Triggering of the TRPV2 channel by cannabidiol sensitizes glioblastoma cells to cytotoxic chemotherapeutic agents. *Carcinogenesis* 34, 48–57. doi: 10.1093/carcin/bgs328
- Nicke, A., Kuan, Y.-H., Masin, M., Rettinger, J., Marquez-Klaka, B., Bender, O., et al. (2009). A functional P2X₇ splice variant with an alternative transmembrane domain 1 escapes gene inactivation in P2X₇ knock-out mice. *J. Biol. Chem.* 284, 25813–25822. doi: 10.1074/jbc.M109.033134
- North, R. A. (2002). Molecular physiology of P2X receptors. *Physiol. Rev.* 82, 1013–1067. doi: 10.1152/physrev.00015.2002
- Nuttall, L. C., and DUBYAK, G. R. (1994). Differential activation of cation channels and non-selective pores by macrophage P2_z purinergic receptors expressed in *Xenopus* oocytes. *J. Biol. Chem.* 269, 13988–13996.
- Pelegrin, P., and Surprenant, A. (2006). Pannexin-1 mediates large pore formation and interleukin-1 β release by the ATP-gated P2X₇ receptor. *EMBO J.* 25, 5071–5082. doi: 10.1038/sj.emboj.7601378
- Pellegatti, P., Falzoni, S., Pinton, P., Rizzuto, R., and Di Virgilio, F. (2005). A novel recombinant plasma membrane-targeted luciferase reveals a new pathway for ATP secretion. *Mol. Biol. Cell* 16, 3659–3665. doi: 10.1091/mbc.e05-03-0222
- Perrais, D., Veran, J., and Mülle, C. (2010). Gating and permeation of kainate receptors: differences unveiled. *Trends Pharmacol. Sci.* 31, 516–522. doi: 10.1016/j.tips.2010.08.004
- Pippel, A., Stolz, M., Woltersdorf, R., Kless, A., Schmalzing, G., and Markwardt, F. (2017). Localization of the gate and selectivity filter of the full-length P2X₇ receptor. *Proc. Natl. Acad. Sci. U S A* 114, E2156–E2165. doi: 10.1073/pnas.1610414114
- Pougnat, J.-T., Toulme, E., Martinez, A., Choquet, D., Hosy, E., and Boué-Grabot, E. (2014). ATP P2X receptors downregulate AMPA receptor trafficking and postsynaptic efficacy in hippocampal neurons. *Neuron* 83, 417–430. doi: 10.1016/j.neuron.2014.06.005
- Puopolo, M., Binshok, A. M., Yao, G.-L., Oh, S. B., Woolf, C. J., and Bean, B. P. (2013). Permeation and block of TRPV1 channels by the cationic lidocaine derivative QX-314. *J. Neurophysiol.* 109, 1704–1712. doi: 10.1152/jn.00012.2013
- Rassendren, F., Buell, G. N., Virginio, C., Collo, G., North, R. A., and Surprenant, A. (1997). The permeabilizing ATP receptor, P2X₇. Cloning and expression of a human cDNA. *J. Biol. Chem.* 272, 5482–5486. doi: 10.1074/jbc.272.9.5482
- Riedel, T., Lozinsky, I., Schmalzing, G., and Markwardt, F. (2007a). Kinetics of P2X₇ receptor-operated single channels currents. *Biophys. J.* 92, 2377–2391. doi: 10.1529/biophysj.106.091413
- Riedel, T., Schmalzing, G., and Markwardt, F. (2007b). Influence of extracellular monovalent cations on pore and gating properties of P2X₇ receptor-operated single-channel currents. *Biophys. J.* 93, 846–858. doi: 10.1529/biophysj.106.103614
- Rokic, M. B., and Stojilkovic, S. S. (2013). Two open states of P2X receptor channels. *Front. Cell. Neurosci.* 7:215. doi: 10.3389/fncel.2013.00215
- Saul, A., Hausmann, R., Kless, A., and Nicke, A. (2013). Heteromeric assembly of P2X subunits. *Front. Cell. Neurosci.* 7:250. doi: 10.3389/fncel.2013.00250
- Savio, L. E. B., de Andrade Mello, P., da Silva, C. G., and Coutinho-Silva, R. (2018). The P2X₇ receptor in inflammatory diseases: angel or demon? *Front. Pharmacol.* 9:52. doi: 10.3389/fphar.2018.00052
- Sluyter, R. (2017). The P2X₇ receptor. *Adv. Exp. Med. Biol.* 1051, 17–53. doi: 10.1007/5584_2017_59

- Solini, A., Cuccato, S., Ferrari, D., Santini, E., Gulinelli, S., Callegari, M. G., et al. (2008). Increased P2X₇ receptor expression and function in thyroid papillary cancer: a new potential marker of the disease? *Endocrinology* 149, 389–396. doi: 10.1210/en.2007-1223
- Sorge, R. E., Trang, T., Dorfman, R., Smith, S. B., Beggs, S., Ritchie, J., et al. (2012). Genetically determined P2X₇ receptor pore formation regulates variability in chronic pain sensitivity. *Nat. Med.* 18, 595–599. doi: 10.1038/nm.2710
- Stanchev, D., Blosa, M., Milius, D., Gerevich, Z., Rubini, P., Schmalzing, G., et al. (2009). Cross-inhibition between native and recombinant TRPV1 and P2X₃ receptors. *Pain* 143, 26–36. doi: 10.1016/j.pain.2009.01.006
- Steinberg, T. H., Newman, A. S., Swanson, J. A., and Silverstein, S. C. (1987). ATP₄-permeabilizes the plasma membrane of mouse macrophages to fluorescent dyes. *J. Biol. Chem.* 262, 8884–8888.
- Steinberg, T. H., and Silverstein, S. C. (1989). “Chapter 3 ATP permeabilization of the plasma membrane,” in *Methods in Cell Biology*, ed. A. M. Tartakoff (New York, NY: Academic Press), 45–61.
- Stephan, G., Huang, L., Tang, Y., Vilotti, S., Fabbretti, E., Yu, Y., et al. (2018). The ASIC3/P2X₃ cognate receptor is a pain-relevant and ligand-gated cationic channel. *Nat. Commun.* 9:1354. doi: 10.1038/s41467-018-03728-5
- Suadicani, S. O., Brosnan, C. F., and Scemes, E. (2006). P2X₇ receptors mediate ATP release and amplification of astrocytic intercellular Ca²⁺ signaling. *J. Neurosci.* 26, 1378–1385. doi: 10.1523/JNEUROSCI.3902-05.2006
- Surprenant, A., Rassendren, F., Kawashima, E., North, R. A., and Buell, G. (1996). The cytolytic P_{2Z} receptor for extracellular ATP identified as a P_{2X} receptor (P2X₇). *Science* 272, 735–738.
- Swayne, L. A., and Boyce, A. K. J. (2017). Regulation of pannexin 1 surface expression by extracellular ATP: potential implications for nervous system function in health and disease. *Front. Cell. Neurosci.* 11:230. doi: 10.3389/fncel.2017.00230
- Takeuchi, T., Harada, Y., Moriyama, S., Furuta, K., Tanaka, S., Miyaji, T., et al. (2017). Vesicular polyamine transporter mediates vesicular storage and release of polyamine from mast cells. *J. Biol. Chem.* 292, 3909–3918. doi: 10.1074/jbc.M116.756197
- Tochitsky, I., Helft, Z., Meseguer, V., Fletcher, R. B., Vessey, K. A., Telias, M., et al. (2016). How azobenzene photoswitches restore visual responses to the blind retina. *Neuron* 92, 100–113. doi: 10.1016/j.neuron.2016.08.038
- Valera, S., Hussy, N., Evans, R. J., Adami, N., North, R. A., Surprenant, A., et al. (1994). A new class of ligand-gated ion channel defined by P2X receptor for extracellular ATP. *Nature* 371, 516–519. doi: 10.1038/371516a0
- Virginio, C., MacKenzie, A., North, R. A., and Surprenant, A. (1999a). Kinetics of cell lysis, dye uptake and permeability changes in cells expressing the rat P2X₇ receptor. *J. Physiol.* 519, 335–346. doi: 10.1111/j.1469-7793.1999.0335m.x
- Virginio, C., MacKenzie, A., Rassendren, F. A., North, R. A., and Surprenant, A. (1999b). Pore dilation of neuronal P2X receptor channels. *Nat. Neurosci.* 2, 315–321. doi: 10.1038/7225
- Wei, L., Caseley, E., Li, D., and Jiang, L.-H. (2016). ATP-induced P2X receptor-dependent large pore formation: how much do we know? *Front. Pharmacol.* 7:5. doi: 10.3389/fphar.2016.00005
- Xu, X. J., Boumechache, M., Robinson, L. E., Marschall, V., Gorecki, D. C., Masin, M., et al. (2012). Splice variants of the P2X₇ receptor reveal differential agonist dependence and functional coupling with pannexin-1. *J. Cell Sci.* 125, 3776–3789. doi: 10.1242/jcs.099374
- Yan, Z., Li, S., Liang, Z., Tomić, M., and Stojilkovic, S. S. (2008). The P2X₇ receptor channel pore dilates under physiological ion conditions. *J. Gen. Physiol.* 132, 563–573. doi: 10.1085/jgp.200810059
- Young, M. T., Pelegrin, P., and Surprenant, A. (2006). Identification of Thr₂₈₃ as a key determinant of P2X₇ receptor function. *Br. J. Pharmacol.* 149, 261–268. doi: 10.1038/sj.bjp.0706880
- Zubcevic, L., Le, S., Yang, H., and Lee, S.-Y. (2018). Conformational plasticity in the selectivity filter of the TRPV2 ion channel. *Nat. Struct. Mol. Biol.* 25, 405–415. doi: 10.1038/s41594-018-0059-z

Conflict of Interest Statement: The authors declare that the research was conducted in the absence of any commercial or financial relationships that could be construed as a potential conflict of interest.

Copyright © 2018 Peverini, Beudez, Dunning, Chataigneau and Grutter. This is an open-access article distributed under the terms of the Creative Commons Attribution License (CC BY). The use, distribution or reproduction in other forums is permitted, provided the original author(s) and the copyright owner(s) are credited and that the original publication in this journal is cited, in accordance with accepted academic practice. No use, distribution or reproduction is permitted which does not comply with these terms.



Invited review

Molecular structure and function of P2X receptors

Chloé Habermacher ^{a, b}, Kate Dunning ^{a, b}, Thierry Chataigneau ^{a, b}, Thomas Grutter ^{a, b, *}^a Centre National de la Recherche Scientifique, Unité Mixte de Recherche 7199, Laboratoire de Conception et Application de Molécules Bioactives, Équipe de Chimie et Neurobiologie Moléculaire, F-67400, Illkirch, France^b Université de Strasbourg, Faculté de Pharmacie, F-67400, Illkirch, France

ARTICLE INFO

Article history:

Received 29 June 2015

Received in revised form

23 July 2015

Accepted 26 July 2015

Available online 29 July 2015

List of chemical compounds:

ATP (PubChem CID: 5957)

Suramin (PubChem CID: 5361)

TNP-ATP (PubChem CID: 3035228)

GW791343 (PubChem CID: 71576670)

Ivermectin (PubChem CID:24278497)

Keywords:

ATP

Gating

Ion channel

Purinergic receptors

Allosteric modulation

ABSTRACT

ATP-gated P2X receptors are trimeric ion channels selective to cations. Recent progress in the molecular biophysics of these channels enables a better understanding of their function. In particular, data obtained from biochemical, electrophysiological and molecular engineering in the light of recent X-ray structures now allow delineation of the principles of ligand binding, channel opening and allosteric modulation. However, although a picture emerges as to how ATP triggers channel opening, there are a number of intriguing questions that remain to be answered, in particular how the pore itself opens in response to ATP and how the intracellular domain, for which structural information is limited, moves during activation. In this review, we provide a summary of functional studies in the context of the post-structure era, aiming to clarify our understanding of the way in which P2X receptors function in response to ATP binding, as well as the mechanism by which allosteric modulators are able to regulate receptor function.

This article is part of the Special Issue entitled 'Purines in Neurodegeneration and Neuroregeneration'.

© 2015 Elsevier Ltd. All rights reserved.

Contents

1. Introduction	19
2. Global architecture	19
2.1. General topology of the ion channel	19
2.2. Location of the ATP sites	21
3. Structural point of view of the gating mechanism	21
3.1. Movement of the binding jaw	21
3.1.1. Reorganization of the binding loops following ATP binding	21
3.1.2. Intermediate activation states	22
3.2. ECD flexibility	23
3.3. Transmembrane motions and pore opening	23
4. Allosteric modulation of P2X receptors	24
4.1. Allosteric regulation within the ectodomain: the case of zinc	24
4.2. Allosteric regulation within the transmembrane domains: the case of ivermectin	25
4.3. Allosteric regulation within the intracellular C-terminus domain: the regulatory effects of phospholipids	26
5. Optogating of P2X receptors	26
6. Conclusion	28
References	28

* Corresponding author. Centre National de la Recherche Scientifique, Unité Mixte de Recherche 7199, Laboratoire de Conception et Application de Molécules Bioactives, Équipe de Chimie et Neurobiologie Moléculaire, F-67400, Illkirch, France.

E-mail address: grutter@unistra.fr (T. Grutter).

1. Introduction

Among the different transmembrane proteins involved in ionic transfer, the ligand-gated ion channels (LGICs) form an essential superfamily owing to the fact that they possess a number of key physiological roles, most notably the mediation of neuronal signalling (Albuquerque et al., 2009; Bardoni et al., 1997; Lalo et al., 2012; Paoletti et al., 2013; Taly et al., 2009). The binding of a ligand in the extracellular domain triggers conformational changes that open the pore and allow the passage of ions along their electrochemical gradients. LGICs comprise three families of receptors, differing primarily in their oligomeric assemblies (Khakh and North, 2006; Lemoine et al., 2012). Among these, trimeric P2X receptors, which are activated by extracellular ATP (Burnstock, 2006; North, 2002), are implicated in a diverse range of physiological and pathological processes, including pain sensation (Wirkner et al., 2007; Zhuo et al., 2011), inflammation (Idzko et al., 2014), taste (Kinnamon and Finger, 2013) and modulation of neurotransmitter release (Khakh and North, 2012; Lalo et al., 2012). These receptors are therefore promising therapeutic targets (Lemoine et al., 2012; North and Jarvis, 2013).

Thus far, seven different P2X subunits (P2X1–7) have been found in mammals, which assemble together in a homomeric and/or heteromeric fashion to form trimeric ion channel structures. Each subunit has several unifying features: C- and N-termini are located intracellularly, linked by two membrane-spanning segments (TM1 and TM2) and a large extracellular domain (ectodomain), where the ATP-binding sites are nestled (Fig. 1A). In response to the binding of extracellular ATP, these receptors switch between different conformational states (Browne et al., 2010; Giniatullin and Nistri, 2013; Jiang et al., 2013; Moffatt and Hume, 2007). Initial agonist binding causes the receptor to progress from a closed, resting state to an open, conducting state (named I1), allowing the flow of Na⁺, K⁺ and Ca²⁺ across the membrane (Egan and Khakh, 2004). Prolonged exposure to ATP leads to the formation of a desensitized state, a temporary inactivation that terminates ion flux despite the fact that ATP remains bound to the receptor. The kinetics of desensitization vary between P2X subtypes – fast desensitization is observed only with P2X1 and P2X3 receptors, whereas slow desensitization is observed for P2X2, P2X4 and P2X5. In contrast, P2X7 receptors exhibit no apparent desensitization (North, 2002). Dissociation of ATP from the desensitized state, in turn, reverts the channel to the initial closed, resting state, in which it is able to be activated once again. This process is known as resensitization. A second conducting state (I2) is also found for selected P2X subtypes, whereby a dilation of the pore occurs, rendering the channel progressively permeable to larger cations and dyes (Khakh et al., 1999a; Virginio et al., 1999) (For a recent review see (Rokic and Stojilkovic, 2013)).

The recent determination of the crystal structures of the zebrafish P2X4 receptor (zfpP2X4) in both an apo, closed-channel state (Kawate et al., 2009) and in an ATP-bound, presumably open-channel state (Hattori and Gouaux, 2012) represented a landmark achievement in the understanding of the molecular architecture of these receptors. These structures allowed the confirmation of a wealth of biochemical and electrophysiological research previously carried out to probe the structure and function of P2X receptors. In addition to this, comparison of structures in the apo and ATP-bound states has enabled identification of the extracellular motions which follow ATP binding, thus providing us with a plausible mechanism for channel activation. However, in addition to these advances, the X-ray structures have also raised a number of intriguing questions. In particular, the molecular mechanism involved in the opening of the transmembrane pore itself still

remains unclear and under debate. This may be due, in part, to the fact that the intracellular domains, known to be of critical importance for P2X function (Allsopp and Evans, 2011; Allsopp et al., 2013; Boue-Grabot et al., 2000; Robinson and Murrell-Lagnado, 2013; Schwarz et al., 2012; Xu et al., 2012), were removed for crystallization purposes. Additional factors, such as crystal packing and the presence of detergents for solubilisation, may also contribute to these uncertainties. This review will provide a summary of functional studies in the context of the post-structure era, aiming to clarify our understanding of the way in which P2X receptors function in response to ATP binding, as well as the mechanism by which allosteric modulators are able to regulate receptor function.

2. Global architecture

2.1. General topology of the ion channel

The concept of purinergic receptors was first proposed by Burnstock in the early seventies (Burnstock, 1972) but sustained studies in this field only began in 1994 following the first molecular identification of P2X receptors (Brake et al., 1994; Valera et al., 1994). As P2X receptors had no sequence homology with other known ion channels, molecular and biochemical studies were first used to extensively explore the molecular structure. The general pattern of hydrophobicity suggested the presence of two domains of sufficient length to span the membrane (Brake et al., 1994; Valera et al., 1994) and complementary approaches such as N-glycosylation site tagging (Newbolt et al., 1998) provided early evidence of the intracellular location of both the N- and C-termini. Substitutions of residues of the putative transmembrane domains to tryptophan (Silberberg et al., 2005), cysteine (Jiang et al., 2001; Rassendren et al., 1997) or alanine (Li et al., 2004) highlighted a relative periodicity compatible with an alpha-helical organization. The peripheral location of TM1 was suggested by calcium permeability studies (Samways and Egan, 2007; Samways et al., 2008), whilst methanethiosulfonate (MTS) accessibility of residues mutated to cysteine (Jiang et al., 2001; Li et al., 2008) showed that TM1 has a limited contribution to the ion conduction pathway. In terms of global receptor structure, the stoichiometry of these receptors was for a long time debated (for a detailed review see (Hausmann et al., 2015)). A trimeric assembly was first proposed following immunohistochemical studies using aldehyde-containing reagent-crosslinked receptors for P2X1 and P2X3 (Nicke et al., 1998), engineered concatemeric receptors of P2X2 (Stoop et al., 1999) and disulphide bond experiments on cysteine-substituted heteromeric P2X2/3 receptors (Jiang et al., 2003). Moreover, functional studies based on Hill slopes obtained from ATP dose–response curves and single-channel recordings (Ding and Sachs, 1999), along with low resolution structures of the receptor by atomic force microscopy and electron microscopy (Barrera et al., 2005; Mio et al., 2005, 2009; Nakazawa et al., 2005; Shinozaki et al., 2009), further supported the originally proposed trimeric assembly of P2X receptors. The determination of crystal structures of a truncated zebrafish P2X4 receptor (Δ zfpP2X4), firstly in 2009 resolved at 3.1 Å in the absence of ATP (Kawate et al., 2009) and subsequently in 2012 bound to ATP at a resolution of 2.8 Å (Hattori and Gouaux, 2012), definitively confirmed this stoichiometry, as well as the global architecture of P2X receptors. These structures revealed the precise three-dimensional organization of the receptor and the folding of each subunit (Fig. 1A–C). The overall shape of each individual subunit is likened to that of a dolphin, consisting of a body, head, tail, dorsal fin and left and right flippers (Fig. 1C). This comparison allows a clear distinction of structurally

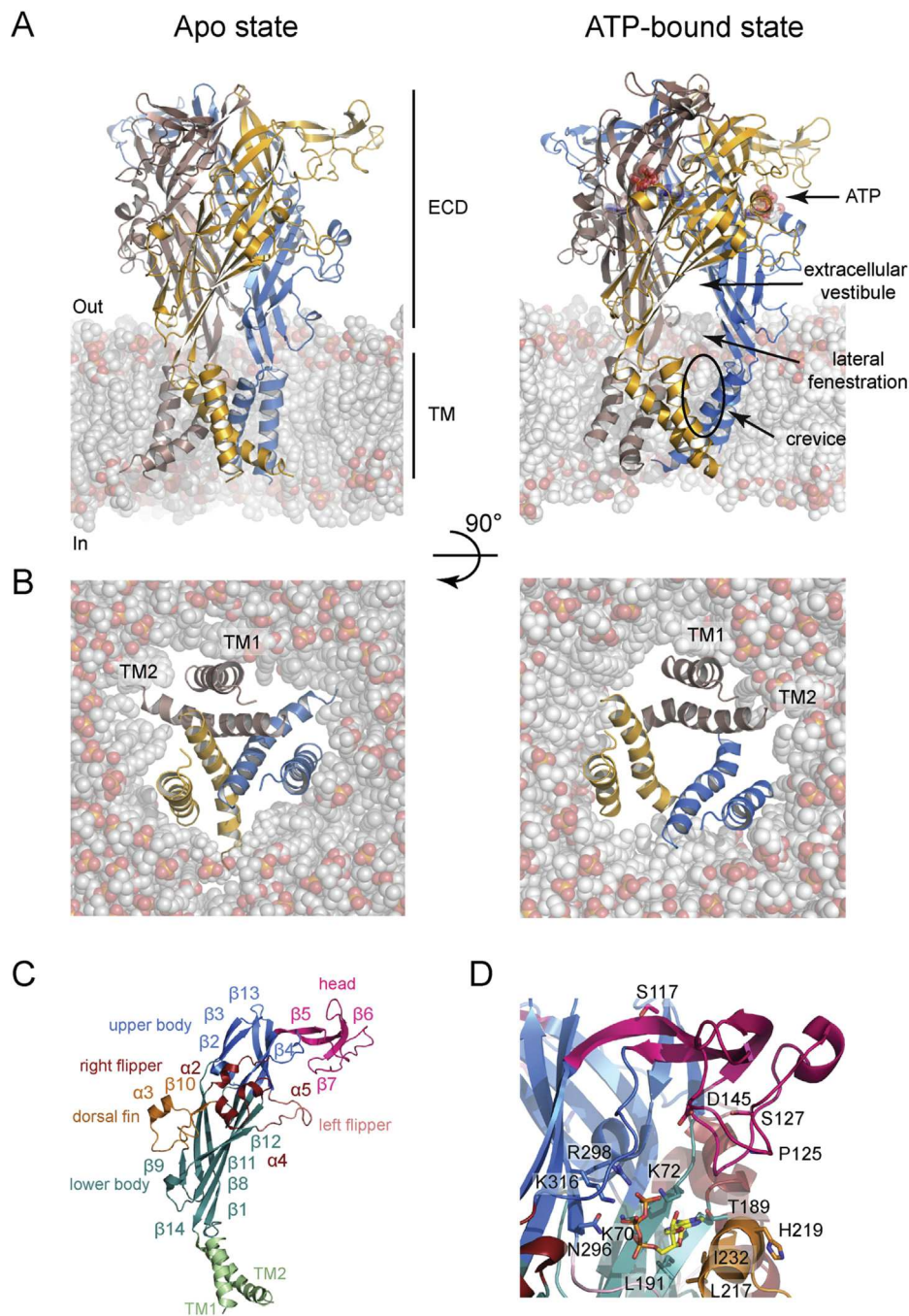


Fig. 1. Molecular organization of P2X receptors. (A) Lateral view of the crystal structures of $\Delta zfp2X4$ receptor in a closed state (left, PDB code 4DW0) and in an ATP-bound state (right, PDB code 4DW1) embedded in a lipid bilayer. The three subunits are depicted in cartoon representation and shown in different colours. ATP is in stick representation, the membrane is represented by red, orange and white spheres. ECD and TM stand for extracellular and transmembrane domains, respectively. (B) The same structures as in (A), viewed from the extracellular side, along the axis of the central channel. (C) Ribbon representation of the folding of one subunit. Each domain is named according to a homology comparison to a dolphin. The extracellular domain is composed of 14 β -sheets and 4 α -helices, whereas 2 α -helices form the transmembrane domain. (D) Close up view of the ATP-binding pocket coloured according to domains as in panel (C), the residues (*zfp2X4* numbering) indicated are discussed in the text.

differing regions. The large glycosylated ectodomain represents the body of the dolphin, and is composed of highly conserved residues, organized into a rigid β -sheet structure and stabilized by five disulphide bonds. Branching out from this core body region are four more structurally flexible domains: the head, dorsal fin, left and right flippers (Fig. 1C). The transmembrane domains, likened to the dolphin tail, were confirmed to be organized into alpha-helices. TM1 is positioned peripherally to TM2 and the ion conducting pore is lined primarily by the association of three TM2 helices,

angled at 45° from the normal of the membrane plane (Fig. 1A and B). The gate of the channel is defined by the hydrophobic region between L340 and A347, centred at the residue A344, approximately halfway down the length of the TM2 helix. The structure of the *zfp2X4* receptor solved in the absence of ATP, presumably in the closed state, reveals inter- and intra-subunit interfaces with extensive interactions in the upper body, each monomer twisting around its neighbours. Two potential pathways through which ions can access the pore were identified: a central pathway, whereby

ions enter the channel vertically *via* three connected vestibules positioned along the central axis of the receptor, or alternatively, a lateral pathway, whereby ions enter the channel through three fenestrations located above the gate region. However, MTS accessibility studies and electrostatic free energy calculations (Kawate et al., 2011; Samways et al., 2011) strongly suggest that extracellular ions use the lateral pathway, entering the channel preferentially through the fenestrations before flowing through the ion pore itself.

2.2. Location of the ATP sites

Systematic site-directed mutagenesis coupled with electrophysiology provided much of the information crucial for locating the ATP binding sites. Several recent reviews focused on this aspect of P2X function (Browne et al., 2010; Chataigneau et al., 2013; Evans, 2009). Briefly, a combination of several studies revealed that there are eight highly conserved residues critical for ATP binding (K70, K72, N96, F188, T189, F297, R298 and K316, zP2X4) insofar as substitutions at these homologous positions inhibit ATP currents in different P2X subtypes (Ennion et al., 2000; Fischer et al., 2007; Jiang et al., 2000; Roberts et al., 2008; Wilkinson et al., 2006; Yan et al., 2006; Zemkova et al., 2007). Evidence that the formation of a ligand-binding site requires the involvement of two subunits was provided by co-expression of rP2X3 with mutated K69A/K308A rP2X2 (a non-functional, “dead” subunit) (Wilkinson et al., 2006), in addition to SDS-page gels of K69C/F289C rP2X2 receptor in both presence and absence of ATP (Marquez-Klaka et al., 2009). Many strategies were also employed to determine the specific residues which are involved in binding ATP. Among them, charge-dependent effects induced by MTS labelling of cysteine introduced at position I67 (Jiang et al., 2000) and activation of the receptor following ADP-ribosylation at position R125 (P2X7) (Adriouch et al., 2008) suggested that these particular residues are in close proximity to the bound agonist. A strategy of site-directed affinity labelling was developed by Jiang et al., using a thiol-reactive probe (8-thiocyno-ATP, NCS-ATP) to demonstrate the involvement of two residues (N140 and L186 in rP2X2) in the coordination of the adenine ring of ATP (Jiang et al., 2011). Voltage-clamp fluorometry (VCF) experiments coupled with site-directed fluorescence labelling allowed Lorinczi et al. to successfully orientate the ribose moiety of the ATP molecule in the binding cavity of rP2X1 (Lorinczi et al., 2012).

The crystal structures of zP2X4 confirm the implication of residues previously identified to bind ATP (Hattori and Gouaux, 2012). These residues form a tight cluster, located within an intersubunit cavity and surrounded by the head and left flipper of one subunit and by the dorsal fin of another (Fig. 1D). Several unanticipated interactions were also revealed: briefly, the residue L217 is involved in the recognition of the solvent-accessible ribose ring, the residues K70, K72, K316, N296 and R298 stabilize the triphosphate tail in an unusual U-shaped structure, K70 and T189 form hydrogen bonds with the adenine base, whilst L191 and I232 coordinate this adenine by means of hydrophobic interactions.

3. Structural point of view of the gating mechanism

Following the resolution of the crystal structures, a key issue for current research is the investigation into how ATP-binding can open the channel. In 2009, Shinozaki et al. provided the first time-lapse imaging of P2X4 receptor's structural changes in response to ATP application using fast-scanning atomic force microscopy (AFM) (Shinozaki et al., 2009). In the presence of ATP, individual subunits were observed, which draw away from one another to form the central pore. Since this study, several functional studies using the

substituted-cysteine accessibility method (SCAM) (Samways et al., 2014), engineered disulphide bonds (Du et al., 2012; Jiang et al., 2001; Kawate et al., 2011; Kowalski et al., 2014; Roberts et al., 2012; Stelmashenko et al., 2014; Zhao et al., 2014) or VCF (Lorinczi et al., 2012) have provided scattered information, giving a glimpse into the gating mechanism. The resolution of an ATP-bound state thus represented a major advance, as it provided an unrivalled picture of an open channel. *In silico* modelling of the two structures provided a basis for further investigations, and a plausible model of gating gradually began to take shape, which can be dissected into 5 key steps: ATP binding, tightening of the so-called binding “jaw”, flexing of the lower body regions, expansion of the lateral fenestrations and subsequent pore opening. ATP binding provokes a global structural movement, whereby subunits bend outward and rotate, inducing an expansion in the lower body region. As the lower body is directly connected to the transmembrane domain, this movement in turn induces a displacement of the outer ends of the TM helices, opening the pore in an iris-like motion (Browne et al., 2010). Here, we will focus on molecular changes in key domains during gating.

3.1. Movement of the binding jaw

3.1.1. Reorganization of the binding loops following ATP binding

The ATP binding site, located in an inter-subunit cavity between the head domain of one subunit, and the dorsal fin of another, is often referred to as the “binding jaw”. Evidence that the closure of this binding jaw plays an important initial role in the gating process has been provided by multiple recent studies. First, the presence of a zinc-binding site, naturally formed by residues H120 and H213 in the rP2X2 receptor, was exploited to display this closing motion of the binding jaw's two lips. ATP-currents on the double cysteine mutant H120C/H213C (rP2X2) are dramatically decreased and DTT treatment rescues a high sensitivity state, indicating that these residues are found in close proximity (Nagaya et al., 2005). However, the distance between these positions as predicted by the closed structure is too great (15 Å) to form a zinc-binding site in the WT receptor or disulphide bridge in the double cysteine mutant, which implies that the head and the dorsal fin domains must come closer together during activation. Whilst this hypothesis readily supports zinc potentiation, it appears that a different mechanism must take place to explain data obtained from the double cysteine mutant. In the latter case, the disulphide bridges may block ATP responsiveness, most likely by locking the receptor in a state for which ATP binding is considerably reduced. VCF experiments coupled with fluorescence labelling of G115C and G124C (hP2X1) also revealed that agonist binding induces a movement of the head domain of P2X1 receptor (Lorinczi et al., 2012), a finding which was further supported by electron microscopy experiments (Roberts et al., 2012). Engineered histidine bridges formed between residues of the head domain and the right-flipper connecting loop (Jiang et al., 2012a), or disulphide bridges formed between the top of the lower body and the right flipper (hP2X1 190C-284C), or between residues of the head region from two different subunits (hP2X1 138C-181C) (Roberts et al., 2012) highlighted the critical role of these segments in ATP function. Finally, using the closed state structure with ATP docked in its binding site according to the results of NCS-ATP labelling (Jiang et al., 2011), two different sets of data were produced by normal mode analysis (NMA) (Du et al., 2012; Jiang et al., 2012a), both suggesting that a decrease in the distance between residues of the binding jaw located in two adjacent subunits occurs following ATP binding. These data combined thus demonstrate that ATP-induced tightening of the binding jaw correlates precisely with an opening of the channel.

Although no structure with a competitive antagonist bound to

the receptor has been resolved to date, several studies suggest that antagonists act by binding to the upper jaw and thus impairing jaw closure. The position K138 of hP2X1 was first identified to be crucial in the binding of suramin (Sim et al., 2008). The use of hP2X1/DdP2X and hP2X1/hP2X2 chimeras subsequently allowed identification of a cluster of positively charged residues (KAKRK), including K138, in the head domain which contribute to suramin sensitivity (El-Ajouz et al., 2012). Moreover, the N140C mutant labelled with the NCS-ATP affinity probe displays decreased ATP-induced currents (Jiang et al., 2011) and binding of TNP-ATP, a presumably competitive P2X antagonist, blocks movement of the binding jaw (Jiang et al., 2012a). A recent study which uses NMA, principal component analysis (PCA) and short molecular dynamics (MD) simulations suggests the presence of at least three sites able to recognize the adenine group of ATP and thus three distinct recognition modes (Huang et al., 2014): the first mode being similar to that found in the ATP-bound crystal structure, the second featuring the adenine group buried in the interface of the rigid lower body domains and finally a third mode whereby adenine is positioned near the base of the head domain, which could explain the previous results obtained by engineered site-directed affinity labelling. Interestingly, only the first recognition mode can promote an effective downward motion of the head domain, whereas the other two modes are only able to induce outward or upward motions of the head. Jaw tightening therefore seems to be an essential step of the gating mechanism.

Other movements following ATP binding which occur in the loop regions surrounding the binding site were also identified as being critical for the initiation of pore opening. In particular, it has been shown that the left flipper must be pushed outward from the ATP binding pocket simultaneously to the cleft closure between the head and dorsal fin domains (Fig. 2A). To this end, Zhao et al. introduced cysteine or histidine residues on the left flipper (e.g. V288C rP2X4) and dorsal fin (e.g. T211C rP2X4) and observed an inter-domain disulphide bond or zinc bridge respectively, which impaired channel gating by preventing the relative motion of the two domains (Zhao et al., 2014). They predict, by MD simulations, that ATP binding may destroy the hydrophobic interactions between the left flipper and dorsal fin domains, induces repelling of V291 (zfp2X4) from the ribose of ATP and provokes closing motions of K193, L217 and I208 around the molecule of ATP, thus causing the downward motion of the left flipper and upward movement of the dorsal fin (Zhao et al., 2014). Other studies have probed the reorganization of the binding pocket by using disulphide bond engineering to restrict movement between the upper body and right flipper domains (N284C/K190C hP2X1) or between the head domain and the adjacent subunit (K138C/E181C hP2X1), revealing that a counter-clockwise rotation of the subunits may occur after ATP binding (Roberts et al., 2012). These results are consistent with MD simulations, which show a leftward motion of the loop F139-G146 (zfp2X4), situated within the head domain, and a rightward movement of the loop P169-A183 (zfp2X4) (Fig. 2A), which is covalently linked to the head (Huang et al., 2014). In agreement with these movements, recent work has suggested that during ATP activation of the P2X2 receptor, a significant rearrangement of residues E167 and R290, which interact electrostatically in the closed state ATP binding site, enables R290 to form a new, strong ionic interaction with the γ -phosphate oxygen of ATP, thus breaking the original salt bridge (Hausmann et al., 2013). This electrostatic switch appears to be a critical step that leads to channel opening.

3.1.2. Intermediate activation states

Some recent works have suggested the existence of intermediate states in P2X receptors which precede pore opening. The idea of

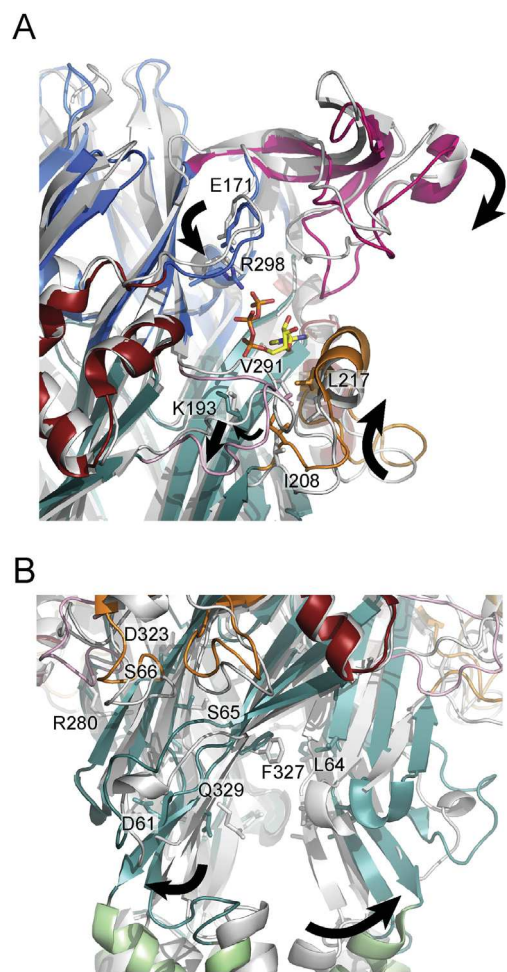


Fig. 2. Structural rearrangements during gating mechanism. Superimposed structures in the resting state (grey) and the ATP-bound state (coloured) at the binding site (A) and the lower body (B). Black arrows show the relevant motions likely to occur during allosteric transition, leading to the opening of the channel. In panel B the indicated pairwise residues (L64-F327; D61-Q329; S65-R280; S66-D323), when mutated into cysteines on different P2X subtypes, are implicated in disulphide locking of the closed state (zfp2X4 numbering).

such primed states in P2X receptors was first introduced by Moffatt and Hume who incorporated a so-called “flipped” intermediate state into the simple allosteric model to explain the delay between ATP-binding and the observation of ionic currents (Moffatt and Hume, 2007). This assumption was later confirmed by two crucial studies. The first of these showed that the agonist NCS-ATP tethered to L186C in rP2X2 receptor in which an allosteric reporter mutation, T339S, was introduced to observe spontaneous channel openings, does not lock the channel in the open state, but instead allows the channel to open in response to zinc (Jiang et al., 2012b), indicating that NCS-ATP actually may trap an intermediate state that precedes channel opening. A second study provides evidence that BzATP tethered in one of the three intersubunit ATP binding sites of P2X7 receptor induced conformational changes in the remaining sites, causing these sites to lose their high selectivity for ATP and to bind other pyrimidine and diphosphate nucleotide analogues (CTP, UTP and ADP) with greater efficiency (Browne and North, 2013).

The molecular movements underlying such primed states remain unclear, but recent works suggest that movements of the head domain may be able to occur not only as a result of ATP-binding, but equally in the absence of agonist. Normal mode

analysis of zfp2X4 and molecular dynamics experiments (Huang et al., 2014; Zhao et al., 2014) showed a possible spontaneous downward motion of the head domain, resulting in the closure of the jaw in the absence of ATP binding. This observation was confirmed by the spontaneous formation of a disulphide bond between residues of the dorsal fin and head domain (K113C and K201C, hP2X3), which impaired binding of a fluorescent ATP derivative, BODIPY-TR ATP (Kowalski et al., 2014). Such spontaneous movements of the binding jaw may therefore be related to the progress of the receptor towards these intermediate states.

It is known that strong cooperativity operates between the three binding sites of P2X receptors (Bhargava et al., 2012; Jiang et al., 2003; Yan et al., 2010), and that ATP association rates increase with the sequential binding of ATP. Experiments from heterotrimeric receptors and concatenated constructs (Stelmashenko et al., 2012) demonstrated that two molecules of agonist seem sufficient to open the channel. If this conclusion also stands true for NCS-ATP, one may speculate that the lack of irreversible trapping of the pore in the open state is due to the irreversible binding of only one NCS-ATP molecule. In this case, the binding of NCS-ATP to one of the three ATP-binding sites would allow the receptor to convert from the closed state to an intermediate state, and subsequent binding of a second molecule would eventually result in the full opening of the channel. Other experiments are needed to further clarify this issue.

3.2. ECD flexibility

The domains which form the ATP binding pocket are structurally coupled to the rigid body domain (Browne et al., 2010). As such, their movements are transmitted across the protein as a whole. But which residues in particular are essential in the gating mechanism? Among studies which explored the orthosteric sites, single-channel recordings revealed a difference in the role of K69 and K308 (rP2X2). Whilst the spontaneous opening of the K69A/T339S receptor was no different than that seen in T339S, this spontaneous activity disappeared in the mutant K308A/T339S (Cao et al., 2007) suggesting a critical role for K308 in channel gating. Interestingly, K308 (rP2X2) is located on the upper ends of β 14, a β strand located in the body domain, which is directly connected to TM2 (Fig. 1C). Du et al. also suggested a crucial role of this β strand and, following NMA simulations, proposed that the upper ends of β strands β 14 and β 1 of adjacent subunits undergo rotation in opposite senses, demonstrated by a decrease in the distance between K70 and K316 residues (zfp2X4). This rotation also causes the lower ends of these β strands to be pulled further apart from one another, a motion which in turn encourages the outward movements required for channel opening (Du et al., 2012).

Other studies have also demonstrated the necessity of this rotational motion of β 1 and β 14 strands of neighbouring subunits: the formation of disulphide bridges between I62C/D320C (hP2X1) (Roberts et al., 2012), E59C/Q321C (rP2X2) (Kawate et al., 2011) or S65C/D315C (rP2X2) (Stelmashenko et al., 2014) results in the inhibition of ATP-currents, which can be restored upon application of DTT. Moreover, in the lower part of the body domain, bridging of β 1 and β 8, which are connected to TM1, in the same subunit causes a decrease in gating (Stelmashenko et al., 2014), which suggests that the lower body region is involved in expansion movements not only between subunits but also within the subunits themselves (Fig. 2B). The flexibility of this region seems to be essential in the gating mechanism, and has been further illustrated by several studies. First, Jiang et al. showed the role of an extracellular salt-bridge between β 1 and β 12 strands (E63/R274 rP2X2) in stabilizing the closed state (Jiang et al., 2010). Second, it has been demonstrated that the segment spanning

G316–I333 (rP2X4) is essential in transmitting the signal for channel opening from the ATP binding site to the TM domains (Rokic et al., 2013). The residue G316 (rP2X4) is crucial for the flexibility of the lower body: an alanine substitution at this position, which rigidifies the structure, results in a decrease of ATP sensitivity as well as slower activation and desensitization kinetics, whereas a proline mutation causes only a variation in kinetics (Yan et al., 2006).

From the crystal structures, it can be seen that no large conformational changes occur in the upper body domain. However, all of the vestibules located in the central part of the trimeric assembly can be seen to expand, whilst the interface of the upper and the central vestibules, near P95 (zfp2X4), is kept relatively narrow. Previous SCAM studies had also suggested the expansion of the central and extracellular vestibules (Allsopp et al., 2011). Interestingly, mutation of F95 to leucine in hP2X7, a residue equivalent to zfp2X4 I94, results in an altered modulation of the ATP response by the allosteric modulator GW791343, and also favours the opening of the channel (Michel et al., 2008).

3.3. Transmembrane motions and pore opening

As previously discussed, combined movements of the head domain, dorsal fin and left flipper cause the rotation and outward flexing of the lower body domains, located near the membrane and connected to the TM helices, which, in turn, induce substantial expansion of the extracellular vestibule and pore opening (Hattori and Gouaux, 2012).

Prior to the publication of the apo and ATP-bound structures, multiple mutagenesis studies focused on the characterization of TM1 and TM2. Extensive SCAM studies provided information about the location of the gate in the TM domain, despite some discrepancies on the exact position of the narrowest point in the channel (for a complete review see (Samways et al., 2014)). From the crystal structures, the gate region can be determined to measure 8 Å in length, spanning from just below L340–N341 on the extracellular side to L346–A347 (zfp2X4) on the intracellular side. SCAM studies were also able to suggest a reorganization of the transmembrane domain, which likely involves extensive repacking and motions of both TM helices. Application of ivermectin (IVM), an allosteric modulator of selected P2X receptors, to mutants obtained by tryptophan scanning mutagenesis provided preliminary information about changes occurring in the interactions of TM1 and TM2 residues during gating, and the results led to the hypothesis that TM1 may rotate relative to TM2 (Silberberg et al., 2007). Following single-channel recordings of TM2 mutants, Cao et al. suggested a counter-clockwise rotation of several tens of degrees and separation of the TM2 helices (Cao et al., 2009). Structural constraints obtained from functional studies predicted conformational rearrangements. The expansion of TM1 and TM2 in the extracellular side was suggested by the inhibition of channel opening resulting from disulphide bond formation between V48C and I328C (rP2X2) (Jiang et al., 2003, 2001). In addition, by engineering metal bridges Li et al. proposed that the TM2 helix does not undergo large rotations, but instead, a relative straightening of TM2 occurs during gating, suggesting that the inner part of the TM2 domain must move toward the central axis of the pore during gating (Li et al., 2010). Moreover, using concatemeric channels carrying one, two or three T339K mutations in rP2X2 receptor, Browne et al. demonstrated that each subunit contributes symmetrically to the opening of the pore (Browne et al., 2011). From the crystal structures, it can be observed that TM1 and TM2 rotate by $\sim 10^\circ$ and $\sim 55^\circ$, respectively, counterclockwise about the central pore axis, perpendicular to the membrane plane, and increase their tilt angle by $\sim 8^\circ$ and $\sim 2^\circ$, respectively, about an axis parallel to the membrane

plane. This implies an iris-like movement, which leads to the opening of a 7 Å-wide pore. However, the large distance separating residues V343 or D349 is not compatible with data from metal bridge experiments in the inner section of the channel, which indicated that these residues should be found in close proximity to one another.

Furthermore, the structure revealed unexpectedly large intersubunit crevices within the transmembrane domain (Fig. 1A). The physiological relevance of these gaps remains unclear, but recent molecular dynamic simulations performed with the ATP-bound state structure indicated that lipids may diffuse into these gaps, thereby blocking the pore, suggesting that these crevices are inconsistent with ion conduction (Heymann et al., 2013).

The lack of cytosolic domain, which was truncated for crystallogenic purposes, may cause the local destabilization of the structure, as well as the absence of intersubunit interactions. A recent study proposes an improved model of the channel in the open state, generated by small rotations and a translation of TM2 toward the central axis, which decreases the size of the crevices and brings the intracellular ends of the TM helices closer together, narrowing the gaps between them. This new packing model restores intersubunit interactions between TM2 helices including the metal bridge formed at the threefold axis by V343C (rP2X2), and intrasubunit interactions between TM2 and TM1 helices (Heymann et al., 2013). These data suggest that the crystal structure most likely does not represent a native, functional open state.

4. Allosteric modulation of P2X receptors

There are many allosteric modulators that regulate P2X function. These modulators can be as small as protons, metals or larger molecules such as IVM, neurosteroids, ethanol, phospholipids and kinases (Coddou et al., 2011a, 2011b; Evans, 2009). Here, we will consider only three examples of allosteric modulators that act on three different loci: the ectodomain, transmembrane domain and intracellular domain. The reader is referred to other extensive reviews for further details (Coddou et al., 2011a, 2011b; Evans, 2009; Huidobro-Toro et al., 2008).

4.1. Allosteric regulation within the ectodomain: the case of zinc

Zinc is the second most abundant trace metal in the body after iron and consistently plays a major role in enzymatic reactions (Huidobro-Toro et al., 2008). In the blood plasma, the concentrations of trace metals including zinc reach 15 µM, and in the brain, zinc concentrations are as high as 100–150 µM. Zinc is co-released with neurotransmitters at some synapses and can act on several post-synaptic targets such as LGICs to modulate neuronal activity (reviewed in Huidobro-Toro et al. (2008), Sensi et al. (2009)).

Extracellular zinc modulates the function of some P2X receptors. It has a biphasic allosteric modulatory effect: at low concentrations (under 100 µM), pre-incubation with zinc has a potentiating effect on ionic currents flowing through rP2X2, rP2X3, rP2X4 and rP2X5 receptors, whereas at higher concentrations, in the millimolar range, zinc mainly has an inhibitory effect (Coddou et al., 2011b; Wildman et al., 2002; Wildman et al., 1998, 1999a, b). In rP2X1 and rP2X7 receptors, zinc exerts a purely concentration-dependent inhibitory effect (Acuna-Castillo et al., 2007; Liu et al., 2008; Virginio et al., 1997; Wildman et al., 2002, 1999b). The inhibitory allosteric effect is dependent upon a pre-incubation period, especially for rP2X2, rP2X3 and rP2X1.

The biphasic effect has been interpreted as a result of the existence of at least two distinct allosteric sites for zinc, one with a high affinity responsible for the potentiating effect and one with a low

affinity involved in the inhibitory control of P2X receptors (Coddou et al., 2011b). Site-directed mutagenesis has been used to solve the role of specific amino acid residues involved in these modulatory effects. It has been observed that the residues H120 and H213 participate primarily to the allosteric metal binding site of rP2X2 receptor responsible for the potentiating effect of zinc (Clyne et al., 2002; Lorca et al., 2005; Nagaya et al., 2005; Tittle et al., 2007). In contrast to the potentiating effect observed on the rat P2X2, zinc inhibits the human P2X2 receptor activity with an IC₅₀ in the micromolar range (Tittle and Hume, 2008), highlighting striking opposite effects between rodents and humans. Analysis of the sequences indicated that only one of the two histidines essential for zinc potentiation in rP2X2 is present at the homologous position to rat H120 in hP2X2 (H132), with the position homologous to rat H213 instead having an arginine (R225). As zinc is likely coordinated directly by the two histidines in rodents, its ability to make such an interaction is abolished in humans because of the presence of the positively charged arginine residue. Notably, mutating R225 to cysteine was sufficient to confer zinc potentiation onto the human orthologue (Tittle and Hume, 2008), suggesting that zinc potentiation uses the same mechanism as that in the wild-type rP2X2 receptor. In the crystal structures, residues homologous to H120 (P125 in zfpP2X4) and H213 (H219 in zfpP2X4) belong to two adjacent subunits and are located, respectively, in the head and dorsal fin domains (Fig. 3A and B), positions which correspond to the two 'lips' of the ATP-binding jaw. In agreement with previous works (Jiang et al., 2012a) and with the recent crystal structure solved in the presence of ATP (Hattori and Gouaux, 2012), ATP binding promotes tightening of the two lips of the binding jaw and zinc stabilizes the conformation of closed jaws through coordination of the two histidine residues (Fig. 3B).

In addition, other histidines (H192 and H245) from rP2X2 (corresponding to R197 and V251 in zfpP2X4, respectively) were also identified as potentially participating to the allosteric potentiating effect of zinc, although to a lesser extent than H120 and H213 (Lorca et al., 2005). However, mapping of the equivalent residues in the crystal structure shows that these residues are not close to each other and are far away from the established potentiating site involving H120 and H213 (Fig. 3A and B). The mechanisms of potentiation involving H192 and H245 thus remain to be clarified.

The location of the zinc inhibition sites also remains unclear. In rP2X2, neither the extracellular histidines nor glutamates or aspartates are required for low affinity zinc inhibition (Clyne et al., 2002; Friday and Hume, 2008). By contrast, mutating H204 and H209 to alanine in the hP2X2 receptor (corresponding to R197 and N202 in zfpP2X4, respectively) has been shown to significantly reduce zinc inhibition, and mutating to cysteine restored wild-type inhibition (Tittle and Hume, 2008). However, the fact that the double alanine mutant was no more deficient than either single mutant, along with the fact that MTS reagents carrying opposite charges were nearly equipotent in affecting zinc effects in cysteine mutants, suggest that H204 and H209 are not directly involved in zinc inhibition. These data reveal the complexity of zinc modulation, since an equivalent position (rP2X2 H192; hP2X2 H204) is involved in either potentiation or inhibition depending on the species.

Additional residues from other P2X subtypes have been identified to be critically involved in zinc allosteric effects. For instance, in rP2X4 receptor, the residue C132 is involved in the potentiating allosteric effect of zinc, whereas D138 and H140 have been determined to participate in the inhibitory allosteric effect of zinc (Coddou et al., 2007, 2003). When mapped on the zfpP2X4 crystal structure, D138 and H140 are close to each other and one may infer that zinc binding to these residues may restrict head domain mobility, and thus may block the ATP-induced response in an

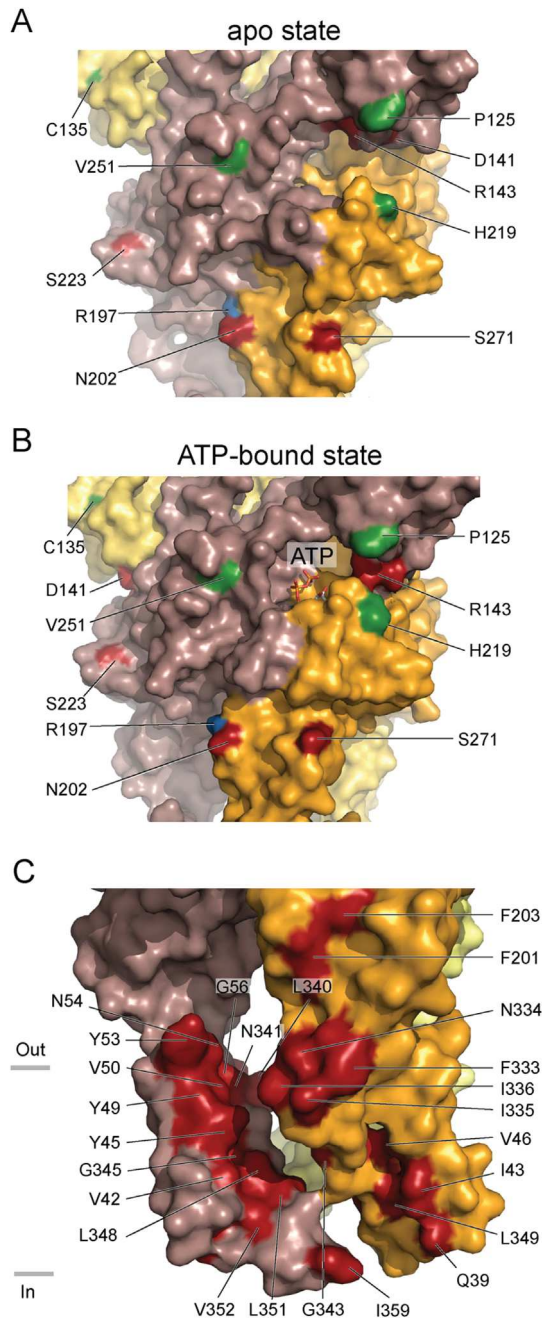


Fig. 3. Mapping of residues implicated in allosteric modulation of P2X activity. Residues contributing to allosteric regulation induced by zinc application on a closed state (A) and an ATP-bound state of $\Delta zfp2x4$ (B). Residues implicated in the production of an inhibitory effect or a potentiation are coloured in red and green, respectively, and positions implicated in both effects are shown in blue. Amino acid residues mapped on the structure of $\Delta zfp2x4$ are indicated in brackets immediately after the equivalent residues of the indicated P2X species that are listed in the text: rP2X2 H120 (P125); rP2X4 C132 (C135); rP2X4 D138 (D141); rP2X4 H140 (R143); rP2X2 H192, hP2X2 H204 (R197); hP2X2 H209 (N202); rP2X2 H213, hP2X2 R225 (H219); rP2X7 H219 (S223); rP2X2 H245 (V251) and rP2X7 H267 (S271). (C) Location of residues associated with IVM potentiation (in red) in the ATP-bound state of $\Delta zfp2x4$. Amino acid residues mapped on the structure of $\Delta zfp2x4$ are indicated in brackets immediately after the equivalent residues of the indicated P2X4 species that are listed in the text: rP2X4 Q36 (Q39); rP2X4 I39 (V42); rP2X4 L40 (I43); rP2X4 Y42, hP2X4 Y42 (Y45); rP2X4 V43, hP2X4 V43 (V46); rP2X4 W46 (Y49); rP2X4 V47 (V50); rP2X4 W50 (Y53); hP2X4 E51 (N54); rP2X4 G53 (G56); rP2X4 F198 (F201); rP2X4 F200 (F203); rP2X4 W330 (F333); rP2X4 D331 (N334); rP2X4 I332 (I335); rP2X4 I333 (I336); rP2X4 I337 (L340); rP2X4 N338 (N341); rP2X4 G340 (G343); rP2X4 G342 (G345); rP2X4 L345 (L348); rP2X4 L346 (L349); rP2X4 V348 (L351); rP2X4 A349 (V352) and rP2X4 I356 (I359). Note that

allosteric manner. Supporting this hypothesis, a recent NMR study of the structure of the rat P2X4 receptor head domain demonstrated that D138 and H140 are directly involved in the binding of zinc and copper, another modulator of the P2X4 receptor (Igawa et al., 2015). However, clear structural interpretation of the zinc potentiation involving the C132 residue is not easy, because this residue (Igawa et al., 2015), and its equivalent in zfp2X4 (Hattori and Gouaux, 2012; Kawate et al., 2009), is already engaged in a naturally occurring disulphide bond. Additional investigations should be carried out in order to understand the specific role of C132 in zinc potentiation in rP2X4 receptor. In rP2X7 receptor, the inhibitory effect of zinc was abolished in H219A and H267A mutants, suggesting a major role of these two amino acids (Acuna-Castillo et al., 2007). As these residues are not conserved among P2X subtypes, these data suggest that P2X7 has undergone a separate adaptation to trace metal coordination (Huidobro-Toro et al., 2008).

4.2. Allosteric regulation within the transmembrane domains: the case of ivermectin

Ivermectin (IVM) is a semi-synthetic macrocyclic lactone used as an antiparasitic in humans and animals (Silberberg et al., 2007). It is a positive allosteric modulator of P2X4 receptors from several different species (Agboh et al., 2004; Khakh et al., 1999b; Priel and Silberberg, 2004) as well as the human P2X7 receptor, but not murine P2X7 receptor (Norenberg et al., 2012). It acts only when applied from the extracellular side of the cell membrane but not from the inside, suggesting that it does not bind to intracellular domains (Norenberg et al., 2012; Priel and Silberberg, 2004). Consistent with its lipophilic character, the effects of IVM are slow to develop, suggesting that it might need first to partition into the membrane before reaching its binding sites, which are likely close to the extracellular face of the membrane. A detailed kinetic analysis suggested that IVM binds to separate sites in hP2X4 receptors. Binding to the higher affinity site increases current amplitude by reducing channel desensitization, whilst binding to the lower affinity site slows the deactivation of the current mainly by stabilizing the open channel state (Priel and Silberberg, 2004). Chimeras made between IVM-sensitive P2X4 receptor and IVM-insensitive P2X2 receptors first confirmed the critical role of the transmembrane domain. It has been initially found that chimeras of the ectodomain of P2X4 with helices and intracellular domains of rP2X2 are not sensitive to IVM (Jelinkova et al., 2006). In contrast, chimeras of the two transmembrane segments of rP2X4 receptor into rP2X2 receptor are sufficient to confer IVM sensitivity (Silberberg et al., 2007), indicating a major role of both transmembrane segments of P2X4 receptor in the positive allosteric effect of the modulator. Consistent with a transmembrane location, site-directed mutagenesis analysis of residues located in the putative TM domains (Jelinkova et al., 2008; Popova et al., 2013; Silberberg et al., 2007) indicated that V28, Q36, I39, L40, Y42, V43, V47, W50 (TM1) and N338, G340, G342, L345, L346, V348, A349, I356 (TM2) in rP2X4 are involved in IVM sensitivity of the channel (Jelinkova et al., 2008; Silberberg et al., 2007). A recent study confirmed the importance of some of these residues (L40, V43, V47 and W50) in the effect of IVM on deactivation in rP2X4, and further identified new ones (W46, G53, F330, D331, I332 and I337) (Zemkova et al., 2015). The mutation to tryptophan of the homologous residues of Y42 and V43 in human P2X4 receptor also reduced the allosteric effect of IVM (Samways et al., 2012). Although these results do not firmly

residue rP2X4 V28 is located out of the truncated crystal structure and therefore cannot be mapped. Each subunit is coloured differently.

demonstrate that these residues contribute directly to IVM binding sites, they support the conclusion that these residues are critically involved in the functional effect of IVM. Interestingly, mapping of the corresponding residues in the zfp2X4 crystal structure bound to ATP reveals that most of them are located on the putative transmembrane helices at the subunit interfaces, with their side chains facing one another (Fig. 3C). This suggests that IVM may indeed bind to these interfaces.

In support of this hypothesis, mutations of the amino acid W46 to other aromatic residues (tyrosine or phenylalanine) in heterologously expressed rP2X4 receptor did not modify IVM-induced potentiation of ATP-dependent currents, whereas substitution with non-aromatic residues (leucine, valine, alanine, asparagine, lysine or aspartate) switched the potentiation to inhibition (Popova et al., 2013). Therefore, it has been suggested that the presence of an aromatic group at position 46 is a critical determinant of IVM-induced allosteric effects, most probably by means of a cation– π interaction (Popova et al., 2013). It was previously suggested that the interaction between W46 and M336 participates in a binding pocket for IVM (Asatryan et al., 2010). However, whilst both individual W46A and M336A mutations as well as the double mutation significantly reduced the inhibitory effect of ethanol, only the mutation W46A (or the combined mutation) modified the positive allosteric effect of IVM (Popova et al., 2013). Finally, the analysis of a new molecular model based on the ATP-bound structure of zfp2X4 suggested a prominent role of the amino acid Y42 of rP2X4 receptor, confirmed by the mutation Y42F which also switched the potentiating allosteric effect of IVM to inhibition (Popova et al., 2013). This is probably due to the lack of a hydrogen bond between IVM and the phenolic OH group of Y42 in the mutation. Interestingly, in another study, the mutation Y42A of rP2X4 receptor mimicked the allosteric action of IVM by decreasing the deactivation rate of the current (Zemkova et al., 2015). It has also been shown that removal of the fixed negative charge of the acidic amino acid E51 of hP2X4 receptor, by the mutation E51Q, markedly reduces the allosteric effect of IVM on current intensity and relative permeability to Ca^{2+} (Samways et al., 2012). As this amino acid is located at the lateral entrance to the transmembrane pore, it has been hypothesized that IVM may change the topology of these lateral portals (Samways et al., 2012).

In agreement with this hypothesis, the allosteric effect of IVM on current deactivation was significantly attenuated by the mutation of F198 and F200, two residues located in the fenestrations (Fig. 3C), whereas the effect was increased by the mutation F330A/S, another amino acid of the region (Gao et al., 2015).

Finally, a recent work investigated the role of IVM on P2X pore dilation (Zemkova et al., 2015). In this study, the influence of IVM on pore dilation was studied in both wild-type rP2X4 receptor and transmembrane domain receptor mutants. IVM-induced receptor dilation in the presence of ATP was reduced or lost in L40A, V43A, W46A, V47A, W50A, G53A, F330A, D331A, I332A, I333A and I337A mutants (Zemkova et al., 2015). The results established that the IVM-induced rescue of rP2X4 receptor from desensitization temporally coincides with pore dilation.

Altogether, these data highlight the notion that there are multiple sites of interaction for IVM in P2X4 receptors (Popova et al., 2013). IVM binding sites are believed to be close to the lateral fenestrations found at the membrane interface (Gao et al., 2015; Jiang et al., 2013). It is thus tempting to speculate that IVM acts by insertion between adjacent transmembrane helices, which are located just below these fenestrations, perhaps by slightly moving apart adjacent helices (Fig. 3C). This mechanism would be consistent with the slight increase of single-channel conductance observed for the lower affinity site and with the slow onset and washout of the effects of IVM (Priel and Silberberg, 2004). Crystal

structures of IVM bound to the receptor in the presence of ATP would definitively resolve this issue.

4.3. Allosteric regulation within the intracellular C-terminus domain: the regulatory effects of phospholipids

The particular allosteric regulation exerted by phospholipids at the carboxy terminal is considered as a post-translational mechanism of regulation of P2X receptor activity. The effects of phosphoinositides (PIPn) on P2X receptors have been reviewed recently (Bernier et al., 2013). PIPn increase P2X currents, most likely through a conformational change of the receptor, leading to an alteration of the gating (Bernier et al., 2013).

There are several important features in the regulatory effect exerted by PIPn on P2X receptors which have been mostly revealed by functional assays using the patch-clamp technique and/or by the binding of GST-fusion proteins containing the C-terminal domains of P2X receptors to PIPn coated on nitrocellulose membranes (PIP strip assays) (Bernier et al., 2013). From these studies, it has been shown that PIPn exert a direct effect on P2X1, P2X2 and P2X4 receptors as well as on the heteromeric P2X1/5 and P2X2/3 receptors (Bernier et al., 2008a, 2008b, 2012; Fujiwara and Kubo, 2006). These studies further identified a dual polybasic cluster motif in the C-terminal region of certain P2X subtypes, in which positively charged residues such as K359 and K364 in rP2X1 (Bernier et al., 2008b), K365 and K369 in rP2X2 (Fujiwara and Kubo, 2006) and K362, K363, K370 and K371 in P2X4 (Bernier et al., 2008a, 2012) play a major role in the binding of PIPn. These adjacent polybasic amino acid clusters, with a net positive charge, are assumed to electrostatically interact with PIPn, which are anionic phospholipids (Bernier et al., 2012). These clusters are located close to the plasma membrane (3 residues from TM2 in the cytosolic region of the C terminal) in close vicinity to the negative phosphate head groups of PIPn in the membrane (Bernier et al., 2012).

The two polybasic clusters are not completely conserved among P2X receptors; in particular, this microdomain is lacking in P2X3, P2X5 and P2X7 subunits (Bernier et al., 2012). However, it has been shown that P2X3 and P2X7 are functionally modulated by PIPn, suggesting that either an indirect regulation mechanism must take place for these receptors (Bernier et al., 2012; Zhao et al., 2007) or these receptors interact with PIPn through other yet unidentified residues. Furthermore, mammalian P2X5 receptors are not sensitive to PIPn regulation (Ase et al., 2010), but negative-to-positive mutations (through mutating negatively-charged residues into positively-charged ones) in the twin clusters were sufficient to confer PIPn-binding and positive regulatory effect on the engineered receptor (Bernier et al., 2012). The identification of the three-dimensional location of these residues is hindered by the lack of intracellular domain structure. Determination of the structure of a full-length receptor, including the intracellular domain, will, therefore, certainly advance in atomic detail the precise molecular mechanism underlying PIPn allosteric regulation.

5. Optogating of P2X receptors

It is clear that a combination of the previously discussed studies, using a range of techniques and methods, has been able to advance our understanding of the molecular structure of P2X receptors and its relationship to their function. And yet, despite the numerous important discoveries made over the years, there are many aspects of P2X structure and function which remain unclear, in particular, the precise mechanism of the gating process and the implications of gating at a molecular level. Progress in these areas is hindered by a lack of pharmacological tools which can be implemented for more in-depth study.

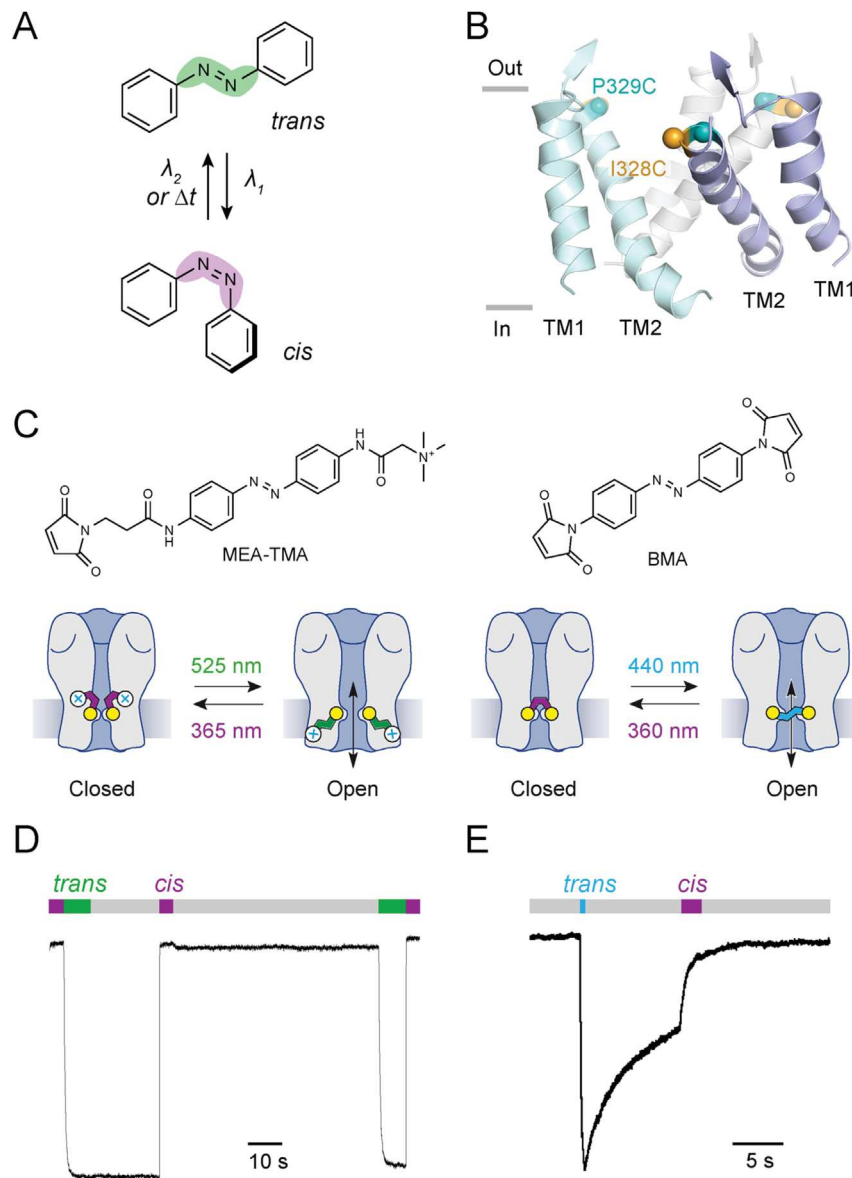


Fig. 4. Optical control of P2X function. (A) Isomerisation of the azobenzene from *trans* to *cis* occurs upon illumination of a particular wavelength λ_1 (usually near UV light) and illumination at a different wavelength λ_2 (in the visible light) or alternatively thermal relaxation (Δt), leads to the isomerisation back to the thermodynamically favoured *trans* isomer. (B) Lateral view of the transmembrane region of a homology model of rP2X2 based on the Δz P2X4 structure bound to ATP (4DW1) showing the location of I328C and P329C mutations that confer light sensitivity to the receptor following labelling with the appropriate photoswitchable probes. (C) Chemical structures of azobenzene compounds used to regulate P2X function by light. The scheme illustrates the light-induced gating mechanism of each photoswitchable probe. (D) Whole-cell currents evoked by light (*trans* induced by 525 nm and *cis* induced by 365 nm) in HEK cells expressing the I328C mutant treated by MEA-TMA (taken from Lemoine et al. (2013)). (E) Whole-cell currents evoked by light (*trans* induced by 440 nm and *cis* induced by 360 nm) in HEK cells expressing the P329C mutant treated by BMA (taken from Browne et al. (2014)).

However, new approaches based on optogenetic pharmacology principles may offer innovative, alternative ways of probing the structure and function of these ion channels. Optogenetic pharmacology, which involves the use of a synthetic photoisomerisable ligand covalently attached to a genetically modified ion channel, has given rise to a number of strategies which allow light-controlled gating of LGICs, such as nAChRs (Tochitsky et al., 2012), GABA_A receptor (Lin et al., 2014) and iGluR6 (Volgraf et al., 2006). Azobenzene-containing reagents are typically employed, as the azobenzene group is well characterised in its photoisomerisation behaviour – isomerisation from *trans* to *cis* occurs upon irradiation of a particular wavelength, λ_1 , and irradiation at a different wavelength, λ_2 , or alternatively thermal relaxation, leads to isomerisation back to the thermodynamically favoured *trans* isomer

(Fig. 4A). The azobenzene group also offers a number of advantages for biological applications (Mourot et al., 2013): *cis* – *trans* isomerisation takes place on the picosecond scale, causes a significant change in geometry of the molecule, and the absorption spectra of the two isomers are sufficiently different to ensure that only one isomer is mostly (but rarely completely) obtained upon irradiation at the required wavelength. Using light as a stimulus for ion channel activation is particularly attractive, as it can be applied with high spatial and temporal precision, and is considered as an orthogonal stimulus unable to trigger other biological processes. Recently, several strategies have also been developed to allow light-controlled gating of P2X receptors.

The first of these is the optogating method, developed by Lemoine et al. in 2013. This strategy uses P2X2 receptors carrying a

genetically encoded cysteine residue in the TM domain, to which is covalently tethered the photoswitchable reagent. In this case, the photoswitch employed is MEA-TMA, comprising a maleimide moiety for tethering to the cysteine, the central azobenzene segment and a positively charged trimethyl ammonium extremity, vital for efficient labelling (Fig. 4C). Irradiation in the visible or near UV region of light, causes the tethered MEA-TMA to undergo isomerisation to the *trans* or *cis* isomer respectively, which in turn induces an opening or closing of the channel (Fig. 4D) (Lemoine et al., 2013). The exact mechanism of optogating remains unknown, but it can be reasonably assumed that the movement involved in this isomerisation process causes a change in the interactions between TM helices, resulting in the gating of the channel (Fig. 4C).

Depending on the exact position at which the tethering cysteine is introduced, the channel may be opened by the molecule in the *cis* or *trans* isomer, giving rise to “*cis*-opener” and “*trans*-opener” positions. The position found to offer the most robust and stable light-induced currents is I328C, a *trans*-opener (Fig. 4D).

An important characteristic of this system is the bistability of the bound MEA-TMA, which ensures a stable photoactivation, sustained in the absence of irradiation. As shown in Fig. 4D, optogated currents induced by isomerisation to the *trans* isomer following irradiation at 525 nm remain stable even when irradiation is ceased and the system left in the dark over the course of 20 s. Only upon irradiation at 365 nm and isomerisation back to the *cis* isomer is a closing of the channel observed. This is particularly pertinent property when considering the possible extension of optogating to *in vivo* systems, as it means that only a transient irradiation would be required, therefore limiting any photodamage to the surrounding tissue.

A second method for achieving light-controlled P2X gating was developed by Browne et al. This strategy, whilst similar to optogating in the choice of an azobenzene compound, BMA, as the photoswitch, differs in that the photoswitch contains two maleimide moieties at the extremities and is thus able to cross-link to two anchoring points of the receptor complex, on different subunits (Fig. 4C). A mechanism of light-induced activation different to that of optogating is therefore at play, whereby light controlled toggling between *cis* and *trans* BMA isomers acts to bring the subunits closer or further apart, thus closing or opening the channel (Fig. 4E) (Browne et al., 2014). Of note, is that this method has been developed using the tethering position P329C, just one residue down from I328C, the position for which the most robust light-gated currents were observed with the optogating strategy (Fig. 4B). This area, located toward the upper end of the TM2 helix, may therefore represent a point in the channel region particularly effective for manipulating the molecular motions involved in channel opening.

As the photoswitches employed here are intrinsically devoid of pharmacological activity, there is the possibility to extend these strategies not only to other P2X variants, but also to other LGICs, offering a flexibility over previously developed optogenetic pharmacology based methods, where photoswitches must feature a pharmacologically active ligand (agonist, antagonist or allosteric modulator) specific for each receptor in question. This has been demonstrated with the BMA system, shown to control gating in P2X3, P2X2/3 heteromers as well as the structurally related ASIC1a channel. Both strategies have also been successfully implemented in P2X2 channels carrying the K69A mutation (Browne et al., 2014; Lemoine et al., 2013), which are known to be rendered unresponsive to their endogenous ligand ATP (Jiang et al., 2000). These systems therefore present the opportunity to study P2X receptors with an exquisite spatiotemporal control, where the only channel activity observed originates from the application of light.

It would be desirable to extend these strategies further, in particular, to the P2X4 and P2X7 subtypes, which have been found to play an important role in a number of disorders such as neuropathic pain (Beggs et al., 2012) and chronic inflammation (Di Virgilio and Vuerich, 2015). An eventual goal which can be envisaged for this work would be the development of systems suitable for use *in vivo*, allowing elucidation of the precise pathological contribution of P2X activation in models of such diseases.

6. Conclusion

In this review, we provided a summary of functional and structural studies on P2X receptors. Although the determination of X-ray structures provided an unprecedented insight into the understanding of the molecular operation of P2X receptors, there are still many questions which are left unanswered. In particular, what is the structure of the intracellular domain and how does it contribute to the function of the receptor? How do the various allosteric modulators regulate the response to ATP? What are the mechanisms of allosteric transition? And how may the pore dynamically change its permeability to cations? Elucidation of the answers to these intriguing questions will better define the functional role of P2X receptors in normal and pathological states.

References

- Acuna-Castillo, C., Coddou, C., Bull, P., Brito, J., Huidobro-Toro, J.P., 2007. Differential role of extracellular histidines in copper, zinc, magnesium and proton modulation of the P2X7 purinergic receptor. *J. Neurochem.* 101, 17–26.
- Adriouch, S., Bannas, P., Schwarz, N., Flieger, R., Guse, A.H., Seman, M., Haag, F., Koch-Nolte, F., 2008. ADP-ribosylation at R125 gates the P2X7 ion channel by presenting a covalent ligand to its nucleotide binding site. *FASEB J.* 22, 861–869.
- Agboh, K.C., Webb, T.E., Evans, R.J., Ennion, S.J., 2004. Functional characterization of a P2X receptor from *Schistosoma mansoni*. *J. Biol. Chem.* 279, 41650–41657.
- Albuquerque, E.X., Pereira, E.F., Alkondon, M., Rogers, S.W., 2009. Mammalian nicotinic acetylcholine receptors: from structure to function. *Physiol. Rev.* 89, 73–120.
- Allsopp, R.C., El Ajouz, S., Schmid, R., Evans, R.J., 2011. Cysteine scanning mutagenesis (residues Glu52–Gly96) of the human P2X1 receptor for ATP: mapping agonist binding and channel gating. *J. Biol. Chem.* 286, 29207–29217.
- Allsopp, R.C., Evans, R.J., 2011. The intracellular amino terminus plays a dominant role in desensitization of ATP-gated P2X receptor ion channels. *J. Biol. Chem.* 286, 44691–44701.
- Allsopp, R.C., Farmer, L.K., Fryatt, A.G., Evans, R.J., 2013. P2X receptor chimeras highlight roles of the amino terminus to partial agonist efficacy, the carboxyl terminus to recovery from desensitization, and independent regulation of channel transitions. *J. Biol. Chem.* 288, 21412–21421.
- Asatryan, L., Popova, M., Perkins, D., Trudell, J.R., Alkana, R.L., Davies, D.L., 2010. Ivermectin antagonizes ethanol inhibition in purinergic P2X4 receptors. *J. Pharmacol. Exp. Ther.* 334, 720–728.
- Ase, A.R., Bernier, L.P., Blais, D., Pankratov, Y., Seguela, P., 2010. Modulation of heteromeric P2X1/5 receptors by phosphoinositides in astrocytes depends on the P2X1 subunit. *J. Neurochem.* 113, 1676–1684.
- Bardoni, R., Goldstein, P.A., Lee, C.J., Gu, J.G., MacDermott, A.B., 1997. ATP P2X receptors mediate fast synaptic transmission in the dorsal horn of the rat spinal cord. *J. Neurosci.* 17, 5297–5304.
- Barrera, N.P., Ormond, S.J., Henderson, R.M., Murrell-Lagnado, R.D., Edwardson, J.M., 2005. Atomic force microscopy imaging demonstrates that P2X2 receptors are trimers but that P2X6 receptor subunits do not oligomerize. *J. Biol. Chem.* 280, 10759–10765.
- Beggs, S., Trang, T., Salter, M.W., 2012. P2X4R+ microglia drive neuropathic pain. *Nat. Neurosci.* 15, 1068–1073.
- Bernier, L.P., Ase, A.R., Chevallier, S., Blais, D., Zhao, Q., Boue-Grabot, E., Logothetis, D., Seguela, P., 2008a. Phosphoinositides regulate P2X4 ATP-gated channels through direct interactions. *J. Neurosci.* 28, 12938–12945.
- Bernier, L.P., Ase, A.R., Seguela, P., 2013. Post-translational regulation of P2X receptor channels: modulation by phospholipids. *Front. Cell. Neurosci.* 7, 226.
- Bernier, L.P., Ase, A.R., Tong, X., Hamel, E., Blais, D., Zhao, Q., Logothetis, D.E., Seguela, P., 2008b. Direct modulation of P2X1 receptor-channels by the lipid phosphatidylinositol 4,5-bisphosphate. *Mol. Pharmacol.* 74, 785–792.
- Bernier, L.P., Blais, D., Boue-Grabot, E., Seguela, P., 2012. A dual polybasic motif determines phosphoinositide binding and regulation in the P2X channel family. *PLoS One* 7, e40595.
- Bhargava, Y., Rettinger, J., Mourot, A., 2012. Allosteric nature of P2X receptor activation probed by photoaffinity labelling. *Br. J. Pharmacol.* 167, 1301–1310.
- Boue-Grabot, E., Archambault, V., Seguela, P., 2000. A protein kinase C site highly conserved in P2X subunits controls the desensitization kinetics of P2X(2) ATP-

- gated channels. *J. Biol. Chem.* 275, 10190–10195.
- Brake, A.J., Wagenbach, M.J., Julius, D., 1994. New structural motif for ligand-gated ion channels defined by an ionotropic ATP receptor. *Nature* 371, 519–523.
- Browne, L.E., Cao, L., Broomhead, H.E., Bragg, L., Wilkinson, W.J., North, R.A., 2011. P2X receptor channels show threefold symmetry in ionic charge selectivity and unitary conductance. *Nat. Neurosci.* 14, 17–18.
- Browne, L.E., Jiang, L.H., North, R.A., 2010. New structure enlivens interest in P2X receptors. *Trends Pharmacol. Sci.* 31, 229–237.
- Browne, L.E., North, R.A., 2013. P2X receptor intermediate activation states have altered nucleotide selectivity. *J. Neurosci.* 33, 14801–14808.
- Browne, L.E., Nunes, J.P., Sim, J.A., Chudasama, V., Bragg, L., Caddick, S., North, R.A., 2014. Optical control of trimeric P2X receptors and acid-sensing ion channels. *Proc. Natl. Acad. Sci. U. S. A.* 111, 521–526.
- Burnstock, G., 1972. Purinergic nerves. *Pharmacol. Rev.* 24, 509–581.
- Burnstock, G., 2006. Historical review: ATP as a neurotransmitter. *Trends Pharmacol. Sci.* 27, 166–176.
- Cao, L., Broomhead, H.E., Young, M.T., North, R.A., 2009. Polar residues in the second transmembrane domain of the rat P2X2 receptor that affect spontaneous gating, unitary conductance, and rectification. *J. Neurosci.* 29, 14257–14264.
- Cao, L., Young, M.T., Broomhead, H.E., Fountain, S.J., North, R.A., 2007. Thr339-to-serine substitution in rat P2X2 receptor second transmembrane domain causes constitutive opening and indicates a gating role for Lys308. *J. Neurosci.* 27, 12916–12923.
- Chataigneau, T., Lemoine, D., Grutter, T., 2013. Exploring the ATP-binding site of P2X receptors. *Front. Cell. Neurosci.* 7, 273.
- Clyne, J.D., LaPointe, L.D., Hume, R.I., 2002. The role of histidine residues in modulation of the rat P2X(2) purinoceptor by zinc and pH. *J. Physiol.* 539, 347–359.
- Coddou, C., Acuna-Castillo, C., Bull, P., Huidobro-Toro, J.P., 2007. Dissecting the facilitator and inhibitor allosteric metal sites of the P2X4 receptor channel: critical roles of CYS132 for zinc potentiation and ASP138 for copper inhibition. *J. Biol. Chem.* 282, 36879–36886.
- Coddou, C., Morales, B., Gonzalez, J., Grauso, M., Gordillo, F., Bull, P., Rassendren, F., Huidobro-Toro, J.P., 2003. Histidine 140 plays a key role in the inhibitory modulation of the P2X4 nucleotide receptor by copper but not zinc. *J. Biol. Chem.* 278, 36777–36785.
- Coddou, C., Stojilkovic, S.S., Huidobro-Toro, J.P., 2011a. Allosteric modulation of ATP-gated P2X receptor channels. *Rev. Neurosci.* 22, 335–354.
- Coddou, C., Yan, Z., Obsil, T., Huidobro-Toro, J.P., Stojilkovic, S.S., 2011b. Activation and regulation of purinergic P2X receptor channels. *Pharmacol. Rev.* 63, 641–683.
- Di Virgilio, F., Vuerich, M., 2015. Purinergic signaling in the immune system. *Auton. Neurosci.* 191, 117–123.
- Ding, S., Sachs, F., 1999. Ion permeation and block of P2X(2) purinoceptors: single channel recordings. *J. Membr. Biol.* 172, 215–223.
- Du, J., Dong, H., Zhou, H.X., 2012. Gating mechanism of a P2X4 receptor developed from normal mode analysis and molecular dynamics simulations. *Proc. Natl. Acad. Sci. U. S. A.* 109, 4140–4145.
- Egan, T.M., Khakh, B.S., 2004. Contribution of calcium ions to P2X channel responses. *J. Neurosci.* 24, 3413–3420.
- El-Ajouz, S., Ray, D., Allsopp, R.C., Evans, R.J., 2012. Molecular basis of selective antagonism of the P2X1 receptor for ATP by NF449 and suramin: contribution of basic amino acids in the cysteine-rich loop. *Br. J. Pharmacol.* 165, 390–400.
- Ennion, S., Hagan, S., Evans, R.J., 2000. The role of positively charged amino acids in ATP recognition by human P2X(1) receptors. *J. Biol. Chem.* 275, 29361–29367.
- Evans, R.J., 2009. Orthosteric and allosteric binding sites of P2X receptors. *Eur. Biophys. J.* 38, 319–327.
- Fischer, W., Zadori, Z., Kullnick, Y., Groger-Arndt, H., Franke, H., Wirkner, K., Illes, P., Mager, P.P., 2007. Conserved lysin and arginin residues in the extracellular loop of P2X(3) receptors are involved in agonist binding. *Eur. J. Pharmacol.* 576, 7–17.
- Friday, S.C., Hume, R.I., 2008. Contribution of extracellular negatively charged residues to ATP action and zinc modulation of rat P2X2 receptors. *J. Neurochem.* 105, 1264–1275.
- Fujiwara, Y., Kubo, Y., 2006. Regulation of the desensitization and ion selectivity of ATP-gated P2X2 channels by phosphoinositides. *J. Physiol.* 576, 135–149.
- Gao, C., Yu, Q., Xu, H., Zhang, L., Liu, J., Jie, Y., Ma, W., Samways, D.S., Li, Z., 2015. Roles of the lateral fenestration residues of the P2X4 receptor that contribute to the channel function and the deactivation effect of ivermectin. *Purinergic Signal.* 11, 229–238.
- Giniatullin, R., Nistri, A., 2013. Desensitization properties of P2X3 receptors shaping pain signaling. *Front. Cell. Neurosci.* 7, 245.
- Hattori, M., Gouaux, E., 2012. Molecular mechanism of ATP binding and ion channel activation in P2X receptors. *Nature* 485, 207–212.
- Hausmann, R., Gunther, J., Kless, A., Kuhlmann, D., Kassack, M.U., Bahrenberg, G., Markwardt, F., Schmalzing, G., 2013. Salt bridge switching from Arg290/Glu167 to Arg290/ATP promotes the closed-to-open transition of the P2X2 receptor. *Mol. Pharmacol.* 83, 73–84.
- Hausmann, R., Kless, A., Schmalzing, G., 2015. Key sites for P2X receptor function and multimerization: overview of mutagenesis studies on a structural basis. *Curr. Med. Chem.* 22, 799–818.
- Heymann, G., Dai, J., Li, M., Silberberg, S.D., Zhou, H.X., Swartz, K.J., 2013. Inter- and intrasubunit interactions between transmembrane helices in the open state of P2X receptor channels. *Proc. Natl. Acad. Sci. U. S. A.* 110, E4045–E4054.
- Huang, L.D., Fan, Y.Z., Tian, Y., Yang, Y., Liu, Y., Wang, J., Zhao, W.S., Zhou, W.C., Cheng, X.Y., Cao, P., Lu, X.Y., Yu, Y., 2014. Inherent dynamics of head domain correlates with ATP-recognition of P2X4 receptors: insights gained from molecular simulations. *PLoS One* 9, e97528.
- Huidobro-Toro, J.P., Lorca, R.A., Coddou, C., 2008. Trace metals in the brain: allosteric modulators of ligand-gated receptor channels, the case of ATP-gated P2X receptors. *Eur. Biophys. J.* 37, 301–314.
- Idzko, M., Ferrari, D., Eltzschig, H.K., 2014. Nucleotide signalling during inflammation. *Nature* 509, 310–317.
- Igawa, T., Abe, Y., Tsuda, M., Inoue, K., Ueda, T., 2015. Solution structure of the rat P2X4 receptor head domain involved in inhibitory metal binding. *FEBS Lett.* 589, 680–686.
- Jelinkova, I., Vavra, V., Jindrichova, M., Obsil, T., Zemkova, H.W., Zemkova, H., Stojilkovic, S.S., 2008. Identification of P2X(4) receptor transmembrane residues contributing to channel gating and interaction with ivermectin. *Pflugers Arch.* 456, 939–950.
- Jelinkova, I., Yan, Z., Liang, Z., Moonat, S., Teisinger, J., Stojilkovic, S.S., Zemkova, H., 2006. Identification of P2X4 receptor-specific residues contributing to the ivermectin effects on channel deactivation. *Biochem. Biophys. Res. Commun.* 349, 619–625.
- Jiang, L.H., Kim, M., Spelta, V., Bo, X., Surprenant, A., North, R.A., 2003. Subunit arrangement in P2X receptors. *J. Neurosci.* 23, 8903–8910.
- Jiang, L.H., Rassendren, F., Spelta, V., Surprenant, A., North, R.A., 2001. Amino acid residues involved in gating identified in the first membrane-spanning domain of the rat P2X(2) receptor. *J. Biol. Chem.* 276, 14902–14908.
- Jiang, L.H., Rassendren, F., Surprenant, A., North, R.A., 2000. Identification of amino acid residues contributing to the ATP-binding site of a purinergic P2X receptor. *J. Biol. Chem.* 275, 34190–34196.
- Jiang, R., Lemoine, D., Martz, A., Taly, A., Gonin, S., Prado de Carvalho, L., Specht, A., Grutter, T., 2011. Agonist trapped in ATP-binding sites of the P2X2 receptor. *Proc. Natl. Acad. Sci. U. S. A.* 108, 9066–9071.
- Jiang, R., Martz, A., Gonin, S., Taly, A., de Carvalho, L.P., Grutter, T., 2010. A putative extracellular salt bridge at the subunit interface contributes to the ion channel function of the ATP-gated P2X2 receptor. *J. Biol. Chem.* 285, 15805–15815.
- Jiang, R., Taly, A., Grutter, T., 2013. Moving through the gate in ATP-activated P2X receptors. *Trends Biochem. Sci.* 38, 20–29.
- Jiang, R., Taly, A., Lemoine, D., Martz, A., Cunrath, O., Grutter, T., 2012a. Tightening of the ATP-binding sites induces the opening of P2X receptor channels. *EMBO J.* 31, 2134–2143.
- Jiang, R., Taly, A., Lemoine, D., Martz, A., Specht, A., Grutter, T., 2012b. Intermediate closed channel state(s) precede(s) activation in the ATP-gated P2X2 receptor. *Channels (Austin)* 6, 398–402.
- Kawate, T., Michel, J.C., Birdsong, W.T., Gouaux, E., 2009. Crystal structure of the ATP-gated P2X(4) ion channel in the closed state. *Nature* 460, 592–598.
- Kawate, T., Robertson, J.L., Li, M., Silberberg, S.D., Swartz, K.J., 2011. Ion access pathway to the transmembrane pore in P2X receptor channels. *J. Gen. Physiol.* 137, 579–590.
- Khakh, B.S., Bao, X.R., Labarca, C., Lester, H.A., 1999a. Neuronal P2X transmitter-gated cation channels change their ion selectivity in seconds. *Nat. Neurosci.* 2, 322–330.
- Khakh, B.S., North, R.A., 2006. P2X receptors as cell-surface ATP sensors in health and disease. *Nature* 442, 527–532.
- Khakh, B.S., North, R.A., 2012. Neuromodulation by extracellular ATP and P2X receptors in the CNS. *Neuron* 76, 51–69.
- Khakh, B.S., Proctor, W.R., Dunwiddie, T.V., Labarca, C., Lester, H.A., 1999b. Allosteric control of gating and kinetics at P2X(4) receptor channels. *J. Neurosci.* 19, 7289–7299.
- Kinnamon, S.C., Finger, T.E., 2013. A taste for ATP: neurotransmission in taste buds. *Front. Cell. Neurosci.* 7, 264.
- Kowalski, M., Hausmann, R., Dopychai, A., Grohmann, M., Franke, H., Nieber, K., Schmalzing, G., Illes, P., Riedel, T., 2014. Conformational flexibility of the agonist binding jaw of the human P2X3 receptor is a prerequisite for channel opening. *Br. J. Pharmacol.* 171, 5093–5112.
- Lalo, U., Verkhatsky, A., Burnstock, G., Pankratov, Y., 2012. P2X receptor-mediated synaptic transmission. *WIREs Membr. Transp. Signal* 1, 297–309.
- Lemoine, D., Habermacher, C., Martz, A., Mery, P.F., Bouquier, N., Diverchy, F., Taly, A., Rassendren, F., Specht, A., Grutter, T., 2013. Optical control of an ion channel gate. *Proc. Natl. Acad. Sci. U. S. A.* 110, 20813–20818.
- Lemoine, D., Jiang, R., Taly, A., Chataigneau, T., Specht, A., Grutter, T., 2012. Ligand-gated ion channels: new insights into neurological disorders and ligand recognition. *Chem. Rev.* 112, 6285–6318.
- Li, M., Chang, T.H., Silberberg, S.D., Swartz, K.J., 2008. Gating the pore of P2X receptor channels. *Nat. Neurosci.* 11, 883–887.
- Li, M., Kawate, T., Silberberg, S.D., Swartz, K.J., 2010. Pore-opening mechanism in trimeric P2X receptor channels. *Nat. Commun.* 1, 44.
- Li, Z., Migita, K., Samways, D.S., Voigt, M.M., Egan, T.M., 2004. Gain and loss of channel function by alanine substitutions in the transmembrane segments of the rat ATP-gated P2X2 receptor. *J. Neurosci.* 24, 7378–7386.
- Lin, W.C., Davenport, C.M., Mourrot, A., Vytla, D., Smith, C.M., Medeiros, K.A., Chambers, J.J., Kramer, R.H., 2014. Engineering a light-regulated GABA_A receptor for optical control of neural inhibition. *ACS Chem. Biol.* 9, 1414–1419.
- Liu, X., Surprenant, A., Mao, H.J., Roger, S., Xia, R., Bradley, H., Jiang, L.H., 2008. Identification of key residues coordinating functional inhibition of P2X7 receptors by zinc and copper. *Mol. Pharmacol.* 73, 252–259.
- Lorca, R.A., Coddou, C., Gazitua, M.C., Bull, P., Arredondo, C., Huidobro-Toro, J.P., 2005. Extracellular histidine residues identify common structural determinants in the copper/zinc P2X2 receptor modulation. *J. Neurochem.* 95, 499–512.
- Lorinczi, E., Bhargava, Y., Marino, S.F., Taly, A., Kaczmarek-Hajek, K., Barrantes-

- Freer, A., Dutertre, S., Grutter, T., Rettinger, J., Nicke, A., 2012. Involvement of the cysteine-rich head domain in activation and desensitization of the P2X1 receptor. *Proc. Natl. Acad. Sci. U. S. A.* 109, 11396–11401.
- Marquez-Klaka, B., Rettinger, J., Nicke, A., 2009. Inter-subunit disulfide cross-linking in homomeric and heteromeric P2X receptors. *Eur. Biophys. J.* 38, 329–338.
- Michel, A.D., Clay, W.C., Ng, S.W., Roman, S., Thompson, K., Condreay, J.P., Hall, M., Holbrook, J., Livermore, D., Senger, S., 2008. Identification of regions of the P2X(7) receptor that contribute to human and rat species differences in antagonist effects. *Br. J. Pharmacol.* 155, 738–751.
- Mio, K., Kubo, Y., Ogura, T., Yamamoto, T., Sato, C., 2005. Visualization of the trimeric P2X2 receptor with a crown-capped extracellular domain. *Biochem. Biophys. Res. Commun.* 337, 998–1005.
- Mio, K., Ogura, T., Yamamoto, T., Hiroaki, Y., Fujiyoshi, Y., Kubo, Y., Sato, C., 2009. Reconstruction of the P2X(2) receptor reveals a vase-shaped structure with lateral tunnels above the membrane. *Structure* 17, 266–275.
- Moffatt, L., Hume, R.I., 2007. Responses of rat P2X2 receptors to ultrashort pulses of ATP provide insights into ATP binding and channel gating. *J. Gen. Physiol.* 130, 183–201.
- Mourat, A., Tochitsky, I., Kramer, R.H., 2013. Light at the end of the channel: optical manipulation of intrinsic neuronal excitability with chemical photoswitches. *Front. Mol. Neurosci.* 6, 5.
- Nagaya, N., Tittle, R.K., Saar, N., Dellal, S.S., Hume, R.I., 2005. An intersubunit zinc binding site in rat P2X2 receptors. *J. Biol. Chem.* 280, 25982–25993.
- Nakazawa, K., Yamakoshi, Y., Tsuchiya, T., Ohno, Y., 2005. Purification and aqueous phase atomic force microscopic observation of recombinant P2X2 receptor. *Eur. J. Pharmacol.* 518, 107–110.
- Newbolt, A., Stoop, R., Virginio, C., Surprenant, A., North, R.A., Buell, G., Rassendren, F., 1998. Membrane topology of an ATP-gated ion channel (P2X receptor). *J. Biol. Chem.* 273, 15177–15182.
- Nicke, A., Baumert, H.G., Rettinger, J., Eichele, A., Lambrecht, G., Mutschler, E., Schmalzing, G., 1998. P2X1 and P2X3 receptors form stable trimers: a novel structural motif of ligand-gated ion channels. *EMBO J.* 17, 3016–3028.
- Norenberg, W., Sobottka, H., Hempel, C., Plotz, T., Fischer, W., Schmalzing, G., Schaefer, M., 2012. Positive allosteric modulation by ivermectin of human but not murine P2X7 receptors. *Br. J. Pharmacol.* 167, 48–66.
- North, R.A., 2002. Molecular physiology of P2X receptors. *Physiol. Rev.* 82, 1013–1067.
- North, R.A., Jarvis, M.F., 2013. P2X receptors as drug targets. *Mol. Pharmacol.* 83, 759–769.
- Paoletti, P., Bellone, C., Zhou, Q., 2013. NMDA receptor subunit diversity: impact on receptor properties, synaptic plasticity and disease. *Nat. Rev. Neurosci.* 14, 383–400.
- Popova, M., Trudell, J., Li, K., Alkana, R., Davies, D., Asatryan, L., 2013. Tryptophan 46 is a site for ethanol and ivermectin action in P2X4 receptors. *Purinergic Signal.* 9, 621–632.
- Priel, A., Silberberg, S.D., 2004. Mechanism of ivermectin facilitation of human P2X4 receptor channels. *J. Gen. Physiol.* 123, 281–293.
- Rassendren, F., Buell, G., Newbolt, A., North, R.A., Surprenant, A., 1997. Identification of amino acid residues contributing to the pore of a P2X receptor. *EMBO J.* 16, 3446–3454.
- Roberts, J.A., Allsopp, R.C., El Ajouz, S., Vial, C., Schmid, R., Young, M.T., Evans, R.J., 2012. Agonist binding evokes extensive conformational changes in the extracellular domain of the ATP-gated human P2X1 receptor ion channel. *Proc. Natl. Acad. Sci. U. S. A.* 109, 4663–4667.
- Roberts, J.A., Digby, H.R., Kara, M., El Ajouz, S., Sutcliffe, M.J., Evans, R.J., 2008. Cysteine substitution mutagenesis and the effects of methanethiosulfonate reagents at P2X2 and P2X4 receptors support a core common mode of ATP action at P2X receptors. *J. Biol. Chem.* 283, 20126–20136.
- Robinson, L.E., Murrell-Lagnado, R.D., 2013. The trafficking and targeting of P2X receptors. *Front. Cell. Neurosci.* 7, 233.
- Rokic, M.B., Stojilkovic, S.S., 2013. Two open states of P2X receptor channels. *Front. Cell. Neurosci.* 7, 215.
- Rokic, M.B., Stojilkovic, S.S., Vavra, V., Kuzuyk, P., Tvrdonova, V., Zemkova, H., 2013. Multiple roles of the extracellular vestibule amino acid residues in the function of the rat P2X4 receptor. *PLoS One* 8, e59411.
- Samways, D.S., Egan, T.M., 2007. Acidic amino acids impart enhanced Ca²⁺ permeability and flux in two members of the ATP-gated P2X receptor family. *J. Gen. Physiol.* 129, 245–256.
- Samways, D.S., Khakh, B.S., Dutertre, S., Egan, T.M., 2011. Preferential use of unobstructed lateral portals as the access route to the pore of human ATP-gated ion channels (P2X receptors). *Proc. Natl. Acad. Sci. U. S. A.* 108, 13800–13805.
- Samways, D.S., Khakh, B.S., Egan, T.M., 2012. Allosteric modulation of Ca²⁺ flux in ligand-gated cation channel (P2X4) by actions on lateral portals. *J. Biol. Chem.* 287, 7594–7602.
- Samways, D.S., Li, Z., Egan, T.M., 2014. Principles and properties of ion flow in P2X receptors. *Front. Cell. Neurosci.* 8, 6.
- Samways, D.S., Migita, K., Li, Z., Egan, T.M., 2008. On the role of the first transmembrane domain in cation permeability and flux of the ATP-gated P2X2 receptor. *J. Biol. Chem.* 283, 5110–5117.
- Schwarz, N., Drouot, L., Nicke, A., Fliegert, R., Boyer, O., Guse, A.H., Haag, F., Adriouch, S., Koch-Nolte, F., 2012. Alternative splicing of the N-terminal cytosolic and transmembrane domains of P2X7 controls gating of the ion channel by ADP-ribosylation. *PLoS One* 7, e41269.
- Sensi, S.L., Paoletti, P., Bush, A.I., Sekler, I., 2009. Zinc in the physiology and pathology of the CNS. *Nat. Rev. Neurosci.* 10, 780–791.
- Shinozaki, Y., Sumitomo, K., Tsuda, M., Koizumi, S., Inoue, K., Torimitsu, K., 2009. Direct observation of ATP-induced conformational changes in single P2X(4) receptors. *PLoS Biol.* 7, e1000103.
- Silberberg, S.D., Chang, T.H., Swartz, K.J., 2005. Secondary structure and gating rearrangements of transmembrane segments in rat P2X4 receptor channels. *J. Gen. Physiol.* 125, 347–359.
- Silberberg, S.D., Li, M., Swartz, K.J., 2007. Ivermectin interaction with transmembrane helices reveals widespread rearrangements during opening of P2X receptor channels. *Neuron* 54, 263–274.
- Sim, J.A., Broomhead, H.E., North, R.A., 2008. Ectodomain lysines and suramin block of P2X1 receptors. *J. Biol. Chem.* 283, 29841–29846.
- Stelmashenko, O., Compan, V., Browne, L.E., North, R.A., 2014. Ectodomain movements of an ATP-gated ion channel (P2X2 receptor) probed by disulfide locking. *J. Biol. Chem.* 289, 9909–9917.
- Stelmashenko, O., Lalo, U., Yang, Y., Bragg, L., North, R.A., Compan, V., 2012. Activation of trimeric P2X2 receptors by fewer than three ATP molecules. *Mol. Pharmacol.* 82, 760–766.
- Stoop, R., Thomas, S., Rassendren, F., Kawashima, E., Buell, G., Surprenant, A., North, R.A., 1999. Contribution of individual subunits to the multimeric P2X(2) receptor: estimates based on methanethiosulfonate block at T336C. *Mol. Pharmacol.* 56, 973–981.
- Taly, A., Corringier, P.J., Guedin, D., Lestage, P., Changeux, J.P., 2009. Nicotinic receptors: allosteric transitions and therapeutic targets in the nervous system. *Nat. Rev. Drug Discov.* 8, 733–750.
- Tittle, R.K., Hume, R.I., 2008. Opposite effects of zinc on human and rat P2X2 receptors. *J. Neurosci.* 28, 11131–11140.
- Tittle, R.K., Power, J.M., Hume, R.I., 2007. A histidine scan to probe the flexibility of the rat P2X2 receptor zinc-binding site. *J. Biol. Chem.* 282, 19526–19533.
- Tochitsky, I., Banghart, M.R., Mourat, A., Yao, J.Z., Gaub, B., Kramer, R.H., Trauner, D., 2012. Optochemical control of genetically engineered neuronal nicotinic acetylcholine receptors. *Nat. Chem.* 4, 105–111.
- Valera, S., Hussy, N., Evans, R.J., Adami, N., North, R.A., Surprenant, A., Buell, G., 1994. A new class of ligand-gated ion channel defined by P2x receptor for extracellular ATP. *Nature* 371, 516–519.
- Virginio, C., Church, D., North, R.A., Surprenant, A., 1997. Effects of divalent cations, protons and calmidazolium at the rat P2X7 receptor. *Neuropharmacology* 36, 1285–1294.
- Virginio, C., MacKenzie, A., Rassendren, F.A., North, R.A., Surprenant, A., 1999. Pore dilation of neuronal P2X receptor channels. *Nat. Neurosci.* 2, 315–321.
- Volgraf, M., Gorostiza, P., Numano, R., Kramer, R.H., Isacoff, E.Y., Trauner, D., 2006. Allosteric control of an ionotropic glutamate receptor with an optical switch. *Nat. Chem. Biol.* 2, 47–52.
- Wildman, S.S., Brown, S.G., Rahman, M., Noel, C.A., Churchill, L., Burnstock, G., Unwin, R.J., King, B.F., 2002. Sensitization by extracellular Ca(2+) of rat P2X(5) receptor and its pharmacological properties compared with rat P2X(1). *Mol. Pharmacol.* 62, 957–966.
- Wildman, S.S., King, B.F., Burnstock, G., 1998. Zn²⁺ modulation of ATP-responses at recombinant P2X2 receptors and its dependence on extracellular pH. *Br. J. Pharmacol.* 123, 1214–1220.
- Wildman, S.S., King, B.F., Burnstock, G., 1999a. Modulation of ATP-responses at recombinant rP2X4 receptors by extracellular pH and zinc. *Br. J. Pharmacol.* 126, 762–768.
- Wildman, S.S., King, B.F., Burnstock, G., 1999b. Modulatory activity of extracellular H⁺ and Zn²⁺ on ATP-responses at rP2X1 and rP2X3 receptors. *Br. J. Pharmacol.* 128, 486–492.
- Wilkinson, W.J., Jiang, L.H., Surprenant, A., North, R.A., 2006. Role of ectodomain lysines in the subunits of the heteromeric P2X2/3 receptor. *Mol. Pharmacol.* 70, 1159–1163.
- Wirkner, K., Sperlagh, B., Illes, P., 2007. P2X3 receptor involvement in pain states. *Mol. Neurobiol.* 36, 165–183.
- Xu, X.J., Boumechache, M., Robinson, L.E., Marschall, V., Gorecki, D.C., Masin, M., Murrell-Lagnado, R.D., 2012. Splice variants of the P2X7 receptor reveal differential agonist dependence and functional coupling with pannexin-1. *J. Cell Sci.* 125, 3776–3789.
- Yan, Z., Khadra, A., Li, S., Tomic, M., Sherman, A., Stojilkovic, S.S., 2010. Experimental characterization and mathematical modeling of P2X7 receptor channel gating. *J. Neurosci.* 30, 14213–14224.
- Yan, Z., Liang, Z., Obsil, T., Stojilkovic, S.S., 2006. Participation of the Lys313-Ile333 sequence of the purinergic P2X4 receptor in agonist binding and transduction of signals to the channel gate. *J. Biol. Chem.* 281, 32649–32659.
- Zemkova, H., Khadra, A., Rokic, M.B., Tvrdonova, V., Sherman, A., Stojilkovic, S.S., 2015. Allosteric regulation of the P2X4 receptor channel pore dilation. *Pflugers Arch.* 467, 713–726.
- Zemkova, H., Yan, Z., Liang, Z., Jelinkova, I., Tomic, M., Stojilkovic, S.S., 2007. Role of aromatic and charged ectodomain residues in the P2X(4) receptor functions. *J. Neurochem.* 102, 1139–1150.
- Zhao, Q., Yang, M., Ting, A.T., Logothetis, D.E., 2007. PIP(2) regulates the ionic current of P2X2 receptors and P2X(7) receptor-mediated cell death. *Channels (Austin)* 1, 46–55.
- Zhao, W.S., Wang, J., Ma, X.J., Yang, Y., Liu, Y., Huang, L.D., Fan, Y.Z., Cheng, X.Y., Chen, H.Z., Wang, R., Yu, Y., 2014. Relative motions between left flipper and dorsal fin domains favour P2X4 receptor activation. *Nat. Commun.* 5, 4189.
- Zhuo, M., Wu, G., Wu, L.J., 2011. Neuronal and microglial mechanisms of neuropathic pain. *Mol. Brain* 4, 31.



UNIVERSITE DE STRASBOURG

RESUME DE LA THESE DE DOCTORAT

Discipline : Sciences de la Vie

Spécialité (facultative) : Neurobiologie moléculaire

Présentée par : DUNNING Kate

Titre : Études structurales et fonctionnelles des récepteurs P2X7

Unité de Recherche : UMR7199, Laboratoire de Conception et Application des Molécules Bioactives

Directeur de Thèse : GRUTTER Thomas, Directeur de recherche CNRS (DR2)

Localisation : Faculté de Pharmacie

ECOLES DOCTORALES :

(cocher la case)

<input type="checkbox"/> ED - Sciences de l'Homme et des sociétés	<input type="checkbox"/> ED 269 - Mathématiques, sciences de l'information et de l'ingénieur
<input type="checkbox"/> ED 99 – Humanités	<input type="checkbox"/> ED 270 – Théologie et sciences religieuses
<input type="checkbox"/> ED 101 – Droit, sciences politique et histoire	<input type="checkbox"/> ED 413 – Sciences de la terre, de l'univers et de l'environnement
<input type="checkbox"/> ED 182 – Physique et chimie physique	<input checked="" type="checkbox"/> ED 414 – Sciences de la vie et de la santé
<input type="checkbox"/> ED 221 – Augustin Cournot	
<input type="checkbox"/> ED 222 - Sciences chimiques	

Introduction

Les récepteurs P2X, activés par l'ATP, font partie de la famille des « Ligand Gated Ion Channels » (LGICs). Ces récepteurs-canaux sont activés par la liaison extracellulaire d'ATP, ce qui provoque un changement conformationnel rapide de la protéine, entraînant l'ouverture d'un canal et le passage de cations à travers la membrane cellulaire, en particulier des ions Ca^{2+} , Na^+ et K^+ . Ce processus s'appelle le « gating ». Cette famille, initialement découverte dans les années 90s^{1,2}, comprend 7 sous-types différents, nommés P2X1–7³. Ces sous-types, malgré des différences subtiles, possèdent tous une structure globale commune, c'est-à-dire un assemblage trimérique, qui peut être homo- ou hétéromérique selon la sous-unité concernée. Chaque monomère est composé de deux segments transmembranaires reliés entre eux par un grand domaine extracellulaire, où se trouve le site de fixation de l'agoniste ATP, ainsi que de deux extrémités N- et C-terminales intracellulaires.

Malgré ces similarités globales, il existe des différences importantes entre les sous-types. Ces différences résident non seulement au niveau de la distribution cellulaire et du rôle physiologique, mais également au niveau du fonctionnement moléculaire. Le sous-type P2X7, en particulier, est considéré comme un récepteur possédant des particularités remarquables qui le distinguent des autres sous-types de la famille, et ce pour de nombreuses raisons. Premièrement, il nécessite des concentrations d'ATP bien plus élevées, de l'ordre du mM, pour activer le récepteur P2X7. Deuxièmement, il présente une très grande extrémité C-terminale contenant 239 amides aminés (aa) et de nombreux motifs de séquence portant des significations biologiques³. L'obtention très récente, en 2019, de la structure du récepteur P2X7 de rat par cryo microscopie électronique (cryo-EM) a montré pour la première fois l'organisation structurale unique de cette région intracellulaire⁴. Outre sa structure, le récepteur P2X7 se démarque des autres sous-types au niveau fonctionnel, notamment à cause de deux phénomènes ; la facilitation des courants induite par une application prolongée ou répétée d'ATP, et la formation d'un macropore ou perméabilisation, qui correspond à une augmentation de perméabilité membranaire aux molécules de grandes tailles (<900 Da).⁵ Ces deux phénomènes sont uniques au récepteur P2X7 et leurs mécanismes sous-jacents restent encore inexpliqués depuis près de quatre décennies. Finalement, ayant un rôle dans de nombreuses pathologies, le récepteur P2X7 est aussi le plus intéressant de la famille d'un point de vue thérapeutique. Ces pathologies comprennent l'inflammation chronique, la douleur neuropathique, le cancer et la maladie d'Alzheimer, pour ne citer que quelques exemples.⁶⁻⁸ Une compréhension profonde de sa structure et de son fonctionnement moléculaire reste donc un défi majeur afin de concevoir de nouvelles solutions thérapeutiques efficaces ciblant ces maladies.

Cette thèse a pour but d'étudier des différents aspects structuraux et fonctionnels des récepteurs P2X7 en employant une combinaison d'approches expérimentales. Trois projets ont été explorés. Premièrement, une étude vers la structure du récepteur P2X7 humain par la technique de cryo-EM. Ensuite, l'utilisation des molécules photoactivables pour des études structurales et mécanistiques du récepteur P2X7. Le troisième axe de cette thèse, qui constitue le projet principal, concerne la résolution des mécanismes moléculaires des phénomènes de facilitation et la formation du macropore qui sont uniques au sous-type P2X7. Ce projet a également permis d'établir l'existence d'un complexe protéique entre la famille de canaux chlores activés par le calcium (CaCC) TMEM16s et le récepteur P2X7, qui module ces deux phénomènes.

1. Vers une structure du hP2X7 par cryoEM

Au début de cette thèse, il n'existait aucune structure cristallographique ou cryo-EM du récepteur P2X7. La technique de cryo-EM a récemment connu une « révolution », ce qui a confirmé son utilité dans l'étude des protéines membranaires qui sont souvent compliquées à isoler et nécessite des troncatures importantes avant l'étape de cristallogenèse. C'était donc dans le but d'obtenir une telle structure cryo-EM que nous avons commencé à travailler sur la production et la purification du récepteur P2X7 humain (hP2X7) dans sa version intégrale.

Pour ce faire, le système de production de protéines de cellules d'insectes Sf9 et baculovirus a été utilisé (Plateforme IGBMC), pour exprimer la construction hP2X7-8His. Malgré une expression de la protéine souhaitée, des tests initiaux d'isolation ont montré que le récepteur rP2X7 subit une agrégation rapide et importante, ce qui rend sa purification et reconstitution compliquée.

Pendant ma thèse, la structure du P2X7 de panda (pdP2X7) tronquée a été résolue⁹, et très récemment, l'équipe de Mansoor a réussi à résoudre la structure complète du récepteur P2X7 de rat (rP2X7), dans les états fermé et ouvert, par cryo-EM.⁴ Cette dernière structure a permis pour la première fois de visualiser l'extrémité C-terminale du récepteur, qui forme une structure nommée

« ballast », propre au sous-type P2X7. Ces travaux apportent des informations précieuses concernant la structure et des modifications post-traductionnelles des récepteurs rP2X7.

Pour ces raisons, nous avons décidé d'interrompre momentanément ce projet, mais qui dans le futur continuera en collaboration avec l'équipe de Dr. R. Wagner (ESBS), en se servant du système d'expression de levure, *P. pastoris*.

2. Utilisation des molécules photoactivables pour étudier le rP2X7

Un autre axe de recherche dans notre laboratoire est l'utilisation des molécules photoactivables pour étudier de manière structurale et fonctionnelle l'activité des récepteurs P2X, en utilisant la lumière en tant que stimulus spécifique et précis. Cette technique repose sur l'incorporation d'un photoswitch par réaction de Michael entre un groupement maléimide et le thiol d'une cystéine sur la protéine cible, introduite préalablement au point d'ancrage souhaité par modification génétique. Deux photoswitches ont été développés au laboratoire, portant un azobenzène central, qui permet l'isomérisation entre deux formes isomères, *cis* et *trans*, de géométrie distinctes, en utilisant des longueurs d'onde différentes (Figure 1a). Le premier de ces photoswitches, nommé MAM, a été développé au laboratoire pour étudier les mouvements moléculaires impliqués dans le processus de gating du récepteur P2X2.^{10,11} Les deux points d'ancrage créent des agrafes moléculaires, capables d'éloigner ou de rapprocher des paires de résidus, pour révéler des mouvements impliqués dans l'ouverture du canal, sans induire des mouvements non-naturels forcés. Le but de ce travail était donc de mettre au point l'utilisation des MAMs de longueurs différentes (MAM-1 à 4) pour étudier et comparer les mouvements moléculaires du récepteur P2X7 et de comparer ces mouvements à ceux du récepteur P2X2.

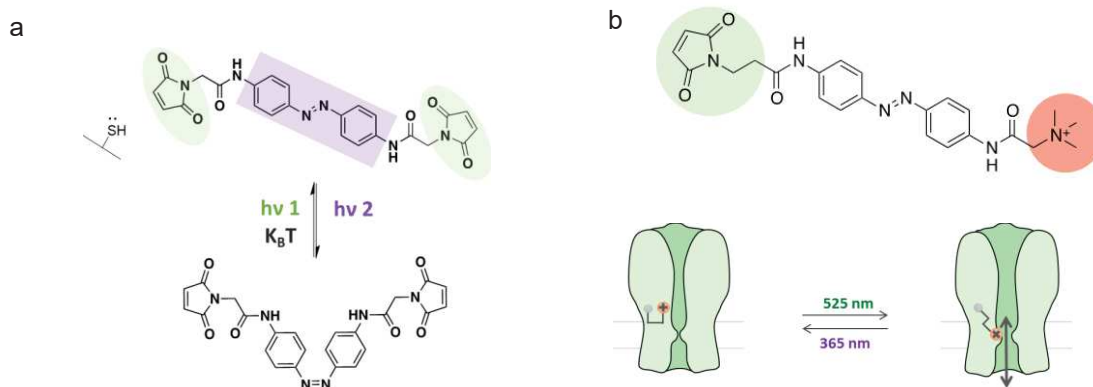


Figure 1. (a) Structure chimique du photoswitch MAM dans sa forme isomère *trans* (haut) et *cis* (bas). Le groupement thiol d'une cystéine cible pouvant réagir avec le groupement maléimide est montré à côté à gauche du MAM. (b) Structure chimique du photoswitch MEA-TMA. En dessous est schématisé son mode de fonctionnement pour contrôler optiquement le gating du récepteur P2X2.

L'utilisation des MAMs sur des récepteurs rP2X7 exprimés dans des cellules HEK293T a montré que plusieurs positions permettent de sonder les mouvements impliqués dans le gating du P2X7. En revanche, une faible photorégulation du récepteur type sauvage (sans introduction de cystéine) est également observée, ce qui complique l'interprétation des résultats. Malgré des efforts pour identifier la cystéine endogène qui réagit avec le MAM, la forte implication de ces cystéines dans le fonctionnement du récepteur limite la possibilité de les muter pour empêcher cette réaction d'avoir lieu. La fixation du MAM-4 dans une position non définie (ailleurs que le point d'ancrage souhaité) limite donc l'utilisation rigoureuse de cet outil pour étudier le sous-type P2X7.

Le deuxième photoswitch utilisé est le MEA-TMA (Figure 1b, en haut). Cette molécule, portant un seul groupement maléimide ainsi qu'une extrémité chargée positivement, se fixe à un seul point d'ancrage dans la partie transmembranaire du récepteur P2X2, et permet d'ouvrir le canal par déstabilisation des interactions entre les hélices (Figure 1b, en bas).¹² Une modulation des courants produits par l'ATP est également possible en isomérisant le photoswitch pour créer un blocage physique dans le canal ou « optoblock ». Cette technique a permis de contrôler optiquement l'ouverture de tous les sous-types P2X, à l'exception du sous-type P2X7. Nous avons donc exploré la mise au point de cet outil pour étudier le récepteur P2X7. Un criblage du deuxième segment transmembranaire a montré qu'aucune position d'ancrage ne permet d'ouvrir le canal de manière robuste en utilisant le MEA-TMA. Par contre, une modulation des réponses ATP par l'effet optoblock est possible sur plusieurs positions. On a donc employé cet optoblock pour étudier le phénomène de la facilitation, où nos

résultats indiquent l'implication de deux populations distinctes qui évoluent de manière différente au cours de la facilitation.

3. Etude des phénomènes de facilitation et « pore formation »

Deux caractéristiques qui font que le récepteur P2X7 est unique dans la famille P2X sont les phénomènes de la facilitation et la « pore formation » ou perméabilisation. La facilitation décrit une augmentation importante de courant produite par une application prolongée ou répétée d'ATP, et qui est connu pour être modulée par le cholestérol membranaire.¹³ La formation du macropore quant à elle concerne une perméabilité aux molécules de taille de l'ordre du nanomètre (<900 Da) à travers la membrane cellulaire suite à l'activation du récepteur P2X7. Le mécanisme de ce dernier processus a été longtemps disputé dans la littérature, en partie dû à une variabilité entre des types cellulaires différents. La possibilité qu'une protéine partenaire serait impliquée à ce phénomène a également été invoquée. Récemment, un lien fonctionnel a été suggéré entre le récepteur P2X7 et le TMEM16F, un membre de la famille de TMEM16s, des canaux chlores activés par le Ca^{2+} .¹⁴

Ces deux phénomènes sont souvent confondus, avec des mécanismes moléculaires peu résolus. Dans ce projet, qui constitue la majeure partie de mon travail de thèse, nous avons voulu aborder les questions suivantes : quels sont les déterminants moléculaires qui caractérisent l'état facilité ? Les phénomènes de la facilitation et la formation du macropore, proviennent-ils d'un même mécanisme commun ? Quelle est l'implication du canal TMEM16F dans ces deux processus ? Pour ce faire, nous avons utilisé une combinaison d'approches dans des cellules HEK293T exprimant le récepteur rP2X7. Notamment, l'électrophysiologie patch clamp, permettant de mesurer les courants produits par une activation du récepteur P2X7, ainsi que le suivi par vidéo-microscopie d'incorporation de YO-PRO-1, un colorant cationique de taille importante qui est souvent utilisé en tant qu'indicateur de perméabilisation membranaire.

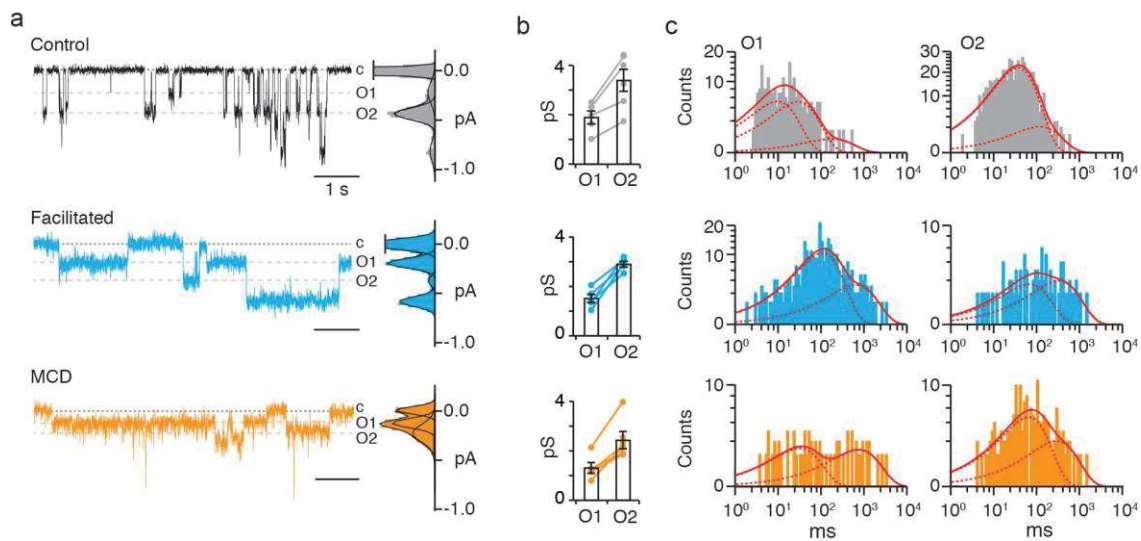


Figure 2. (a) Traces électrophysiologiques des courants induits par un analogue d'ATP, le BzATP, en configuration canal unique des récepteurs rP2X7 en conditions control (noir), facilité (bleu) et traité au MCD (orange). (b) Histogrammes représentant des conductances (en pS) des états O1 et O2 dans chaque condition. (c) Histogrammes du temps de résidence des ouvertures, dont le « fit » par des exponentiels permet de calculer le temps moyen d'ouverture de chaque condition.

Dans un premier temps nous avons étudié la facilitation en utilisant la technique d'électrophysiologie patch clamp dans la configuration « outside-out », qui permet d'enregistrer les courants passants par un canal unique (Figure 2). Nous avons enregistré des courants de canal unique dans des patches non-traités, des patches ayant été préalablement facilités à l'ATP et des patches ayant été traités par le méthyl- β -cyclodextrine (MCD), un agent chélateur de cholestérol membranaire. Grâce à cette technique, nous avons pu mettre en évidence deux conductances distinctes, nommées O1 et O2. Ces deux conductances sont conservées dans chaque condition testée ; par contre, nous avons pu déterminer que les récepteurs canaux facilités ont une probabilité d'ouverture (NP_o) augmentée de ~ 2.9 fois comparés aux récepteurs naïfs. Le traitement MCD, qui produit des patches de membranes appauvries en cholestérol, produit la même tendance d'augmentation d'activité du récepteur. Ces résultats montrent que le phénomène de la facilitation se produit suite à une augmentation de la

probabilité d'ouverture des canaux P2X7, probablement en conséquence de la dépletion de cholestérol.

Ensuite nous avons pu établir que les courants P2X7 sont inhibés par des inhibiteurs non-spécifiques des canaux chlores, tels que l'acide tannique, dans la configuration cellule entière ou « whole-cell » ainsi qu'en canal unique (Figure 3). Cette inhibition touche également aux récepteurs facilités. Que cette inhibition soit conservée dans des patchs membranaires excisés montre qu'une interaction forte et stable entre ces deux protéines existe. La présence d'une telle interaction est soutenue par des expériences de biochimie, qui démontrent une co-immunoprécipitation du récepteur rP2X7 par le rTMEM16F quand ces deux protéines sont co-exprimées dans des cellules HEK293T.

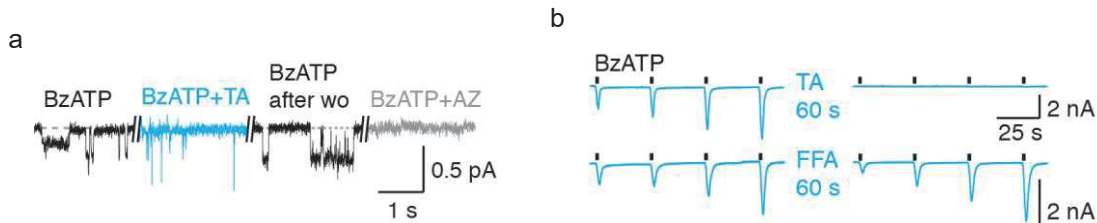


Figure 3. (a) Enregistrement électrophysiologique en canal unique des courants rP2X7 induits par le BzATP, et leur modulation par l'acide tannique (TA), un inhibiteur des canaux chlores, ainsi que le AZ10606120 (AZ) un inhibiteur spécifique du récepteur P2X7. (b) Enregistrements en configuration whole cell qui montrent l'inhibition des courants P2X7 facilités par le TA et l'acide flufenamique (FFA), des inhibiteurs de canaux chlores.

Pour étudier plus précisément le rôle de TMEM16F, nous avons établi une lignée de cellules HEK293T dépourvue de TMEM16F endogène (16F-null) en utilisant le système de CRISPR/Cas9. Une combinaison de mesures électrophysiologiques ainsi que des expériences d'incorporation de YO-PRO-1 a démontré que l'absence du TMEM16F n'a aucune incidence sur la facilitation observée en patch clamp, mais mène à une réduction significative de l'incorporation de YO-PRO-1 (Figure 3 a – c). Ces résultats montrent que i) le TMEM16F contribue au phénomène de la formation du macropore, et non au phénomène de la facilitation, ce qui suggère des voies mécanistiques différentes de ces deux processus et ii) le TMEM16F n'est pas le seul TMEM16 à être impliqué dans le complexe P2X7/TMEM16.

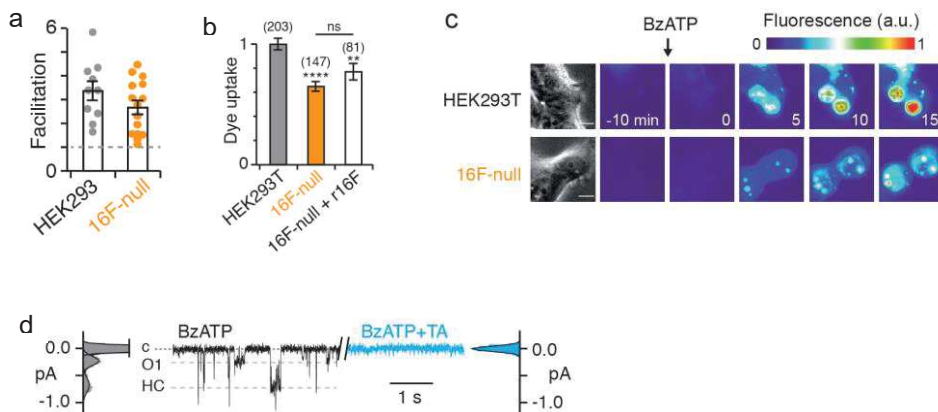


Figure 4. (a) Histogrammes montrant que le niveau de facilitation observée en présence (HEK293T) et absence (16F-null) du TMEM16F reste similaire. (b) Histogrammes montrant que l'incorporation de YO-PRO-1 observée dans des cellules 16F-null est significativement réduite par rapport à celles dans les cellules HEK293T. (c) Image de fluorescence de type « time series » montrant la fluorescence au cours de l'incorporation de YO-PRO-1 dans les deux lignées cellulaires. (d) Les courants unitaires provenant des récepteurs rP2X7 exprimés dans des cellules 16F-null restent sensibles aux inhibiteurs de canaux chlores, comme le TA.

Nous avons également identifié une mutation, P451L, de type Single-Nucleotide Polymorphism (SNP) dans l'extrémité C-terminale du récepteur P2X7, qui permet de séparer mécanistiquement une fois de plus les deux phénomènes.

Ces résultats permettent donc d'éclairer les mécanismes moléculaires de la facilitation et la formation du macropore. Malgré ces deux mécanismes différents, les deux processus sont modulés par un complexe entre le P2X7/TMEM16, y compris le TMEM16F, dans des cellules HEK293T. Ce travail a été soumis dans un journal à fort impact.

1. Brake, A. J., Wagenbach, M. J. & Julius, D. New structural motif for ligand-gated ion channels defined by an ionotropic ATP receptor. *Nature* **371**, 519–523 (1994).
2. Valera, S. *et al.* A new class of ligand-gated ion channel defined by P₂X₇ receptor for extracellular ATP. *Nature* **371**, 516–519 (1994).
3. North, R. A. Molecular physiology of P₂X₇ receptors. *Physiol. Rev.* **82**, 1013–1067 (2002).
4. McCarthy, A. E., Yoshioka, C. & Mansoor, S. E. Full-Length P₂X₇ Structures Reveal How Palmitoylation Prevents Channel Desensitization. *Cell* **179**, 659-670.e13 (2019).
5. Surprenant, A., Rassendren, F., Kawashima, E., North, R. A. & Buell, G. The Cytolytic P₂Z₂ Receptor for Extracellular ATP Identified as a P₂X₇ Receptor (P₂X₇). *Science* **272**, 735 (1996).
6. Hughes, J. P., Hatcher, J. P. & Chessell, I. P. The role of P₂X₇ in pain and inflammation. *Purinergic Signal.* **3**, 163–169 (2007).
7. Godoy, P. A., Ramírez-Molina, O. & Fuentealba, J. Exploring the Role of P₂X₇ Receptors in Alzheimer's Disease. *Front. Pharmacol.* **10**, (2019).
8. Burnstock, G. & Knight, G. E. The potential of P₂X₇ receptors as a therapeutic target, including inflammation and tumour progression. *Purinergic Signal.* **14**, 1–18 (2018).
9. Karasawa, A. & Kawate, T. Structural basis for subtype-specific inhibition of the P₂X₇ receptor. *eLife* **5**, e22153 (2016).
10. Habermacher, C. *et al.* Photo-switchable tweezers illuminate pore-opening motions of an ATP-gated P₂X₇ ion channel. *eLife* **5**, e11050 (2016).
11. Harkat, M. *et al.* On the permeation of large organic cations through the pore of ATP-gated P₂X₇ receptors. *Proc. Natl. Acad. Sci. U. S. A.* **114**, E3786–E3795 (2017).
12. Lemoine, D. *et al.* Optical control of an ion channel gate. *Proc. Natl. Acad. Sci.* **110**, 20813–20818 (2013).
13. Robinson, L. E., Shridar, M., Smith, P. & Murrell-Lagnado, R. D. Plasma membrane cholesterol as a regulator of human and rodent P₂X₇ receptor activation and sensitization. *J. Biol. Chem.* **289**, 31983–31994 (2014).
14. Ousingsawat, J. *et al.* Anoctamin 6 mediates effects essential for innate immunity downstream of P₂X₇ receptors in macrophages. *Nat. Commun.* **6**, 6245 (2015).

Publications :

- **Dunning, K.***, Martz, A.*, Peralta, F.A., Cevoli, F., Boué-Grabot, E., Taly, A., Compan, V., Gautherat, F., Wolf, P., Chataigneau, T., Grutter, T., P2X7 Receptors and TMEM16 Form a Regulating Hub with Implications for Macropore Formation and Current Facilitation, *soumis*
- Peverini, L., Beudez, J., **Dunning, K.**, Chataigneau, T., Grutter, T., (2018) New Insights Into Permeation of Large Cations Through ATP-gated P2X Receptors, *Front. Mol. Neurosci.*, *11*, 265
- Harkat, M.*, Peverini, L.*, Cerdan, A.H., **Dunning, K.**, Beudez, J., Martz, A., Calimet, N., Specht, A., Cecchini, M., Chataigneau, T., Grutter, T., (2017) On the permeation of large organic cations through the pore of ATP-gated P2X receptors, *Proc. Natl. Acad. Sci.*, *114*, 19, E3786-E3795
- Habermacher, C., **Dunning, K.**, Chataigneau, T., Grutter, T., (2015) Molecular structure and function of P2X receptors, *104*, 18 – 30

* = these authors contributed equally to this work.

Communications orales et par affiches :

- Communication orale: Studies on the sensitisation phenomenon of P2X7 receptors by use of photoisomerisable tools, International Symposium on Photopharmacology, Barcelona, 2018
- Communication par affiche: **Dunning, K.**, Grutter, T., Studies on the sensitisation phenomenon of P2X7 receptors by use of photoisomerisable tools, International Symposium on Photopharmacology, Barcelone, Espagne, 2018
- Communication par affiche: **Dunning, K.**, Grutter, T., Studies on the sensitization phenomenon of P2X7 receptors, Ligand Gated Ion Channels from structure to synaptic transmission (conférence Jacques Monod), Roscoff, France, 2019